

A new species of *Gaillardiellus* Guinot, 1976 (Crustacea, Brachyura, Xanthidae) from the coral reefs of the South China Sea

Yuan Ziming^{1,2,3,4}, Jiang Wei^{1,2,3,4}, Sha Zhongli^{1,2,3,4}

¹ Department of Marine Organism Taxonomy and Phylogeny, Institute of Oceanology, Chinese Academy of Sciences, Qingdao 266071, China

² Laboratory for Marine Biology and Biotechnology, Qingdao Marine Science and Technology Center, Qingdao 266237, China

³ Shandong Province Key Laboratory of Experimental Marine Biology, Institute of Oceanology, Chinese Academy of Sciences, Qingdao 266071, China

⁴ University of Chinese Academy of Sciences, Beijing 100049, China

Corresponding author: Sha Zhongli (shazl@qdio.ac.cn)

Abstract

A new xanthid species of *Gaillardiellus* Guinot, 1976, is described from the coral reefs of the Xisha and Nansha Islands in the South China Sea. The new species, *Gaillardiellus magiruber* sp. nov., closely resembles *G. rueppellii* (Krauss, 1843) but can be distinguished mainly by its closer proximity of the outer orbital angle and anterolateral margin, which lacks an accessory lobe, a broader and non-protruding front, and notable differences in live coloration and size. Molecular analysis of mitochondrial cytochrome c oxidase I (COI) sequences further corroborates the validity of this new species. An updated identification key for *Gaillardiellus* is provided.

Key words: Actaeinae, COI, *Gaillardiellus*, identification key, morphology, new species, rock crabs, taxonomy



Academic editor: Sameer Pati

Received: 10 December 2024

Accepted: 19 February 2025

Published: 8 April 2025

ZooBank: <https://zoobank.org/E5C71E6F-577A-45F8-8B44-7D2DBEE09299>

Citation: Ziming Y, Wei J, Zhongli S (2025) A new species of *Gaillardiellus* Guinot, 1976 (Crustacea, Brachyura, Xanthidae) from the coral reefs of the South China Sea. ZooKeys 1234: 1–17. <https://doi.org/10.3897/zookeys.1234.144026>

Copyright: © Yuan Ziming et al.
This is an open access article distributed under terms of the Creative Commons Attribution License (Attribution 4.0 International – CC BY 4.0).

Introduction

The xanthid genus *Gaillardiellus* was first described by Guinot (1976), who included four species (including *G. rueppellii* (Krauss, 1843) as the type species), which were previously known under *Actaea* De Haan, 1833. The main distinguishing characteristics of *Gaillardiellus* include a carapace divided into distinct regions, an anterolateral margin subdivided into three or four lobes, pereopods that lack nodules except for those on the carpus of the chelipeds, and distinctly sinuous margins of male pleonites 3–5, which fit closely with the corresponding parts of the thoracic sternum (Guinot 1976).

Currently, six species of *Gaillardiellus* are known worldwide: *G. rueppellii*, *G. alphonsi* (Nobili, 1905), *G. orientalis* (Odhnor, 1925), *G. superciliaris* (Odhnor, 1925), *G. bathus* Davie, 1997, and *G. holthuisi* Takeda & Komatsu, 2010 (Ng et al. 2008; Takeda and Komatsu 2010). These species inhabit the Indo-West Pacific region, ranging from intertidal zone to bathyal zone exceeding 300 m depth (Davie 1997).

In a recent coral reef biodiversity survey, a new species of *Gaillardiellus*, *G. magiruber* sp. nov., was discovered from the Xisha and Nansha Islands in the

South China Sea. Here, we provide a detailed description of this species, supported by mitochondrial cytochrome c oxidase I (COI) sequence data to confirm its validity. Additionally, we present an updated identification key for the genus.

Material and methods

Morphological analyses

Material was collected by diving or remotely operated vehicle (ROV) from coral reefs in the South China Sea and preserved in 70% ethanol. The specimens were deposited at the Marine Biological Museum, Chinese Academy of Sciences (MBMCAS) in Qingdao, China, and were assigned catalogue numbers with the MBM prefix. A specimen from the Institute of Zoology, Chinese Academy of Sciences, was also examined and assigned catalogue numbers with the IOZ prefix. Morphological characteristics were observed using a ZEISS SteREO Discovery V20 stereoscopic microscope. Photographs were taken with a Canon EOS 6D camera equipped with a Canon MP-E 65 mm lens or a ZEISS Axiocam 506 microscope camera.

The terminology used primarily follows Serène (1984) and Davie et al. (2015). The following abbreviations are used in the text: CW = maximum carapace width; CL = median carapace length; G1 = first gonopod of male; G2 = second gonopod of male.

Phylogenetic analyses

Genomic DNAs were extracted from muscle tissue by OMEGA EZNA Tissue DNA Kit. Mitochondrial cytochrome c oxidase I (COI, 658 bp) sequences were obtained for molecular phylogenetic analyses and amplified by polymerase chain reaction (PCR) with the primers jgLCO1490 and jgHCO2198 (Geller et al. 2013) or Pano-F and Pano-R (Thoma et al. 2014). The PCR 25 µl volumes contained: 1 µl (3–200 ng) of genomic DNA template, 1 µl (10 pM) of each primer, 12 µl of 2×PCR Mix (Dongsheng Biotech, Guangzhou, China), and 10 µl ultrapure water. Reactions were carried out with initial denaturation at 94 °C for 3 min, 35 cycles for denaturation at 94 °C for 30 s, annealing at 48 °C for 45 s, extension at 72 °C for 45 s, and final extension at 72 °C for 10 min.

Sixteen sequences representing 10 species were used for the analysis (Table 1). The sequences with the ZRC prefix originated from specimens from the Zoological Reference Collection of the Lee Kong Chian Natural History Museum (LKCNHM), National University of Singapore, Singapore. The nucleotide sequences were aligned using Muscle default settings in MEGA v. 6.06 (Tamura et al. 2013). The phylogenetic trees were reconstructed using maximum likelihood (ML) and Bayesian Inference (BI) algorithms. The best-fitting model was selected using jModeltest v. 0.1.1 under the Akaike information criterion (AIC) (Posada 2008). The BI analyses were performed using MrBayes v. 3.2.7 (Huelsenbeck and Ronquist 2001), utilizing a Markov Chain Monte Carlo (MCMC) algorithm. Two independent runs were conducted, each comprising four chains over 1,000,000 generations, with tree sampling every 500 generations, resulting in 2000 sampled trees. The first 500 trees were discarded as burn-in, and posterior probabilities were calculated based on the remaining

Table 1. Species and sequences used in the phylogenetic analysis with GenBank accession numbers.

| Catalogue number | Voucher ID | GenBank accession number | Species | Location | Reference |
|------------------|--|--------------------------|---|---|------------------|
| MBM288134 | NS-MJ-2022-1859 | PQ195874 | <i>Gaillardiiellus magiruber</i> sp. nov. | China: Mischief Reef, Nansha Islands | present study |
| MBM288135 | XS-QL-2022-1030 | PQ195876 | <i>Gaillardiiellus magiruber</i> sp. nov. | China: Qilianyu Islands, Xisha Islands | present study |
| MBM288142 | G01 | PQ195869 | <i>Gaillardiiellus orientalis</i> (Odhnér, 1925) | China: Qingdao, Shandong | present study |
| ZRC 2000.1196 | ZRC 2000.1196 | HM750987 | <i>Gaillardiiellus orientalis</i> (Odhnér, 1925) | Singapore: Palau Seringat | Lai et al. 2011 |
| MBM283642 | MBM283642 | PQ195870 | <i>Gaillardiiellus rueppellii</i> (Krauss, 1843) | China: Weizhou Island, Guangxi | present study |
| ZRC 2010.0162 | ZRC 2010.0162 | HM750988 | <i>Gaillardiiellus rueppellii</i> (Krauss, 1843) | Philippines: Bohol Island | Lai et al. 2011 |
| N.A. | PH | OP759455 | <i>Gaillardiiellus rueppellii</i> (Krauss, 1843) | South Korea: Jodo Island, Yeongdo-gu, Busan | unpublished |
| MBM288143 | 2404188881 | PQ195868 | <i>Gaillardiiellus superciliaris</i> (Odhnér, 1925) | China: Zhongbei Shoal, Zhongsha Islands | present study |
| N.A. | UF:Invertebrate Zoology:45484-Arthropoda | MW277787 | <i>Gaillardiiellus superciliaris</i> (Odhnér, 1925) | USA: Patch Reef, Kaneohe Bay, Oahu, Hawaii | unpublished |
| MBM288144 | XS-QL-2022-1108 | PQ195877 | <i>Paractaea tumulosa</i> (Odhnér, 1925) | China: Qilianyu Islands, Xisha Islands | present study |
| MBM288145 | G03 | PQ195871 | <i>Paractaea</i> cf. <i>excentrica</i> Guinot, 1969 | China: Tree Island, Xisha Islands | present study |
| MBM288146 | JN01 | PQ195872 | <i>Paractaea retusa</i> (Nobili, 1906) | China: Fiery Cross Reef, Nansha Islands | present study |
| MBM288147 | JN02 | PQ195873 | <i>Paractaea retusa</i> (Nobili, 1906) | China: Tree Island, Xisha Islands | present study |
| MBM288148 | NI01 | PQ195875 | <i>Paractaea plumosa</i> Guinot in Sakai, 1976 | China: Phoenix Island, Hainan | present study |
| MBM288149 | ZS-MB-2022-1022 | OP718532 | <i>Trapezia lutea</i> Castro, 1997 | China: Walker Shoal, Zhongsha Islands | Yuan et al. 2023 |
| MBM288150 | XS-YL-2022-1012 | OP718531 | <i>Trapezia digitalis</i> Latreille, 1828 | China: Yongle Islands, Xisha Islands | Yuan et al. 2023 |

trees. The ML analyses were conducted online using W-IQ-TREE (<http://iqtree.cibiv.univie.ac.at/>) (Trifinopoulos et al. 2016), with clade support evaluated via 10,000 ML bootstrap replications.

Multiple species delimitation methods were employed to evaluate the hypothesis that the specimens represent a distinct species. COI data were analyzed using the Automated Barcode Gap Discovery (ABGD) method via the ABGD web-based platform (<https://bioinfo.mnhn.fr/abi/public/abgd/abgdweb.html>) as described by Puillandre et al. (2012). The analysis was performed using the Kimura 2-parameter substitution model (TS/TV = 2.0), with the prior for maximum intraspecific divergence set between 0.001 and 0.1, over 10 recursive steps, and a relative gap width (X) of 1.0. Additionally, the Bayesian implementation of the Poisson Tree Processes (bPTP) species delimitation model was applied following Zhang et al. (2013). This analysis was conducted on the web server of the Heidelberg Institute for Theoretical Studies, Germany (<http://species.h-its.org/>), utilizing BI phylogenetic trees as input data.

Taxonomic account

Family Xanthidae MacLeay, 1838

Subfamily Actaeinae Alcock, 1898

Genus *Gaillardiiellus* Guinot, 1976

Gaillardiiellus magiruber sp. nov.

<https://zoobank.org/0D5CECEE-4112-4E55-8537-620637B3BE52>

Figs 1–5, Suppl. material 1

Material examined. *Holotype*: CHINA • ♂, 5.9 × 4.4 mm; Xisha Islands, Tree Island; depth 58 m; 2 Jul. 1977; Dong Dong leg.; MBM288133. *Paratypes*: CHINA • 1 ♀, 9.8 × 7.1 mm; Nansha Islands, Mischief reef; 9°54'N, 115°34'E; depth 1 m; 11 May 2022; Yuan Ziming, Sun Yuli, Ma Shaobo leg.; MBM288134 • 1 ♀, 9.5 × 6.4 mm; Nansha Islands, Banyue Reef; 29 Sep. 1994; MBM164284 • 1 ♀, 5.7 × 4.2 mm; Xisha Islands, Qilianyu Islands; 16°58'N, 112°16'E; depth 10 m; 19 May 2022; Yuan Ziming, Sun Yuli, Ma Shaobo leg.; MBM288135 • 1 juvenile ♂, 4.5 × 3.5 mm; Xisha Islands, North Reef; depth 30 m; 1 Sep. 2024; Dong Dong leg.; MBM288136 • 1 juvenile ♂, 4.2 × 3.3 mm; Xisha Islands, Huaguang Reef; depth 31 m; 26 Aug. 2024; Dong Dong leg.; MBM288137 • 1 juvenile ♀, 4.5 × 3.4 mm; Xisha Islands, Yagong Island; depth 33 m; 19 Aug. 2024; Dong Dong leg.; MBM288138 • 1 juvenile ♀, 4.1 × 3.0 mm; Xisha Islands, Yagong Island; depth 31 m; 20 Aug. 2024; Dong Dong leg.; MBM288139.

Comparative material. *Gaillardiiellus rueppellii* (Krauss, 1843) (Figs 6A, B, 7) CHINA • 1 ♂; Xisha Islands, Money Island; 17 Mar. 1977; IOZ31604-01-4 • 1 ♂; Hainan, Dachan Island; 25 Mar. 2018; MBM288140 • 1 ♂; Hainan, Lingao Bay; depth 15–30 m; 20 Aug. 2018; Pan Yunhao leg.; MBM288141 • 1 ♂; Guangxi, Weizhou Island; 19 Nov. 2018; MBM283642. CW 25.3–45.6 mm, CL 19.4–34.4 mm. *Gaillardiiellus orientalis* (Odhner, 1925) (Fig. 6C, D) CHINA • 1 ♂, 34.9 × 25.8 mm; Shandong, Qingdao; 22 Jul. 2015; Yang Bin leg.; MBM288142. *Gaillardiiellus superciliaris* (Odhner, 1925) (Fig. 6E, F) CHINA • 1 ♂, 11.6 × 7.9 mm; Zhongsha Islands, Zhongbei Shoal; 16°5'N, 114°25'E; 6 May 2024; Yuan Ziming leg.; MBM288143.

Diagnosis. Carapace (Figs 1A, B, 2A, 3A, B, 4A, B) transversely oval, regions clearly defined, short setae present within grooves and between granules, long setae scattered between granules; front not protruding, slightly curved downwards, divided into 2 lobes by broad V-shaped notch; anterolateral margin divided into 4 granular lobes, first lobe small, slightly larger than outer orbital angle, adjacent to latter; posterolateral margin shorter than anterolateral margin, distinctly concave. Thoracic sternum (Figs 1D, 3D) with low granules, sternites 1 to 4 covered with soft setae. Male pleonite 6 (Figs 1D, 2B) with expanded lateral distal angles, wider than long; telson wider than long, terminal end blunt. G1 (Fig. 2F, G, J, K) curved outwards, distal third with small spines, long setae near distal end, terminal lobe slender. Orange-red to vibrant bright red in life (Fig. 5).

Description of male holotype. Carapace (Figs 1A, B, 2A) transversely oval, CW about 1.3 times CL, dorsal surface slightly elevated, regions clearly defined, covered with granules, grooves wide and deep; short setae present within grooves and between granules, long setae scattered between granules; regions 1–3M distinct, 2M completely divided into 2 lobes, 3M

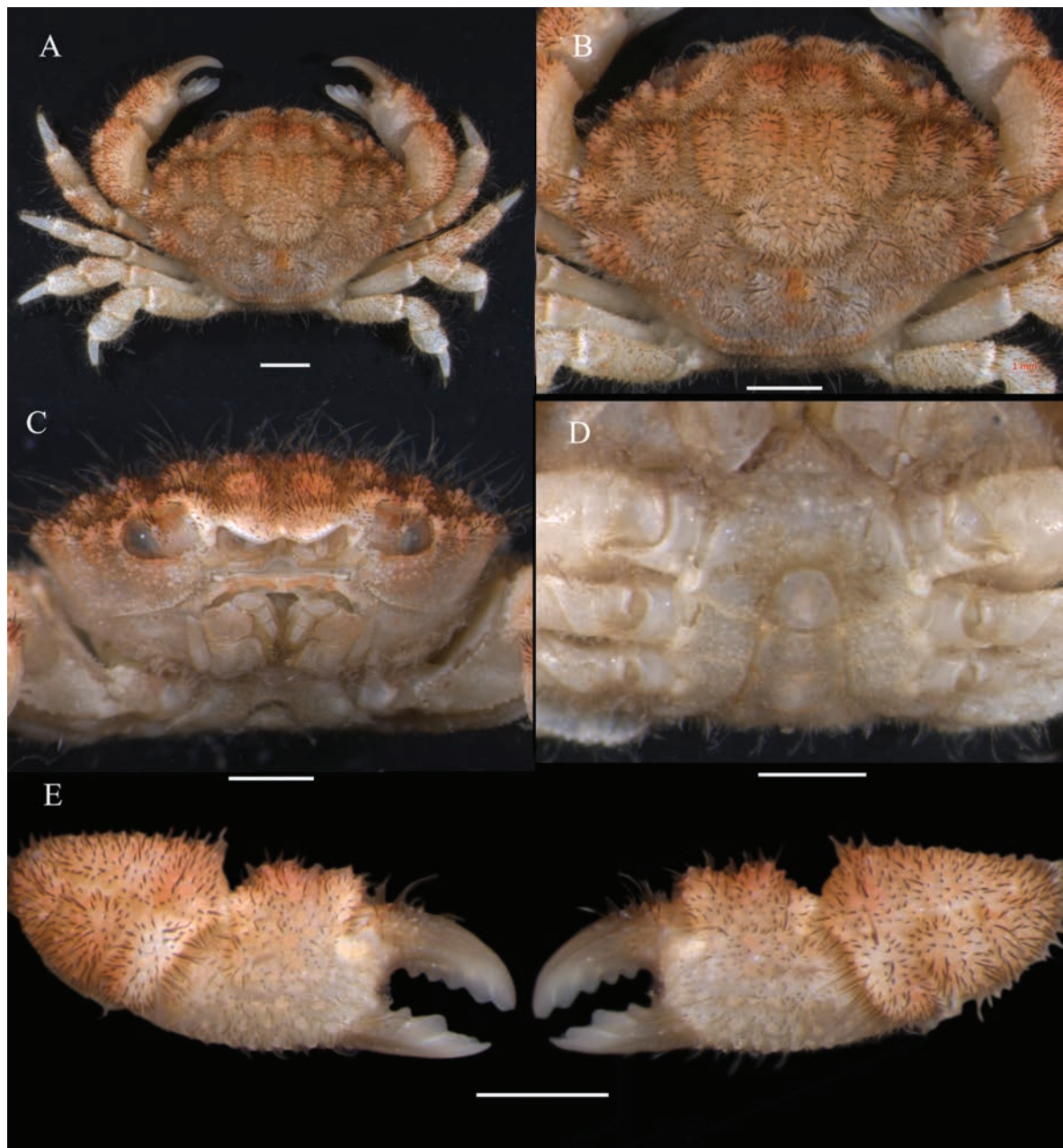


Figure 1. *Gaillardiiellus magiruber* sp. nov., male holotype (5.9 × 4.4 mm) (MBM288133) **A** overall dorsal view **B** dorsal view of cephalothorax **C** frontal view of cephalothorax **D** thoracic sternites, pleon and telson **E** outer view of chelipeds. Scale bar: 1 mm.

intact, 4M indistinct; regions 2–6L distinct, 1P distinct, 2P indistinct; front about 0.3 times CW, not protruding, slightly curved downwards, divided into 2 lobes by broad V-shaped notch, inner lobes rounded and more prominent, outer lobes smaller and flatter, separated from inner orbital angle by notch; dorsal orbital margin with 2 sutures; eyestalks with setae and granules near cornea. Outer orbital angle not fused with anterolateral margin; anterolateral margin divided into 4 granular lobes, first lobe small, slightly larger than outer orbital angle, adjacent to latter, second and third lobes broader, fourth lobe smaller than third; posterolateral margin shorter than anterolateral margin, distinctly concave; subhepatic region with granules and short setae; pterygostomial region smooth with soft setae.

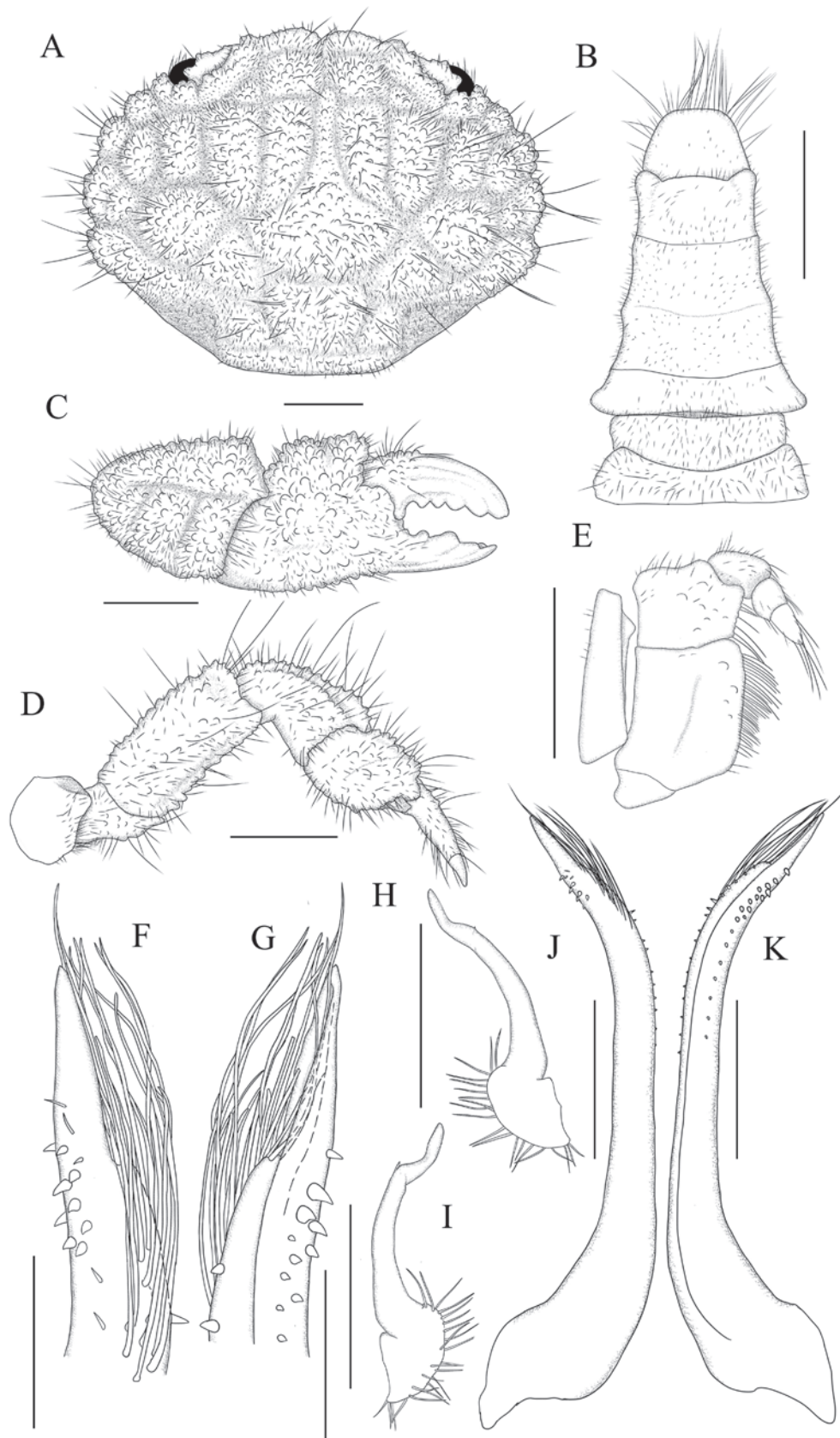


Figure 2. *Gaillardiiellus magiruber* sp. nov., male holotype (5.9 × 4.4 mm) (MBM288133) **A** dorsal view of cephalothorax **B** pleon and telson **C** outer view of right cheliped **D** right pereopod **E** right third maxilliped **F** dorsal view of left G1 distal part **G** ventral view of left G1 distal part **H** dorsal view of left G2 **I** ventral view of left G2 **J** dorsal view of left G1 **K** ventral view of left G1. Scale bars: 1 mm (**A–E**); 0.2 mm (**F, G**); 0.5 mm (**H–K**).

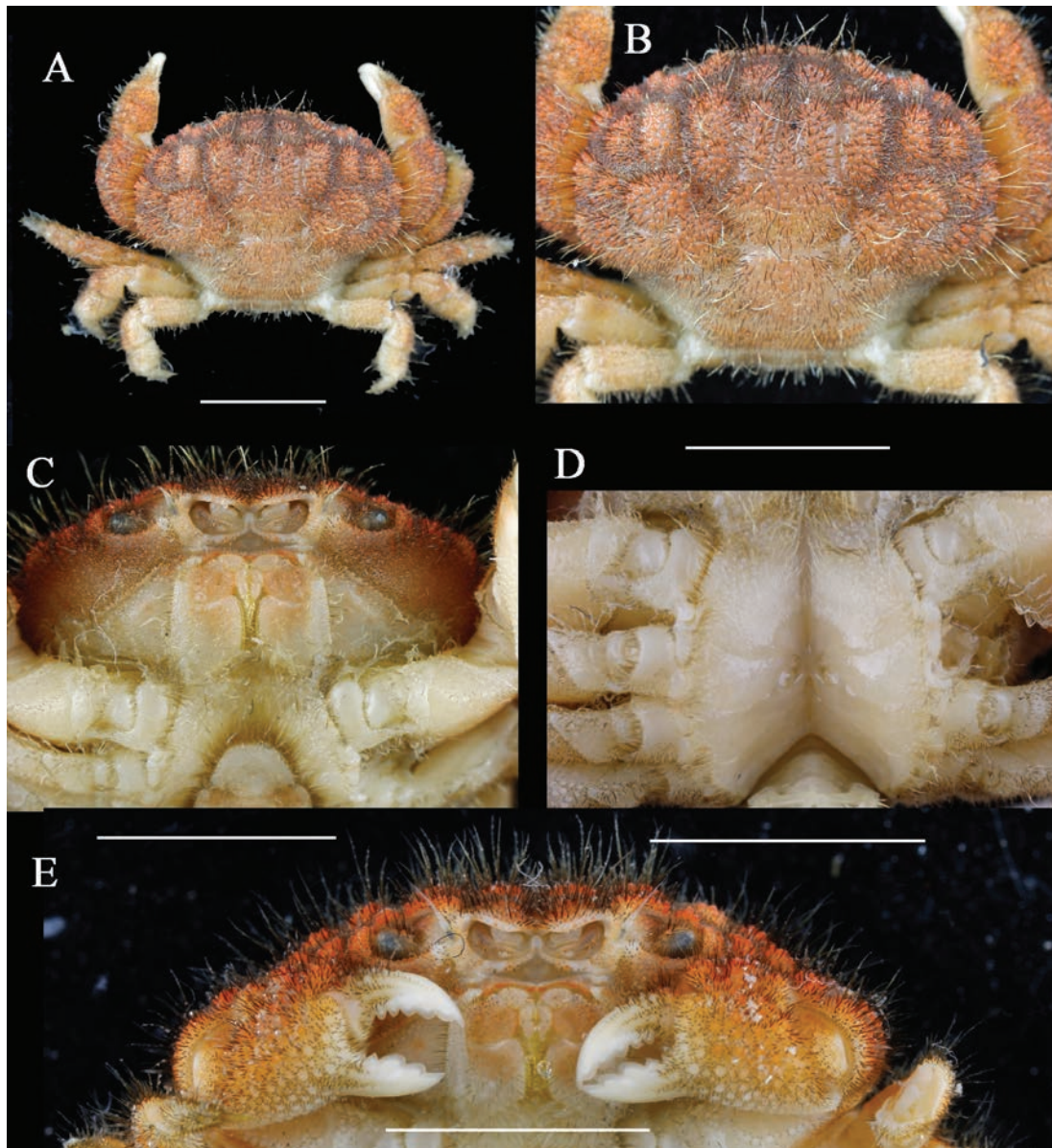


Figure 3. *Gaillardiiellus magiruber* sp. nov., female paratype (9.8 × 7.1 mm) (MBM288134) **A** overall dorsal view **B** dorsal view of cephalothorax **C** subhepatic and pterygostomial regions **D** thoracic sternum showing vulvae **E** outer view of chelipeds. Scale bar: 5 mm.

Antennule (Fig. 1C) folding transversely, antennular fossa subrectangular; basal segment of antenna subrectangular, filling orbital hiatus, antennal flagellum fitting into orbital hiatus. Epistome (Fig. 1C) central region with a strong median projection on posterior margin. Third maxilliped merus subquadrate, with low granules, anterior margin slightly indented, outer distal angle slightly expanded; ischium subrectangular, with submedian groove.

Chelipeds (Figs 1E, 2C) symmetrical, merus margins with low granules and soft setae; carpus robust, densely covered with granules and long setae, dorsolateral surface with grooves; palm densely covered with granules and setae on dorsal and lateral surfaces, ventral and medial surfaces smoother with low granules, dorsal surface with 2 granular tubercles; gap present when fingers closed; basal part of movable finger with granules, dorsal surface with 2 grooves, 3–5 rounded teeth between fingers, tips slightly concave.

Ambulatory legs (Figs 1A, 2D) densely covered with setae and granules; merus concave near terminal end of dorsal margin; carpus with groove near anterior margin, slightly swollen near terminal end; propodus nearly rhomboid; dactylus almost as long as propodus, terminal end chitinous, long, and sharp, with underdeveloped dactylo-propodal lock.

Thoracic sternum (Fig. 1D) with low granules, sternites 1 to 4 covered with soft setae; sternites 1 and 2 fused, suture between sternites 2 and 3 straight, suture between sternites 3 and 4 visible at margins, extending as shallow groove towards center, slightly curving backwards, with sternite 4 partially covered by telson, central groove beneath telson; tubercle of sterno-pleonal lock (press-button mechanism) located on anterior margin of sternite 5.

Pleon (Figs 1D, 2B) relatively short, pleonites 3 to 5 fused, fusion lines visible, margins concave and sinuous, fitting closely to corresponding part of thoracic sternum; pleonite 6 with expanded lateral distal angles, wider than long; telson (Figs 1D, 2B) wider than long, terminal end blunt, with long soft setae.

G1 (Fig. 2F, G, J, K) curved outward, distal third with small spines, long setae near distal end, terminal lobe slender. G2 (Fig. 2H, I) about one-third length of G1, curved outwards, terminal lobe longer and curved upwards.

Note on paratypes. In the current paratypes, an adult female exhibits the largest body size (9.8 × 7.1 mm; MBM288134, Figs 3, 4, 5A, B). Compared to the male holotype, the female paratype possesses a broader and more expanded carapace and a more concave posterior margin (Figs 3A, B, 4A), which may reflect a higher level of maturity in this species. In smaller individuals and juveniles, the carapace is narrower.

The overall morphology of the female is similar to that of the male, with the following sexual dimorphic characteristics: female pleon broad, oval-shaped (Fig. 4F); telson terminal end blunt (Fig. 4F); and vulva located at the anterior margin of the sternite 6, with an oval-shaped cover (Figs 3D, 4G).

Colour in life. In the current specimens, as body size increases, the coloration changes from a lighter orange-red with bright red spots (Fig. 5C) to a totally vibrant bright red (Fig. 5A). The cheliped fingers change from having a white distal half and a brown base (Fig. 5C) to being entirely white along their length (Fig. 5A).

Etymology. The new species is named after the fiery Stand “Magician’s Red” from the manga “JoJo’s Bizarre Adventure”, wielded by the character Muhammad Avdol. This name alludes to the species’ changing flame-like red coloration.

Remarks. *Gaillardiiellus magiruber* sp. nov. should be placed within *Gaillardiiellus* based on the well-defined regions on the dorsal carapace, the morphology of the granules and setae, the presence of four granular rounded lobes on the anterolateral margin (Figs 1B, 2A), the absence of nodules on the ambulatory legs (Figs 1A, 2D), and the sinuous margins of male pleonites 3–5, along with the overall morphology of the thoracic sternum (Fig. 2B). The anterolateral margin of *G. magiruber* sp. nov. is completely separated from the outer orbital angle (Figs. 1A, 2A, 3B, 4A), which distinguishes it clearly from *G. superciliaris* and *G. alphonsi* as their outer orbital angle is fused with the first anterolateral lobe (cf. Guinot 1976: pl. 16 figs 4, 5). Additionally, the well-developed long setae on the dorsal surface of the carapace and the evenly rounded teeth on the immovable finger of the cheliped further differentiate this new species from *G. holthuisi* and *G. bathus*. In contrast, *G. holthuisi* and *G. bathus* have only sparse long setae, and they also differ in the placement of a strong tooth: in *G. holthuisi*, it is near the tip

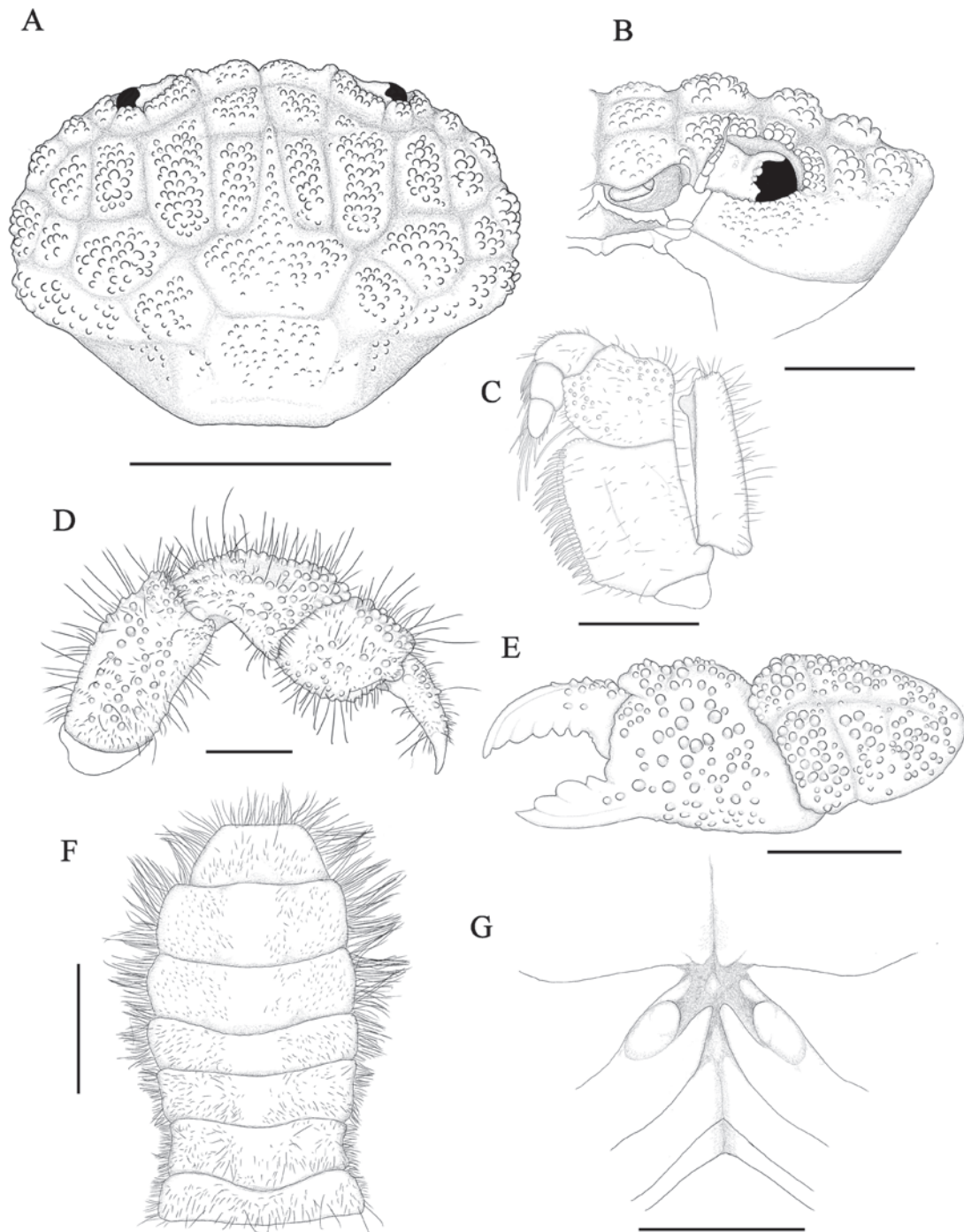


Figure 4. *Gaillardiiellus magiruber* sp. nov., female paratype (9.8 × 7.1 mm) (MBM288134) **A** dorsal view of cephalothorax, setae removed **B** frontal view of left half of cephalothorax, setae removed **C** left third maxilliped **D** right pereopod 5 **E** outer view of left cheliped, setae removed **F** pleon and telson **G** vulvae. Scale bars: 5 mm (**A**); 2 mm (**B**, **E**, **F**); 1 mm (**C**, **D**, **G**).

of the immovable finger, while in *G. bathus*, it is in the middle part of the immovable finger (cf. Davie 1997: figs 1b, 15c; Takeda and Komatsu 2010: figs 1, 2B).

Gaillardiiellus magiruber sp. nov. is most similar to two closely related congeners, i.e., *G. rueppellii* and *G. orientalis*. Considering the scattered distribution of setae on the dorsal surface of the carapace, rather than the distinct tufted clusters in *G. orientalis* (cf. Guinot 1976: pl. 16, fig. 2), *G. magiruber* sp. nov. is especially similar to *G. rueppellii* and could be confused with it. *Gaillardiiellus rueppellii* was first reported from Natal, South Africa and is widely known in the Indo-West



Figure 5. *Gaillardiiellus magiruber* sp. nov., live coloration **A, B** female paratype (9.8 × 7.1 mm) (MBM288134) **C** female paratype (5.7 × 4.2 mm) (MBM288135). Scale bar: 5 mm.

Pacific region (Krauss 1843; Guinot 1976; Serène 1984). Guinot (1976) provided a detailed redescription of the type specimen, accompanied by refined photographs and illustrations (cf. Guinot 1976: figs 42A, 43A, 43a, 44B, pl. 16, fig. 1, 1a), enhancing the understanding of *G. rueppellii*. *Gaillardiiellus magiruber* sp. nov. can be distinguished from *G. rueppellii* by the following characteristics: the front being broader and non-protruding, about 0.3 times CW (Figs 1B, 2A) (vs. front narrower and protruding, about 0.2 times CW in *G. rueppellii*; Fig. 6A; cf. Guinot 1976: pl. 16, fig. 1); the first anterolateral lobe is almost adjacent to the outer orbital angle, with no additional lobe underneath (Figs 1B, C, 2A) (vs. a wider gap between the first anterolateral lobe and outer orbital angle, with an

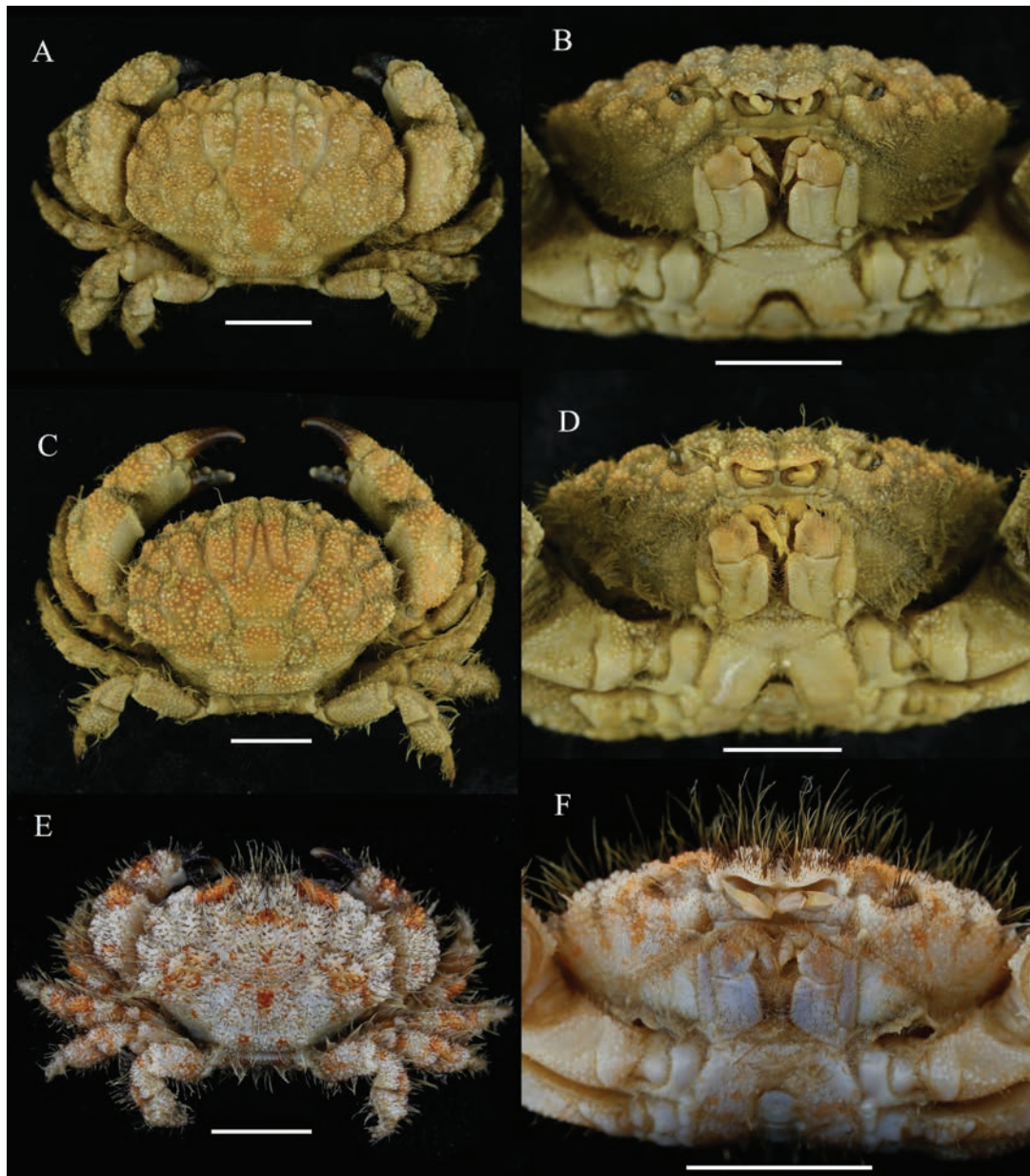


Figure 6. Comparative material of *Gaillardiiellus* species: *Gaillardiiellus rueppellii* (Krauss, 1843), male (38.6 × 28.2 mm) (MBM283642) (**A, B**) *Gaillardiiellus orientalis* (Odhner, 1925), male (34.9 × 25.8 mm) (MBM288142) (**C, D**) *Gaillardiiellus superciliaris* (Odhner, 1925), male (11.6 × 7.9 mm) (MBM288143) (**E, F**) **A, C, E** overall dorsal view **B, D, F** frontal view of cephalothorax. Scale bars: 10 mm (**A–D**); 5 mm (**E, F**).

accessory lobe underneath in *G. rueppellii*; Fig. 6B; cf. Guinot 1976: pl. 16, fig. 1); the male and female thoracic sternum with long soft setae on sternites 1–4 (Figs 1D, 3D) (vs. only sparse short setae in *G. rueppellii*; Fig. 6B); the male pleon is shorter, the pleonite 6 and telson being broader than long, and the telson with long soft setae on tip (Figs 1D, 2B) (vs. male pleon is longer, the pleonite 6 and telson are nearly equal in length and width, and the telson without long soft setae in *G. rueppellii*; cf. Guinot 1976: fig. 62A); the G1 is shorter and stouter (Fig. 2J, K) (vs. G1 slender in *G. rueppellii*; cf. Guinot 1976: fig. 63A). Additionally, *G. magiruber* sp. nov. has a more vibrant bright red live coloration (Fig. 5) (vs. duller coloration, appearing brownish in *G. rueppellii*; Fig. 7).



Figure 7. *Gaillardiiellus rueppellii* (Krauss, 1843), live coloration, photo by Zhang Xu.

Furthermore, although the present specimens of *G. magiruber* sp. nov. include some juvenile individuals, considering the body size of the two female specimens displaying distinct maturity traits, such as the well-developed pleon and vulva, the new species is relatively smaller in size (CW less than 10 mm) compared to most congeners.

It is worth noting that *G. rueppellii* has two early synonyms: *Actaea pilosa* Stimpson, 1858, from Hong Kong, and *Aegle rugata* Adams & White, 1849 (not H. Milne Edwards, 1834), from the Philippine Islands. Unfortunately, the type specimen of *Aegle rugata* is no longer traceable (Dr Paul Clark, Natural History Museum, personal communication), and the type specimen of *Actaea pilosa* was likely lost in the infamous fire. The identities of these two specimens remain uncertain. However, based on the limited available illustrations (Stimpson 1907: pl. 5 fig. 6; Adams and White 1849: pl. 8, fig. 5), both species exhibit a prominently lobed frontal margin, suggesting closer affinity to *G. rueppellii* rather than *G. magiruber* sp. nov. Due to the similarities between the two species, *G. magiruber* sp. nov.

may be mistakenly identified as a juvenile of *G. rueppellii*. Further extensive examination will help clarify the distribution ranges of both species.

In the COI-based molecular analysis, the BI (Fig. 8) and ML (Suppl. material 2) trees exhibited similar topologies. *Gaillardieillus magiruber* sp. nov. is most closely related to *G. orientalis*, followed by clustering with *G. rueppellii*. Species delimitation based on ABGD and bPTP further supports the validity of the new species.

In addition, *Paractaea* Guinot, 1969, is not monophyletic in the current study, with *P. tumulosa* (Odhner, 1925) and *P. cf. excentrica* (Guinot, 1969) forming a single clade. Serène (1984) previously suggested transferring *P. tumulosa* to *Paractaeopsis* Serène, 1984 (see Takeda and Komatsu 2018). Further research is needed to clarify the phylogenetic relationships among species within *Paractaea*.

Geographic distribution. Xisha and Nansha Islands, South China Sea.

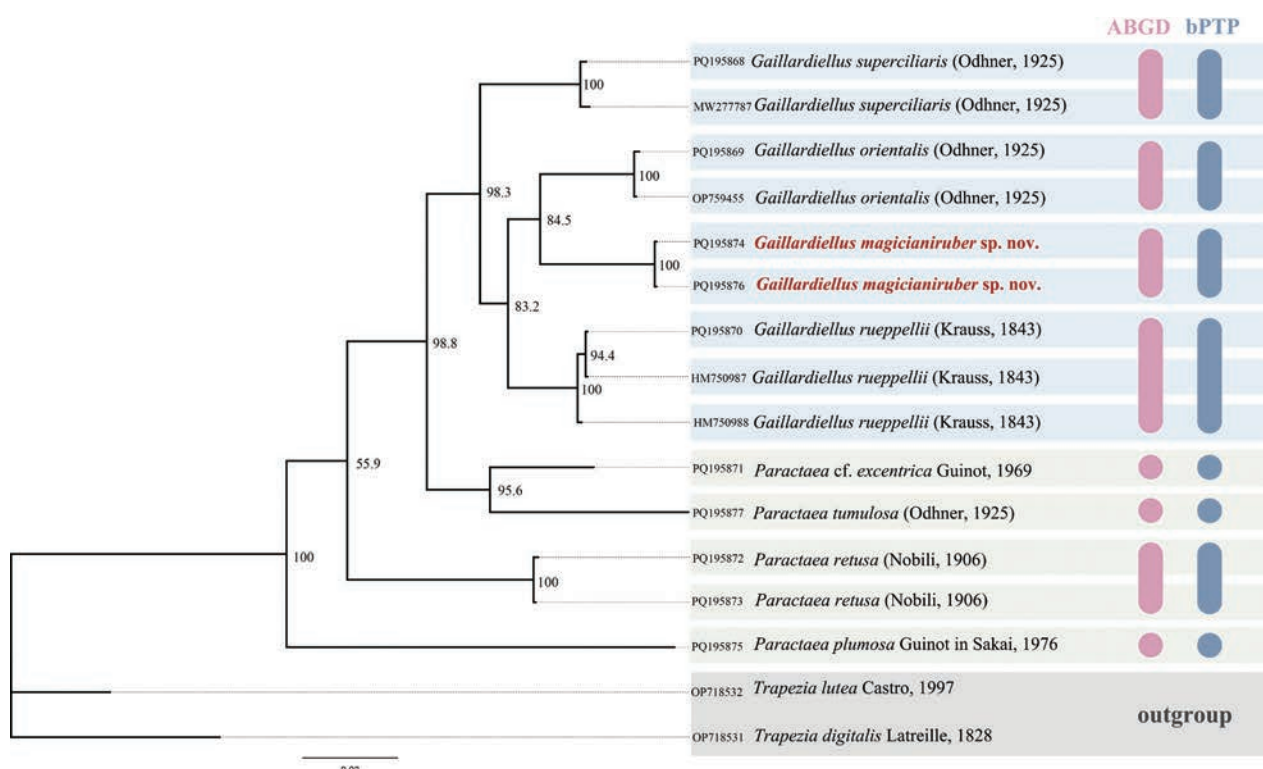


Figure 8. Bayesian inference (BI) phylogenetic tree based on COI showing the phylogenetic relationship between *Gaillardieillus magiruber* sp. nov. and related species, with bootstrap replications (BS) labeled. The results of Automated Barcode Gap Discovery (ABGD) and Bayesian implementation of the Poisson Tree Processes (bPTP) species delimitation methods are shown on the right margin of the figure, each circle or capsule shape represents one species.

Key to species of *Gaillardieillus* (adapted from Serène 1984)

- 1 Carapace anterolateral margin with 3 distinct lobes behind outer orbital angle, anterior lobe fused with outer orbital angle; 3M faintly divided into 3 parts ***G. superciliaris* and *G. alphonsi* [possibly synonyms; see also Guinot 1976]**
- Carapace anterolateral margin with 4 distinct lobes behind outer orbital angle, anterior lobe not fused with outer orbital angle; 3M intact.....**2**
- 2 Cheliped immovable finger with strong tooth**3**
- Cheliped immovable finger without strong tooth.....**4**
- 3 Cheliped with strong tooth near tip of immovable finger***G. holthuisi***
- Cheliped with strong tooth in middle part of immovable finger...***G. bathus***

- 4 Carapace dorsal surface with tufts of long, plumose setae.....***G. orientalis***
- Carapace dorsal surface with scattered sort and long setae**5**
- 5 Carapace first anterolateral lobe widely separated from outer orbital angle, with accessory lobe located in-between.....***G. rueppellii***
- Carapace first anterolateral lobe almost adjacent to outer orbital angle, with no additional lobe underneath.....***G. magiruber* sp. nov.**

Acknowledgements

The authors would like to express their sincere gratitude to Dong Dong, Pan Yunhao, and Yang Bin for collecting and generously providing specimens of the new species and comparative material. The authors also extend thanks to Ma Shaobo and Sun Yuli for their assistance during the expedition and their valuable contributions to the collection of specimens. The authors also thank Zhang Xu for providing the live photographs of *G. rueppellii*. The authors express their gratitude to Dr Paul Clark (Natural History Museum) for his assistance and patience in locating the specimens. The authors would like to thank Kai Meng (Institute of Zoology, Chinese Academy of Sciences) for his assistance with specimen examination. Finally, the authors express their gratitude to the anonymous reviewer and subject editor for their valuable suggestions on revising this paper.

Additional information

Conflict of interest

The authors have declared that no competing interests exist.

Ethical statement

No ethical statement was reported.

Funding

This work was supported by the Ministry of Science and Technology of China (2021YFF0502801), the National Science & Technology Fundamental Resources Investigation Program of China (2022FY100603), the National Natural Science Foundation of China (42176138), and the Qingdao New Energy Shandong Laboratory Open Project (QNESL OP202306).

Author contributions

Conceptualization: YZ. Data curation: YZ. Funding acquisition: SZ, JW. Project administration: SZ. Writing - original draft: YZ.

Author ORCIDs

Yuan Ziming  <https://orcid.org/0009-0008-0009-2693>

Jiang Wei  <https://orcid.org/0000-0003-4767-8196>

Sha Zhongli  <https://orcid.org/0000-0002-2192-3758>

Data availability

All of the data that support the findings of this study are available in the main text or Supplementary Information.

References

- Adams A, White A (1849) Crustacea, Part II. In: Adams A (Eds) The Zoology of the Voyage of H.M.S. Samarang; Under the Command of Captain Sir Edward Belcher, C.B., F.R.A.S., F.G.S., During the Years 1843–1846. Reeve, Benham, and Reeve, Covent Garden, London, viii + 33–66. [pls 7–13] <https://doi.org/10.5962/bhl.title.120176>
- Davie PJF (1997) Crustacea Decapoda: Deep water Xanthoidea from the South-Western Pacific and the Western Indian Ocean. In: Crosnier A (Ed.) Résultats des Campagnes MUSORSTOM 18. Mémoires du Muséum national d'Histoire naturelle, Série A, Zoologie 176: 337–387.
- Davie PJF, Guinot D, Ng PKL (2015) Anatomy and functional morphology of Brachyura. In: Castro P, Davie PJF, Guinot D, Schram FR, von Vaupel Klein JC (Eds) Treatise on Zoology-Anatomy, Taxonomy, Biology-The Crustacea, Complementary to the Volumes Translated from the French of the Traité de Zoologie 9(C)(I), Decapoda: Brachyura. Part 2. Brill, Leiden, 11–163. https://doi.org/10.1163/9789004190832_004
- Geller J, Meyer C, Parker M, Hawk H (2013) Redesign of PCR primers for mitochondrial cytochrome c oxidase sub-unit I for marine invertebrates and application in all-taxa biotic surveys. Molecular Ecology Research 13: 851–861. <https://doi.org/10.1111/1755-0998.12138>
- Guinot D (1976) Constitution de quelques groupes naturels chez les Crustacés Décapodes Brachyours. I. La superfamille des Bellioidea Dana et trois sous-familles de Xanthidae (Polydectinae Dana, Trichiinae de Haan, Actaeinae Alcock). Mémoires du Muséum national d'Histoire naturelle, séries A 97: 1–308. [figs 1–47, pls 1–19]
- Huelsenbeck JP, Ronquist F (2001) MRBAYES: Bayesian inference of phylogeny. Bioinformatics 17: 754–755. <https://doi.org/10.1093/bioinformatics/17.8.754>
- Krauss CFF (1843) Die Südafrikanischen Crustaceen. Eine Zusammenstellung aller bekannten Malacostraca, Bemerkungen über deren Lebensweise und geographische Verbreitung, nebst Beschreibung und Abbildung mehrerer neuen Arten. Stuttgart, Schweizerbartsche, 1–68. [pls 1–4] <https://doi.org/10.5962/bhl.title.4825>
- Trifinopoulos J, Nguyen LT, Haeseler AV, Minh BQ (2016) W-iq-tree: a fast online phylogenetic tool for maximum likelihood analysis. Nucleic Acids Research (W1): W232–W235. <https://doi.org/10.1093/nar/gkw256>
- Lai JCY, Mendoza JCE, Guinot D, Clark PF, Ng PKL (2011) Xanthidae MacLeay, 1838 (Decapoda: Brachyura: Xanthoidea) systematics: A multi-gene approach with support from adult and zoeal morphology. Zoologischer Anzeiger 250: 407–448. <https://doi.org/10.1016/j.jcz.2011.07.002>
- Ng PKL, Guinot D, Davie PJF (2008) Systema Brachyurorum: Part I. An annotated checklist of the extant brachyuran crabs of the world. Raffles Bulletin of Zoology 17: 1–286.
- Posada D (2008) jModelTest: Phylogenetic model averaging. Molecular Biology and Evolution 25: 1253–1256. <https://doi.org/10.1093/molbev/msn083>
- Puillandre N, Lambert A, Brouillet S, Achaz G (2012) ABGD, automatic barcode gap discovery for primary species delimitation. Molecular Ecology 21: 1864–1877. <https://doi.org/10.1111/j.1365-294X.2011.05239.x>
- Serène R (1984) Crustacés Décapodes Brachyours de l'Océan Indien Occidental et de la Mer Rouge, Xanthoidea: Xanthidae et Trapeziidae. Faune Tropicale 24: 1–349. [figs A–C + 1–243, pls 1–48]
- Stimpson W (1907) Report on the Crustacea (Brachyura and Anomura) collected by the North Pacific Exploring Expedition, 1853–1856. Smithsonian Miscellaneous Collections 49: 1–240. [pls 1–26] <https://doi.org/10.5962/bhl.title.51448>

- Takeda M, Komatsu H (2010) A new xanthid crab (Decapoda, Brachyura) from a submarine cave in the Philippines. In: Fransen CHJM, De Grave S, Ng PKL (Eds) Studies on Malacostraca: Lipke Bijdeley Holthuis Memorial Volume. Crustaceana Monographs 14: 677–683. https://doi.org/10.1163/9789047427759_049
- Takeda M, Komatsu H (2018) Offshore crabs of the family Xanthidae and some related families (Crustacea, Decapoda, Brachyura) from the Ogasawara Islands, Japan. Memoirs of the National Science Museum 52: 153–189.
- Tamura K, Stecher G, Peterson D, Filipinski A, Kumar S (2013) MEGA6: Molecular Evolutionary Genetics Analysis version 6.0. Molecular Biology and Evolution 30: 2725–2729. <https://doi.org/10.1093/molbev/mst197>
- Thoma BP, Danièle G, Felder DL (2014) Evolutionary relationships among American mud crabs (Crustacea: Decapoda: Brachyura: Xanthoidea inferred from nuclear and mitochondrial markers, with comments on adult morphology. Zoological Journal of the Linnean Society 1: 86–109. <https://doi.org/10.1111/zoj.12093>
- Yuan ZM, Jiang W, Sha ZL (2023) A new species of the coral-symbiont crab genus *Cymo* de Haan, 1833 (Decapoda, Brachyura, Xanthidae) from Nansha Islands, the South China Sea. Zootaxa 5361(2): 275–286. <https://doi.org/10.11646/zootaxa.5361.2.8>
- Zhang J, Kapli P, Pavlidis P, Stamatakis A (2013) A general Species delimitation method with applications to phylogenetic placements. Bioinformatics 29: 2869–2876. <https://doi.org/10.1093/bioinformatics/btt499>

Supplementary material 1

Gaillardiiellus magiruber sp. nov.

Authors: Yuan Ziming, Jiang Wei, Sha Zhongli

Data type: jpg

Explanation note: Juvenile male paratype (4.5 × 3.5 mm) (MBM288136) (**A–C**); juvenile male paratype (4.2 × 3.3 mm) (MBM288137) (**D–F**). **A, D** dorsal view **B, E** ventral view **C, F** immature G1 and G2. Scale bars: 1 mm (**A, B, D, E**), 0.2 mm (**C, F**).

Copyright notice: This dataset is made available under the Open Database License (<http://opendatacommons.org/licenses/odbl/1.0/>). The Open Database License (ODbL) is a license agreement intended to allow users to freely share, modify, and use this Dataset while maintaining this same freedom for others, provided that the original source and author(s) are credited.

Link: <https://doi.org/10.3897/zookeys.1234.144026.suppl1>

Supplementary material 2

Maximum likelihood (ML) phylogenetic tree based on COI showing the phylogenetic relationship between *Gaillardieillus magiruber* sp. nov. and related species

Authors: Yuan Ziming, Jiang Wei, Sha Zhongli

Data type: jpg

Copyright notice: This dataset is made available under the Open Database License (<http://opendatacommons.org/licenses/odbl/1.0/>). The Open Database License (ODbL) is a license agreement intended to allow users to freely share, modify, and use this Dataset while maintaining this same freedom for others, provided that the original source and author(s) are credited.

Link: <https://doi.org/10.3897/zookeys.1234.144026.suppl2>

Systematic review of the genus *Pseudognaptorina* Kaszab, 1977 (Coleoptera, Tenebrionidae, Blaptinae, Blaptini) from the Qinghai-Xizang Plateau, with description of six new species

Xiu-Min Li¹, Bao-Yue Zhang¹, Ji-Gang Li¹, Zhao Pan¹

¹ Key Laboratory of Zoological Systematics and Application of Hebei Province, College of Life Sciences, Institute of Life Science and Green Development, Hebei University, Baoding 071002, China

Corresponding authors: Ji-Gang Li (lijigang@hbu.edu.cn); Zhao Pan (panzhao86@yeah.net)

Abstract

The genus *Pseudognaptorina*, with four described species, is endemic to the Qinghai-Xizang Plateau. In this study, *Pseudognaptorina* is reviewed based on a combination of molecular and morphological datasets. A preliminary phylogenetic tree is reconstructed based on COI sequences of four related genera within the subtribe Gnaptorinina. Additionally, the geographical distribution of *Pseudognaptorina* is presented. Six new species are described and illustrated: *P. banbarica* X.-M. Li, **sp. nov.**, *P. himalayana* X.-M. Li, **sp. nov.**, *P. migana* X.-M. Li, **sp. nov.**, *P. oblonga* X.-M. Li, **sp. nov.**, *P. rectangularis* X.-M. Li, **sp. nov.**, and *P. reni* X.-M. Li, **sp. nov.** This work provides valuable molecular, morphological, and distributional data for the study of species evolution in the subtribe Gnaptorinina.

Key words: China, COI gene, darkling beetle, morphology



Academic editor: Patrice Bouchard
Received: 24 September 2024
Accepted: 24 February 2025
Published: 8 April 2025

ZooBank: <https://zoobank.org/4322717B-32FF-4BDA-AC70-E48306179D34>

Citation: Li X-M, Zhang B-Y, Li J-G, Pan Z (2025) Systematic review of the genus *Pseudognaptorina* Kaszab, 1977 (Coleoptera, Tenebrionidae, Blaptinae, Blaptini) from the Qinghai-Xizang Plateau, with description of six new species. ZooKeys 1234: 19–46. <https://doi.org/10.3897/zookeys.1234.137739>

Copyright: © Xiu-Min Li et al.
This is an open access article distributed under terms of the Creative Commons Attribution License (Attribution 4.0 International – CC BY 4.0).

Introduction

The subtribe Gnaptorinina Medvedev, 2001 belongs to the tribe Blaptini Leach, 1815 within the subfamily Blaptinae. It consists of 189 species in 12 genera, which are mainly distributed at high-elevations of the Qinghai-Xizang Plateau. These genera are *Agnaptoria* Reitter, 1887 (36 species and subspecies), *Asidoblaps* Fairmaire, 1886 (56 species), *Blaptogonia* Medvedev, 1998 (five species), *Colasia* Koch, 1965 (seven species and subspecies), *Gnaptorina* Reitter, 1887 (39 species), *Itagonia* Reitter, 1887 (24 species), *Montagona* Medvedev, 1998 (three species), *Nepalindia* Medvedev, 1998 (five species), *Pseudognaptorina* Kaszab, 1977 (four species), *Sintagona* Medvedev, 1998 (one species), *Tagonoides* Fairmaire, 1886 (eight species), and *Viettagona* Medvedev & Merkl, 2003 (one species) (Medvedev and Merkl 2002; Medvedev 2004; Ren et al. 2016; Li et al. 2018, 2019; Chigray 2019; Bai et al. 2020, 2023; Nabozhenko and Chigray 2020; Ji et al. 2024).

Pseudognaptorina was established by Kaszab (1977), with the type species *P. nepalica* Kaszab, 1977 (Fig. 1) from Nepal. Later, three species (*P. exsertogena* Shi, Ren & Merkl, 2005, *P. flata* Liu & Ren, 2009, and *P. obtusa* Shi, Ren & Merkl, 2005) were described from Xizang and Sichuan, China (Shi et al. 2005; Liu and Ren 2009). *Pseudognaptorina* is morphologically similar to the genus *Gnaptorina*

but differs in the following characters: protibial spurs subequal in length; ventral surface of male protarsomeres I–III and at least mesotarsomere I with hair brushes; aedeagus with moderately elongate parameres, at least twice as long as wide. *Pseudognaptorina* is also related to *Montagona* but can be distinguished by the following characters: epipleural carina visible in dorsal view at apex; elytra without longitudinal carina or smooth bulge; ventral surface of male protarsomeres I–III and at least mesotarsomere I with hair brushes; lobes of ovipositor transverse. Medvedev (2009) proposed that the genus *Pseudognaptorina* likely comprises only the type species, *P. nepalica*. The generic taxonomic status of *P. exsertogena* and *P. obtusa* is doubtful, as these two species are found in east-central Xizang, China, which is considerably distant from the type locality of the type species. Notably, *P. flata* has been discovered in Sichuan, China, which is geographically close to *P. exsertogena* (Liu and Ren 2009). To date, the genus *Pseudognaptorina* has not been studied using molecular data. Consequently, the taxonomic status of these species requires evaluation within the framework of molecular phylogeny.

In this study, six new species are described and illustrated. In addition, we construct a phylogenetic tree for four related genera to investigate the monophyly of the genus *Pseudognaptorina*. This study provides valuable molecular and distributional data on *Pseudognaptorina*, which can be used to study the richness of endemic insects in the surrounding areas of the Qinghai-Xizang Plateau.

Materials and methods

Morphological examination

Nine species (108 specimens) of the genus *Pseudognaptorina* were examined for this study and deposited at the Museum of Hebei University, Baoding, China (MHBV) and Hungarian Natural History Museum, Budapest, Hungary (HNHM). The specimens were photographed using a Canon EOS 5D Mark III (Canon Inc., Tokyo, Japan) with a Laowa FF 100 mm F2.8 CA-Dreamer Macro 2 × lens, or Laowa FF 25 mm F2.8 Ultra Macro 2.5–5 × lens (Anhui Changgeng Optics Technology Co., Ltd, Hefei, China).

Label data are presented verbatim. A slash (/) separates text on lines of the label.

Taxon sampling, DNA extraction, PCR amplification, and sequencing

Specimens were collected in the field on the Qinghai-Xizang Plateau. Molecular data were collected from 148 individuals and includes previously published sequences from 72 individuals of the genus *Gnaptorina* (Li et al. 2021; Ji et al. 2024).

DNA was extracted from the leg muscle tissue of adults using the Insect DNA isolation Kit (BIOMIGA, Dalian, China) following the manufacturer's protocols. The DNA extracted was stored at -20 °C. The fragment of the mitochondrial molecular marker (cytochrome oxidase subunit I, COI) was amplified with the primers F 2183 and R 3014 (Folmer et al. 1994). The profile of the PCR amplification consisted of an initial denaturation step at 94 °C for 4 min, 35 cycles of denaturation at 94 °C for 1 min, annealing for 45 s, an extension at 72 °C for 1 min, and a final 8 min extension step at 72 °C. PCR was performed using TaKaRa Ex Taq (TaKaRa, Dalian, China). PCR products were subsequently checked by 1% agarose gel electrophoresis and sequenced at General Biol Co. (Chuzhou, China).

Phylogenetic analyses

In total, 148 sequences from 70 species were used for the phylogenetic analyses including 72 new sequences from four genera: *Agnaptoria*, *Asidoblaps*, *Gnaptoriana*, and *Pseudognaptorina*. Detailed information on the new samples in this study is provided in Suppl. material 1, and the previously published sequence numbers were labeled on the phylogenetic tree. The tribe Platyscelidini was selected as the outgroup, which was considered to be most closely related to the tribe Blaptini (Kamiński et al. 2021).

Phylogenetic analysis was based on the COI gene fragment using maximum likelihood (ML). A best-fit model was tested according to the corrected Akaike's Information Criterion (AICc) using ModelFinder (included in IQ-TREE) with PhyloSuite v. 1.2.2 (Zhang et al. 2020). The ML tree search was performed in IQ-TREE v. 1.6.8 (Nguyen et al. 2015). The ML tree was inferred using an edge-linked partition model for 5000 ultrafast bootstraps (1000 replicates) (Minh et al. 2013). Support for each node is represented by ultrafast bootstrap values (uBV).

Results

Morphological study

Key to males of *Pseudognaptorina* species

- 1 Lateral margins of pronotum regularly arcuate. Elytral surface densely covered with rather smooth punctation, without coarse wrinkles. Ventral surface of protarsomeres I–II with hair brushes, protarsomere III with small hairy tuft; mesotarsomere I with hair brushes, mesotarsomere II with small hairy tuft..... ***P. nepalica***
- Lateral margins of pronotum arcuate at anterior half. Elytra densely covered with indistinct punctation and coarse wrinkles. Ventral surface of protarsomeres I–III with hair brushes, mesotarsomeres I–III with hair brushes or tufts **2**
- 2 Pronotum transverse, surface flattened. Ventral surface of mesotarsomeres I–II with hair brushes, mesotarsomere III with small hairy tuft..... ***P. rectangularis* sp. nov.**
- Pronotum transverse, surface slightly convex. Ventral surface of mesotarsomeres I–III with hair brushes..... **3**
- 3 Posterior angles of pronotum slightly obtuse. Parameres strongly elongate, 2.78 times as long as wide..... ***P. obtusa***
- Posterior angles of pronotum almost rectangular. Parameres not strongly elongate **4**
- 4 Lateral margins of pronotum arcuately narrowed at basal 2/3..... ***P. flata***
- Lateral margins of pronotum arcuately narrowed at basal 1/2..... **5**
- 5 Surface of elytra with fine punctures and irregular wrinkles ***P. oblonga* sp. nov.**
- Surface of elytra with fine punctures and without regular wrinkles..... **6**
- 6 Antennomeres VIII–X nearly cylindrical..... **7**
- Antennomeres VIII–X nearly spherical **8**

- 7 Ventral surface of mesotarsomeres I–II with hair brushes, mesotarsomere III with small, hairy tuft ***P. banbarica* sp. nov.**
- Ventral surface of mesotarsomeres I–III with hair brushes **9**
- 8 Pronotum 1.28 times as wide as long. Surface of elytra with fine punctures and irregular wrinkles ***P. exsertogena***
- Pronotum 1.50 times as wide as long. Surface of elytra with fine punctures and without regular wrinkles ***P. reni* sp. nov.**
- 9 Pronotum 1.34 times as wide as long, lateral margins arcuately narrowed at basal 2/3. Ventral surface of mesotarsomeres I–III with hair brushes...
..... ***P. migana* sp. nov.**
- Pronotum 1.29 times as wide as long, lateral margins of pronotum regularly arcuate. Mesotarsomeres I–II with hair brushes, mesotarsomere III with small, hairy tuft ***P. himalayana* sp. nov.**

Key to females of *Pseudognaptorina* species

- 1 Antennae long, reaching base of pronotum posteriad **2**
- Antennae short, not reaching base of pronotum posteriad **3**
- 2 Pronotum 1.38 times as wide as long. Ratio of width at anterior margin to its maximum width and to width at posterior margin 0.58: 1.00: 0.89
..... ***P. nepalica***
- Pronotum 1.56 times as wide as long. Ratio of width at anterior margin to its maximum width and width at posterior margin 0.55: 1.00: 0.97
..... ***P. reni* sp. nov.**
- 3 Protibial spurs rounded apically ***P. banbarica* sp. nov.**
- Protibial spurs small and pointed **4**
- 4 Posterior angles of pronotum slightly obtuse **5**
- Posterior angles of pronotum almost rectangular **6**
- 5 Elytra wider (1.36 times as long as wide), densely covered with irregular wrinkles ***P. flata***
- Elytra elongate-oval (1.28–1.29 times as long as wide), sparsely covered with fine punctures and irregular wrinkles ***P. obtusa***
- 6 Antennomere VII short. Pronotum slightly convex ***P. exsertogena***
- Antennomere VII long. Pronotum flattened **7**
- 7 Pronotum with fine punctuation; stem of spiculum long ***P. migana* sp. nov.**
- Pronotum with very dense punctuation; stem of spiculum short
..... ***P. oblonga* sp. nov.**

Genus *Pseudognaptorina* Kaszab, 1977

Pseudognaptorina Kaszab, 1977: 250; Shi et al. 2005: 163; Liu and Ren 2009.

Type species. *Pseudognaptorina nepalica* Kaszab, 1977, by original designation, by monotypy.

Generic diagnosis. Antennomere VII narrower than VIII; epipleural carina visible in dorsal view at basal part and apex; all tibiae narrow, dilated apically, tarsi slender, ventral surface of male protarsomeres I–III and at least mesotarsomeres I–II with hair brushes; protibial spurs subequal in length; parameres



Figure 1. *Pseudognaptorina nepalica* Kaszab, 1977, male.

moderately elongate, at least 1.8 times as long as wide; apical part of ovipositor short, 1–1.4 times as long as wide, lobes transverse.

Distribution. Nepal and China.

Pseudognaptorina exsertogena Shi, Ren & Merkl, 2005

Type material examined. Holotype: CHINA • ♂ (MHBU XZ04062848): Yangbajain, Damxung County, Xizang/ 30°06'N, 90°30'E/ 3700–4100 m/ 2004-VI-28/ Yi-Bin Ba & Ai-Min Shi leg. **Paratypes:** CHINA • 15♂♂, 23♀♀ (MHBU XZ04062843–04062847, 04062849–04062871): same as holotype; CHINA • 4♂♂, 1♀ (MHBU XZ02070511–02070515): Maizhokunggar County, Xizang/ 29°48'N, 91°48'E/ 4100 m/ 2002-VII-5/ Guo-Dong Ren leg.

Distribution. Xizang, China.

Pseudognaptorina flata Liu & Ren, 2009

Type material examined. Holotype: CHINA • ♂ (MHBU XZ08071698): Batang, Sichuan/ 30°07' N, 99°02' E/ 3850 m/ 2008-VII-16/ Guo-Dong Ren leg. **Paratype:** CHINA • 1♀ (MHBU XZ08071697): same data as the holotype.

Distribution. Sichuan, China.

Pseudognaptorina nepalica Kaszab, 1977

Type material examined. Paratypes: 1♀ (HNHM SMF C 14534): “Nepal. Expeditionen Jochen Martens,” “Gompabei Tarakot/ 3300–3400 m/ 1970-V-11–16”, “*Tagonoides (Pseudognaptorina) nepalica* Kasz., det. N. Skopin, 1976”; 1♂ (HNHM SMF C 14539), “Dolpo, Tal der oberen Barbung Khola, zwischen Terang und Tukot/ 4000 m/ 1970-VI-19”; 1♂ (HNHM SMF C 14537), “Dolpo, Weg von Kangar nach Shimen/ 4300–4500 m/ 1973-VI-18”;

1♂ (HNHM SMF C 14532), "Dolpo, Tal der oberen Barbung Khola, Charka/ 4300–4400 m/ 20–25.VI.1973".

Distribution. Nepal.

***Pseudognaptorina obtusa* Shi, Ren & Merkl, 2005**

Type material examined. Holotype: CHINA • ♂ (MHBU XZ04061237): Markam County, Xizang/ 29°36'N, 98°24'E/ 3800–4000 m/ 2004-VI-12/ Ai-Min Shi & Yi-Bin Ba leg. **Paratypes:** CHINA • 2♀♀ (MHBU XZ04061238–04061239): same data as holotype.

Distribution. Xizang, China.

***Pseudognaptorina banbarica* X.-M. Li, sp. nov.**

<https://zoobank.org/8BEDBC76-29B9-4860-93AA-B9B858BF2D73>

Type materials. Holotype: CHINA • ♂ (MHBU HBU(E)339867): Marxog Township, Banbar County, Xizang/ 31°01.410' N, 94°37.152' E/ Alt. 4400 m/ 2019-VII-31/ Guo-Dong Ren, Ya-Lin Li & Xing-Long Bai leg. **Paratypes:** CHINA • 3♂♂, 7♀♀ (MHBU HBU(E)339868–339877): same data as holotype.

Description. Male (Figs 2, 3A–C). Body length 10.5–11.0 mm, width 4.9–5.0 mm; shiny, black or brownish; antennae, palpi, and tarsi brown.

Head (Fig. 2A, B). Anterior margin of clypeus slightly sinuate. Head widest at eye level. Lateral margin of head with pair of projections between antennal base and oculus, brownish red. Genal margin arcuately converging before eyes. Eyes barely protruding beyond contour of head. Vertex flat or slightly convex, with uniform punctures. Antennae (Fig. 2D) slender and long, reaching beyond pronotal base when posteriorly extended, antennomeres III very long, 3.2 times as long as antennomeres II, antennomeres VIII–X oval, XI spindle-shaped. Length (width) ratio of antennomeres II–XI as follows: 10.9(10.0): 27.6(10.0): 13.9(10.0): 14.3(10.0): 15.0(10.0): 15.7(10.0): 12.6(12.7): 11.3(12.6): 11.7(14.3): 18.0(14.4).

Prothorax. Pronotum (Fig. 2C) transverse, 1.28 times as wide as long, widest in middle, 1.78 times as wide as head. Ratio of width at anterior margin to its maximum width and posterior margin 0.60: 1.00: 0.97. Lateral margins of pronotum arcuately narrowing to anterior margin, bordered along entire length; posterior margin straight; anterior margin slightly emarginate; anterior angles widely obtuse-angled, posterior angles almost rectangular. Surface of pronotum slightly convex between lateral margins, covered with fine dense punctation. Hypomera covered shallow longitudinal wrinkles and granules. Prosternum before procoxae gently sloping. Prosternal process gently sloping behind procoxae, forming obtuse projection.

Pterothorax. Elytra oblong-oval and convex, 1.37–1.39 times as long as wide, 1.38–1.39 times as wide as pronotum, widest in apical third. Dorsal surface of elytra passing into outer (deflexed) surface without traces of humeral carina. Outer margin of epipleura visible in dorsal view at basal third and apex. Surface of elytra with dense, rather smooth punctation and wrinkles almost vanishing on apical declivity.

Legs (Fig. 2E–J). Femora and tibiae moderately thickened. Ratio of length (width) of pro-, meso-, and metatibiae: 43.8(6.6): 43.2(7.1): 69.6(8.0).

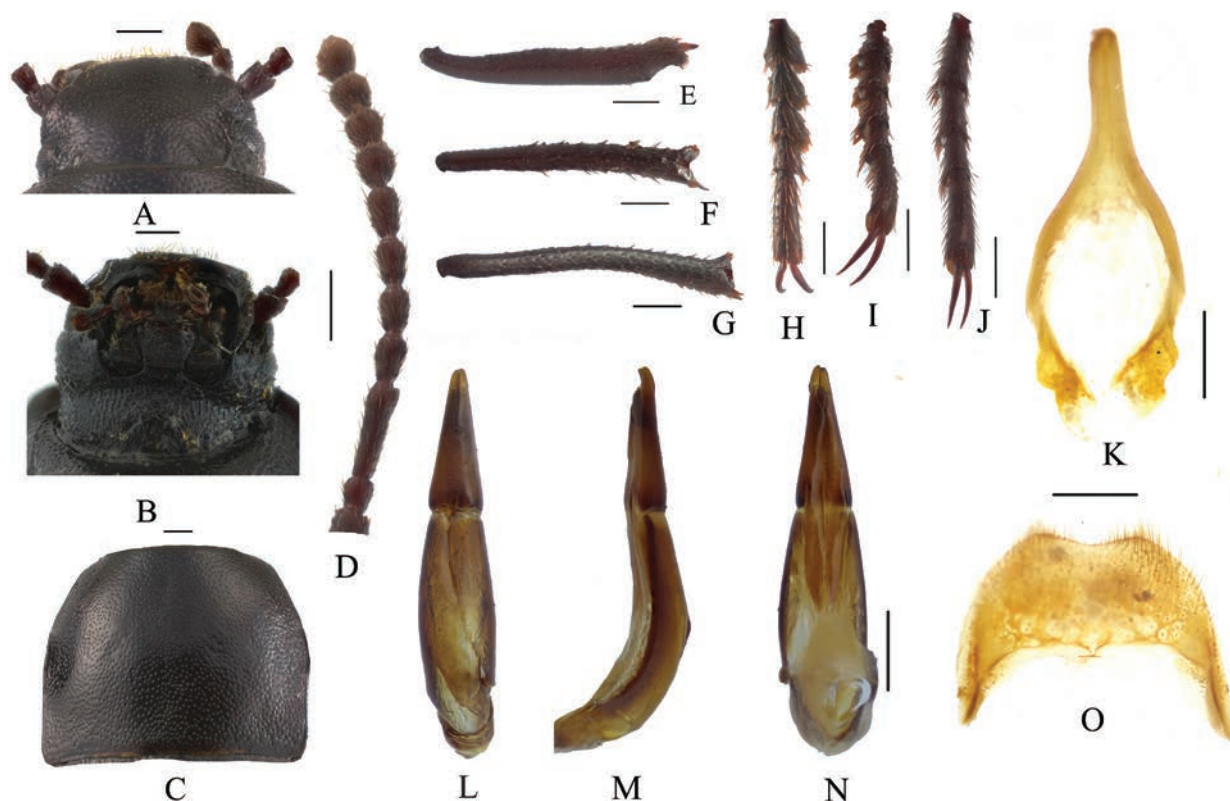


Figure 2. *Pseudognaptorina banbarica* X.-M. Li, sp. nov., male **A** head, dorsal view **B** head, ventral view **C** pronotum **D** antenna **E** protibia **F** mesotibia **G** metatibia **H** protarsus **I** mesotarsus **J** metatarsus **K** spiculum gastrale **L–N** aedeagus **L** dorsal view **M** lateral view **N** ventral view **O** abdominal sternite VIII. Scale bars: 0.5 mm.

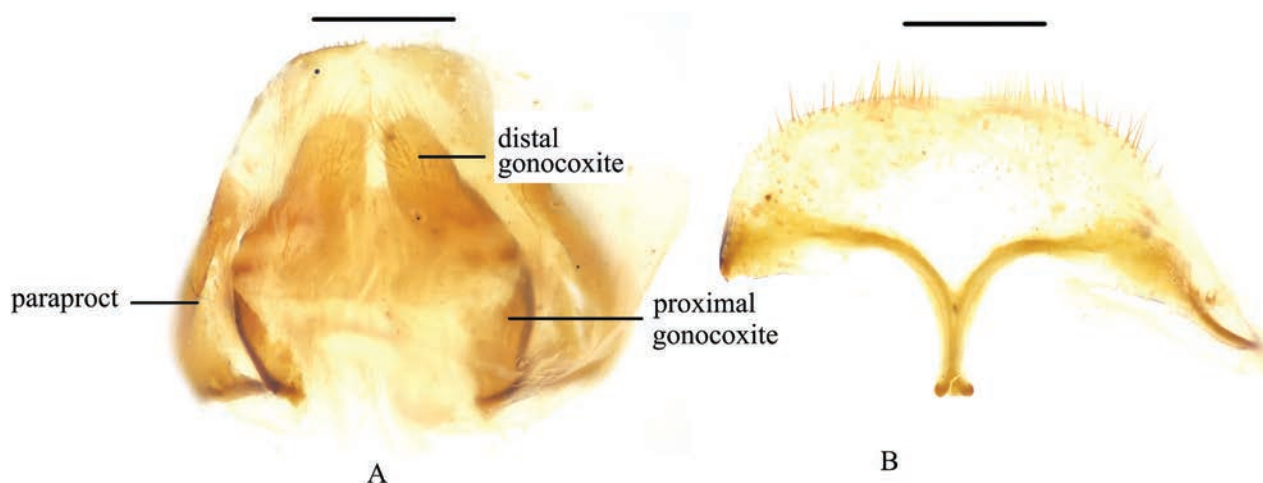


Figure 3. *Pseudognaptorina banbarica* X.-M. Li, sp. nov., female **A** ovipositor **B** spiculum ventrale. Scale bars: 0.5 mm.

Protibiae straight with shorter spurs, inner surface of protibiae slightly widened at basal third; mesotibiae slightly curved; metatibiae curved, narrow. Ventral surface of protarsomeres I–III with hairy brush; ventral surface of mesotarsomeres I–II with hairy brush. Ratio of length (width) of metatarsomeres I–IV: 24.0(9.8): 18.7(8.8): 15.6(8.3): 30.8(8.3).

Abdomen. Abdominal ventrites rather sparsely covered with minute, pale, recumbent setae.

Aedeagus. (Fig. 2K–O) Length of aedeagus 2.31 mm, width 0.42 mm; length of parameres 0.87 mm, width 0.29 mm. Slightly curved to ventral side apically in lateral

view. Parameres strongly elongate, widest at base, regularly narrowing towards apex; outer margins slightly curved to ventral side apically in lateral view. Spiculum gastrale as in Fig. 2K. Posterior margin of abdominal sternite VIII sinuate (Fig. 2O).

Female (Figs 3A, B, 4D–F). Body larger and wider than male, length 12.6–14.4 mm, width 6.9–7.4 mm. Antennae shorter than male, not posteriorly reaching base of pronotum when posteriorly extended. Pronotum 1.52 times as wide as long, widest in middle, lateral margins subparallel from base to middle

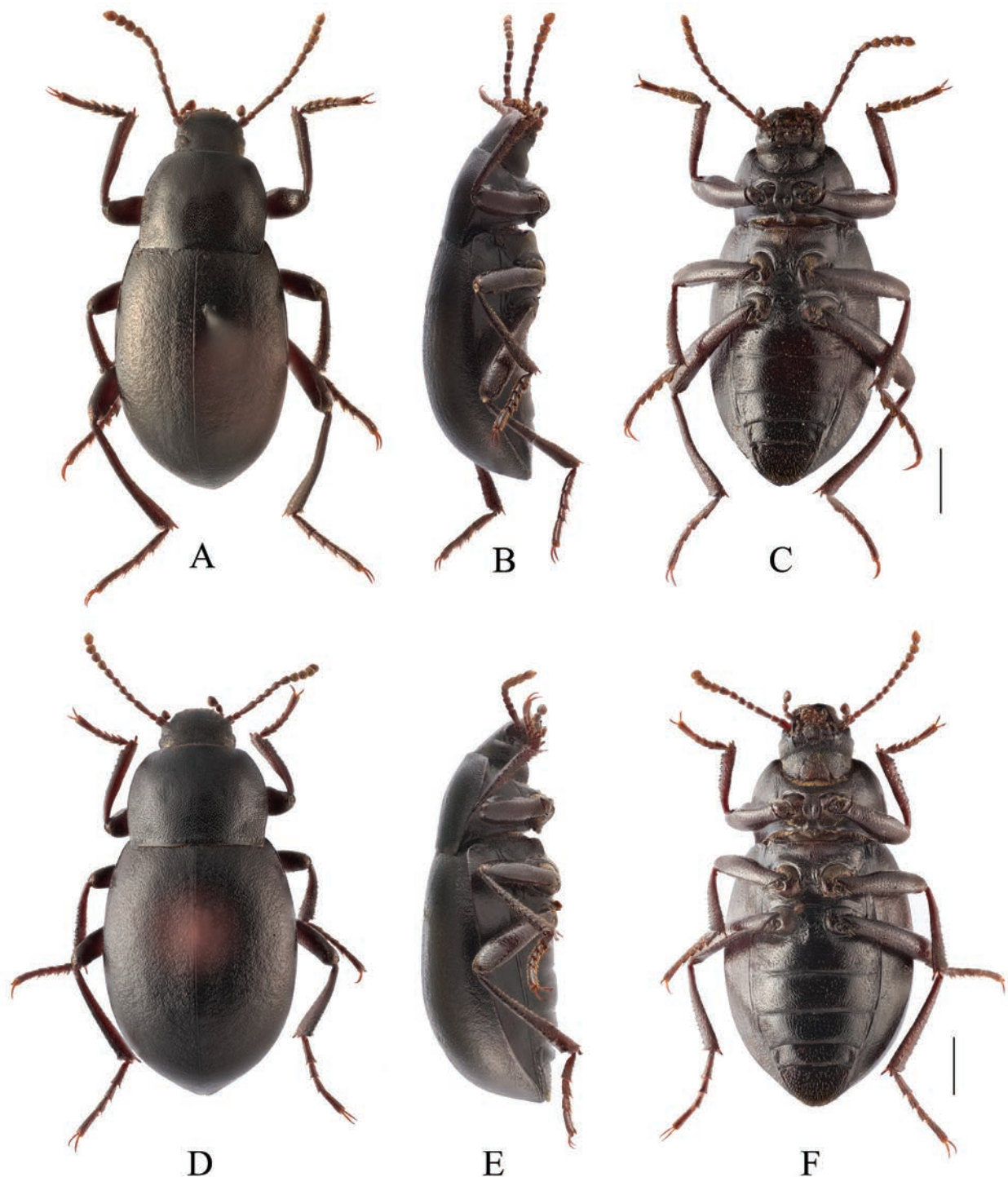


Figure 4. Habitus of *Pseudognaptorina banbarica* X.-M. Li, sp. nov. **A–C** male, holotype **D–F** female, paratype **A, D** dorsal views **B, E** lateral views **C, F** ventral views. Scale bars: 2.0 mm.

and arcuately narrowing toward anterior angles, sides of pronotum slightly convex, 1.79 times as wide as head, with very dense punctation. Elytra oval, more convex than male, 1.34 times as long as wide. Protibial spurs rounded at apex. Distal gonocoxite (Fig. 3A) rounded apically, densely covered with setae; spiculum ventrale as in Fig. 3B.

Diagnosis. This new species is morphologically similar to *P. oblonga*, but can be distinguished from it by the following male character states: ventral surface of mesotarsomeres I–II with hair brushes, mesotarsomere III with small hairy tuft (ventral surface of mesotarsomeres I–III with hairy brush in *P. oblonga*); surface of elytra with dense, rather smooth punctation and regular wrinkle (surface of elytra with fine punctures and irregular wrinkles in *P. oblonga*); parameres strongly elongate, 3.0 times as long as wide (parameres elongate, 2.75 times as long as wide in *P. oblonga*).

Etymology. This species is named for Banbar County, where the type locality is located.

Distribution. Banbar County, Xizang, China.

***Pseudognaptorina himalayana* X.-M. Li, sp. nov.**

<https://zoobank.org/2AD0AE17-2347-47BA-94A7-1674F0633791>

Type materials. Holotype: CHINA • ♂ (MHBU HBU(E)339877): Qucho Mountain, Lhunze County, Xizang/ 28°19.562' N, 92°19.112' E/ Alt. 4824 m/ 2019-VII-30/ Xiu-Min Li & Zhao Pan leg.

Description. Male (Figs 5, 6A–C). Body length 10.3 mm, width 4.9 mm; shiny, brownish; antennae, palpi, and tarsi brown.

Head (Fig. 5A, B). Anterior margin of clypeus slightly sinuate. Head widest at eye level. Lateral margin of head with pair of projections between antennal base and oculus, brownish red. Genal margin arcuately converging before eyes. Eyes barely protruding beyond contour of head. Vertex flat or slightly convex, with uniform punctures. Antennae (Fig. 5D) slender, long, and reaching beyond pronotal base when posteriorly extended; antennomeres VIII–X oval, XI spindle-shaped. Length (width) ratio of antennomeres II–XI as follows: 11.0(10.0): 27.7(10.0): 12.5(10.0): 12.5(10.0): 12.5(10.0): 13.4(10.0): 10.4(12.5): 10.4(14.8): 10.4(15.6): 15.5(15.8).

Prothorax. Pronotum (Fig. 5C) transverse, 1.29 times as wide as long, widest in middle, 1.72 times as wide as head. Ratio of width on anterior margin to its maximum width and posterior margin 0.58: 1.00: 0.92. Lateral margins of pronotum arcuately narrowing in middle, bordered along entire length; posterior margin straight; anterior margin slightly emarginate; anterior angles widely obtuse, posterior angles slightly obtuse. Surface of pronotum very narrowly flattened along lateral margins from base nearly to anterior angles, covered with dense punctation. Hypomera covered shallow longitudinal wrinkles and granules. Prosternum before procoxae gently sloping. Prosternal process gently sloping behind procoxae, forming obtuse projection.

Pterothorax. Elytra oblong-oval and convex, 1.32–1.33 times as long as wide, 1.38–1.41 times as wide as pronotum, widest in apical third. Dorsal surface of elytra passing into outer (deflexed) surface without traces of humeral carina. Outer margin of epipleura visible in dorsal view at basal third and apex.

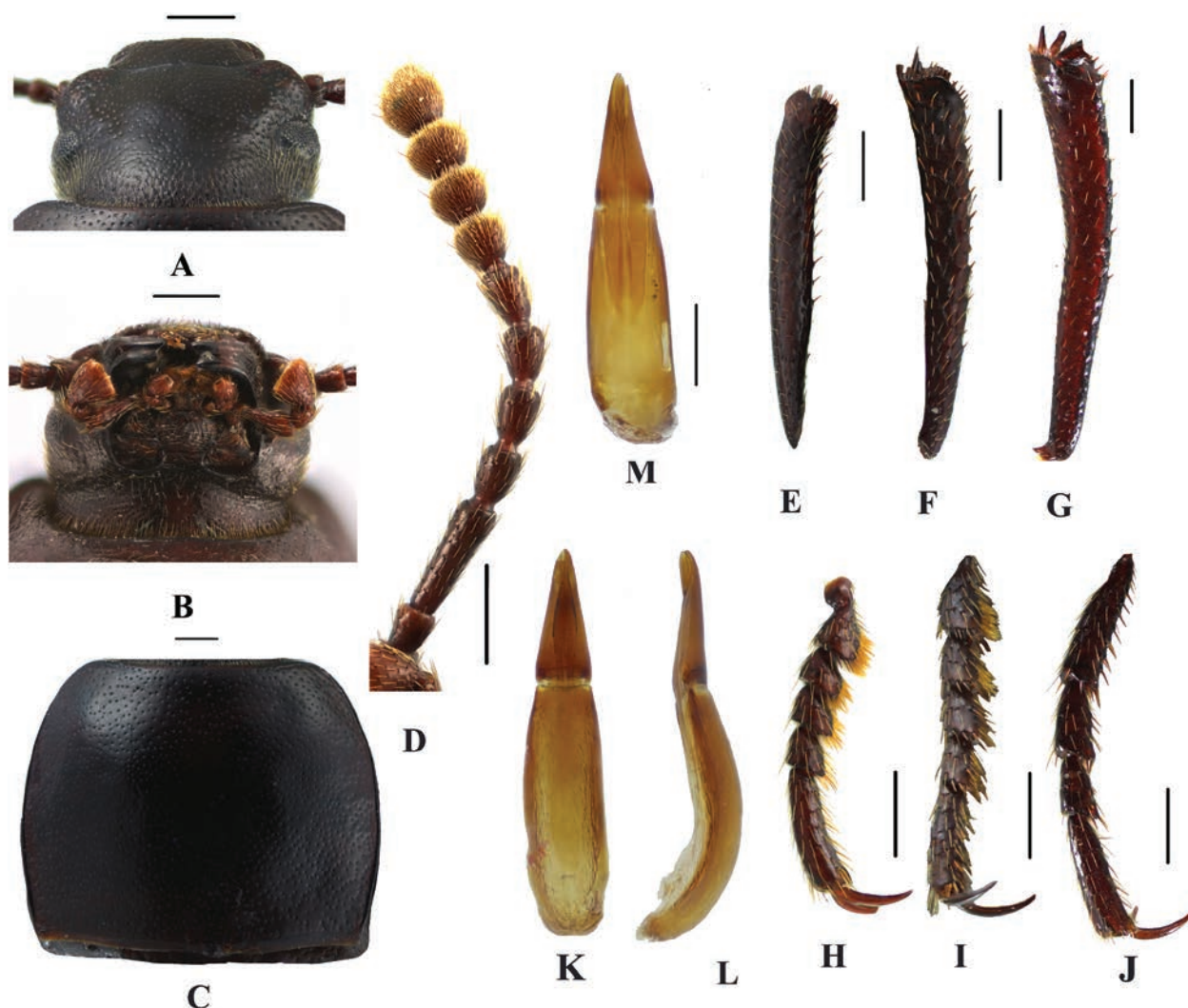


Figure 5. *Pseudognaptorina himalayana* X.-M. Li, sp. nov., male **A** head, dorsal view **B** head, ventral view **C** pronotum **D** antenna **E** protibia **F** mesotibia **G** metatibia **H** protarsus **I** mesotarsus **J** metatarsus **K–M** aedeagus **K** dorsal view **L** lateral view **M** ventral view. Scale bars: 0.5 mm.

Surface of elytra with dense, rather smooth punctation and wrinkles almost vanishing on apical declivity.

Legs (Fig. 5E–J). Femora and tibiae moderately thickened. Ratio of length (width) of pro-, meso-, and metatibiae: 45.0(6.5): 50.0(7.5): 82.5(8.0). Protibiae narrow, straight with shorter spurs; mesotibiae slightly arcuately curved; metatibiae arcuately curved, narrow. Ventral surface of protarsomeres I–III with hairy brush; ventral surface of mesotarsomeres I–II with hairy brush. Ratio of length(width) of metatarsomeres I–IV: 32.0(9.5): 17.0(10.0): 13.5(9.0): 30.0(8.5).

Abdomen. Abdominal ventrites rather sparsely covered with minute, pale, recumbent setae.

Aedeagus (Fig. 5K–M). Length of aedeagus 2.30 mm, width 0.48 mm; length of parameres 0.83 mm, width 0.34 mm. Slightly curved to ventral side apically in lateral view. Parameres moderately elongate, regularly narrowing towards apex; outer margins slightly curved to ventral side apically in lateral view.

Diagnosis. This new species is morphologically similar to *P. migana* but can be distinguished from it by the following male character states:



Figure 6. Habitus of *Pseudognaptorina himalayana* X.-M. Li, sp. nov., male, holotype. **A** dorsal view **B** lateral view **C** ventral view. Scale bar: 2.0 mm.

pronotum 1.34 times as wide as long, lateral margins arcuately narrowed at basal 2/3 (pronotum 1.29 times as wide as long, lateral margins of pronotum regularly arcuate in *P. migana*); ventral surface of mesotarsomeres I–III with hair brushes (mesotarsomeres I–II with hair brushes, mesotarsomere III with small hairy tuft in *P. migana*); parameres moderately elongate, regularly narrowing towards apex, more obtuse from basal half to apex (parameres strongly elongate, widest at base, regularly narrowing towards apex, more acute from basal half to apex in *P. migana*).

Etymology. This species is named for the Himalayas, where the type locality of the species is located.

Distribution. Lhunze County, Xizang, China.

***Pseudognaptorina migana* X.-M. Li, sp. nov.**

<https://zoobank.org/A3F1F50C-5F43-4F93-80B1-99960E9A47FA>

Type materials. Holotype: CHINA • ♂ (MHBU HBU(E)339879): Miga Mountain pass, Gongbogyamda County, Xizang/ 29°84.105' N, 92°33.422' E/ Alt. 4775 m/ 2023-VII-18/ Xiu-Min Li & Tong-Yang Guo leg. **Paratypes:** CHINA • 10♂♂, 20♀♀ (MHBU HBU(E)339880–339909): same data as holotype; CHINA • 1♂, 1♀ (MHBU HBU(E)339910–339911): Miga pass, Gongbogyamda County, Xizang/ 29°84.105' N, 92°33.422' E/ Alt. 4750 m/ 2019-VII-26/ Xiu-Min Li & Zhao Pan leg.

Description. Male (Fig. 7, 8A–C). Body length 10.5–11.3 mm, width 4.9–5.2 mm; shiny, black or brownish; antennae, palpi, and tarsi brown.



Figure 7. *Pseudognaptorina migana* X.-M. Li, sp. nov., male **A** head, dorsal view **B** head, ventral view **C** pronotum **D** antenna **E** protibia **F** mesotibia **G** metatibia **H** protarsus **I** mesotarsus **J** metatarsus **K** spiculum gastrale **L–N** aedeagus **L** dorsal view **M** lateral view **N** ventral view **O** abdominal sternite VIII. Scale bars: 0.5 mm.

Head (Fig. 7A, B). Anterior margin of clypeus slightly sinuate. Head widest at eye level. Lateral margin of head with pair of projections between antennal base and oculus, brownish red. Genal margin arcuately converging before eyes. Eyes barely protruding beyond contour of head. Vertex flat or slightly convex, with uniform punctures. Antennae (Fig. 7D) slender and long, reaching pronotal base when posteriorly extended, antennomere III very long, 2.4 times as long as antennomeres II, antennomeres VIII–X oval, XI spindle-shaped. Length (width) ratio of antennomeres II–XI as follows: 11.8(10.0): 28.1(10.0): 14.5(10.0): 14.5(10.0): 14.5(10.0): 14.5(10.0): 13.3(12.0): 13.3(13.0): 13.3(14.0): 19.5(14.0).

Prothorax. Pronotum (Fig. 7C) transverse, 1.34 times as wide as long, widest in middle, 1.71 times as wide as head. Ratio of width on anterior margin to its maximum width and posterior margin 0.52: 1.00: 0.92. Lateral margins of pronotum arcuately narrowing to anterior margin, bordered along entire length; posterior margin straight; anterior margin slightly emarginate; anterior angles widely, obtusely angled; posterior angles almost rectangular. Surface of pronotum slightly convex between lateral margins, covered with fine, dense punctation. Hypomera covered shallow, longitudinal wrinkles and granules. Prosternum before procoxae gently sloping. Prosternal process gently sloping behind procoxae, forming obtuse projection.

Pterothorax. Elytra oblong-oval and convex, 1.38–1.40 times as long as wide, 1.35–1.37 times as wide as pronotum, widest in apical third. Dorsal surface of elytra passing into outer (deflexed) surface without traces of humeral carina. Outer margin of epipleura visible in dorsal view at basal third and apex. Surface of elytra with dense, rather smooth punctation and wrinkles almost vanishing on apical declivity.

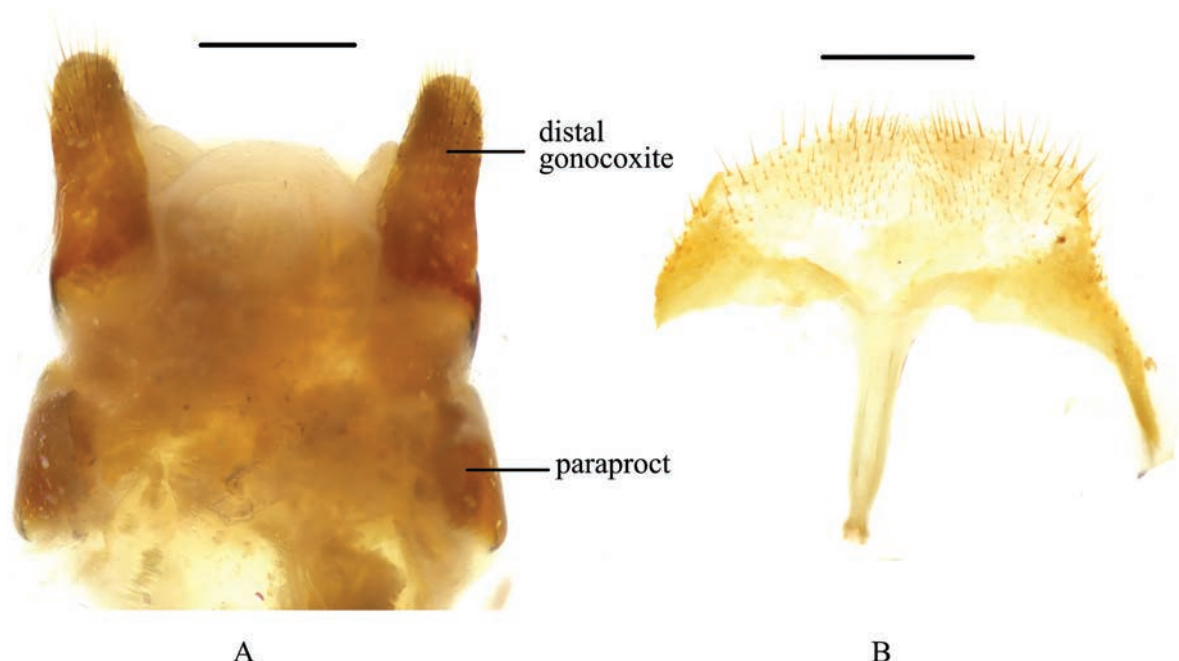


Figure 8. *Pseudognaptorina migana* X.-M. Li, sp. nov., female **A** ovipositor **B** spiculum ventrale. Scale bars: 0.5 mm.

Legs (Fig. 7E–J). Femora and tibiae moderately thickened. Ratio of length (width) pro-, meso-, and metatibiae: 56.2(9.1): 55.8(9.5): 94.1(11.0). Protibiae straight with shorter spurs, inner surface of protibiae slightly widened at basal third; mesotibiae slightly arcuately curved; metatibiae arcuately curved, narrow. Ventral surface of protarsomeres I–III with hairy brush; ventral surface of mesotarsomeres I–II with hairy brush. Ratio of length (width) of metatarsomeres I–IV: 29.9(10.0): 19.5(10.0): 17.1(10.0): 29.4(7.9).

Abdomen. Abdominal ventrites rather sparsely covered with minute, pale, recumbent setae.

Aedeagus (Fig. 7K–O). Length of aedeagus 2.34 mm, width 0.46 mm; length of parameres 0.89 mm, width 0.35 mm. Slightly curved to ventral side apically in lateral view. Parameres strongly elongate, widest at base, regularly narrowing towards apex; outer margins slightly curved to ventral side apically in lateral view. Spiculum gastrale as in Fig. 7K. Posterior margin of abdominal sternite VIII sinuate (Fig. 7O).

Female (Figs 8A, B, 9D–F). Body larger and wider than male, length 12.1–12.7 mm, width 6.0–6.4 mm. Antennae shorter than male, not posteriorly reaching base of pronotum when posteriorly extended. Pronotum 1.5 times as wide as long, widest in middle, lateral margins subparallel from base to middle and narrowing toward anterior angles curved, sides of pronotum slightly convex; 1.73 times as wide as head; with very dense punctation. Elytra oval, more convex than male, 1.37 times as long as wide. Protibial spurs with small, pointed at apex. Distal gonocoxite (Fig. 8A) rounded apically, densely covered with setae; spiculum ventrale as in Fig. 8B.

Diagnosis. This new species is morphologically similar to *P. himalayana*, but can be distinguished from it by the following male character states: pronotum 1.29 times as wide as long, lateral margins of pronotum regularly arcuate (pronotum 1.34 times as wide as long, lateral margins arcuately narrowed at basal 2/3 in *P. himalayana*); mesotarsomeres I–II with hair brushes, mesotarsomere III with small hairy tuft (ventral surface of mesotarsomeres I–III with hair

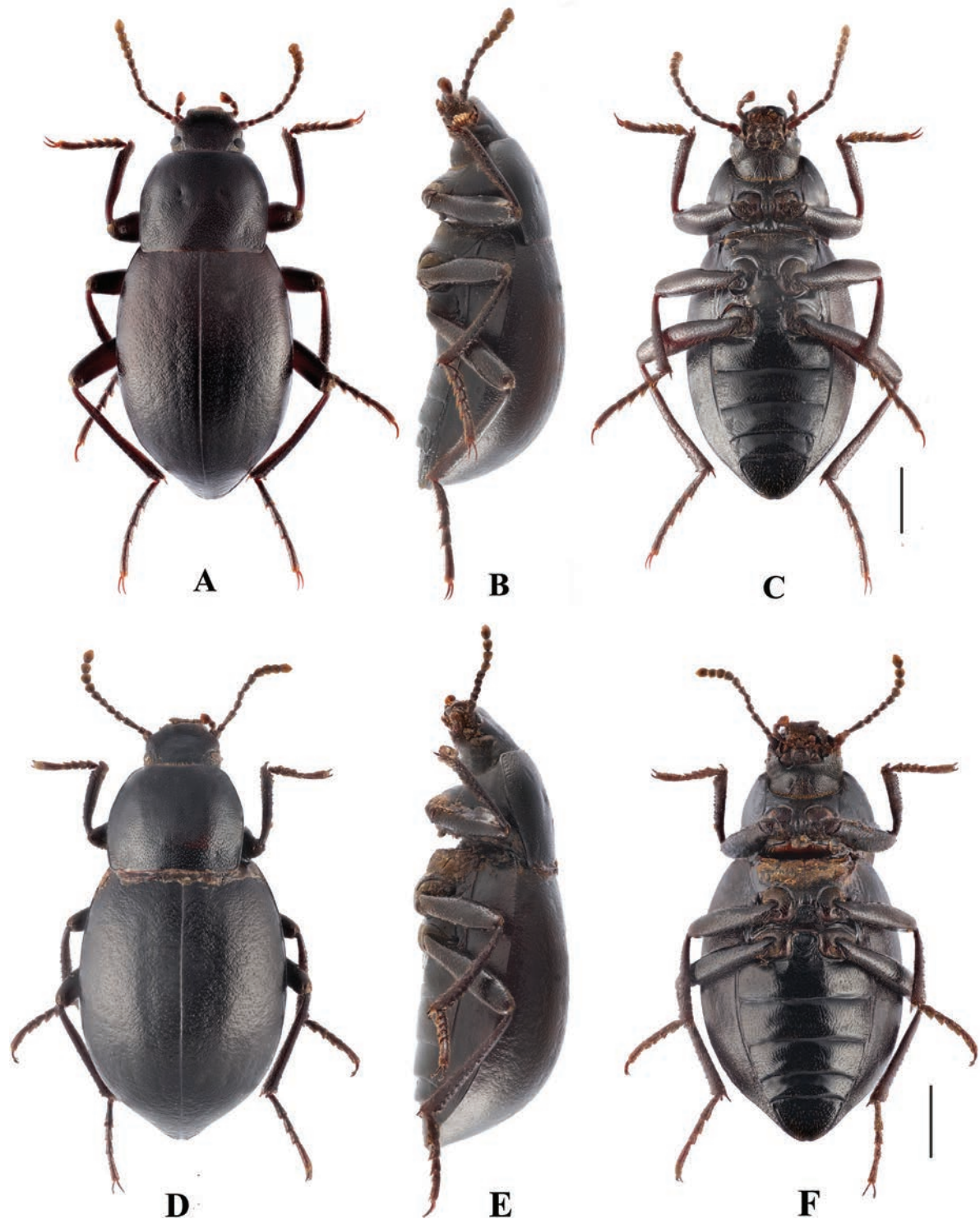


Figure 9. Habitus of *Pseudognaptorina migana* X.-M. Li, sp. nov. **A–C** male, holotype **D–F** female, paratype **A, D** dorsal views **B, E** lateral views **C, F** ventral views. Scale bars: 2.0 mm.

brushes in *P. himalayana*); parameres strongly elongate, widest at base, regularly narrowing towards apex, more acute from basal half to apex (parameres moderately elongate, regularly narrowing towards apex, more obtuse from basal half to apex in *P. himalayana*).

Etymology. This species is named after the type locality, Miga Pass.

Distribution. Gongbogyamda County, Xizang, China.

***Pseudognaptorina oblonga* X.-M. Li, sp. nov.**

<https://zoobank.org/460ECFD4-85F7-410A-9D6D-D74A2A6DD9CD>

Type materials. Holotype: CHINA • ♂ (MHBU HBU(E)339912): Lhari County, Xizang / 2013-VII-22/ Xing-Long Bai & Jun-Sheng Shan leg. **Paratypes:** CHINA • 2♂♂, 4♀♀ (MHBU HBU(E)339913–339918): same data as holotype; CHINA • 4♂♂, 5♀♀ (MHBU HBU(E)339919–339927): Arza Township, Lhari County, Xizang/ 30°37.104'N, 93°24.307'E/ Alt. 4300 m/ 2019-VIII-9/ Guo-Dong Ren, Ya-Lin Li & Xing-Long Bai leg.; CHINA • 1♂ (MHBU HBU(E)339928): Lhari County, Xizang/ 30°45.225'N, 93°13.162'E/ Alt. 4762 m/ 2023-VII-17/ Xiu-Min Li & Tong-Yang Guo leg.

Description. Male (Figs 10, 11A–C). Body length 10.8–11.3 mm, width 5.0–5.1 mm; shiny, black or brownish; antennae, palpi, and tarsi brown.

Head (Fig. 10A, B). Anterior margin of clypeus slightly sinuate. Head widest at eye level. Lateral margin of head with pair of projections between antennal base and oculus, brownish red. Genal margin arcuately converging before eyes. Eyes barely protruding beyond contour of head. Vertex flat or slightly convex, with uniform punctures. Antennae (Fig. 10D) slender and long, reaching beyond pronotal base when posteriorly extended, antennomere III very long, 3.1 times as long as antennomere II, antennomeres VIII–X oval, XI spindle-shaped. Length (width) ratio of antennomeres II–XI as follows: 10.0(10.0): 31.3(10.0): 15.9(10.0): 15.1(10.0): 16.2(10.0): 16.2(10.3): 15.3(12.5): 15.3(12.5): 14.8(12.5): 19.8(13.8).

Prothorax. Pronotum (Fig. 10C) transverse, 1.40 times as wide as long, widest in middle, 1.67 times as wide as head. Ratio of width on anterior margin to its maximum width and posterior margin 0.57: 1.00: 0.96. Lateral margins of pronotum arcuately narrowing to anterior margin, bordered along entire length; posterior margin straight; anterior margin slightly emarginate; anterior angles widely, obtusely angled; posterior angles almost rectangular. Surface of pronotum very narrowly flattened along lateral margins from base nearly to anterior angles, covered with dense punctation. Hypomera covered shallow longitudinal wrinkles and granules. Prosternum before procoxae gently sloping. Prosternal process gently sloping behind procoxae, forming obtuse projection.

Pterothorax. Elytra oblong-oval and convex, 1.45–1.49 times as long as wide, 1.44–1.46 times as wide as pronotum, widest at apical third. Dorsal surface of elytra passing into outer (deflexed) surface without traces of humeral carina. Outer margin of epipleura visible in dorsal view at basal third and apex. Surface of elytra with dense, rather smooth punctation and wrinkle almost vanishing on apical declivity.

Legs (Fig. 10E–J). Femora and tibiae moderately thickened. Ratio of length(width) of pro-, meso-, and metatibiae: 46.8(6.5): 64.6(7.5): 94.1(8.0). Protibiae straight with shorter spur, inner surface of protibiae slightly widen in basal 1/3; mesotibiae slightly arcuately curved; metatibiae arcuately curved, narrow. Ventral surface of protarsomeres I–III with hairy brush; ventral surface of mesotarsomere I–III with hairy brush. Ratio of length(width) of metatarsomeres I–IV segments: 27.5(9.9): 25.0(9.1): 17.5(8.6): 37.5(9.3).

Abdomen. Abdominal ventrites rather sparsely covered with minute, pale, recumbent setae.

Aedeagus (Fig. 10K–O). Length of aedeagus 2.77 mm, width 0.53 mm; length of parameres 0.88 mm, width 0.32 mm. Slightly curved to ventral side apically in lateral view. Parameres strongly elongate, widest at base, regularly narrowing

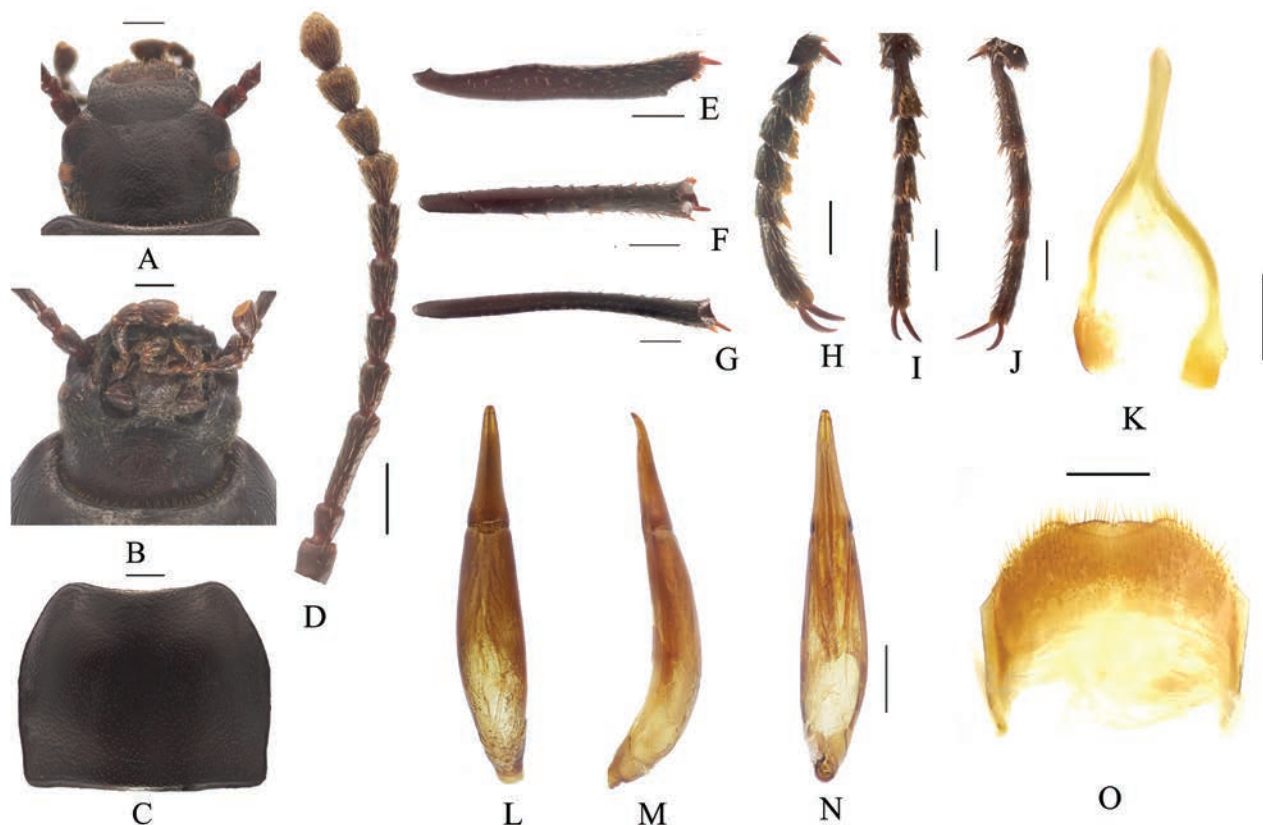


Figure 10. *Pseudognaptorina oblonga* X.-M. Li, sp. nov., male **A** head, dorsal view **B** head, ventral view **C** pronotum **D** antenna **E** protibia **F** mesotibia **G** metatibia **H** protarsus **I** mesotarsus **J** metatarsus **K** spiculum gastrale **L–N** aedeagus **L** dorsal view **M** lateral view **N** ventral view **O** abdominal sternite VIII. Scale bars: 0.5 mm.

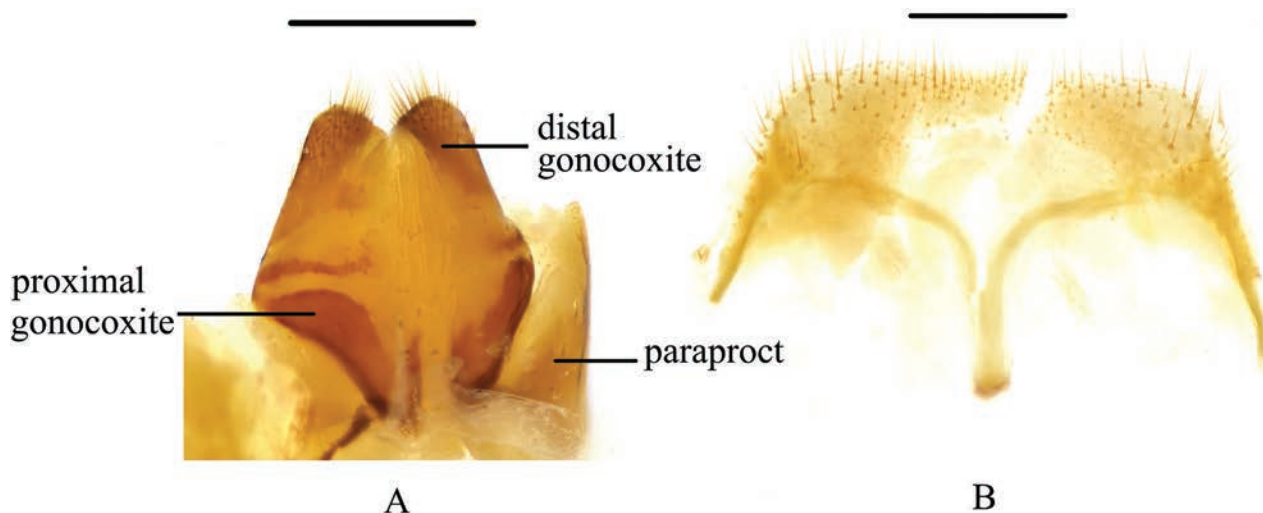


Figure 11. *Pseudognaptorina oblonga* X.-M. Li, sp. nov., female. **A** ovipositor **B** spiculum ventrale. Scale bars: 0.5 mm.

towards apex; outer margins slightly curved to ventral side apically in lateral view. Spiculum gastrale as in Fig. 10K. Posterior margin of abdominal sternite VIII sinuate (Fig. 10O).

Female (Fig. 11A, B, 12D–F). Body larger and wider than male, length 12.1–12.5 mm, width 5.9–6.1 mm. Outer margin of head above base of antennae with widely, obtusely angled emargination, less sharp than in male. Antennae shorter than in male, not posteriorly reaching base of pronotum when

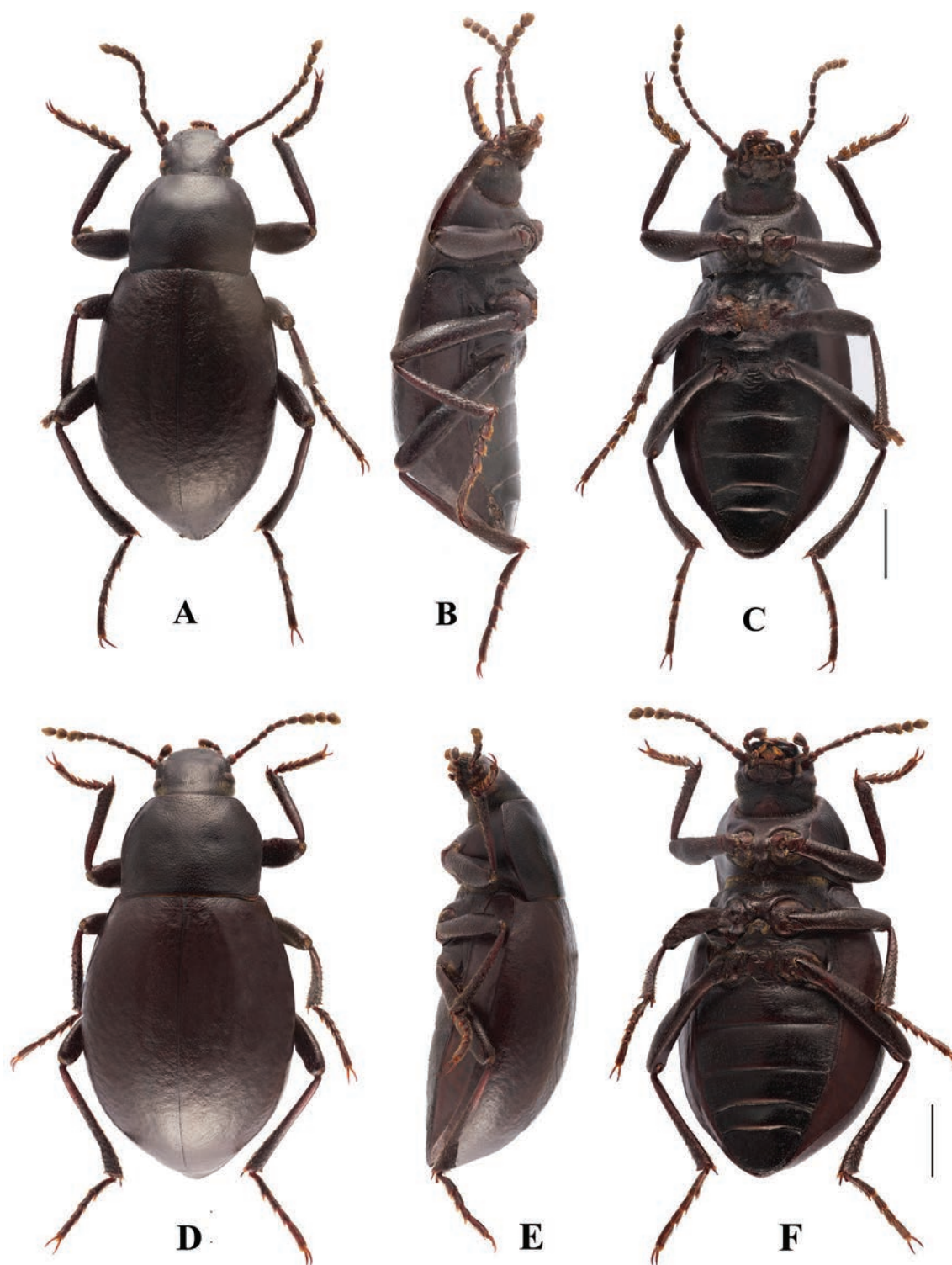


Figure 12. Habitus of *Pseudognaptorina oblonga* X.-M. Li, sp. nov. **A–C** male, holotype **D–F** female, paratype **A, D** dorsal views **B, E** lateral views **C, F** ventral views. Scale bars: 2.0 mm.

posteriorly extended. Pronotum 1.45 times as wide as long, widest in middle, lateral margins subparallel from base to middle and narrowing toward anterior angles arcuately, sides of pronotum slightly convex; 1.72 times as wide as head; with very dense punctation. Elytra oval, more convex than male, 1.32 times as long as wide. Protibial spurs small, pointed at apex. Distal gonocoxite (Fig. 11A) rounded apically, densely covered with setae; spiculum ventrale as in Fig. 11B.

Diagnosis. This new species is morphologically similar to *P. banbarica*, but can be distinguished from it by the following male character states: ventral surface of mesotarsomeres I–III with hairy brush (ventral surface of mesotarsomeres I–II with hair brushes, mesotarsomere III with small hairy tuft in *P. banbarica*); surface of elytra with fine punctures and irregular wrinkles (surface of elytra with dense, rather smooth punctation and wrinkle in *P. banbarica*).

Etymology. This species is named from the Latin adjective “oblonga”, in reference to its elongate aedeagus.

Distribution. Lhari County, Xizang, China.

***Pseudognaptorina rectangularis* X.-M. Li, sp. nov.**

<https://zoobank.org/2AF10B93-D9D1-4DE2-AEA5-480ABF9D4098>

Type materials. Holotype: CHINA • ♂ (MHBU HBU(E)339929): Hongyuan County, Sichuan/ 32°01.96'N, 102°01.99'E/ Alt. 3451 m/ 2021-VII-20/ Xiu-Min Li leg.

Description. Male (Figs 13, 14A–C). Body length 12.6 mm, width 6.2 mm; shiny, black; antennae, palpi, and tarsi brown.

Head (Fig. 13A, B). Anterior margin of clypeus slightly sinuate. Head widest at eye level. Lateral margin of head with pair of projections between antennal base and oculus, brownish red. Genal margin arcuately converging before eyes. Eyes barely protruding beyond contour of head. Vertex flat or slightly convex, with uniform punctures. Antennae (Fig. 13D) slender, long, and reaching pronotal base when posteriorly extended; antennomere III very long, 2.9 times as long as antennomere II; antennomeres VIII–X oval; XI spindle-shaped. Length (width) ratio of antennomeres II–XI as follows: 10.9(9.4): 27.1(10.7): 14.8(10.0): 16.2(10.0): 15.5(10.0): 18.9(10.0): 15.1(11.5): 13.9(13.3): 13.9(13.3): 15.2(13.9).

Prothorax. Pronotum (Fig. 13C) transverse, 1.52 times as wide as long, widest in middle, 1.84 times as wide as head. Ratio of width on anterior margin to its maximum width and posterior margin 0.55: 1.00: 0.97. Lateral margins of pronotum arcuately narrowing to anterior margin, bordered along entire length; posterior margin straight; anterior margin slightly emarginate; anterior angles widely, obtusely angled; posterior angles almost rectangular. Surface of pronotum very narrowly flattened along lateral margins from base nearly to anterior angles, covered with dense punctation. Hypomera covered shallow longitudinal wrinkles and granules; inner part covered with longitudinal rugae. Prosternum gently sloping before procoxae. Prosternal process gently sloping behind procoxae, forming obtuse projection.

Pterothorax. Elytra oblong-oval and convex, 1.31 times as long as wide, 1.43 times as wide as pronotum, widest at apical third. Dorsal surface of elytra passing into outer (deflexed) surface without traces of humeral carina. Outer margin of epipleura visible in dorsal view at basal third and apex. Surface of elytra with dense, rather smooth punctation and wrinkles almost vanishing on apical declivity.

Legs (Fig. 13E–J). Femora and tibiae moderately thickened. Ratio of length (width) of pro-, meso-, and metatibiae: 57.2(9.2): 59.1(9.4): 77.9(10.3). Protibiae straight with shorter spur, inner surface of protibiae nearly flat; mesotibiae slightly curved; metatibiae slightly curved. Ventral surface of protarsomeres I–III with hairy brush; ventral surface of mesotarsomeres I–II with hairy brush. Ratio of length(width) of metatarsomeres I–IV: 34.5(9.7): 22.5(10.0): 22.8(10.0): 31.9(7.7).

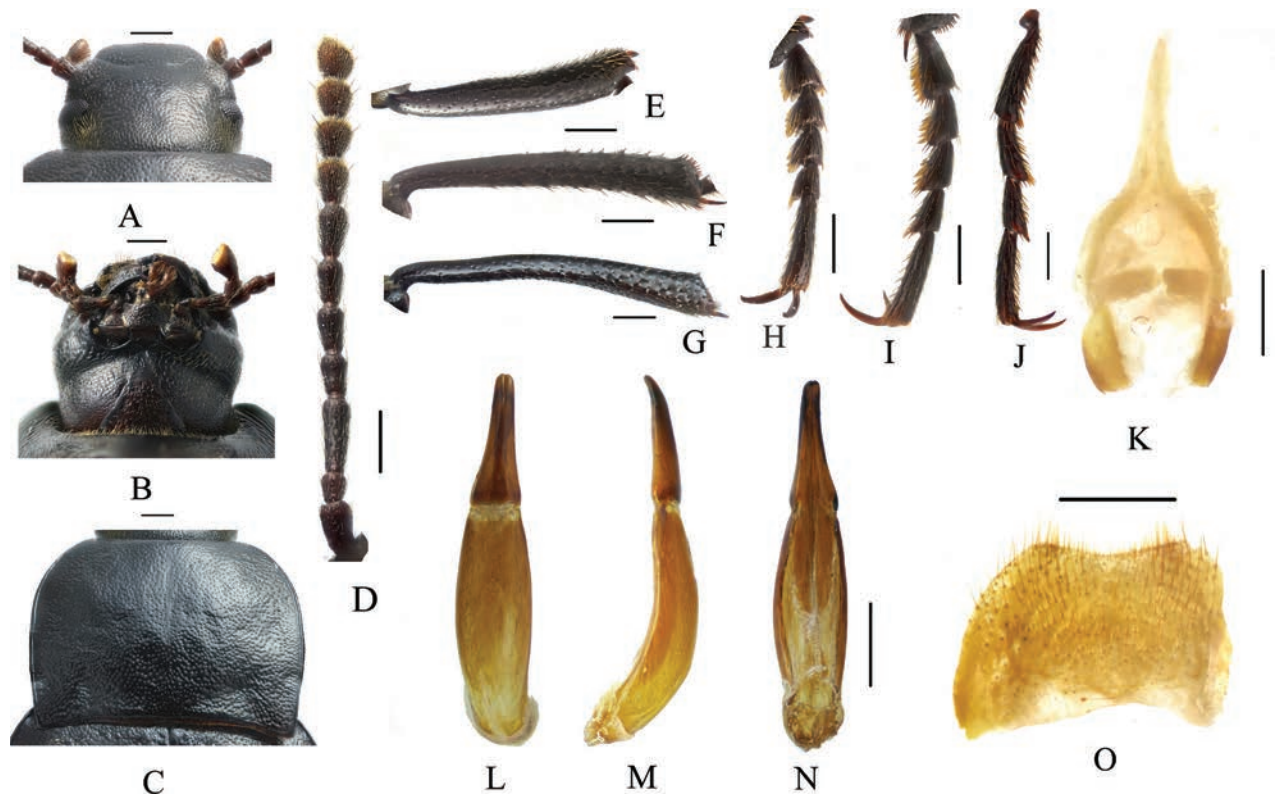


Figure 13. *Pseudognaptorina rectangularis* X.-M. Li, sp. nov., male A head, dorsal view B head, ventral view C pronotum D antenna E protibia F mesotibia G metatibia H protarsus I mesotarsus J metatarsus K spiculum gastrale L–N aedeagus L dorsal view M lateral view N ventral view O abdominal sternite VIII. Scale bars: 0.5 mm.

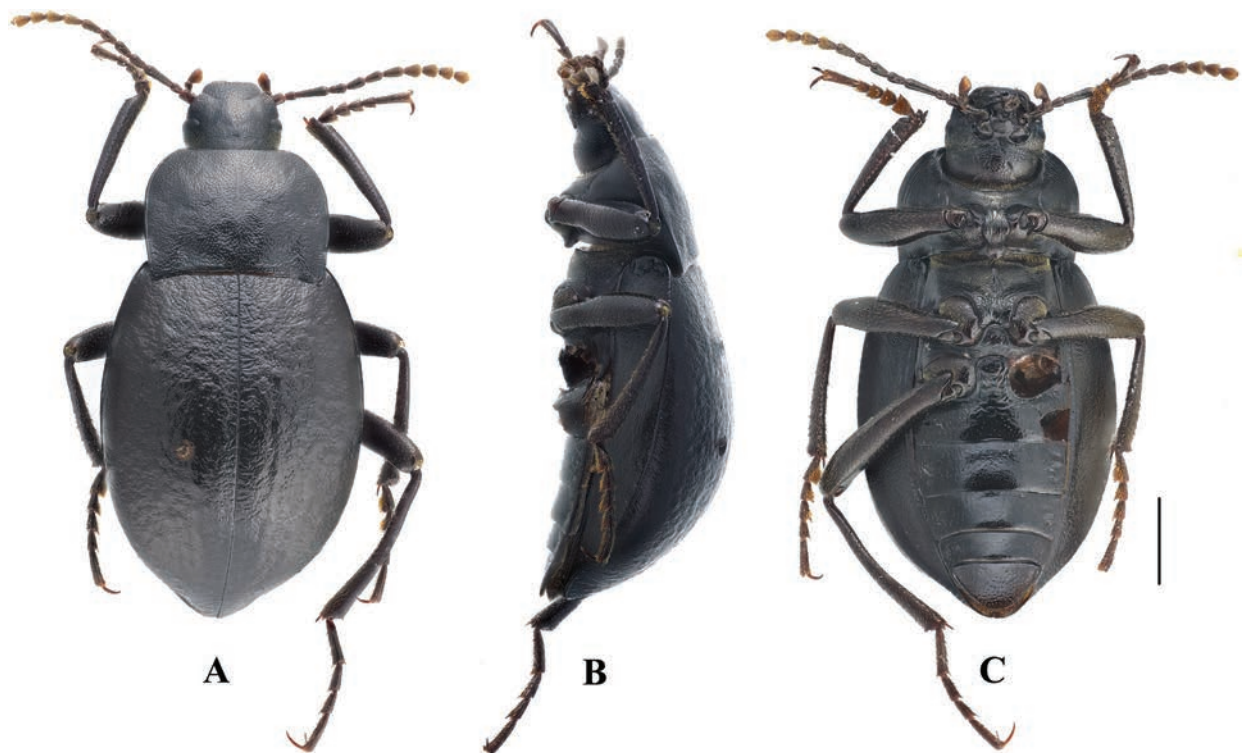


Figure 14. Habitus of *Pseudognaptorina rectangularis* X.-M. Li, sp. nov., male, holotype A dorsal view B lateral view C ventral view. Scale bar: 2.0 mm.

Aedeagus (Fig. 13K–O). Length of aedeagus 2.18 mm, width 0.46 mm; length of parameres 0.79 mm, width 0.31 mm. Slightly curved to ventral side apically in lateral view. Parameres strongly elongate, widest at base, regularly narrowing towards apex; outer margins slightly curved to ventral side apically in lateral view. Spiculum gastrale as in Fig. 13K. Posterior margin of abdominal sternite VIII sinuate (Fig. 13O).

Diagnosis. This new species is morphologically similar to *P. flata*, but can be distinguished from it by the following male character states: pronotum transverse, 1.52 times as wide as long, surface flatted, posterior angles nearly rectangular (pronotum transverse, 1.36 times as wide as long, surface explanate and slightly concave, posterior angles obtusely rounded in *P. flata*); ventral surface of mesotarsomeres I–II with hair brushes, mesotarsomere III with small hairy tuft (ventral surface of mesotarsomeres I–III with hair brushes in *P. flata*).

Etymology. This species is named from the Latin adjective “*rectangularis*”, in reference to its sub-rectangular prothorax.

Distribution. Hongyuan County, Sichuan, China.

***Pseudognaptorina reni* X.-M. Li, sp. nov.**

<https://zoobank.org/62A03392-4ADE-414F-9E21-00E41A071DAA>

Type materials. Holotype: CHINA • ♂ (MHBU HBU(E)339930): Vajra Mountain pass, Zadowa County, Qinghai/ 32°47.98' N, 95°09.26' E/ Alt. 4718 m/ 2019-VII-26/ Guo-Dong Ren & Yi-Ping Niu leg. **Paratypes:** CHINA • 10♂♂, 20♀♀ (MHBU HBU(E)339931–339960): same data as holotype; CHINA • 3♂♂, 10♀♀ (MHBU HBU(E)339961–339973): Konge township, Bachan County, Xizang/ 32°31.50' N, 94°43.31' E/ Alt. 4556 m/ 2022-VII-4/ Guo-Dong Ren & Yi-Ping Niu leg.

Description. Male (Figs 15, 16A–C). Body length 13.6–14.1 mm, width 6.30–6.58 mm; black, slightly shiny, oval-oblong.

Head (Fig. 15A, B). Anterior margin of clypeus slightly sinuate. Head widest at eye level. Lateral margin of head with pair of projections between antennal base and oculus, brownish red. Genal margin arcuately converging before eyes. Eyes barely protruding beyond contour of head. Vertex flat or slightly convex, with uniform punctures. Antennae (Fig. 15D) slender and long, reaching pronotal base when posteriorly extended, antennomere III very long, 2.7 times as long as antennomere II, antennomeres VIII–X oval, XI spindle-shaped. Length (width) ratio of antennomeres II–XI as follows: 12.5(10.0): 33.4(10.0): 16.6(10.0): 15.7(10.0): 14.8(10.0): 16.4(10.0): 14.1(12.9): 14.1(14.1): 14.1(14.7): 18.8(15.5).

Prothorax. Pronotum (Fig. 15C) transverse, 1.50 times as wide as long, widest in middle, 1.72 times as wide as head. Ratio of width on anterior margin to its maximum width and posterior margin 0.54: 1.00: 0.95. Lateral margins of pronotum arcuately narrowing to anterior margin, bordered along entire length; posterior margin straight; anterior margin slightly emarginate; anterior angles widely, obtusely angled; posterior angles almost rectangular. Surface of pronotum slightly convex between lateral margins, very narrowly flattened along lateral margins from base nearly to anterior angles, covered with fine, dense punctation. Hypomera covered shallow, longitudinal wrinkles and granules. Prosternum before procoxae gently sloping. Prosternal process gently sloping behind procoxae, forming obtuse projection.



Figure 15. *Pseudognaptorina reni* X.-M. Li, sp. nov., male **A** head, dorsal view **B** head, ventral view **C** pronotum **D** antenna **E** protibia **F** mesotibia **G** metatibia **H** protarsus **I** mesotarsus **J** metatarsus **K** spiculum gastrale **L–N** aedeagus **L** dorsal view **M** lateral view **N** ventral view **O** abdominal sternite VIII. Scale bars: 0.5 mm.

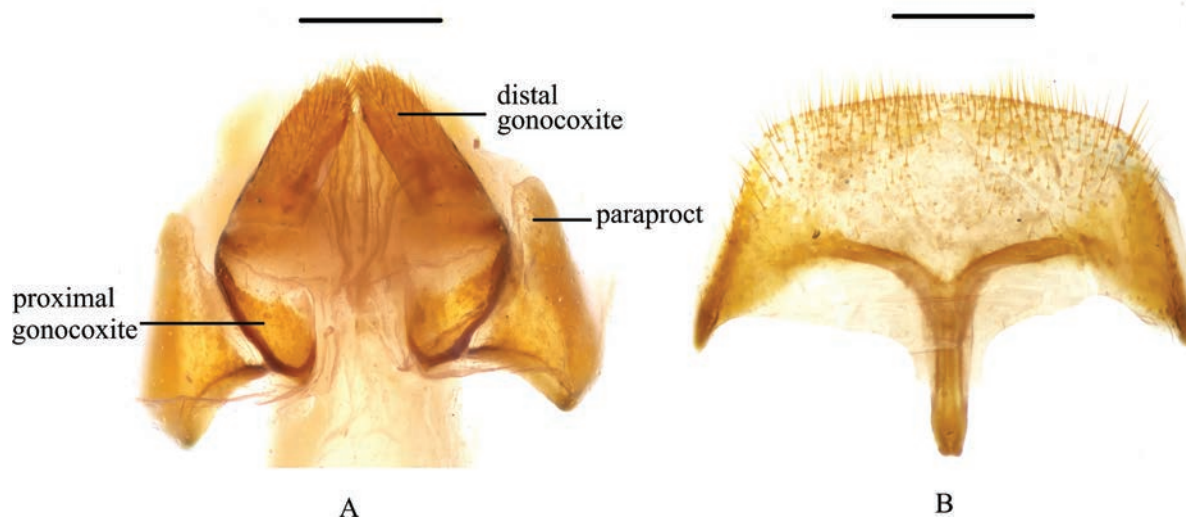


Figure 16. *Pseudognaptorina reni* X.-M. Li, sp. nov., female. **A** ovipositor **B** spiculum ventrale. Scale bars: 0.5 mm.

Pterothorax. Elytra oblong-oval and convex, 1.43–1.48 times as long as wide, 1.39–1.41 times as wide as pronotum, widest at apical third. Dorsal surface of elytra passing into outer (deflexed) surface without traces of humeral carina. Outer margin of epipleura visible in dorsal view at basal third and apex. Surface of elytra with dense, rather smooth punctation and wrinkles almost vanishing on apical declivity.

Legs (Fig. 15E–J). Femora and tibiae moderately thickened. Ratio of length (width) of pro-, meso-, and metatibiae: 56.0(8.6): 49.6(7.6): 68.0(8.6). Protibiae straight with shorter spur, inner surface of protibiae slightly widened at basal

third; mesotibiae slightly arcuately curved; metatibiae curved, narrow. Ventral surface of protarsomeres I–III with hairy brush; ventral surface of mesotarsomeres I–II with hairy brush. Ratio of length (width) of metatarsomeres I–IV: 38.7(11.5): 21.1(10.0): 19.6(10.0): 31.1(10.0).

Abdomen. Abdominal ventrites rather sparsely covered with minute, pale, recumbent setae.

Aedeagus (Fig. 15K–O). Length of aedeagus 2.31 mm, width 0.51 mm; length of parameres 0.76 mm, width 0.33 mm. Slightly curved to ventral side apically in lateral view. Parameres strongly elongate, widest at base, regularly narrowing towards apex; outer margins slightly curved to ventral side apically in lateral view. Spiculum gastrale as in Fig. 15K. Posterior margin of abdominal sternite VIII sinuate (Fig. 15O).

Female (Figs 16A, B, 17D–F). Body larger and wider than male, length 14.1–15.0 mm, width 7.0–7.7 mm. Antennae shorter than in male, reaching base of pronotum when posteriorly extended. Pronotum 1.56 times as wide as long, widest in middle, lateral margins subparallel from base to middle and arcuately narrowing toward anterior angles, sides of pronotum slightly convex; 1.83 times as wide as head, with very dense punctation. Elytra oval, more convex than in male, 1.37 times as long as wide. Protibial spurs small, pointed at apex. Distal gonocoxite (Fig. 16A) rounded apically, densely covered with setae; spiculum ventrale as in Fig. 16B.

Diagnosis. This new species is morphologically similar to *P. exsertogena*, but can be distinguished from it by the following male character states: pronotum 1.50 times as wide as long (pronotum 1.28 times as wide as long in *P. exsertogena*); surface of elytra with fine punctures and without regular wrinkles (surface of elytra with fine punctures and irregular wrinkles in *P. exsertogena*).

Etymology. This species is named after Prof. Guo-Dong Ren, in recognition to his contributions in collecting specimens of *Pseudognaptorina*.

Distribution. Zadowa and Bachen Counties, Xizang, China.

Phylogenetic relationships

The preliminary phylogenetic relationships were hypothesized from 147 samples of four genera (*Agnaptoria*, 31 samples; *Asidoblaps*, 22 samples; *Pseudognaptorina*, 17 samples; *Gnaptorina*, 77 samples) (Fig. 18). The ML tree exhibited a satisfactory correlation between these major clades and the current four genera. The individuals were grouped into four well-supported clades: clade C1 (*Gnaptorina*, uBV = 98), clade C2 (*Pseudognaptorina*, uBV = 98), clade C3 (*Agnaptoria*, uBV = 99), and clade C4 (*Asidoblaps*, uBV = 100).

Geographical distribution and bionomics

Species of *Pseudognaptorina* exhibit distinctive distribution patterns within the geographical range of the genus. The genus has a wide distribution, mainly in Xizang, Sichuan, and Qinghai, China, except *P. nepalica* occurring in Nepal (Fig. 19).

All *Pseudognaptorina* species were found on the Qinghai-Xizang Plateau. Interestingly, these species have a narrow range on hillsides in subhumid environments. They were often found around the roots of underbrush and under stones or clods, and they probably feed on decaying plant roots or leaves (Fig. 20).

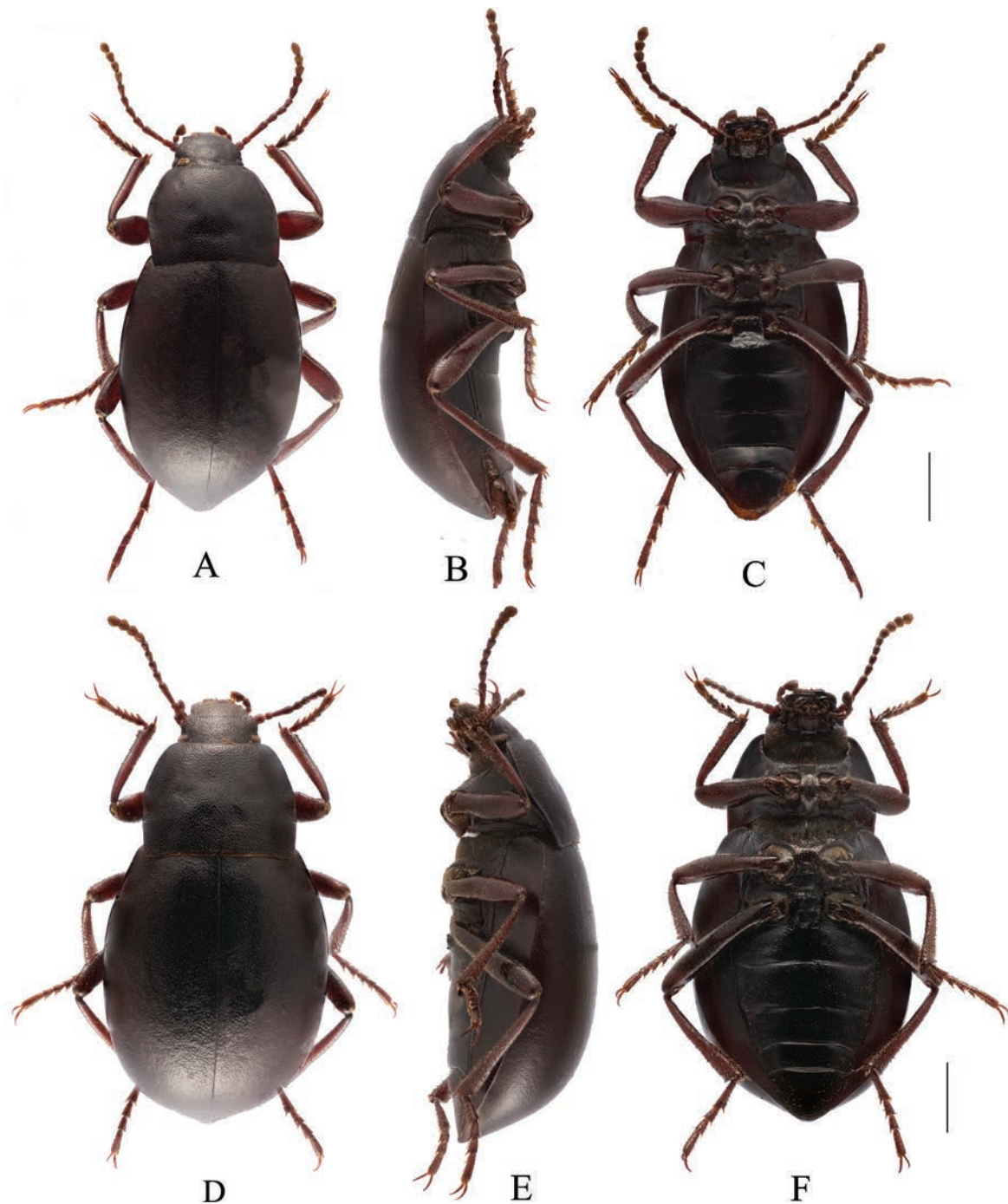
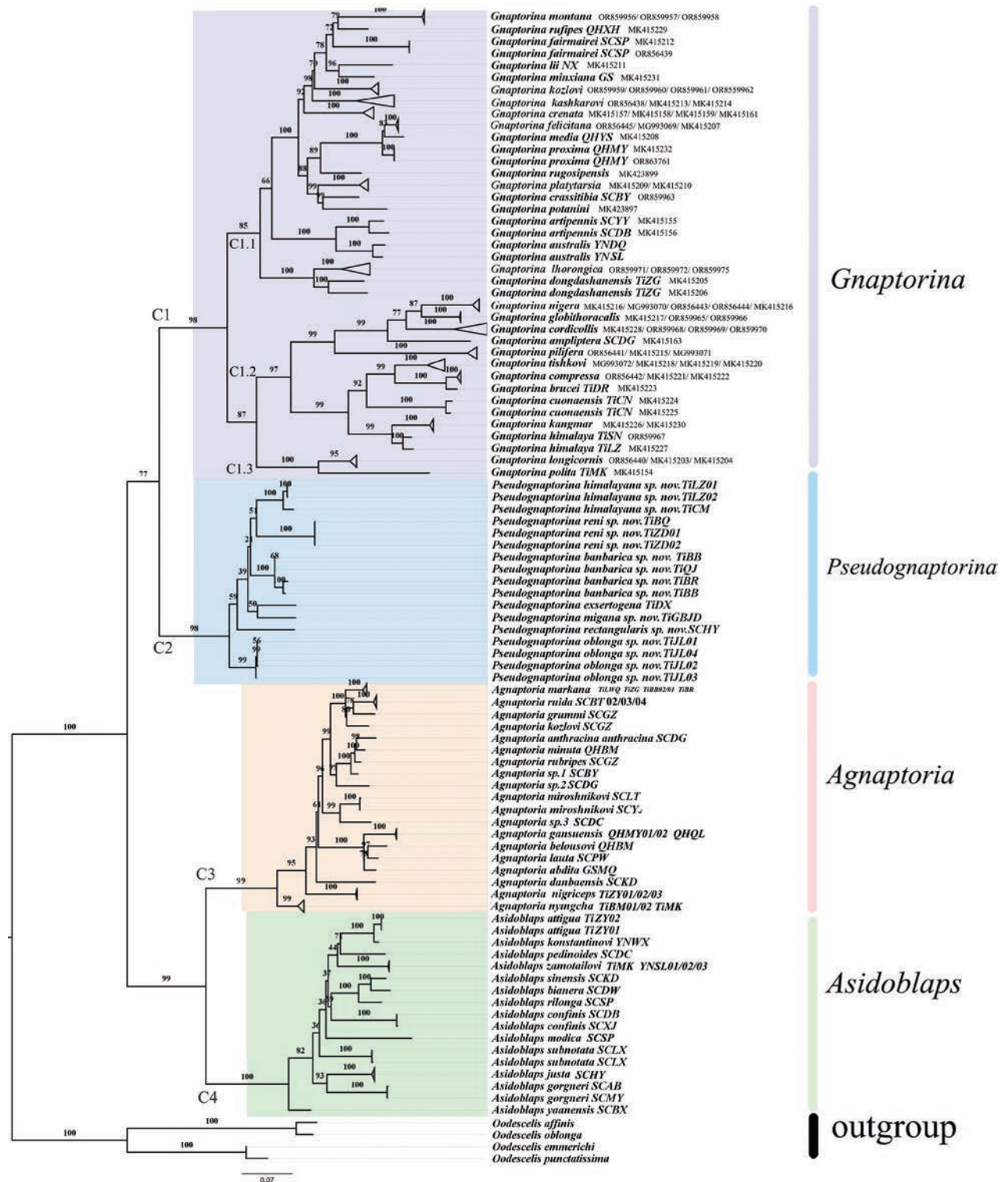


Figure 17. Habitus of *Pseudognaptorina reni* X.-M. Li, sp. nov. **A–C** male, holotype **D–F** female, paratype **A, D** dorsal views **B, E** lateral views **C, F** ventral views. Scale bar: 2.0 mm.

Discussion

Gnaptorinina is a species-rich subtribe of Blaptini consisting of 189 species in 12 genera. These species are primarily distributed in deserts, semi-deserts, grasslands, meadows, woodlands, and high-elevation environments across the Qinghai-Xizang Plateau. We constructed the phylogenetic relationships of four genera within the subtribe Gnaptorinina based on COI gene sequences. Our analyses provide the first phylogenetic tree for the genus *Pseudognaptorina*, which is confirmed to be monophyletic. The distribution



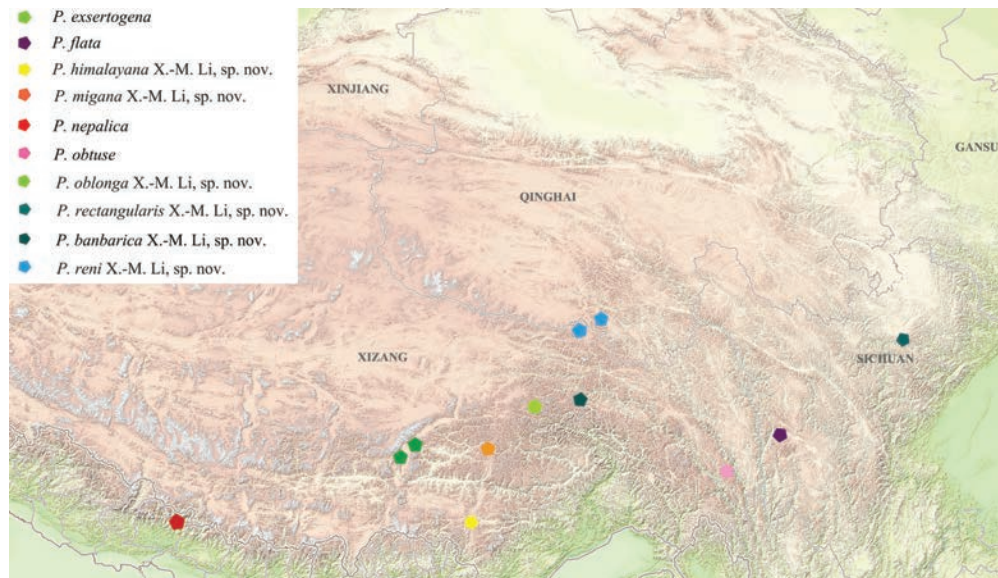


Figure 19. Geographical distribution of ten *Pseudognaptorina* species in this study.



Figure 20. Habitat for *P. migana* X.-M. Li, sp. nov. Photographed by Xiu-Min Li, at Miga Mountain pass, Gongbogyamda County, Xizang, China, on June 26, 2019 and July 18, 2023.

2021), whereas *Pseudognaptorina* primarily inhabits more humid valley environments traversed by the Yarlung Tsangpo, Lancang, and Nujiang rivers. We hypothesize that these species dispersed along river systems and formed their current geographical distribution patterns during the uplift of the Qinghai-Xizang Plateau. What is the relationship between species dispersal and the uplift of the Qinghai-Xizang Plateau? We will provide a comprehensive analysis and discussion of this issue in a forthcoming paper based on genomic data.

Acknowledgements

We are very grateful to the editor and anonymous reviewers for their constructive comments on the manuscript.

Additional information

Conflict of interest

The authors have declared that no competing interests exist.

Ethical statement

No ethical statement was reported.

Funding


This work was supported by the Natural Science Foundation of Hebei (C2024201003), the National Natural Science Foundation of China (32170477), and the Survey of Wildlife Resources in Key Areas of Tibet (ZL202203601).

Author contributions

Conceptualization: B-Y Z, X-M L and Z P. Data curation: X-M L, J-G L. Formal analysis: X-M L, J-G L. Writing-original draft: X-M L, Z P. Visualization: X-M L, Z P. Funding acquisition: X-M L. Writing-review and editing: B-Y Z, Z P and X-M L.

Author ORCIDs

Xiu-Min Li  <https://orcid.org/0000-0003-0575-1869>

Bao-Yue Zhang  <https://orcid.org/0009-0008-9251-4792>

Ji-Gang Li  <https://orcid.org/0000-0001-8662-0734>

Zhao Pan  <https://orcid.org/0000-0001-7798-0009>

Data availability

All data that support the findings of this study are available in the Supplementary file.

References

- Bai XL, Li XM, Ren GD (2020) Description of a new subgenus and four new species of *Gnaptorina* Reitter, 1887 (Coleoptera: Tenebrionidae: Blaptini) from China. *Zootaxa* 4809(1): 165–176. <https://doi.org/10.11646/zootaxa.4809.1.10>
- Bai XL, Liu JZ, Ren GD (2023) Revision of the genus *Colasia* Koch, 1965 (= *Belousovia* Medvedev, 2007, syn. nov.) (Coleoptera, Tenebrionidae, Blaptini). *ZooKeys* 1161: 143–167. <https://doi.org/10.3897/zookeys.1161.97440>

- Chigray IA (2019) A new genus and species of darkling beetles of the tribe Blaptini (Coleoptera: Tenebrionidae) from Afghanistan and taxonomic changes in the tribe. *Entomological Review* 99: 914–923. <https://doi.org/10.1134/S0013873819070054>
- Folmer O, Black M, Hoeh W, Lutz R, Vrijenhoek R (1994) DNA primers for amplification of mitochondrial cytochrome c oxidase subunit I from diverse metazoan invertebrates. *Molecular Marine Biology and Biotechnology* 3: 294–299.
- Ji BY, Ma XT, Rong JD, Ren GD, Pan Z, Li XM (2024) The adult, pupa, and larva of a new species of *Gnaptorina* Reitter, 1887 (Coleoptera, Tenebrionidae, Blaptini) from the Tibetan Plateau, with molecular phylogenetic inferences. *ZooKeys* 1190: 91–106. <https://doi.org/10.3897/zookeys.1190.113126>
- Kamiński MJ, Lumen R, Kanda K, Iwan D, Johnston MA, Kergoat GJ, Bouchard P, Bai XL, Li XM, Ren GD, Smith AD (2021) Reevaluation of Blapimorpha and Opatrinae: addressing a major phylogeny-classification gap in darkling beetles (Coleoptera: Tenebrionidae: Blaptinae). *Systematic Entomology* 46: 140–156. <https://doi.org/10.1111/syen.12453>
- Kaszab Z (1977) Tenebrionidae der Nepal-Expeditionen von Dr. J. Martens (1969–1974) *Senckenbergiana Biologica* 57: 241–283.
- Li XM, Bai XL, Ren GD (2018) A new species of the genus *Blaptogonia* from the Himalayas with four DNA markers (Coleoptera, Tenebrionidae, Blaptini). *ZooKeys* 773: 69–78. <https://doi.org/10.3897/zookeys.773.24656>
- Li XM, Bai XL, Ren GD (2019) Two new species of the genus *Gnaptorina* Reitter from the Hengduan Mountains, China (Coleoptera: Tenebrionidae: Blaptini). *Zootaxa* 4695(1): 83–89. <https://doi.org/10.11646/zootaxa.4695.1.7>
- Li XM, Bai XL, Kergoat GJ, Pan Z, Ren GD (2021) Phylogenetics, historical biogeography and molecular species delimitation of *Gnaptorina* Reitter (Coleoptera: Tenebrionidae: Blaptini). *Systematic Entomology* 46(1): 239–251. <https://doi.org/10.1111/syen.12459>
- Liu HY, Ren GD (2009) Review of the genus *Pseudognaptorina* Kaszab from China (Coleoptera, Tenebrionidae). *Zootaxa* 2174: 45–50. <https://doi.org/10.11646/zootaxa.2174.1.5>
- Medvedev GS (2004) New species of the darkling-beetle tribe Blaptini (Coleoptera, Tenebrionidae) from India, Nepal and China. *Entomologicheskoe Obozrenie* 83: 163–189. [In Russian, English translation: *Entomological Review* 84: 78–99].
- Medvedev GS (2009) Composition of the genera *Gnaptorina* Reitter and *Pseudognaptorina* Kaszab of the tribe Blaptini (Coleoptera, Tenebrionidae). *Entomologicheskoe Obozrenie* 88: 416–429. [In Russian, English translation: *Entomological Review* 89: 451–461]. <https://doi.org/10.1134/S0013873809040095>
- Medvedev GS, Merkl O (2002) *Viettagona vietnamensis* gen. et sp. n. from Vietnam (Coleoptera, Tenebrionidae: Blaptini). *Acta Zoologica Academiae Scientiarum Hungaricae* 48(4): 317–332.
- Minh BQ, Nguyen MAT, von Haeseler A (2013) Ultrafast approximation for phylogenetic bootstrap. *Molecular Biology and Evolution* 30(5): 1188–1195. <https://doi.org/10.1093/molbev/mst024>
- Nabozhenko M, Chigray IA (2020) Tribe Blaptini Leach, 1815: 268–296. In: Iwan D, Löbl I (Eds) *Catalogue of Palaearctic Coleoptera* (Vol. 5). Tenebrionoidea. Revised and Up dated Second Edition. Koninklijke Brill NV, Leiden/Boston, 945 pp. https://doi.org/10.1163/9789004434998_004
- Nguyen LT, Schmidt HA, Von Haeseler A, Minh BQ (2015) IQ-TREE: a fast and effective stochastic algorithm for estimating maximum-likelihood phylogenies. *Molecular Biology and Evolution* 32(1): 268–274. <https://doi.org/10.1093/molbev/msu300>

- Ren GD, Ba YB, Liu HY, Niu YP, Zhu XC, Li Z, Shi AM (2016) Coleoptera: Tenebrionidae (I); Fauna Sinica: Insecta, Volume 63. Science Press, Beijing, 532 pp.
- Shi AM, Ren GD, Merkl O (2005) Two new species of *pseudognaptorina* Kaszab (Coleoptera, Tenebrionidae: Blaptini) from the Tibet plateau. Acta Zoologica Academiae Scientiarum Hungaricae 51(3): 163–170.
- Zhang D, Gao FL, Jakovlić I, Zou H, Zhang J, Li WX, Wang GT (2020) PhyloSuite: an integrated and scalable desktop platform for streamlined molecular sequence data management and evolutionary phylogenetics studies. Molecular Ecology Resources 20(1): 348–355. <https://doi.org/10.1111/1755-0998.13096>

Supplementary material 1

List of specimens

Author: Xiu-Min Li






Data type: doc

Explanation note: List of specimens used in this study with the corresponding accession number.

Copyright notice: This dataset is made available under the Open Database License (<http://opendatacommons.org/licenses/odbl/1.0/>). The Open Database License (ODbL) is a license agreement intended to allow users to freely share, modify, and use this Dataset while maintaining this same freedom for others, provided that the original source and author(s) are credited.

Link: <https://doi.org/10.3897/zookeys.1234.137739.suppl1>

Complete mitogenome of the critically endangered Asian king vulture (*Sarcogyps calvus*) (Aves, Accipitriformes, Accipitridae): evolutionary insights and comparative analysis

Wannapol Buthasane¹, Sithichoke Tangphatsornruang², Piroon Jenjaroenpun³,
Thidathip Wongsurawat³, Saowaphang Sanannu⁴, Vorasuk Shotelersuk^{5,6}, Gunnaporn Suriyaphol¹

¹ Biochemistry Unit, Department of Physiology, Faculty of Veterinary Science, Chulalongkorn University, Bangkok 10330, Thailand

² National Omics Center, National Center for Genetic Engineering and Biotechnology (BIOTEC), National Science and Technology Development Agency, Pathum Thani 12120, Thailand

³ Division of Medical Bioinformatics, Research Department, Faculty of Medicine Siriraj Hospital, Mahidol University, Bangkok 10700, Thailand

⁴ Animal Conservation and Research Institute, The Zoological Park Organization of Thailand, Bangkok 10300, Thailand

⁵ Center of Excellence for Medical Genomics, Medical Genomics Cluster, Department of Pediatrics, Faculty of Medicine, Chulalongkorn University, Bangkok 10330, Thailand

⁶ Excellence Center for Genomics and Precision Medicine, King Chulalongkorn Memorial Hospital, The Thai Red Cross Society, Bangkok 10330, Thailand

Corresponding author: Gunnaporn Suriyaphol (Gunnaporn.V@chula.ac.th)



Academic editor: George Sangster

Received: 12 October 2024

Accepted: 14 February 2025

Published: 8 April 2025

ZooBank: <https://zoobank.org/4753D591-718F-431B-9757-D7374401A2D8>

Citation: Buthasane W, Tangphatsornruang S, Jenjaroenpun P, Wongsurawat T, Sanannu S, Shotelersuk V, Suriyaphol G (2025) Complete mitogenome of the critically endangered Asian king vulture (*Sarcogyps calvus*) (Aves, Accipitriformes, Accipitridae): evolutionary insights and comparative analysis. ZooKeys 1234: 47–65. <https://doi.org/10.3897/zookeys.1234.138722>

Abstract

The Asian king vulture (*Sarcogyps calvus*), also known as the red-headed vulture, is an Old World vulture (Gypini) facing severe population declines. This study aimed to assemble the complete mitogenome of *S. calvus*, explore its phylogenetic relationships, estimate divergence times, and examine genetic distances and amino acid substitutions. The mitogenome was de novo assembled from genomic DNA extracted from the blood of a female *S. calvus*. Phylogenetic and pairwise genetic distance analyses were conducted, comparing *S. calvus* with other members of Gypini, New World vultures (Cathartidae) and various other birds. The assembled mitogenome was 17,750 base pairs in length, comprising 13 protein-coding genes (PCGs), 22 transfer RNA genes, two ribosomal RNA genes and two control regions. Most PCGs used the ATG start codon, except for cytochrome c oxidase subunit 1 (*COX1*), which employed GTG. Phylogenetic analysis revealed a close genetic relationship between *S. calvus* and other members of Gypini, with an estimated divergence time of 16.7 million years ago. Genetic distance analysis indicated that *S. calvus* was more closely related to other Gypini, as well as to *Spilornis cheela* and *Circaetus pectoralis* (Circaetini), than to Cathartidae. Conserved amino acid substitutions between Gypini and Cathartidae were primarily observed in the NADH-ubiquinone oxidoreductase chain 1 (*ND1*) gene. This study provided the first complete mitogenome of *S. calvus*, offering new insights into its genomic structure, evolutionary history, and genetic relationships.

Key words: Asian king vulture, comparative analysis, evolution, mitogenome, *Sarcogyps calvus*

Introduction

The Asian king vulture (*Sarcogyps calvus* Scopoli, 1786), also known as the red-headed vulture, belongs to the Old World vulture group (tribe Gypini) within the order Accipitriformes and the family Accipitridae. Classified as Critically Endangered by the International Union for Conservation of Nature (IUCN) Red List of Threatened Species, *S. calvus* is also listed under Appendix II of the Convention on International Trade in Endangered Species of Wild Fauna and Flora (CITES) (BirdLife International 2021; CITES 2024). Additionally, the species is protected under Thailand's Wild Animal Conservation and Protection Act, B.E. 2562 (2019) (FAOLEX Database 2019). Gypini are distributed across Africa, Asia, and Europe, while New World vultures (Cathartidae) inhabit the Americas. Currently, the global population of *S. calvus* in the wild is estimated to be between 2,500 and 9,999 individuals, while in Thailand, the species is possibly extinct in the wild and only seven individuals remain in captivity (BirdLife International 2021; Buthasane et al. 2024).

The mitogenome (mitochondrial genome) is a valuable tool for investigating phylogenetic relationships, molecular identification, and adaptive evolution (De Panis et al. 2021; Kong et al. 2024). Mitogenomes of four species of Gypini have been reported, i.e., those of the Eurasian griffon (*Gyps fulvus* Hablizl, 1783), cape vulture (*Gyps coprotheres* Forster, 1798), cinereous vulture (*Aegypius monachus* Linnaeus, 1766) and Himalayan griffon (*Gyps himalayensis* Hume, 1869) (Li et al. 2015; Mereu et al. 2017; Jiang et al. 2019; Adawaren et al. 2020). For Cathartidae, seven mitogenomes from six species have been documented, i.e. the Andean condor (*Vultur gryphus* Linnaeus, 1758), king vulture (*Sarcorampus papa* Linnaeus, 1758), California condor (*Gymnogyps californianus* Shaw, 1797), lesser yellow-headed vulture (*Cathartes burrovianus* Cassin, 1845), turkey vulture (*Cathartes aura* Linnaeus, 1758) and black vulture (*Coragyps atratus* Bechstein, 1793) (Slack et al. 2007; De Panis et al. 2021; Urantówka et al. 2021). In addition, 11 mitogenomes from other species in the family Accipitridae have been reported, including those of the golden eagle (*Aquila chrysaetos* Linnaeus, 1758), common buzzard (*Buteo buteo* Linnaeus, 1758) and black kite (*Milvus migrans* Boddaert, 1783) (Haring et al. 2001; Jeon et al. 2018; Mead et al. 2021). The genome of *S. calvus* has recently been published (Buthasane et al. 2024). However, no mitogenomic data are currently available for *S. calvus*, and its mitochondrial features remain understudied. This study aimed to elucidate the complete mitogenome of *S. calvus* and provide a comprehensive analysis of its structure, phylogenetic position, and the divergence time from other vultures. This research offers valuable insights into the mitochondrial profiles, evolutionary relationships, and population genetics of *S. calvus* in relation to other Gypini, Cathartidae and related species.

Materials and methods

Whole blood samples were obtained from a female *S. calvus*, approximately 25 years old, at Nakhon Ratchasima Zoo, the Zoological Park Organization of Thailand (ZPOT). Sampling was conducted in compliance with the ethical guidelines under the Chulalongkorn University Animal Care and Use Committee

(CU-ACUC), Thailand (approval number 2131005). Total DNA was extracted from the whole blood sample using the Wizard HMW DNA Extraction Kit (Promega, Madison, WI, USA). The DNA concentration was determined using a NanoDrop One Microvolume UV-Vis Spectrophotometer (Thermo Fisher Scientific, Waltham, MA, USA).

The mitochondrial genome was sequenced using the short-read MGISEQ-2000 platform (MGI Tech, Shenzhen, China) and assembled with NOVOPlasty v. 3.8.2 (Dierckxsens et al. 2017). Annotation was carried out using the MITOS WebServer (Bernt et al. 2013). Protein-coding, rRNA and tRNA genes were further identified using the NCBI Basic Local Alignment Search Tool (BLAST) (Altschul et al. 1990). The circular structure of the mitogenome was visualized with OrganellarGenomeDRAW (OGDRAW) v. 1.3.122 (Greiner et al. 2019). Analyses of nucleotide and amino acid composition were conducted using MEGA X (Kumar et al. 2018). Simple sequence repeats (SSRs) of 1–6 bp in length were identified using the Microsatellite identification tool (Beier et al. 2017).

Mitogenomes from 39 bird species, representing the orders Accipitriformes (Old World vultures, hawks, eagles, and kites), Cathartiformes (New World vultures), Falconiformes (falcons), Strigiformes (owls), Anseriformes (ducks and relatives) and Galliformes (chickens and relatives), were used for phylogeny reconstruction, comparative codon usage analyses (Table 1) and divergence time estimation. These mitogenomes, along with the newly sequenced mitogenome of *S. calvus*, were analyzed. Multiple sequence alignments of 13 conserved protein-coding genes (PCGs)—cytochrome B (*CYTB*), NADH dehydrogenase subunits 1 (*ND1*), *ND2*, *ND3*, *ND4*, *ND4L*, *ND5*, *ND6*, cytochrome c oxidase subunits 1 (*COX1*), *COX2*, *COX3*, ATP synthase F0 subunit 6 (*ATP6*) and *ATP8*—were performed using PRANK v170427. The best-fit model, mt-Ver+I+R4, was selected using ModelFinder, and maximum likelihood phylogenies were constructed using IQ-TREE v. 2.2.0.3 with 1,000 ultrafast bootstrap replications (Nguyen LT et al. 2014; Hoang et al. 2017). The phylogenetic tree was visualized with Figtree v. 1.4.4 (Rambaut 2018). Several species of Anseriformes and Galliformes were used as outgroups. Divergence times were estimated using MCMCTree in the PAML 4.9j package, with the Hessian matrix computed via CODEML and a burn-in of 2,000 iterations. Fossil calibration times were obtained from the TimeTree database (Kumar et al. 2022). Genetic distance analyses were conducted using MEGA X and visualized using ggplot2 and ggtree in R (Wickham 2016; Yu et al. 2017; Kumar et al. 2018). The nomenclature for higher taxa follows Gregory et al. (2024).

Relative synonymous codon usage (RSCU) values for *S. calvus* mitochondrial protein-coding genes were calculated using MEGA X (Kumar et al. 2018). RSCU values reflect codon bias, with values greater than one indicating positive codon bias, values less than one indicating a negative codon bias, and values equal to one indicating random codon usage (Wong et al. 2010).

Amino acid sequences from 13 mitochondrial protein-coding genes in the mitogenomes of Gypini (*Aegypius monachus*, *Gyps coprotheres*, *Gyps fulvus*, *Gyps himalayensis*, *S. calvus*) and Cathartidae (*Cathartes aura*, *Cathartes burrovianus*, *Coragyps atratus*, *Gymnogyps californianus*, *Sarcoramphus papa*, *Vultur gryphus*) were aligned using the Unipro UGENE Multiple Alignment Editor (Okonechnikov et al. 2012).

Table 1. List of 39 avian species employed for comparative mitogenome analyses in this study, along with their corresponding GenBank accession numbers.

| Scientific name | Order | Family | Accession number | Sequence length (bp) | Reference |
|---------------------------------|-----------------|----------------|------------------|----------------------|------------------------|
| <i>Accipiter gentilis</i> | Accipitriformes | Accipitridae | NC_011818.1 | 18,266 | Unpublished |
| <i>Accipiter virgatus</i> | Accipitriformes | Accipitridae | NC_026082.1 | 17,952 | Song et al. 2015 |
| <i>Aegypius monachus</i> | Accipitriformes | Accipitridae | KF682364.1 | 17,811 | Li et al. 2015 |
| <i>Aquila chrysaetos</i> | Accipitriformes | Accipitridae | NC_024087.1 | 17,332 | Doyle et al. 2014 |
| <i>Buteo buteo</i> | Accipitriformes | Accipitridae | NC_003128.3 | 18,674 | Haring et al. 2001 |
| <i>Circetus pectoralis</i> | Accipitriformes | Accipitridae | NC_052805.1 | 17,473 | Feng et al. 2020 |
| <i>Circus melanoleucos</i> | Accipitriformes | Accipitridae | NC_035801.1 | 17,749 | Unpublished |
| <i>Gyps coprotheres</i> | Accipitriformes | Accipitridae | MF683387.1 | 16,908 | Adawaren et al. 2020 |
| <i>Gyps fulvus</i> | Accipitriformes | Accipitridae | NC_036050.1 | 18,094 | Mereu et al. 2017 |
| <i>Gyps himalayensis</i> | Accipitriformes | Accipitridae | KY594709.1 | 17,381 | Jiang et al. 2019 |
| <i>Haliaeetus albicilla</i> | Accipitriformes | Accipitridae | NC_040858.1 | 17,719 | Kim et al. 2019 |
| <i>Haliastur indus</i> | Accipitriformes | Accipitridae | NC_066800.1 | 19,055 | Sonongbua et al. 2024 |
| <i>Milvus migrans</i> | Accipitriformes | Accipitridae | NC_038195.1 | 18,016 | Jeon et al. 2018 |
| <i>Spilornis cheela</i> | Accipitriformes | Accipitridae | NC_015887.1 | 18,291 | Unpublished |
| <i>Spizaetus tyrannus</i> | Accipitriformes | Accipitridae | NC_052803.1 | 17,479 | Feng et al. 2020 |
| <i>Pandion haliaetus</i> | Accipitriformes | Pandionidae | NC_008550.1 | 19,285 | Gibb et al. 2007 |
| <i>Sagittarius serpentarius</i> | Accipitriformes | Sagittariidae | NC_023788.1 | 19,329 | Mahmood et al. 2014 |
| <i>Anser cygnoides</i> | Anseriformes | Anatidae | NC_023832.1 | 19,302 | Mu et al. 2014 |
| <i>Branta canadensis</i> | Anseriformes | Anatidae | NC_007011.1 | 16,808 | Snyder et al. 2015 |
| <i>Anseranas semipalmata</i> | Anseriformes | Anseranatidae | NC_005933.1 | 16,870 | Harrison et al. 2004 |
| <i>Cathartes aura</i> | Cathartiformes | Cathartidae | NC_007628.1 | 16,870 | Slack et al. 2007 |
| <i>Cathartes burrovianus</i> | Cathartiformes | Cathartidae | NC_063526.1 | 16,779 | Urantowska et al. 2021 |
| <i>Coragyps atratus</i> | Cathartiformes | Cathartidae | NC_063525.1 | 17,864 | Urantowska et al. 2021 |
| <i>Gymnogyps californianus</i> | Cathartiformes | Cathartidae | BK059163.1 | 16,760 | De Panis et al. 2021 |
| <i>Sarcoramphus papa</i> | Cathartiformes | Cathartidae | NC_063527.1 | 16,773 | Urantowska et al. 2021 |
| <i>Vultur gryphus</i> | Cathartiformes | Cathartidae | NC_058600.1 | 16,739 | De Panis et al. 2021 |
| <i>Caracara plancus</i> | Falconiformes | Falconidae | NC_044672.1 | 17,077 | Oswald et al. 2019 |
| <i>Falco peregrinus</i> | Falconiformes | Falconidae | NC_000878.1 | 18,068 | Mindell et al. 1997 |
| <i>Alectura lathami</i> | Galliformes | Megapodiidae | NC_007227.1 | 16,698 | Slack et al. 2007 |
| <i>Crax rubra</i> | Galliformes | Cracidae | NC_024618.1 | 16,666 | Meiklejohn et al. 2014 |
| <i>Callipepla squamata</i> | Galliformes | Odontophoridae | NC_029340.1 | 16,701 | Halley et al. 2015 |
| <i>Gallus gallus</i> | Galliformes | Phasianidae | NC_053523.1 | 16,784 | Unpublished |
| <i>Numida meleagris</i> | Galliformes | Numididae | NC_034374.1 | 16,785 | Unpublished |
| <i>Asio otus</i> | Strigiformes | Strigidae | NC_039736.1 | 17,555 | Lee et al. 2018 |
| <i>Bubo bubo</i> | Strigiformes | Strigidae | NC_038219.1 | 18,952 | Kang et al. 2018 |
| <i>Glaucidium cuculoides</i> | Strigiformes | Strigidae | NC_034296.1 | 17,392 | Unpublished |
| <i>Otus sunia</i> | Strigiformes | Strigidae | NC_041422.1 | 17,835 | Zhou et al. 2019 |
| <i>Strix uralensis</i> | Strigiformes | Strigidae | NC_038218.1 | 18,708 | Kang et al. 2018 |
| <i>Phodilus badius</i> | Strigiformes | Tytonidae | NC_023787.1 | 17,086 | Mahmood et al. 2014 |

Results

The complete mitogenome of *S. calvus* was determined to be 17,750 base pairs (bp) in length and was assigned GenBank accession number OR896160. The circular structure of the mitogenome of *S. calvus* is illustrated in Fig. 1. This mitogenome contained 13 PCGs, 22 transfer RNA genes (tRNAs), two ribosomal RNA genes and two putative control regions (CRs), also referred to as D-loop regions (Table 2). The nucleotide composition was characterized by 54.1% adenine and thymine (AT) and 45.9% guanine and cytosine (GC).

The protein-coding regions spanned 11,407 bp, accounting for 64.26% of the length of the complete mitogenome of *S. calvus*. All PCGs, except for *ND6*, were transcribed on the plus strand. The predominant start codon for most PCGs

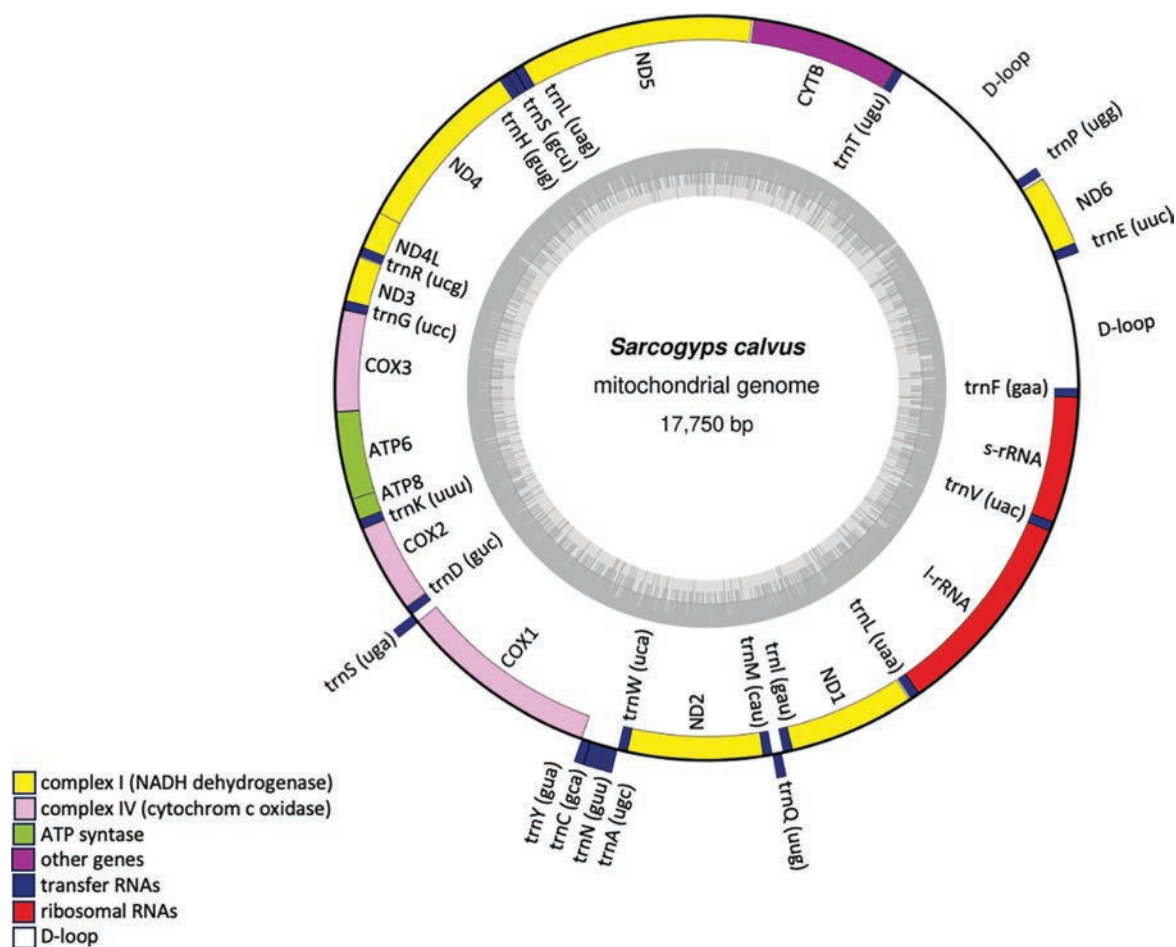


Figure 1. Circular mitogenome map of Asian king vulture. The complex I (NADH dehydrogenase), complex IV (cytochrome c oxidase), ATP synthase, ribosomal RNAs, transfer RNAs, cytochrome b and control region (D-loop) are annotated. Genes located outside the circle are transcribed in a clockwise direction, whilefig. genes inside are transcribed counterclockwise. The inner ring shadow denotes the GC content of the genome.

was ATG, except for *COX1*, which utilized GTG as the start codon (Table 2). A detailed overview of the RSCU and codon distribution in the protein-coding genes of the mitogenome of *S. calvus* is provided. The codons CUA (L), CCU (P), and CUC (L) exhibited the highest frequency of occurrence (Fig. 2). A total of 1,257 SSRs were identified in the mitogenome, comprising 314 (24.98%) mono-, 529 (42.08%) di-, 301 (23.95%) tri-, 78 (6.21%) tetra-, 24 (1.91%) penta- and 11 (0.88%) hexanucleotide repeats. The ND5 gene contained the highest number of SSRs with 135 repeats (Table 3).

The mitogenome of *S. calvus* was aligned with 39 previously published mitogenomes of bird species from the orders Accipitriformes, Cathartiformes, Falconiformes, Strigiformes, Anseriformes and Galliformes. Maximum likelihood phylogenies are illustrated in Fig. 3. The mitogenome of *S. calvus* was part of a clade formed by the tribe Gypini (*Gyps fulvus*, *Gyps coprotheres*, *Gyps himalayensis* and *Aegypius monachus*). Gypini formed a sister group with the serpent-eagles of the tribe Circaetini (*Spilornis cheela* Latham, 1790 and *Circaetus pectoralis* Smith, 1829). Gypini and Circaetini formed the sister-group of a clade comprising the subfamilies Accipitrinae and Aquilinae. The subfamily Aquilinae included the species *Spizaetus tyrannus* Wied, 1820 and *Aquila chrysaetos*, whereas the subfamily Accipitrinae included the tribe Accipitrini

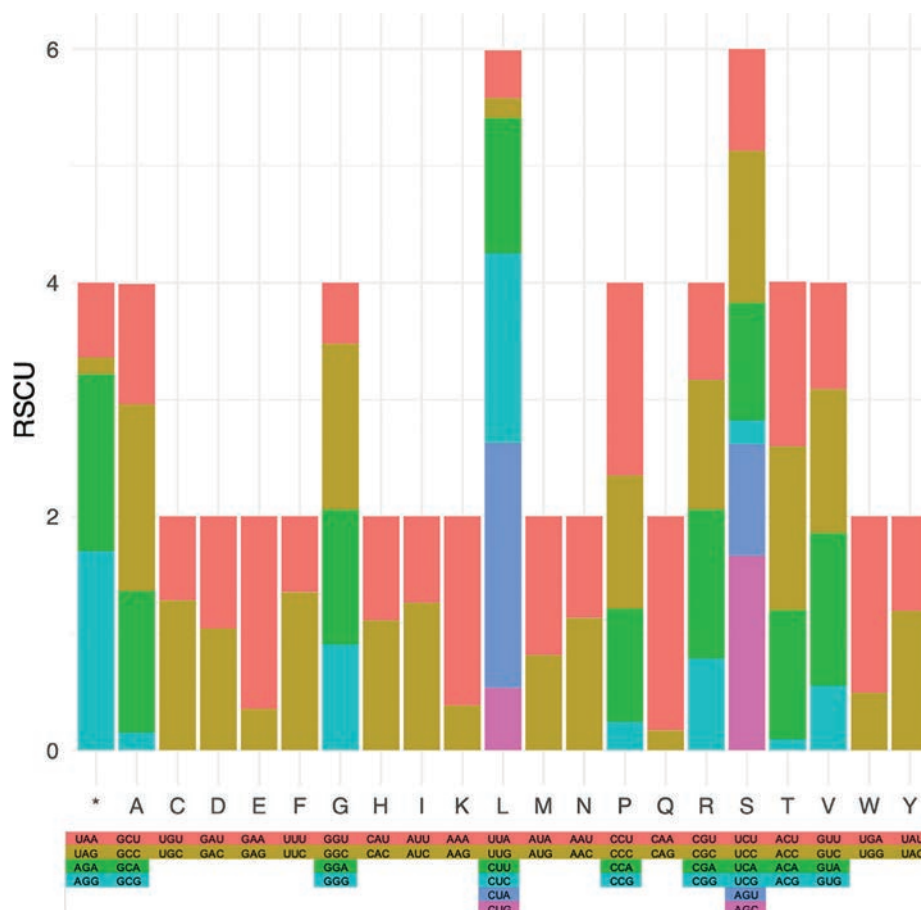


Figure 2. The relative synonymous codon usage (RSCU) and codon distribution of the Asian king vulture mitogenome. The different colors in the column chart symbolize distinct codon families associated with the amino acids listed below. Consistent coloring is applied to maintain representation uniformity across the same codon families. Bar chart showed relative synonymous codon usage in all protein-coding genes of the mitogenome of *S. calvus*.

(*Accipiter virgatus* Temminck, 1822, *Accipiter gentilis* and *Circus melanoleucos* Forster, 1795) and the tribe Buteonini (*Milvus migrans*, *Haliaeetus albicilla* and *Buteo buteo*) (Fig. 3A). The estimated evolutionary divergence time between *S. calvus* and its sister taxa, based on mitochondrial data, was approximately 22.2 million years ago (Mya) (95% highest posterior density (HPD): 2.8–43.8 Mya) (Fig. 3B). Fossil calibration constraints were applied to several groups, including Accipitriformes and Falconiformes, as well as Accipitriformes and Galliformes, among others. The estimated divergence times for these groups ranged from 6.2 to 101.5 Mya. Genetic distance analysis showed that the genetic distance between *S. calvus* and other Gypini ranged from 4.02% to 5.17%, while the distance between *S. calvus* and Cathartidae ranged from 10.90% to 12.26% (Suppl. material 1: table S1).

A total of 138 conserved amino acid substitution sites were observed between Old World vulture (Gypini) and New World vulture (Cathartidae) groups. The largest number of substitutions was found in the *ND5* gene (23 sites), whereas the smallest number occurred in *ATP6* (3 sites) (Suppl. material 1: table S2). Among these, 67 sites displayed substitutions between different amino acid chemical groups, with *ND1* showing the highest number of such substitutions (11 sites). Special case amino acid substitutions were found in *ATP8* (1 site), *COX1* (1 site), *COX2* (1 site), *CYTB* (2 sites), *ND1* (2 sites), *ND3* (2 sites),

Table 2. Characteristics of the mitogenome of *Sarcogyps calvus*.

| Start | End | Length (bp) | Direction | Type | Gene name | Gene product | Anti-codon | Start codon | Stop codon |
|-------|-------|-------------|-----------|----------------|------------------|----------------------------------|------------|-------------|------------|
| 1 | 987 | 987 | + | control region | - | - | - | - | - |
| 988 | 1058 | 71 | + | tRNA | <i>trnE(uuc)</i> | tRNA-Glu | TTC | - | - |
| 1059 | 1577 | 519 | + | CDS | <i>ND6</i> | NADH dehydrogenase subunit 6 | - | ATG | TAG |
| 1599 | 1668 | 70 | + | tRNA | <i>trnP(ugg)</i> | tRNA-Pro | TGG | - | - |
| 1669 | 2863 | 1195 | + | control region | | | | | |
| 2931 | 2864 | 68 | - | tRNA | <i>trnT(ugu)</i> | tRNA-Thr | TGT | | |
| 4076 | 2934 | 1143 | - | CDS | <i>CYTb</i> | cytochrome b | - | ATG | TAA |
| 5903 | 4089 | 1815 | - | CDS | <i>ND5</i> | NADH dehydrogenase subunit 5 | - | ATG | TAA |
| 5974 | 5904 | 71 | - | tRNA | <i>trnL(uag)</i> | tRNA-Leu | TAG | - | - |
| 6039 | 5975 | 65 | - | tRNA | <i>trnS(gcu)</i> | tRNA-Ser | GCT | - | - |
| 6110 | 6041 | 70 | - | tRNA | <i>trnH(gug)</i> | tRNA-His | GTG | - | - |
| 7488 | 6106 | 1383 | - | CDS | <i>ND4</i> | NADH dehydrogenase subunit 4 | - | ATG | AGG |
| 7778 | 7482 | 297 | - | CDS | <i>ND4L</i> | NADH dehydrogenase subunit 4L | - | ATG | TAA |
| 7848 | 7780 | 69 | - | tRNA | <i>trnR(ucg)</i> | tRNA-Arg | TCG | - | - |
| 8204 | 7854 | 354 | - | CDS | <i>ND3</i> | NADH dehydrogenase subunit 3 | - | ATG | AGG |
| 8273 | 8205 | 69 | - | tRNA | <i>trnG(ucc)</i> | tRNA-Gly | TCC | - | - |
| 9057 | 8274 | 784 | - | CDS | <i>COX3</i> | cytochrome c oxidase subunit III | - | ATG | CCT |
| 9740 | 9057 | 684 | - | CDS | <i>ATP6</i> | ATP synthase F0 subunit 6 | - | ATG | TAA |
| 9898 | 9731 | 168 | - | CDS | <i>ATP8</i> | ATP synthase F0 subunit 8 | - | ATG | TAA |
| 9970 | 9900 | 71 | - | tRNA | <i>trnK(uuu)</i> | tRNA-Lys | TTT | - | - |
| 10655 | 9972 | 684 | - | CDS | <i>COX2</i> | cytochrome c oxidase subunit II | - | ATG | TAA |
| 10726 | 10658 | 69 | - | tRNA | <i>trnD(guc)</i> | tRNA-Asp | GTC | - | - |
| 10731 | 10802 | 72 | + | tRNA | <i>trnS(uga)</i> | tRNA-Ser | TGA | - | - |
| 12344 | 10794 | 1551 | - | CDS | <i>COX1</i> | cytochrome c oxidase subunit I | - | GTG | AGG |
| 12346 | 12415 | 70 | + | tRNA | <i>trnY(gua)</i> | tRNA-Tyr | GTA | - | - |
| 12416 | 12482 | 67 | + | tRNA | <i>trnC(gca)</i> | tRNA-Cys | GCA | - | - |
| 12485 | 12557 | 73 | + | tRNA | <i>trnN(guu)</i> | tRNA-Asn | GTT | - | - |
| 12560 | 12628 | 69 | + | tRNA | <i>trnA(ugc)</i> | tRNA-Ala | TGC | - | - |
| 12702 | 12630 | 73 | - | tRNA | <i>trnW(uca)</i> | tRNA-Trp | TCA | - | - |
| 13747 | 12701 | 1047 | - | CDS | <i>ND2</i> | NADH dehydrogenase subunit 2 | - | ATG | TAG |
| 13816 | 13748 | 69 | - | tRNA | <i>trnM(cau)</i> | tRNA-Met | CAT | - | - |
| 13816 | 13886 | 71 | + | tRNA | <i>trnQ(uug)</i> | tRNA-Gln | TTG | - | - |
| 13971 | 13900 | 72 | - | tRNA | <i>trnI(gau)</i> | tRNA-Ile | GAU | - | - |
| 14947 | 13970 | 978 | - | CDS | <i>ND1</i> | NADH dehydrogenase subunit 1 | - | ATG | AGG |
| 15030 | 14957 | 74 | - | tRNA | <i>trnL(uaa)</i> | tRNA-Leu | TAA | - | - |
| 16634 | 15030 | 1605 | - | rRNA | <i>l-rRNA</i> | 16S ribosomal RNA | - | - | - |
| 16706 | 16635 | 72 | - | tRNA | <i>trnV(uac)</i> | tRNA-Val | TAC | - | - |
| 17681 | 16706 | 976 | - | rRNA | <i>s-rRNA</i> | 12S ribosomal RNA | - | - | - |
| 17750 | 17681 | 70 | - | tRNA | <i>trnF(gaa)</i> | tRNA-Phe | GAA | - | - |

Table 3. Number of short sequence repeats in mitochondrial genome of *Sarcogyps calvus*. Abbreviations: MRS, monomeric repeated sequences; DRS, dinomeric repeated sequences; TriRS, trimeric repeated sequences; TetRS, tetrameric repeated sequences.

| Region | MRS | DRS | TriRS | TetRS | Microsatellite sequences | Total |
|-----------------------|-----|-----|-------|-------|--------------------------|-------|
| (unidentified region) | 7 | 0 | 4 | 0 | 2 | 13 |
| ATP6 | 7 | 18 | 14 | 3 | 3 | 45 |
| ATP8 | 4 | 4 | 5 | 1 | 0 | 14 |
| COX1 | 11 | 56 | 28 | 7 | 2 | 104 |
| COX2 | 7 | 15 | 14 | 4 | 1 | 41 |
| COX3 | 10 | 27 | 16 | 2 | 1 | 56 |
| CR1 | 22 | 46 | 15 | 3 | 2 | 88 |
| CR2 | 24 | 44 | 16 | 2 | 4 | 90 |
| CYTB | 18 | 37 | 16 | 6 | 3 | 80 |
| <i>I</i> -rRNA | 43 | 49 | 18 | 5 | 0 | 115 |
| ND1 | 17 | 38 | 15 | 2 | 3 | 75 |
| ND2 | 18 | 28 | 20 | 4 | 5 | 75 |
| ND3 | 3 | 9 | 3 | 2 | 0 | 17 |
| ND4 | 27 | 41 | 34 | 2 | 1 | 105 |
| ND4L | 1 | 10 | 3 | 2 | 0 | 16 |
| ND5 | 32 | 53 | 41 | 7 | 2 | 135 |
| ND6 | 14 | 10 | 12 | 5 | 5 | 46 |
| <i>s</i> -rRNA | 20 | 22 | 10 | 3 | 1 | 56 |
| <i>trn</i> A | 1 | 1 | 0 | 1 | 0 | 3 |
| <i>trn</i> C | 0 | 3 | 0 | 0 | 0 | 3 |
| <i>trn</i> D | 1 | 1 | 0 | 0 | 0 | 2 |
| <i>trn</i> E(uuc) | 2 | 1 | 1 | 0 | 0 | 4 |
| <i>trn</i> G | 2 | 5 | 2 | 0 | 0 | 9 |
| <i>trn</i> H(gug) | 1 | 1 | 0 | 2 | 0 | 4 |
| <i>trn</i> I | 0 | 4 | 0 | 0 | 0 | 4 |
| <i>trn</i> K | 1 | 2 | 4 | 0 | 0 | 7 |
| <i>trn</i> L | 1 | 3 | 0 | 0 | 0 | 4 |
| <i>trn</i> L(uag) | 1 | 0 | 0 | 0 | 0 | 1 |
| <i>trn</i> M | 2 | 0 | 2 | 0 | 0 | 4 |
| <i>trn</i> N | 1 | 0 | 0 | 1 | 0 | 2 |
| <i>trn</i> P(ugg) | 2 | 2 | 0 | 0 | 0 | 4 |
| <i>trn</i> Q | 2 | 3 | 2 | 0 | 0 | 7 |
| <i>trn</i> R | 0 | 1 | 0 | 1 | 0 | 2 |
| <i>trn</i> S | 0 | 1 | 1 | 2 | 0 | 4 |
| <i>trn</i> S(gcu) | 2 | 1 | 0 | 0 | 0 | 3 |
| <i>trn</i> T(ugu) | 2 | 4 | 0 | 0 | 0 | 6 |
| <i>trn</i> V | 0 | 1 | 3 | 2 | 0 | 6 |
| <i>trn</i> W | 1 | 2 | 0 | 0 | 0 | 3 |
| <i>trn</i> Y | 4 | 0 | 0 | 0 | 0 | 4 |
| Total | 311 | 543 | 299 | 69 | 35 | 1257 |

ND4 (1 site), ND4L (1 site) and ND6 (5 sites). Among these, Pro was the most frequently substituted amino acid, with 7 substitutions across ATP8, CYTB, ND1, ND3 and ND6, followed by Cys (5 sites) and Gly (4 sites) (Table 4). In the Old World vulture clade, 43 amino acid substitution sites were identified between *S. calvus* and other Gypini. The largest number of substitutions was found in CYTB (9 sites), while the smallest number occurred in COX1, COX2 and ND4L (1 site each) (Table 5). Unique amino acid chemical groups were found at 15 sites in *S. calvus*, with the largest number located in ND5 (5 sites). Pro was the most frequently substituted amino acid in this group (3 sites in ATP8, CYTB and ND4), with Gly ranking second (1 site in ND5) (Table 5).

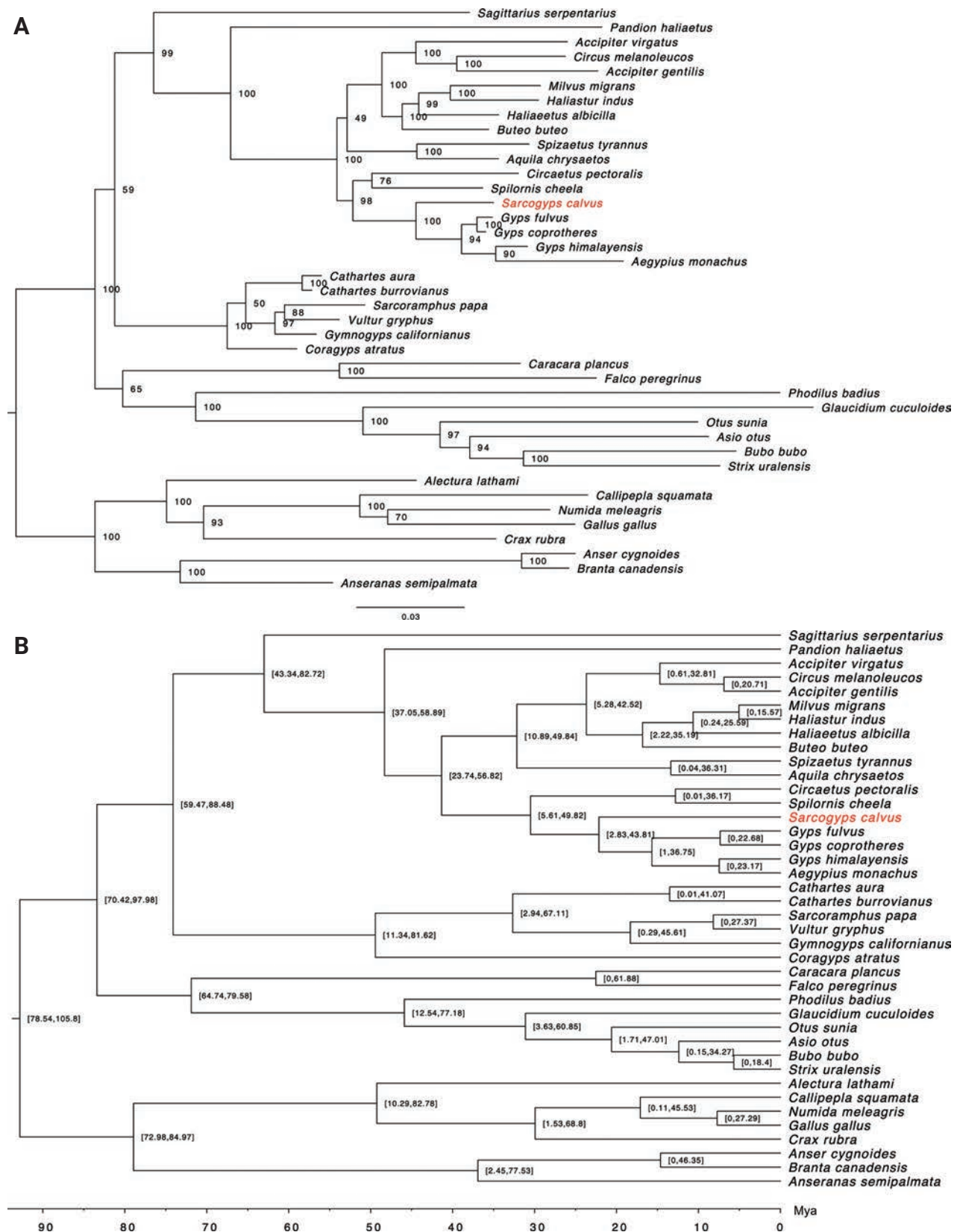


Table 4. Amino acid substitution with different side chain property between Old World vultures (OWVs) and New World vultures (NWVs).

| Gene | Position | OWV | NWV | Side chain property | |
|------|----------|-----|-----|---------------------|-----------------|
| | | | | OWV | NWV |
| ATP8 | 7 | A | N | Hydrophobic | Polar uncharged |
| | 30 | P | S | Special case | Polar uncharged |
| COX1 | 1 | G | A | Special case | Hydrophobic |
| | 3 | S | F | Polar uncharged | Hydrophobic |
| COX2 | 4 | H | N | Positive | Polar uncharged |
| | 43 | A | T | Hydrophobic | Polar uncharged |
| | 90 | N | D | Polar uncharged | Negative |
| | 156 | N | G | Polar uncharged | Special case |
| | 161 | A | S | Hydrophobic | Polar uncharged |
| | 166 | A | T | Hydrophobic | Polar uncharged |
| COX3 | 152 | M | T | Hydrophobic | Polar uncharged |
| | 224 | N | K | Polar uncharged | Positive |
| CYTB | 5 | P | I | Special case | Hydrophobic |
| | 376 | M | T | Hydrophobic | Polar uncharged |
| | 378 | C | Y | Special case | Hydrophobic |
| | 381 | T | K | Polar uncharged | Positive |
| ND1 | 9 | H | Y | Positive | Hydrophobic |
| | 79 | T | I | Polar uncharged | Hydrophobic |
| | 81 | M | T | Hydrophobic | Polar uncharged |
| | 160 | V | T | Hydrophobic | Polar uncharged |
| | 171 | A | T | Hydrophobic | Polar uncharged |
| | 173 | T | A | Polar uncharged | Hydrophobic |
| | 189 | T | A | Polar uncharged | Hydrophobic |
| | 260 | Q | E | Polar uncharged | Negative |
| | 263 | T | P | Polar uncharged | Special case |
| | 312 | I | T | Hydrophobic | Polar uncharged |
| | 323 | C | Y | Special case | Hydrophobic |
| ND2 | 5 | T | A | Polar uncharged | Hydrophobic |
| | 56 | T | A | Polar uncharged | Hydrophobic |
| | 65 | T | A | Polar uncharged | Hydrophobic |
| | 140 | V | T | Hydrophobic | Polar uncharged |
| | 185 | A | S | Hydrophobic | Polar uncharged |
| | 229 | T | M | Polar uncharged | Hydrophobic |
| | 299 | H | Y | Positive | Hydrophobic |
| ND3 | 7 | T | M | Polar uncharged | Hydrophobic |
| | 19 | I | T | Hydrophobic | Polar uncharged |
| | 64 | L | P | Hydrophobic | Special case |
| | 77 | T | P | Polar uncharged | Special case |
| ND4 | 8 | T | M | Polar uncharged | Hydrophobic |
| | 40 | H | Q | Positive | Polar uncharged |
| | 57 | C | G | Special case | Special case |
| | 63 | S | A | Polar uncharged | Hydrophobic |
| | 112 | A | T | Hydrophobic | Polar uncharged |
| | 170 | H | Q | Positive | Polar uncharged |

| Gene | Position | OWV | NWV | Side chain property | |
|------|----------|-----|-----|---------------------|-----------------|
| | | | | OWV | NWV |
| | 171 | I | T | Hydrophobic | Polar uncharged |
| | 195 | L | S | Hydrophobic | Polar uncharged |
| | 201 | M | T | Hydrophobic | Polar uncharged |
| ND4L | 11 | S | A | Polar uncharged | Hydrophobic |
| | 16 | C | S | Special case | Polar uncharged |
| | 43 | T | A | Polar uncharged | Hydrophobic |
| ND5 | 16 | A | T | Hydrophobic | Polar uncharged |
| | 61 | S | M | Polar uncharged | Hydrophobic |
| | 71 | I | T | Hydrophobic | Polar uncharged |
| | 332 | T | M | Polar uncharged | Hydrophobic |
| | 350 | A | N | Hydrophobic | Polar uncharged |
| | 382 | M | T | Hydrophobic | Polar uncharged |
| | 407 | A | T | Hydrophobic | Polar uncharged |
| | 438 | M | T | Hydrophobic | Polar uncharged |
| | 597 | T | I | Polar uncharged | Hydrophobic |
| ND6 | 36 | G | A | Special case | Hydrophobic |
| | 50 | P | S | Special case | Polar uncharged |
| | 53 | A | S | Hydrophobic | Polar uncharged |
| | 73 | C | S | Special case | Polar uncharged |
| | 78 | L | P | Hydrophobic | Special case |
| | 107 | E | G | Negative | Special case |
| | 126 | V | S | Hydrophobic | Polar uncharged |
| | 140 | W | R | Hydrophobic | Positive |

Discussion

The present study has, for the first time, characterized the complete mitogenome of *S. calvus* and compared it with 39 other avian mitogenomes. The mitogenome of *S. calvus* included 13 PCGs, 22 tRNA genes, two rRNA genes and two putative CR regions, consistent with the mitogenomes of the *Gyps himalayensis* and *Aepygius cinereus* (Li et al. 2015; Jiang et al. 2019). The total length of the PCG region of *S. calvus* was 11,407 base pairs (bp), which fell within the range observed in other members of Accipitriformes (11,377–11,920 bp). We observed that mitogenomes are subject to weaker translational selection compared to nuclear genomes (dos Reis et al. 2004). Regarding the GTG initiation codon of *COX1*, a previous study has reported the utilization of GTG as a start codon in the ribosomal protein L16 (rpl16) gene in some plant mitochondria (Bock et al. 1994). Additionally, RNA editing could also be a factor, as it has been observed in chicken mitochondria (Yokobori and Pääbo 1997). In the context of RSCU values, we identified AGG and AGA as the preferred stop codons in the mitogenome of *S. calvus*, with the RSCU values of 1.7 and 1.52, respectively. AGG has been identified as a stop codon for the NADH dehydrogenase 1 (*ND1*) and cytochrome c oxidase subunit 1 (*COX1*) mitochondrial genes in the cinereous vulture and Himalayan griffon (Li et al. 2015; Jiang et al. 2019). Similarly, AGA has been shown to function as a stop codon for the NADH dehydrogenase subunit 3 (*NADH3*) and NADH dehydrogenase subunit 5 (*NADH5*) mitochondrial genes in the ostrich (Härlid et al. 1997). In contrast, UAA and

Table 5. Amino acid substitution with different side chain property between Old World vultures (OWVs) and New World vultures (NWVs).

| Gene | Position | OWV | NWV | Side chain property | |
|------|----------|-----|-----|---------------------|-----------------|
| | | | | OWV | NWV |
| ATP6 | 31 | F | I | Hydrophobic | Hydrophobic |
| | 83 | I | I | Hydrophobic | Hydrophobic |
| | 139 | I | I | Hydrophobic | Hydrophobic |
| ATP8 | 24 | I | I | Hydrophobic | Hydrophobic |
| | 50 | S | P | Polar uncharged | Special case |
| COX1 | 468 | M | M | Hydrophobic | Hydrophobic |
| COX2 | 70 | I | I | Hydrophobic | Hydrophobic |
| CYTB | 15 | I | I | Hydrophobic | Hydrophobic |
| | 26 | P | S | Special case | Polar uncharged |
| | 47 | L | L | Hydrophobic | Hydrophobic |
| | 213 | I | V | Hydrophobic | Hydrophobic |
| | 220 | P | P | Special case | Special case |
| | 307 | F | F | Hydrophobic | Hydrophobic |
| | 310 | K | K | Positive | Positive |
| | 321 | L | L | Hydrophobic | Hydrophobic |
| | 370 | T | L | Polar uncharged | Hydrophobic |
| ND1 | 15 | S | S | Polar uncharged | Polar uncharged |
| | 179 | L | L | Hydrophobic | Hydrophobic |
| ND2 | 19 | I | I | Hydrophobic | Hydrophobic |
| | 22 | S | S | Polar uncharged | Polar uncharged |
| | 122 | S | S | Polar uncharged | Polar uncharged |
| | 325 | T | T | Polar uncharged | Polar uncharged |
| | 327 | I | T | Hydrophobic | Polar uncharged |
| | 335 | I | L | Hydrophobic | Hydrophobic |
| ND3 | 1 | I | I | Hydrophobic | Hydrophobic |
| | 108 | T | N | Hydrophobic | Polar uncharged |
| ND4 | 43 | L | L | Hydrophobic | Hydrophobic |
| | 90 | A | T | Hydrophobic | Polar uncharged |
| | 183 | H | P | Positive | Special case |
| | 263 | T | T | Polar uncharged | Polar uncharged |
| | 357 | T | T | Polar uncharged | Polar uncharged |
| | 394 | I | I | Hydrophobic | Hydrophobic |
| | 418 | T | T | Polar uncharged | Polar uncharged |
| ND4L | 73 | T | T | Polar uncharged | Polar uncharged |
| ND5 | 30 | T | T | Polar uncharged | Polar uncharged |
| | 74 | M | T | Hydrophobic | Polar uncharged |
| | 291 | T | T | Polar uncharged | Polar uncharged |
| | 404 | Y | Y | Hydrophobic | Hydrophobic |
| | 434 | E | G | Negative | Special case |
| | 600 | I | I | Hydrophobic | Hydrophobic |
| ND6 | 3 | A | T | Hydrophobic | Polar uncharged |
| | 142 | A | A | Hydrophobic | Hydrophobic |
| | 166 | M | L | Hydrophobic | Hydrophobic |

UAG stop codons exhibited a negative bias, with RSCU values of 0.64 and 0.14, respectively. Additionally, we detected a negative bias against guanine at the third codon position across all 13 PCGs, consistent with findings in the cinereous vulture and Himalayan griffon (Li et al. 2015; Jiang et al. 2019).

Our results corroborate the position of *S. calvus* within the Old World vulture clade (Gypini), consistent with previous studies (Seibold and Helbig 1995; Lerner and Mindell 2005; Mindell et al. 2018; Khatri et al. 2019; Catanach et al. 2024). We estimated that *S. calvus* diverged from its sister clade (*Gyps* and *Aegypius*) approximately 22 Mya, while the divergence between Gypini and Cathartidae was estimated to have occurred around 74.1 Mya. This estimate closely aligns with previous findings (De Panis et al. 2021). Our analysis of amino acid substitutions, particularly those involving different chemical groups, suggests that these changes could potentially influence protein structure and function (Teng et al. 2010). Substitutions involving Cys, Pro, and Gly are particularly significant due to their unique roles in protein structure and stability. In this study, we observed transitions from Cys, which forms disulfide bonds critical for protein stability, to hydrophobic residues, potentially affecting protein folding and stability (Zavodszky et al. 2001; Alvares et al. 2013). Additionally, we detected changes involving Pro, known to restrict backbone flexibility, and Gly, which contributes to protein folding due to its small size, and may disrupt protein dynamics (Wilman et al. 2014; Senthil et al. 2019). We also noticed substitutions from hydrophobic to polar uncharged residues, such as Ser and Thr, across mitochondrial genes. These residues enhance hydrogen bonding and stability in aqueous environments, although transitions between similar residues (e.g., Ser to Thr) likely have minimal structural impact (Saeki et al. 2013). The observed amino acid changes may reflect functional adaptations and divergence within Gypini, with implications for mitochondrial function and the conservation of *S. calvus*. Future studies should explore these findings using structural modeling to better understand their impact.

Conclusions

Our study documents the characteristics of the complete mitogenome of *S. calvus*. Phylogenetic analysis corroborated its evolutionary relationships within Accipitriformes. *S. calvus* was most closely related to a clade formed by *Aegypius monachus* and species of *Gyps*. Additionally, we identified conserved amino acid changes between Gypini and Cathartidae, as well as unique amino acid substitutions specific to the *S. calvus*. These findings enhance our understanding of the evolutionary history and functional genomics of this critically endangered species.

Acknowledgements

We extended our sincere gratitude to the staffs at Khao Kheow Open Zoo for their assistance with sample collection. Special thanks to the staff from the National Omics Center and the National Biobank of Thailand for their valuable suggestions on data analysis. We are grateful to the reviewers for their helpful comments.

Additional information

Conflict of interest

The authors have declared that no competing interests exist.

Ethical statement

Sampling was conducted in compliance with the ethical guidelines under the Chulalongkorn University Animal Care and Use Committee (CU-ACUC), Thailand (approval number 2131005).

Funding

This work was supported by the Second Century Fund (C2F), Chulalongkorn University; the 90th Anniversary of Chulalongkorn University Scholarship (grant number GCU-GR1125652078D). The funders had no role in the design of the study, data collection, analysis, interpretation, or manuscript preparation.

Author contributions

Wannapol Buthasane: investigation; formal analysis; data curation; methodology; visualization; funding acquisition; writing – original draft. Sithichoke Tangphatsornruang: methodology; software; validation; formal analysis. Piroon Jenjaroenpun: data curation; formal analysis; investigation; methodology; software; validation. Thidathip Wongsurawat: data curation; formal analysis; investigation; methodology; software; validation. Saowaphang Sanannu: resources. Vorasuk Shotelersuk: methodology; software. Gunnaporn Suriyaphol: Conceptualization; funding acquisition; project administration; validation; supervision; writing – original draft; writing – review and editing.


Author ORCIDs

Sithichoke Tangphatsornruang  <https://orcid.org/0000-0003-2673-0012>

Piroon Jenjaroenpun  <https://orcid.org/0000-0002-1555-401X>

Thidathip Wongsurawat  <https://orcid.org/0000-0002-3659-2074>

Vorasuk Shotelersuk  <https://orcid.org/0000-0002-1856-0589>

Gunnaporn Suriyaphol  <https://orcid.org/0000-0002-8961-5970>

Data availability

All of the data that support the findings of this study are available in the main text or Supplementary Information.

References

- Adawaren EO, Du Plessis M, Suleman E, Kindler D, Oosthuizen AO, Mukandiwa L, Naidoo V (2020) The complete mitochondrial genome of *Gyps coprotheres* (Aves, Accipitridae, Accipitriformes): phylogenetic analysis of mitogenome among raptors. PeerJ 8: e10034. <https://doi.org/10.7717/peerj.10034>
- Altschul SF, Gish W, Miller W, Myers EW, Lipman DJ (1990) Basic local alignment search tool. Journal of Molecular Biology 215: 403–410. [https://doi.org/10.1016/S0022-2836\(05\)80360-2](https://doi.org/10.1016/S0022-2836(05)80360-2)
- Alvares RDA, Tulumello DV, Macdonald PM, Deber CM, Prosser RS (2013) Effects of a polar amino acid substitution on helix formation and aggregate size along the

- detergent-induced peptide folding pathway. *Biochimica et Biophysica Acta* 1828: 373–381. <https://doi.org/10.1016/j.bbamem.2012.09.024>
- Beier S, Thiel T, Münch T, Scholz U, Mascher M (2017) MISA-web: a web server for microsatellite prediction. *Bioinformatics* 33: 2583–2585. <https://doi.org/10.1093/bioinformatics/btx198>
- Bernt M, Donath A, Jühling F, Externbrink F, Florentz C, Fritzsche G, Pütz J, Middendorf M, Stadler PF (2013) MITOS: improved de novo metazoan mitochondrial genome annotation. *Molecular Phylogenetics and Evolution* 69: 313–319. <https://doi.org/10.1016/j.ympev.2012.08.023>
- BirdLife International (2021) *Sarcogyps calvus*. The IUCN Red List of Threatened Species 2021: e.T22695254A205031246. <http://datazone.birdlife.org/species/factsheet/red-headed-vulture-sarcogyps-calvus> [accessed on 30 June 2024]
- Bock H, Brennicke A, Schuster W (1994) Rps3 and rpl16 genes do not overlap in *Oenothera* mitochondria: GTG as a potential translation initiation codon in plant mitochondria? *Plant Molecular Biology* 24: 811–818. <https://doi.org/10.1007/BF00029863>
- Buthasane W, Shotelersuk V, Chetruengchai W, Srichomthong C, Assawapitaksakul A, Tangphatsornruang S, Pootakham W, Sonthirod C, Tongshima S, Wangkumhang P, Wilantho A, Thongphakdee A, Sanannu S, Poksawat C, Nipanunt T, Kasornorkbua C, Koepfli K-P, Pukazhenthi BS, Suriyaphol P, Wongsurawat T, Jenjaroenpun P, Suriyaphol G (2024) Comprehensive genome assembly reveals genetic diversity and carcass consumption insights in critically endangered Asian king vultures. *Scientific Reports* 14: 9455. <https://doi.org/10.1038/s41598-024-59990-9>
- Catanach TA, Halley MR, Pirro S (2024) Enigmas no longer: using ultraconserved elements to place several unusual hawk taxa and address the non-monophyly of the genus *Accipiter* (Accipitriformes: Accipitridae). *Biological Journal of the Linnean Society*, blae028.
- CITES (2024) The CITES Appendices I, II and III. <https://cites.org/eng/app/appendices.php> [accessed on 5 December 2024]
- FAOLEX Database (2019) Wild Animal Conservation and Protection Act, B.E. 2562 (2019). FAOLEX No. LEX-FAOC201932. <http://www.fao.org/faolex/results/details/en/c/LEX-FAOC201932> [accessed on 30 June 2024]
- De Panis D, Lambertucci SA, Wiemeyer G, Dopazo H, Almeida FC, Mazzoni CJ, Gut M, Gut I, Padró J (2021) Mitogenomic analysis of extant condor species provides insight into the molecular evolution of vultures. *Scientific Reports* 11: 17109. <https://doi.org/10.1038/s41598-021-96080-6>
- Dierckxsens N, Mardulyn P, Smits G (2017) NOVOPlasty: de novo assembly of organelle genomes from whole genome data. *Nucleic Acids Research* 45: e18.
- dos Reis M, Savva R, Wernisch L (2004) Solving the riddle of codon usage preferences: a test for translational selection. *Nucleic Acids Research* 32: 5036–5044. <https://doi.org/10.1093/nar/gkh834>
- Doyle JM, Katzner TE, Bloom PH, Ji Y, Wijayawardena BK, DeWoody JA (2014) The genome sequence of a widespread apex predator, the golden eagle (*Aquila chrysaetos*). *PLoS ONE* 9(4): e95599. <https://doi.org/10.1371/journal.pone.0095599>
- Feng S, Stiller J, Deng Y, Armstrong J, Fang Q, Reeve AH, Xie D, Chen G, Guo C, Faircloth BC, Petersen B, Wang Z, Zhou Q, Diekhans M, Chen W, Andreu-Sánchez S, Margaryan A, Howard JT, Parent C, Pacheco G, Sinding MS, Puetz L, Cavill E, Ribeiro ÂM, Eckhart L, Fjeldså J, Hosner PA, Brumfield RT, Christidis L, Bertelsen MF, Sicheritz-Ponten T, Tietze DT, Robertson BC, Song G, Borgia G, Claramunt S, Lovette IJ, Cowen SJ, Njoroge P, Dumbacher JP, Ryder OA, Fuchs J, Bunce M, Burt DW, Cracraft J, Meng G, Hackett

- SJ, Ryan PG, Jönsson KA, Jamieson IG, da Fonseca RR, Braun EL, Houde P, Mirarab S, Suh A, Hansson B, Ponnikas S, Sigeman H, Stervander M, Frandsen PB, van der Zwan H, van der Sluis R, Visser C, Balakrishnan CN, Clark AG, Fitzpatrick JW, Bowman R, Chen N, Cloutier A, Sackton TB, Edwards SV, Foote DJ, Shakya SB, Sheldon FH, Vignal A, Soares AER, Shapiro B, González-Solís J, Ferrer-Obiol J, Rozas J, Riutort M, Tigano A, Friesen V, Dalén L, Urrutia AO, Székely T, Liu Y, Campana MG, Corvelo A, Fleischer RC, Rutherford KM, Gemmell NJ, Dussex N, Mouritsen H, Thiele N, Delmore K, Liedvogel M, Franke A, Hoepfner MP, Krone O, Fudickar AM, Milá B, Ketterson ED, Fidler AE, Friis G, Parody-Merino ÁM, Battley PF, Cox MP, Lima NCB, Prosdociimi F, Parchman TL, Schlinger BA, Loiselle BA, Blake JG, Lim HC, Day LB, Fuxjager MJ, Baldwin MW, Braun MJ, Wirthlin M, Dikow RB, Ryder TB, Camenisch G, Keller LF, DaCosta JM, Hauber ME, Louder MIM, Witt CC, McGuire JA, Mudge J, Megna LC, Carling MD, Wang B, Taylor SA, Del-Rio G, Aleixo A, Vasconcelos ATR, Mello CV, Weir JT, Haussler D, Li Q, Yang H, Wang J, Lei F, Rahbek C, Gilbert MTP, Graves GR, Jarvis ED, Paten B, Zhang G (2020) Dense sampling of bird diversity increases power of comparative genomics. *Nature* 587: 252–257. <https://doi.org/10.1038/s41586-020-2873-9>
- Gibb GC, Kardailsky O, Kimball RT, Braun EL, Penny D (2007) Mitochondrial genomes and avian phylogeny: complex characters and resolvability without explosive radiations. *Molecular Biology and Evolution* 24: 269–280. <https://doi.org/10.1093/molbev/msl158>
- Gregory SMS, Sangster G, Trevor HW, Scofield RP (2024) Falling through the cracks: a family-group name for a clade of hawks and eagles (Accipitridae) including *Morphnus* Dumont, 1816, *Harpia* Vieillot, 1816, *Harpyopsis* Salvadori, 1875 and *Macheiramphus* Bonaparte, 1850. *Avian Systematics* 2: N5–N17.
- Greiner S, Lehwark P, Bock R (2019) OrganellarGenomeDRAW (OGDRAW) version 1.3.1: expanded toolkit for the graphical visualization of organellar genomes. *Nucleic Acids Research* 47: W59–W64. <https://doi.org/10.1093/nar/gkz238>
- Halley YA, Oldeschulte DL, Bhattarai EK, Hill J, Metz RP, Johnson CD, Presley SM, Ruzicka RE, Rollins D, Peterson MJ, Murphy WJ, Seabury CM (2015) Northern Bobwhite (*Colinus virginianus*) mitochondrial population genomics reveals structure, divergence, and evidence for heteroplasmy. *PLOS ONE* 10: e0144913. <https://doi.org/10.1371/journal.pone.0144913>
- Haring E, Kruckenhauser L, Gamauf A, Riesing MJ, Pinsker W (2001) The complete sequence of the mitochondrial genome of *Buteo buteo* (Aves, Accipitridae) indicates an early split in the phylogeny of raptors. *Molecular Biology and Evolution* 18: 1892–1904. <https://doi.org/10.1093/oxfordjournals.molbev.a003730>
- Härlid A, Janke A, Arnason U (1997) The mtDNA sequence of the ostrich and the divergence between paleognathous and neognathous birds. *Molecular Biology and Evolution* 14: 754–761. <https://doi.org/10.1093/oxfordjournals.molbev.a025815>
- Hoang DT, Chernomor O, von Haeseler A, Minh BQ, Vinh LS (2017) UFBoot2: Improving the Ultrafast Bootstrap Approximation. *Molecular Biology and Evolution* 35: 518–522. <https://doi.org/10.1093/molbev/msx281>
- Jeon HS, Myeong H, Kang SG, Kim JA, Lee SH, Lee MY, An J (2018) The mitochondrial genome of *Milvus migrans* (Aves, Accipitriformes, Accipitridae), an endangered species from South Korea. *Mitochondrial DNA Part B: Resources* 3: 498–499. <https://doi.org/10.1080/23802359.2018.1450678>
- Jiang L, Peng L, Tang M, You Z, Zhang M, West A, Ruan Q, Chen W, Merilä J (2019) Complete mitochondrial genome sequence of the Himalayan Griffon, *Gyps himalayensis* (Accipitriformes: Accipitridae): Sequence, structure, and phylogenetic analyses. *Ecology and Evolution* 9: 8813–8828. <https://doi.org/10.1002/ece3.5433>

- Kang H, Li B, Ma X, Xu Y (2018) Evolutionary progression of mitochondrial gene rearrangements and phylogenetic relationships in Strigidae (Strigiformes). *Gene* 674: 8–14. <https://doi.org/10.1016/j.gene.2018.06.066>
- Khatri H, Ghosh A, Jabin G, Basu S, Singh S, Chandra K, Sharma L, Thakur M (2019) Mass mortality of birds on railway track genetically identified as critically endangered Red-headed Vulture (*Sarcogyps calvus*) in Ranipur Wildlife Sanctuary, Uttar Pradesh, India. *Conservation Genetics Resources* 12: 3.
- Kim JA, Kang SG, Jeon HS, Jeon JH, Jang JH, Kim S, An J (2019) Complete mitogenomes of two Accipitridae, *Haliaeetus albicilla*, and *Pernis ptilorhynchus*. *Mitochondrial DNA Part B: Resources* 4: 391–392. <https://doi.org/10.1080/23802359.2018.1547155>
- Kong D, Gan Z, Li X (2024) Phylogenetic relationships and adaptation in deep-sea carideans revealed by mitogenomes. *Gene* 896: 148054. <https://doi.org/10.1016/j.gene.2023.148054>
- Kumar S, Stecher G, Li M, Knyaz C, Tamura K (2018) MEGA X: Molecular Evolutionary Genetics Analysis across Computing Platforms. *Molecular Biology and Evolution* 35: 1547–1549. <https://doi.org/10.1093/molbev/msy096>
- Kumar S, Suleski M, Craig JM, Kasprowicz AE, Sanderford M, Li M, Stecher G, Hedges SB (2022) TimeTree 5: An Expanded Resource for Species Divergence Times. *Molecular Biology and Evolution* 39(8): msac174. <https://doi.org/10.1093/molbev/msac174>
- Lee MY, Lee SM, Jeon HS, Lee SH, Park JY, An J (2018) Complete mitochondrial genome of the Northern Long-eared Owl (*Asio otus* Linnaeus, 1758) determined using next-generation sequencing. *Mitochondrial DNA Part B: Resources* 3: 494–495. <https://doi.org/10.1080/23802359.2018.1451260>
- Lerner HR, Mindell DP (2005) Phylogeny of eagles, Old World vultures, and other Accipitridae based on nuclear and mitochondrial DNA. *Molecular Phylogenetics and Evolution* 37: 327–346. <https://doi.org/10.1016/j.ympev.2005.04.010>
- Li B, Liu G, Zhou L, Gu C (2015) Complete mitochondrial genome of Cinereous vulture *Aegypius monachus* (Falconiformes: Accipitridae). *Mitochondrial DNA* 26: 910–911. <https://doi.org/10.3109/19401736.2013.863286>
- Mahmood MT, McLenachan PA, Gibb GC, Penny D (2014) Phylogenetic position of avian nocturnal and diurnal raptors. *Genome Biology and Evolution* 6: 326–332. <https://doi.org/10.1093/gbe/evu016>
- Mead D, Ogden R, Meredith A, Peniche G, Smith M, Corton C, Oliver K, Skelton J, Betteridge E, Doultan J, Holmes N, Wright V, Loose M, Quail MA, McCarthy SA, Howe K, Chow W, Torrance J, Collins J, Challis R, Durbin R, Blaxter M (2021) The genome sequence of the European golden eagle, *Aquila chrysaetos chrysaetos* Linnaeus 1758. *Wellcome Open Research* 6: 112. <https://doi.org/10.12688/wellcomeopenres.16631.1>
- Meiklejohn KA, Danielson MJ, Faircloth BC, Glenn TC, Braun EL, Kimball RT (2014) Incongruence among different mitochondrial regions: A case study using complete mitogenomes. *Molecular Phylogenetics and Evolution* 78: 314–323. <https://doi.org/10.1016/j.ympev.2014.06.003>
- Mereu P, Satta V, Frongia GN, Berlinguer F, Muzzeddu M, Campus A, Decandia L, Pirastru M, Manca L, Naitana S, Leoni GG (2017) The complete mtDNA sequence of the griffon vulture (*Gyps fulvus*): Phylogenetic analysis and haplotype frequency variations after restocking in the Sardinian population. *Biological Conservation* 214: 195–205. <https://doi.org/10.1016/j.biocon.2017.08.017>
- Mindell DP, Sorenson MD, Huddleston CJ, Miranda HC, Knight A, Sawchuk SJ, Yuri T (1997) Phylogenetic relationships among and within select avian orders based on

- mitochondrial DNA. In: Mindell DP (Ed.) Avian Molecular Evolution and Systematics. Academic Press, San Diego, 213–247.
- Mindell DP, Fuchs J, Johnson JA (2018) Phylogeny, taxonomy, and geographic diversity of diurnal Raptors: Falconiformes, Accipitriformes, and Cathartiformes. In: Sarasola JH, Grande JM, Negro JJ (Eds) Birds of Prey: Biology and Conservation in the XXI Century. Springer International Publishing, Cham, 3–32.
- Mu CY, Huang ZY, Chen Y, Wang B, Su YH, Li Y, Sun ZM, Xu Q, Zhao WM, Chen GH (2014) Complete sequencing and gene organization of the *Anser cygnoides* mitochondrial genome. Journal of Agricultural Biotechnology 22: 1482–1493. [In Chinese]
- Nguyen LT, Schmidt HA, von Haeseler A, Minh BQ (2014) IQ-TREE: a fast and effective stochastic algorithm for estimating maximum-likelihood phylogenies. Molecular Biology and Evolution 32: 268–274. <https://doi.org/10.1093/molbev/msu300>
- Okonechnikov K, Golosova O, Fursov M (2012) Unipro UGENE: a unified bioinformatics toolkit. Bioinformatics 28: 1166–1167. <https://doi.org/10.1093/bioinformatics/bts091>
- Oswald JA, Allen JM, Witt KE, Folk RA, Albury NA, Steadman DW, Guralnick RP (2019) Ancient DNA from a 2,500-year-old Caribbean fossil places an extinct bird (*Caracara creightoni*) in a phylogenetic context. Molecular Phylogenetics and Evolution 140: 106576. <https://doi.org/10.1016/j.ympev.2019.106576>
- Rambaut A (2018) FigTree v1.4.4. <http://tree.bio.ed.ac.uk/software/figtree/> [Accessed on May 31, 2024]
- Saeki T, Sato K, Ito S, Ikeda K, Kanamoto R (2013) Importance of uncharged polar residues and proline in the proximal two-thirds (Pro107-Ser128) of the highly conserved region of mouse ileal Na⁺-dependent bile acid transporter, Slc10a2, in transport activity and cellular expression. BMC Physiology 13: 4. <https://doi.org/10.1186/1472-6793-13-4>
- Seibold I, Helbig AJ (1995) Evolutionary history of New and Old World vultures inferred from nucleotide sequences of the mitochondrial cytochrome b gene. Philosophical Transactions of the Royal Society of London. Series B, Biological Sciences 350: 163–178. <https://doi.org/10.1098/rstb.1995.0150>
- Senthil R, Usha S, Saravanan KM (2019) Importance of fluctuating amino acid residues in folding and binding of proteins. Avicenna Journal of Medical Biotechnology 11: 339–343. <https://pmc.ncbi.nlm.nih.gov/articles/PMC6925403/>
- Slack KE, Delsuc F, McLenachan PA, Arnason U, Penny D (2007) Resolving the root of the avian mitogenomic tree by breaking up long branches. Molecular Phylogenetics and Evolution 42: 1–13. <https://doi.org/10.1016/j.ympev.2006.06.002>
- Snyder JC, Mackaness CA, Sopher MR, Huber JP, Disantis EJ, Senecal AJ, Vaughn BP, Desantis RS, Tobelmann PE, Balauff NM, Barry PM, Show MD, Speering LH, Genareo CA, Brenner FJ, Ray DB (2015) The complete mitochondrial genome sequence of the Canada goose (*Branta canadensis*). Mitochondrial DNA 26: 672–673. <https://doi.org/10.3109/19401736.2013.840601>
- Song X, Huang J, Yan C, Xu G, Zhang X, Yue B (2015) The complete mitochondrial genome of *Accipiter virgatus* and evolutionary history of the pseudo-control regions in Falconiformes. Biochemical Systematics and Ecology 58: 75–84. <https://doi.org/10.1016/j.bse.2014.10.013>
- Sonongbua J, Thong T, Panthum T, Budi T, Singchat W, Kraichak E, Chaiyes A, Muangmai N, Duengkhae P, Sitdhibutr R, Kasorndorkbua C, Srikulnath K (2024) Insights into mitochondrial rearrangements and selection in accipitrid mitogenomes, with new data on *Haliastur indus* and *Accipiter badius poliopsis*. Genes 15: 1439. <https://doi.org/10.3390/genes15111439>

- Teng S, Srivastava AK, Schwartz CE, Alexov E, Wang L (2010) Structural assessment of the effects of amino acid substitutions on protein stability and protein protein interaction. *International Journal of Computational Biology and Drug Design* 3: 334–349. <https://doi.org/10.1504/IJCBDD.2010.038396>
- Urantówka AD, Krocak A, Strzała T, Zaniewicz G, Kurkowski M, Mackiewicz P (2021) Mitogenomes of Accipitriformes and Cathartiformes were subjected to ancestral and recent duplications followed by gradual degeneration. *Genome Biology and Evolution* 13: evab193. <https://doi.org/10.1093/gbe/evab193>
- Wickham H (2016) *ggplot2: Elegant Graphics for Data Analysis*. Springer-Verlag New York. pp. ISBN 978-3-319-24277-4. <https://ggplot2.tidyverse.org>
- Wilman HR, Shi J, Deane CM (2014) Helix kinks are equally prevalent in soluble and membrane proteins. *Proteins* 82: 1960–1970. <https://doi.org/10.1002/prot.24550>
- Wong EH, Smith DK, Rabadan R, Peiris M, Poon LL (2010) Codon usage bias and the evolution of influenza A viruses. *Codon Usage Biases of Influenza Virus*. *BMC Evolutionary Biology* 10: 253. <https://doi.org/10.1186/1471-2148-10-253>
- Yokobori S-i, Pääbo S (1997) Polyadenylation creates the discriminator nucleotide of chicken mitochondrial tRNA^{Tyr}11 Edited by J. Karn. *Journal of Molecular Biology* 265: 95–99.
- Yu G, Smith DK, Zhu H, Guan Y, Lam TT-Y (2017) *ggtree: an r package for visualization and annotation of phylogenetic trees with their covariates and other associated data*. *Methods in Ecology and Evolution* 8: 28–36. <https://doi.org/10.1111/2041-210X.12628>
- Zavodszky M, Chen CW, Huang JK, Zolkiewski M, Wen L, Krishnamoorthi R (2001) Disulfide bond effects on protein stability: designed variants of *Cucurbita maxima* trypsin inhibitor-V. *Protein Science* 10: 149–160. <https://doi.org/10.1110/ps.26801>
- Zhou C, Chen Y, Hao Y, Meng Y, Yue B, Zeng, T (2019) Characterization of the complete mitochondrial genome and phylogenetic analysis of *Otus sunia* (Strigiformes: Strigidae). *Mitochondrial DNA Part B: Resources* 4: 804–805. <https://doi.org/10.1080/23802359.2019.1574643>

Supplementary material 1

Additional tables

Authors: Wannapol Buthasane, Sithichoke Tangphatsornruang, Piroon Jenjaroenpun, Thidathip Wongsurawat, Saowaphang Sanannu, Vorasuk Shotelersuk, Gunnaporn Suriyaphol







Data type: pdf

Explanation note: **table S1**. Pairwise genetic distances of *Sarcogyps calvus* and related species. Abbreviations: OWV, Old World vulture; NWV, New World vulture. **table S2**. Conserved amino acid substitution between Old World vultures (OWV) and New World vultures (NWV).

Copyright notice: This dataset is made available under the Open Database License (<http://opendatacommons.org/licenses/odbl/1.0/>). The Open Database License (ODbL) is a license agreement intended to allow users to freely share, modify, and use this Dataset while maintaining this same freedom for others, provided that the original source and author(s) are credited.

Link: <https://doi.org/10.3897/zookeys.1234.138722.suppl1>

Systematics of the braconid wasp subfamily Rhysipolinae (Hymenoptera, Braconidae) based on UCE data, with the description of a new Neotropical genus

Gerardo Y. García-Acosta¹, Rubén Castañeda-Osorio¹, Sergey A. Belokobylskij²,
Eduardo M. Shimbori^{1,3,4}, Jovana M. Jasso-Martínez¹, Angélica M. Pentead-Dias³,
Alejandro Zaldívar-Riverón¹

1 Colección Nacional de Insectos, Departamento de Zoología, Instituto de Biología, Universidad Nacional Autónoma de México, 3er circuito exterior s/n, Ciudad Universitaria, Coyoacán, Ciudad de México, Mexico

2 Zoological Institute of the Russian Academy of Sciences, Universitetskaya naberezhnaya 1, Saint Petersburg, Russia

3 Departamento de Ecologia e Biologia Evolutiva, Universidade Federal de São Carlos, São Carlos, São Paulo, Brazil

4 Centre de coopération internationale en recherche agronomique pour le développement (CIRAD), Centre de Biologie pour la Gestion de Populations (CBGP), Montpellier, F-34398, France

Corresponding author: Alejandro Zaldívar-Riverón (azaldivar@ib.unam.mx)



Academic editor: Kees van Achterberg

Received: 25 January 2025

Accepted: 27 February 2025

Published: 8 April 2025

ZooBank: <https://zoobank.org/DEBD2828-252B-4F0C-8170-F36FF28AC839>

Citation: García-Acosta GY, Castañeda-Osorio R, Belokobylskij SA, Shimbori EM, Jasso-Martínez JM, Pentead-Dias AM, Zaldívar-Riverón A (2025) Systematics of the braconid wasp subfamily Rhysipolinae (Hymenoptera, Braconidae) based on UCE data, with the description of a new Neotropical genus. ZooKeys 1234: 67–87. <https://doi.org/10.3897/zookeys.1234.147859>

Copyright: © Gerardo Y. García-Acosta et al.
This is an open access article distributed under terms of the Creative Commons Attribution License (Attribution 4.0 International – CC BY 4.0).

Abstract

Rhysipolinae is a small cosmopolitan cyclostome subfamily of braconid wasps, currently comprising 10 genera and more than 80 species. The two species of the subfamily whose biology has been confirmed are koinobiont ectoparasitoids of lepidopteran larvae, deviating from the two common parasitoid strategies in Braconidae (koinobiont-endoparasitoid, idiobiont-ectoparasitoid). Defining the limits of Rhysipolinae has been challenging due to the lack of exclusive morphological features and difficulties in resolving its phylogenetic relationships based on both morphological and Sanger DNA sequence data. However, recent phylogenomic studies using nuclear ultraconserved elements (UCEs) and mitochondrial genome sequences have begun to clarify its relationships, although various generic boundaries remain unclear. Here a phylogenomic analysis based on UCE data was performed including 32 species of nine rhysipoline genera to assess the monophyly of the subfamily as well as its generic limits. Our phylogenetic analysis confirmed the monophyly of Rhysipolinae, but no unique external morphological features were found for its diagnosis. Most genera were recovered as monophyletic except *Rhysipolis* Förster, 1863, whose clade included *Cerophanes* Tobias, 1971 and *Troporhysipolis* Quicke, Belokobylskij & Butcher, 2016. Based on our molecular and morphological evidence, we synonymise *Cerophanes* **syn. nov.** with *Rhysipolis* and describe the new genus and species *Rogapolis nomai* García-Acosta, Shimbori, Castañeda-Osorio & Zaldívar-Riverón **gen. et sp. nov.**, which is mainly characterised by a median longitudinal carina on the second metasomal tergum, a feature previously predominantly occurring in Rogadinae. Moreover, *Pseudavga* Tobias, 1964 **syn. nov.** is proposed as a subgenus of *Pachystigmus* Hellén, 1927. A taxonomic diagnosis for Rhysipolinae and a key to its currently valid genera are also provided.

Key words: Cyclostome, Ichneumonoidea, new genus, phylogeny, ultraconserved elements

Introduction

Rhysipolinae Belokobylskij, 1984 is a small cosmopolitan cyclostome subfamily of braconid wasps, currently comprising 10 genera and over 80 extant species (Yu et al. 2016; Quicke et al. 2016; Jasso-Martínez et al. 2021, 2022a). Its type genus, *Rhysipolis* Förster, 1863, is the most widespread and speciose, comprising 22 valid species distributed across the Palaearctic, Nearctic, Neotropical, Oriental, and Australasian regions (Yu et al. 2016). While the biology of most rhysipoline species remains unknown, two species with well-documented strategies, *Rh. decorator* (Haliday, 1836) and *Pseudavga flavicoxa* Tobias, 1964, are known to be koinobiont ectoparasitoids of lepidopteran larvae from the families Crambidae, Gelechiidae, Gracillariidae, Momphidae, and Bucculatricidae (Shaw 1983; Shaw and Sims 2015; Yu et al. 2016; Shaw 2017). This parasitoid strategy represents a notable deviation from the typical koinobiont-endoparasitoid and idiobiont-ectoparasitoid strategies observed in Braconidae (Shaw 1983). It has been proposed that this behaviour might constitute an evolutionary intermediate stage between ectoparasitoid idiobiosis and endoparasitoid koinobiosis (Gauld 1988). Additionally, the biology of three species from other rhysipoline genera, *Cantharoctonus* Viereck, 1912, *Pachystigmus* Hellén, 1927, and *Parachremylus* Granger, 1949 is partially known, with all being reported as ectoparasitoids of lepidopteran larvae (Belokobylskij and Tobias 1986; Whitfield and Wagner 1991; Belokobylskij and Maeto 2006).

The taxonomic definition of Rhysipolinae has historically been challenging due to the absence of exclusive morphological features and the difficulty in consistently delineating its generic limits, composition, and phylogenetic relationships among its genera based on external morphology (Whitfield and van Achterberg 1987; Whitfield 1992; Wharton 1993; Spencer and Whitfield 1999; Scatolini et al. 2002; Quicke 2015) and Sanger DNA sequence data (Sharanowski et al. 2011; Zaldívar-Riverón et al. 2006). Recent studies using genomic-scale data, including nuclear ultraconserved elements (UCEs; Jasso-Martínez et al. 2021, 2022a) and mitochondrial genome sequences (Jasso-Martínez et al. 2022b), have significantly advanced the understanding of the generic composition and phylogenetic relationships within this group. These phylogenomic analyses consistently place Rhysipolinae as sister to the Hormiinae + Rogadinae clade, incorporating the taxonomically problematic genera *Allobracon* Gahan, 1915 and *Parachremylus* Granger, 1949, which were previously classified within the subfamily Hormiinae (Hormiini) due to their unsclerotised terga (Belokobylskij 1993; Wharton 1993).

Currently, Rhysipolinae lacks exclusive external morphological features that reliably distinguish it from other braconid subfamilies, and instead it is diagnosed by a combination of plesiomorphic and partly apomorphic features (Spencer and Whitfield 1999). For instance, Rhysipolinae shares with Hormiinae, Exothecinae, and Rogadinae several features, including an occipital carina that does not join the hypostomal carina ventrally, the presence of epicnemial carina, and sometimes costate sculpture on the second metasomal tergum (Sharkey 1997; Whitfield and Wharton 1997). However, these features vary considerably among rhysipoline genera and their sister groups (van Achterberg 1995; Quicke 2015).

In this study, we employed nuclear ultraconserved element (UCE) data for nine of the ten currently recognised rhysipoline genera, representing the first phylogenetic study specifically focused on this subfamily. Using the reconstructed phylogenetic framework and external morphological features, we evaluated the validity of the examined genera and proposed corresponding taxonomic changes. Moreover, the integration of phylogenetic and morphological evidence led to the description of a new rhysipoline genus and species, *Rogapolis nomai* gen. et sp. nov., characterised by a distinctive feature mainly known in the cyclostome subfamily Rogadinae: a median longitudinal carina on the second metasomal tergum. Finally, we provide an identification key to the valid genera of Rhysipolinae.

Materials and methods

Taxon sampling

We analysed UCE data from 29 species representing nine of the 11 rhysipolinae genera: *Rhysipolis*, 15 spp.; *Cantharoctonus*, 1 sp.; *Pachystigmus*, 2 spp., *Pseudavga* Tobias, 1964, 2 spp., *Parachremylus*, 2 spp.; *Allobracon*, 3 spp.; *Pseudorhysipolis* Scatolini, Pentead-Dias & van Achterberg, 2002, 2 spp.; *Cerophanes* Tobias, 1971, 1 sp.; and *Troporhysipolis* Quicke, Belokobylskij & Butcher, 2023, 1 sp. As outgroups, we included 28 species belonging to 23 genera of the subfamilies Hormiinae and Rogadinae, as these groups have consistently been recovered as sisters to Rhysipolinae in previous UCE-based studies (Jasso-Martínez et al. 2021; Jasso-Martínez et al. 2022a, b). We also included one specimen with uncertain generic assignment (DNA sample voucher: USNMENT01322932).

New UCE data were generated for 24 ingroup and outgroup species, while data for the remaining species were obtained from four previously published studies (Jasso-Martínez et al. 2021, 2022a, b; Shimbori et al. 2024). Detailed information of the specimens examined in this study, their species assignment, locality, DNA voucher, and SRA accession numbers are available in the Suppl. material 1.

Morphological examination

We examined the external morphology of the sequenced and additional specimens, all of which are deposited in the following collections: Colección Nacional de Insectos del Instituto de Biología de la Universidad Nacional Autónoma de México (CNIN IB-UNAM); Zoological Institute of the Russian Academy of Sciences, St Petersburg, Russia (ZISP); and Coleção Entomológica, Departamento de Ecologia e Biologia Evolutiva, Universidade Federal de São Carlos, São Carlos, SP, Brazil (DCBU). Morphological terminology follows van Achterberg (1988), except for wing venation and microsculpture features, which follow Sharkey and Wharton (1997) and Harris (1979), respectively. Digital images of representative species from various rhysipoline genera were taken at the Zoological Institute of the Russian Academy of Sciences using a Canon EOS 70D digital camera mounted on an Olympus SZX10 microscope, and at the Laboratorio Nacional de Biodiversidad (LANABIO) at IBUNAM using a ZEISS® AXIO ZoomV16 stereoscopic microscope, an AxioCam MRc5 (5 megapixels) camera, and the ZEN 2012 (Blue Edition) software.

DNA extraction protocol and library preparation

Genomic DNA was extracted from ethanol-preserved and pinned specimens using a non-destructive technique (Ceccarelli et al. 2012) with the EZ-10 Spin Column Genomic DNA minipreps Kit (BIOBasic, Toronto, ON, Canada). Specimens were digested overnight, and subsequently removed from digestion, washed with distilled water, and remounted. DNA quantification was performed using a Qubit 4.0 fluorometer (v.4.0, Invitrogen, Life Technologies, Carlsbad, CA, USA) and the High Sensitivity Kit (Invitrogen, Life Technologies, Carlsbad, CA, USA).

Twenty-two genomic libraries were prepared following the protocol described by Branstetter et al. (2017), using the Kapa Hyper Prep Kit (Kapa Biosystems Inc., Wilmington, MA, USA) and custom TruSeq-style dual-indexing barcodes adapters (Glenn et al. 2019) for *in silico* demultiplexing. For library preparation, up to 150 ng of input DNA per sample was resuspended in 100 µl of ultrapure water. DNA was sheared into ~ 200–600 bp fragments using a BioRuptor Pico sonicator, applying one to three cycles of 15–90-second on/off pulses, depending on the collection date and condition of each specimen. Samples were pooled at equimolar concentrations in groups of 7–10 libraries for enrichment, with a total input of 2,000 ng of DNA per enrichment reaction. The UCE enrichment was performed using the RNA probe set Hym v.2 designed for Hymenoptera (Branstetter et al. 2017), which includes 31,829 baits targeting 2,590 UCE loci, following the standard enrichment protocol (www.ultraconserved.org). Post-enrichment DNA pools were quantified using the Qubit 4.0 fluorometer with the Broad Range Kit (Invitrogen, Life Technologies, Carlsbad, CA, USA), combined at equimolar ratios, and sent for sequencing to Admera Health BioPharma Services (South Plainfield, NJ, USA) employing an Illumina NovaSeqX instrument (PE150, v4 chemistry). Sequenced libraries produced 150-bp paired-end reads.

Two additional libraries belonging to two species of *Pseudorhysipolis* were generated using the NEBNext Ultra II FS DNA Library Prep kit (New England Biolabs, Ipswich, MA, USA) according to the manufacturer's protocol, scaled to a 1:15 ratio. Up to 10 ng of DNA, resuspended in 2.6 µL of ultrapure water, was used as input. DNA was fragmented for 5 minutes to achieve a mean fragment size of 200–500 bp. Amplified and purified libraries were quantified using Qubit, pooled at equimolar concentrations, and sent for sequencing to Admera Health BioPharma Services (South Plainfield, NJ, USA). Sequencing was performed on an Illumina NovaSeqX instrument (PE150, v4 chemistry). Sequenced libraries produced 150-bp paired-end reads. Raw sequence data for all newly generated samples are available in the NCBI Sequence Read Archive (NCBI-SRA) under BioProject accession number PRJNA1228065.

UCE data processing

Bioinformatic processing was performed using the Beagle HPC supercomputer at the Instituto de Biología, Universidad Nacional Autónoma de México (IB-UNAM). Raw reads were cleaned of adapters, and low-quality sequences were filtered using Trimmomatic v. 0.39 (Bolger et al. 2014). Reads assembly was performed on the web server Galaxy (usegalaxy.org) using either SPAdes or RNAspades (Bankevich et al. 2012; Bushmanova et al. 2019). Contigs were processed following the Phyluce v. 1.7.1 pipeline (Faircloth 2016).

UCE contigs were identified using the Hymenoptera-v2 probe set (Branstetter et al. 2017) and subsequently extracted. Individual UCE loci were aligned using MAFFT (Katoh and Toh 2008) implemented in Phyluce, and poorly aligned regions were removed using GBLOCKS v. 0.91 (Talavera and Castresana 2007) with relaxed stringency values (0.5, 0.5, 12, and 7 for the b1-b4 parameters, respectively). This bioinformatic pipeline was applied to both target and non-target enrichment samples. Finally, we built completeness matrices with thresholds of 50, 60, 70%.

Phylogenetic analyses

We used the SWSC-EN algorithm (Tagliacollo and Lanfear 2018) to define partitions within each UCE locus. The optimal partition scheme and appropriate evolutionary model for each partition was determined using ModelFinder in IQTREE v2.2.0 (Minh et al. 2020) with the `-rclusterf` option, which is suitable for our data matrices (Lanfear et al. 2017) and the `-TESTMERGEONLY` command, which implements the greedy algorithm of PartitionFinder. We also used the Bayesian information criterion (BIC) to identify the best partition scheme. Maximum likelihood (ML) analyses were conducted using IQTREE v. 2.2.0 (Minh et al. 2020) with 1,000 ultra-fast bootstrap replicates (Hoang et al. 2018) to assess clade support and generate a consensus tree (Soltis and Soltis 2003).

All completeness matrices with their respective partition schemes and their derived phylogenetic trees are available in the FigShare repository (10.6084/m9.figshare.28489664).

Results

UCE performance and alignment statistics

An average of 1,618,742 reads were obtained for the newly processed samples prior to filtering and trimming. After trimming, an average of 1,290,498 clean reads were obtained. The cleaned reads produced an average of 95,360 assembled contigs (min. 33,351 – max. 470,913). We recovered a total of 2,460 UCE loci from the 2,590 available loci in the Hymenoptera-v2 probe set across all samples, including outgroups. The recovered loci had a mean length of 333.60 bp after aligning and trimming. The average number of UCE loci recovered was 1,192.1. *Parachremylus* sp. and *Soraya alencarae* had the lowest (99) and highest (1898) number of loci, respectively, across all samples. The alignment summary for each completeness matrix is provided in Table 1.

Phylogenetic relationships

The ML phylograms derived from the analyses conducted with the 50%, 60% and 70% completeness matrices are provided in Fig. 1 and Suppl. material 2. We recovered similar topologies for the analyses across the three completeness matrices, with topological differences primarily observed among species of the *Rhysipolis* + *Cerophanes* + *Troporhysipolis* clade. The topology from the 50% completeness matrix had the highest number of nodes supported by bootstrap (BTP) values of 100 (all but one node within the ingroup), and we thus only describe its relationships.

Table 1. Alignments summary for the matrices with different completeness percentages.

| Matrix | No. of taxa | UCE loci | Loci mean length (bp) [min-max] | Matrix length (bp) | Informative sites | Nucleotide positions |
|--------|-------------|----------|---------------------------------|--------------------|-------------------|----------------------|
| 50% | 61 | 1,232 | 371.07 [172-614] | 457,160 | 218,966 | 15,871,303 |
| 60% | 61 | 827 | 379.36 [200-614] | 313,727 | 160,106 | 12,249,152 |
| 70% | 61 | 642 | 388.45 [200-614] | 249,388 | 132,562 | 10,357,365 |

The subfamily Rhysipolinae and most of its genera were recovered as monophyletic, except for *Rhysipolis*, which was paraphyletic with respect to the only species of *Cerophanes* and *Troporhysipolis*: *C. kerzhneri* Tobias and *T. antefurcalis* (Granger). The *Rhysipolis* clade was divided into two main subclades. The first included *C. kerzhneri* deeply nested along with most *Rhysipolis* species from the Palaearctic and one from the Nearctic regions. The second subclade comprised *Rhysipolis* species from the Palaearctic, Oriental, and Neotropical regions, with the Afrotropical *T. antefurcalis* placed as sister to all of them.

The species with problematic assignment was recovered as sister to the *Pseudorhysipolis* + *Allobracon* clade, with these three taxa being sister to the remaining rhysipoline genera. *Parachremylus* was also recovered as monophyletic and sister to the *Cantharoctonus* + (*Pseudavga* + *Pachystigmus*) and the *Rhysipolis* + *Cerophanes* + *Troporhysipolis* clades. *Cantharoctonus*, on the other hand, was sister to the *Pseudavga* + *Pachystigmus* clade.

Taxonomic inferences

Our taxon sampling confirmed the monophyly of Rhysipolinae and of most of its genera. However, *Rhysipolis* was recovered as paraphyletic with respect to *Cerophanes* Tobias and *Troporhysipolis*. These two genera are morphologically similar to *Rhysipolis*, sharing all the diagnostic features of this genus, including a complete occipital carina not joining the hypostomal carina, epicnemial carina complete, and first to third terga never striated. *Cerophanes* is distinguished from *Rhysipolis* by the presence of a large inner horn-like process on the scapus (absent in *Rhysipolis*) (Tobias 1971; Belokobylskij and Tobias 1986; Whitfield and Wagner 1991), whereas *Troporhysipolis* is distinguished by the vein 1cu-a antefurcal to the veins 1M and 2CUb arising distinctly before the middle of distal margin of second subdiscal cell (vein 1cu-a postfurcal to vein 1M and vein 2CUb usually arising behind or in the middle of distal margin of second subdiscal cell in *Rhysipolis*) (Quicke et al. 2016). Our best-supported phylogenetic estimate placed *Cerophanes* deeply nested within *Rhysipolis*, whereas *Troporhysipolis* appeared at the base of one of the two main subclades of *Rhysipolis*. Based on these relationships and on the aforementioned morphological features, we propose *Cerophanes* syn. nov. as a junior synonym of *Rhysipolis*. Further molecular phylogenetic studies including additional species of *Troporhysipolis* are needed to confirm its generic status.

Our best phylogenetic estimate recovered the members of *Pachystigmus* and *Pseudavga* as reciprocally monophyletic, which is congruent with their morphology. Species of both genera share several features, including a short first metasomal tergum, typically not longer than its posterior width, basal sternal plate not longer than its posterior width, vein CU1a of fore wing arising from middle of distal margin of second subdiscal cell, and vein m-cu of hind wing usually present. Tobias (1964) described *Pseudavga* and distinguishing it from *Avga* Nixon, 1940

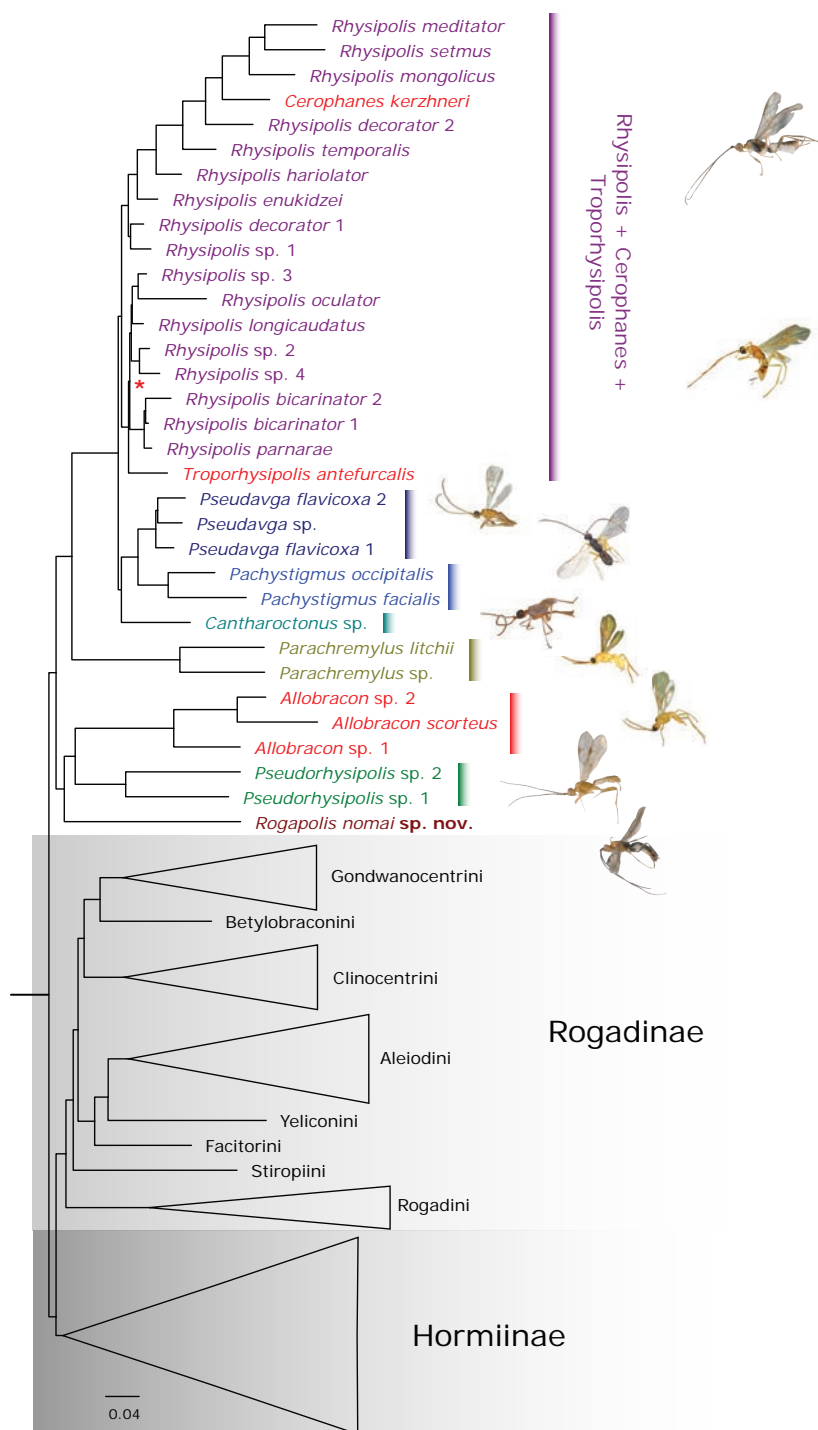


Figure 1. ML phylogram derived from the 50% completeness matrix. Coloured clades correspond to the different rhysipoline genera, except for the *Rhysipolis* (violet), *Cerophanes* (red) and *Troporhysipolis* (red) clade. Asterisks (*) near branches indicate bootstrap support values < 100. Nodes without labels are supported by BTP support values of 100.

and *Hormius* Nees, 1919, though overlooked the genus *Noserus* Foerster, 1863 (= *Pachystigmus* Hellén, 1927), whose status was unclear at that time. A subsequent study of the type material and additional specimens of the genotype *Noserus facialis* Förster, 1863 (Belokobylskij and Tobias 1986) revealed that this genus and *Pseudavga* did not have external morphological differences, and thus the former was regarded a synonym of the second. Recently, the restoration of

the generic status of *Pseudavga* was proposed after studying its biology and subtle morphological features (Shaw and Sims 2015). However, based on our recovered relationships, molecular evidence, and on the consistent morphological similarity of these two taxa, we propose *Pseudavga* syn. nov. to be treated as a synonym of *Pachystigmus* and consider it a subgenus within the latter.

Based on the recovered phylogenetic relationships and the morphological examination of the studied specimens, we propose that the specimen with problematic assignment, which is sister to *Allobracon* + *Pseudorhysipolis*, represents an undescribed genus and species. Below, we describe this genus, provide a diagnosis for Rhysipolinae, and a key to the currently valid genera of this subfamily. Digital pictures of representative species belonging to all the rhysipoline genera recognised in this study except *Rogapolis* gen. nov. are provided in the Suppl. material 3.

Systematic accounts

Family Braconidae Nees, 1811

Subfamily Rhysipolinae Belokobylskij, 1984

Diagnosis. Head with subcircular or weakly oval hypoclypeal cavity; occipital carina usually present (except *Allobracon*), complete, not joining hypostomal carina ventrally, distinctly removed from it and separately reaching lower margin of head capsule near mandible, or sometimes incomplete ventrally; postgenal bridge always absent; maxillary palpus 6-segmented, labial palpus 4-segmented, third segment of labial palpus never shortened. Antenna often setiform, sometimes curled into ring apically in dried specimens; first flagellar segment not shorter than second segment. Mesosoma: notauli on mesoscutum complete or often absent in posterior half of mesoscutum, usually without longitudinal furrow medio-posteriorly; prepectal carina and precoxal sulcus present and distinct, but sometimes some of these structures absent (*Allobracon* and *Parachremylus*); propodeum often without areola, but sometimes with mid-longitudinal carina or with relatively several distinct areas (at least posteriorly) delineated by rather distinct carinae. Fore wing with marginal cell always closed distally, usually not shortened and reaching wing apex. Vein m-cu usually antefurcal to vein 2-SR; veins 2SR and r-m present; discal cell petiolate anteriorly; second subbasal cell always closed distally by vein CU1b; vein CU1a never interstitial; vein a always absent. Hind wing with three hamuli; vein m-cu usually present, but sometimes short, or absent; vein cu-a always present and closing subbasal cell. Subbasal cell medium-sized or short. Fore tibia without spines; hind coxa suboval, without basoventral corner and tubercle; hind femur long and narrow; claws simple and small. First metasomal tergum always with dorsope, though sometimes small; acrosternite (basal sternal plate) of first segment predominantly short, rarely (*Cantharoctonus*) elongated; dorsal carinae usually distinct at least in basal half, fused or not fused subbasally. Following terga usually relatively soft, mainly smooth, but sometimes second and third terga rather distinctly sclerotised, shagreened, granulate or even partly striate (*Afro-rhysipolis*, *Rogapolis* and *Pseudorhysipolis*); laterotergites of second tergum often not separated, but usually with inflection and crease; spiracles of second and third terga situated dorso-laterally, slightly above crease; suture between

second and third terga usually present, distinct, or almost indistinct. Ovipositor short, distinctly shorter than metasoma, usually slightly widened subapically, with dorsal node, often without serration ventro-apically.

Included genera. *Afrorhysipolis*, *Allobracon*, *Cantharoctonus*, *Pachystigmus* (= *Pseudavga*, *Noserus*), *Parachremylus*, *Pseudorhysipolis*, *Rhysipolis* (= *Cerophanes*), *Rogapolis*, *Troporhysipolis* (Table 2).

Comments. The genus *Neoavga* Belokobylskij, 1989 was originally included within Hormiinae (Hormiini; Belokobylskij 1989) and it was subsequently transferred to Rhysipolinae (van Achterberg 1995; Yu et al. 2016), though Wharton (1993) previously suggested that this genus belonged to Exothecini. More recently, in the redefinition of the Mesostoinae (Shimbori et al. 2017), *Neoavga* was proposed to belong to this subfamily mainly based on the presence of the crossvein a in the fore wing, and the epicnemial carina present only laterally and absent ventrally. This placement was later confirmed by Quicke et al. (2020) in a molecular phylogenetic study that focused on the cyclostome braconid subfamilies.

***Rogapolis* García-Acosta, Shimbori, Castañeda-Osorio & Zaldívar-Riverón, gen. nov.**

<https://zoobank.org/499133C5-4432-4361-B0FE-1296986DCA14>

Type species. *Rogapolis nomai* sp. nov.

Diagnosis. *Rogapolis* can be morphologically distinguished from the remaining members of Rhysipolinae by having the second metasomal terga with a basal triangular median area followed by a longitudinal carina, a feature that had been mainly observed in most members of the subfamily Rogadinae and some Braconinae.

Description. Head: Antenna with at least 45 flagellomeres. Basal flagellomeres long, distal flagellomeres shorter. Distal margin of scapus strongly oblique (ventral length of pedicellus as long as ventral length of scapus). Frons, vertex, temple, and gena smooth and polished. Eyes glabrous, large, and oval-shaped. Malar space relatively short, distinctly shorter than eye. Face considerably pilose, with long setae. Hypoclypeal depression small and rounded. Malar suture present. Frons depressed, flat, with an indistinct median transversal carina. Ocelli small. Occipital carina incomplete medio-dorsally, ventrally not joining hypostomal carina.

Mesosoma: Mostly smooth and polished, except metapleuron and propodeum, which are rugose areolate. Propleuron with posterior flange. Notauli deep, wide, not joining posteriorly, finishing in the middle of mesoscutum. Mid pit absent. Scutellar sulcus with six complete carinae. Epicnemial carina present. Precoxal sulcus deep, scrobiculate, extended at least two thirds length of mesopleuron. Metanotum with complete mid-longitudinal carina, posterior margin not protruding. Propodeum angled in lateral view, with median longitudinal carina present.

Wings: Forewing vein r as long as vein (RS+M)a, inserted in the proximal part of the pterostigma, slightly oblique; second submarginal cell moderately large, rectangular, distinctly narrowing proximally, vein r-m present but spectral; vein 1RS short; vein (RS+M)a slightly sinuate; vein M+CU completely tubular and almost straight; 1cu-a postfurcal; vein 2cu-a present and long. Hindwing veins RS and M present; vein M+CU as long as vein 1-M; second subdiscal cell long and closed distally; vein m-cu present and distinctly sclerotised.

Table 2. List of valid rhysipoline genera after this study, including author, geographic distribution, and number of their described species (Yu et al. 2016; Jasso-Martínez et al. 2021, 2022a, b).

| Genera | Author and year | Geographic distribution | No. described species |
|---|---|--|-----------------------|
| <i>Afrorhysipolis</i> | Belokobylskij, 1999 | Afrotropical | 1 |
| <i>Allobracon</i> | Gahan, 1915 | Nearctic, Neotropical | 24 |
| <i>Cantharoctonus</i> | Viereck, 1912 | Nearctic, Neotropical | 9 |
| <i>Pachystigmus</i> (<i>Pseudavga</i> syn. nov.) | Hellén, 1927 | Afrotropical, Palaearctic | 6 |
| <i>Parachremylus</i> | Granger, 1949 | Afrotropical, Oriental | 4 |
| <i>Pseudorhysipolis</i> | Scatolini, Penteado-Dias & van Achterberg, 2002 | Neotropical | 10 |
| <i>Rhysipolis</i> (<i>Cerophanes</i> syn. nov.) | Förster, 1863 | Neotropical, Nearctic, Oriental, Palaearctic | 24 |
| <i>Rogapolis</i> | gen. nov. | Neotropical | |
| <i>Troporhysipolis</i> | Quicke, Belokobylskij & Butcher, 2016 | Afrotropical, Australasian | 4 |

Legs: Coxae mostly smooth, with long setae. Hind tibial spurs slightly curved and with few setae. Claws simple, without distinct basal lobe or pecten.

Metasoma: First and second terga longitudinally costate; first tergum with a median longitudinal carina; second tergum with a basal triangular median area followed by median longitudinal carina. Exposed part of ovipositor sheath short, 0.5× as long as hind tibia.

Biology. Unknown.

Geographic distribution. This genus is known only from the type locality, a cloud forest region in the state of Acre, northern Brazil.

Etymology. The genus name *Rogapolis* is formed by combining Rogadinae, a subfamily that includes morphologically similar genera, and *Rhysipolis*, a genus within Rhysipolinae, the subfamily to which this new genus belongs. The gender of the genus is feminine, following the grammatical treatment of taxonomic names ending in *-polis*.

***Rogapolis nomai* García-Acosta, Shimbori, Castañeda-Osorio & Zaldívar-Riverón, sp. nov.**

<https://zoobank.org/9AC078D0-A04E-4004-B2B1-39CF12AD842C>

Fig. 2A–I

Type material. *Holotype*, female (USNMENT01322932) “BRAZIL, Mâncio Lima, AC / 20.IV.2006 / Menezes col” (DCBU 22093).

Description. Female, body length 4 mm, fore wing 4 mm; antenna 6.1 mm.

Head. Face without mid-longitudinal ridge, smooth and polished. Frons, occiput, temples, and malar space smooth and polished. Frons depressed behind antennal sockets, flat, with a an almost indistinct median transversal carina. Occipital carina medio-dorsally incomplete, ventrally present, and not joining hypostomal carina above the base of mandible. Temple narrow and receding (dorsal view), about as long as eyes. Head in dorsal view 1.25× wider than mesoscutum height. POL 0.57× OD, 0.238× OOL. Face width 1.51× longer than high. Hypoclypeal cavity nearly round. Diameter of hypoclypeal cavity 0.69× shorter than distance between cavity and eye margin. Hypoclypeal cavity moderate to strongly convex dorsally. Antenna 1.5× longer than body. Flagellum with 45 flagellomeres (one broken). Apical (lighter) flagellomeres somewhat

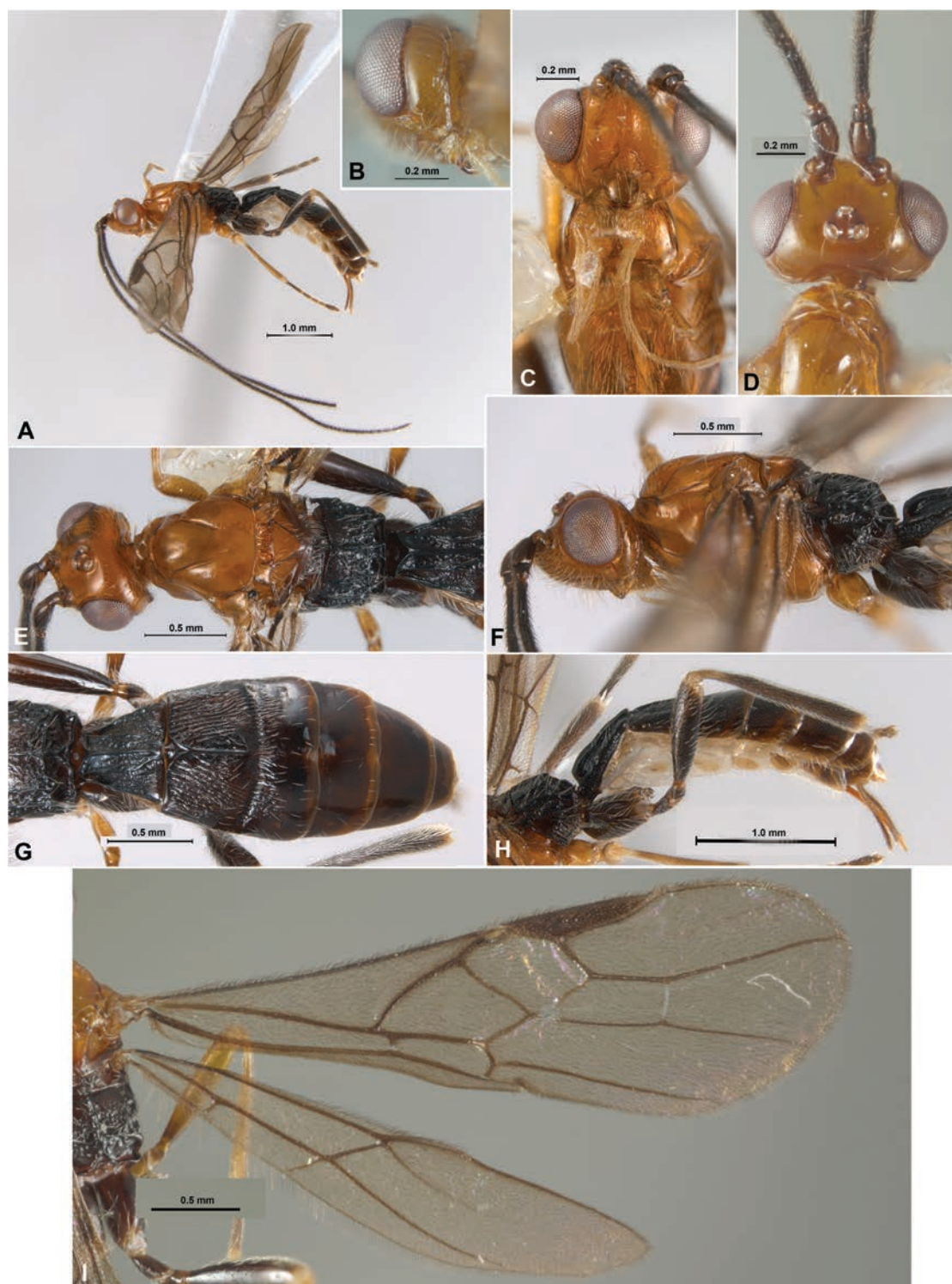


Figure 2. *Rogapolis nomai* García-Acosta, Shimbori, Castañeda-Osorio & Zaldívar-Riverón, gen. et sp. nov. Holotype, female **A** habitus, lateral view **B** head, posterolateral view (shown hypostomal carina not reaching occipital carina) **C** head, front view **D** head, dorsal view **E** head and mesosoma, dorsal view **F** head and mesosoma, lateral view **G** metasoma, dorsal view **H** metasoma, lateral view **I** wings.

widening in comparison with basal ones. First flagellomere 3.4× longer than wide, 1.55× longer than the second and 1.65× third.

Mesosoma. Pronotal collar forming a distinct neck. Pronotum smooth and polished. Pronope and subpronopes present. Pronope forming a wide concave

area. Mesosoma 1.79× longer than high, 2.2× longer than width in dorsal view. Mesoscutum and scutellum smooth and polished. Mesoscutum 0.97× longer than high. Scutellum 1.9× wider than long. Scutellar sulcus 0.4× as long as wide.

Wings. Forewing: pterostigma relatively small, 5.4× longer than maximum width. Vein 2RS 1.4× longer than vein r. Vein 3RSa 1.17× longer than 2RS. Vein 3RSb 2.3× longer than 3RSa; vein 1CUa around same size than vein 1cu-a; vein (RS+M)a straight. Hind wing: vein 1M 1.31× longer than M+CU. Vein 1M 3.2× longer than m-cu.

Legs. Mid and hind coxae smooth and polished. Hind legs with tarsi broken. Ventral margin of hind tibia without dense comb of setae. Hind tibial spurs slightly curved with few setae.

Metasoma. First metasomal tergum short, 2.1× longer than subbasal width, 0.8× as long as distal width. First and second terga longitudinally costate. Third tergum longitudinally costate anteriorly. Ovipositor sheaths uniformly setose, short, 0.5× as long as hind tibia.

Colour. Head, mesoscutum, scutellum, and mesopleuron honey yellow, propodeum and metasoma dark brown to black. Antenna, fore and mid coxae, and tibiae honey yellow. Hind leg and fore and middle tarsi dark brown to black. Wings dusky; veins and pterostigma brown to dark brown. Ovipositor sheaths dark brown. Ovipositor honey yellow.

Male. Unknown.

Etymology. This species was named after a fictional alien race called Nomai, from the 'Outer Wilds' video game.

Key to Rhysipolinae genera

- 1 Prepectal carina present and complete. Occipital carina usually complete, sometimes reduced ventrally. First metasomal tergum entirely coarsely sclerotised, without membranous areas in posterior half. Mesoscutum usually mostly smooth.....**2**
- Prepectal carina absent. Occipital carina incomplete, reduced dorsally and ventrally, or sometimes entirely absent. First metasomal tergum with two large, membranous areas in posterior half. Mesoscutum densely finely granulate**8**
- 2 Vein m-cu of fore wing distinctly postfurcal to vein 2-SR. Mesoscutum densely granulate. Second and third metasomal terga distinctly sclerotised and mainly rugose-striate. Afrotropical region.....***Afrorhysipolis* Belokobylskij, 1999**
- Vein m-cu of fore wing distinctly antefurcal to vein 2-SR. Other characters variable.....**3**
- 3 First and second metasomal terga with posteriorly acuminate subtriangular basal areas and with high medial carinae prolonged to posterior margins of terga. First and second metasomal terga entirely and third tergum in basal half distinctly striate with reticulation between striae. Neotropical region***Rogapolis* gen. nov.**
- First and second metasomal terga usually without acuminate subtriangular basal areas and usually without high medial carinae prolonged to posterior margins of terga. First to third metasomal terga never striate, usually smooth and often weakly sclerotised, but sometimes shagreened or granulate (some *Pseudorhysipolis* species)**4**

- 4 Vein cu-a of fore wing distinctly antefurcal to vein 1-M. Second subdiscal cell of fore wing concave, widened medially. Vein 2-CU1 thickened. Vein CU1 of fore wing arising before or from middle of distal margin of second subdiscal cell. Afrotropical region..... ***Troporhysipolis* Quicke, Belokobylskij & Butcher, 2016**
- Vein cu-a of fore wing distinctly postfurcal to vein 1-M (basal). Second subdiscal (brachial) cell of fore wing not widened medially. Vein 2-CU1 not thickened. Vein CU1 of fore wing variable..... **5**
- 5 Inner apex of hind tibia with conspicuous comb of setae. Vertex, mesoscutum and propodeum antero-dorsally granulate. Vein 1-M of hind wing 1.5–2.2× as long as vein M+CU. Second metasomal terga often entirely and most part of third tergum strongly sclerotised and densely granulate. Neotropical region..... ***Pseudorhysipolis* Scatolini, Penteado-Dias & van Achterberg, 2002**
- Inner apex of hind tibia without comb or with a comparatively narrow comb of setae. Vertex, mesoscutum and propodeum without granulation. Vein 1-M of hind wing 1.3× as long as vein M+CU or less. Second and third terga always weakly sclerotised and smooth or faintly shagreened..... **6**
- 6 Setose part of ovipositor sheath longer than half of metasoma. Second subdiscal cell of fore wing wide. Vein CU1a of fore wing arising from posterior 0.3 of distal margin of second subdiscal cell. Occipital carina present and complete, not fused below with hypostomal carina, removed from it and separately reaching lower margin of head capsule near mandible. Vein r of fore wing arising near middle of pterostigma. Rarely scapus of antenna modified, with distinct and acuminate inner lateral process. Nearctic, Neotropical, Oriental, and Palaearctic regions ***Rhysipolis* Foerster, 1863** [*Cerophanes* Tobias, 1960, syn. nov.]
- Setose part of ovipositor sheath short or very short, not or only slightly longer than first metasomal tergum. Second subdiscal cell of fore wing narrow. Vein CU1a arising from or before middle of distal margin of second subdiscal cell. Occipital carina present, fused with hypostomal carina, or not fused, removed from it and separately reaching lower margin of head capsule near mandible. Vein r of fore wing usually arising distal to middle of pterostigma, often from its distal 0.3–0.4. Scapus never modified **7**
- 7 Propodeum with wide, transverse groove anteriorly. First metasomal tergum long, 1.5–1.8× longer than its posterior width; basal sternal plate elongated. Vein CU1a of fore wing often arising before middle of distal margin of second subdiscal cell. Vein m-cu of hind wing absent. Pterostigma of male never enlarged. Nearctic and Neotropical regions..... ***Cantharoctonus* Viereck, 1912**
- Propodeum usually without transverse groove anteriorly, sometimes only with narrow sulcus. First metasomal tergum short, usually not longer than its posterior width; basal sternal plate never elongated. Vein CU1a of fore wing always arising from middle of distal margin of second subdiscal cell. Vein m-cu of hind wing usually present. Pterostigma of male sometimes enlarged. Afrotropical and Palaearctic regions ***Pachystigmus* Hellen, 1927** [including *Pseudavga* Tobias, 1964 as subgenus]

- 8 Occipital carina completely absent. Vertex smooth. Precoxal sulcus absent. Propodeum without areola, with distinct and almost complete longitudinal keel. Second and third metasomal terga without longitudinal carina, rarely second tergum basally with short carina. Nearctic and Neotropical regions..... ***Allobracon* Gahan, 1915**
- Occipital carina present laterally, absent dorsally and sometimes ventrally. Vertex densely granulate-coriaceous. Precoxal sulcus present. Propodeum with large areola delineated by distinct carinae, longitudinal carina absent or, if present, short basally. Second and third metasomal terga with distinct median longitudinal carina. Afrotropical and Oriental regions
..... ***Parachremylus* Granger, 1949**

Discussion

This study represents the first effort to delineate the limits of the subfamily Rhysipolinae using nuclear genome-wide data. As a small and historically overlooked braconid subfamily with a global distribution, our findings also provide a phylogenetic framework to assess the validity of its genera. Our best phylogenetic estimate consistently supports the monophyly of the subfamily with the inclusion of the newly described genus *Rogapolis*. However, our morphological revision failed to identify any diagnostic morphological feature exclusive to Rhysipolinae, leaving its monophyly currently supported solely by molecular data.

A putative synapomorphy of Rhysipolinae is their biology as koinobiont ectoparasitoids of leaf-miners and leaf-rollers. However, evidence supporting this trait is scarce and limited to only two of the nine genera (Shaw 1983; Shaw and Sims 2015; Shaw 2017). While host associations are documented for *Allobracon*, *Parachremylus*, and *Troporhysipolis*, the available information is incomplete. *Allobracon* is associated with leaf-miners, but its parasitism strategy remains unknown (Muesebeck 1958; Belokobylskij and Maeto 2006; Quicke et al. 2016). Similarly, *Troporhysipolis* has hosts among leaf-tying Lepidoptera rather than leaf-miners, and no further details on its biology are available (Quicke et al. 2016). A second putative synapomorphy of this subfamily is the presence of large abdominal exocrine glands in males, a feature originally described by Buckingham and Sharkey (1988) in *Rhysipolis* (though not examined in other rhysipoline genera). These glands are morphologically similar to the so-called Hagen's glands observed in the subfamilies Opiinae, Alysiinae, and Telengaiinae (formerly Gnamptodontinae), and thus their presence was interpreted as indicative of a phylogenetic affinity between Rhysipolinae and the latter three subfamilies (Buckingham and Sharkey 1988). However, this hypothesis has been refuted based on recent molecular-phylogenetic evidence (Jasso-Martínez et al. 2022a, b). Notably, Buckingham and Sharkey (1988) highlighted key anatomical differences, particularly in the position of the gland openings, underscoring their morphological significance. Given the potential phylogenetic relevance of this structure, further investigation into its prevalence within Rhysipolinae could provide additional insights into the evolutionary history of this group.

Despite the absence of known exclusive diagnostic morphological features, a combination of previously proposed characters can help distin-

guish Rhysipolinae from its closely related subfamilies Hormiinae, Exothecinae and Rogadinae (Belokobylskij 1993; Wharton 1993; van Achterberg 1995). These characters include the occipital carina not merging with hypostomal carina, complete epicnemial carina, vein m-cu of fore wing usually antefurcal to vein 2-SR, vein cu-a of fore wing usually postfurcal to vein 1-M, submedian vein of forewing not strongly decurved, and a weakly developed forewing SR.

Following the taxonomic changes proposed in this study, we recognise nine genera within Rhysipolinae (Table 2), several of which possess distinctive diagnostic features. For example, *Rogapolis* is mainly defined by a median longitudinal carina on the second metasomal tergum, a feature that is present in most rogadine genera (Sharkey 1997), but that within Rhysipolinae is only shared with *Parachremylus*. *Pseudorhysipolis*, on the other hand, is distinguished by a conspicuous comb of modified bristles on the hind tibia and an often granulate sculpture of mesosoma (Scatolini et al. 2002), while *Allobracon* is characterised by the complete absence of an occipital carina and a partially unsclerotised first metasomal tergum (as in *Parachremylus*) (Belokobylskij 1993; Wharton 1993).

Our phylogenetic reconstruction revealed geographic patterns in the distribution of some clades within Rhysipolinae. Two main clades can be distinguished within the subfamily. The first only includes genera with a New World (Neotropical and Nearctic) distribution—*Rogapolis*, *Pseudorhysipolis*, and *Allobracon*—, whereas the second consists of genera primarily distributed across the Afrotropical, Oriental, and Palaearctic regions—*Pachystigmus*, *Parachremylus*, *Rhysipolis*, and *Troporhysipolis*— though it also contains the Neotropical and Nearctic genus *Cantharoctonus*.

The fossil subgenus of *Rhysipolis*, *Rhysipolis* (*Granulopolis*) *simutniki* Belokobylskij, 2024, was recently described from inclusion of the late Eocene Baltic amber, revealing that this genus was already extant during the late Eocene, 37–34 Mya (Belokobylskij and Manukyan 2024). All previous records of rhysipoline (in current sense) fossil taxa from the Baltic amber, amber from the Tarkeshwar lignite mine in Gujarat, India, and imprints of Rott am Siebengebirge. Mount and Aix-en-Provence in France, are unconfirmed and therefore doubtful (Belokobylskij and Manukyan 2024). Further UCE-based phylogenomic studies incorporating more rhysipoline species from different continents are therefore necessary to evaluate the origin and subsequent diversification of Rhysipolinae across the New and Old Worlds.

Acknowledgements

We thank Cristina Mayorga for her help with the curation of the specimens deposited at the CNIN IBUNAM; Andrea Jiménez, Laura Márquez, and Nelly López for their help in the laboratory; David Velázquez, Alfredo Wong and Cristian Cervantes for the access to the HPC infrastructure at the Unidad TIC, IBUNAM (CONACy Proyecto Fronteras de la Ciencias 2016-01-1867); and Susana Guzmán for her help with the digital images taken at IBUNAM. This study was carried out by GYGA to obtain his BSc degree at the faculty of Sciences of the National Autonomous University of Mexico.

Additional information

Conflict of interest

The authors have declared that no competing interests exist.

Ethical statement

No ethical statement was reported.

Funding

This study was supported by a grant given by DGAPA-UNAM, Mexico (PAPIIT convocatorias 2022, 2025, project numbers IN201622, IN216725) to AZR, by grants given by the Conselho Nacional de Desenvolvimento Científico e Tecnológico (CNPq, Brazil; process 201050/2022-6) and Instituto Nacional de Ciência e Tecnologia dos Hymenoptera Parasitoides Project to EMS, and by the Russian State Research (project No. 125012901042-9) to SAB.

Author contributions

Conceptualization: AZR. Data curation: SAB, EMS, AMPD, GYGA, JMJM, RCO. Formal analysis: RCO, GYGA, EMS. Funding acquisition: AZR, AMPD. Investigation: AZR, RCO, SAB, EMS, AMPD. Methodology: GYGA, RCO. Project administration: AZR. Resources: SAB, JMJM, AZR. Supervision: SAB. Validation: AZR. Visualization: AZR. Writing - original draft: GYGA. Writing - review and editing: SAB, RCO, EMS, AMPD, AZR, JMJM.

Author ORCIDs

Rubén Castañeda-Osorio  <https://orcid.org/0000-0003-0507-5477>

Sergey A. Belokobylskij  <https://orcid.org/0000-0002-3646-3459>

Eduardo M. Shimbori  <https://orcid.org/0000-0003-4655-2591>

Jovana M. Jasso-Martínez  <https://orcid.org/0000-0001-6497-7150>

Angélica M. Penteado-Dias  <https://orcid.org/0000-0002-8371-5591>

Alejandro Zaldívar-Riverón  <https://orcid.org/0000-0001-5837-1929>

Data availability

All of the data that support the findings of this study are available in the main text or Supplementary Information.

References

- Bankevich A, Nurk S, Antipov D, Gurevich AA, Dvorkin M, Kulikov AS, Lesin VM, Nikolenko SI, Pham S, Prjibelski AD, Pyshkin AV, Sirotkin AV, Vyahhi N, Tesler G, Alekseyev MA, Pevzner PA (2012) SPAdes: a new genome assembly algorithm and its applications to single-cell sequencing. *Journal of Computational Biology* 19: 455–477. <https://doi.org/10.1089/cmb.2012.0021>
- Belokobylskij SA (1989) The braconid wasps of the tribe Hormiini (Hymenoptera, Braconidae) from Australia. *Entomologicheskoe Obozrenie* 68: 376–392. [In Russian]
- Belokobylskij SA (1993) On the classification and phylogeny of the braconid wasps of subfamilies Doryctinae and Exothecinae (Hymenoptera, Braconidae). Part I. On the classification, 2. *Entomologicheskoe Obozrenie*. 72: 143–164. [In Russian]
- Belokobylskij SA, Maeto K (2006) A new species of the genus *Parachremylus* Granger (Hymenoptera: Braconidae), a parasitoid of *Conopomorpha* lychee pests (Lepidoptera: Gracillariidae) in Thailand. *Journal of Hymenoptera Research* 15: 181–186.

- Belokobylskij SA, Manukyan AR (2024) First reliable fossil record of the subfamily Rhysipolinae (Hymenoptera: Braconidae): a new subgenus and species of the genus *Rhysipolis* Foerster, 1863 from Baltic amber. *Zootaxa* 5448: 591–600. <https://doi.org/10.11646/zootaxa.5448.4.10>
- Belokobylskij SA, Tobias VI (1986) Subfam. Doryctinae. In: Medvedev GS (Ed.) *Opre-delitel' Nasekomykh Evrospeiskoy Chasti SSSR*, 3, Pereponchatokrylye, 4, 21–72. [In Russian]
- Bolger AM, Lohse M, Usadel B (2014) Trimmomatic: a flexible trimmer for Illumina sequence data. *Bioinformatics* 30: 2114–2120. <https://doi.org/10.1093/bioinformatics/btu170>
- Branstetter MG, Longino JT, Ward PS, Faircloth BC (2017) Enriching the ant tree of life: enhanced UCE bait set for genome-scale phylogenetics of ants and other Hymenoptera. *Methods in Ecology and Evolution* 8: 768–776. <https://doi.org/10.1111/2041-210X.12742>
- Buckingham GR, Sharkey MJ (1988) Abdominal exocrine glands in Braconidae (Hymenoptera). *Advances in Parasitic Hymenoptera Research* 1988: 199–242.
- Bushmanova E, Antipov D, Lapidus A, Pribelski AD (2019) rnaSPAdes: a de novo transcriptome assembler and its application to RNA-Seq data. *GigaScience* 8: giz100. <https://doi.org/10.1093/gigascience/giz100>
- Ceccarelli FS, Sharkey MJ, Zaldívar-Riverón A (2012) Species identification in the taxonomically neglected, highly diverse, Neotropical parasitoid wasp genus *Notiospathius* (Braconidae: Doryctinae) based on an integrative molecular and morphological approach. *Molecular Phylogenetics and Evolution* 62: 485–495. <https://doi.org/10.1016/j.ympev.2011.10.018>
- Faircloth BC (2016) PHYLUCE is a software package for the analysis of conserved genomic loci. *Bioinformatics* 32: 786–788. <https://doi.org/10.1093/bioinformatics/btv646>
- Gauld ID (1988) Evolutionary patterns of host utilization by ichneumonoid parasitoids (Hymenoptera: Ichneumonidae and Braconidae). *Biological Journal of the Linnean Society* 35: 351–377. <https://doi.org/10.1111/j.1095-8312.1988.tb00476.x>
- Glenn TC, Nilsen RA, Kieran TJ, Sanders JG, Bayona-Vásquez NJ, Finger JW, Pierson TW, Bentley KE, Hoffberg SL, Louha S, Garcia- De Leon FJ, del Rio Portilla MA, Reed KD, Anderson JL, Meece JK, Aggrey SE, Rekaya R, Alabady M, Belanger M, Winker K, Faircloth BC (2019) Adapterama I: universal stubs and primers for 384 unique dual-indexed or 147,456 combinatorially indexed Illumina libraries (iTru & iNext). *PeerJ* 7: e7755. <https://doi.org/10.7717/peerj.7755>
- Harris RA (1979) A glossary of surface sculpturing. *Occasional Papers in Entomology*, State of California Department of Food and Agriculture 28: 1–31.
- Hoang DT, Chernomor O, Von Haeseler A, Minh BQ, Vinh LS (2018) UFBoot2: improving the ultrafast bootstrap approximation. *Molecular Biology and Evolution* 35: 518–522. <https://doi.org/10.1093/molbev/msx281>
- Jasso-Martínez JM, Quicke DL, Belokobylskij SA, Meza-Lázaro RN, Zaldívar-Riverón A (2021) Phylogenomics of the lepidopteran endoparasitoid wasp subfamily Rogadiinae (Hymenoptera: Braconidae) and related subfamilies. *Systematic Entomology* 46: 83–95. <https://doi.org/10.1111/syen.12449>
- Jasso-Martínez JM, Quicke DL, Belokobylskij SA, Santos BF, Fernández-Triana JL, Kula RR, Zaldívar-Riverón A (2022a) Mitochondrial phylogenomics and mitogenome organization in the parasitoid wasp family Braconidae (Hymenoptera: Ichneumonoidea). *BMC Ecology and Evolution* 22: 1–15. <https://doi.org/10.1186/s12862-022-01983-1>

- Jasso-Martínez JM, Santos BF, Zaldívar-Riverón A, Fernández-Triana JL, Sharanowski BJ, Richter R, Dettman JR, Blaimer BB, Brady SG, Kula RR (2022b) Phylogenomics of braconid wasps (Hymenoptera, Braconidae) sheds light on classification and the evolution of parasitoid life history traits. *Molecular Phylogenetics and Evolution* 173: 107452. <https://doi.org/10.1016/j.ympev.2022.107452>
- Katoh K, Toh H (2008) Recent developments in the MAFFT multiple sequence alignment program. *Briefings in Bioinformatics* 9: 286–298. <https://doi.org/10.1093/bib/bbn013>
- Lanfear R, Frandsen PB, Wright AM, Senfeld T, Calcott B (2017) PartitionFinder 2: new methods for selecting partitioned models of evolution for molecular and morphological phylogenetic analyses. *Molecular Biology and Evolution* 34: 772–773. <https://doi.org/10.1093/molbev/msw260>
- Minh BQ, Schmidt HA, Chernomor O, Schrempf D, Woodhams MD, von Haeseler A, Lanfear R (2020) IQ-TREE 2: new models and efficient methods for phylogenetic inference in the genomic era. *Molecular Biology and Evolution* 37: 1530–1534. <https://doi.org/10.1093/molbev/msaa015>
- Muesebeck CFW (1958) New Neotropical wasps of the family Braconidae (Hymenoptera) in the U.S. National Museum. *Proceedings of the United States National Museum* 107: 405–461. <https://doi.org/10.5479/si.00963801.108-3389.405>
- Quicke DL (2015) *The Braconid and Ichneumonid Parasitoid Wasps: Biology, Systematics, Evolution and Ecology*. John Wiley & Sons, Chichester, U.K. <https://doi.org/10.1002/9781118907085>
- Quicke DLJ, Belokobylskij SA, Smith MA, Rota J, Hrcek J, Butcher BA (2016) A new genus of rhysipoline wasp (Hymenoptera: Braconidae) with modified wing venation from Africa and Papua New Guinea, parasitoid of Choreutidae (Lepidoptera). *Annales Zoologici* 66: 173–192. <https://doi.org/10.3161/00034541ANZ2016.66.2.003>
- Quicke DLJ, Belokobylskij SA, Braet Y, van Achterberg C, Hebert PDN, Prosser SWJ, Austin AD, Fagan-Jeffries EP, Ward DF, Shaw MR, Butcher BA (2020) Phylogenetic reassignment of basal cyclostome braconid parasitoid wasps (Hymenoptera) with description of a new, enigmatic Afrotropical tribe with a highly anomalous 28S D2 secondary structure. *Zoological Journal of the Linnean Society* 190: 1002–1019. <https://doi.org/10.1093/zoolinnean/zlaa037>
- Scatolini D, Pentead-Dias AM, van Achterberg C (2002) *Pseudorhysipolis* gen. nov. (Hymenoptera: Braconidae: Rhysipolinae), with nine new species from Brazil, Suriname and Panama. *Zoologische Mededelingen* 76: 109–131.
- Sharanowski BJ, Dowling AP, Sharkey MJ (2011) Molecular phylogenetics of Braconidae (Hymenoptera: Ichneumonoidea), based on multiple nuclear genes, and implications for classification. *Systematic Entomology* 36: 549–572. <https://doi.org/10.1111/j.1365-3113.2011.00580.x>
- Sharkey MJ (1997) Key to New World subfamilies of the family Braconidae. In: *Manual of the New World genera of the family Braconidae (Hymenoptera)*. International Society of Hymenopterists, Special Publ. 1, Washington, DC, 39–63.
- Sharkey MJ, Wharton RA (1997) Morphology & terminology. In: *Manual of the New World genera of the family Braconidae (Hymenoptera)*. International Society of Hymenopterists Special Publ. 1, Washington, DC, 19–37.
- Shaw MR (1983) On [One] evolution of endoparasitism: the biology of some genera of Rogadinae (Braconidae). *Contributions of the American Entomological Institute* 20: 307–328.
- Shaw MR (2017) Further notes on the biology of *Pseudavga flavicoxa* Tobias, 1964 (Hymenoptera, Braconidae, Rhysipolinae). *Journal of Hymenoptera Research* 54: 113–128. <https://doi.org/10.3897/jhr.54.10789>

- Shaw MR, Sims I (2015) Notes on the biology, morphology, nomenclature and classification of *Pseudavga flavicoxa* Tobias, 1964 (Hymenoptera, Braconidae, Rhysipolinae), a genus and species new to Britain parasitizing *Bucculatrix thoracella* (Thunberg) (Lepidoptera, Bucculatricidae). *Journal of Hymenoptera Research* 42: 21–32. <https://doi.org/10.3897/JHR.42.8935>
- Shimbori EM, Souza-Gessner CSS, Pentead-Dias AM, Shaw SR (2017) A revision of the genus *Andesipolis* (Hymenoptera: Braconidae: Mesostoinae) and redefinition of the subfamily Mesostoinae. *Zootaxa* 4216(2): 101–152. <https://doi.org/10.11646/zootaxa.4216.2.1>
- Shimbori EM, Castañeda-Osorio R, Jasso-Martínez JM, Pentead-Dias AM, Gadelha SS, Brady SG, Quicke DLJ, Kula RR, Zaldívar-Riverón A (2024) UCE-based phylogenomics of the lepidopteran endoparasitoid wasp subfamily Rogadinae (Hymenoptera: Braconidae) unveils a new Neotropical tribe. *Invertebrate Systematics* 38: IS24040. <https://doi.org/10.1071/IS24040>
- Soltis PS, Soltis DE (2003) Applying the bootstrap in phylogeny reconstruction. *Statistical Science* 18: 256–267. <https://doi.org/10.1214/ss/1063994980>
- Spencer L, Whitfield JB (1999) Revision of the Nearctic Species of *Rhysipolis* Förster (Hymenoptera: Braconidae). *Transactions of the American Entomological Society* (1890) 125: 295–324. <http://www.jstor.org/stable/25078684>
- Tagliacollo VA, Lanfear R (2018) Estimating improved partitioning schemes for ultra-conserved elements. *Molecular Biology and Evolution* 35: 1798–1811. <https://doi.org/10.1093/molbev/msy069>
- Talavera G, Castresana J (2007) Improvement of phylogenies after removing divergent and ambiguously aligned blocks from protein sequence alignments. *Systematic Biology* 56: 564–577. <https://doi.org/10.1080/10635150701472164>
- Tobias VI (1964) Novye vidy I rod braconid (Hymenoptera, Braconidae) iz Tadzhikistana. *Izvestiya Akademii Nauk Tadzhikskoi SSR* 2: 58–65. [In Russian]
- Tobias VI (1971) Review of the Braconidae (Hymenoptera) of the U.S.S.R. *Proceedings of the All-Union Entomological Society* 54: 156–268. [In Russian]
- van Achterberg C (1995) Generic revision of the subfamily Betylobraconinae (Hymenoptera: Braconidae) and other groups with modified fore tarsus. *Zoologische Verhandelingen* 298: 1–242.
- van Achterberg C (1988) Revision of the subfamily Blacinae Foerster (Hymenoptera: Braconidae). *Zoologische Verhandelingen* 64: 1–20.
- Wharton RA (1993) Review of the Hormiini (Hymenoptera: Braconidae) with a description of new taxa. *Journal of Natural History* 27: 107–171. <https://doi.org/10.1080/00222939300770061>
- Whitfield JB (1992) The polyphyletic origin of endoparasitism in the cyclostome lineages of Braconidae (Hymenoptera). *Systematic Entomology* 17: 273–286. <https://doi.org/10.1111/j.1365-3113.1992.tb00338.x>
- Whitfield JB, van Achterberg C (1987) Clarification of the taxonomic status of the genera *Cantharoctonus* Viereck, *Noserus* Foerster and *Pseudavga* Tobias (Hymenoptera: Braconidae). *Systematic Entomology* 12: 509–518. <https://doi.org/10.1111/j.1365-3113.1987.tb00221.x>
- Whitfield JB, Wagner DL (1991) Annotated key to the genera of Braconidae (Hymenoptera) attacking leafmining Lepidoptera in the Holarctic Region. *Journal of Natural History* 25: 733–754. <https://doi.org/10.1080/00222939100770481>
- Whitfield JB, Wharton RA (1997) Subfamily Horminae. In: Wharton RA, Marsh PM, Sharkey MJ (Eds) *Manual of the New World Genera of the Family Braconidae*

(Hymenoptera). International Society of Hymenopterists, Special Publ. 1, Washington, DC, 285–302.

Yu DSK, van Achterberg C, Horstmann K (2016) Taxapad, Ichneumonoidea 2015. Database on flash-drive, Ottawa, Ontario. <http://www.taxapad.com/>

Zaldívar-Riverón A, Mori M, Quicke DL (2006) Systematics of the cyclostome subfamilies of braconid parasitic wasps (Hymenoptera: Ichneumonoidea): a simultaneous molecular and morphological Bayesian approach. *Molecular Phylogenetics and Evolution* 38: 130–145. <https://doi.org/10.1016/j.ympev.2005.08.006>

Supplementary material 1

Species assignment, locality, DNA voucher number, and GenBank and SRA accession numbers of the specimens examined in this study

Authors: Gerardo Y. García-Acosta, Rubén Castañeda-Osorio, Sergey A. Belokobylskij, Eduardo M. Shimbori, Jovana M. Jasso-Martínez, Angélica M. Penteado-Dias, Alejandro Zaldívar-Riverón

Data type: xlsx

Copyright notice: This dataset is made available under the Open Database License (<http://opendatacommons.org/licenses/odbl/1.0/>). The Open Database License (ODbL) is a license agreement intended to allow users to freely share, modify, and use this Dataset while maintaining this same freedom for others, provided that the original source and author(s) are credited.

Link: <https://doi.org/10.3897/zookeys.1234.147859.suppl1>

Supplementary material 2

ML phylograms derived from the 60% and 70% completeness matrices (1 and 2, respectively)

Authors: Gerardo Y. García-Acosta, Rubén Castañeda-Osorio, Sergey A. Belokobylskij, Eduardo M. Shimbori, Jovana M. Jasso-Martínez, Angélica M. Penteado-Dias, Alejandro Zaldívar-Riverón

Data type: pdf

Explanation note: Numbers near branches indicate bootstrap support values. Nodes without labels are supported by BTP support values of 100.

Copyright notice: This dataset is made available under the Open Database License (<http://opendatacommons.org/licenses/odbl/1.0/>). The Open Database License (ODbL) is a license agreement intended to allow users to freely share, modify, and use this Dataset while maintaining this same freedom for others, provided that the original source and author(s) are credited.

Link: <https://doi.org/10.3897/zookeys.1234.147859.suppl2>

Supplementary material 3

Digital pictures of representative species belonging to all the rhysipoline genera recognised in this study except *Rogapolis*

Authors: Gerardo Y. García-Acosta, Rubén Castañeda-Osorio, Sergey A. Belokobylskij, Eduardo M. Shimbori, Jovana M. Jasso-Martínez, Angélica M. Penteado-Dias, Alejandro Zaldívar-Riverón






Data type: pdf

Explanation note: **fig. 1.** *Afrorhysipolis intermedius* Belokobylskij, 1999. Female, paratype. **A** habitus, lateral view **B** face **C** head, dorsal view **D** antenna, apical segments **E** antenna, scapus and pedicel **F** head and mesosoma, lateral view **G** mesosoma, dorsal view **H** metasoma, dorsal view **I** metasoma, lateral view **J** fore and hind wings **K** legs. **fig. 2.** *Allobracon primus* (Muesebeck, 1958). Female, paratype. **A** habitus, lateral view **B** face **C** head, dorsal view **D** antenna, scapus and pedicel **E** head and mesosoma, lateral view **F** mesosoma, dorsal view **G** metasoma, dorsal view **H** metasoma, lateral view **I** fore and hind wings **J** hind legs. **fig. 3.** *Cantharoctonus stramineus* Viereck, 1912. Female, paratype. **A** habitus, dorsal view **B** face **C** head, dorsal view **D** antenna, scapus and pedicel **F** head and mesosoma, lateral view **G** mesosoma, dorsal view **H** metasoma, dorsal view **I** metasoma, ventral view **J** fore and hind wings **K** hind leg. **fig. 4.** *Pachystigmus facialis* (Förster, 1863). Female. **A** habitus, dorsal view **B** face **C** head, dorsal view **D** antenna, apical segments **E** antenna, scapus and pedicel **F** head and mesosoma, lateral view **G** mesosoma, dorsal view **H** propodeum and metasoma, dorsal view **I** metasoma, lateral view **J** legs **K** fore and hind wings **L** part of male fore wing. **fig. 5.** *Pseudavga flavicoxa* Tobias, 1964. Female. **A** habitus **B** face **C** head, dorsal view **D** antenna, apical segments **E** antenna, scapus and pedicel **F** mesosoma, lateral view **G** mesosoma, dorsal view **H** propodeum and metasoma, dorsal view **I** metasoma, lateral view **J** fore and hind wings **K** hind coxa and femur **L** hind tibia. **fig. 6.** *Parachremylus litchii* Belokobylskij & Maeto, 2006. Female. **A** habitus, lateral view **B** face **C** head, dorsal view **D** antenna, scapus and pedicel **E** antenna, apical segments **F** mesosoma, lateral view **G** mesosoma dorsal view **H** propodeum and metasoma, dorsal view **I** metasoma, lateral view **J** fore wing **K** hind wing **L** hind legs. **fig. 7.** *Pseudorhysipolis (Pararhysipolis)* sp. Female. **A** habitus, lateral view **B** head, dorsal view **C** face **D** head and mesosoma, dorsal view **E** head and mesosoma, lateral view **F** propodeum and metasoma, dorsal view **G** metasoma, lateral view **H** fore and hind wings. **fig. 8.** *Pseudorhysipolis (Pseudorhysipolis)* sp. Female. **A** habitus, lateral view **B** head, dorsal view **C** face **D** head and mesosoma, dorsal view **E** head and mesosoma, lateral view **F** propodeum and metasoma, dorsal view **G** metasoma, lateral view **H** fore wing **I** hind wing. **fig. 9.** *Rhysipolis meditator* (Haliday, 1836). Female. **A** habitus, lateral view **B** face **C** head, dorsal view **D** antenna, scapus and pedicel **E** head and mesosoma, lateral view **F** mesosoma, dorsal view **G** metasoma, dorsal view **H** metasoma, lateral view **I** fore and hind wings **J** legs. **fig. 10.** *Troporhysipolis antefurcalis* (Granger, 1949). Female. **A** habitus, lateral view **B** face **C** head, dorsal view **D** antenna, scapus and pedicel **E** mesosoma, dorsal view **F** mesosoma, lateral view **G** propodeum and metasoma, dorsal view **H** metasoma, lateral view **I** fore and hind wings **J** first metasomal tergum.

Copyright notice: This dataset is made available under the Open Database License (<http://opendatacommons.org/licenses/odbl/1.0/>). The Open Database License (ODbL) is a license agreement intended to allow users to freely share, modify, and use this Dataset while maintaining this same freedom for others, provided that the original source and author(s) are credited.

Link: <https://doi.org/10.3897/zookeys.1234.147859.suppl3>

Discovering diversity of Central Asian and Himalayan *Epeorus* (*Caucasiron*) mayflies (Ephemeroptera, Heptageniidae) using DNA barcoding and morphology

Ľuboš Hrivniak¹, Pavel Sroka², Roman J. Godunko^{2,3}, Alexander V. Martynov⁴, Dmitry M. Palatov⁵, Jindřiška Bojková¹

¹ Department of Botany and Zoology, Faculty of Science, Masaryk University, Kotlářská 2, 61137 Brno, Czech Republic

² Biology Centre of the Czech Academy of Sciences, Institute of Entomology, Branišovská 31, 370 05 České Budějovice, Czech Republic

³ Department of Invertebrate Zoology and Hydrobiology, Faculty of Biology and Environmental Protection, University of Lodz, Banacha 12/16, 90237 Łódź, Poland

⁴ National Museum of Natural History, National Academy of Sciences of Ukraine, Bohdan Khmelnytsky str., 15, 01030, Kyiv, Ukraine

⁵ Independent researcher

Corresponding author: Ľuboš Hrivniak (lubos.hrivniak@gmail.com)



Academic editor:

Lyndall Pereira-da-Conceicao

Received: 22 November 2024

Accepted: 14 February 2025

Published: 9 April 2025

ZooBank: <https://zoobank.org/260E4DE4-553D-43FF-BEEA-68356C23F13F>

Citation: Hrivniak Ľ, Sroka P, Godunko RJ, Martynov AV, Palatov DM, Bojková J (2025) Discovering diversity of Central Asian and Himalayan *Epeorus* (*Caucasiron*) mayflies (Ephemeroptera, Heptageniidae) using DNA barcoding and morphology. ZooKeys 1234: 89–125. <https://doi.org/10.3897/zookeys.1234.141196>

Copyright: © Ľuboš Hrivniak et al.
This is an open access article distributed under terms of the Creative Commons Attribution License (Attribution 4.0 International – CC BY 4.0).

Abstract

The mayflies of the genus *Epeorus* Eaton, 1881 subgenus *Caucasiron* Kluge, 1997 are distributed from the eastern Mediterranean to the mountains of south-west China. In contrast to the Caucasus, the Mediterranean and Irano-Anatolian regions, where *E. (Caucasiron)* represents one of the most extensively studied mayfly taxa, the species diversity in the more eastern mountains of Asia has been studied only sporadically. In this study, the species diversity of *E. (Caucasiron)* from the mountains of Central Asia (Pamir, Tian Shan) and the western part of the Himalayas was analysed using DNA barcoding and the morphology of larvae and adults. The distance- and phylogenetic tree-based molecular species delimitation analyses revealed five *E. (Caucasiron)* species occurring in the study area. Three of them did not correspond morphologically to any known species of the genus *Epeorus*. These species were described herein as *E. (C.) himalayensis* Hrivniak & Sroka, **sp. nov.**, *E. (C.) lanceolatus* Hrivniak & Sroka, **sp. nov.** and *E. (C.) lineatus* Hrivniak & Sroka, **sp. nov.** All new species were compared with other representatives of the subgenus and other related species of the genus *Epeorus*, and appropriate morphological diagnostic characters were provided. Morphological revision, main diagnostic characters, and information on the distribution of *E. (C.) guttatus* Braasch & Soldán, 1979 and two other potentially related *Epeorus* species from the area, *E. psi* Eaton, 1885 and *E. suspicatus* (Braasch, 2006), are also given.

Key words: Aquatic insects, integrative taxonomy, mountains, species delimitation

Introduction

The genus *Epeorus* Eaton, 1881, subgenus *Caucasiron* Kluge, 1997, represents a charismatic group of mountain mayflies distributed in the Palaearctic (Hrivniak et al. 2020a). Its highest diversity is to be found in the Caucasus region, where it represents one of the most species-rich groups of mayflies (Hrivniak et al. 2024). Its larvae inhabit rapids of montane and submontane streams, as well

as rivers with stony substrates, and are among the most important indicators of high water quality (Türkmen 2023). The distribution range of *E. (Caucasiron)* can be divided into two separate areas. The western part includes the Eastern Mediterranean (Samos and Cyprus Islands), the Caucasus and the Irano-Anatolian mountain ranges (Hrivniak et al. 2020b), while the eastern part includes the mountains of Central Asia, the Himalayas, and the mountains of south-west China (Fig. 1). The species diversity of the western part of the area was already intensively studied from 1938 to 1981 (Tshernova 1938; Sinitschenkova 1976; Braasch 1978, 1979, 1980a, 1983a; Braasch and Soldán 1979; Braasch and Zimmerman 1979) and altogether ten species were described based on morphology. Since 2017, a further eight species have been described using an integrative taxonomic approach (Hrivniak et al. 2017, 2019, 2020a, 2021, 2022, 2024), when the analysis of morphological traits proposed by Braasch and Soldán (1979) and Hrivniak et al. (2020b) were combined with the DNA barcoding (sequences of cytochrome c oxidase subunit I; hereafter COI) and molecular species delimitation (e.g. Fujisawa and Barraclough 2013; Puillandre et al. 2021). To date, the research has resulted in 18 described species (listed in Hrivniak et al. 2020b, 2024), a comprehensive DNA barcoding dataset of all species (deposited in NCBI GenBank, <https://www.ncbi.nlm.nih.gov/genbank>) and a guide for the identification of larvae to the species level (Hrivniak et al. 2020b, 2024).

In contrast to the western part of the area, only two species reliably attributed to *E. (Caucasiron)* are known from the eastern part of the area, namely *E. (C.) guttatus* (Braasch & Soldán, 1979) distributed in the mountains of Central Asia (Tian Shan and Pamir) (Braasch and Soldán 1979; Kluge 2015) and *E. (C.) extraordinarius* Chen, Wang & Zhou, 2010 known from south-west China (Yunnan-Guizhou Plateau) (Chen et al. 2010; Ma and Zhou 2022) (Fig. 1). The recent study by Vasanth et al. (2021) summarised the diversity and distribution of the genus *Epeorus* in India and placed three additional species in the subgenus *E. (Caucasiron)*. These included *E. psi* Eaton, 1885 distributed in the Himalayas and Mountains of south-west China (Braasch 1980b, 1981; Vasanth et al. 2021; Ma and Zhou 2022), and *E. kapurkripalanorum* (Braasch, 1983) and *E. suspicatus* (Braasch, 2006), both of which are known from the Himalayas (Kapur and Kripalani 1963; Braasch 2006a) (Fig. 1). However, this was based solely on larval morphology or on original descriptions of larvae, but not on the analysis of molecular data or the examination of adults, which are essential for the assignment of species to species groups/subgenera (Braasch 2006a). Therefore, the subgeneric classification of these species within the genus *Epeorus* remains uncertain (Kluge 2004; Braasch 2006a) and a reliable taxonomic revision is required to clarify their systematic position. In this study, we retain the assignment of *E. psi*, *E. kapurkripalanorum* and *E. suspicatus* to the genus level, while we consider the assignment to the subgenus *E. (Caucasiron)* to be uncertain.

Considering the geographical extent and topographical complexity of the eastern part of the area, more species of *E. (Caucasiron)* can be expected there. Therefore, we aim to investigate its species diversity in Central Asia and the Himalayas using an integrative taxonomic approach that has proven successful in the species delimitation of *E. (Caucasiron)* mayflies in the western part of the area. Since species identification based on the original descriptions is often complicated and inaccurate, we also aim to revise the morphology of insufficiently described species.

This study summarises the recent knowledge on *E. (Caucasion)* from the eastern part of its range, focusing on the mountains of Central Asia (Tian Shan and Pamir) and the western part of the Himalayas (Fig. 1). The main objectives are (i) to study the species diversity of the subgenus in Central Asia and the Himalayas using molecular species delimitation tools and morphology, (ii) to describe the morphology of new species and provide their key diagnostic characters, and (iii) to provide basic information on their distribution and habitat requirements. In addition, we provide information on larval morphology, diagnostic characters, and distribution of three species of the genus *Epeorus* known from the area, *E. (C.) guttatus*, *E. suspicatus*, and *E. psi*.

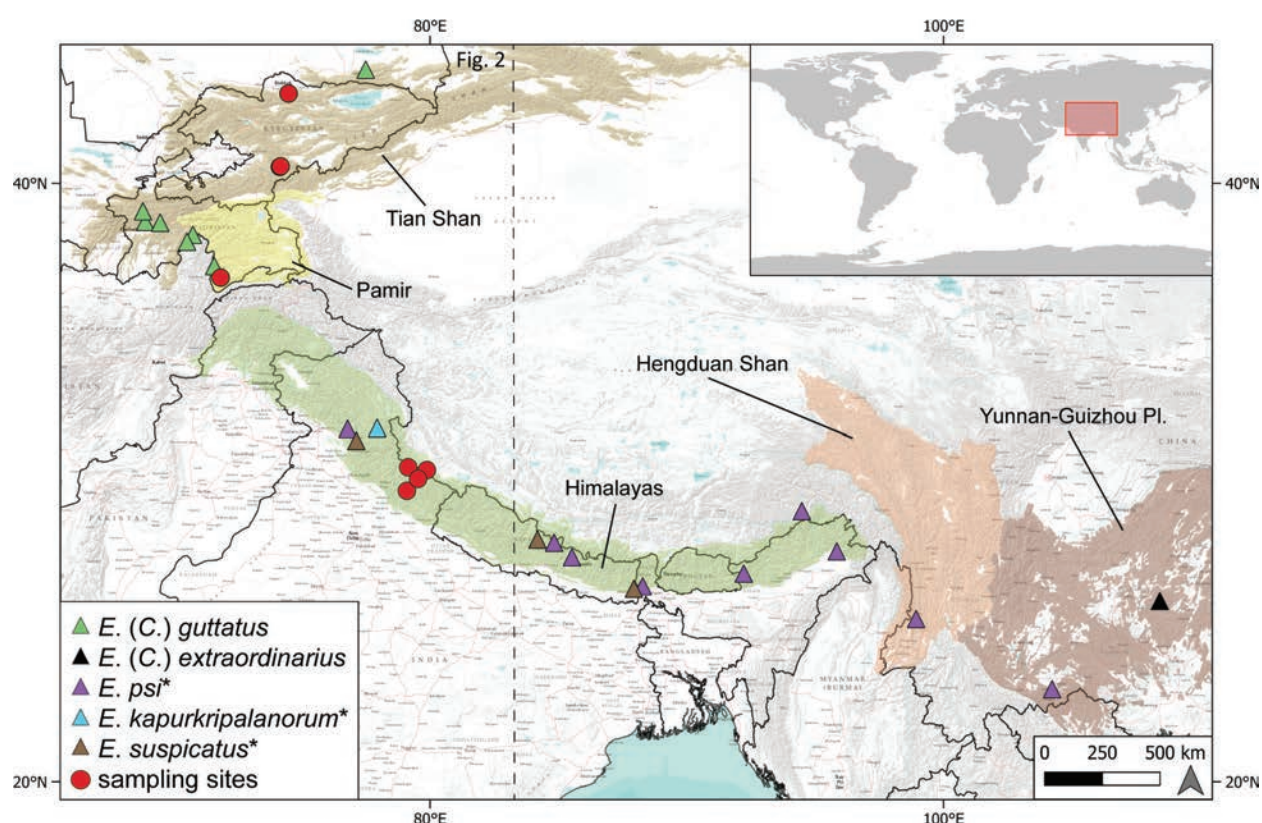


Figure 1. Distribution of studied *Epeorus* spp. across Asian mountains. Triangles refer to localities in the literature; our sampling sites are marked with red dots. A species name marked with an asterisk indicates the unclear systematic position of the species within the genus *Epeorus*. Dashed line represents the frame of the detailed map in Fig. 2. Boundaries of mountain ranges were adopted from Snethlage et al. (2022).

Materials and methods

The specimens of *E. (Caucasion)* examined in this study were collected in Tajikistan, Kyrgyzstan, and India in 2016–2018. The larvae were collected by hand net and the winged stages were reared from larvae in the field. The material was preserved in 96% EtOH and stored in the laboratory at -20 °C. The collection is deposited at the Zoological Survey of India (**ZSI**), Kolkata (The Ministry of Environment, Forest and Climate Change, India), Biology Centre of the Czech Academy of Sciences, Institute of Entomology, České Budějovice, Czech Republic (**IECA**) and National Museum of Natural History, National Academy of Sciences of Ukraine (**NMNH NASU**). Other species used for morphological comparison were obtained from the IECA. These included all species from the

Caucasus, the Mediterranean region and Irano-Anatolian region, *E. psi* and the type material (paratype) of *E. (C.) guttatus* (Braasch & Soldán, 1979). The type material (holotype and paratypes) of *E. suspicatus* (Braasch, 2006) was obtained from the State Museum of Natural History, Stuttgart, Germany (**SMNS**).

Morphological examination and terminology

Parts of specimens were mounted on microscopic slides using HydroMatrix (MicroTech Lab, Graz, Austria) mounting medium. To remove the muscle tissue for an investigation of the cuticular structures, specimens were left overnight in a 10% solution of NaOH prior to slide mounting. Drawings were made using a stereomicroscope Olympus SZX7 and a microscope Olympus BX41, both equipped with a drawing tube. Photographs were obtained using Leica DFC450 camera fitted with macroscope Leica Z16 APO. Photographs were stacked in Helicon Focus v. 5.3. All photographs were subsequently enhanced with Adobe Photoshop v. CS5. Specimens assignable to already described species were identified using original descriptions/redescriptions of individual species (Kapur and Kripalani 1963; Braasch 1980b, 2006a; Chen et al. 2010; Kluge 2015; Vasanth et al. 2021) and comparative material. Adults were associated with larvae by rearing in the field and analyses of COI. Morphological traits for the description of larvae and adults were adopted from Braasch (1980a) and Hrivniak et al. (2020).

A term “late instar larva” refers to the larva with well-developed wing pads (as on Fig. 3A) or the larva with body length exceeding 10 mm without cerci. A term “extralimital species” used in sections “Affinities” includes species from the western part of *E. (Caucasion)* range (i.e., the Caucasus, Mediterranean and Irano-Anatolian regions). The systematic classification follows the concept of Kluge (1997, 2015), where several subgenera within the genus *Epeorus* are recognised. Species with unclear subgeneric position are classified to the genus level only.

DNA extraction, PCR, sequencing, and alignment

Total genomic DNA of 25 specimens was extracted from legs using the DEP-25 DNA Extraction Kit (Top-Bio) or DNeasy Blood & Tissue Kit (QIAGEN). COI was sequenced according to Hrivniak et al. (2017). COI sequences of other *E. (Caucasion)* species used in the species delimitation analyses were obtained from Hrivniak et al. (2020a, 2021, 2022, 2024) and Ma and Zhou (2022). The final dataset contained 123 specimens, all species from the Caucasus, Mediterranean, and Irano-Anatolian regions, and a single species from south-west China (*E. (C.) extraordinarius*). Sequences were assembled in Jalview v. 2 (Waterhouse et al. 2009) and aligned in the same software using the Mafft v. 7 plugin (Katoh and Standley 2013). Newly obtained sequences are deposited in GenBank with accession numbers PV330270–PV330294.

Molecular species delimitation

Molecular delimitation of individual species was performed using the single threshold General Mixed Yule Coalescent model (GMYC, Pons et al. 2006; Fujisawa and Barraclough 2013) and the Assemble Species by Automatic Partitioning (ASAP; Puillandre et al. 2021). The COI gene tree for GMYC model was recon-

structured using BEAST v. 2.6.7. (Bouckaert et al. 2019) with settings described in Hrivniak et al. (2020a). Two analyses were run on CIPRES Science Gateway (Miller et al. 2010) for 100 million generations sampled every 10,000 generations. Convergence and effective sample size (ESS > 200) were verified using Tracer v. 1.7. (Rambaut et al. 2018). The first 10% of trees from each run were discarded as burn-in. Files from both independent runs were combined using LogCombiner v. 2.6.7. The maximum clade credibility tree was constructed from 18,000 trees using TreeAnnotator v. 1.8.4. with default settings. GMYC model was performed at <https://species.h-its.org/gmyc/>. ASAP was performed at <https://bioinfo.mnhn.fr/abi/public/asap/>. The input dataset was the aligned fasta file and a simple pairwise genetic distances were selected. Inter- and intraspecific pairwise genetic distances were calculated in MEGA X (Kumar et al. 2018).

Results and discussion

Molecular and morphological species delimitation

The final alignment contained 631 base pairs and 226 variable positions, from which 211 were parsimony informative. The GMYC model revealed 26 species units (confidence interval: 23–31). The most probable scenario of ASAP species delimitation (ASAP score of partition 1: 1.50; threshold distance: 0.043582) was congruent with GMYC model (Fig. 2). All species clusters were supported by posterior probability (> 0.95) from BEAST 2. Specimens from Central Asia and the Himalayas were delimited into five species units. Two of them morphologically corresponded to *E. (C.) guttatus* and *E. psi*. The remaining three species units did not correspond to any previously known *E. (Caucasiron)* species. They also differed from similar species with unclear subgeneric attribution occurring in the same area, *E. kapurkripalanorum* and *E. suspicatus*. Therefore, we have named the three new species *E. (C.) himalayensis* sp. nov., *E. (C.) lanceolatus* sp. nov., and *E. (C.) lineatus* sp. nov. and their morphology is described below.

Interspecific pairwise genetic distances of the dataset restricted to species from Central Asia, the Himalayas and south-west China ranged from 5.07 to 18.07% and maximum intraspecific distances reached 1.59%. Interspecific pairwise genetic distances of morphologically well-defined species distributed in the Caucasus, Mediterranean and Irano-Anatolian region ranged from 5.24 to 16.03% and maximum intraspecific distances reached 3.53%.

The newly proposed species *E. (C.) himalayensis* sp. nov. differed from all other species included in the analysis by 6.25–17.49% (*E. (C.) lanceolatus* sp. nov.: 6.25–6.83% and *E. psi*: 16.51–17.49%), *E. (C.) lineatus* sp. nov. differed by 5.07–18.07% (*E. (C.) guttatus*: 5.07–5.71% and *E. psi*: 16.83–18.07%), and *E. (C.) lanceolatus* sp. nov. differed by 6.25–17.27% (*E. (C.) himalayensis* sp. nov.: 6.25–6.83% and *E. psi*: 16.32–17.27%).

Descriptions of the new species

All species described below were assigned to the subgenus *Caucasiron* within the genus *Epeorus* based on the following morphological characters: larva: i) presence of a projection on the costal margin of gill plates II–VII, and ii) mediodorsal

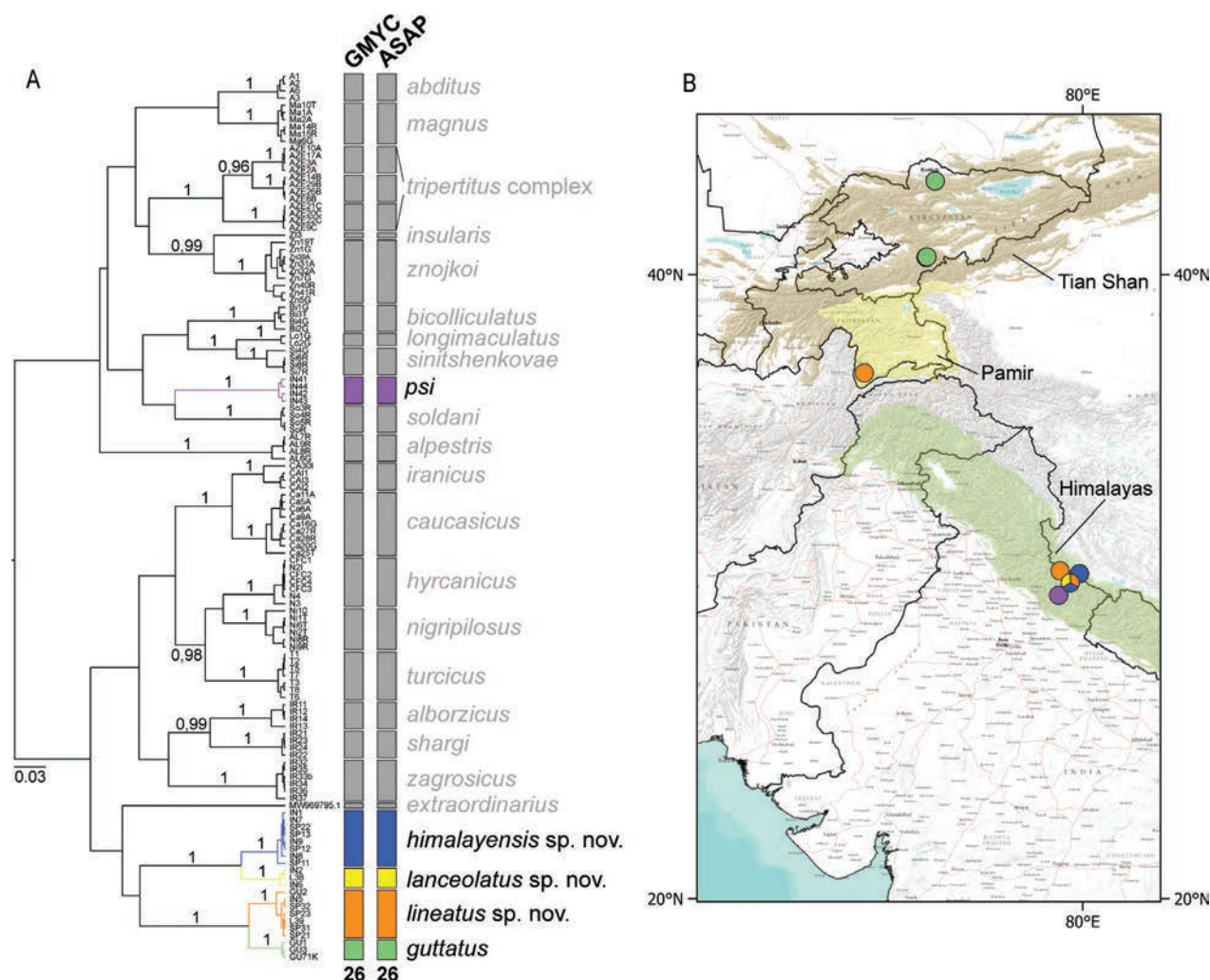


Figure 2. A COI gene tree generated in BEAST 2 and results of GMYC and ASAP species delimitation analyses. Numbers on the tree branches refer to the posterior probability. Species delimited from our sampling sites in Central Asia and the Himalayas are highlighted and colored B occurrence of delimited species in the study area (colors correspond to A).

directed hair-like setae along the anterior margin of the head; male imago: iii) penis lobes cylindrical, without latero-apical spines, and iv) median titillators well developed. The holotypes are deposited in ZSI, paratypes in IECA and NMNH NASU.

***Epeorus* (Caucasion) *himalayensis* Hrivniak & Sroka, sp. nov.**

<https://zoobank.org/8A4B0D7A-B2FD-42B8-85DB-87FCFC1D2140>

Figs 3–6

Type material. Holotype: • male larva: INDIA: Uttarakhand Pradesh, vicinity of Pandukeshwar village, left tributary of Alakananda River, 2099 m a.s.l., 30°38.901'N, 79°32.108'E (codes: IND2018/7; 39Gang); 9–11.05.2018, Martynov A.V., Palatov D.M. leg. **Paratypes:** • 12 larvae (barcoded specimens: IN1, SP11 - labrum and mandibular incisors mounted on slide, SP12), 4 male imagoes (reared from larvae; barcoded specimens: IN7 - genitalia and larval exuvia mounted on slide, IN8, IN9), 3 female imagoes (reared from larva; two larval exuviae mounted on slide), 1 male subimago (reared from larva): same data as holotype. • 2 larvae (barcoded specimens: SP13, SP22): INDIA: Uttarakhand Pradesh, vicinity of

Lambagad village, Alaknanda River, 1998 m a.s.l.; 30°38.64198'N, 79°32.02500'E (codes: IND2018/8; 40Gang); 9–11.05.2018, Martynov A.V., Palatov D.M. leg.

Etymology. The species name *himalayensis* (Latin) refers to the distribution in the Himalayas.

Description of larva. General coloration yellowish brown with dark brown maculation (Fig. 3). Body length (BL) of late-instar larvae: 15.0 mm (female; $n = 1$), 11.8–13.1 mm (male; $n = 3$). Length of cerci approximately $1.2 \times$ body length.

Head. Shape trapezoidal, slightly rounded (Fig. 3D, E). Head dimensions of late-instar larvae: length 3.3 mm, width 5.0 mm in female; length 2.5–2.6 mm, width 4.0–4.1 mm in male. Width/length ratio: 1.48–1.57 (female; $n = 8$), 1.48–1.64 (male; $n = 8$). Coloration pattern of dorsal surface consists of: i) paired stripe-like and rounded maculae along epicranial suture, ii) pair of triangular (or blurred) macula near inner edges of eyes, iii) pair of rounded maculae ventrally to lateral ocelli, iv) pale stripes extending from lateral ocelli to lateral edges of head, v) rectangular macula between ocelli, vi) stripe-like and rounded maculae ventrally to median ocellus. Antennae yellowish brown, scapus and pedicellus darkened (Fig. 3D, E). Dorsal surface covered with short rounded spatulate setae (as on abdominal terga; Fig. 4E), fine hair-like setae and stick-like setae. Sparse longer and fine hair-like setae located posteriorly to eyes.

Mouthparts. Labrum (Fig. 4A) widened anteriorly; anterior margin slightly rounded or nearly straight. Lateral angles rounded. Dorsal surface covered with setae of different size, 4–6 longer bristle-like setae located antero-medially and two bristles antero-laterally (Fig. 4A, left half). Epipharynx with longer, slightly plumose bristles situated along lateral to anterior margin, cluster of fine, hair-like setae medially (not figured), and group of 6–12 setae of various size (Fig. 4A, right half). Outer incisors of both mandibles with three apical teeth; outer tooth blunt in both mandibles. Inner incisor of left mandible with three apical teeth (Fig. 4B), right inner incisor bifurcated (Fig. 4C).

Thorax. Prothorax anteriorly narrowed, lateral edges slightly rounded. Metanotum with small blunt posterior-median projection. Dorsal surface covered with hair-like setae, stick-like setae and short rounded spatulate setae (as on abdominal terga and head). Sparse longer, hair-like setae along pro-, meso- and metanotal suture.

Legs. Coloration on Fig. 3H, I. Femora with median hypodermal spot, often transversely extended. Base and apex of femora darkened; patella-tibial suture darkened; tarsi proximally and distally darkened. Dorsal surface of femora covered by short rounded spatulate setae (Fig. 4D), hair-like setae and sparsely distributed stick-like setae. Dorsal edge of femora with blade-like setae. Dorsal margin of tibiae and tarsi with row of dense hair-like setae; ventral margin with irregular row of distally accumulated spines. Tarsal claws with two or three denticles.

Abdominal terga. Color pattern of abdominal terga consists of transversal stripe along anterior margin of terga I–IX (X), medially extending to: i) triangular or blurred macula on terga II–IV and ii) triangular or T-shaped macula on terga V–IX (median macula on terga VIII and IX widened) (Fig. 3F, G). Pair of short stripes or spots present antero-laterally to median maculae. Lateral margins with oblique stripe-like maculae on terga I–IX (often dorso-posteriorly extended). Denticles along posterior margin of terga dense, irregular, and pointed (Fig. 4F). Surface of terga covered with hair-like setae, stick-like setae and



Figure 3. *Epeorus* (*Caucasion*) *himalayensis* sp. nov., larva **A** habitus in dorsal view **B** habitus in ventral view **C** habitus in lateral view **D** head of male in dorsal view **E** head of female in dorsal view **F, G** coloration of abdominal terga **H, I** middle leg in dorsal view **J** distal part of abdomen in ventral view **K–M** coloration of abdominal sterna.

rounded spatulate setae (Fig. 4E, F). Tergum X with short posterolateral projections (Fig. 4L, arrow). Terga with longitudinal median row of hair-like setae.

More or less developed posteromedian spine (best expressed on terga VII–IX as on Fig. 11M, N) were observed in larvae of BL 6.0–8.2 mm (barcoded specimens SP12, SP13, SP22). Tergal spines were not observed in late instar larvae and last instar larval exuvia from reared adults (barcoded specimens: IN1, IN7, IN8, IN9).

Abdominal sterna. Yellowish, with a pattern consisting of more or less defined triangular maculae (Fig. 3K–N). Nerve ganglia darkened. Sternum IX of female with V-shaped median emargination and numerous hair-like setae (Fig. 4M).

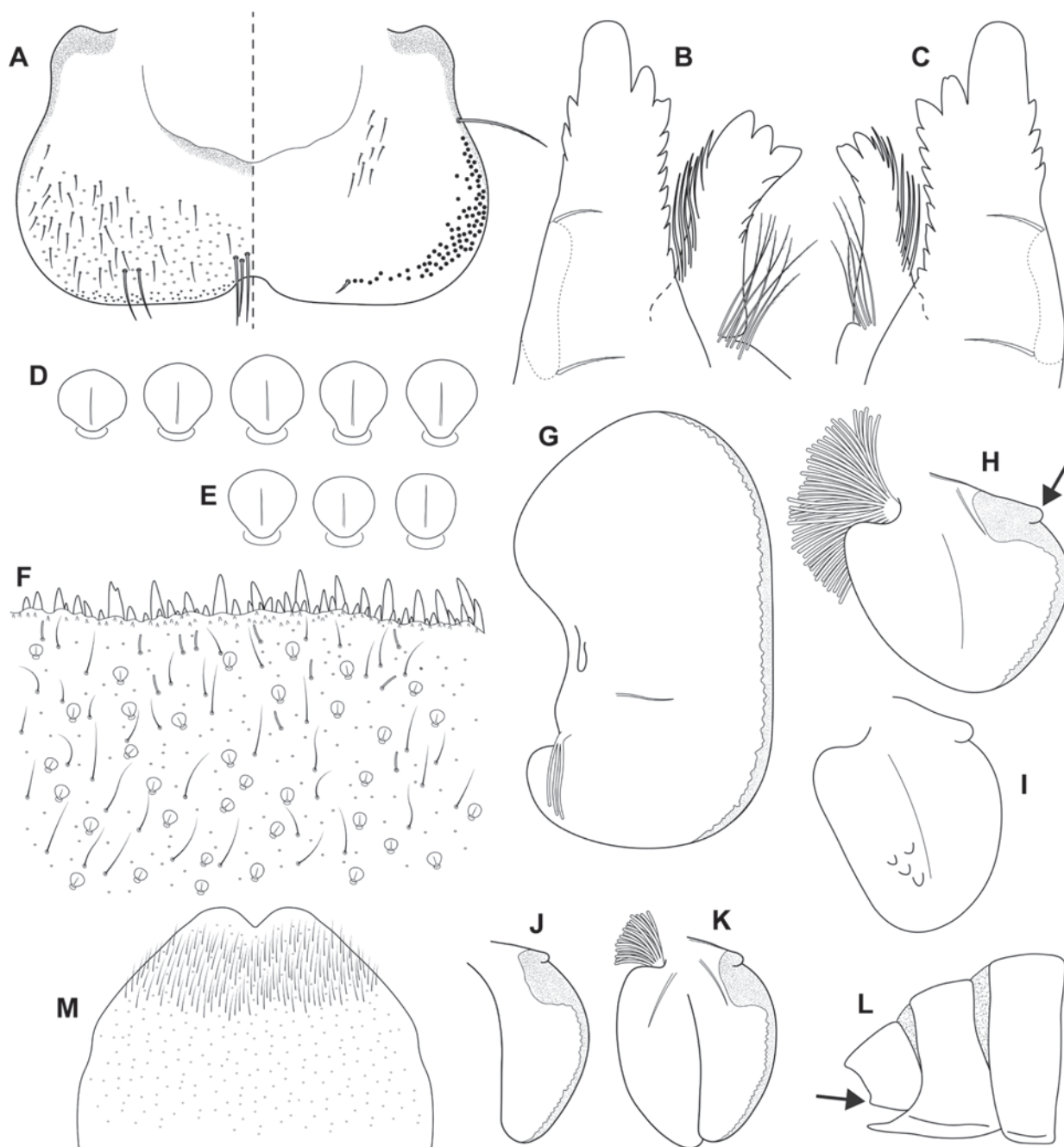


Figure 4. *Epeorus* (*Caucasion*) *himalayensis* sp. nov., larva **A** labrum, left half in dorsal view, right half in ventral view (black dots correspond to setae along antero-lateral margin) **B** incisors of left mandible **C** incisors of right mandible (both flattened on slide; dashed polygons correspond to area covered by setae) **D** setae on dorsal surface of femora **E** setae on surface of tergum VII **F** surface and posterior margin of abdominal tergum VII **G** gill I **H** gill III (arrow shows projection on costal margin) **I** gill plate VI in dorsal view **J** gill plate VII in ventral view **K** gill VII (flattened on slide) **L** abdominal segments VIII–X in lateral view (arrow shows posterolateral projection of tergum X) **M** sternum IX of female. Drawn from late instar larvae and last instar larval exuvium.

Gills. Dorsal surface of gill plate I yellowish and of gill plates II–VII greyish on anterior half, brownish on posterior half. Ventral margin of all gill plates yellowish brown, sometimes pinkish. Projection on gill plate III well developed (Fig. 4H, arrow). Gill plate VII narrow (in natural position of ventral view, Figs 3J, 4J). Dorsal margin of gill plates IV–VII with more or less developed papillae; best expressed on gill plates VI–VII (Fig. 4I).

Cerci. Yellowish brown, basally darkened.

Description of male imago. General coloration yellowish brown with dark brown maculation (Fig. 5A). Body length 11.5–13.0 mm ($n = 2$); length of cerci approximately $2 \times$ body length. Length of fore wings 14.0–15.3 mm, hind wings 4.5–5.1 mm.

Head. Frons yellowish brown; frontal fold dark brown. Antennae yellowish; scapus and pedicellus darkened. Ocelli basally blackish, apically whitish. Compound eyes greyish brown, basally darkened (Fig. 5B, C). Compound eyes not touching each other (distance between eyes 0.10–0.66 of median ocellus; $n = 3$) or touching each other ($n = 1$).

Thorax. Pronotum dark brown; meso- and metathorax yellowish brown with dark brown maculation. Dorsal surface of mesothorax yellowish brown, median longitudinal suture darkened. Mesothoracic fucasternum yellowish brown to brown. Metathorax with blunt posteromedian projection.

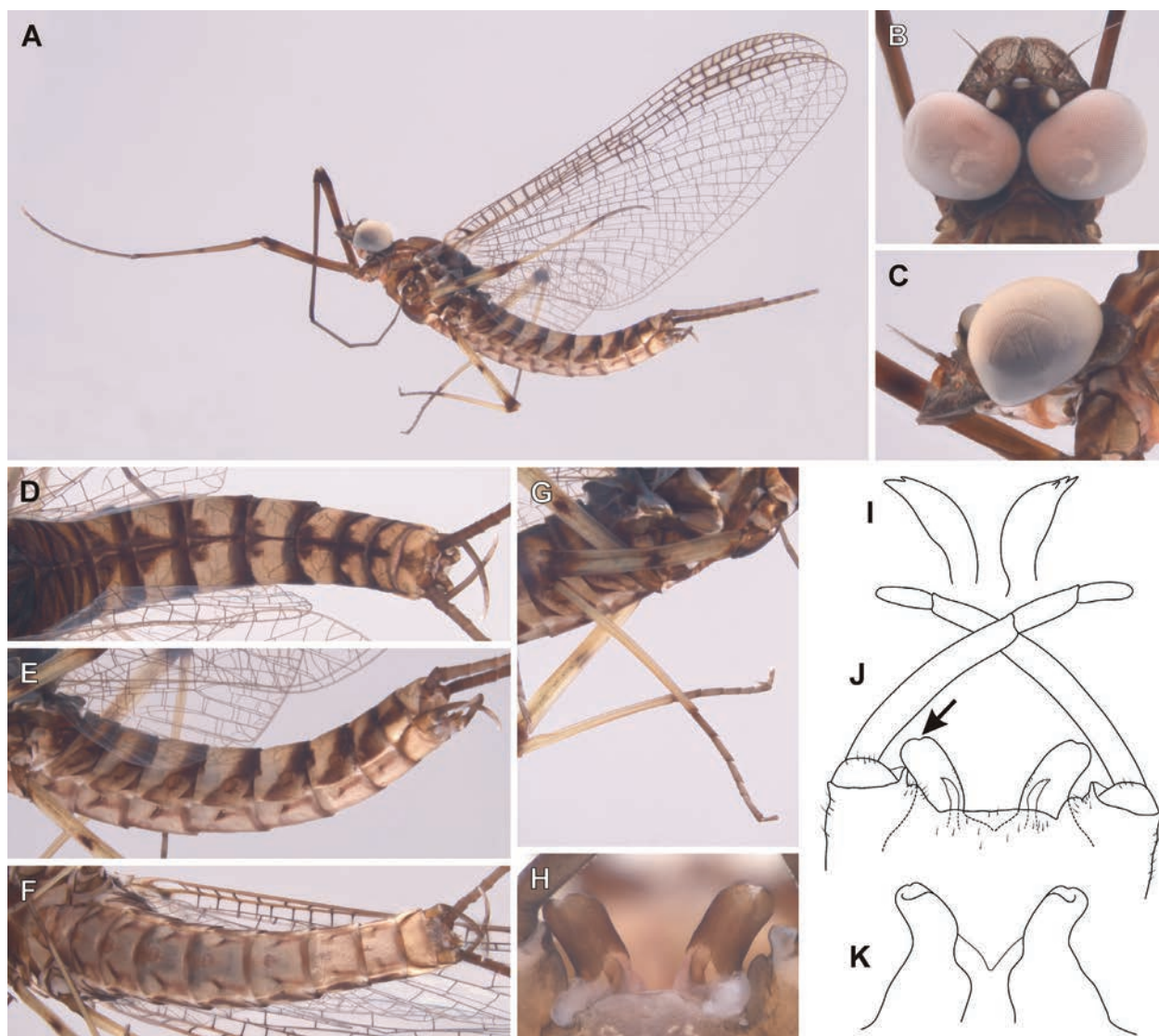


Figure 5. *Epeorus* (*Caucasion*) *himalayensis* sp. nov., male imago **A** habitus in lateral view **B** head in dorsal view **C** head in lateral view **D** abdomen in dorsal view **E** abdomen in lateral view **F** abdomen in ventral view **G** middle leg in dorsal view **H** penis in ventral view **I** titillators **J** male genitalia in ventral view (arrow points on shallow medio-apical emargination) **K** penis in dorsal view.

Wing membrane colorless. Veins dark brown, basally paler. Pterostigmatic area cloudy, with simple cross veins. Costal brace dark brown (Fig. 5A). Hind wings with short triangular costal projection.

Femora basally and apically darkened, median spot present. Tibiae basally darkened; claws dark brown (Fig. 5A, G). Fore legs darker than middle and hind legs. One claw blunt, one claw pointed.

Abdomen. Color pattern of abdominal terga as described in larva. Tergum X with median macula (Fig. 5D). Lateral margins with oblique stripe-like maculae on terga I–IX extending dorso-posteriorly, forming transversal stripe-like macula along posterior margin of terga (Fig. 5D, E). Abdominal sterna with narrow triangular maculae (Fig. 5F). Styliger yellowish brown; medially slightly convex and sparsely covered by hair-like setae (Fig. 5H, J). Forceps brown or yellowish, apically paler. Penis lobes brown and basally paler or yellowish, with shallow medio-apical notch (Fig. 5H, J, arrow), and short spine-like setae on interior edges. Titillators well developed and apically serrated (Fig. 5H, I). Titillators reach 0.30–0.44 of respective penis lobe length.

Cerci. Yellowish, basally darkened.

Description of female imago. General coloration yellowish brown with dark brown maculation (Fig. 6A). Body length 13.0–15.5 mm ($n = 2$); length of cerci $2.3 \times$ body length. Length of fore wings 18.2–19.5 mm, hind wings 5.6–6.3 mm.

Head. Frons yellowish brown; frontal fold brownish. Antennae yellowish; scapus and pedicellus darkened. Ocelli basally blackish, apically whitish. Eyes greyish (Fig. 6B, C).

Thorax. Coloration as described in male imago. Wing membrane colorless (area around bullae sometimes darkened; Fig. 6A). Veins dark brown, basally paler. Pterostigmatic area cloudy, with mostly simple cross veins. Costal brace dark brown. Hind wings with short triangular costal projection. Coloration of legs as in male imago.

Abdomen. Coloration pattern of abdominal terga and sterna as in male imago (Fig. 6D–F). Subgenital plate apically narrowed, posterior margin rounded or slightly concave (Fig. 6G–I). Subanal plate with shallow U-shaped median emargination.

Description of eggs. Oval shaped, dimensions approximately $188 \times 101 \mu\text{m}$ (average values from 6 eggs). Chorionic surface slightly granulated (Fig. 6K), without distinct structures. One or two visible micropyle, shallow and rounded, located in subequatorial position ($\sim 12.5 \mu\text{m}$ in width) (Fig. 6J, K).

Main morphological diagnostics of larva. i) abdominal sterna with more or less defined triangular maculae (Fig. 3K–N), ii) coloration of abdominal terga as on Fig. 3F, G, iii) femora with median spot (Fig. 3H, I), iv) gill plates VII narrow (in natural position from ventral view; Figs 3J, 4J), v) tergum X with short posterolateral projections (Fig. 4L, arrow), vi) abdominal terga and dorsal surface of femora with rounded spatulate setae (Fig. 4D–F); denticles along posterior margin of abdominal terga dense, irregular and pointed (Fig. 4F).

Main morphological diagnostics of imago. i) abdominal sterna with narrow triangular maculae (Figs 5F, 6F), ii) coloration of abdominal terga as on Figs 5D, E, 6D, E, iii) femora with median spot (Fig. 5G), iv) wing membrane colourless (Figs 5A, 6A) (area of bullae sometimes darkened in female), v) subgenital plate of female rounded or slightly concave (Fig. 6G–I), vi) subanal plate with shallow median emargination (Fig. 6H, I), vii) penis lobes not apically widened,

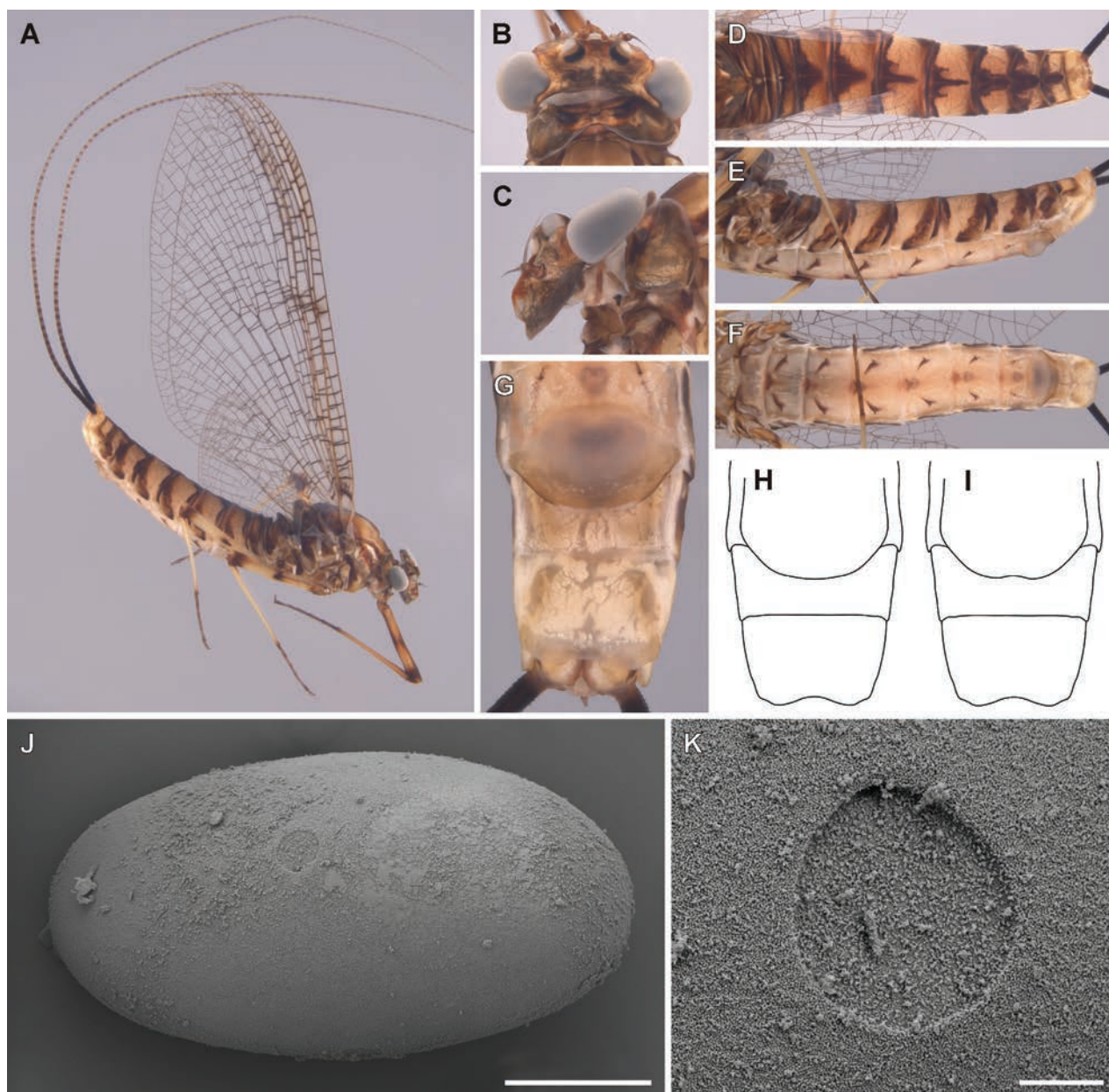


Figure 6. *Epeorus* (*Caucasion*) *himalayensis* sp. nov., female imago and egg **A** habitus in lateral view **B** head in dorsal view **C** head in lateral view **D** abdomen in dorsal view **E** abdomen in lateral view **F** abdomen in ventral view **G–I** subgenital and subanal plates **J** egg **K** detail of micropyle. Scale bars: 5 μ m (**K**); 50 μ m (**J**).

with shallow medio-apical notch (Fig. 5J, arrow), viii) titillators well developed, apically serrated, reaching to 0.30–0.44 of penis lobes in length (Fig. 5H, J).

Morphological affinities. Larva. *Epeorus* (*C.*) *himalayensis* sp. nov. is characterised by more or less defined triangular maculae on the abdominal sterna (Fig. 3K–M). This feature distinguishes *E. (C.) himalayensis* sp. nov. from *E. (C.) guttatus*, with a pair of oblique stripes and a large median macula (Fig. 13H), and *E. (C.) extraordinarius*, with a longitudinal reddish-brown median macula (Chen et al. 2010). The triangular maculae on abdominal sterna of *E. (C.) himalayensis* sp. nov. may be narrowed (Fig. 3N). Similar oblique stripes are present in *E. (C.) lanceolatus* sp. nov. (Fig. 7F) and *E. (C.) lineatus* sp. nov. (Fig. 10Q). *E. (C.) himalayensis* sp. nov. can be distinguished from these species based on rounded spatulate setae on abdominal terga, which are lanceolate in

E. (C.) lanceolatus sp. nov. (Fig. 8E, F) and elongated spatulate in *E. (C.) lineatus* sp. nov. (Fig. 11E, F). In addition, *E. (C.) himalayensis* sp. nov. differs from the latter species by the absence of a median longitudinal line on abdominal sterna (or posteromedian macula; Fig. 10N–Q). The combination of all morphological characters that distinguish *E. (C.) himalayensis* sp. nov. from both related species are given in the section “Main morphological diagnostics of the larva”.

Three other species occur within the eastern part of (*E.*) *Caucasion* range (Fig. 1), which may belong to *E. (Caucasion)* based on the morphology of larvae. Of these, *E. suspicatus* possess oblique stripes on abdominal sterna (Fig. 15I). However, this species has sparse larger denticles separated by shorter denticles along the posterior margin of abdominal terga (Fig. 16F), in contrast to dense, irregular, and pointed denticles (Fig. 4F) in *E. (C.) himalayensis* sp. nov. Denticulation along abdominal terga separates *E. (C.) himalayensis* sp. nov. also from *E. psi*, with basally denticulate spines and shorter denticles (Fig. 18F). Additionally, *E. (C.) himalayensis* sp. nov. differs by a short dorso-apical projection on femora (Fig. 3H, I) from *E. psi* with an elongate and pointed dorso-apical projection on femora (Figs 17F, 18M).

Morphological characters separating *E. kapurkripalanorum* from *E. (C.) himalayensis* sp. nov. are given in the section “Remarks on *Iron paraguttatus* (Braasch, 1983) and *E. kapurkripalanorum* (Braasch, 1983)”. Considering *E. (Caucasion)* species from the western part of the area, *E. (C.) himalayensis* sp. nov. can be easily distinguished by the shape of setae on abdominal terga. It is characterised by rounded spatulate setae, while the extralimital species have fine or basally widened hair-like setae (Hrivniak et al. 2020b).

Imago. In the eastern part of *E. (Caucasion)* area, adults of four species have been described so far, namely *E. (C.) guttatus* (male and female), *E. (C.) extraordinarius* (male and female), *E. psi* (male and female) and *E. (C.) lanceolatus* sp. nov. (female). *E. (C.) himalayensis* sp. nov. can be distinguished from them by the colouration pattern of abdominal sterna, each consisting of a narrow triangular macula (Fig. 6F). This is in contrast to *E. (C.) guttatus* with a pair of oblique stripes and large median macula (Kluge 2015), *E. (C.) extraordinarius* with a longitudinal reddish-brown median macula (Chen et al. 2010) and *E. (C.) lanceolatus* sp. nov. with fine, slightly curved oblique stripes (Fig. 9F). From the latter species, *E. (C.) himalayensis* sp. nov. can be separated also by a shallow emargination on the posterior margin of subanal plate in female imago (Fig. 6G–I), which contrasts with the straight posterior margin in *E. (C.) lanceolatus* sp. nov. (Fig. 9H, I).

Based on male genitalia, *E. (C.) himalayensis* sp. nov. differs from *E. (C.) guttatus* by longer titillators, reaching at least 1/3 of the penis lobes (Fig. 5H, J), in contrast to short titillators not exceeding styliger in *E. (C.) guttatus* (Kluge 2015). The shape of penis lobes with a shallow medio-apical notch allows *E. (C.) himalayensis* sp. nov. to be distinguished from *E. psi*, which has apically bifurcated penis lobes with extended latero-apical tip (Eaton 1883–1888; Braasch 2006b).

Among the extralimital species, *E. (C.) nigripilosus* and *E. (C.) caucasicus* show similar coloration pattern of abdominal sterna. *Epeorus (C.) himalayensis* sp. nov. can be distinguished from them by relatively narrow penis lobes with a shallow medio-apical notch, because both species have apically widened penis lobes and a deeper medio-apical notch (Braasch 1979).

***Epeorus* (*Caucasion*) *lanceolatus* Hrivniak & Sroka, sp. nov.**

<https://zoobank.org/4DFD1C17-701E-4BEF-9793-00F79F574355>

Figs 7–9

Type material. Holotype: • female larva (barcoded specimen: IN6 - labrum, leg and tergum VII mounted on slide): INDIA Uttarakhand Pradesh, vicinity of Lambagad village, Alaknanda River, 1998 m a.s.l.; 30°38.64198'N, 79°32.02500'E (codes: IND2018/8; 40Gang); 9–11.05.2018, Martynov A.V., Palatov D. M. leg.

Paratypes: • 1 larva (barcoded specimen: IN2 - labrum, mandibular incisors and tergum VII mounted on slide), 1 female imago (reared from larva; barcoded specimen: L38 - larval exuvium mounted on slide): same data as holotype.

Etymology. The species name *lanceolatus* (Latin) refers to lanceolate setae on abdominal terga and dorsal surface of femora characteristic for larvae.

Description of larva. General coloration yellowish brown with dark brown to blackish maculation (Fig. 7). BL of late-instar larva 13.87 mm (female; $n = 1$); male unknown. Length of cerci unknown.

Head. Shape oval to trapezoidal (Fig. 7A). Head dimensions of late-instar larva: length 3.5 mm, width 5.7 mm (female; $n = 1$), male unknown. Head width/length ratio: 1.53 (female; $n = 1$), male unknown. Coloration pattern of dorsal surface consists of: i) paired stripe-like and rounded maculae along epicranial suture, ii) pair of triangular (or blurred) maculae near inner edges of eyes, iii) pair of rounded maculae ventrally to lateral ocelli, iv) pale stripes extending from lateral ocelli to lateral edges of head, v) blurred or rectangular maculae between ocelli, vi) scattered maculae ventrally to median ocellus. Antennae yellowish brown, scapus and pedicellus darkened. Dorsal surface of head densely covered with elongated lanceolate setae (as on abdominal terga; Fig. 8E, F), fine hair-like setae and stick-like setae. Sparse longer and fine hair-like setae located posteriorly to eyes.

Mouthparts. Labrum (Fig. 8A) widened anteriorly; anterior margin slightly rounded or straight. Lateral angles rounded. Dorsal surface sparsely covered with setae of different size, five or six longer bristle-like setae located antero-medially, and two bristles antero-laterally (Fig. 8A, left half). Epipharynx with longer, slightly plumose bristles situated along lateral to anterior margin, cluster of fine, hair-like setae medially (not figured), and group of 4–6 setae of various size (Fig. 8A, right half). Outer incisors of both mandibles with three apical teeth; outer tooth blunt in both mandibles. Inner incisor of left mandible with three apical teeth (Fig. 8B), right inner incisor bifurcated (Fig. 8C).

Thorax. Prothorax anteriorly narrowed, lateral edges slightly rounded. Metanotum with small blunt posteromedian projection. Dorsal surface covered with hair-like setae, stick-like setae, and lanceolate setae (as on abdominal terga and head, Fig. 8E, F); sparse longer, hair-like setae along pro-, meso- and metanotal suture.

Legs. Coloration on Fig. 7B. Femora with medial hypodermal spot, often transversely extended. Base and apex of femora darkened; patella-tibial suture darkened; tarsi proximally and distally darkened. Dorsal surface of femora covered by lanceolate setae, hair-like setae, and sparsely distributed stick-like setae (Fig. 8E; drawn from late-instar larvae and last instar larval exuvium). Dorsal edge of femora with blade-like setae. Dorsal margin of tibiae and tarsi with row of dense hair-like setae; ventral margin with irregular row of distally accumulated spines. Tarsal claws with 3–4 denticles.

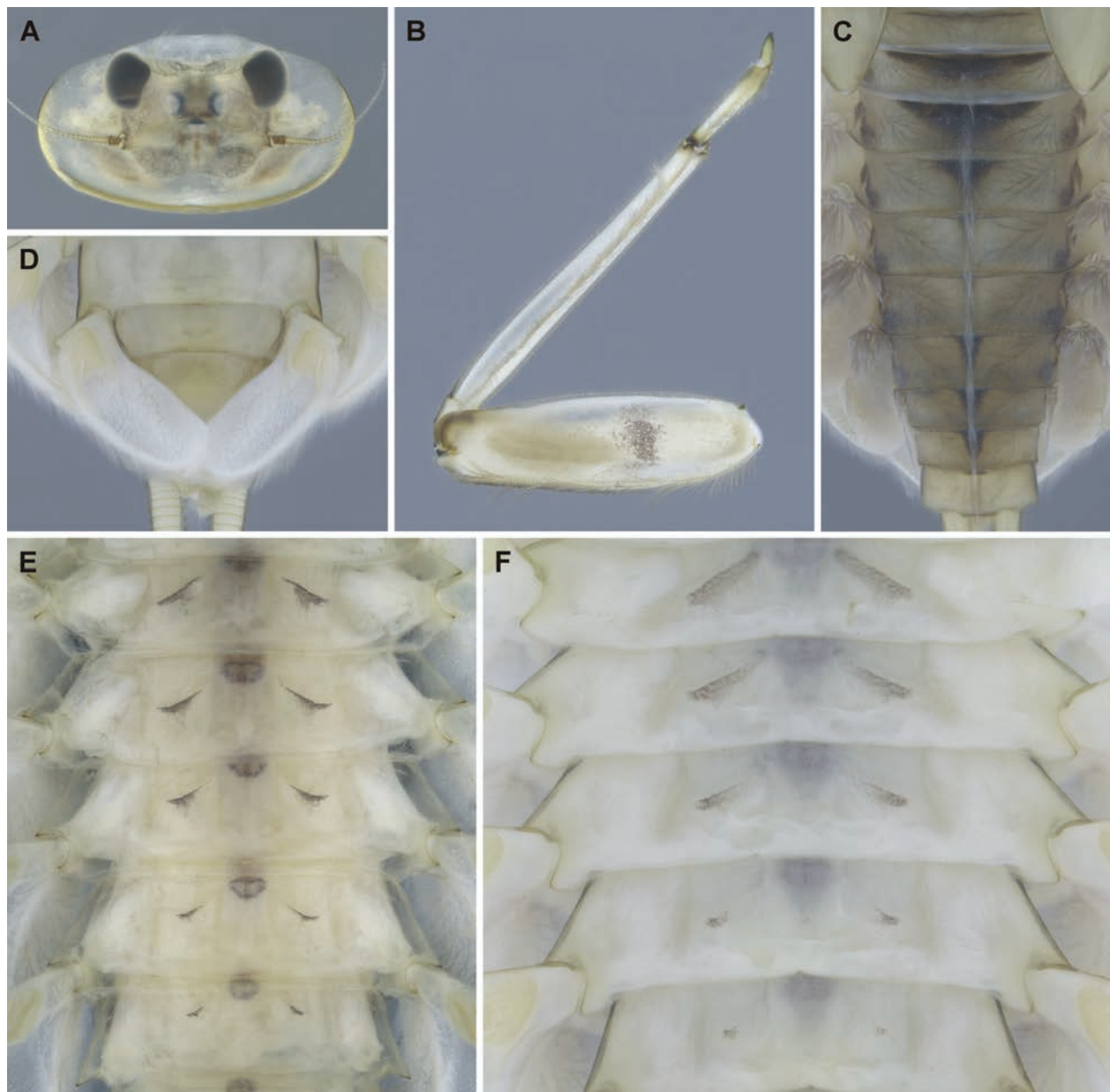


Figure 7. *Epeorus* (*Caucasion*) *lanceolatus* sp. nov., larva **A** head of female in dorsal view (holotype) **B** fore leg in dorsal view **C** coloration of abdominal terga **D** distal part of abdomen in ventral view **E, F** coloration of abdominal sterna II–VI (**E** holotype).

Abdominal terga. Colour pattern of abdominal terga consists of transverse stripe along anterior margin of terga I–IX (X) medially extending to: i) triangular macula on terga II–IV, ii) T-shaped macula on terga V–VI (VII), and iii) triangular macula on terga (VII) VIII–IX (Fig. 7C). Pair of short stripes sometimes present antero-laterally to median macula. Lateral margins with oblique stripe-like maculae on terga I–IX. Denticles along posterior margin on terga dense, relatively narrow, irregular, and pointed (Fig. 8F). Surface of terga covered with hair-like setae, stick-like setae, and lanceolate (sporadically narrow spatulate) setae (Fig. 8E, F; drawn from late-instar larvae and last instar larval exuvium). Tergum X with well-developed posterolateral projections (Fig. 8L, M, arrow). Terga with longitudinal median row of hair-like setae. Tergal spines not observed in late-instar larvae and larval exuvium from reared adult.

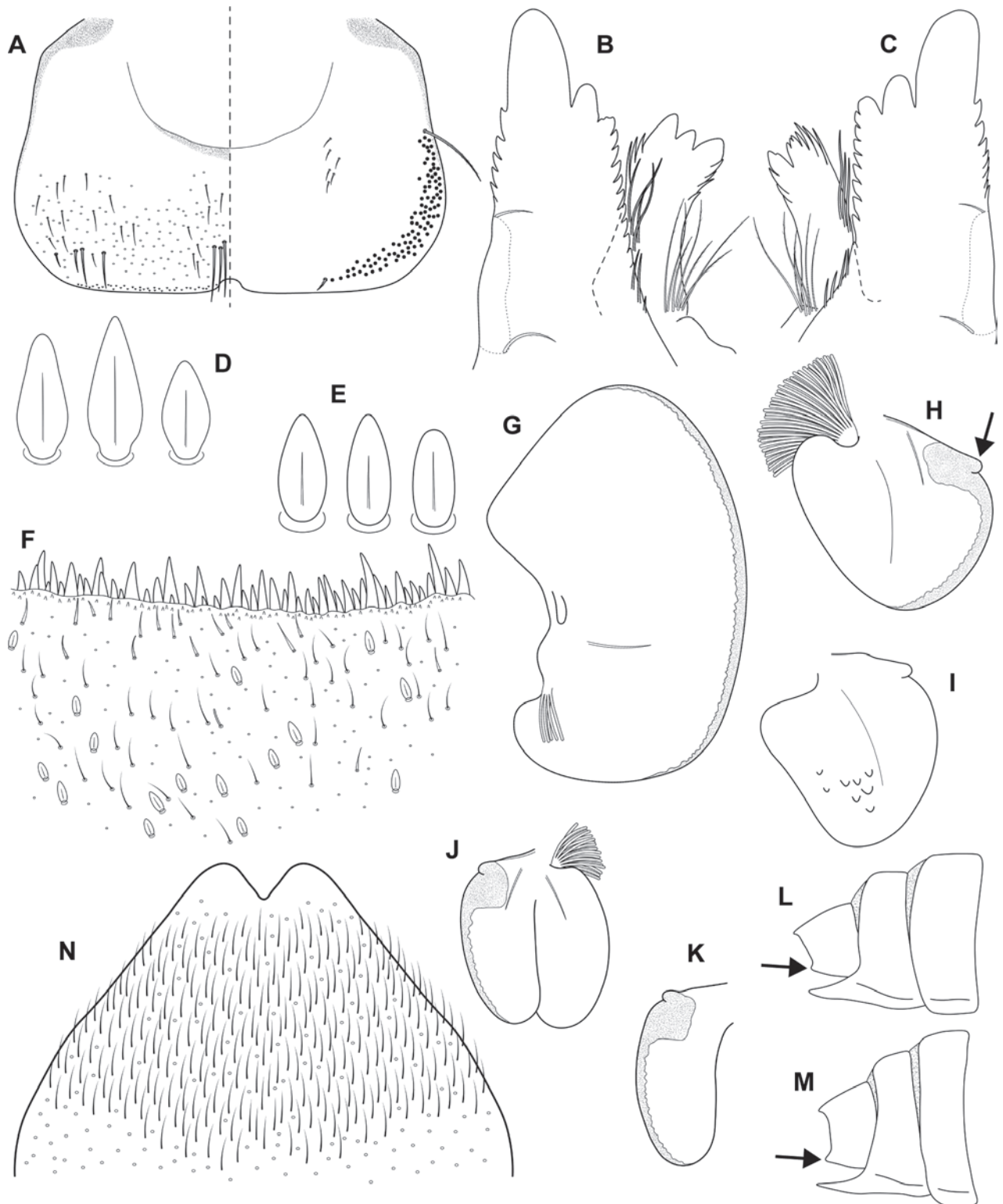


Figure 8. *Epeorus* (*Caucasion*) *lanceolatus* sp. nov., larva **A** labrum, left half in dorsal view, right half in ventral view (black dots correspond to setae along antero-lateral margin) **B** incisors of left mandible **C** incisors of right mandible (both flattened on slide; dashed polygons correspond to area covered by setae) **D** setae on dorsal surface of femora **E** setae on surface of tergum VII **F** surface and posterior margin of abdominal tergum VII (holotype) **G** gill I **H** gill III (arrow shows projection on costal margin) **I** gill plate VI in dorsal view **J** gill VII (flattened on slide) **K** gill plate VII in ventral view **L, M** abdominal segments VIII–X in lateral view (arrow shows posterolateral projection of tergum X) **N** sternum IX of female. Drawn from late instar larva and last instar larval exuvium.

Abdominal sterna. Yellowish, with fine oblique stripes (slightly curved in late-instar larvae; Fig. 7E, F). Nerve ganglia darkened. Sternum IX of female with V-shaped median emargination and numerous hair-like setae (Fig. 8N).

Gills. Dorsal surface of gill plate I yellowish; of gill plates II–VII brownish on anterior half, greyish to brownish on posterior half. Ventral margin of all gill plates yellowish. Projection of gill plate III well developed (Fig. 8H, arrow). Gill plate VII narrow (in natural position of ventral view, Figs 7D, 8K). Dorsal margin of gill plates IV–VII with more or less developed papillae; best expressed on gill plates VI and VII (Fig. 8I).

Cerci. Yellowish brown, basally darkened.

Description of female imago. General coloration yellowish brown with dark brown to blackish maculation (Fig. 9A–F). Body length 14.0 mm ($n = 1$); length of cerci unknown. Length of fore wings 17.5 mm, length of hind wings unknown (broken).

Head. Frons brownish; frontal fold dark brown (Fig. 9B, C). Antennae yellowish brown; scapus and pedicellus darkened. Eyes greyish, ocelli basally blackish, apically whitish.

Thorax. Prothorax dark brown. Mesothorax yellowish brown; median longitudinal suture darkened. Metathorax with short posterior-median blunt projection. Furcasternum dark brown. Wing membrane of fore wings in subimago cloudy, cross veins darkened (Fig. 9A); hind wings unknown. Femora apically and basally darkened; median spot present (Fig. 9G). Tibiae apically and basally darkened, tarsi brownish. One claw blunt, one claw pointed.

Abdomen. Coloration pattern of abdominal terga similar as in late-instar larvae (Fig. 9 D–F). Tergum X with medial macula. Lateral margins with oblique stripe-like maculae on terga I–IX extending dorso-posteriorly, forming transversal stripe-like macula along posterior margin of terga (Fig. 9D, E). Abdominal sterna with fine, slightly curved oblique stripes (Fig. 9F). Nerve ganglia darkened. Subgenital plate posteriorly narrowed, posterior margin slightly rounded. Subanal plate posteriorly narrowed; posterior margin straight (Fig. 9I).

Cerci. Unknown.

Description of eggs. Oval shaped, dimensions approximately $186 \times 110 \mu\text{m}$ (average values from 7 eggs). Chorionic surface with texture as on Fig. 9L. One to three visible micropyle shallow and rounded, located in subequatorial position ($\sim 12.5 \mu\text{m}$ in width) (Fig. 9J, K).

Male imago. Unknown.

Main morphological diagnostics of larva. i) abdominal sterna with fine oblique stripes (slightly curved in late-instar larvae; Fig. 7E, F), ii) coloration of abdominal terga as on Fig. 7C, iii) femora with femur spot (Fig. 7B), iv) dorsal surface of femora with lanceolate setae (Fig. 8D), v) abdominal terga with lanceolate (sporadically narrow spatulate) setae (Fig. 8E, F), vi) tergum X with well-developed posterolateral projections (Fig. 8L, M, arrow), vii) gill plates VII narrow (in natural position from ventral view; Figs 7D, 8K), viii) denticles along posterior margin of abdominal terga dense, relatively narrow, irregular and pointed (Fig. 8F).

Main morphological diagnostics of imago (female). i) abdominal sterna with fine, slightly curved oblique stripes (Fig. 9F), ii) femora with a median spot (Fig. 9G), iii) wing membrane colourless, iv) subgenital plate posteriorly slightly rounded, iv) subanal plate posteriorly straight (Fig. 9H, I).

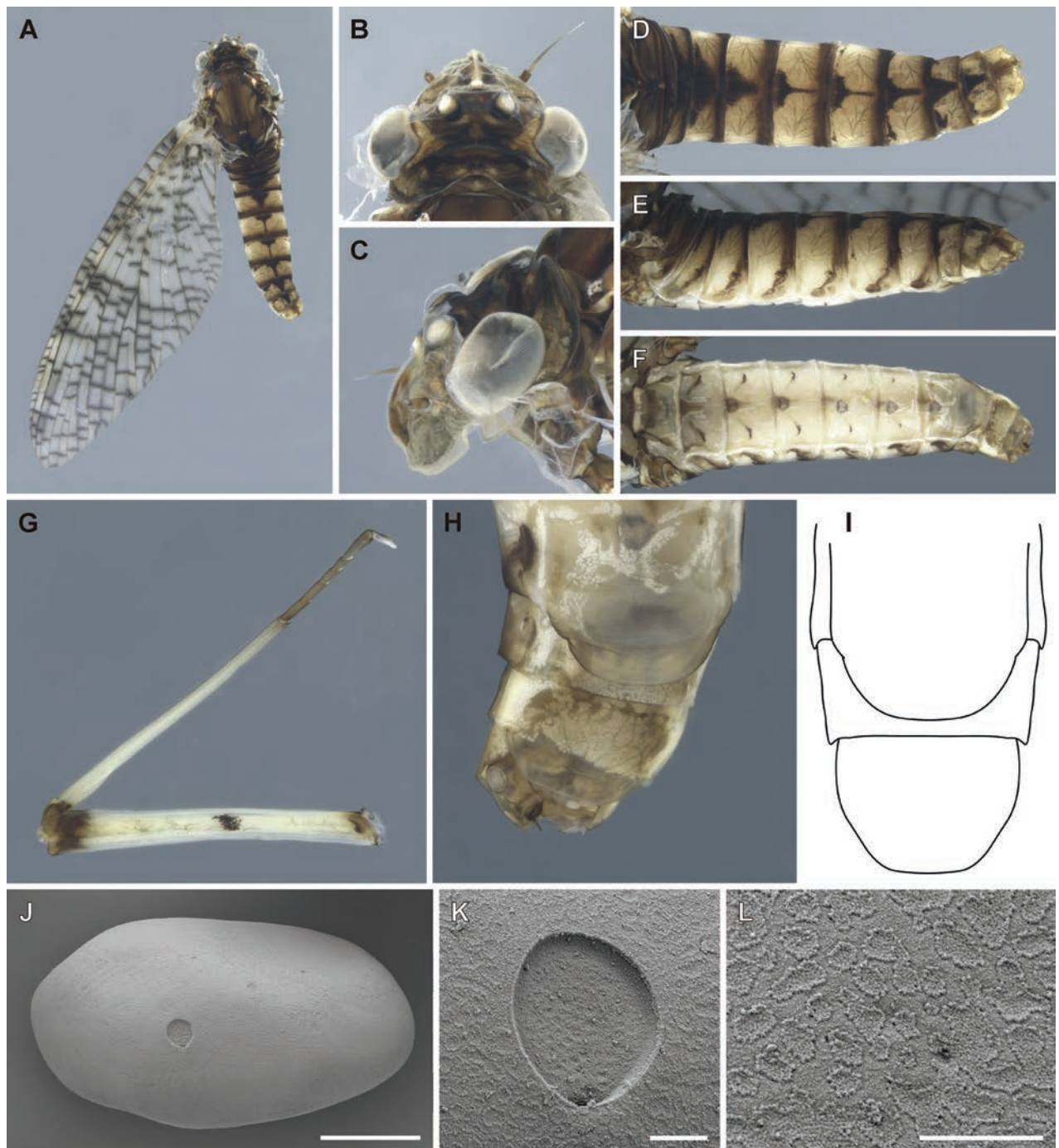


Figure 9. *Epeorus (Caucasiron) lanceolatus* sp. nov., female imago (wing and head not fully molted from subimago) **A** habitus in dorsal view **B** head in dorsal view **C** head in lateral view **D** abdomen in dorsal view **E** abdomen in lateral view **F** abdomen in ventral view **G** middle leg **H, I** subgenital and subanal plates **J** egg **K** detail of micropyle **L** texture on the surface of egg. Scale bars: 50 μ m (**J**); 5 μ m (**K, L**).

Morphological affinities. Larva. *Epeorus* (C.) *lanceolatus* sp. nov. is characterised by lanceolate setae on the dorsal surface of femora and abdominal terga (Fig. 8D, E). This trait, together with the remaining seven traits, given above distinguishes the species from all *E. (Caucasiron)* species described so far and also from *E. suspicatus*, whose attribution to the subgenus *Caucasiron* is uncertain (Figs 15, 16). Similar lanceolate setae on the dorsal surface of femora are present in *E. psi* (Fig. 18D). *Epeorus* (C.) *lanceolatus* sp. nov.

differs from this species by dense, relatively narrow, irregular, and pointed denticles along the posterior margin of abdominal terga (Fig. 8F) and by a short dorso-apical projection of femora (Fig. 7B), in contrast to *E. psi* with basally denticulate spines and shorter denticles along abdominal terga (Fig. 18F) and an elongated pointed dorso-apical projection of femora (Figs 17F, 18M). The characters distinguishing *E. kapurkripalanorum* from *E. (C.) lanceolatus* sp. nov. are given in the section “Remarks on *Iron paraguttatus* (Braasch, 1983) and *E. kapurkripalanorum* (Braasch, 1983)”.

Female imago. The presence of the fine, slightly curved oblique stripes on abdominal sterna (Fig. 9F) separates *E. (C.) lanceolatus* sp. nov. from *E. (C.) guttatus*, with a pair of oblique stripes and a large median macula on abdominal sterna (Kluge 2015), *E. (C.) extraordinarius*, with an longitudinal reddish brown median macula on abdominal sterna (Chen et al. 2010), *E. (C.) himalayensis* sp. nov., with narrow triangular maculae (Fig. 6F) and *E. psi*, with a fine longitudinal median line (sometimes reduced anteriorly) and a pair of oblique stripes on abdominal sterna (Eaton 1883–1888). In addition, *E. (C.) lanceolatus* sp. nov. can be distinguished from *E. (C.) himalayensis* sp. nov. by the straight posterior margin of subanal plate (Fig. 9H, I), in contrast to *E. (C.) himalayensis* sp. nov. with a shallow emargination (Fig. 6G–I).

Among the extralimital species, *E. (C.) caucasicus* and *E. (C.) nigripilosus* show similar coloration pattern on abdominal sterna (Braasch 1979). However, the female imagoes of both species have not been described, thus female genitalia cannot be compared with *E. (C.) lanceolatus* sp. nov. *Epeorus (C.) lanceolatus* sp. nov. can be separated by fine and slightly curved oblique stripes on abdominal sterna (Fig. 9F), in contrast to *E. (C.) caucasicus* and *E. (C.) nigripilosus* with well pigmented pattern (Braasch 1979). Moreover, both species are geographically restricted to the western part of the *E. (Caucasion)* range (Hrivniak et al. 2020b).

***Epeorus (Caucasion) lineatus* Hrivniak & Sroka, sp. nov.**

<https://zoobank.org/6698815A-1AEE-4174-9573-91B5747B3DD8>

Figs 10, 11

Type material. Holotype: • female larva: INDIA: Uttarakhand Pradesh, vicinity of Badrinath town, Rishi Ganga River, right tributary of Alaknanda River, 3141 m a.s.l.; 30°44.44800'N, 79°29.34600'E; (codes: IND2018/9; 41Gang); 12–13.05.2018, Martynov A.V., Palatov D.M. leg. **Paratypes:** • 27 larvae (barcoded specimens: L39, SP31, SP32; three larvae mounted on slide): same data as holotype. • 5 larvae (barcoded specimens: IN5 - mounted on slide, SP21, SP23): INDIA: Uttarakhand Pradesh, vicinity of Lambagad village, Alaknanda River, 1998 m a.s.l.; 30°38.64198'N, 79°32.02500'E (codes: IND2018/8, 40Gang); 9–11.05.2018, Martynov A.V., Palatov D.M. leg. • 1 larva (barcoded specimen: GU2 - mounted on slide): TAJIKISTAN: Gorno-Badakhshan Autonomous Region, Roshtqal'a District, left tributary of Badamdara River, 3070 m a.s.l.; 37°07.70617'N, 071°50.52000'E (code: 252Tj); 30.06.2016, Palatov D.M. leg.

Etymology. The species name *lineatus* (Latin) refers to a median line on abdominal sterna characteristic for larvae.

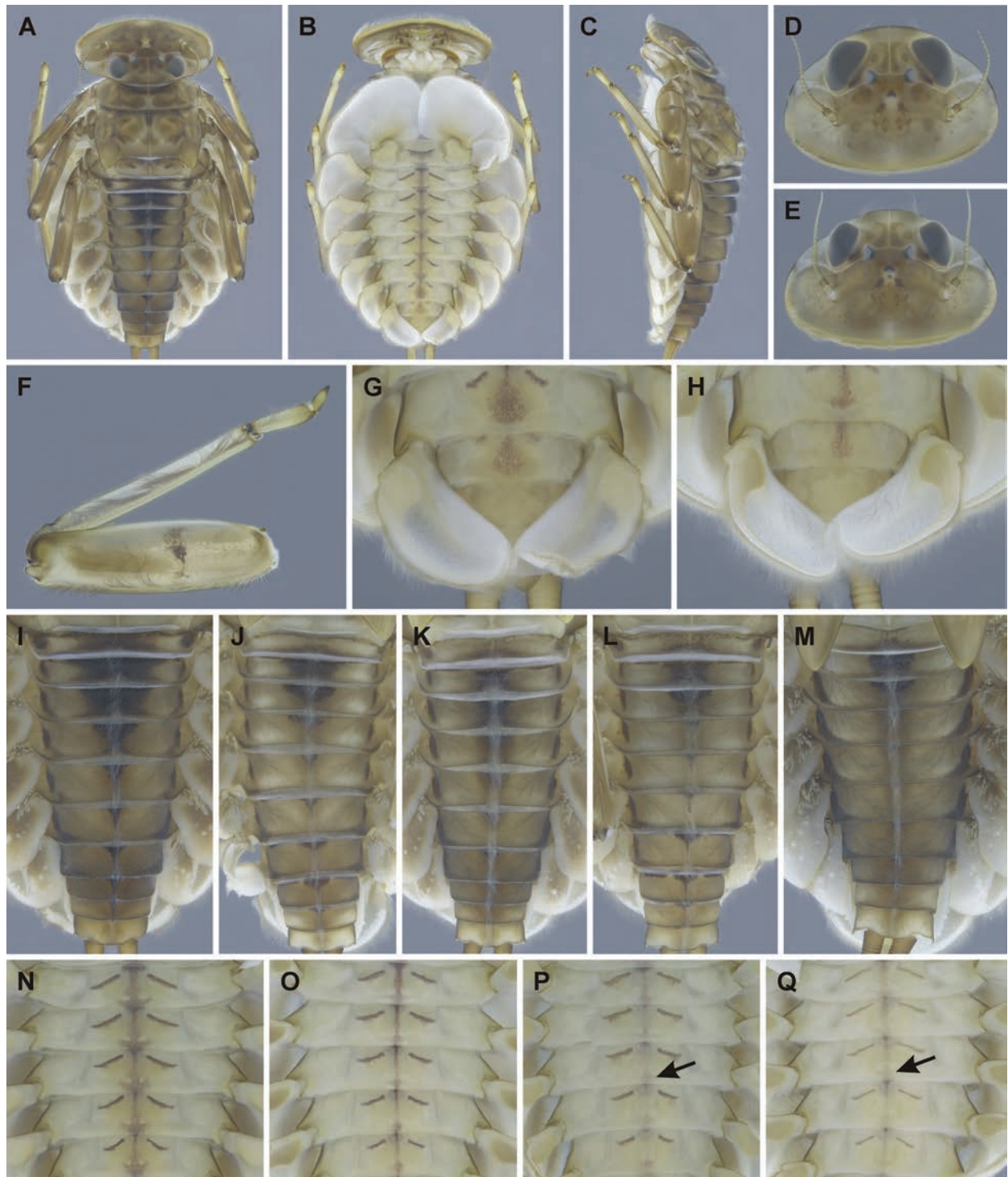


Figure 10. *Epeorus* (*Caucasiron*) *lineatus* sp. nov., larva **A** habitus in dorsal view **B** habitus in ventral view **C** habitus in lateral view **D** head of male in dorsal view **E** head of female in dorsal view **F** middle leg in dorsal view **G**, **H** distal part of abdomen in ventral view **I–M** coloration of abdominal terga **N–Q** coloration of abdominal sterna II–VI.

Description of larva. General coloration yellowish brown with dark brown to blackish maculation (Fig. 10). Body length of late-instar larva unknown. Maximum body length of examined larvae 14.0 mm (female), 9.30 mm (male). Length of cerci $\sim 1.2 \times$ body length.

Head. Shape trapezoidal (Fig. 10D, E). Head width/length ratio: 1.49–1.56 (female; $n = 6$), 1.50–1.57 (male; $n = 2$). Coloration pattern of dorsal surface con-

sists of: i) paired stripe-like and rounded maculae along epicranial suture, ii) pair of triangular (or blurred) maculae near inner edges of eyes, iii) pair of rounded maculae ventrally to lateral ocelli, iv) pale stripes extending from lateral ocelli to lateral edges of head, v) rectangular or blurred macula between ocelli, vi) scattered smaller maculae ventrally to median ocellus. Antennae yellowish brown, scapus and pedicellus darkened. Dorsal surface covered with elongated spatulate setae (as on abdominal terga; Fig. 11E), fine hair-like setae and stick-like setae. Sparse longer and fine hair-like setae located posteriorly to eyes.

Mouthparts. Labrum (Fig. 11A) widened anteriorly; anterior margin slightly rounded or nearly straight. Lateral angles rounded. Dorsal surface sparsely covered with setae of different size, 5–6 longer bristle-like setae located antero-medially, and two bristles antero-laterally (Fig. 11A, left half). Epipharynx with longer, slightly plumose bristles situated along lateral to anterior margin, cluster of fine hair-like setae medially (not figured), and 5–9 setae of various size (Fig. 11A, right half). Outer incisors of both mandibles with three apical teeth; outer tooth blunt in both mandibles. Inner incisor of left mandible with three apical teeth (Fig. 11B), right inner incisor bifurcated (Fig. 11C).

Thorax. Prothorax anteriorly narrowed, lateral edges slightly rounded. Metanotum with small blunt posteromedian projection. Dorsal surface covered with hair-like setae, stick-like setae and elongated spatulate setae (as on abdominal terga and head); sparse longer, hair-like setae along pro-, meso-, and metanotal suture.

Legs. Coloration as on Fig. 10F. Femora with medial hypodermal spot, often transversely extended. Base and apex of femora darkened; patella-tibial suture darkened; tarsi proximally and distally darkened. Dorsal surface of femora covered by rounded (sporadically apically narrowed) spatulate setae (Fig. 11D), hair-like setae, and sparsely distributed stick-like setae. Dorsal edge of femora with blade-like setae. Dorsal margin of tibiae and tarsi with row of dense hair-like setae; ventral margin with irregular row of distally accumulated spines. Tarsal claws with 2–3 denticles.

Abdominal terga. Colour pattern of abdominal terga consists of transversal stripe along anterior margin of terga I–IX (X) medially extending to: i) triangular, rounded, or anteriorly and posteriorly widened macula on terga II–IV; and ii) triangular or T-shaped macula on terga V–IX (Fig. 10I–M). Lateral margins with oblique stripe-like maculae on terga I–IX, sometimes dorso-posteriorly extended. Denticles along posterior margin on terga dense, irregular, and pointed (Fig. 11F). Surface of terga covered with hair-like setae, stick-like setae, and elongated (sporadically rounded) spatulate setae (Fig. 11E, F) (dominantly rounded spatulate setae can be present in younger instars). Tergum X with well-developed posterolateral projections (Fig. 11L, arrow). Terga with longitudinal median row of hair-like setae. More or less developed posteromedian spine (most expressed on terga VII–IX (Fig. 11M, N). Posteromedian tergal spine observed only in larvae of BL 4.6–11.2 mm ($n = 22$; barcoded specimens SP21, SP31, L39, SP23, IN5), not observed in larger larvae of BL 11.2–14.0 ($n = 5$; barcoded specimens: GU2, SP32).

Abdominal sterna. Yellowish, with a pattern consisting of oblique stripes and median line extending from anterior to posterior margin (Fig. 10N–Q). Median line often posteriorly widened (Fig. 11N) or reduced to posteromedian macula (Fig. 11P, Q, arrows). Sternum IX of female apically narrowed, with V-shaped median emargination, and numerous hair-like setae (Fig. 11O).

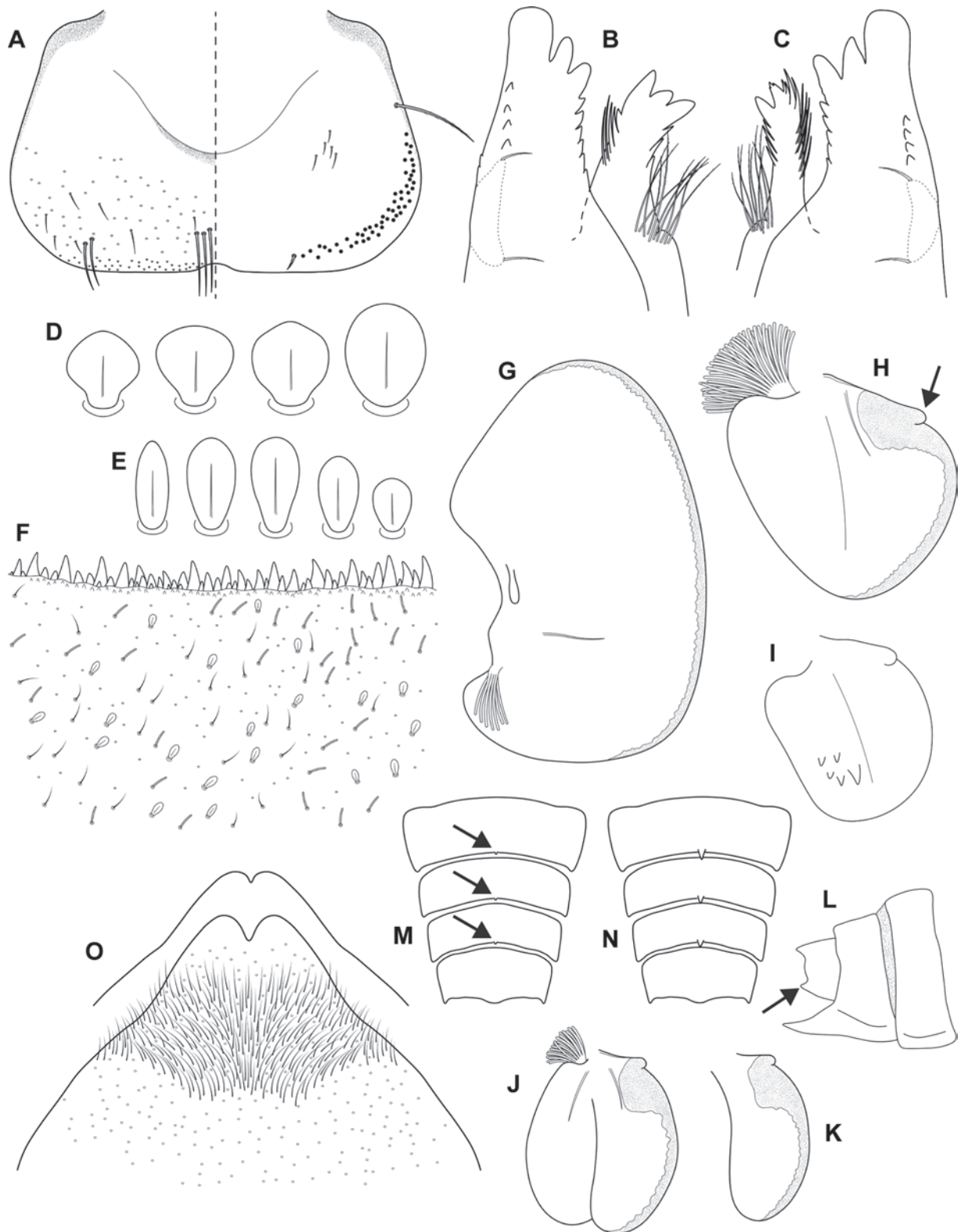


Figure 11. *Epeorus* (*Caucasion*) *lineatus* sp. nov., larva **A** labrum, left half in dorsal view, right half in ventral view (black dots correspond to setae along antero-lateral margin) **B** incisors of left mandible **C** incisors of right mandible (both flattened on slide; dashed polygons correspond to area covered by setae) **D** setae on dorsal surface of femora **E** setae on surface of tergum VII (drawn from late-instar larva) **F** surface and posterior margin of abdominal tergum VII **G** gill I **H** gill III (arrow shows projection on costal margin) **I** gill plate VI in dorsal view **J** gill plate VII (flattened on slide) **K** gill plate VII in ventral view **L** abdominal segments VIII–X in lateral view (arrow shows posterolateral projection of tergum X) **M** abdominal terga VIII–X with short spines (arrows) **N** abdominal terga VIII–X with well-developed spines **O** sternum IX of female. Drawn from late instar larvae.

Gills. Dorsal surface of gill plate I yellowish; of gill plates II–VII brownish. Ventral margin of all gill plates yellowish. Projection of gill plate III well-developed (Fig. 11H, arrow). Gill plate VII wide (in natural position of ventral view, Figs 10G, H, 11K). Dorsal margin of gill plates (III) IV–VII with more or less developed papillae; best expressed on gill plates VI and VII (Fig. 11I).

Cerci. Yellowish brown, basally darkened.

Imagoes and eggs. Unknown.

Main morphological diagnostics of the larva. i) abdominal sterna with oblique stripes and more or less developed median line (Fig. 10N–Q), ii) coloration of abdominal terga as on Fig. 10I–M, iii) femora with median spot (Fig. 10F), iv) gill plates VII wide (in natural position from ventral view; Figs 10G, H, 11K), v) tergum X with well-developed posterolateral projections (Fig. 11L, arrow), vi) abdominal terga with elongated (sporadically rounded) spatulate setae (Fig. 11E, F), vii) dorsal surface of femora with rounded spatulate setae (Fig. 11D), viii) denticles along posterior margin on terga dense, irregular and pointed (Fig. 11F).

Morphological affinities. Larva. Based on the coloration pattern of abdominal sterna consisting of oblique stripes and more or less developed longitudinal median line, *E. (C.) lineatus* sp. nov. can be distinguished from *E. (C.) extraordinarius*, with a longitudinal reddish brown median macula (Chen et al. 2010) and *E. (C.) himalayensis* sp. nov., with more or less defined triangular maculae (Fig. 3K–N). In addition, *E. (C.) lineatus* sp. nov. differs from the latter species by elongated spatulate setae on abdominal terga (Fig. 11E, F) and wide shape of gill plates VII (Figs 10G, H, 11K), in contrast to rounded spatulate setae and narrow gill plates VII in *E. (C.) himalayensis* sp. nov. (Figs 3J, 4J).

Elongated spatulate setae on abdominal terga separate *E. (C.) lineatus* sp. nov. from *E. (C.) lanceolatus* sp. nov., with lanceolate setae on abdominal terga (Fig. 8E). Other characters distinguishing *E. (C.) lineatus* sp. nov. from *E. (C.) himalayensis* sp. nov. and *E. (C.) lanceolatus* sp. nov. are given in the section “Main morphological diagnostics of the larva”.

Epeorus (C.) lineatus sp. nov. is most similar to Central Asian *E. (C.) guttatus*. Both species possess elongated spatulate setae on the dorsal margin of abdominal terga, well-developed posterolateral projection on tergum X, wide gill plates VII and similar coloration of abdominal terga and legs. *Epeorus (C.) lineatus* sp. nov. can be distinguished by the presence of more or less developed longitudinal median line on abdominal sterna (Fig. 10N–Q), in contrast to *E. (C.) guttatus* with large median macula (Fig. 13H). A longitudinal median line in *E. (C.) lineatus* sp. nov. is sometimes posteriorly widened (Fig. 10N). When it is pronounced, reaching oblique stripes, the pattern may resemble that of *E. (C.) guttatus*. This was observed in a specimen collected in Tajikistan (barcoded specimen: GU2).

Epeorus (C.) lineatus sp. nov. differs from other *Epeorus* species, which could represent the subgenus *Caucasion* based on larval morphology (Fig. 1), by dense, irregular, and pointed denticles along posterior margin of abdominal terga (Fig. 11F). *Epeorus suspicatus* possesses sparse larger denticles separated by shorter denticles (Fig. 16F) and *E. psi* basally denticulate spines and short denticles (Fig. 18F). The latter species additionally differs by a long and pointed dorso-apical projection of femora (Figs 17F, 18M). Morphological diagnostics of *E. kapurkripalanorum* are given in the section “Remarks on *Iron paraguttatus* (Braasch, 1983) and *E. kapurkripalanorum* (Braasch, 1983)”.

Epeorus (*C.*) *lineatus* sp. nov. differs from all extralimital species of the subgenus *Caucasiron* by the presence of spatulate setae on abdominal terga, in contrast to fine or basally widened hair-like setae present in *E.* (*Caucasiron*) from the western part of its range (Hrivniak et al. 2020b).

Distribution and habitat of the new *Epeorus* (*Caucasiron*) species

Epeorus (*C.*) *himalayensis* sp. nov. and *E.* (*C.*) *lanceolatus* sp. nov. are currently known only from the western part of the Himalayas in north-west India (Fig. 2). *Epeorus* (*C.*) *lineatus* sp. nov. was recorded in the Himalayas (north-west India) and in the Pamir Mountains in Central Asia (Tajikistan; Fig. 2). All species inhabit mountain streams and rivers with stony bed substrate and predominant riffles with turbulent flow. *Epeorus* (*C.*) *himalayensis* sp. nov. was found between 1998 and 2099 m a. s. l. (Fig. 12A, B), while *E.* (*C.*) *lineatus* sp. nov. occurred in India at altitudes of 1998 and 3141 m a. s. l. and in Tajikistan at 3070 m a. s. l. (Fig. 12B–D). *Epeorus* (*C.*) *lanceolatus* sp. nov. was only found in one river at an altitude of 1998 m a. s. l. (Fig. 12B) and was absent from the smaller streams investigated in the area. Adults of *E.* (*C.*) *himalayensis* sp. nov. and *E.* (*C.*) *lanceolatus* sp. nov. were reared in the field in May.

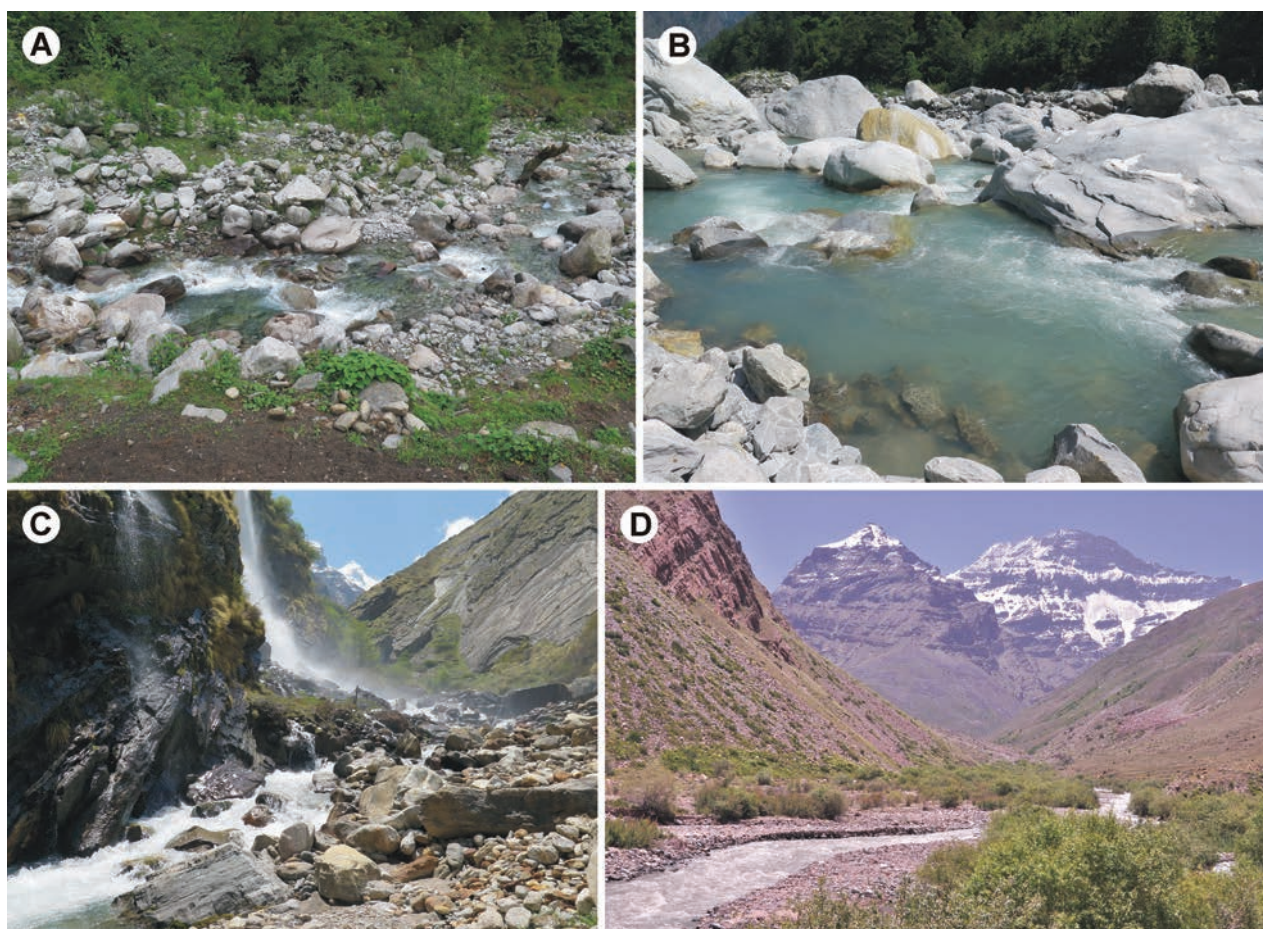


Figure 12. Streams and rivers inhabited by *Epeorus* (*Caucasiron*) spp. in the Himalayas (**A–C**) and the Pamir Mountains (**D**) **A** the type locality of *E.* (*C.*) *himalayensis* sp. nov. **B** locality of *E.* (*C.*) *himalayensis* sp. nov., *E.* (*C.*) *lineatus* sp. nov. and *E.* (*C.*) *lanceolatus* sp. nov. (type locality) **C, D** localities of *E.* (*C.*) *lineatus* sp. nov. (**C** type locality).

Morphological revisions

In this section, we provide the list of main diagnostic characters, drawings, and photographs of previously described species attributable to *E. (Caucasiron)* from our study area (Central Asian mountains and the Himalayas). The subgeneric attribution is regarded as uncertain for *E. suspicatus* and *E. psi* (see below). The purpose of this chapter is to facilitate the direct comparison of all potential *E. (Caucasiron)* species from our study area based on the same set of characters.

Epeorus (Caucasiron) guttatus (Braasch & Soldán, 1979)

Figs 13, 14

Iron guttatus Braasch & Soldán, 1979.

Epeorus (Iron) guttatus (Braasch & Soldán, 1979): Kluge 1988: 296.

Epeorus (Caucasiron) guttatus (Braasch & Soldán, 1979): Kluge 1997: 234.

Iron (Caucasiron) guttatus (Braasch & Soldán, 1979): Braasch 2006b: 87.

Type locality. KAZAKHSTAN: Issyk River near Alma-Ata.

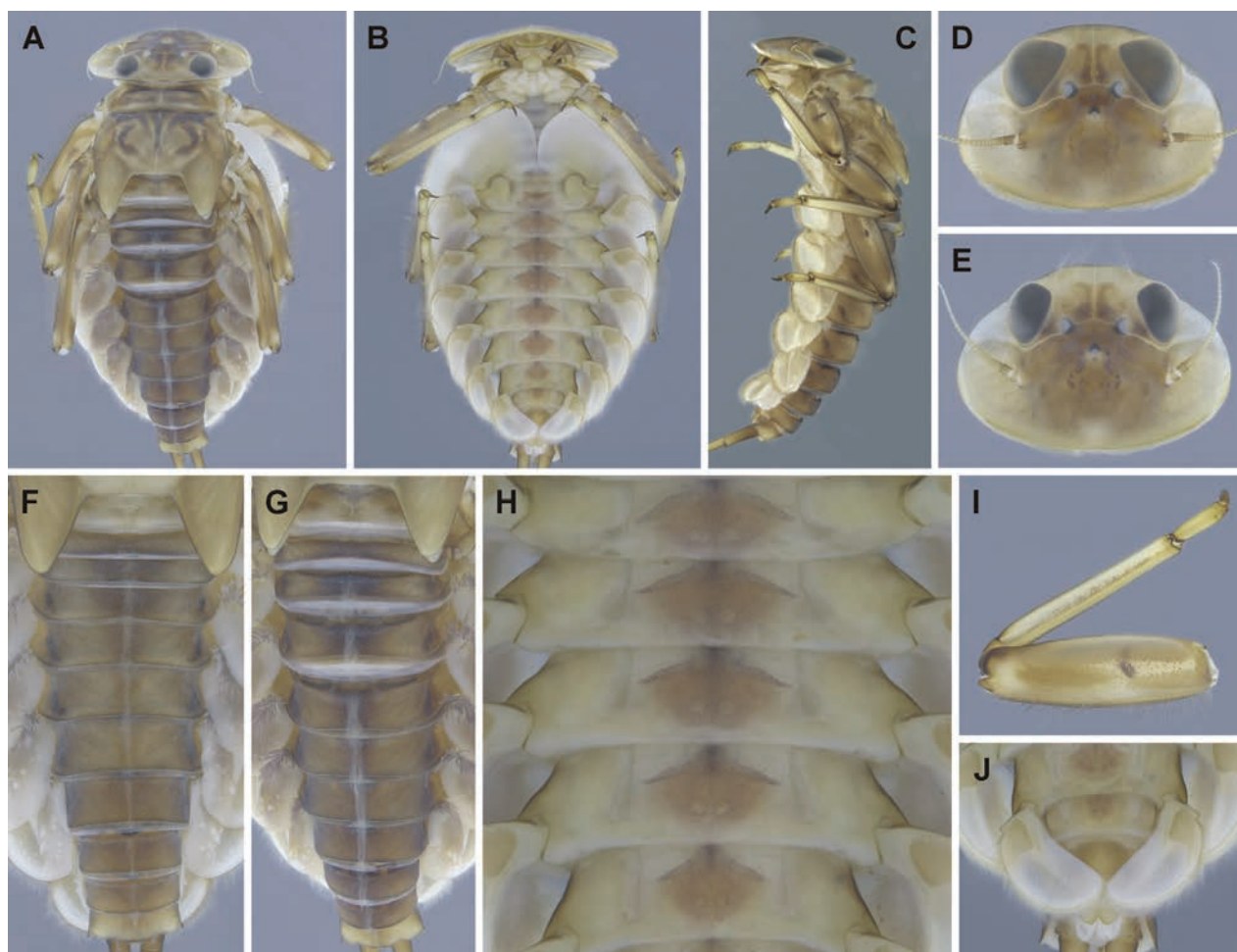


Figure 13. *Epeorus (Caucasiron) guttatus*, larva **A** habitus in dorsal view **B** habitus in ventral view **C** habitus in lateral view **D** head of male in dorsal view **E** head of female in dorsal view **F, G** coloration of abdominal terga **H** coloration of abdominal sterna II–VI **I** middle leg in dorsal view **J** distal part of abdomen in ventral view.

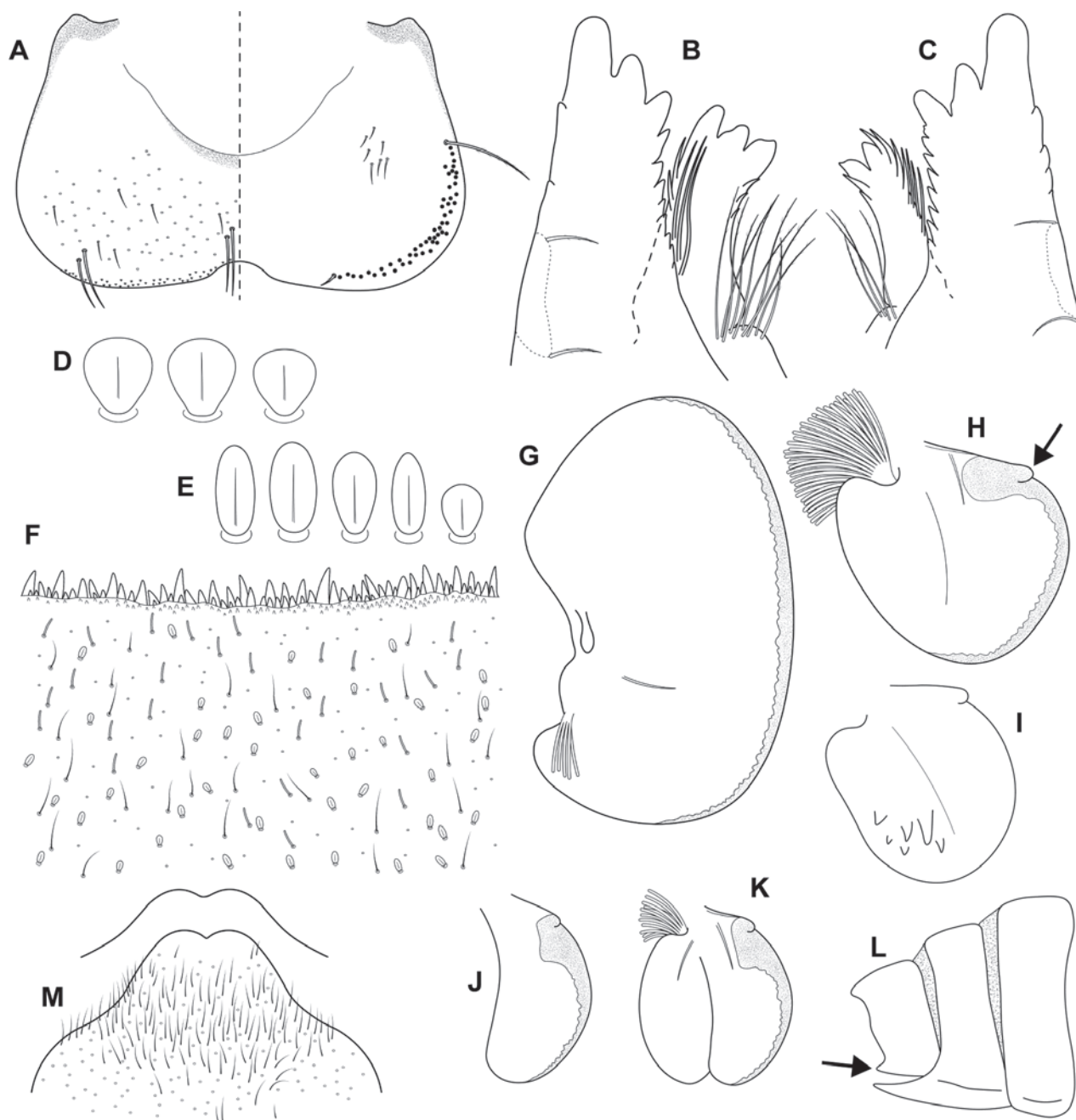


Figure 14. *Epeorus* (*Caucasion*) *guttatus*, larva **A** labrum, left half in dorsal view, right half in ventral view (black dots correspond to setae along antero-lateral margin) **B** incisors of left mandible **C** incisors of right mandible (both flattened on slide; dashed polygons correspond to area covered by setae) **D** setae on dorsal surface of femora **E** setae on surface of tergum VII **F** surface and posterior margin of abdominal tergum VII (paratype) **G** gill I **H** gill III (arrow shows projection on costal margin) **I** gill plate VI in dorsal view **J** gill plate VII in ventral view **K** gill VII (flattened on slide) **L** abdominal segments VIII–X in lateral view (arrow shows posterolateral projection of tergum X) **M** sternum IX of female. Drawn from late instar larvae.

Examined material (deposited in IECA). • 1 larva: paratype from type locality.
 • 1 larva (barcoded specimen: GU3): KYRGYZSTAN: Chuy Region, left tributary of Ala-Archa River, 1717 m a. s. l., 42°37.743'N, 74°29.293'E (code: 1Kyrgyz), 26. 05. 2016, Palatov D.M. leg. • 6 larvae (barcoded specimen: GU71K): KYRGYZSTAN: Osh Region, right tributary of Kulun River, 2060 m a. s. l., 40°29.516'N, 74°09.077'E

(code: 71Kyrgyz), 01. 05. 2017, Palatov D.M. leg. • 3 larvae (barcoded specimen: GU1): KYRGYZSTAN: Osh Region Kara-Bel River, 2135 m. a. s. l., 40°30.300'N, 74°10.621'E (code: 73Kyrgyz), 01. 05. 2017, Palatov D. M. leg.

Distribution, habitat, and biology. Tian Shan: Kazakhstan (Braasch and Soldán 1979; Kluge 2015), Kyrgyzstan; Pamir: Tajikistan (Kluge 2015) (Fig. 1). The species inhabits mountain streams with rapid turbulent flow and bed substrate formed by stones and boulders (Kluge 2015). The altitude of our sampling sites ranged between 1717 and 2135 m a.s.l. Adults were recorded from May to September (Kluge 2015).

Main morphological diagnostics of the larva. i) femora with a median spot (Fig. 13I), ii) abdominal sterna with a pair of oblique stripes and a large median macula (Fig. 13H), iii) coloration of abdominal terga as on Fig. 13F, G, iv) tergum X with a well-developed posterolateral projection (Fig. 14L, arrow), v) dorsal surface of femora with rounded spatulate setae (Fig. 14D), vi) abdominal terga with elongated (sporadically rounded) spatulate setae (Fig. 14E, F), vii) gill plates VII wide (in natural position from ventral view) (Figs 13J, 14J), viii) projection on gill plates III well-developed (Fig. 14H), ix) denticles along posterior margin of abdominal terga dense, irregular, and pointed (Fig. 14F).

Remarks. Morphology. Description of adult stages in Kluge (2015).

***Epeorus* (*Caucasiron*?) *susplicatus* (Braasch, 2006)**

Figs 15, 16

Iron susplicatus Braasch, 2006.

Epeorus (*Caucasiron*) *susplicatus* (Braasch, 2006): Vasanth et al. 2021: 519.

Type locality. NEPAL: Tal, Marshyangdi River (orig. Marsyandi-Tal, Thangja) (2400 m a. s. l.).

Examined material (deposited in SMNS). • 2 larvae: holotype and paratype from type locality. • 1 larva (paratype): NEPAL: Marsyandi-Tal, Bagarchap, ca. 2100 m a. s. l., 21.05.1980, leg. Sivec.

Distribution, habitat, and biology. Himalayas: Nepal and India (Fig. 1). The species inhabits rhithral zones of mountain streams. The altitude of the sampling sites ranged between 2000 and 2400 m a. s. l. Late-instar larvae were recorded in May (Braasch 2006a).

Main morphological diagnostics of the larva. i) abdominal sterna with a pair of oblique stripes and a postero-median macula (Fig. 15I), ii) coloration of abdominal terga as on Fig. 15G, H, iii) posterior margin of abdominal terga with sparse larger denticles separated by shorter denticles (Fig. 16F), iv) tergum X with a short posterolateral projection (Fig. 16L, arrow), v) gill plates VII narrow (in natural position from ventral view) (Figs 15K, L, 16K), vi) projection on gill plates III well-developed (Fig. 16H, arrow), vii) femora with a median spot (Fig. 15F), viii) dorsal surface of femora with rounded spatulate setae (Fig. 16D), ix) abdominal terga with elongated (oval) and rounded spatulate setae (Fig. 16E, F).

Remarks. Morphology. Adult stages undescribed.

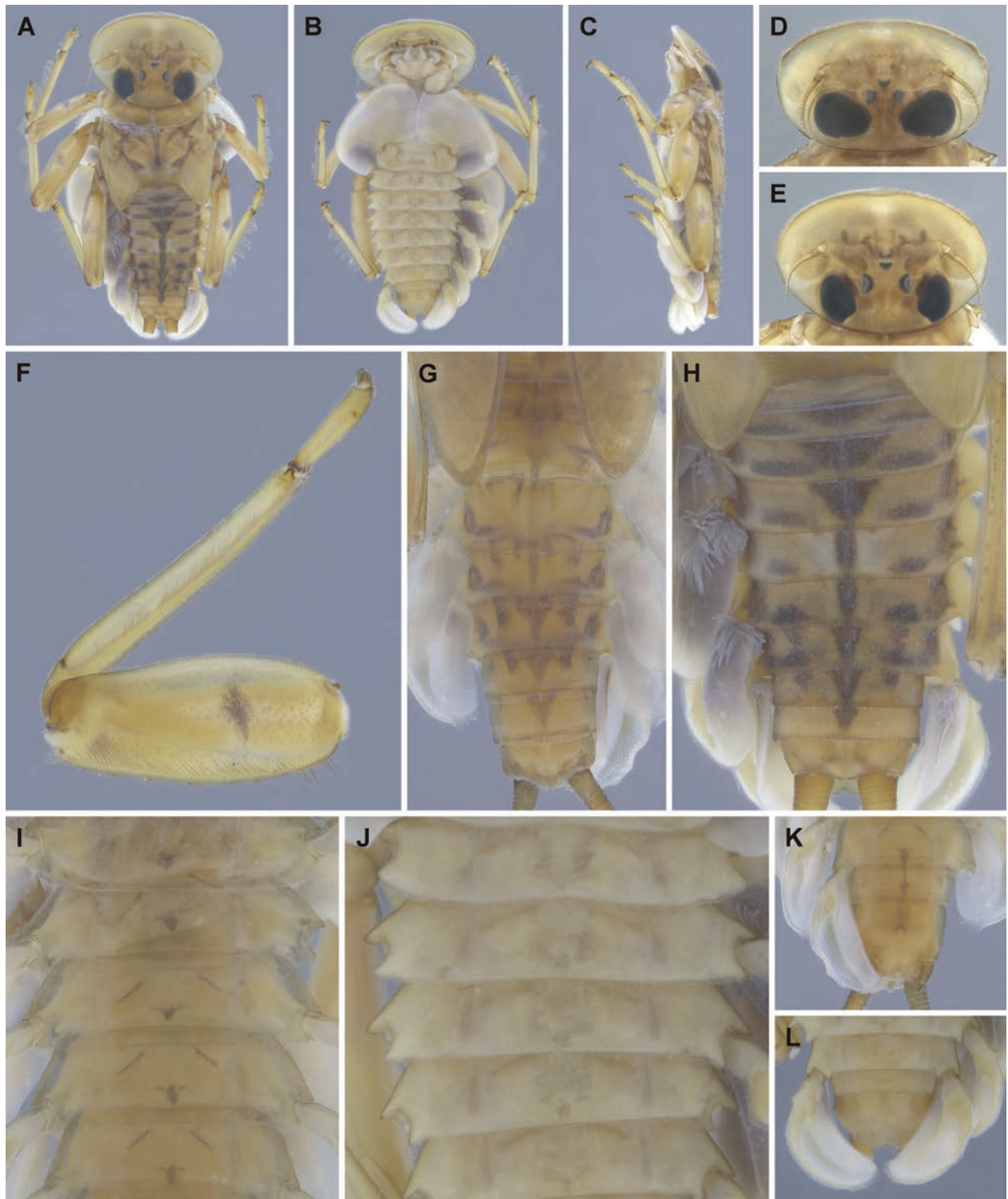


Figure 15. *Epeorus* (*Caucasiron*?) *suspicatus*, larva **A** habitus in dorsal view **B** habitus in ventral view **C** habitus in lateral view **D** head of male in dorsal view (holotype) **E** head of female in dorsal view **F** middle leg in dorsal view **G, H** coloration of abdominal terga (**G** holotype) **I–J** coloration of abdominal sterna II–VI (**I** holotype) **K, L** distal part of abdomen in ventral view (**K** holotype).

Taxonomy. The attribution of the species to the subgenus *E. (Caucasiron)* by Vasanth et al. (2021) was not confirmed by male genitalia or molecular data and hence remains unclear.

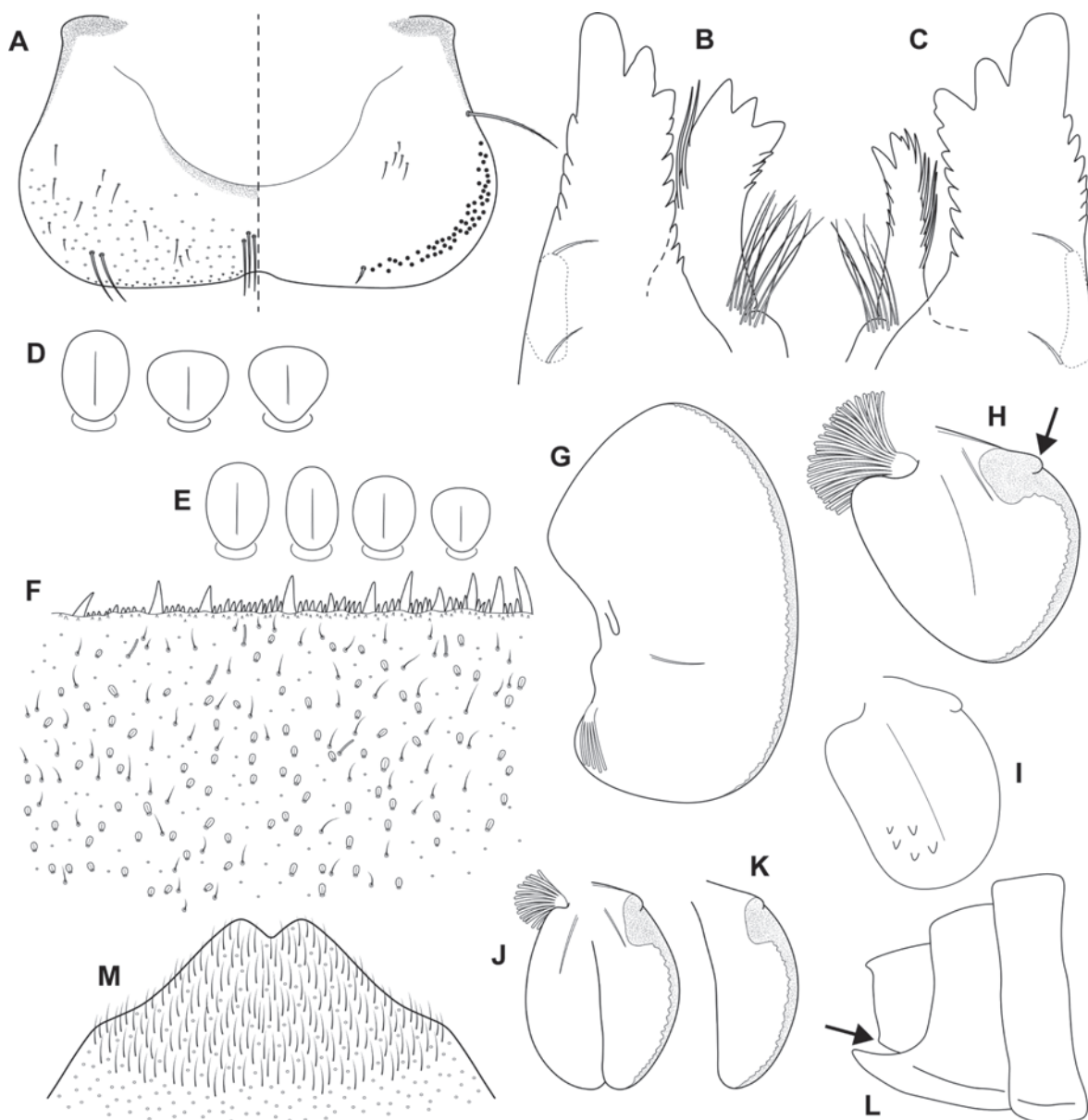


Figure 16. *Epeorus* (*Caucasiron*?) *suspicatus*, larva **A** labrum, left half in dorsal view, right half in ventral view (black dots correspond to setae along antero-lateral margin) **B** incisors of left mandible **C** incisors of right mandible (both flattened on slide; dashed polygons correspond to area covered by setae) **D** setae on dorsal surface of femora **E** setae on surface of tergum VII **F** surface and posterior margin of abdominal tergum VII **G** gill I **H** gill III (arrow shows projection on costal margin) **I** gill plate VI in dorsal view **J** gill plate VII (flattened on slide) **K** gill plate VII in ventral view **L** abdominal segments VIII–X in lateral view (arrow shows indistinct posterolateral projection of tergum X) **M** sternum IX of female. Drawn from late instar larvae.

***Epeorus* (*Caucasiron*?) *psi* (Eaton, 1885)**

Figs 17, 18

Iron psi? (Eaton, 1885): Braasch 1980b: 58.

Epeorus (*Belovius*) *psi* (Eaton, 1885): Tshernova 1981: 332.

Epeorus (*Caucasiron*) *psi* (Eaton, 1885): Vasanth et al. 2021: 516–519.

Type locality. INDIA: Kullu district (orig. Kooloo, Himalaya) (Eaton 1883–1888).

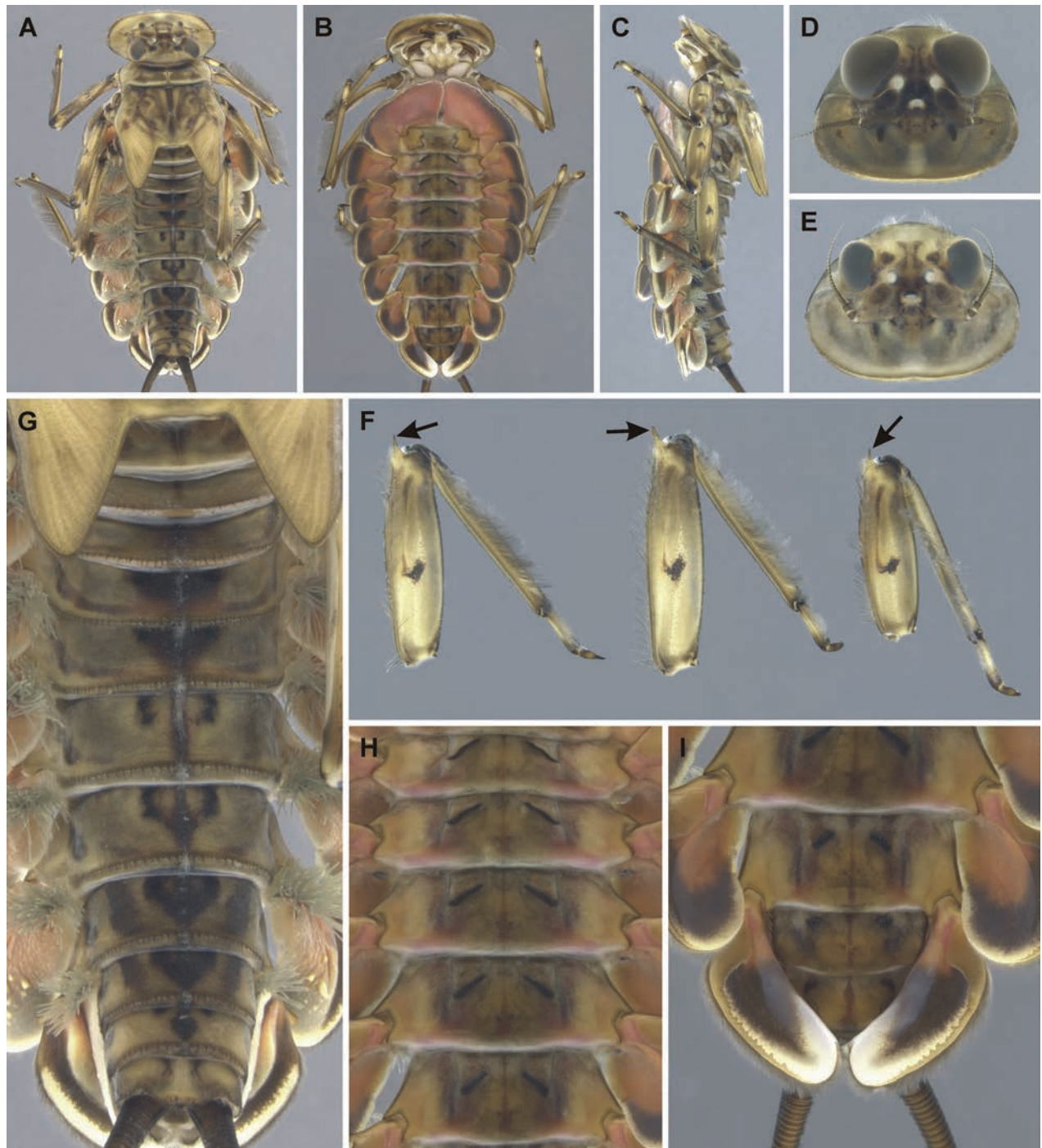


Figure 17. *Epeorus* (*Caucasion*?) *psi*, larva **A** habitus in dorsal view **B** habitus in ventral view **C** habitus in lateral view **D** head of male in dorsal view **E** head of female in dorsal view **F** legs in dorsal view (arrows point to elongated and pointed dorso-apical projections) **G** coloration of abdominal terga **H** coloration of abdominal sterna II–VI **I** distal part of abdomen in ventral view.

Examined material (deposited in IECA and NMNH NASU). • 20 larvae (bar-coded specimens: IN4, IN42 - both mounted on slide), 2 male subimagos (bar-coded specimen: IN44 - genitalia mounted on slide): INDIA: Uttarakhand state, vicinity of Guptkashi town, Madhyamaheshwar Ganga Mandahishvar River – left tributary of Mandakini River, 30°32.27700'N, 79°05.95698'E, 1102 m a.s.l., 15.–16.5.2018, Martynov A.V. leg. (code: IND2018/11). • 5 larvae (bar-coded specimen: IN43 - mounted on slide): INDIA: Uttarakhand Pradesh,

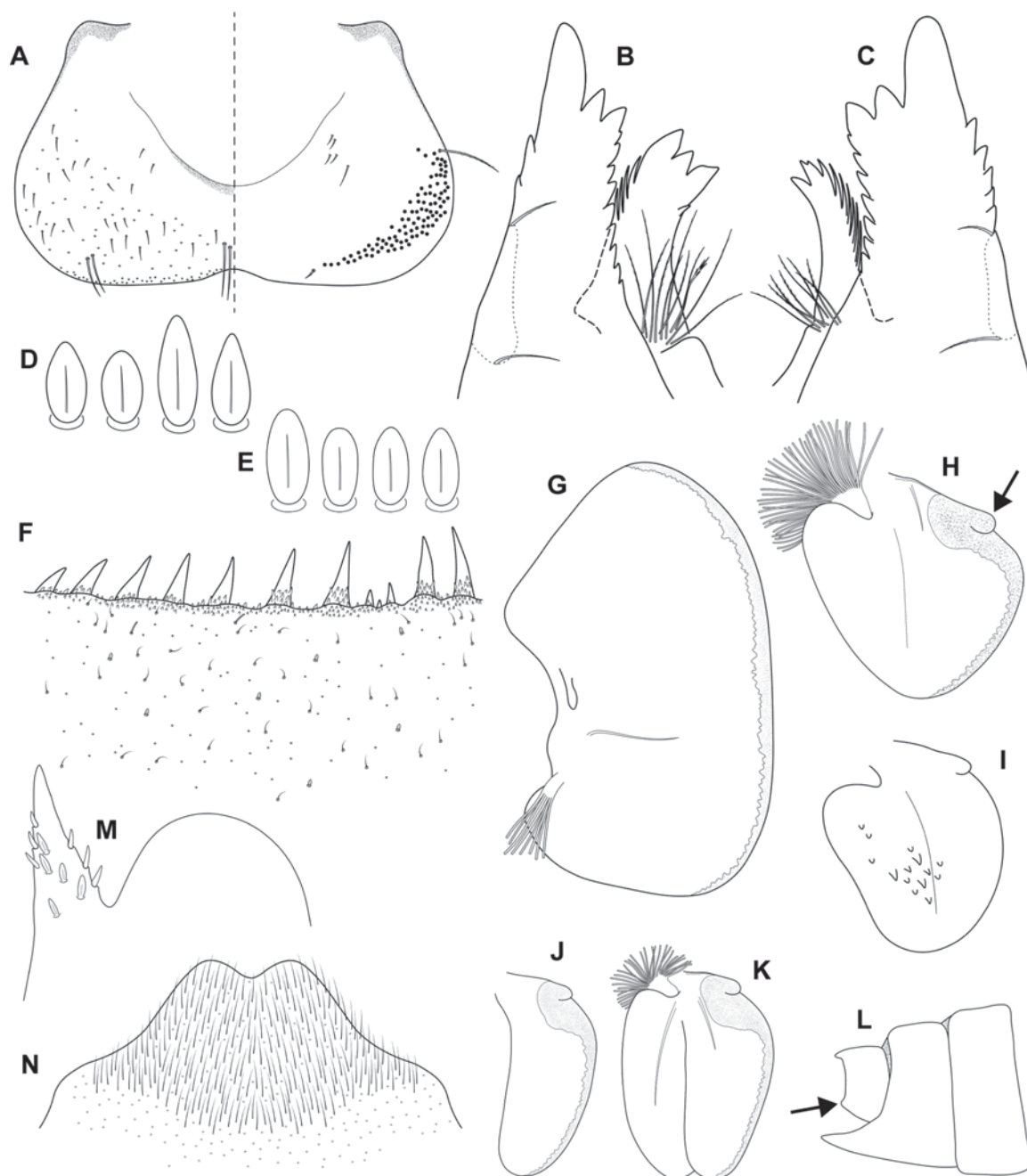


Figure 18. *Epeorus* (*Caucasion*?) *psi*, larva **A** labrum, left half in dorsal view, right half in ventral view (black dots correspond to setae along antero-lateral margin) **B** incisors of left mandible **C** incisors of right mandible (both flattened on slide; dashed polygons correspond to area covered by setae) **D** setae on dorsal surface of femora **E** setae on surface of tergum VII **F** surface and posterior margin of abdominal tergum VII **G** gill I **H** gill III (arrow shows projection on costal margin) **I** gill plate VI in dorsal view **J** gill plate VII in ventral view **K** gill plate VII (flattened on slide) **L** abdominal segments VIII–X in lateral view (arrow shows posterolateral projection of tergum X) **M** detail of dorso-apical projection of femora (middle leg) **N** sternum IX of female. Drawn from late instar larvae.

vicinity of Guptkashi village, Mandakini River, 1087 m a.s.l., 30°32.24700'N, 79°05.73900'E, 16.05.2018, Martynov A.V. leg. (code: IND 2018/12).

Distribution, habitat, and biology. Himalayas: India (Eaton 1883–1888; Vasanth et al. 2021), Nepal (Braasch 1980b, 1981), south-east Tibet (Ma and Zhou 2022); Hengduan Shan and Yunnan-Guizhou Plateau: China (Ma and Zhou 2022) (Fig. 1). The species inhabits mountain streams and rivers in relatively

wide altitudinal range. The altitude of the sampling sites ranged between 488 and 2100 m a.s.l. (our data; Braasch 1980b, 1981; Vasanth et al. 2021). Adults were recorded in May (Braasch 1980b).

Main morphological diagnostics of the larva. i) abdominal sterna with a pair of oblique stripes and a longitudinal median line (sometimes reduced anteriorly) (Fig. 17H), ii) coloration of abdominal terga as on Fig. 17G), posterior margin of abdominal terga with basally denticulate spines and shorter denticles (Fig. 18F), iv) tergum X with a short posterolateral projection (Fig. 18L, arrow), v) gill plates VII narrow (in natural position from ventral view) (Figs 17I, 18J), vi) projection on gill plates III well-developed (Fig. 18H, arrow), vii) femora with median femur spot (Fig. 17F), viii) dorsal surface of femora with lanceolate (sporadically elongated spatulate) setae (Fig. 18D), ix) abdominal terga with elongated spatulate and lanceolate setae (Fig. 18E), femora with an extended and pointed dorso-apical projection (Figs 17F, 18M).

Remarks. Morphology. The species was originally described by Eaton (1883–1888) based on male and female imago. The larva and the male subimago were later described by Braasch (1980b) from Nepal. Association with imagoes of *E. psi* was based on the specific pattern of colouration on abdomen and the shape of penis lobes.

Taxonomy. The species was attributed to the subgenus *Iron* within its own species group “*Iron psi-Gruppe*” (Braasch 1980b, 2006b). Vasanth et al. (2021) examined the morphology of larvae and assigned the species to the subgenus *Caucasiron* based on “the shape of gills II–VII with an outer thumb-like projection”. Although the shape of gill plates II–VII is similar to those of *E. (Caucasiron)*, male genitalia with bifurcated penis lobes and extended latero-apical tip, as figured by Eaton (1883–1888) and described by Braasch (1980b, 2006b), are not consistent with the diagnosis of *E. (Caucasiron)* as given by Kluge (1997, 2015). Therefore, the systematic position of *E. psi* remains unclear until the systematic revision based on molecular data is available.

Distribution. Specimens from Taiwan identified as *E. psi* by Ulmer (1912) were later described as *E. erratus* Braasch, 1981.

Remarks on *E. paraguttatus* (Braasch, 1983) and *E. kapurkripalanorum* (Braasch, 1983)

Two other species from our study area have been assigned to *E. (Caucasiron)* in the literature; however, their systematic position is rather doubtful. Braasch (1981) attributed a single larva, a male and a female imago as well as two female subimagoes from Nepal to *E. (C.) guttatus*. Later, Braasch (1983b) re-evaluated these specimens as a new species that he described as *Iron paraguttatus* Braasch, 1983. The gill plate III of *I. paraguttatus* larvae bears a projection on the costal margin (Braasch 1983b: 196, fig. 2), which corresponds to the diagnosis of the subgenus *Epeorus* (*Caucasiron*). Therefore, the species was classified as *Iron (Caucasiron?) paraguttatus* in Braasch (2006b). However, its subgeneric attribution was marked as uncertain (Kluge 2015), because the male genitalia of the holotype (Braasch 1981: 106, fig. 1r, s, t) possesses penis lobes with a latero-apical spine, which is not consistent with the definition of *E. (Caucasiron)* according to Kluge (1997, 2015). For this reason, we assume that *I. paraguttatus* does not belong to *E. (Caucasiron)* and was excluded from our study.

Assuming from the shape of genitalia as figured in Braasch (1981), *I. paraguttatus* can most likely be attributed to the *montanus* species group within the subgenus *E. (Iron)* (Brodsky 1930; Kluge 2015). Importantly, the larva assigned to *I. paraguttatus* does not belong to the type series of this species. It was collected in different locality than the adults and was associated with them only based on the similarity in the coloration pattern of the abdomen. We assume that the larva represents a different species than the adults described as *I. paraguttatus*. According to the description of Braasch (1981, 1983b), the larva is characterised by: the absence of coloration pattern on abdominal sterna, the presence of a triangular median macula on terga VI–VIII, the shape of the gill plate VII, and the shape of tarsal claws. These larval morphological characters are not consistent with any of the species described herein and it may indicate that another unnamed species of *E. (Caucasiron)* occurs in the Himalayas.

Another problematic species, *Epeorus kapurkripalanorum*, was originally described from the western Himalayas (Spiti Valley) as *Ironopsis* sp. 1. (Kapur and Kripalani 1963). Braasch (1983b) assigned these specimens to the name *Iron kapurkripalanorum* Braasch, 1983, relying solely on the original description and figures from Kapur and Kripalani (1963), but not on the investigation of the material. Vasanth et al. (2021) attributed this species to *E. (Caucasiron)* based on the presence of a projection on the costal margin of gill plates II figured in the original description (Kapur and Kripalani 1969: 213, fig. 14b, c). *Epeorus kapurkripalanorum* was not included in our molecular analyses and morphological investigation due to the lack of available material. As the adult stages are not known, its systematic position in *E. (Caucasiron)* remains unclear. Moreover, the larva was insufficiently described and significant morphological traits necessary for species identification, such as the coloration of abdominal sterna or the shape of setae on the surface of femora and abdominal terga, were not provided. Nevertheless, based on the original description by Kapur and Kripalani (1963) and the statements of other authors (Braasch 2006a; Vasanth et al. 2021), the larva of *E. kapurkripalanorum* differs from all species described here by the absence of a median spot on the dorsal surface of femora, the presence of a median longitudinal dense row of long hair-like setae and distinctly “over-bent” tarsal claw of fore legs (Kapur and Kripalani 1963: 215, fig. 16a, d). The median longitudinal dense row of long hair-like setae and a shallow convexity on the costal margin of gill plates II–VII are characteristic of *E. rheophilus*, which is distributed in Central Asia (Kluge 2015) and the Himalayas (unpublished data). Therefore, it cannot be ruled out that *E. kapurkripalanorum* is related to *E. rheophilus*, rather than to *E. (Caucasiron)*.

Conclusions

Our study confirms that the diversity of *E. (Caucasiron)* in the Central Asian mountains and the Himalayas is higher than previously known. This is supported by the descriptions of three new species, namely *E. (C.) himalayensis* sp. nov., *E. (C.) lanceolatus* sp. nov. and *E. (C.) lineatus* sp. nov., discovered in relatively restricted area in Pamir and the western part of the Himalayas. In addition to the morphological descriptions and DNA barcoding of the new species, we present the main larval diagnostic characters of the already known *E. (C.) guttatus* and two other species, *E. psi* and *E. suspicatus*, possibly related to *E. (Caucasiron)*.

The DNA barcodes for *E. (C.) guttatus* and *E. psi* are provided, which may facilitate direct comparison between the species and the discovery of greater diversity of this mayfly lineage in Central Asia and the Himalayas. The literature review of dubious species indicates that *E. paraguttatus* does not belong to *E. (Caucasion)*. The systematic position of *E. kapurkripalanorum* remains unclear.

Additional information

Conflict of interest

The authors have declared that no competing interests exist.

Ethical statement

No ethical statement was reported.

Funding

The study was funded by the institutional support of Institute of Entomology, Biology Centre of the Czech Academy of Sciences (RVO: 60077344).

Author contributions

Conceptualization: ĽH. Formal analysis: ĽH. Investigation: ĽH. Methodology: ĽH, PS. Resources: AM, DP. Visualization: PS, ĽH, RG. Writing – original draft: ĽH, PS, JB. Review and editing: RG, AV, DP.

Author ORCIDs

Ľuboš Hrivniak  <https://orcid.org/0000-0002-9327-1314>

Pavel Sroka  <https://orcid.org/0000-0003-4367-6564>

Roman J. Godunko  <https://orcid.org/0000-0003-2196-3327>

Alexander V. Martynov  <https://orcid.org/0000-0002-6506-5134>

Jindřiška Bojková  <https://orcid.org/0000-0003-0996-3308>

Data availability

All data are publicly freely available in GenBank database (<https://www.ncbi.nlm.nih.gov>).

References

- Bouckaert R, Vaughan TG, Barido-Sottani J, Duchêne S, Fourment M, Gavryushkina A, Heled J, Jones G, Kühnert D, De Maio N, Matschiner M, Mendes FK, Müller NF, Ogilvie HA, du Plessis L, Popinga A, Rambaut A, Rasmussen D, Siveroni I, Suchard MA, Wu C-H, Xie D, Zhang C, Stadler T, Drummond AJ (2019) BEAST 2.5: An advanced software platform for Bayesian evolutionary analysis. *PLOS Computational Biology* 15(4): e1006650. <https://doi.org/10.1371/journal.pcbi.1006650>
- Braasch D (1978) *Epeorus znojko* Tshernova und *Iron magnus* n. sp. (Heptageniidae, Ephemeroptera) aus dem Kaukasus. *Entomologische Nachrichten* 22(5): 65–70.
- Braasch D (1979) Beitrag zur Kenntnis der Gattung *Iron* Eaton im Kaukasus (UdSSR) (III) (Ephemeroptera, Heptageniidae). *Reichenbachia* 17(33): 283–294.
- Braasch D (1980a) Beitrag zur Kenntnis der Gattung *Iron* Eaton (Heptageniidae, Ephemeroptera) im Kaukasus (UdSSR), 2. *Entomologische Nachrichten* 24(10–11): 166–173.

- Braasch D (1980b) Eintagsfliegen (Gattungen *Epeorus* und *Iron*) aus Nepal (Ephemeroptera, Heptageniidae). Reichenbachia 18: 55–65.
- Braasch D (1981) Eintagsfliegen (Gattungen *Epeorus* und *Iron*) aus Nepal (II) (Ephemeroptera, Heptageniidae). Reichenbachia 19(18): 105–110.
- Braasch D (1983a) Zwei neue Heptageniidae von den griechischen Inseln (Ephemeroptera). Reichenbachia 21(11): 69–74.
- Braasch D (1983b) Eintagsfliegen (Gattungen *Epeorus* und *Iron*) aus Nepal und Indien (Ephemeroptera, Heptageniidae). Reichenbachia 21(34): 195–196.
- Braasch D (2006a) *Iron suspicatus* n. sp. (Ephemeroptera, Heptageniidae) aus Nepal und aus dem Kulu-Valley des Himalaja in Indien. Entomologische Nachrichten und Berichte 50(3): 125–128.
- Braasch D (2006b) Neue Eintagsfliegen der Gattungen *Epeorus* und *Iron* aus dem Himalaja (Ephemeroptera, Heptageniidae). Entomologische Nachrichten und Berichte 50: 79–88.
- Braasch D, Soldán T (1979) Neue Heptageniidae aus Asien (Ephemeroptera). Reichenbachia 17(31): 261–272.
- Braasch D, Zimmermann W (1979) *Iron sinitschenkovi* sp.n. – eine neue Heptageniide (Ephemeroptera) aus dem Kaukasus. Entomologische Nachrichten 23(7): 103–107.
- Brodsky K (1930) Zur Kenntnis der mittelasiatischen Ephemeropteren I. (Imagines). Zoologische Jahrbücher 59: 681–720.
- Chen P, Wang Y, Zhou C-F (2010) A New Mayfly Species of *Epeorus* (*Caucasion*) from Southwestern China (Ephemeroptera: Heptageniidae). Zootaxa 2527: 61–68. <https://doi.org/10.11646/zootaxa.2527.1.4>
- Eaton AE (1881) An announcement of new genera of the Ephemeridae. Entomologist's Monthly Magazine 18: 21–27.
- Eaton AE (1883–1888) A revisional monograph of recent Ephemeridae or mayflies. Transactions of the Linnean Society of London (2) 3: 1–352. <https://doi.org/10.1111/j.1096-3642.1883.tb01550a.x>
- Fujisawa T, Barraclough TG (2013) Delimiting species using single locus data and the generalized mixed yule coalescent approach: a revised method and evaluation on simulated datasets. Systematic Biology 62: 707–724. <https://doi.org/10.1093/sysbio/syt033>
- Hrivniak L, Sroka P, Godunko RJ, Žurovcová M (2017) Mayflies of the genus *Epeorus* Eaton, 1881 s.l. (Ephemeroptera: Heptageniidae) from the Caucasus Mountains: a new species of *Caucasion* Kluge, 1997 from Georgia and Turkey. Zootaxa 4341(3): 353–374. <https://doi.org/10.11646/zootaxa.4341.3.2>
- Hrivniak L, Sroka P, Türkmen G, Godunko RJ, Kazancı N (2019) A new *Epeorus* (*Caucasion*) (Ephemeroptera: Heptageniidae) species from Turkey based on molecular and morphological evidence. Zootaxa 4550(1): 58–70. <https://doi.org/10.11646/zootaxa.4550.1.2>
- Hrivniak L, Sroka P, Bojková J, Godunko RJ, Imanpour Namin J, Bagheri S, Nejat F, Abdoli A, Staniczek AH (2020a) Diversity and distribution of *Epeorus* (*Caucasion*) (Ephemeroptera, Heptageniidae) in Iran, with descriptions of three new species. ZooKeys 947: 71–102. <https://doi.org/10.3897/zookeys.947.51259>
- Hrivniak L, Sroka P, Bojková J, Godunko RJ (2020b) Identification guide to larvae of Caucasian *Epeorus* (*Caucasion*) (Ephemeroptera, Heptageniidae). ZooKeys 986: 1–53. <https://doi.org/10.3897/zookeys.986.56276>
- Hrivniak L, Sroka P, Bojková J, Manko P, Godunko RJ (2021) A new species of *Epeorus* (*Caucasion*) (Ephemeroptera: Heptageniidae) from Azerbaijan and Iran. ZooKeys 1068: 13–26. <https://doi.org/10.3897/zookeys.1068.70717>

- Hrivniak Ľ, Sroka P, Godunko RJ, Manko P, Bojková J (2022) Diversification in Caucasian *Epeorus* (Caucasion) mayflies (Ephemeroptera: Heptageniidae) follows topographic deformation along the Greater Caucasus range. *Systematic Entomology* 47(4): 603–617. <https://doi.org/10.1111/syen.12551>
- Hrivniak Ľ, Sroka P, Türkmen G, Martynov AV, Bojková J (2024) Integrative delimitation of a new *Epeorus* (Caucasion) (Ephemeroptera, Heptageniidae) from the Caucasus with a supplement to the identification guide of Caucasian and Irano-Anatolian species. *Zookeys* 1214: 265–279. <https://doi.org/10.3897/zookeys.1214.131266>
- Kapur AP, Kripalani MB (1963) The mayflies (Ephemeroptera) from the north-western Himalaya. *Records of the Indian Museum* 59(1–2): 183–221. <https://doi.org/10.26515/rzsi/v59/i1-2/1961/161581>
- Katoh K, Standley DM (2013) MAFFT multiple sequence alignment software version 7: improvements in performance and usability. *Molecular Biology and Evolution* 30(4): 772–780. <https://doi.org/10.1093/molbev/mst010>
- Kluge NJ (1997) New subgenera of Holarctic mayflies (Ephemeroptera: Heptageniidae, Leptophlebiidae, Ephemerellidae). *Zoosystematica Rossica* 5: 233–235.
- Kluge NJ (2004) *The phylogenetic system of Ephemeroptera*. Springer, Dordrecht, 456 pp. <https://doi.org/10.1007/978-94-007-0872-3>
- Kluge NJ (2015) Central Asian mountain Rhithrogenini (Ephemeroptera: Heptageniidae) with pointed and ephemeropteroid claws in the winged stages. *Zootaxa* 3994(3): 301–353. <https://doi.org/10.11646/zootaxa.3994.3.1>
- Kumar S, Stecher G, Li M, Knyaz C, Tamura K (2018) MEGA X: Molecular Evolutionary Genetics Analysis across computing platforms. *Molecular Biology and Evolution* 35(6): 1547–1549. <https://doi.org/10.1093/molbev/msy096>
- Ma Z, Zhou C (2022) A new subgenus of *Epeorus* and its five species from China (Ephemeroptera: Heptageniidae). *Insect Systematics & Evolution* 53: 1–40. <https://doi.org/10.1163/1876312X-bja10028>
- Miller MA, Pfeiffer W, Schwartz T (2010) Creating the CIPRES science gateway for inference of large phylogenetic trees. In: *Proceedings of the gateway computing environments workshop (GCE)*. New Orleans: IEEE: 1–8. <https://doi.org/10.1109/GCE.2010.5676129>
- Pons J, Barraclough TG, Gomez-Zurita J, Cardoso A, Duran DP, Hazell S, Kamoun S, Sumlin WD, Vogler AP (2006) Sequence-based species delimitation for the DNA taxonomy of undescribed insects. *Systematic Biology*, 55: 595–609. <https://doi.org/10.1080/10635150600852011>
- Puillandre N, Brouillet S, Achaz G (2021) ASAP: Assemble species by automatic partitioning. *Molecular Ecology Resources* 21(2): 609–620. <https://doi.org/10.1111/1755-0998.13281>
- Rambaut A, Drummond AJ, Xie D, Baele G, Suchard MA (2018) Posterior summarisation in Bayesian phylogenetics using Tracer 1.7. *Systematic Biology* 67(5): 901–904. <https://doi.org/10.1093/sysbio/syy032>
- Sinitshenkova ND (1976) Mayflies of the Genus *Iron* Eaton (Ephemeroptera, Heptageniidae) in the Fauna of the Caucasus. *Entomologicheskoye obozreniye* 55(4): 853–862.
- Snethlage MA, Geschke J, Spehn EM, Ranipeta A, Yoccoz NG, Körner Ch, Jetz W, Fischer M, Urbach D (2022) A hierarchical inventory of the world's mountains for global comparative mountain science. *Scientific Data* 9: 149. <https://doi.org/10.1038/s41597-022-01256-y>
- Tshernova OA (1938) Zur Kenntnis der Ephemeropteren Ost-Transkaukasien. *Trudy Azerbajdshanskogo Filiala AN SSSR, Baku* 7(42): 55–64.

- Tshernova OA (1981) On the systematics of adult mayflies of the genus *Epeorus* Eaton, 1881 (Ephemeroptera, Heptageniidae). Entomologicheskoe Obozrenie 60(2): 323–336.
- Türkmen G (2023). Biomonitoring in the Caucasus Biodiversity Hotspot: The ecological and habitat preferences of *Epeorus* (*Caucasion*) *znojko*i (Ephemeroptera, Heptageniidae) from Northeastern Turkey. Kuwait Journal of Science 50(3): 313–321. <https://doi.org/10.1016/j.kjs.2022.11.002>
- Ulmer G (1912) H. Sauter's Formosa-Ausbeute. Ephemeriden. Entomologische Mitteilungen 1: 369–375. <https://doi.org/10.5962/bhl.part.25902>
- Vasanth M, Selvakumar C, Subramanian KA, Sivaramakrishnan KG, Sinha B (2021) Contribution to the study of *Epeorus* Eaton, 1881 (Ephemeroptera: Heptageniidae) from India. Zootaxa 4991: 499–522. <https://doi.org/10.11646/zootaxa.4991.3.4>
- Waterhouse AM, Procter JB, Martin DMA, Clamp M, Barton GJ (2009) Jalview Version 2 - a multiple sequence alignment editor and analysis workbench Bioinformatics 25(9): 1189–1191. <https://doi.org/10.1093/bioinformatics/btp033>

Six new species and a new synonym of the mesh-web spider genus *Sudesna* Lehtinen, 1967 (Araneae, Dictynidae) from China

Lu-Yu Wang¹, Xian-Jin Peng², Zhi-Sheng Zhang¹

¹ Key Laboratory of Eco-environments in Three Gorges Reservoir Region (Ministry of Education), School of Life Sciences, Southwest University, Chongqing 400715, China

² College of Life Sciences, Hunan Normal University, Changsha 410081, Hunan, China

Corresponding author: Zhi-Sheng Zhang (zhangzs327@qq.com)

Abstract

Six new species of the genus *Sudesna* are described from South China: *S. cangshan* sp. nov. (♀, Yunnan), *S. dali* sp. nov. (♂♀, Yunnan), *S. haiboi* sp. nov. (♂♀, Yunnan), *S. hainan* sp. nov. (♂♀, Hainan), *S. shangrila* sp. nov. (♂♀, Yunnan) and *S. yangi* sp. nov. (♂♀, Yunnan). *Dictyna yongshun* Yin, Bao & Kim, 2001 is proposed here as a junior synonym of *S. hedini* (Schenkel, 1936). Detailed descriptions, photographs, along with illustrations of genital organs, somatic features, and a distribution map of *Sudesna* species in China are provided.

Key words: Description, Dictyninae, morphology, taxonomy



Academic editor: Dimitar Dimitrov

Received: 25 December 2024

Accepted: 14 March 2025

Published: 9 April 2025

ZooBank: <https://zoobank.org/6DB976C7-4B5C-42C7-AA7E-D239CF3241CB>

Citation: Wang L-Y, Peng X-J, Zhang Z-S (2025) Six new species and a new synonym of the mesh-web spider genus *Sudesna* Lehtinen, 1967 (Araneae, Dictynidae) from China. ZooKeys 1234: 127–149. <https://doi.org/10.3897/zookeys.1234.145300>

Copyright: © Lu-Yu Wang et al.
This is an open access article distributed under terms of the Creative Commons Attribution License (Attribution 4.0 International – CC BY 4.0).

Introduction

The mesh-web spider genus *Sudesna* Lehtinen, 1967 was established by Lehtinen (1967) based on the type species, *S. hedini* (Schenkel, 1936) (both sexes), from China and three other species, *S. anaulax* (Simon, 1908) (male only) from Australia, *S. grammica* (Simon, 1893) (female only) from Philippines, and *S. grossa* (Simon, 1906) (female only) from India. These species' distributions indicate that *Sudesna* may be endemic to Australia, South and Southeast Asia. Additional exploration should be done to find the other sex of the aforementioned three species, and likely more species will also be found. Zhang and Li (2011) described two species from Xishuangbanna, Yunnan, China, a small tropical area, indicating that *Sudesna* has a relatively high diversity in South China. Esysunin and Sozontov (2016) transferred a seventh species to *Sudesna*, *S. flavipes* (Hu, 2001) (female only), after their analysis of the morphological characters of some Palearctic *Dictyna* Sundevall, 1833 species.

Based on newly collected material from China, we propose six new species and suggest a new synonym of the type species, *S. hedini* from Hunan Province. Thus, the genus *Sudesna* contains 13 species from Australia and South, Southeast and East Asia. Except for the type species, which has been recorded from China and South Korea, each *Sudesna* species is known only from their

type locality. Our field observations indicate that *Sudesna* species prefer to live in small mesh-webs on the underside of leaves, and they have been collected by beating leaves (Zhang and Wang 2017).

Materials and methods

All specimens are preserved in 75% ethanol and were examined, illustrated, photographed, and measured using a Leica M205A stereomicroscope equipped with a drawing tube, a Leica DFC450 Camera, and LAS v. 4.6 software. Male palps and epigynes were examined and illustrated after dissection. Epigynes were cleared by immersing them in a pancreatin solution (Álvarez-Padilla and Hormiga 2007). Eye sizes were measured as the maximum dorsal diameter. Leg measurements are shown as: total length (femur, patella and tibia, metatarsus, tarsus). All measurements are in millimetres. Specimens examined here are deposited in the Collection of Spiders, School of Life Sciences, Southwest University, Chongqing, China (**SWUC**) and in the Hunan Normal University (**HNU**).

Abbreviations used in the text: **ALE**, anterior lateral eye; **AME**, anterior median eye; **MOA**, median ocular area; **PLE**, posterior lateral eye; **PME**, posterior median eye.

Taxonomy

Family Dictynidae O. Pickard-Cambridge, 1871 (卷叶蛛科)

Subfamily Dictyninae O. Pickard-Cambridge, 1871 (卷叶蛛亚科)

Genus *Sudesna* Lehtinen, 1967

(苏蛛属)

Type species. *Dictyna hedini* Schenkel, 1936.

Diagnosis. *Sudesna* can be distinguished from *Dictyna* by the reduced or absent spur of the male palpal tibia, the anteriorly located, widely separated epigynal copulatory openings, the tube-like copulatory ducts, and the laterally located spermathecal heads (Zhang and Li 2011).

Description. Diminutive in size (1.60–4.57). Dorsum of prosoma pale darker to brown, with high cephalic area. Fovea absent. Cervical groove distinct, radial furrows indistinct. Eight eyes in 2 rows; eyes located on eye tubercles; eye tubercles coloured same as carapace. Chelicerae stout, yellowish to brown, with small yellow lateral condyles, 3–4 promarginal and 1–3 retromarginal teeth. Endites yellow, longer than wide. Labium yellow-brown, as long as wide. Sternum yellow-brown, with truncated anterior margin and blunt posterior margin. Legs yellowish to brown, patella with a small protrusion. Opisthosoma oval. Dorsum pale to darker brown, with some small, white, scale-like markings near midline. Venter of abdomen yellow-brown, with small, undivided cribellum. Spinnerets short and yellowish brown.

Palp with droplet-shaped cymbium. Tibia dorsally with two ctenidia or absent (*S. circularis* Zhang & Li, 2011 and *S. yangi* sp. nov.). Retrolateral tibial apophysis triangular or hook-shaped. Embolus semicircular and originating at about 8:00 to 11:30 o'clock position. Anterior arm of conductor (AA) short and membranous; posterior arm (PA) finger-shaped or twisted, usually with scaly tip.

Epigyne with widely separated copulatory openings. Copulatory openings with pronounced inner margins. Copulatory ducts short or long, usually twisted, and membranous or slightly sclerotized. Spermathecae sclerotized, irregularly shaped. Spermathecal heads spherical or oval. Fertilization ducts thin, long, extending from the anterior parts of spermathecae, curving and pointing laterally.

Key to species

| | | |
|----|--|-----------------------------------|
| 1 | Male..... | 2 |
| – | Female..... | 7 |
| 2 | Tibia without ctenidia..... | <i>S. yangi</i> sp. nov. |
| – | Tibia with ctenidia | 3 |
| 3 | Posterior arm of conductor straight..... | <i>S. dali</i> sp. nov. |
| – | Posterior arm of conductor twisted | 4 |
| 4 | Embolus originating at about the 11:30 o'clock position... <i>S. hainan</i> sp. nov. | |
| – | Embolus originating at about the 8:30 to 10:00 o'clock position | 5 |
| 5 | Opisthosoma dark | <i>S. haiboi</i> sp. nov. |
| – | Opisthosoma pale | 6 |
| 6 | Posterior arm of the conductor strongly curved ... <i>S. hedini</i> (Schenkel, 1936) | |
| – | Posterior arm of the conductor slightly curved | <i>S. shangrila</i> sp. nov. |
| 7 | Spermatheca bifurcate | <i>S. cangshan</i> sp. nov. |
| – | Spermatheca simple | 8 |
| 8 | Spermathecal heads oval; spermatheca spiral | <i>S. haiboi</i> sp. nov. |
| – | Spermathecal heads spherical; spermatheca not spiral | 9 |
| 9 | Copulatory ducts short, slightly curved | 10 |
| – | Copulatory ducts long, strongly curved | 12 |
| 10 | Edges of spermatheca tuberculate | <i>S. dali</i> sp. nov. |
| – | Edges of spermatheca smooth | 11 |
| 11 | Diameter of spermathecal heads equal to width of copulatory openings.... | <i>S. hainan</i> sp. nov. |
| – | Diameter of spermathecal heads greater than width of copulatory openings..... | <i>S. shangrila</i> sp. nov. |
| 12 | Diameter of spermathecal heads equal to width of spermatheca..... | <i>S. yangi</i> sp. nov. |
| – | Diameter of spermathecal heads less than width of spermatheca | <i>S. hedini</i> (Schenkel, 1936) |

Sudesna cangshan sp. nov.

<https://zoobank.org/D8657831-FABF-41DE-9754-3350542064DF>

Figs 1, 2, 15

(苍山苏蛛)

Type material. Holotype: CHINA • ♀ (SWUC-T-DI-14-01); Yunnan Province; Dali City, Mount Cangshan, Dapoqing; 25°34'38"N, 100°07'51"E; elev. 2043 m; 30 August 2009; Z.Z. Yang leg.

Etymology. The specific name is derived from the county where the type locality is located; used as a noun in apposition.

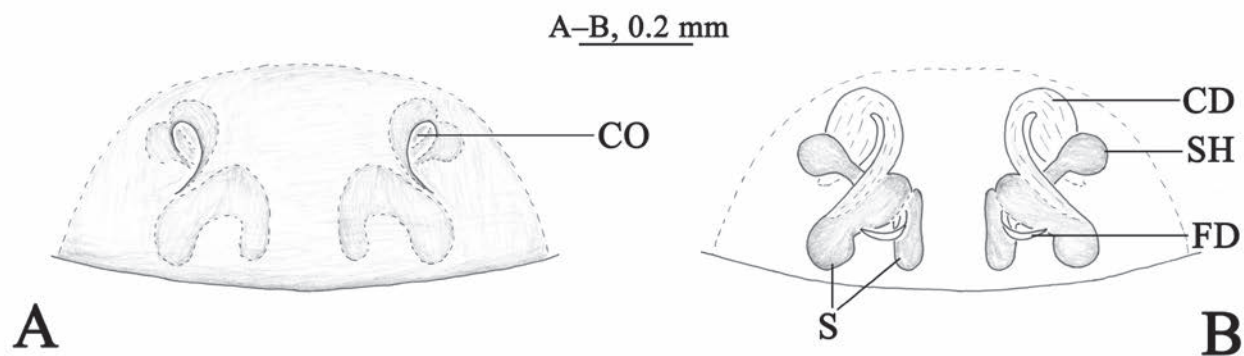


Figure 1. *Sudesna cangshan* sp. nov. holotype female **A** epigyne, ventral view **B** vulva, dorsal view. Abbreviations: CD = copulatory duct; CO = copulatory opening; FD = fertilization duct; S = spermatheca; SH = spermathecal head.



Figure 2. *Sudesna cangshan* sp. nov. holotype female **A** habitus, dorsal view **B** epigyne, ventral view **C** vulva, dorsal view.

Diagnosis. The female of this new species is similar to *S. yangi* sp. nov. (Figs 13, 14) in having a pale body and 9-shaped copulatory openings, but it can be distinguished by having copulatory openings as large as the spermathecal head (vs twice as large), gently curved copulatory ducts (vs abruptly bent at an acute angle), and bifurcate spermatheca (vs clavate) (Figs 1, 2B, C).

Description. Female holotype (Fig. 2A) total length 3.31. Prosoma 1.27 long, 1.16 wide; Opisthosoma 2.23 long, 1.65 wide. Dorsum of prosoma pale, with high cephalic area. Eye sizes and interdistances: AME 0.05, ALE 0.08, PME 0.08, PLE 0.07; AME–AME 0.11, AME–ALE 0.09, PME–PME 0.13, PME–PLE

0.12, ALE–PLE 0.02. MOA 0.20 long, anterior width 0.20, posterior width 0.27. Clypeus height 0.12. Chelicerae stout, yellowish brown, with 3 promarginal and 3 retromarginal teeth. Legs yellowish. Leg measurements: I 3.73 (1.04, 1.58, 0.70, 0.41); II 3.28 (1.04, 1.17, 0.68, 0.39), III 2.72 (0.92, 0.91, 0.58, 0.31), IV 3.20 (1.02, 1.12, 0.75, 0.31). Leg formula: 1243. Opisthosoma oval. Dorsum and venter pale. Spinnerets short and yellowish brown.

Epigyne (Figs 1, 2B, C). Copulatory openings somewhat 9-shaped and facing away from each other, separated by about 6 times their width. Copulatory ducts membranous, gently curved, longer than spermathecal length. Spermatheca bifurcate, spermathecal heads spherical. Fertilization ducts thin, curved, directed laterally.

Male unknown.

Distribution. Known only from the type locality, Yunnan, China (Fig. 15).

***Sudesna dali* sp. nov.**

<https://zoobank.org/CE4698DA-3BB0-4BFF-8815-C8C8F84B0AF9>

Figs 3, 4, 15

(大理苏蛛)

Type material. **Holotype** ♂ (SWUC-T-DI-15-01); **Yunnan Province**; Dali City, Mount Cangshan, Dapoqing; 25°34'59"N, 100°08'09"E; elev. 2500 m; 8 November 2009; T.B. Yang leg. **Paratypes**: 1 ♂ 3 ♀ (SWUC-T-DI-15-02 to 05); same data as for holotype • 3 ♂ 2 ♀ (SWUC-T-DI-15-06 to 10); Mount Cangshan, Yujufeng; 25°42'14"N, 100°07'09"E; elev. 2700 m; 10 April 2011; L. Yang leg. • 2 ♀ (SWUC-T-DI-15-11 to 12); Mount Cangshan; elev. 2500 m; 15 January 2009; Z.Z. Yang leg. • 4 ♂ 16 ♀ (SWUC-T-DI-15-13 to 32); Mount Cangshan, Xieyangfeng; 25°36'04"N, 100°11'11"E; elev. 2559 m; 14 June 2011; K.C. Zhang leg. • 1 ♂ (SWUC-T-DI-15-33); Mount Cangshan, Xieyangfeng; 25°35'54"N, 100°11'13"E; elev. 2700 m; 14 June 2011; Z.X. Bao leg. • 1 ♂ (SWUC-T-DI-15-34); Mount Cangshan; Xieyangfeng; 25°35'58"N, 100°11'7"E; elev. 2500 m; 10 April 2011; N.J. Li leg. • 1 ♂ 1 ♀ (SWUC-T-DI-15-35 to 36); Mount Cangshan, Xieyangfeng; 25°35'54"N, 100°11'13"E; elev. 2615 m; 15 January 2009; Z.Z. Yang leg.

Etymology. The specific name is derived from the county where the type locality is located; used as a noun in apposition.

Diagnosis. This new species is similar to *S. hainan* sp. nov. (Figs 7, 8) in having a semicircular embolus and short copulatory ducts, but it can be distinguished by the triangular (dorsal view) retrolateral tibial apophysis (vs semicircular, lamellate), the finger-shaped and untwisted posterior arm (PA) of the conductor (vs somewhat S-shaped) (Figs 3A–C, 4C–E), and the absence of a stem of the spermathecal head (vs present) (Figs 3E, 4G).

Description. **Male holotype** (Fig. 4A) total length 2.00. Prosoma 0.86 long, 0.78 wide; Opisthosoma 1.20 long, 0.75 wide. Dorsum of prosoma brown, with high cephalic area. Eye sizes and interdistances: AME 0.03, ALE 0.04, PME 0.04, PLE, 0.04; AME–AME 0.09, AME–ALE 0.06, PME–PME 0.08, PME–PLE 0.10, ALE–PLE 0.02. MOA 0.14 long, anterior width 0.14, posterior width 0.16. Clypeus height 0.09. Chelicerae stout, yellow-brown, with 3 promarginal teeth and 1 retromarginal tooth. Legs yellowish. Leg measurements: I 2.76 (0.84, 0.95, 0.59, 0.38); II 2.56 (0.78, 0.88, 0.50, 0.40); III 2.03 (0.62, 0.65, 0.46, 0.30);

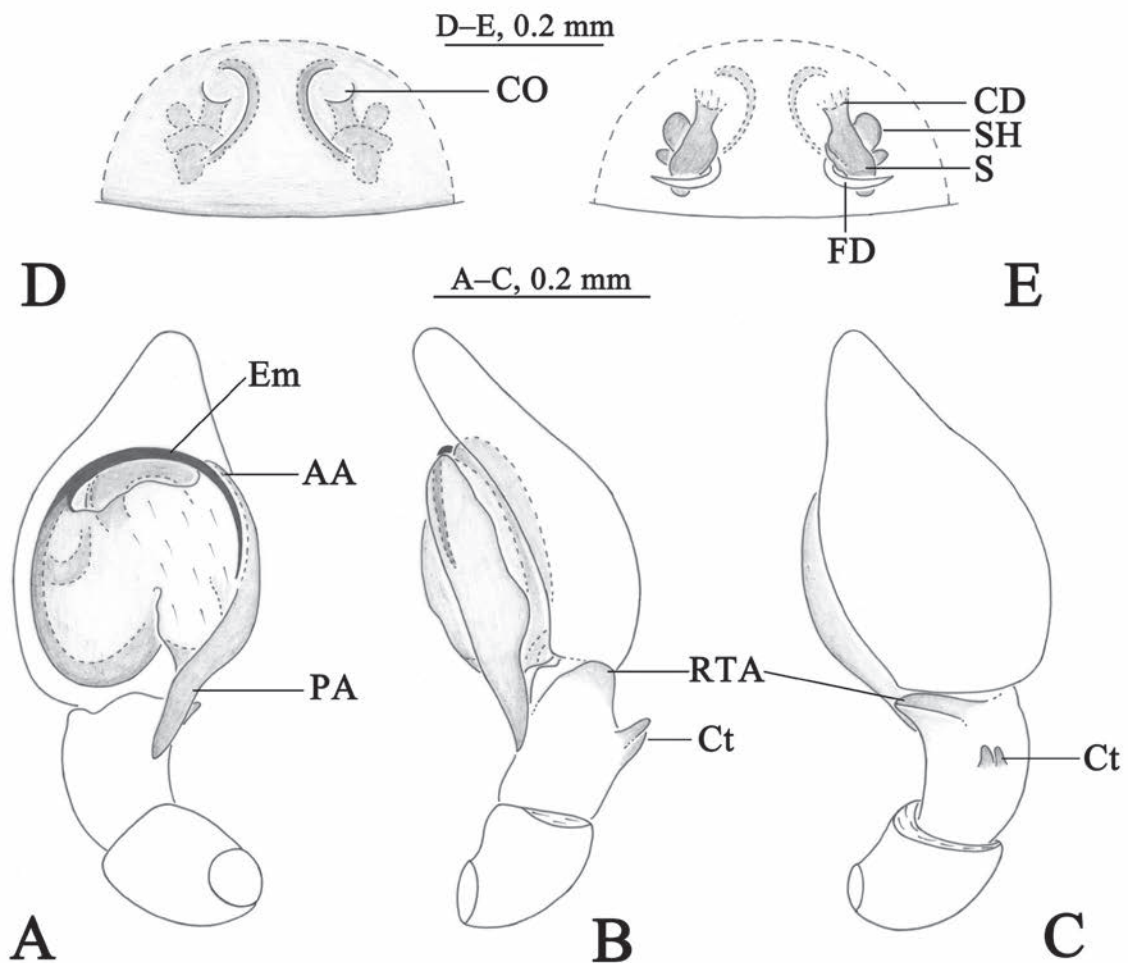


Figure 3. *Sudesna dali* sp. nov. holotype male (A–C) and paratype female (D, E). **A** Left male palp, ventral view **B** same, retrolateral view **C** same, dorsal view **D** epigyne, ventral view **E** vulva, dorsal view. Abbreviations: AA = anterior arm of conductor; CD = copulatory duct; CO = copulatory opening; Ct = ctenidia; Em = embolus; FD = fertilization duct; PA = posterior arm of conductor; RTA = retrolateral tibial apophysis; S = spermatheca; SH = spermathecal head.

IV 2.28 (0.73, 0.69, 0.55, 0.31). Leg formula: 1243. Opisthosoma oval. Dorsum with black and white markings. Venter yellow brown. Spinnerets short and yellow-brown, with black markings.

Palp (Figs 3A, B, 4C–E). Tibia dorsally with 2 ctenidia, located at 1/3 length of tibia from the distal-most part. Retrolateral tibial apophysis triangular in dorsal view. Embolus semicircular and originating at about the 10:00 o'clock position and terminating at about the 4:30 o'clock position. Anterior arm of conductor (AA) short and membranous; posterior arm (PA) finger-shaped with sharply pointed tip.

Female paratype (SWUC-T-DI-15-02, Fig. 4B) total length 2.46. Prosoma 0.86 long, 0.81 wide; opisthosoma 1.64 long, 1.30 wide. Dorsum of prosoma yellow-brown, with high cephalic area. Eye sizes and interdistances: AME 0.04, ALE 0.04, PME 0.04, PLE 0.04; AME–AME 0.07, AME–ALE 0.06, PME–PME 0.08, PME–PLE 0.08, ALE–PLE 0.02. MOA 0.13 long, anterior width 0.14, posterior width 0.16. Clypeus height 0.06. Leg measurements: I 2.41 (0.75, 0.81, 0.49, 0.36); II 2.32 (0.71, 0.79, 0.48, 0.34); III 1.98 (0.62, 0.63, 0.46, 0.27); IV 2.29 (0.72, 0.78, 0.51, 0.28). Legs yellowish. Leg formula: 1243. Opisthosoma oval. Dorsum yellow-brown, with white scaly markings. Venter yellow-brown. Spinnerets short and yellow brown.

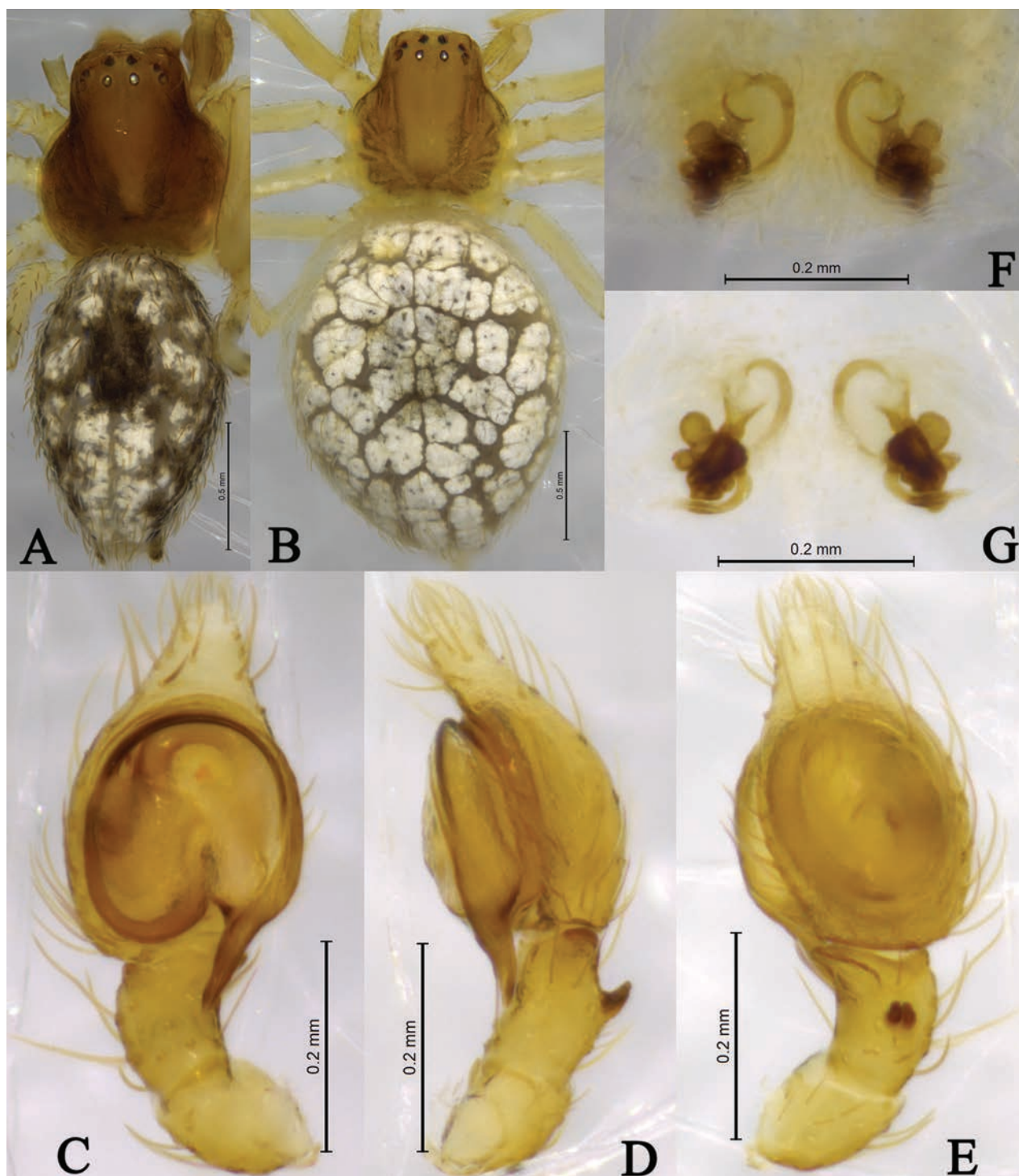


Figure 4. *Sudesna dali* sp. nov. holotype male (**A**, **C–E**) and paratype female (**B**, **F**, **G**). **A** Male habitus, dorsal view **B** female habitus, dorsal view **C** left male palp, ventral view **D** same, retrolateral view **E** same, dorsal view **F** epigyne, ventral view **G** vulva, dorsal view.

Epigyne (Figs 3C, D, 4F, G). Copulatory openings semicircular, facing each other, separated by about 4 times their width. Copulatory ducts membranous, short, as long as width. Spermatheca peanut-shaped, spermathecal heads somewhat ball-shaped. Fertilization ducts semicircular, directed laterally, the length is 2.5 times the width of the copulatory openings.

Variation. Male ($n = 12$) total length 1.87–2.13; female ($n = 24$) total length 2.18–2.71.

Distribution. Known only from the type locality, Yunnan, China (Fig. 14).

***Sudesna haiboi* sp. nov.**

<https://zoobank.org/823D83E1-E618-4AB5-9A32-DD970521E5C4>

Figs 5, 6, 15

(海波苏蛛)

Type materials. *Holotype* ♂ (SWUC-T-DI-16-01); **Yunnan Province**; Dali City, Mount Cangshan, Southern Slopes; 25°34'27"N, 100°7'49"E; elev. 2320 m; May 2010; H.B. Pu and Z.Z. Yang leg. *Paratypes*: 9 ♂ 10 ♀ (SWUC-T-DI-16-02 to 20); same data as holotype.

Etymology. The specific name honours Mr Haibo Pu, who was of tremendous assistance in the field; a noun in genitive case.

Diagnosis. This species is similar to *S. shangrila* sp. nov. (Figs 11, 12) in having a hook-shaped retrolateral tibial apophysis, a long anterior arm of

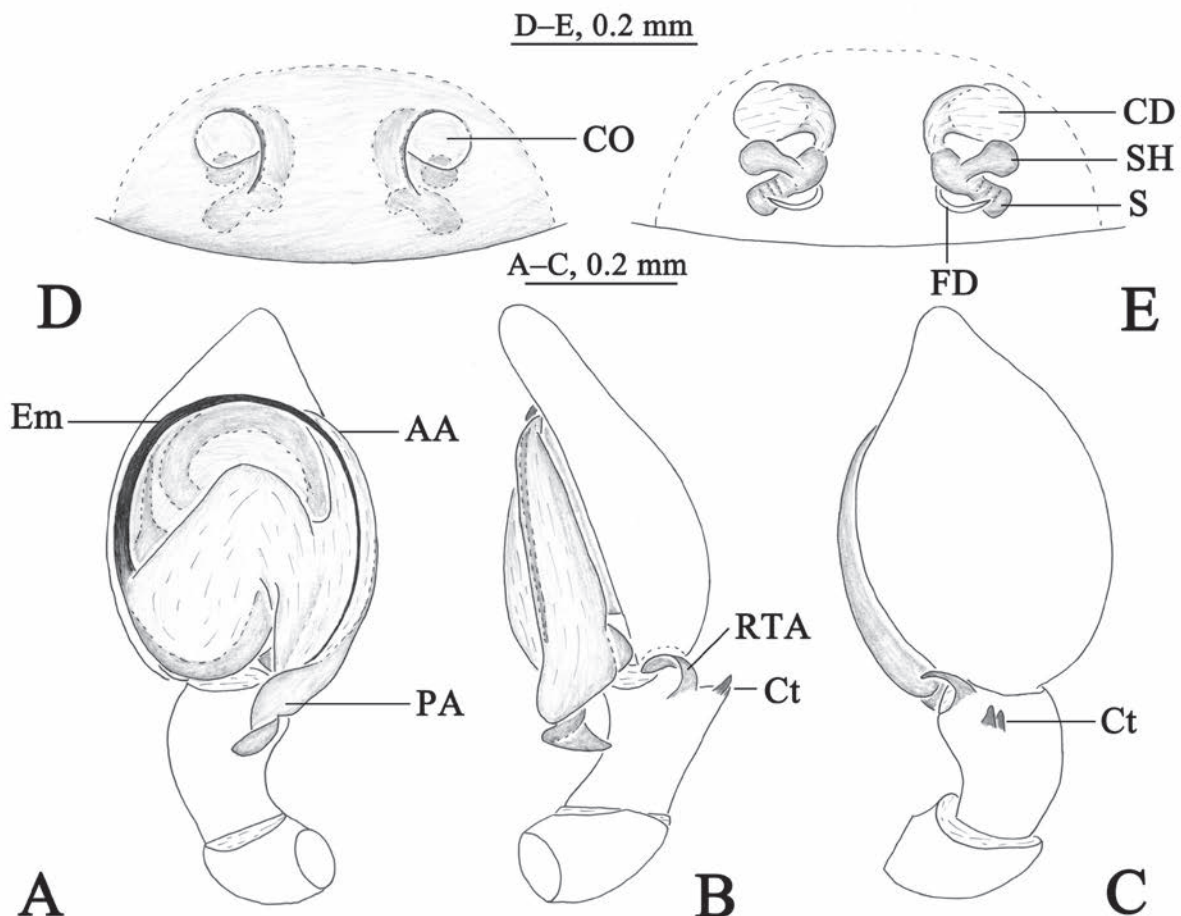


Figure 5. *Sudesna haiboi* sp. nov. holotype male (A–C) and paratype female (D, E). **A** Left male palp, ventral view **B** same, retrolateral view **C** same, dorsal view **D** epigyne, ventral view **E** vulva, dorsal view. Abbreviations: AA = anterior arm of conductor; CD = copulatory duct; CO = copulatory opening; Ct = ctenidia; Em = embolus; FD = fertilization duct; PA = posterior arm of conductor; RTA = retrolateral tibial apophysis; S = spermathecal; SH = spermathecal head.

conductor, and cylindrical spermatheca, but it can be distinguished by the embolus originating at about the 8:30 o'clock position (vs 9:30), the lack of a scaly tip on the posterior arm of the conductor (vs present) (Figs 5A–C, 6C–E), and long, curved copulatory ducts (vs short and straight) (Figs 5E, 6G).

Description. Male holotype (Fig. 6A) total length 2.01. Prosoma 0.94 long, 0.87 wide; opisthosoma 1.14 long, 0.76 wide. Dorsum of prosoma brown, with high cephalic area. Eye sizes and interdistances: AME 0.05, ALE 0.05, PME 0.06, PLE, 0.07; AME–AME 0.08, AME–ALE 0.07, PME–PME 0.09, PME–PLE 0.08, ALE–PLE 0.01. MOA 0.16 long, anterior width 0.16, posterior width 0.19.

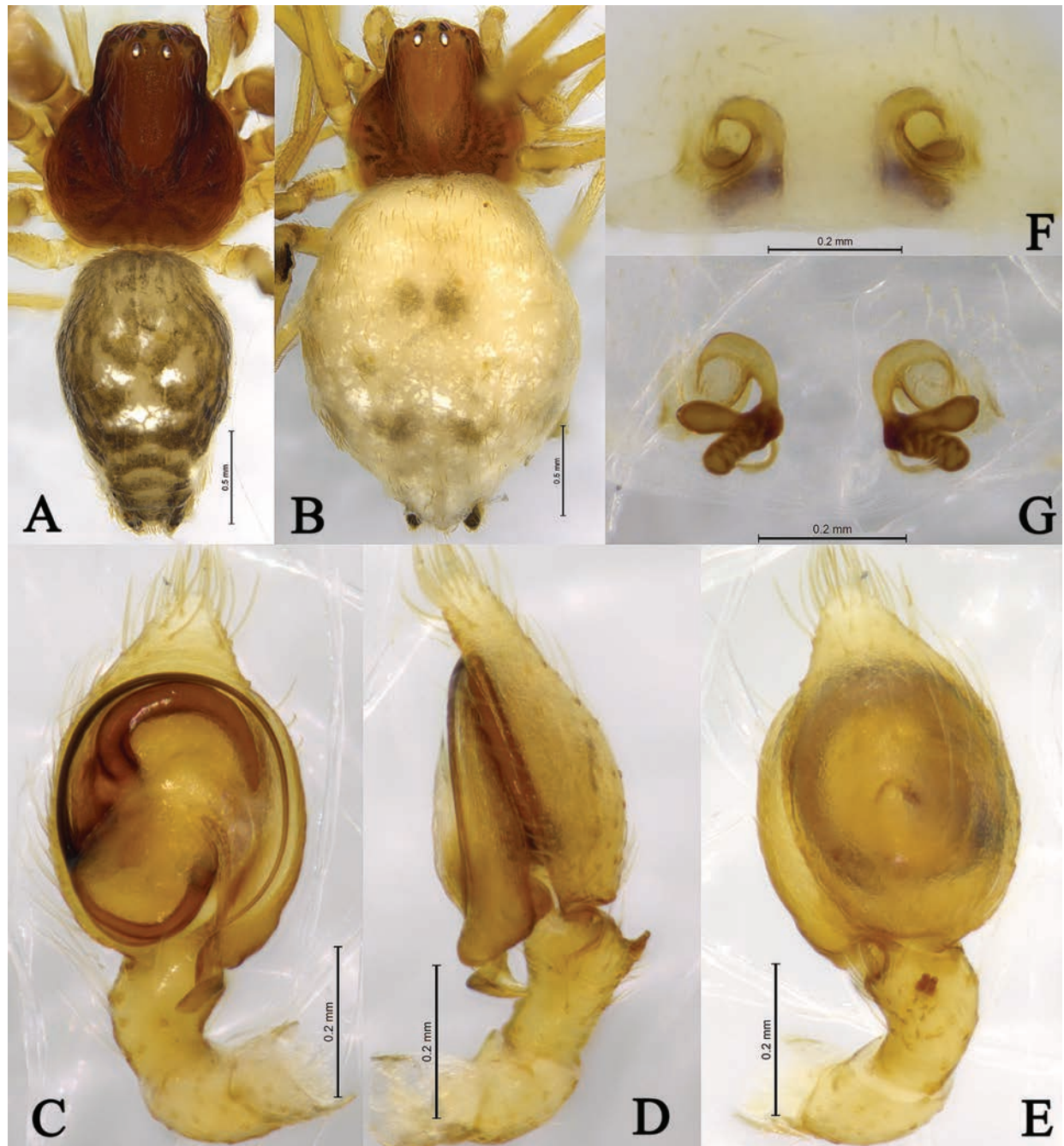


Figure 6. *Sudesna haibo* sp. nov. holotype male (A, C–E) and paratype female (B, F, G). A Male habitus, dorsal view B female habitus, dorsal view C left male palp, ventral view D same, retrolateral view E same, dorsal view F epigyne, ventral view G vulva, dorsal view.

Clypeus height 0.12. Chelicerae stout, brown, with 3 promarginal teeth and 1 retromarginal tooth. Legs yellow-brown. Leg measurements: I 3.45 (1.09, 1.12, 0.80, 0.44), II 3.34 (1.05, 1.08, 0.78, 0.44), III 2.51 (0.79, 0.77, 0.60, 0.35), IV 2.72 (0.83, 0.87, 0.67, 0.35). Leg formula: 1243. Opisthosoma oval. Dorsum yellowish brown, with black and white markings. Venter yellow-brown. Spinnerets short and yellow-brown, with black markings.

Palp (Figs 5A, B, 6C–E). Tibia dorsally with two ctenidia, located 1/3 from distal-most portion of tibia. Retrolateral tibia apophysis hook-shaped. Embolus somewhat O-shaped, originating at about the 8:30 o'clock position and terminating at about the 5:30 o'clock position. Anterior arm of conductor (AA) tapering and terminating at about the 1:00 o'clock position; posterior arm (PA) spiral, with blunt tip.

Female paratype (SWUC-T-DI-16-02, Fig. 6B) total length 2.27. Prosoma 0.82 long, 0.83 wide; opisthosoma 1.54 long, 1.27 wide. Dorsum of prosoma yellow-brown, with high cephalic area. Eye sizes and interdistances: AME 0.04, ALE 0.06, PME 0.05, PLE 0.05; AME–AME 0.08, AME–ALE 0.05, PME–PME 0.08, PME–PLE 0.09, ALE–PLE 0.02. MOA 0.14 long, anterior width 0.14, posterior width 0.16. Clypeus height 0.06. Legs yellow-brown. Leg measurements: I 2.96 (0.95, 0.95, 0.67, 0.39), II 2.86 (0.92, 0.92, 0.64, 0.38), III 2.39 (0.77, 0.75, 0.55, 0.32), IV 2.62 (0.82, 0.86, 0.63, 0.31). Leg formula: 1243. Opisthosoma oval. Dorsum yellowish brown, with a few black markings and lots of white scaly markings. Venter yellowish brown. Spinnerets short and yellow-brown, with black markings.

Epigyne (Figs 5C, D, 6F, G). Copulatory openings nearly 9-shaped, facing away from each other, separated by about 2.5 times their width. Copulatory ducts long, membranous, semicircular. Spermatheca spiral; spermathecal heads oval. Fertilization ducts semicircular, laterally directed and as long as width of copulatory openings.

Variation. Male ($n = 10$) total length 1.92–2.10; female ($n = 10$) total length 2.15–2.35.

Distribution. Known only from the type locality, Yunnan, China (Fig. 15).

***Sudesna hainan* sp. nov.**

<https://zoobank.org/C7C6A794-7C79-4A8D-85CF-A17C4EF6694D>

Figs 7, 8, 15

(海南苏蛛)

Type materials. **Holotype** ♂ (SWUC-T-DI-17-01); **Hainan Province**; Changjiang County, Bawangling; 19°07'51"N, 109°03'22"E; elev. 739 m; 21 May 2009; G.X. Han leg. **Paratypes:** 1 ♂ 13 ♀ (SWUC-T-DI-17-02 to 15); same data as holotype • 2 ♀ (SWUC-T-DI-17-16 to 17); Bawangling, Yajia; 19°04'46"N, 109°07'35"E; elev. 624 m; 19 May 2009; G.X. Han leg. • 2 ♀ (SWUC-T-DI-17-18 to 19); Diaolushan National Nature Reserve; 18°40'08"N, 109°53'53"E; elev. 2225 m; June 2009; G.X. Han leg. • 3 ♀ (SWUC-T-DI-17-20 to 22); Jianfengling National Nature Reserve, Zhufeng; 18°42'35"N, 108°52'35"E; elev. 960 m; 31 May 2009; G.X. Han leg. • 5 ♀ (SWUC-T-DI-17-23 to 27); Jianfengling National Nature Reserve, Tianchi; 18°44'38"N, 108°51'43"E; elev. 811 m; 29 May 2009; G.X. Han leg. • 2 ♂ 7 ♀ (SWUC-T-DI-17-28 to 36); Jianfengling National Nature Reserve, Yulingu; 18°44'59"N, 108°55'16"E; elev. 680 m; 1 June 2009; G.X. Han leg. • 2 ♂ 4 ♀ (SWUC-T-DI-17-37 to 42); Tunchang County, Xichang Town; 19°25'55"N,

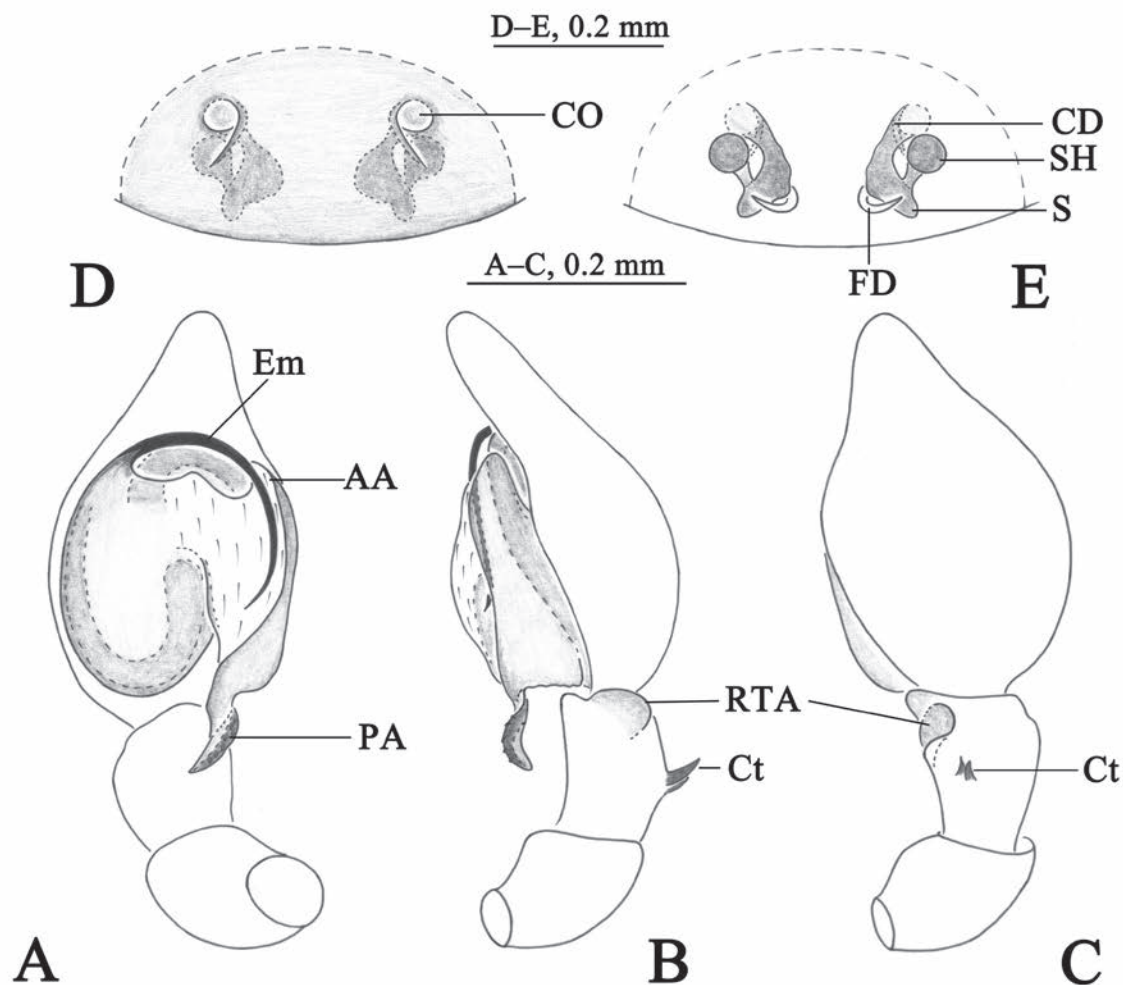


Figure 7. *Sudesna hainan* sp. nov. holotype male (**A–C**) and paratype female (**D, E**). **A** Left male palp, ventral view **B** same, retrolateral view **C** same, dorsal view **D** epigyne, ventral view **E** vulva, dorsal view. Abbreviations: AA = anterior arm of conductor; CD = copulatory duct; CO = copulatory opening; Ct = ctenidia; Em = embolus; FD = fertilization duct; PA = posterior arm of conductor; RTA = retrolateral tibial apophysis; S = spermathecal; SH = spermathecal head.

110°2'48"E; elev. 124 m; 11 June 2009; G.X. Han leg. • 1 ♂ 1 ♀ (SWUC-T-DI-17-43 to 44); Wuzhishan City, Shuiman Township, Wuzhishan National Nature Reserve; 18°54'23"N, 109°40'51"E; elev. 747 m; Q.L. Lu leg.

Etymology. The specific name is derived from the county where the type locality is located; used as a noun in apposition.

Diagnosis. See the diagnosis of *S. dali* sp. nov.

Description. Male holotype (Fig. 8A) total length 2.30. Prosoma 0.91 long, 0.84 wide; opisthosoma 1.48 long, 0.98 wide. Dorsum of prosoma brown, with white high cephalic area. Eye sizes and interdistances: AME 0.04, ALE 0.10, PME 0.08, PLE 0.09; AME–AME 0.07, AME–ALE 0.04, PME–PME 0.06, PME–PLE 0.10, ALE–PLE 0.02. MOA 0.20 long, anterior width 0.15, posterior width 0.22. Clypeus height 0.04. Chelicerae stout, brown, with 3 promarginal teeth and 1 retromarginal tooth. Legs yellow-brown (femur I brown). Leg measurements: I 3.27 (1.04, 1.16, 0.62, 0.45); II 3.05 (1.03, 1.02, 0.57, 0.43); III 2.35 (0.75, 0.74, 0.50, 0.36); IV 2.59 (0.81, 0.85, 0.54, 0.39). Leg formula: 1243. Opisthosoma almost pyriform. Dorsum white, with a few short, strong spines. Venter yellowish brown. Spinnerets short and yellowish brown with black markings.

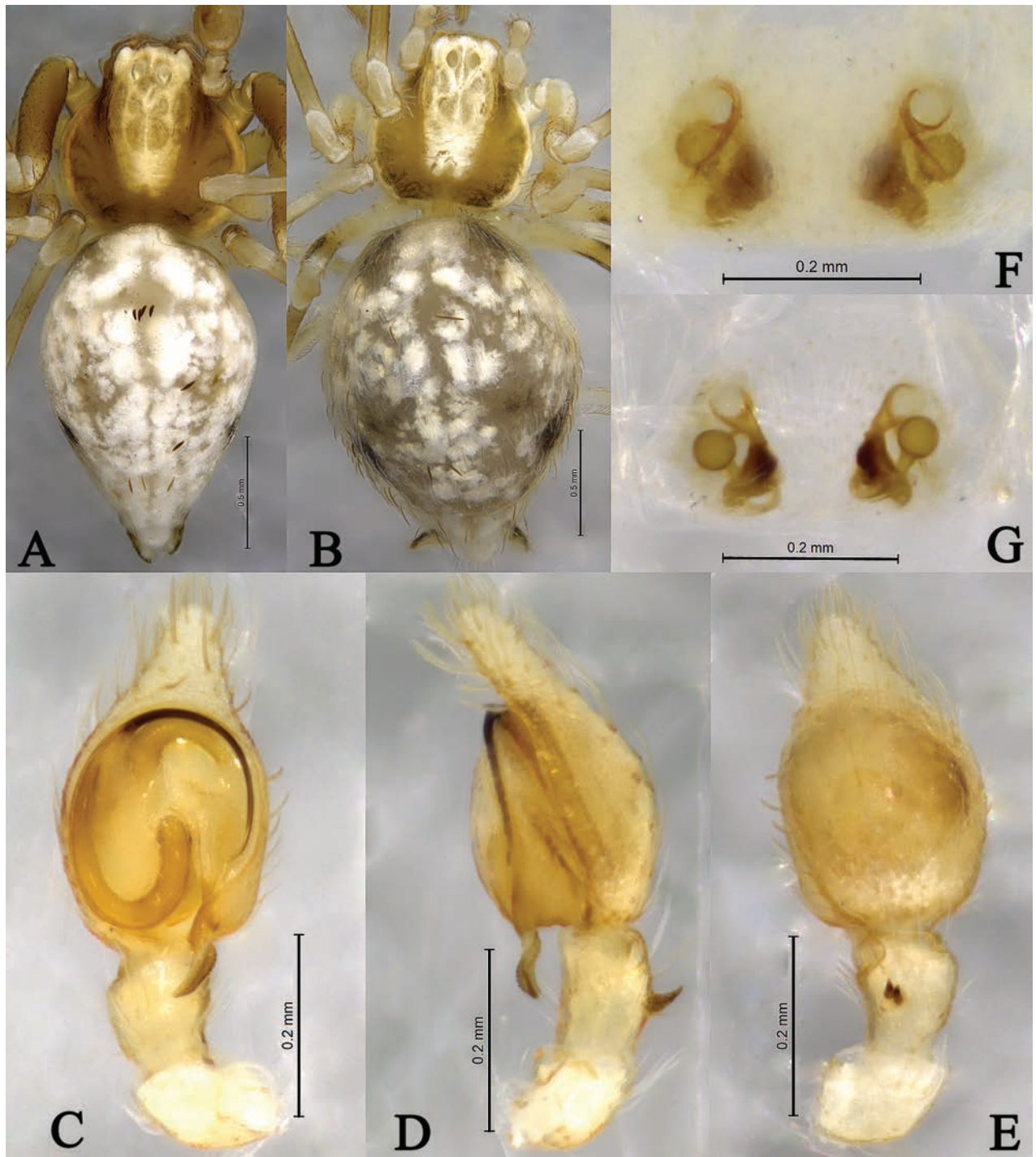


Figure 8. *Sudesna hainan* sp. nov. holotype male (**A**, **C–E**) and paratype female (**B**, **F**, **G**). **A** Male habitus, dorsal view **B** female habitus, dorsal view **C** left male palp, ventral view **D** same, retrolateral view **E** same, dorsal view **F** epigyne, ventral view **G** vulva, dorsal view.

Palp (Figs 7A, B, 8C–E). Tibia dorsally with 2 ctenidia, located at middle. Retro-lateral tibia apophysis lamellate. Embolus semicircular and originating at about the 11:30 o'clock position, terminating at about the 4:00 o'clock position. Anterior arm of conductor (AA) membranous, terminating at about the 1:30 o'clock position; posterior arm (PA) backwards S-shaped in retrolateral view, with a blunt, scaly tip.

Female paratype (SWUC-T-DI-17-02, Fig. 8B) total length 2.42. Prosoma 0.85 long, 0.79 wide; opisthosoma 1.58 long, 1.24 wide. Dorsum of prosoma

yellowish brown, with white high cephalic area. Eye sizes and interdistances: AME 0.03, ALE 0.08, PME 0.07, PLE, 0.08; AME–AME 0.06, AME–ALE 0.03, PME–PME 0.05, PME–PLE 0.07, ALE–PLE 0.02. MOA 0.17 long, anterior width 0.11, posterior width 0.17. Clypeus height 0.04. Legs yellowish brown, with black markings. Leg measurements: I 2.87 (0.87, 1.00, 0.60, 0.40); II 2.85 (0.93, 0.94, 0.57, 0.41); III 2.25 (0.70, 0.70, 0.51, 0.34); IV 2.55 (0.77, 0.84, 0.54, 0.40). Leg formula: 1243. Opisthosoma oval. Dorsum yellowish brown, with a few black markings and many white scaly markings. Venter yellowish brown. Spinnerets short and yellow-brown with black markings.

Epigyne (Figs 7C, D, 8F, G). Copulatory openings nearly 9-shaped, facing away from each other, separated by about 4.5 times their width. Copulatory ducts slightly sclerotized, short, slightly curved. Spermatheca curved, spermathecal heads round. Fertilization ducts thin, semicircular, and directed laterally.

Variation. Male ($n = 5$) total length 1.91–2.30; female ($n = 37$) total length 2.24–2.42.

Distribution. China (Hainan) (Fig. 15).

***Sudesna hedini* (Schenkel, 1936)**

Figs 9, 10, 15

(赫氏苏蛛)

Dictyna hedini Schenkel, 1936: 14, f. 2 (♂♀); Paik 1979: 423, figs 11–21 (♂♀); Zhu and Shi 1985: 57, figs 46a–c (♀).

Sudesna hedini: Lehtinen, 1967: 265, figs 305, 318 (♂♀); Song and Lu 1985: 80, fig. 4A, B (♀); Song 1987: 79, fig. 43 (♀); Feng 1990: 37, fig. 12 (♀); Song et al. 1999: 365, fig. 216D, E (♀); Song et al. 2001: 288, fig. 182A, B (♀); Namkung 2002: 385, fig. 27.10a, b (♂♀); Namkung 2003: 387, fig. 27.10a, b (♂♀); Marusik et al. 2006: 355, fig. 5 (♂); Zhang and Li 2011: 30, fig. 7A–H (♂♀); Esyunin and Sozontov 2016: 204, fig. 13 (♀); Kim and Lee 2017: 49, fig. 28A, B (♀).

Dictyna yongshun Yin, Bao & Kim, 2001: 170, figs 1–4 (♂); Yin et al. 2012: 976, fig. 496a–d (♂). syn. nov.

Material examined. **Hunan:** 1 ♂ (holotype of *Dictyna yongshun* Yin, Bao & Kim, 2001), Yongshun County, Buermen; 12 September 1996; C.M. Yin leg. (HNU) • **Guizhou:** 1 ♀ (SWUC-DI-SH-01); Guiyang City, Qianling Park; 26°35'55"N, 106°41'35"E; elev. 1172 m; 8 October 2012; L.Y. Wang, X.K. Jiang leg. • 1 ♂ (SWUC-DI-SH-02), Guiding County, Yanxia Town; 26°23'00"N, 107°18'13"E; elev. 1173 m; 8 August 2007; Z.S. Zhang leg.; • 2 ♂ (SWUC-DI-SH-03 to 04); Xishui County, Tucheng Town; 28°16'40"N, 105°59'48"E; elev. 307 m; 17 September 2016; Z.Z. Yang leg. • 6 ♀ (SWUC-DI-SH-05 to 10); Kaili City, Leishan County, Leigongshan National Nature Reserve, Xiaodanjiang; 26°21'21"N, 108°09'30"E; elev. 1409 m; 17 September 2005; Z.S. Zhang, H.M. Chen leg. • **Hebei:** 1 ♀ (SWUC-DI-SH-11); Xiaowutai Mountain, Yangjiaping, 39°56'10"N, 114°56'43"E; elev. 1440 m; 30 July 2012; F. Zhang leg. • **Hubei:** 1 ♀ (SWUC-DI-SH-12); Shennongjia, Muyuping; 31°27'54"N, 110°23'53"E; elev. 1207m; 24 September 2001; M.S. Zhu leg. • **Liaoning:** 1 ♂ (SWUC-DI-SH-13); Dandong City, Jinjiangshan Park; 40°08'02"N, 124°22'32"E; elev. 84 m; 16 August 2009; H.M. Chen, Z. Li, H.P. Wang leg. • 1 ♀ (SWUC-DI-SH-14); Benxi City, Huanren County, Wunvshan; 41°19'38"N,

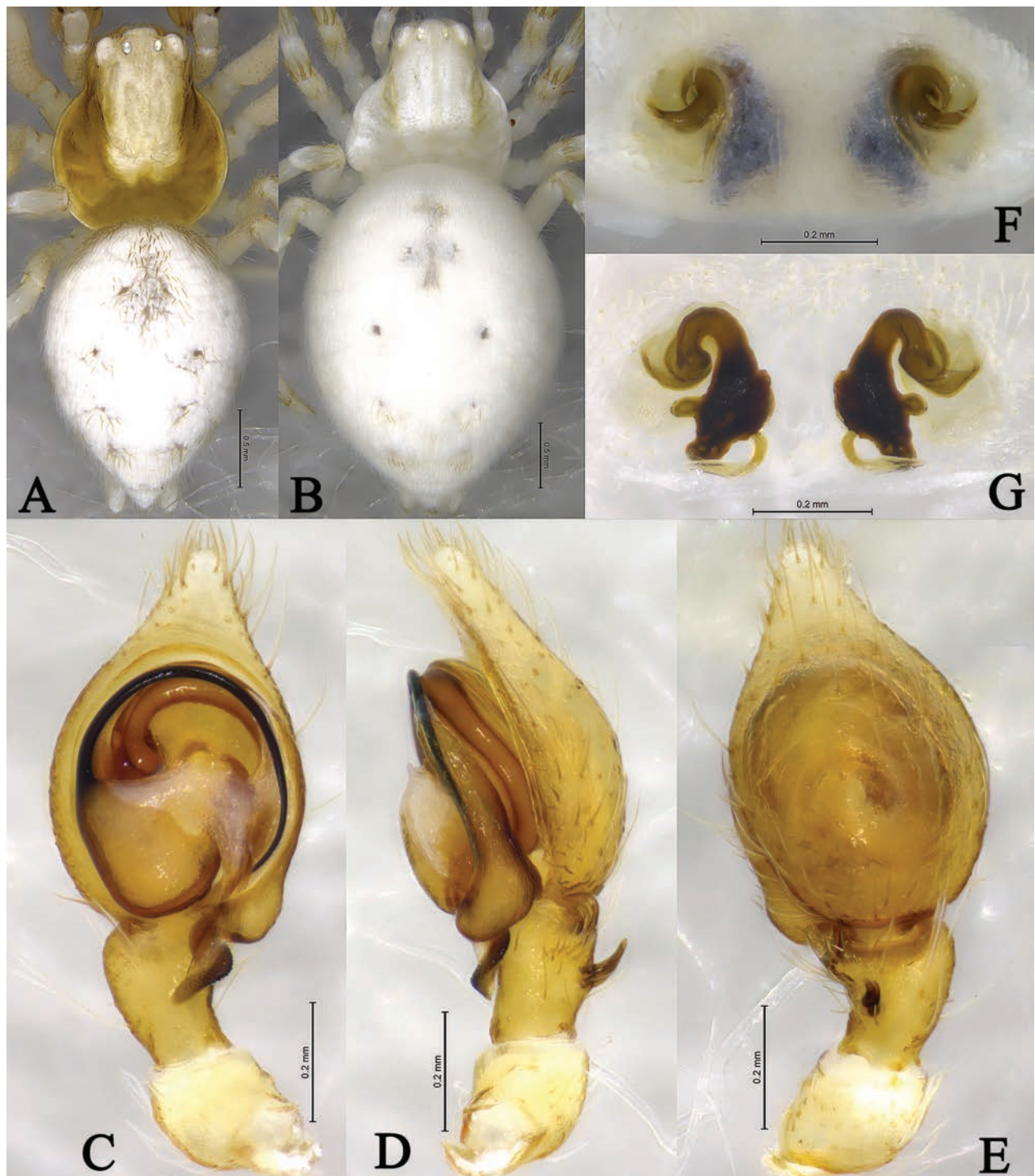


Figure 9. *Sudesna hedini* (Schenkel, 1936) male (SWUC-DI-SH-56, **A, C–E**) and female (SWUC-DI-SH-57, **B, F, G**). **A** Male habitus, dorsal view **B** female habitus, dorsal view **C** left male palp, ventral view **D** same, retrolateral view **E** same, dorsal view **F** epigyne, ventral view **G** vulva, dorsal view.

125°25'01"E; elev. 627 m; 21 August 2009; H.M. Chen, Z. Li, H.P. Wang leg. • 4 ♂
 14 ♀ (SWUC-DI-SH-15 to 32); Benxi City, Huanren County, Wangtiandong Scenic
 Spot; 41°11'24"N, 125°16'04"E; elev. 280 m; 20 August 2009; H.M. Chen, Z. Li,
 H.P. Wang leg. • 1 ♂ (SWUC-DI-SH-33); Kuandian County, Tianhuashan Scenic
 Spot; 41°05'06"N, 124°34'50"E; elev. 724 m; 17 August 2009; H.M. Chen, Z. Li,
 H.P. Wang leg. • **Shaanxi**: 1 ♂ (SWUC-DI-SH-34); Mei County, Tangyu, Taibaishan;



Figure 10. *Sudesna hedini* (Schenkel, 1936) (holotype of *Dictyna yongshun* Yin, Bao & Kim, 2001). **A** Left male palp, ventral view **B** same, retrolateral view.

34°07'46"N, 107°53'50"E; elev. 703 m; 10 September 2004; Z.S. Zhang, H.M. Chen leg. • 2 ♀ (SWUC-DI-SH-35 to 36); Zhouzhi County, Houzhenzi Town; 33°50'49"N, 107°50'01"E; elev. 1305 m; 14 September 2011; L.Y. Wang, Z. Li, D. Wang leg. • **Sichuan:** 8 ♂ 11 ♀ (SWUC-DI-SH-37 to 55); Jiulong County, Wanba Town; 29°04'16"N, 102°03'09"E; elev. 2078 m; 28 September 2008; H.M. Chen leg. • 1 ♂ 2 ♀ (SWUC-DI-SH-56 to 58); Luding County, Moxi Town; 29°39'04"N, 102°06'53"E; elev. 1572 m; 12 November 2019; Z.S. Zhang, L.Y. Wang leg.

Diagnosis. This species is similar to *S. shangrila* sp. nov. (Figs 11, 12) in having a hook-shaped retrolateral tibial apophysis and spiraled copulatory openings, but it can be distinguished by the spiral posterior arm of the conductor (vs slightly twisted), the curved copulatory duct (vs columnar), and the bud-shaped spermathecal head (vs round).

Distribution. China (Beijing, Gansu, Guizhou, Hebei, Hubei, Hunan, Liaoning, Shanxi, Shaanxi, Sichuan, Zhejiang) (Fig. 15).

Remarks. Although we did not examine the type of *S. hedini*, the published figures of it (Schenkel 1936; Lehtinen 1967) are clear enough. We carefully compared *D. yongshun* (type examined, Fig. 10) and *S. hedini* (Fig. 9), and found that these two species share the same structures, such as the helical posterior arm

of conductor, the semicircular embolus originating at about the 9:00 o'clock position, and two ctenidia located dorso-medially on the tibia. Therefore, we consider *D. yongshun* to be a junior synonym of *S. hedini* (Schenkel, 1936).

***Sudesna shangrila* sp. nov.**

<https://zoobank.org/6CB767CD-9CBC-4E37-B45E-73F1B9FF087D>

Figs 11, 12, 15

(香格里拉苏蛛)

Type material. *Holotype* ♂ (SWUC-T-DI-18-01); **Yunnan Province**; Shangrila, Tianshengqiao, Geothermal park; 27°47'53"N, 99°48'46"E; elev. 3406 m; 21 August 2009; Z.X. Li and L.Y. Wang leg. *Paratypes*: 1 ♂ 7 ♀, (SWUC-T-DI-18-02 to 09); same data as holotype.

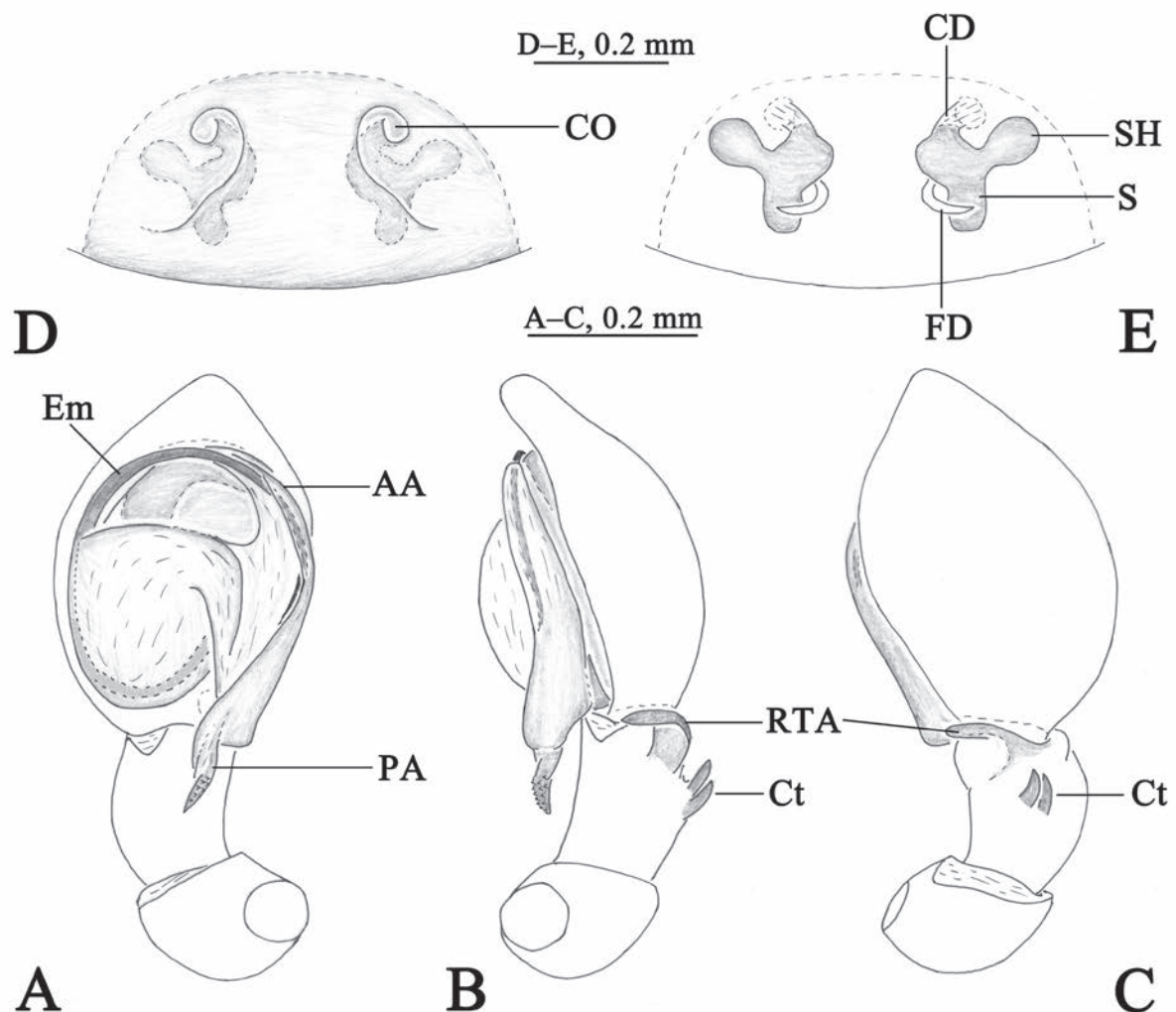


Figure 11. *Sudesna shangrila* sp. nov. holotype male (**A–C**) and paratype female (**D, E**). **A** Left male palp, ventral view **B** same, retrolateral view **C** same, dorsal view **D** epigyne, ventral view **E** vulva, dorsal view. Abbreviations: AA = anterior arm of conductor; CD = copulatory duct; CO = copulatory opening; Ct = ctenidia; Em = embolus; FD = fertilization duct; PA = posterior arm of conductor; RTA = retrolateral tibial apophysis; S = spermathecal; SH = spermathecal head.

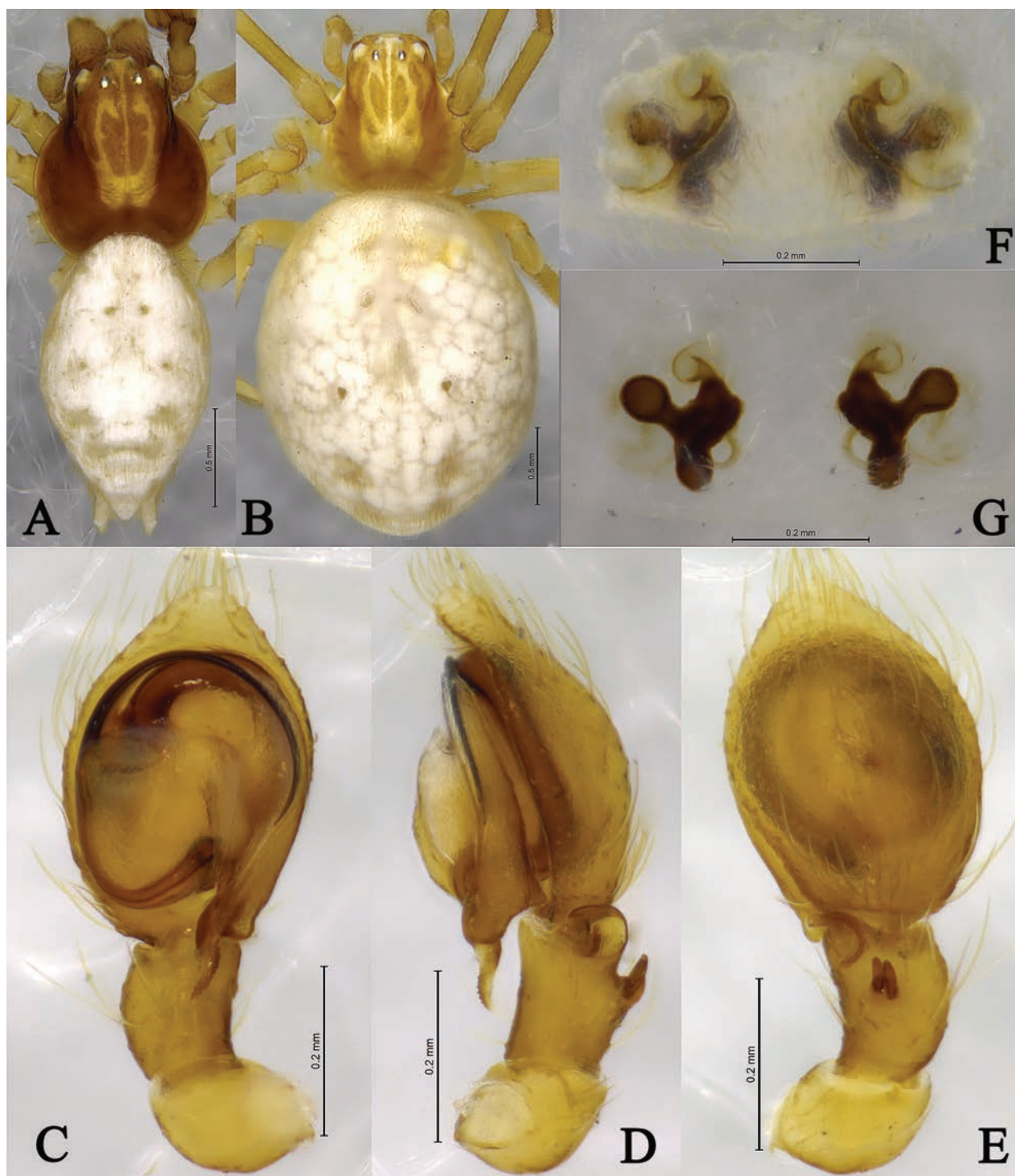


Figure 12. *Sudesna shangrila* sp. nov. holotype male (**A**, **C–E**) and paratype female (**B**, **F**, **G**). **A** Male habitus, dorsal view **B** female habitus, dorsal view **C** left male palp, ventral view **D** same, retrolateral view **E** same, dorsal view **F** epigyne, ventral view **G** vulva, dorsal view.

Etymology. The specific name is derived from the county where the type locality is located; used as a noun in apposition.

Diagnosis. See the diagnosis of *S. haiboi* sp. nov.

Description. **Male holotype** (Fig. 12A) total length 2.30. Prosoma 1.04 long, 0.90 wide; opisthosoma 1.38 long, 0.86 wide. Dorsum of prosoma brown, with

white high cephalic area. Eye sizes and interdistances: AME 0.05, ALE 0.07, PME 0.05, PLE 0.07; AME–AME 0.12, AME–ALE 0.08, PME–PME 0.13, PME–PLE 0.13, ALE–PLE 0.03. MOA 0.18 long, anterior width 0.19, posterior width 0.24. Clypeus height 0.11. Chelicerae stout, yellow-brown, with 3 promarginal and 2 retromarginal teeth. Legs yellow brown. Leg measurements: I 2.94 (0.92, 0.99, 0.62, 0.41), II 2.83 (0.87, 0.95, 0.60, 0.41), III 2.25 (0.74, 0.72, 0.48, 0.31), IV 2.49 (0.77, 0.85, 0.58, 0.29). Leg formula: 1243. Opisthosoma oval. Dorsum yellowish brown, with white markings. Venter yellowish brown. Spinnerets short and yellowish brown.

Palp (Figs 11A, B, 12C–E). Tibia dorsally with 2 ctenidia, located 1/3 from distalmost part of tibia. Retrolateral tibia apophysis hook-shaped. Embolus semicircular, originating near the 9:30 o'clock position, terminating at about the 4:00 o'clock position. Anterior arm of conductor (AA) membranous and terminating near the 12:00 o'clock position; posterior arm (PA) slightly twisted with a pointed, scaly tip.

Female paratype (SWUC-T-DI-18-02, Fig. 12B) total length 3.76. Prosoma 1.36 long, 1.13 wide; opisthosoma 2.64 long, 1.97 wide. Dorsum of prosoma yellowish brown, with white high cephalic area. Eye sizes and interdistances: AME 0.06, ALE 0.07, PME 0.06, PLE 0.07; AME–AME 0.16, AME–ALE 0.12, PME–PME 0.17, PME–PLE 0.16, ALE–PLE 0.04. MOA 0.21 long, anterior width 0.25, posterior width 0.29. Clypeus height 0.12. Legs yellowish brown. Leg measurements: I 3.48 (1.09, 1.16, 0.75, 0.48), II 3.47 (1.05, 1.15, 0.70, 0.47), III 2.90 (0.94, 0.98, 0.64, 0.34), IV 3.51 (1.12, 1.25, 0.80, 0.34). Leg formula: 1243. Opisthosoma oval. Dorsum yellowish brown, with white scaly markings. Venter yellowish brown. Spinnerets short and yellowish brown.

Epigyne (Figs 11C, D, 12F, G). Copulatory openings nearly spiral, facing away from each other, separated by about 4 times their width. Copulatory ducts short, slightly sclerotized. Spermatheca cylindrical; spermathecal heads round. Fertilization ducts thin, semicircular, and directed laterally.

Variation. Male ($n = 2$) total length 2.06–2.30; female ($n = 7$) total length 2.65–3.76.

Distribution. Known only from the type locality, Yunnan, China (Fig. 15).

***Sudesna yangi* sp. nov.**

<https://zoobank.org/8D303C1E-237D-4A68-8EB3-7EED0A0B6413>

Figs 13, 14, 15

(杨氏苏蛛)

Type material. **Holotype** ♂ (SWUC-T-DI-19-01); **Yunnan Province**; Dali City, Mount Cangshan, Xieyangfeng; 25°35'39"N, 100°11'23"E; elev. 2573 m; 11 September 2011; Z.Z. Yang leg. **Paratypes**: 3 ♂ 6 ♀ (SWUC-T-DI-19-02 to 10); same data as holotype. • 1 ♀ (SWUC-T-DI-19-11); Mount Cangshan, Dapoqing; 25°34'38"N, 100°07'51"E; elev. 2043 m; 30 August 2009; Z.Z. Yang leg. • 6 ♂ 4 ♀ (SWUC-T-DI-19-12 to 21); Mount Cangshan, Yujufeng; 25°42'21"N, 100°7'7"E; elev. 2600 m; 13 September 2009; Z.Z. Yang leg. • 1 ♂ (SWUC-T-DI-19-22); Mount Cangshan, Xieyangfeng; 25°35'24"N, 100°11'47"E; elev. 2500 m; 22 November 2011; P. Feng leg. • 2 ♀ (SWUC-T-DI-19-23 to 24); Mount Cangshan, Xieyangfeng; 5°35'40"N, 100°11'21"E; elev. 2500 m; 14 June 2011; Y. He leg. • 3 ♀ (SWUC-T-DI-19-25 to 27); Eyuan County, Cibi Township,

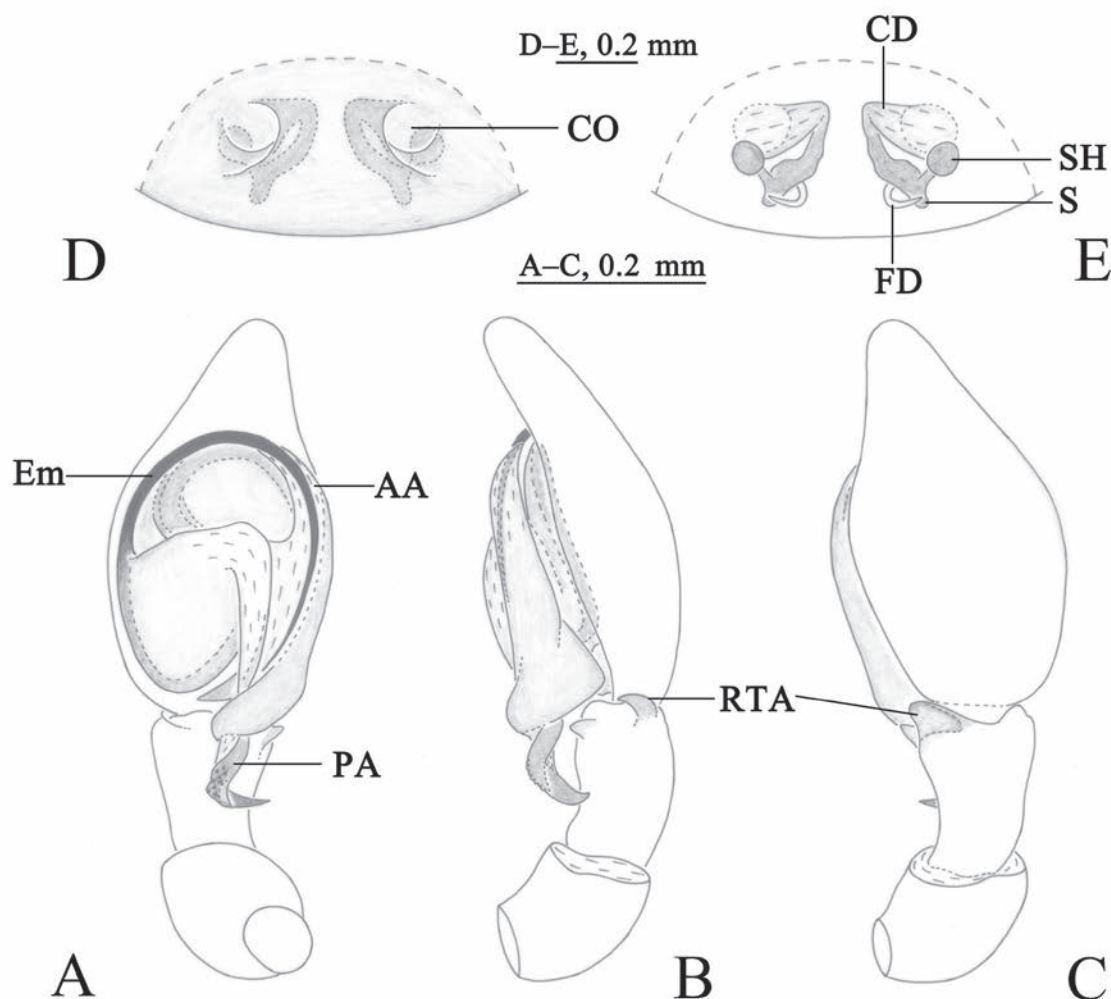


Figure 13. *Sudesna yangi* sp. nov. holotype male (**A–C**) and paratype female (**D, E**). **A** Left male palp, ventral view **B** same, retrolateral view **C** same, dorsal view **D** epigyne, ventral view **E** vulva, dorsal view. Abbreviations: AA = anterior arm of conductor; CD = copulatory duct; CO = copulatory opening; Ct = ctenidia; Em = embolus; FD = fertilization duct; PA = posterior arm of conductor; RTA = retrolateral tibial apophysis; S = spermathecal; SH = spermathecal head.

Biaoshan; 26°09'41"N, 99°54'21"E; elev. 2310 m; 17 August 2009; Z.X. Li and L.Y. Wang leg. • 1 ♂ (SWUC-T-DI-19-28); Kunming City, Mount Xishan, Maomaoqing; 24°57'20"N, 102°37'54"E; elev. 2204 m; 13 October 2016; G.Q. Huang, X.B. Guo and Y.C. Wang leg. • 1 ♀ (SWUC-T-DI-19-29); Baoshan City, Longyang District, Mangkuan Township, Mount Gaoligong; 25°18'27"N, 98°47'42"E; elev. 1496 m; 6 October 2015; T. Lu and Y.C. Zhou leg. • 2 ♀ (SWUC-T-DI-19-30 to 31); Baoshan City, Longyang District, Mangkuan Township, Mount Gaoligong; 25°18'05"N, 98°47'24"E; elev. 1793 m; 8 October 2015; T. Lu and Y.C. Zhou leg.

Etymology. This species is named after the collector of the holotype and some paratype material; a noun in genitive case.

Diagnosis. The male of this new species is similar to *S. circularis* Zhang & Li, 2011 (Zhang and Li 2011: 30, figs 8A–C, 9A–F) in having a long embolus and lacking tibial ctenidia, but it can be distinguished by the pale opisthosoma (vs yellow-brown with black markings) (Fig. 14A) and the embolus originating at the 9:00 o'clock position (vs 8:30) (Figs 13A–C, 14C–E). For the diagnosis of the female of *S. yangi*, see *S. cangshan* sp. nov. part.



Figure 14. *Sudesna shangrila* sp. nov. holotype male (**A, C–E**) and paratype female (**B, F, G**). **A** Male habitus, dorsal view **B** female habitus, dorsal view **C** left male palp, ventral view **D** same, retrolateral view **E** same, dorsal view **F** epigyne, ventral view **G** vulva, dorsal view.

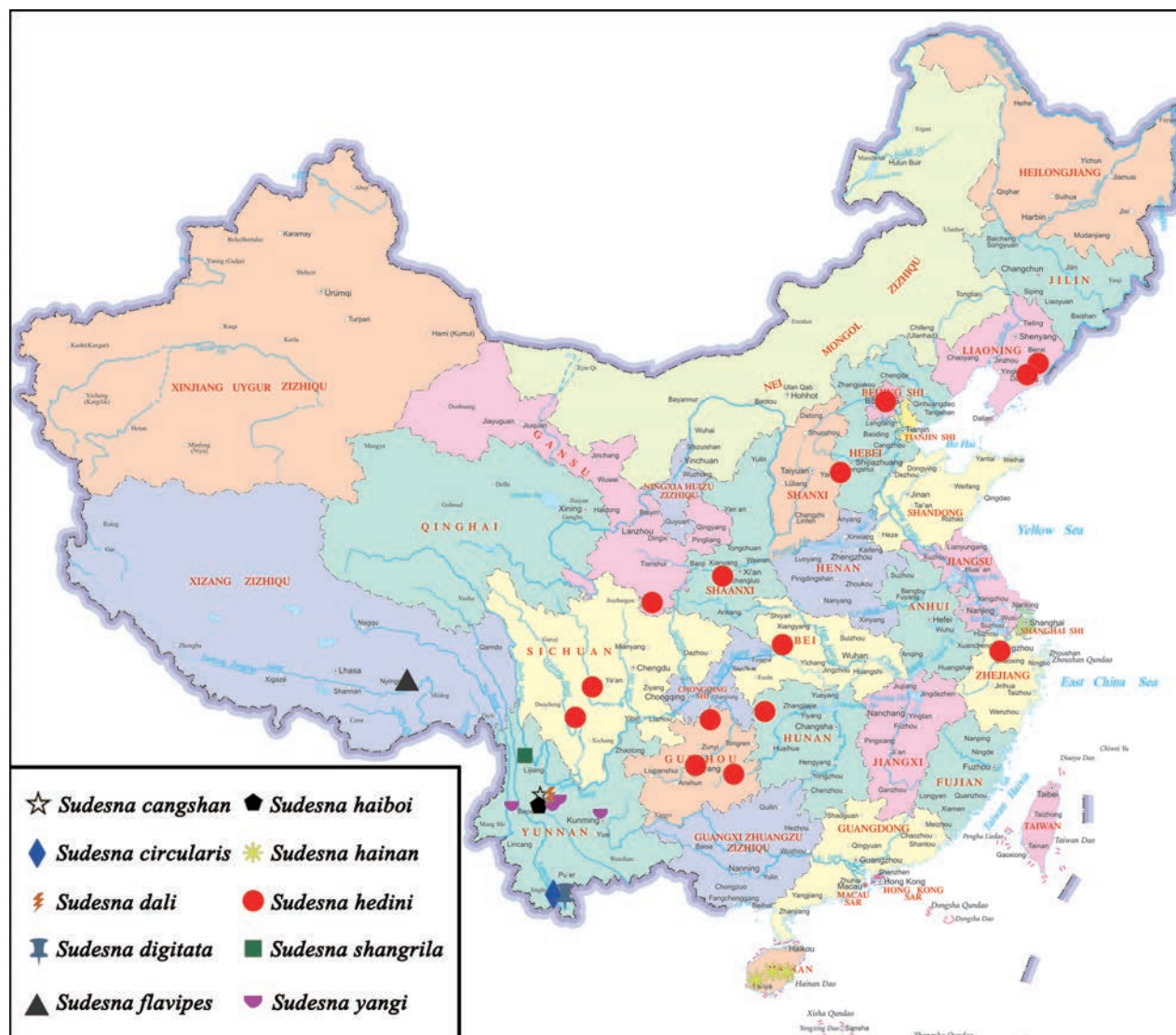


Figure 15. Distribution of *Sudesna* species in China.

Description. **Male holotype** (Fig. 14A) total length 3.76. Prosoma 1.70 long, 1.42 wide; opisthosoma 2.13 long, 1.48 wide. Dorsum of prosoma brown, with high cephalic area. Eye sizes and interdistances: AME 0.07, ALE 0.11, PME 0.10, PLE, 0.11; AME–AME 0.14, AME–ALE 0.11, PME–PME 0.15, PME–PLE 0.16, ALE–PLE 0.02. MOA 0.29 long, anterior width 0.26, posterior width 0.32. Clypeus height 0.16. Chelicerae stout, brown, with 4 promarginal and 3 retro-marginal teeth. Legs yellow-brown. Leg measurements: I 6.08 (1.86, 2.18, 1.28, 0.76); II 6.34 (1.72, 2.02, 1.90, 0.70); III 4.02 (1.27, 1.28, 0.93, 0.54); IV 4.48 (1.36, 1.54, 1.08, 0.50). Leg formula: 1243. Opisthosoma oval. Dorsum and venter pale. Spinnerets short and yellowish brown.

Palp (Figs 13A, B, 14C–E). Tibia without ctenidia. Retrolateral tibial apophysis hook-shaped in retrolateral view. Embolus somewhat O-shaped and originating at about the 9:00 o'clock position, terminating at about the 5:00 o'clock position. Anterior arm of conductor (AA) tapering and distally reaching the 12:30 o'clock position; posterior arm (PA) spiral, with a pointed, scaly tip.

Female paratype (SWUC-T-DI-19-02, Fig. 14B) total length 3.78. Prosoma 1.36 long, 1.13 wide; opisthosoma 2.67 long, 1.99 wide. Dorsum of prosoma yellowish brown, with high cephalic area. Eye sizes and interdistances: AME 0.05, ALE 0.10, PME 0.09, PLE, 0.09; AME–AME 0.13, AME–ALE 0.10, PME–PME 0.14, PME–PLE 0.15, ALE–PLE 0.05. MOA 0.25 long, anterior width 0.23, posterior width 0.31. Clypeus height 0.14. Legs yellow-brown. Leg measurements: I 5.14 (1.61, 1.75, 1.07, 0.71); II 4.66 (1.52, 1.52, 1.00, 0.62); III 3.81 (1.20, 1.24, 0.85, 0.52); IV 4.58 (1.41, 1.59, 1.06, 0.52). Leg formula: 1243. Opisthosoma oval. Dorsum and venter pale. Spinnerets short and yellowish brown.

Epigyne (Figs 13C, D, 14F, G). Copulatory openings large, 9-shaped, facing away from each other, separated by about 1.7 times their width. Copulatory ducts slightly sclerotized, long and abruptly bent. Spermatheca clavate, spermathecal heads round. Fertilization ducts semicircular, directed laterally.

Variation. Male ($n = 12$) total length 3.76–4.15; female ($n = 16$) total length 3.78–4.57.

Distribution. China (Yunnan) (Fig. 15).

Acknowledgements

Great thanks are given to the subject editor, Dr. Dimitar Dimitrov, and two reviewers, Dr. Sarah Crews and Martin Ramirez for their helpful comments. Many thanks are given to Prof. Feng Zhang (College of Life Sciences, Hebei University, Baoding, China) and Prof. Zi-Zhong Yang (Yunnan Provincial Key Laboratory of Entomological Biopharmaceutical R & D, Dali University, Dali, China) for sending specimens as gifts.

Additional information

Conflict of interest

The authors have declared that no competing interests exist.

Ethical statement

No ethical statement was reported.

Funding


This work was supported by the National Natural Science Foundation of China (31060070) to Zi-Zhong Yang.


Author contributions

All authors have contributed equally.

Author ORCIDs

Lu-Yu Wang  <https://orcid.org/0000-0002-5250-3473>

Xian-Jin Peng  <https://orcid.org/0000-0002-2614-3910>

Zhi-Sheng Zhang  <https://orcid.org/0000-0002-9304-1789>



Data availability

All of the data that support the findings of this study are available in the main text.

References

- Álvarez-Padilla F, Hormiga G (2007) A protocol for digesting internal soft tissues and mounting spiders for scanning electron microscopy. *Journal of Arachnology* 35: 538–542. <https://doi.org/10.1636/Sh06-55.1>
- Esyunin SL, Sozontov AN (2016) On a new Eurasian species of *Dictyna* Sundevall, 1833 (Aranei: Dictynidae), with taxonomic notes on poorly known Palaearctic *Dictyna* species. *Arthropoda Selecta* 25(2): 199–206. <https://doi.org/10.15298/arthscl.25.2.06>
- Feng ZQ (1990) *Spiders of China in Colour*. Hunan Science and Technology Publishing House, Changsha, 256 pp.
- Kim ST, Lee SY (2017) Arthropoda: Arachnida: Araneae [sic]: Oecobiidae, Oxyopidae, Cybaeidae, Dictynidae, Sparassidae, Philodromidae. *Spiders II. Invertebrate Fauna of Korea* 21(42): 1–122.
- Lehtinen PT (1967) Classification of the cribellate spiders and some allied families, with notes on the evolution of the suborder Araneomorpha. *Annales Zoologici Fennici* 4: 199–468.
- Marusik YM, Ovtchinnikov SV, Koponen S (2006) Uncommon conformation of the male palp in common Holarctic spiders belonging to the *Lathys stigmatisata* group (Araneae, Dictynidae). *Bulletin of the British Arachnological Society* 13(9): 353–360.
- Namkung J (2002) *The Spiders of Korea*. Kyo-Hak Publishing, Seoul, 648 pp.
- Namkung J (2003) *The Spiders of Korea*, 2nd ed. Kyo-Hak Publishing, Seoul, 648 pp.
- Paik KY (1979) Korean spiders of family Dictynidae. *Research Review of Kyungpook National University* 27: 419–431.
- Schenkel E (1936) Schwedisch-chinesische wissenschaftliche Expedition nach den nordwestlichen Provinzen Chinas, unter Leitung von Dr. Sven Hedin und Prof. Sü Pingchang. Araneae gesammelt vom schwedischen Arzt der Expedition Dr. David Hummel 1927–1930. *Arkiv för Zoologi* 29(A1): 1–314.
- Song DX (1987) *Spiders from agricultural regions of China* (Arachnida: Araneae). Agriculture Publishing House, Beijing, 376 pp.
- Song DX, Lu L (1985) On some dictynids from China (Araneae: Dictynidae). *Sinozoologia* 3: 77–83.
- Song DX, Zhu MS, Chen J (1999) *The Spiders of China*. Hebei Science and Technology Publishing House, Shijiazhuang, 640 pp.
- Song DX, Zhu MS, Chen J (2001) *The Fauna of Hebei, China: Araneae*. Hebei Science and Technology Publishing House, Shijiazhuang, 510 pp.
- Yin CM, Bao YH, Kim JP (2001) A new species of the genus *Dictyna* from China (Araneae: Dictynidae). *Korean Arachnology* 17: 169–172.
- Yin CM, Peng XJ, Yan HM, Bao YH, Xu X, Tang G, Zhou QS, Liu P (2012) *Fauna Hunan: Araneae in Hunan, China*. Hunan Science and Technology Press, Changsha, 1590 pp.
- Zhang ZS, Li SQ (2011) On four new canopy spiders of Dictynidae (Araneae) from Xishuangbanna rainforest, China. *Zootaxa* 3066: 21–36. <https://doi.org/10.11646/zootaxa.3066.1.2>
- Zhang ZS, Wang LY (2017) *Chinese Spiders Illustrated*. Chongqing University Press, Chongqing, 954 pp.
- Zhu MS, Shi JG (1985) Crop field spiders of Shanxi Province. *Agriculture Planning Committee of Shanxi Province* 1983: 239 pp.

Caribbean Amphipoda (Crustacea) of Panama. Part IV: parvorder Caprellidira

Sally J. Sir¹ , Kristine N. White¹ 

¹ Aquatic Sciences Center, Department of Biological and Environmental Sciences, Georgia College & State University, Milledgeville, GA 31061, USA
Corresponding author: Sally J. Sir (sally.sir13@gmail.com)

Abstract

The parvorder Caprellidira includes 1,244 described species in 17 families. The diverse morphology of caprellidiran amphipods ranges from thread-like to more typical laterally compressed body forms. Caprellidiran amphipods are associated with coral rubble, sea-grasses, sponges, algae, and sand and typically feed on detritus from the water column. Twenty species from five families within the parvorder are documented from Bocas del Toro, Panama. Five species are new to science and a range extension is documented for 15 species. All species are diagnosed, new species are described, and an identification key to the Caprellidira amphipods of Panama is provided herein.

Resumen

El parvorden Caprellidira incluye 1,244 especies descritas, distribuidas en 17 familias, con una morfología que varía desde formas corporales filiformes hasta las típicamente comprimidas lateralmente. Estas especies están asociadas a hábitats como escombros de coral, pastos marinos, esponjas, algas y sedimentos arenosos, donde suelen alimentarse de detritos en la columna de agua. En Bocas del Toro, Panamá, se han registrado 20 especies pertenecientes a cinco familias, de las cuales cinco representan descubrimientos nuevos para la ciencia, y se ha documentado una expansión del rango de distribución para 15 especies. Se diagnostican todas las especies, se describen nuevas especies y se proporciona una clave de identificación de los anfípodos Caprellidiran de Panamá.

Key words: Bocas del Toro, Caprellidae, Caprellidira, identification key, Ischyroceridae, Neomegamphopidae, Photidae, Podoceridae



This article is part of:
Caribbean Amphipoda of Panama
Edited by Kristine N. White

Academic editor: Alan Myers
Received: 3 January 2025
Accepted: 31 January 2025
Published: 10 April 2025

ZooBank: <https://zoobank.org/015A0803-9479-4905-8A7D-FECF01495883>

Citation: Sir SJ, White KN (2025) Caribbean Amphipoda (Crustacea) of Panama. Part IV: parvorder Caprellidira. ZooKeys 1234: 151–205. <https://doi.org/10.3897/zookeys.1234.145826>

Copyright: © Sally J. Sir & Kristine N. White.
This is an open access article distributed under terms of the Creative Commons Attribution License (Attribution 4.0 International – CC BY 4.0).

Introduction

Caprellidira Leach, 1814 (sensu Lowry and Myers 2013) is a parvorder consisting of 1,224 species distributed in a cosmopolitan manner (Horton et al. 2024). The parvorder Caprellidira was originally classified as infraorder Caprellida (Myers and Lowry 2003) based on the hypothesis that ancestors of these species consumed suspended matter found in the water column. This feeding behavior is reflected in several families such as Caprellidae which hold

on to substrate with pereopods 5–7 and catch suspended matter as it drifts by. Amphipods in the genus *Cerapus* have a thick article 1 on antenna 1, which may provide extra strength to collect suspended matter with their antennae. Morphology varies drastically in the Caprellidira, with members of Caprellidae exhibiting threadlike bodies and other families with laterally compressed or subcylindrical bodies. Caprellida was reclassified as the parvorder Caprellidira by Lowry and Myers (2013).

The Caprellidira comprises 17 families: Aetiopedesidae Myers & Lowry, 2003 (one sp.); Australomicrotopodidae Myers, Lowry & Billingham, 2016 (one sp.); Caprellidae Leach 1814 (452 spp.); Caprogammaridae Kudrjashov & Vassilenko, 1966 (two spp.); Cyamidae Rafinesque, 1815 (29 spp.); Dulichiidae Dana, 1849 (30 spp.); Isaeidae Dana, 1852 (seven spp.); Ischyroceridae Stebbing, 1899 (293 spp.); Kamakidae Myers & Lowry, 2003 (43 spp.); Microtopodidae Myers & Lowry, 2003 (five spp.); Neomegamphopidae Myers, 1981 (22 spp.); Paragammaropsidae Myers & Lowry, 2003 (two spp.); Photidae Boeck, 1871 (238 spp.); Podoceridae Leach, 1814 (93 spp.); Priscosmilitaridae Hirayama, 1988 (three spp.); Protodulichiidae Ariyama, 2019, in Ariyama and Hoshino 2019 (one sp.); Rakiroidae Myers & Lowry, 2003 (one sp.).

Prior to this study, 70 caprellidiran species in six families were documented from Caribbean waters: Caprellidae, Ischyroceridae, Kamakidae, Neomegamphopidae, Photidae, and Podoceridae (LeCroy et al. 2009; Miloslavich et al. 2010; Martín et al. 2013). *Paracaprella barnardi* (McCain, 1967) is the only species previously documented from Caribbean Panama and *Posophotis seri* Barnard, 1979 was previously documented from the canal zone on the Pacific side of Panama (Barnard 1979). Twenty Caprellidira species were collected during this study, including five species new to science.

Materials and methods

Coral rubble, algae, sand, seagrass, hydroids, sponges, and buoy scrapings were collected at 13 sites around Bocas del Toro, Panama at depths of 0.2–15 m. Substrates were elutriated with freshwater and amphipods were sorted into morphospecies while alive. Live specimens were placed in clove oil for imaging and preserved in 99.5% EtOH. Preserved specimens were examined in glycerol after being measured from the tip of the rostrum to the base of the telson. Amphipods were dissected using a stereomicroscope and illustrated using an Olympus BH2 differential interference contrast microscope with an Olympus BH2-DA drawing tube attached. Pencil drawings were digitally inked using a Wacom® Intuos Pro Pen tablet following the methods of Coleman (2003) in Adobe Illustrator 2020. Abbreviations used in figures are as follows: **H**, habitus; **Hd**, head; **A**, antenna; **Mx**, maxilla; **Md**, mandible; **UL**, upper lip; **LL**, lower lip; **Xpd**, maxilliped; **C**, coxa; **G**, gnathopod; **P**, pereopod; **E**, epimeron; **Pl**, pleopod; **U**, uropod; **T**, telson; **R**, right; **L**, left. Size ranges of each species collected from Bocas del Toro, Panama are provided at the beginning of each material examined section. Specimens are deposited in the Smithsonian Institution, U.S. National Museum of Natural History (**USNM**) and the Gulf Coast Research Laboratory Museum (**GCRL**).

Results

Taxonomic account

Parvorder Caprellidira Leach, 1814 (sensu Lowry & Myers, 2013)

Superfamily Caprelloidea Leach, 1814

Family Caprellidae Leach, 1814

Genus *Deutella* Mayer, 1890

Diagnosis. Antenna 2 flagellum bi-articulate, lacking swimming setae. Mandibular palp tri-articulate. Maxilliped inner lobe shorter than outer lobe. Pereopod 5 with six articles, distinctly thinner than pereopods 6 and 7. Male abdomen with two appendages.

***Deutella caribensis* Guerra-García, Krapp-Schickel & Müller, 2006**

Figs 1, 31A

Deutella caribensis Guerra-García, Krapp-Schickel & Müller, 2006: 161–164, figs 7, 8.

Material examined. PANAMA • 3.5 mm • 1 ♀; Bocas del Toro, Bocas del Drago; 9.4134°N, 82.3334°W; depth 1–3 m, among coral rubble, 23 June 2023; K.N. White leg.; USNM 1743942.

Diagnosis. Head with paired dorsal projections. Body without lateral projections; pereonites 2–4 with dorsal projections. Pereopods 3 and 4 uni-articulate. Pereopod 5 longer than pereonite 5.

Distribution. Colombia: Bahía Concha (Guerra-García et al. 2006); Panama: Bocas del Toro (present study).

Ecology and remarks. This species occurs among algae and coral rubble at depths of 1–3 m. Panamanian specimens agree closely with the original description of this species. This is the first record of this species since the original description suggesting that the range of this species is much larger than previously known. Live specimens are yellow-brown in color with a red eye.

***Deutella* cf. *pseudoincerta* Winfield & Guerra-García, 2021**

Figs 2, 31B

Deutella pseudoincerta Winfield & Guerra-García, 2021: 4–8, figs 2–6.

Material examined. PANAMA • 2.2–2.8 mm • 3 ♂, 1 ♀; Bocas del Toro, Crawl Caye; 9.2459°N, 82.1369°W; depth 1–4 m, among coral rubble, 25 June 2023; K.N. White leg.; USNM 174393.

Diagnosis. Head and pereonites 2 and 3 with dorsal projections; pereonite 4 with posterodorsal hump; pereonites with minute setae. Male gnathopod 2 propodus with distinct excavation and single grasping spine proximally. Pereopods 3 and 4 minute, bi-articulate, ~ 0.3 × length of gills. Pereopod 5

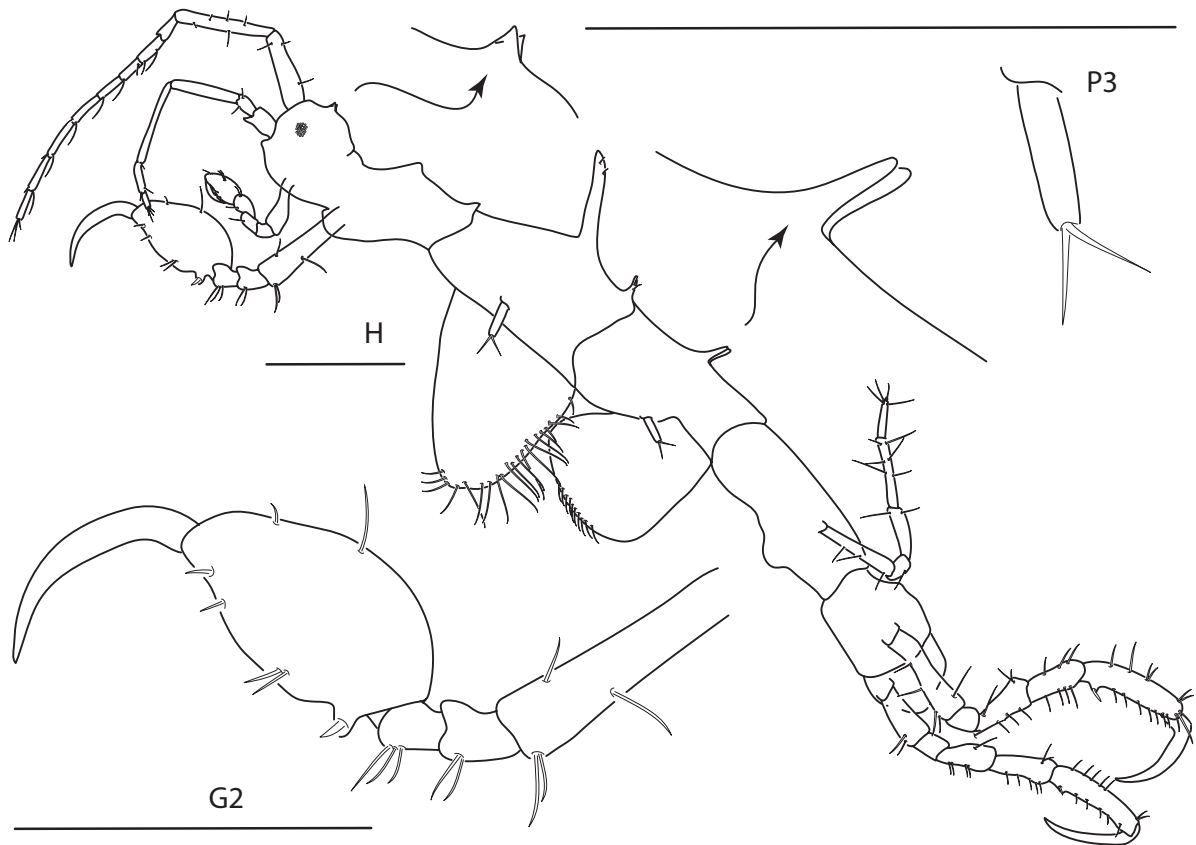


Figure 1. *Deutella caribensis*, female, 3.5 mm, habitus, gnathopod 2 lateral, and pereopod 3. Scale bars: 0.5 mm.

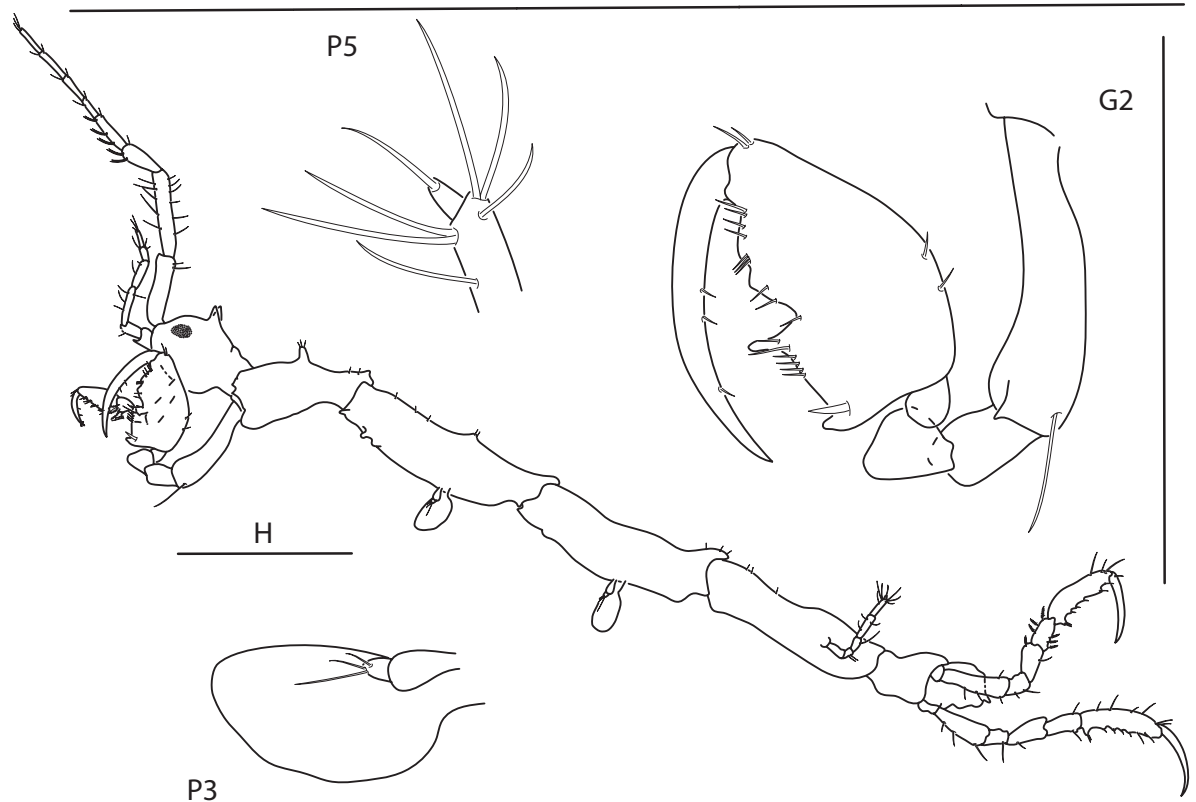


Figure 2. *Deutella* cf. *pseudoincerta*, male, 2.8 mm, habitus, gnathopod 2 medial, pereopod 3, and pereopod 5 dactylus. Scale bars: 0.5 mm.

dactylus reduced to minute article. Male abdomen with two setose lobes and two setose appendages.

Distribution. Mexico: Veracruz State (Winfield and Guerra-García 2021); Panama: Bocas del Toro (present study).

Ecology and remarks. This species occurs among coral rubble at depths of 1–4 m. Panamanian specimens agree closely with previous descriptions of the species except for having five flagellar segments on antenna 1 (8 in original description) and more apically rounded pereopods 3 and 4 (triangular in original description). The size of pereopod 5 in illustrated specimen seems to be an anomaly, as all other specimens were missing pereopod 5. Variation among specimens collected in Panama includes differences in dorsal projections on body and proximal projections on gnathopod 2 and pereopods 6 and 7. Due to the morphological variation in specimens, comparison with type material is necessary to confirm the species identification. Live specimens are white in color with purple-brown splotches and a red eye.

Genus *Paracaprella* Mayer, 1890

Diagnosis. Pereopods 3 and 4 bi-articulate. Maxilliped outer lobes significantly larger than inner lobes, not fused, bearing few setae. Mandibular palp reduced.

Paracaprella pusilla Mayer, 1890

Figs 3, 31C

Caprella nigra: Reid 1951: 283–284, 289, fig. 58.

Paracaprella pusilla Mayer, 1890: 41, taf. 1, figs 28–30, taf. 3, figs 45–47, taf. 5, fig. 48–49, taf. 6, fig. 10; Mayer 1903: 67, taf. 2, figs 36, 37, taf 7, fig. 52; Steinberg and Dougherty 1957: 283–284, figs 16, 19, 24, 30; McCain 1968: 82–86, figs 41, 42; Wakabara et al. 1991: 73; Guerra-García et al. 2006: 175, figs 17–19; Díaz et al. 2005: 6, 7, 22, fig. 13; Ros and Guerra-García 2012: 137; Ros et al. 2013: 677, fig. 2.

Material examined. PANAMA • 3.2–3.8 mm • 2 ♂, 2 ♀; Bocas del Toro, Hospital Point; 9.3333°N, 82.2185°W; depth 11 m; from buoy scrapings, 26 June 2023; K.N. White leg; USNM 1743944.

Diagnosis. Body lacking dorsal projections. Male pereonite 2 with large, triangular anteroventral projection. Gnathopod 1 dactylus reaching ~ 1/2 of propodus length. Male gnathopod 2 basis with posteroproximal bump.

Distribution. Africa: West Africa (Reid 1951); Brazil: Rio de Janeiro (Wakabara et al. 1991); Chile: Coquimbo (Guerra-García and Thiel 2001); Colombia: Magdalena (Guerra-García et al. 2006); Mediterranean Sea: Balearic Islands (Ros et al. 2013); Mexico: Gulf of Mexico (Steinberg and Dougherty 1957; Winfield et al. 2006); U.S.A.: Florida (Camp 1998); Venezuela: Falcón, Carabobo, Aragua, Sucre, Nueva Esparta (Díaz et al. 2005); Western North Atlantic (McCain 1968); Spain: Cadiz (Ros and Guerra-García 2012); Panama: Bocas del Toro (present study).

Ecology and remarks. This species occurs among mangrove roots, seagrasses, hydroids, ascidians, gravel bottoms, ropes, mussels, oysters, and

shallow waters (McCain 1968; Díaz et al. 2005; Guerra-García et al. 2006). In Bocas del Toro, this species was collected from buoy scrapings at 11 m depth. Panamanian specimens agree closely with the original description of the species; however, several descriptions show variation in the shape of the male gnathopod 2 propodus. This species has recently been documented as spreading in several non-indigenous regions (Ros and Guerra-García 2012; Ros et al. 2013). Live specimens are yellow-brown in color with brown spots and a brown eye.

Family Ischyroceridae Stebbing, 1899

Genus *Caribboecetes* Just, 1983

Diagnosis. Body subcylindrical. Rostrum pointed. Gnathopods 1 and 2 simple. Coxae 3 and 4 distal margins dentate, setose. Pereopods 5–7 lacking accessory tooth. Urosomite 3 fused to telson. Uropod 1 biramous, inner ramus shorter than outer ramus. Uropod 2 absent. Uropod 3 rami absent.

Caribboecetes intermedius Just, 1984

Figs 4, 31D

Caribboecetes intermedius Just, 1984: 48, 49, figs 9, 10.

Caribboecetes sp.: Ortiz and Lemaitre 1994: 124.

Caribboecetes justii: Ortiz and Lemaitre 1997: 82–85, figs 10–14.

Material examined. PANAMA • 1.1–4 mm • 7 ♂, 11 ♀, 12 juveniles; Bocas del Toro, Crawl Caye, 9.2449°N, 82.1383°W; depth 1.5–2.4 m, in sand; 11 Aug 2021; K.N. White leg.; USNM 1743945 • 3 ♂, 3 ♀, 7 juveniles; Bocas del Toro, Crawl Caye; 9.2475°N, 82.1290°W; depth 4.6 m, in sand; 12 Aug 2021; K.N. White leg.; USNM 1743946 • 1 ♀; Bocas del Toro, Bocas del Drago; 9.4134°N, 82.3334°W; depth 1–3 m, in sand; 23 June 2023; K.N. White leg.; USNM 1743947 • 3 ♂, 7 ♀; Bocas del Toro, Drago Beach; 9.4171°N, 82.3248°W; 0–1 m, in sand; 27 June 2023; K.N. White leg.; USNM 1743948.

Diagnosis. Rostrum acute, reaching beyond eye lobes. Coxae 1–4 ventral margin with long setae; coxa 2 with plumose setae; coxae 3 and 4 anterodistal margins subtruncate. Gnathopod 2 propodus posterior margin with 1–3 robust setae. Pereopod 7 anterior and posterior margins with long, plumose setae.

Distribution. Barbados: Bath (Just 1984); Colombia: Barú, Islas del Rosario, Gulf of Morrosquillo (Ortiz and Lemaitre 1997); Panama: Bocas del Toro (present study).

Ecology and remarks. *Caribboecetes intermedius* is a tube dwelling species that occurs in sand at depths of 1–3 m. Gnathopod 2, propodus posterior margin with robust setae (number of robust setae varying with size). After observing the type specimens for *Caribboecetes justii* and *Caribboecetes intermedius*, we believe that they are the same species. Panamanian specimens agree closely with previous descriptions of both species. Live specimens are yellow-white in color with brown markings on head and antennae.

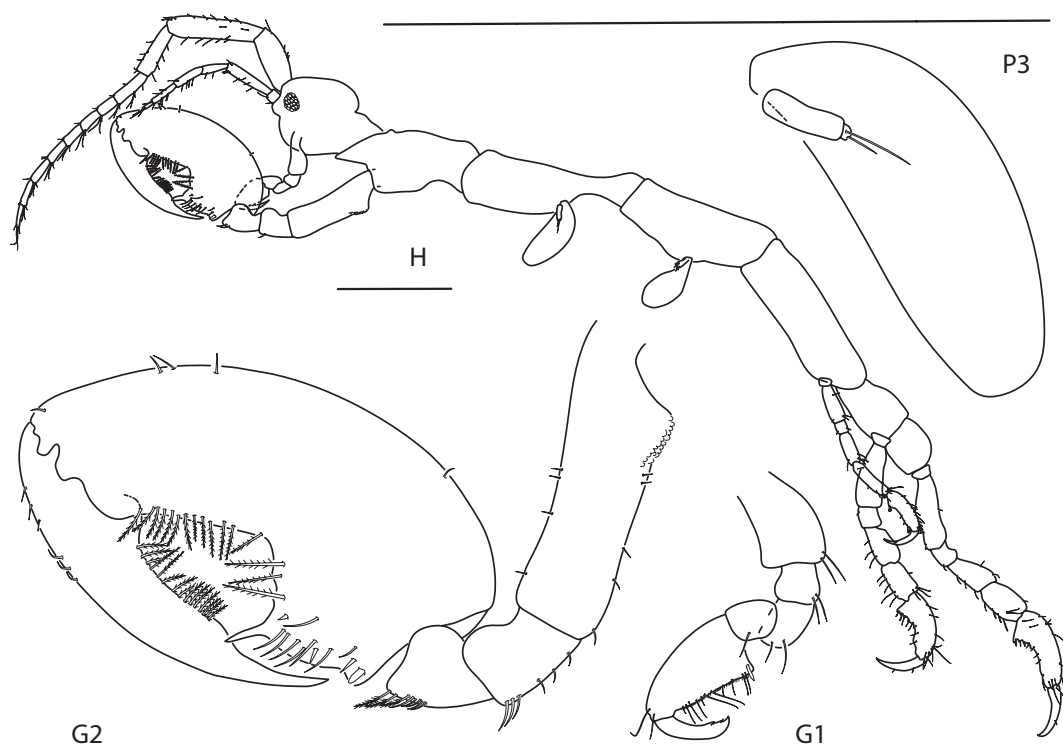


Figure 3. *Paracaprella pusilla*, male, 3.8 mm, habitus, gnathopod 2 lateral, gnathopod 1 lateral, and pereopod 3. Scale bars: 0.5 mm.

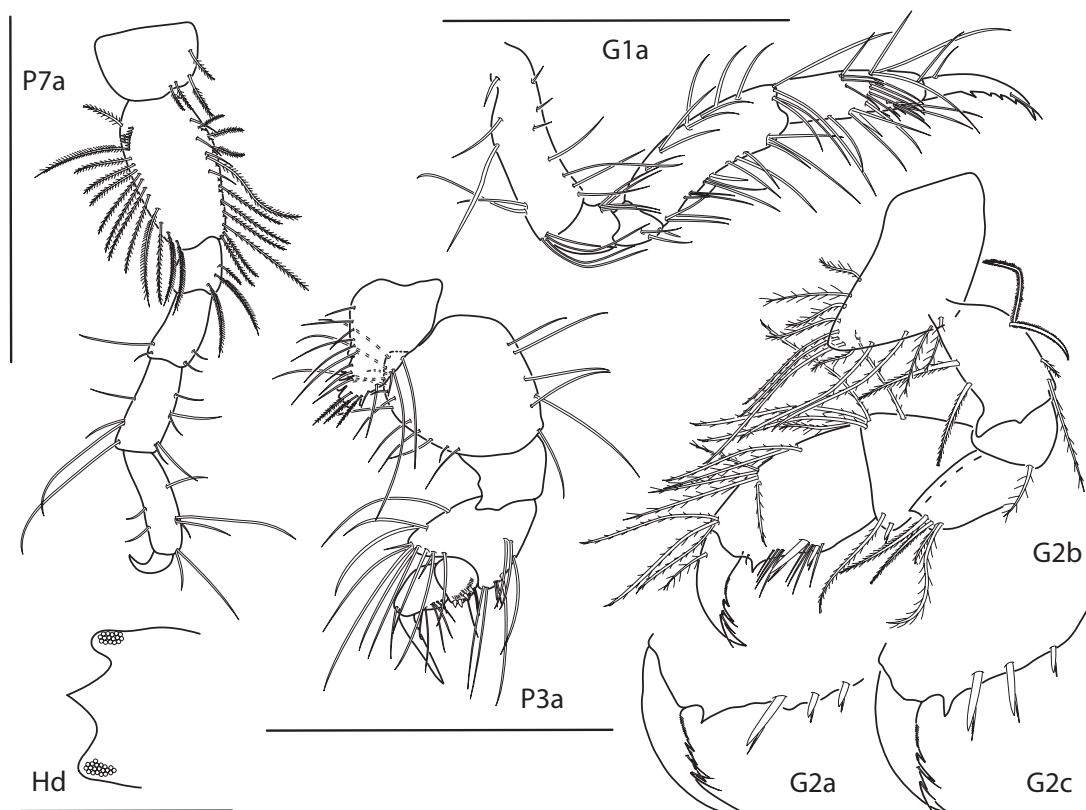


Figure 4. *Caribboecetes intermedius*, male "a" 3.0 mm, pereopod 7, pereopod 3, gnathopod 1 lateral, gnathopod 2 medial; female 2.4 mm, head; male "b" 1.4 mm, gnathopod 2 propodus and dactylus; male "c" 2.1 mm, gnathopod 2 propodus and dactylus. Scale bars: 0.5 mm.

Genus *Cerapus* Say, 1817

Diagnosis. Body subcylindrical. Rostrum produced. Antenna 1 peduncle article 1 expanded, wider than articles 2–3. Mandibular palp reaching beyond incisor process, tri-articulate. Coxae 1–4 discontinuous. Gnathopod 1 subchelate. Male gnathopod 2 carpochelate. Female gnathopod 2 subchelate, lacking stout setae. Pereopod 5 geniculate at merus; merus posteroventral margin produced. Pereopod 7 longer than pereopod 6. Pleopods 2 and 3 inner ramus shorter than outer. Uropod 1 inner ramus shorter than outer ramus. Uropods 2 and 3 uniramous. Telson cleft.

Cerapus benthophilus Thomas & Heard, 1979

Figs 5, 31E

Cerapus sp.: Thomas 1976: 92, 93.

Cerapus benthophilus Thomas & Heard, 1979: 98–104, figs 1–4; LeCroy 2007: 552, fig. 475.

Material examined. PANAMA • 5.4 mm • 1 ♀; Bocas del Toro, Chiriqui Grande, Laguna de Chiriqui; 8.9396°N, 82.1105°W; depth 0.2–1.5 m, among *Thalassia*; 10 Aug 2005; S. LeCroy leg.; GCRL 6661.

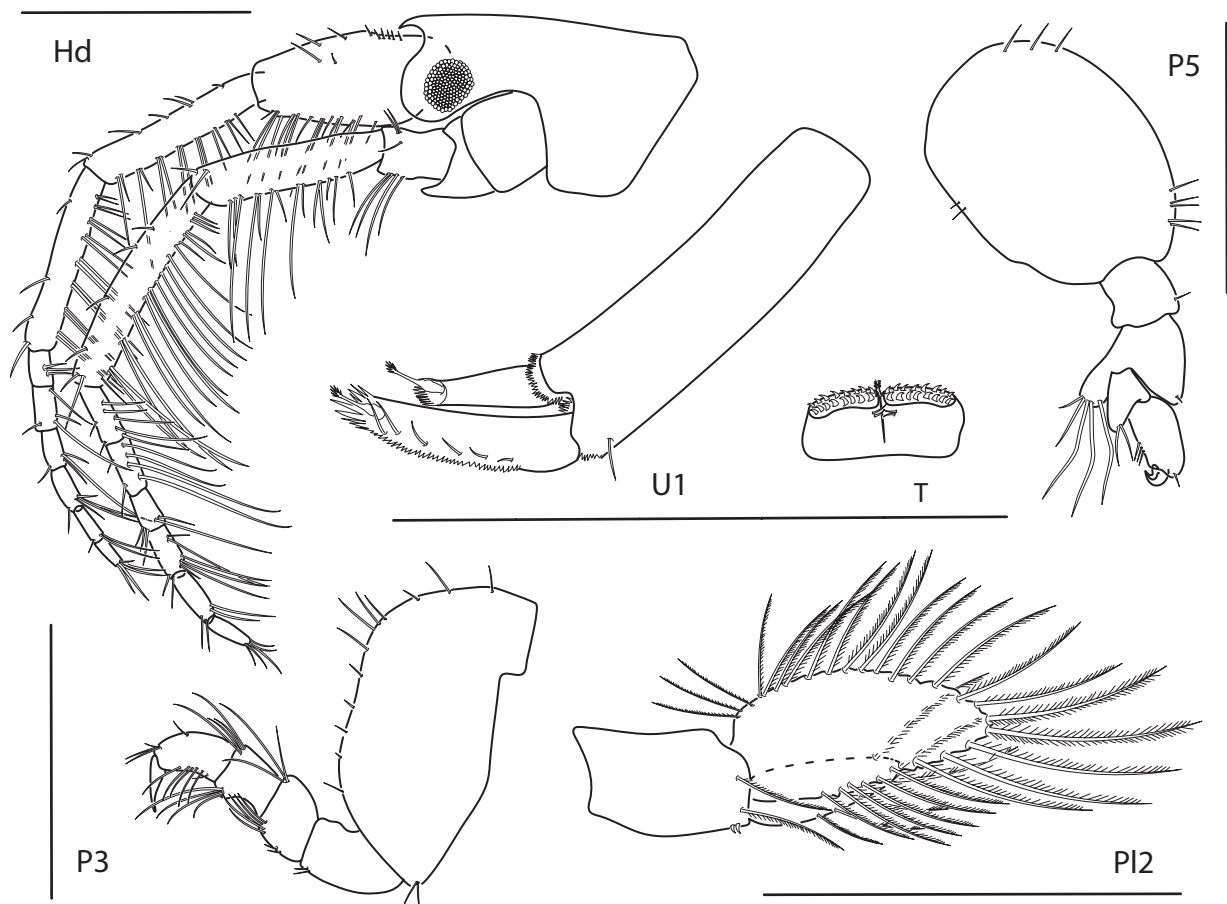


Figure 5. *Cerapus benthophilus*, female, 5.4 mm, head, uropod 1, telson, pereopod 5, pereopod 3, and pleopod 2. Scale bars: 0.5 mm.

Diagnosis. Head ocular lobe posteriorly upturned; rostrum slightly produced. Antenna 1 flagellum 6-articulate. Pleopod 2 outer ramus unsegmented; inner ramus with marginal plumose setae. Uropod 1 outer ramus wide, apical margin not narrowing distally; inner ramus with apical robust seta, distal margin of seta narrowing unevenly.

Distribution. U.S.A.: Ocean Springs, Mississippi (Thomas and Heard 1979), Indian River Lagoon, St. Lucie River, Biscayne Bay, southeastern Gulf of Mexico between Cape Sable and Cape Romano, Estero Bay and Cocohatchee River, Withalacoochee Bay, Florida panhandle to Louisiana, Florida (Nelson 1995; Thomas 1993; LeCroy 2007); Mexico: Laguna de Alvarado, Veracruz (Winfield et al. 1997, 2001), Laguna de Términos, Campeche (Ledoyer 1986); Panama: Chiriqui Grande, Laguna de Chiriqui (present study).

Ecology and remarks. This species occurs among *Thalassia* at depths of 0.2–1.5 m. This species can be difficult to identify with only female specimens. Previously, male specimens have been identified based on the following characteristics: coxa 3 with small anterior lobe, reaching body lengths longer than most *Cerapus* species, ranging from 4–13 mm, male pereon segment 1 with lateral keel, male gnathopod 2 basis, anterodorsal margin with numerous, long setae, antennae 1 and 2, 7–12 segmented (LeCroy 2007; Thomas and Heard 1979). The number of antennae segments seems variable based on size, as seen with the specimens described herein and by Drumm (2018). Panamanian specimens agree closely with the original description of *Cerapus benthophilus* Thomas & Heard, 1979. Ethanol-preserved specimens retained purple coloration on most of the body, especially on the head.

***Cerapus slayeri* Drumm, 2018**

Figs 6, 31F

Cerapus sp B.: LeCroy 2007: 556, fig. 481.

Cerapus slayeri Drumm, 2018: 496–503, figs 1–6.

Material examined. PANAMA • 1.4–2 mm • 3 juvenile ♀; Bocas del Toro, Pidgeon Key Reef; 9.2693°N, 82.2489°W, depth 0.5–1 m, among *Halimeda*, *Thalassia*; 9 August 2005; S. LeCroy leg.; GCRL 6662.

Diagnosis. Head ocular lobe posterior margin even, reaching ~ 1/2 of head length; rostrum short, acute. Antennae 1 and 2 flagella tri-articulate. Pereopod 7 basis posterior margin with spinules; carpus antero- and posterodistal margins with long, plumose setae. Pleopod 2 outer ramus tri-articulate; inner ramus with marginal setules. Uropod 1 inner ramus with apical robust seta, distal margin of seta narrowing evenly; both rami with marginal setules.

Distribution. USA: Delaware Bay, Delaware and Great South Bay, New York (Drumm 2018); Florida (LeCroy 2007); Panama: Bocas del Toro (present study).

Ecology and remarks. This species occurs among *Halimeda*, *Thalassia*, and mangrove roots at depths of 0.5–1 m. Panamanian specimens agree closely with previous descriptions of *Cerapus slayeri*, despite being juveniles. Notable exceptions include female uropod 1 peduncle with distoventral robust seta and pleopod 2 with plumose setae (simple in original description). We did not

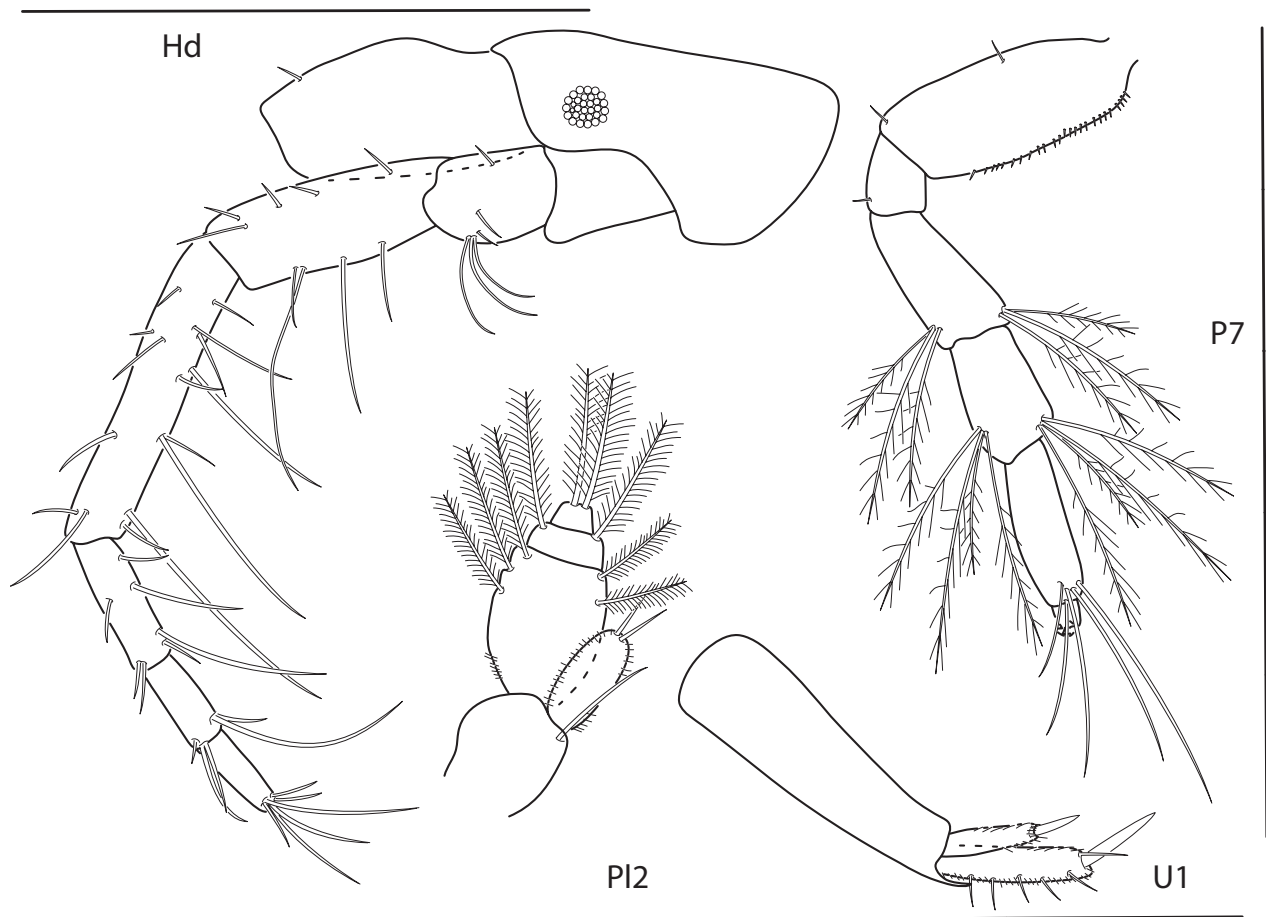


Figure 6. *Cerapus slayeri*, female, 2.0 mm, head, pleopod 2, pereopod 7, uropod 1. Scale bars: 0.5 mm.

collect male specimens of *C. slayeri*, but diagnostic characters described previously include: antenna 1 peduncle 3 × as long as flagellum, peduncle articles 2 and 3 slender, subequal; flagellum 3- or 4-articulate. Antenna 2 flagellum tri-articulate. Pereonite 1 lateral keel absent. Gnathopod 2 carpus with process where the dactylus closes on propodus. Uropod 1 peduncle with large distoventral hook. Ethanol-preserved specimens retained purple coloration on most of the body, especially stripes on antennae.

***Cerapus thomasi* Ortiz & Lemaitre, 1997**

Figs 7, 31G

Cerapus sp.: Ortiz and Lemaitre 1994: 124.

Cerapus thomasi Ortiz & Lemaitre, 1997: 86–90, figs 15–20.

Material examined. PANAMA • 1.6–2.7 mm • 1 ♀; Bocas del Toro, Crawl Caye; 9.2376°N, 82.1438°W, depth 1.5–3 m, among *Halimeda*, 11 Aug 2021; K.N. White leg.; USNM 1743949 • 1 ♀; Bocas del Drago; 9.4180°N, 82.3375°W; depth 2–3 m, among red algae, 9 Aug 2021; K.N. White leg.; USNM 1743950.

Diagnosis. Head ocular lobe posterior margin even, reaching ~ 1/3 head length; rostrum slightly produced. Antenna 1 and 2 flagella bi- and tri-articulate.

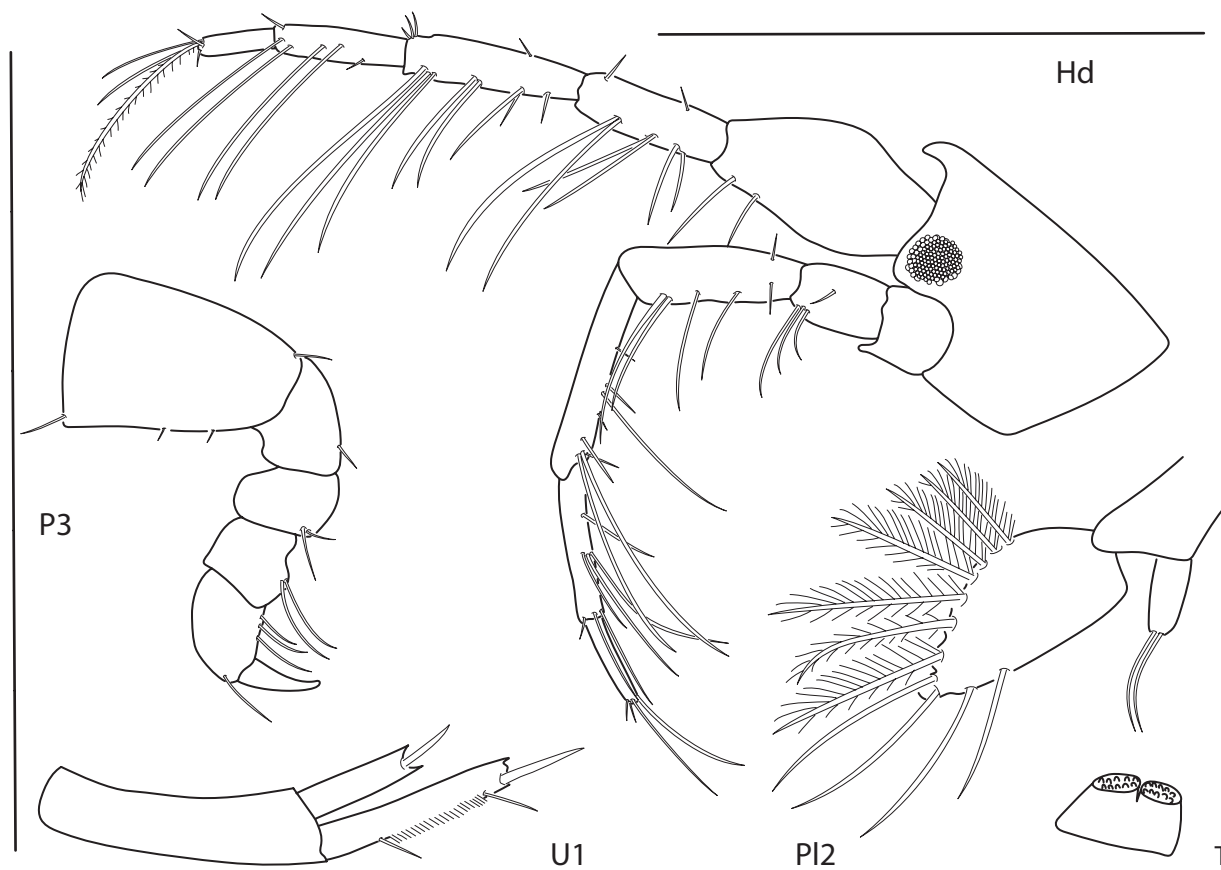


Figure 7. *Cerapus thomasi*, female, 1.6 mm, pereopod 3, head, uropod 1, pleopod 2, telson. Scale bars: 0.5 mm.

Pereopod 3 basis anteroproximal corner rectangular. Pleopod 2 outer ramus uni-articulate; inner ramus with two apical setae. Telson partially cleft. Ethanol-preserved specimens retained brown coloration on most of body, especially stripes on antennae.

Distribution. Colombia: Barú, Bahía de Cispatá, Gulf of Morrosquillo, South of Punta Comisario (Ortiz and Lemaitre 1994, 1997); Panama: Bocas del Toro (present study).

Ecology and remarks. This species occurs among *Halimeda* and red algae at depths of 1.5–3 m. Panamanian specimens agree closely with previous descriptions of *Cerapus thomasi* with the following exceptions: antenna 2 number of flagellar articles and antennae color pattern.

Genus *Erichthonius* H. Milne Edwards, 1830

Diagnosis. Body subcylindrical. Antennae 1 and 2 peduncular articles 1–3 not broadly expanded, similar in width; antenna 1 accessory flagellum minute. Male coxa 2 distinctly separate from coxa 3; longer than wide in hyperadults. Gnathopod 1 subchelate, smaller than gnathopod 2. Male gnathopod 2 carpocheate. Pereopod 5 not geniculate. Pleopods 1–3 outer ramus thin; pleopods 2–3 rami not reduced, subequal. Uropod 2 bi-ramous. Uropod 3 uniramous, ramus with distal hook. Telson entire with dorsal recurved spines.

***Erichthonius brasiliensis* (Dana, 1853)**

Figs 8, 31H

Pyctilus brasiliensis Dana, 1853: 976, fig. 5a–h.

Erichthonius brasiliensis: Bousfield 1973: 195, pl 59, fig. 2; Myers 1982: 200, 201, figs 136, 137; Myers and McGrath 1984: 382–385, figs 1, 2; Thomas 1993: 49, fig. 6; LeCroy 2007: 561, fig. 483.

Material examined. PANAMA • 1.8–5.7 mm • 1 ♂; Bocas del Toro, Crawl Caye; 9.2504°N, 82.1316°W; depth 10 m, among coral rubble and red sponge; 7 Aug 2005; S. DeGrave, M. Salazar leg.; GCRL 6663 • 3 ♂, 2 ♀; Bocas del Toro, Hospital Point; 9.3048°N, 82.1316°W; depth 1.5 m, among sponges, coral rubble, and sand; 7 Aug 2005; T.A. Haney leg.; GCRL 6664 • 1 ♂, 5 ♀; Bocas del Toro, 100 m west of STRI dock; 14 m; 8 Aug 2005; T.A. Haney leg.; GCRL 6665 • 1 ♂, 1 ♀; Bocas del Toro, Isla San Cristobal; 9.2625°N, 82.1897°W; depth 0.2 m, 9 Aug 2005; S. LeCroy leg.; GCRL 6666 • 6 ♀; Bocas del Toro, Crawl Caye; 9.2376°N, 82.1438°W; depth 1.5–3 m, among *Halimeda*, 11 Aug 2021; K.N. White leg.; USNM 1743951 • 1 ♂, 1 ♀; Bocas del Toro, Crawl Caye; 9.2459°N, 82.1369°W; depth 1–4 m; 25 June 2023; K.N. White leg.; USNM 1743952 • 11 ♂, 17 ♀; Bocas del Toro, Hospital Point; 9.3333°N, 82.2185°W; depth 11 m, from buoy scrapings, 26 June 2023; K.N. White leg.; USNM 1743955 • 1 ♀; Bocas del Toro, Swan Cay; 9.4536°N, 82.3000°W; 27 June 2023; K.N. White leg.; USNM 1743956 • 3 ♀; Bocas del Toro, Cayo Zapatilla; 9.2699°N, 82.0587°W; depth 10–11 m; 28

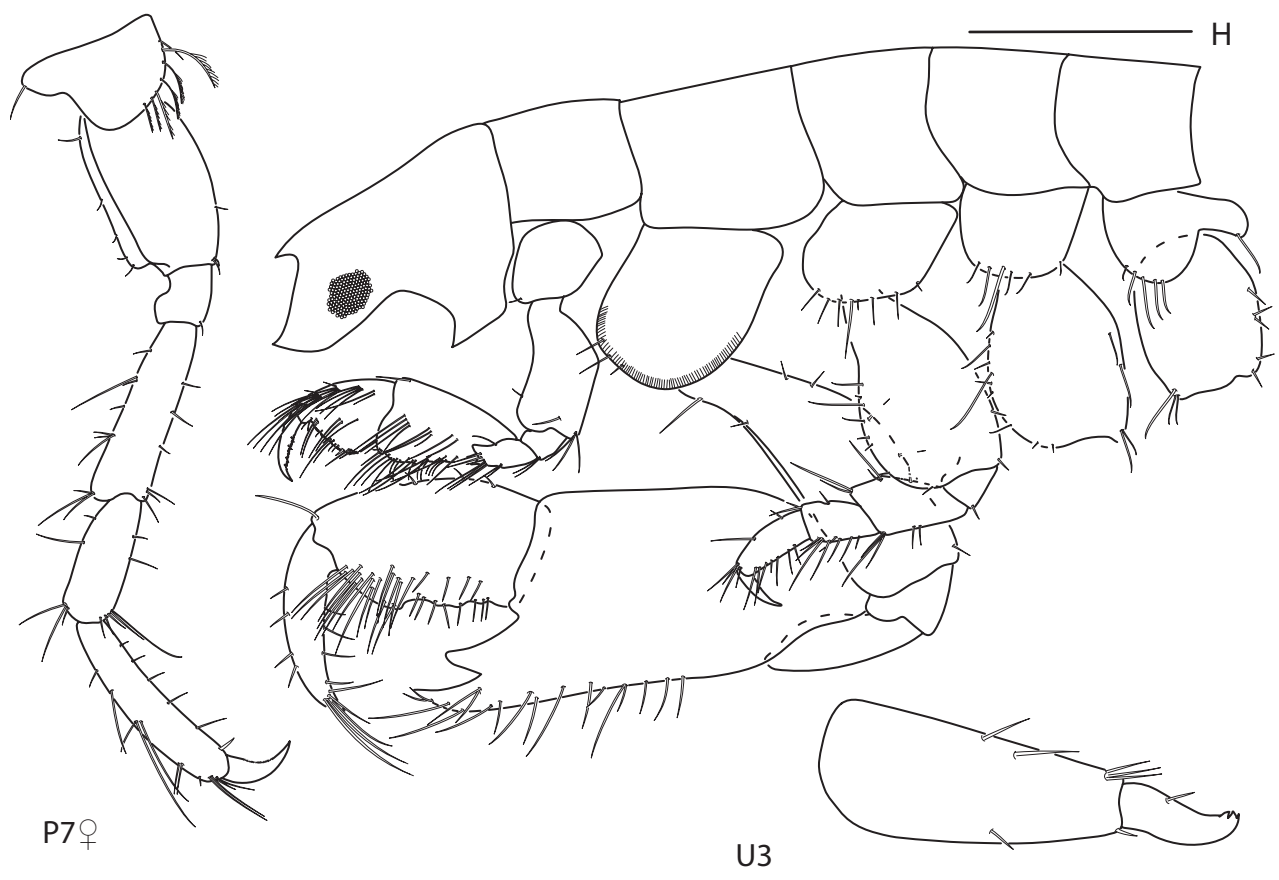


Figure 8. *Erichthonius brasiliensis*, female, 5.3 mm, pereopod 7; male 5.5 mm, habitus (in part); uropod 3. Scale bars: 0.5 mm.

June 2023; K.N. White leg.; USNM 1743953 • 4 ♂, 6 ♀; Cayo Zapatilla, Bocas del Toro; 9.2699°N, 82.0587°W; depth 0 m, in sand; 29 June 2023; K.N. White leg.; USNM 1743954 • 1 ♂; Crawl Caye, Bocas del Toro; 9.2502°N, 82.1318°W; depth 5–13 m, among coral rubble; 29 June 2023; K.N. White leg.; USNM 1743957.

Diagnosis. Male gnathopod 1 basis widely expanded posterodistally. Coxa 2 anteroventral margin rounded, with vertical stridulating ridges, without long plumose setae. Male gnathopod 2 carpus anterodistal margin with two large distal projections. Coxa 3 evenly rounded distally, basis strongly expanded anterodistally. Pereopod 4 basis strongly expanded. Male pereopod 5 basis not produced into wing-like projection. Uropod 3 ramus slender.

Distribution. Brazil: Rio De Janeiro (Dana 1853); U.S.A.: Cape Cod to Chesapeake Bay, Florida, Gulf states (Bousfield 1973); Italy: Thau, Napoli, Venezia, Lipari-Castello, Messina, Bosphorus (Myers 1982); France: Banyuls-sur-Mer (Myers 1982); Cosmopolitan (Thomas 1993; LeCroy 2007); Panama: Bocas del Toro (present study).

Ecology and remarks. This species occurs among coral rubble, red sponges, sand, and from buoy scrapings at depths of 0–11 m. Variation between Panamanian specimens has been seen in the following characters: size of posterior hump on basis; male gnathopod 2 basis posterior margin with fewer setae than previously described; uropod 3 more setose than previously described; color pattern (possibly due to differences in preservation). Variation within this species is further discussed in Myers and McGrath (1984). Panamanian specimens agree closely with specimens described by Bousfield (1973). Live specimens have brown stripes covering entire body with a red eye.

Family Neomegamphopidae Myers, 1981

Genus *Konatopus* Barnard, 1970

Diagnosis. Antenna 1 accessory flagellum short, bi-articulate. Eye slightly smaller than ocular lobe. Mandibular palp article 3 stout, clavate. Coxae overlapping. Male coxa 1 subovate, larger than remaining coxae. Female coxa 1 equally long as broad. Male gnathopod 1 carpus elongate with posterodistal tooth. Gnathopod 2 smaller than gnathopod 1, carpus longer than propodus. Uropod 1 peduncle with interramal spine. Uropod 3 biramous, rami slightly longer than peduncle, outer ramus with small barrel-shaped article. Telson broader than long, slightly concave.

Konatopus tridens sp. nov.

<https://zoobank.org/EF59C1A6-B4A2-4E59-86C5-0C3E1DFC968A>

Figs 9–11, 32A

Type locality. Bocas del Toro, Panama: Crawl Caye, 9.2459°N, 82.1369°W, depth 1–4 m, in sand.

Distribution. Panama: Bocas del Toro (present study).

Material examined. Holotype: PANAMA • 1 ♂, 4.2 mm; Bocas del Toro, Crawl Caye; 9.2459°N, 82.1369°W; depth 1–4 m, in sand; 25 June 2023; K.N. White leg.; USNM 1743958. **Paratype:** PANAMA • 1 ♀, 4.7 mm; same station data as for preceding; USNM 1743959. **Other material:** PANAMA • 1 ♂ juvenile, 3.0 mm; same station data as for preceding; USNM 1743960.

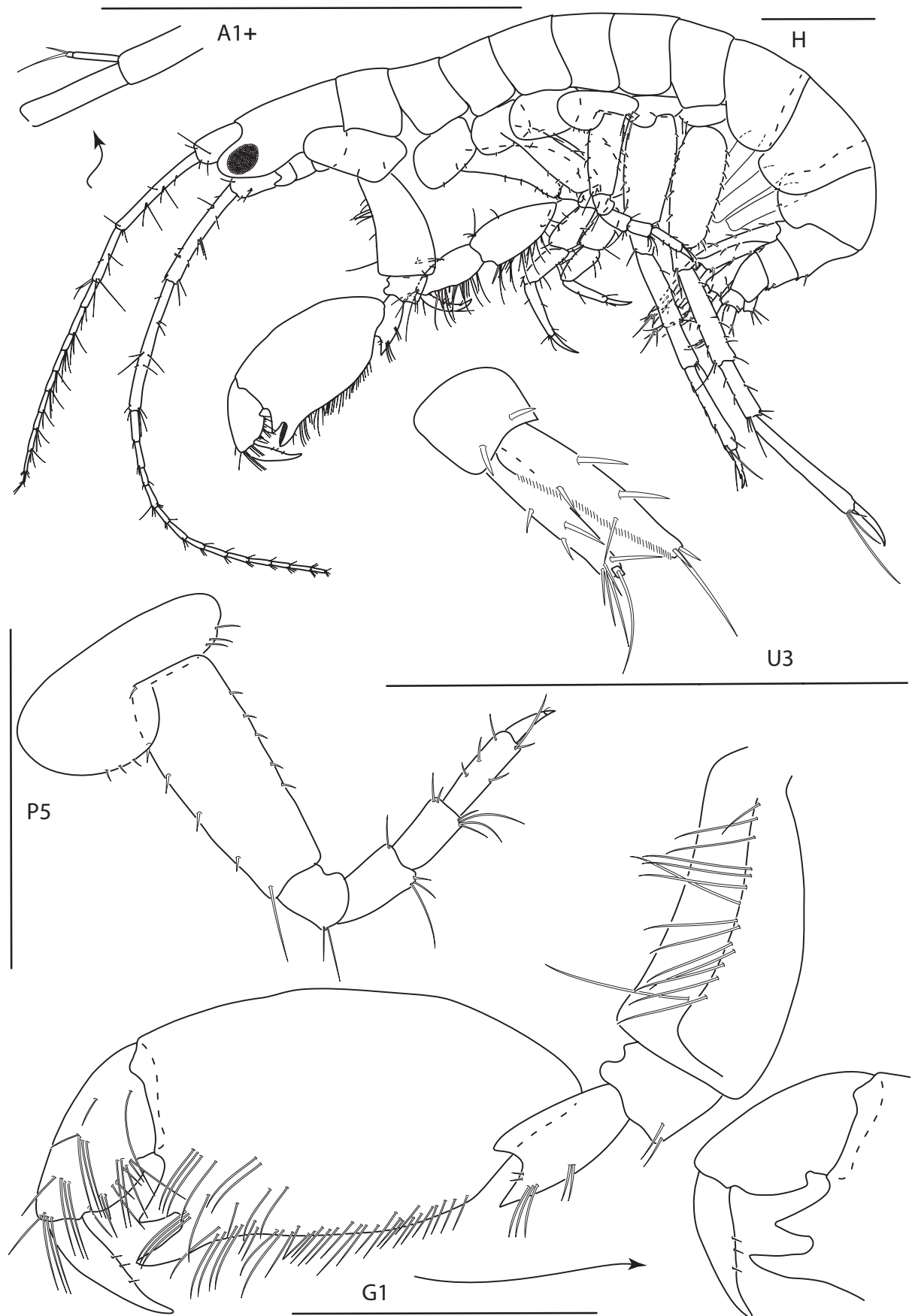


Figure 9. *Konatopus tridens* sp. nov., male holotype, 4.2 mm, habitus, antenna 1 accessory flagellum, uropod 3, pereopod 5, gnathopod 1 medial. Scale bars: 0.5 mm.

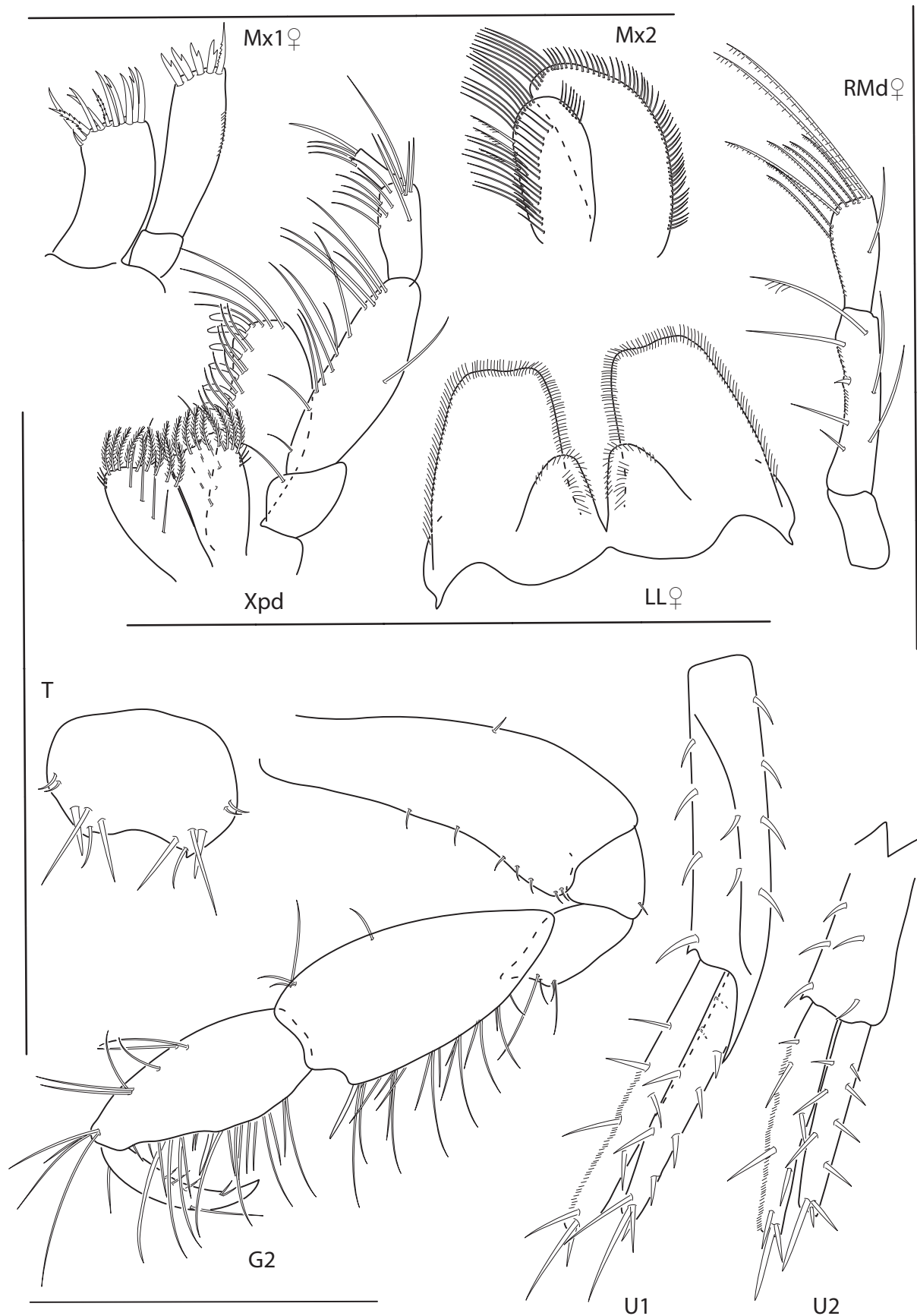


Figure 10. *Konatopus tridens* sp. nov., female paratype, 4.7 mm, maxilla 1, lower lip, right mandibular palp; male holotype, 4.2 mm, maxilla 2, maxilliped, telson, gnathopod 2 lateral, uropod 1, uropod 2 (broken). Scale bars: 0.5 mm.

Diagnosis. Male gnathopod 1 basis stout, merus with large anterodistal U-shaped excavation, carpus with three triangular anterodistal processes increasing in size distally, with deep U-shaped excavation between two lower processes, propodus subovate with large proximal notch. Pereopod 5 basis length $2.7 \times$ width. Uropod 3 peduncle $\sim 0.5 \times$ length of outer ramus.

Description. Male (holotype, 4.2 mm). **Head.** Ocular lobe rounded, eye ovate with many small ommatidia. Antenna 1 shorter than antenna 2, peduncle article 2 $1.9 \times$ length of article 1 and 3; flagellum setose with aesthetascs. Antenna 2 $\sim 1.4 \times$ length of antenna 1, flagellum moderately setose. Maxilliped inner plate with nine apical plumose setae, outer plate lined with long thin setae and six stout setae. Maxilla 1 missing. Maxilla 2 inner plate with row of facial setae, margin lined with dense setae. Upper lip missing. Lower lip rounded, apically setose. Mandibles similar; palp article 3 stout, clavate.

Pereon. Coxae 1 large, subovate; coxae 2–4 subrectangular. Gnathopod 1 carpocheate; basis stout, with row of long facial setae; merus with large anterodistal U-shaped excavation, carpus with three triangular anterodistal processes increasing in size, with deep U-shaped excavation between two lower processes, propodus subovate with large proximal notch; dactylus thick, closing on carpus, marginally setose. Gnathopod 2 subchelate, much smaller than gnathopod 1; basis widened distally, anterior margin with sparse setae, carpus distally setose with one robust anterodistal seta, propodus distally setose with one distal robust seta. Pereopods 3–7 basis and propodus narrow, elongate. Pereopods 3 and 4 dactylus narrow, elongate. Pereopod 5 dactylus short, stout. Pereopods 6 and 7 much longer than pereopod 5; dactylus long, narrow.

Pleon. Epimera 1–3 rounded, with few distal setae. Uropod 1 with interrampal spine, peduncle subequal in length with inner ramus, both margins lined with robust setae, with facial row of robust setae; inner ramus $1.1 \times$ length of outer ramus, lined with robust setae, medial margin lined with fine setae, apical margin with three robust setae; outer ramus both margins lined with robust setae, apical margin with four robust setae. Uropod 2 peduncle broken, with several robust setae, medio-distal margin with acute point; inner ramus $1.2 \times$ length of outer ramus, both margins lined with robust setae, medial margin lined with fine setae, apical margin with three robust setae; outer ramus both margins lined with robust setae, apical margin with three. Uropod 3 peduncle $0.5 \times$ length of inner ramus, with two distal robust setae, medio-distal margin with acute point; inner ramus $1.1 \times$ length of outer ramus, both margins with few robust setae, lateral margin lined with fine setae, apical margin with three robust setae; outer ramus bi-articulate, article 1 margins with few robust setae, apical margin with four robust setae, article 2 with one long seta. Telson apical margin slightly concave with acute lateral points, each point surrounded by four robust setae, lateral margins each with two setae.

Female (paratype, 4.7 mm). Similar in all aspects to the male with the exception of the following: Lower lip outer lobes lined with setae; mandibular lobes long, pointed. Maxilla 1 inner plate apical margin lined with bifurcate setae; palp bi-articulate, article 2 apical margin with four bifurcate robust setae and one serrate robust seta, outer margin with fine setules. Gnathopod 1 weakly subchelate, merus, carpus, propodus, and dactylus densely setose, propodus and dactylus lateral margins lined with fine setae. Gnathopod 2 missing.

Etymology. After the Latin *tridens*, meaning fork with three tines and referring to the three triangular process on the gnathopod 2 carpus of males of this species.

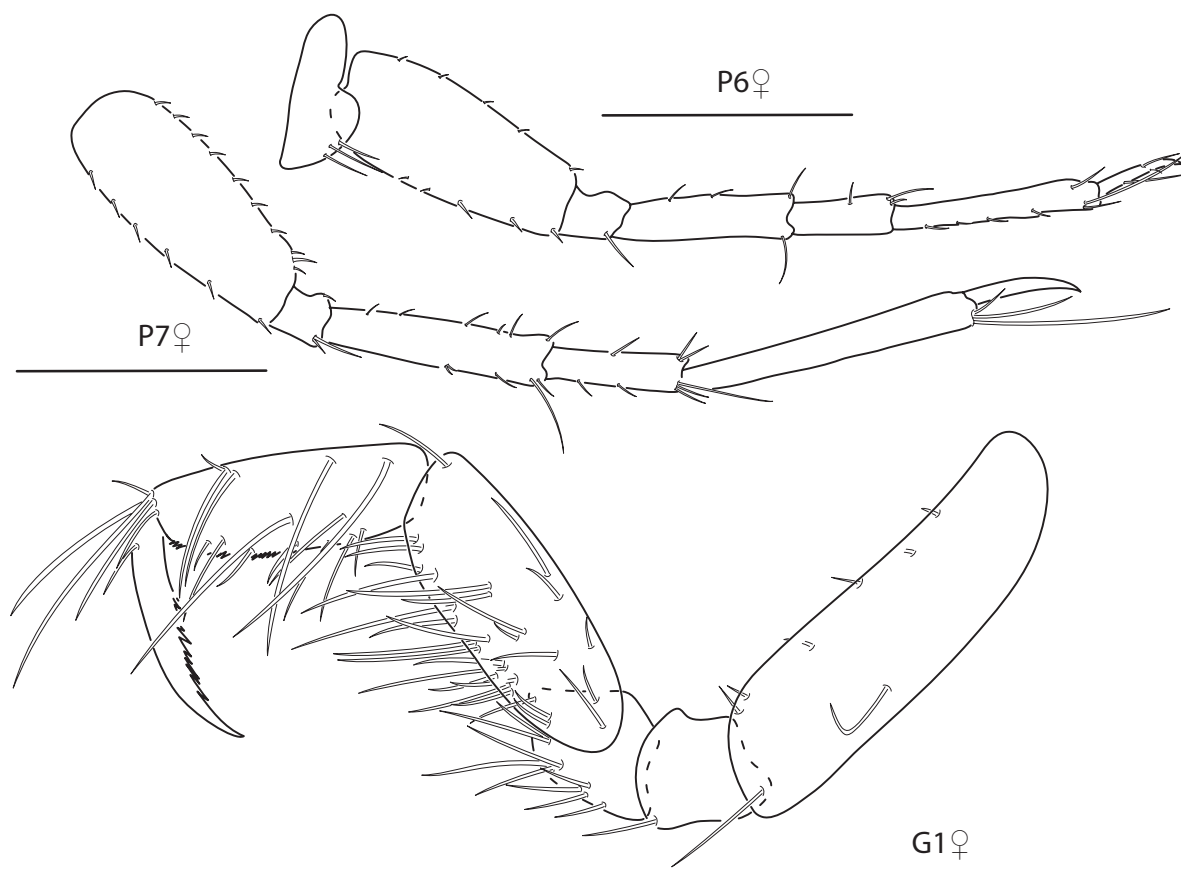


Figure 11. *Konatopus tridens* sp. nov., female paratype, 4.7 mm, gnathopod 1 lateral, pereopod 6, pereopod 7. Scale bars: 0.5 mm.

Ecology and remarks. This species occurs among sand at depths of 1–4 m. This species most closely resembles *Konatopus tulearensis* Ledoyer, 1982 in sharing the male gnathopod 1 stout basis with a subovate propodus with proximal notch. The new species can be distinguished from *K. tulearensis* based on male gnathopod 1 merus with short acute distal lobe (vs large lobe), carpus with three triangular anterodistal processes increasing in size, lowest process with deep U-shaped excavation (vs 1 process and small excavation), propodus subovate with large proximal notch (vs subrectangular with small proximal notch), and pereopod 5 basis length $2.7 \times$ width (vs $1.3 \times$ width). The new species can be distinguished from all other described *Konatopus* species based on the shape of the gnathopod 1 carpus: with one large distal subacute process in *Konatopus latipalmus* Ledoyer, 1979; with one slight distal process in *Konatopus pao* J.L. Barnard, 1970; and produced into a rounded lobe distally in *Konatopus storeyae* Myers, 2002. Live specimens are white in color with brown splotches.

Genus *Varohios* J.L. Barnard, 1979

Diagnosis. Male coxa 1 subquadrate. Male gnathopod 1 chelate, carpus and propodus fused, dactylus with posteroproximal tooth. Gnathopod 2 smaller than gnathopod 1, propodus longer than carpus. Uropod 1 with large interrampal spine. Uropod 3 rami subequal in length with peduncle, outer ramus with small barrel-shaped article 2.

***Varohios topianus* Barnard, 1979**

Figs 12, 32B

Varohios topianus Barnard, 1979: 35–37, figs 13, 14.

Material examined. PANAMA • 2.3 mm • 1 ♂; Bocas del Toro, Crawl Caye; 9.2699°N, 82.0587°W, depth 1–4 m, among coral rubble; K.N. White leg.; USNM 1743961.

Diagnosis. Gnathopod 1 basis with rows of anterior, posterior, and facial setae; dactylus posteroproximal tooth longer than wide. Male pereopod 5 basis length $1.4 \times$ width. Uropod 1 interramal spine subequal in length with peduncle; inner ramus with robust setae on both margins, lateral margin lined with small setae; outer ramus with two robust setae on lateral margin. Uropod 3 rami subequal, rami subequal to peduncle, outer ramus with small barrel shaped article 2. Telson apex convex, dorsal surface with excavation. Live specimens are white in color with brown splotches.

Distribution. U.S.A.: Gulf of California (Barnard 1979); Ecuador: Galápagos Islands (Barnard 1979); Panama: Bocas del Toro (present study).

Ecology and remarks. This species occurs among coral rubble at depths of 1–4 m. Panamanian specimen agrees closely with specimens described by Barnard (1979) with the exception of fewer setae on the gnathopod 1 basis and carpus/propodus, fewer robust setae on uropod 1 rami; both of which could be variation based on size. This species has previously only been collected from the Pacific Ocean.

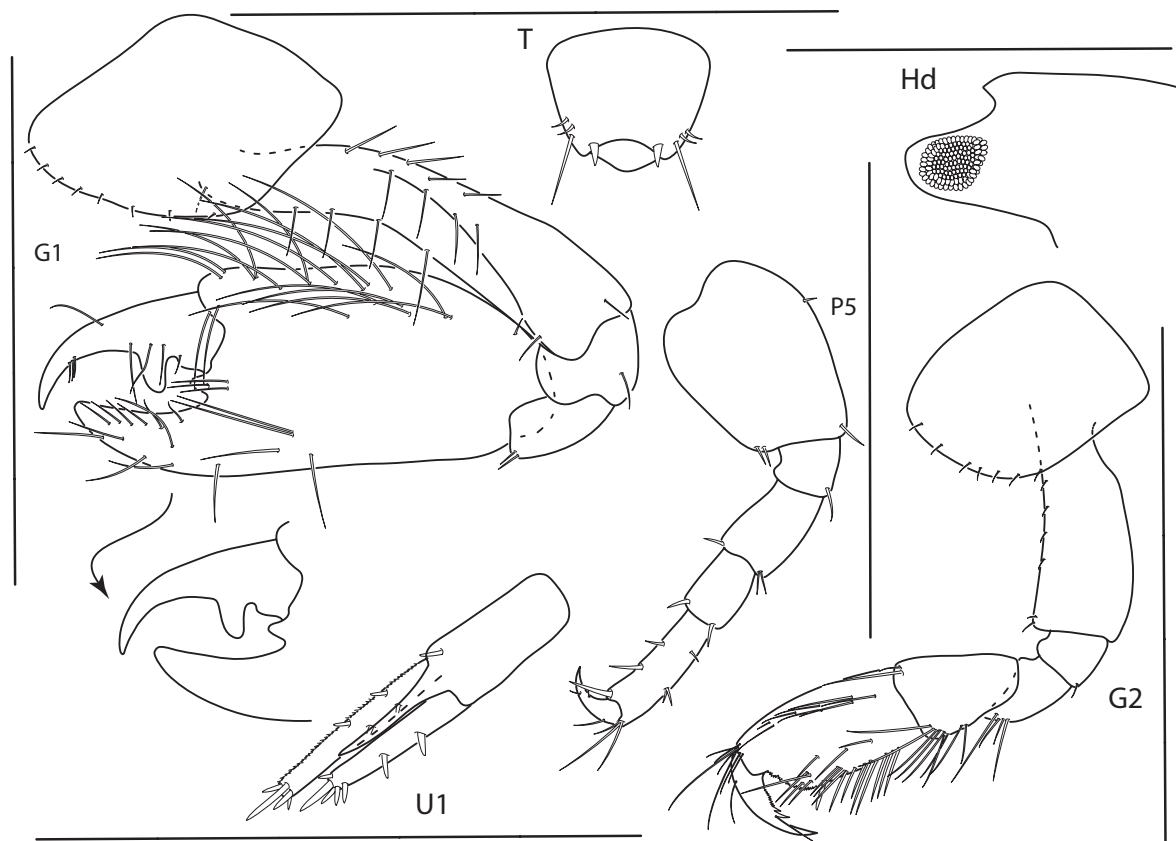


Figure 12. *Varohios topianus*, male, 2.3 mm, gnathopod 1 medial, telson, uropod 1, pereopod 5, head, gnathopod 2 medial. Scale bars: 0.5 mm.

Family Photidae Boeck, 1871

Genus *Audulla* Chevreux, 1901

Diagnosis. Head ocular lobe narrowly rounded anteriorly, inferior antennal sinus deeply recessed for insertion of antenna 2. Antenna 1 peduncle article 3 subequal to article 1 in length, accessory flagellum 5- or 6-articulate. Male antenna 2 flagellum dorsoventrally flattened. Male gnathopod 2 minutely chelate, propodus subrectangular, palm uncurving, with distal margin extending anteriorly. Female gnathopod 2 larger than gnathopod 1; propodus anterior margin with dense rows of setae. Uropod 3 biramous, rami subequal in length, peduncle longer than telson.

Audulla chelifera (Chevreux, 1901)

Figs 13, 33C

Gammaropsis chelifera Chevreux, 1901: 432–436, figs 56–65.

Eurystheus lina: Kunkel 1910: 81–83, fig. 31.

Eurystheus semichelatus: K.H. Barnard 1957: 8, fig. 5.

Gammaropsis lina: Lazo-Wasem and Gable 1987: 331–335, figs 7–9.

Audulla chelifera: Thomas and Barnard 1987: 364–369, figs 1–4; LeCroy 2000: 125, fig. 163.

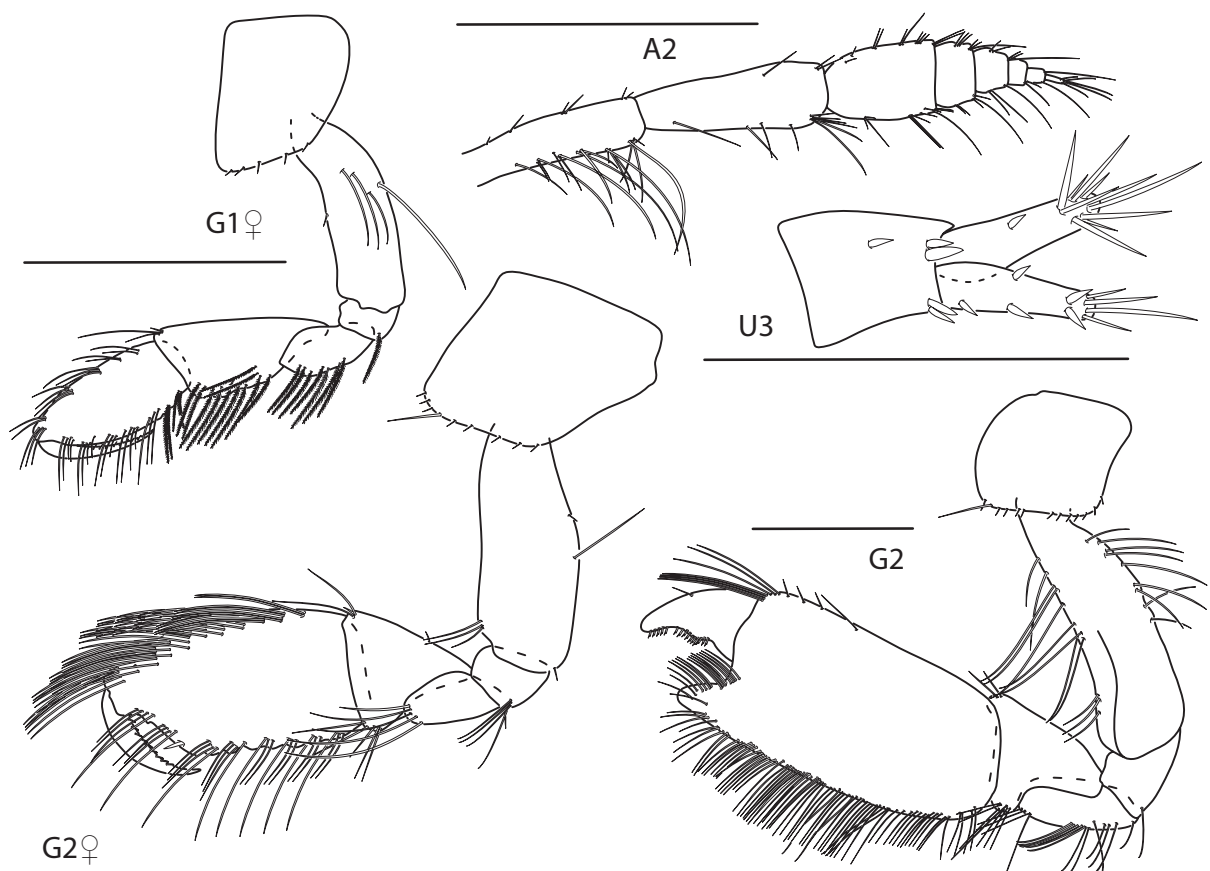


Figure 13. *Audulla chelifera*, female, 4.8 mm, gnathopod 1 medial, gnathopod 2 medial; male, 4.9 mm, antenna 2, uropod 3, gnathopod 2 lateral. Scale bars: 0.5 mm.

Material examined. PANAMA • 4.2–5.8 mm • 7 ♂, 5 ♀ • Bocas del Toro, Lime Point; 9.414°N, 82.3323°W; depth 0.2–0.5 m, among coral rubble and red algae; 5 Aug 2005; S. DeGrave, M. Salazar leg.; GCRL 6667.

Diagnosis. Male antenna 2 flagellum dorsoventrally flattened. Male gnathopod 2 minutely chelate, basis anterior and posterior margins with long setae; propodus subrectangular with rounded projection at palmar angle, densely setose. Female gnathopod 1 smaller than gnathopod 2; ischium, merus, carpus, with plumose setae. Gnathopod 2 propodus anterior margin densely setose. Uropod 3 rami subequal in length.

Distribution. South Africa: St. Helena Bay (K.H. Barnard 1957); Bermuda: exact location unknown (Kunkel 1910, Lazo-Wasem and Gable 1987); USA: Florida (LeCroy 2000), Gulf of Mexico (LeCroy et al. 2009); Caribbean Sea (Barnard and Karaman 1991); Belize: Curlew Cay (Thomas and Barnard 1987); Mexico: Yucatan (McKinney 1977); Seychelles Islands: La Digue (Chevreux 1901; Ledoyer 1982; Barnard and Karaman 1991); Panama: Bocas del Toro (present study).

Ecology and remarks. This species occurs among coral rubble and red algae at depths of 0.2–5.8 m. Panamanian specimens agree closely with previous descriptions of *Audulla chelifera*.

Genus *Latigammaropsis* Myers, 2009

Diagnosis. Head cephalic lobes rounded, anteroventral margin surpassing posterior margin of eye; eyes at least partially situated within cephalic lobe. Antenna 2 flagellum longer than peduncle article 5. Uropod 3 peduncle stout; outer ramus bi-articulate, second article vestigial, subtruncate with two fine setae; inner ramus subequal to or shorter than outer ramus, narrowing distally, with one stout apical seta.

Latigammaropsis atlantica (Stebbing, 1888)

Figs 14, 32D

Gammaropsis atlantica Stebbing, 1888: 1101, fig. 114; Myers 1985: 80, fig. 60; LeCroy 2000: 135, fig. 176.

Gammaropsis zeylanicus: Walker 1904: 282, 283, fig. 41.

Gammaropsis gardineri: Walker 1905: 929, 930, figs 11–14, 16–17.

Eurystheus atlantica: Stebbing 1906: 611.

Latigammaropsis atlantica: Myers 2009: 777.

Material examined. PANAMA • 2.4–3 mm • 3 ♂; Bocas del Toro, Hospital Point, Cayo Solarte; 9.3336°N, 82.2188°W; depth 15 m, among coral rubble and *Halimeda*; 6 Aug 2005; S. DeGrave leg.; GCRL 6668 • 2 ♂; Bocas del Toro, Crawl Caye, 9.2459°N, 82.1369°W; depth 1–4 m, among coral rubble; 25 Jun 2023; K.N. White leg.; USNM 1743962.

Diagnosis. Male gnathopod 2 propodus distinctly longer than carpus, robust seta present at palmar angle; dactylus subequal in length with propodus palm. Coxae 3 and 4 subquadrate. Epimera 2 and 3 posteroventral margins subquadrate with weak notches.

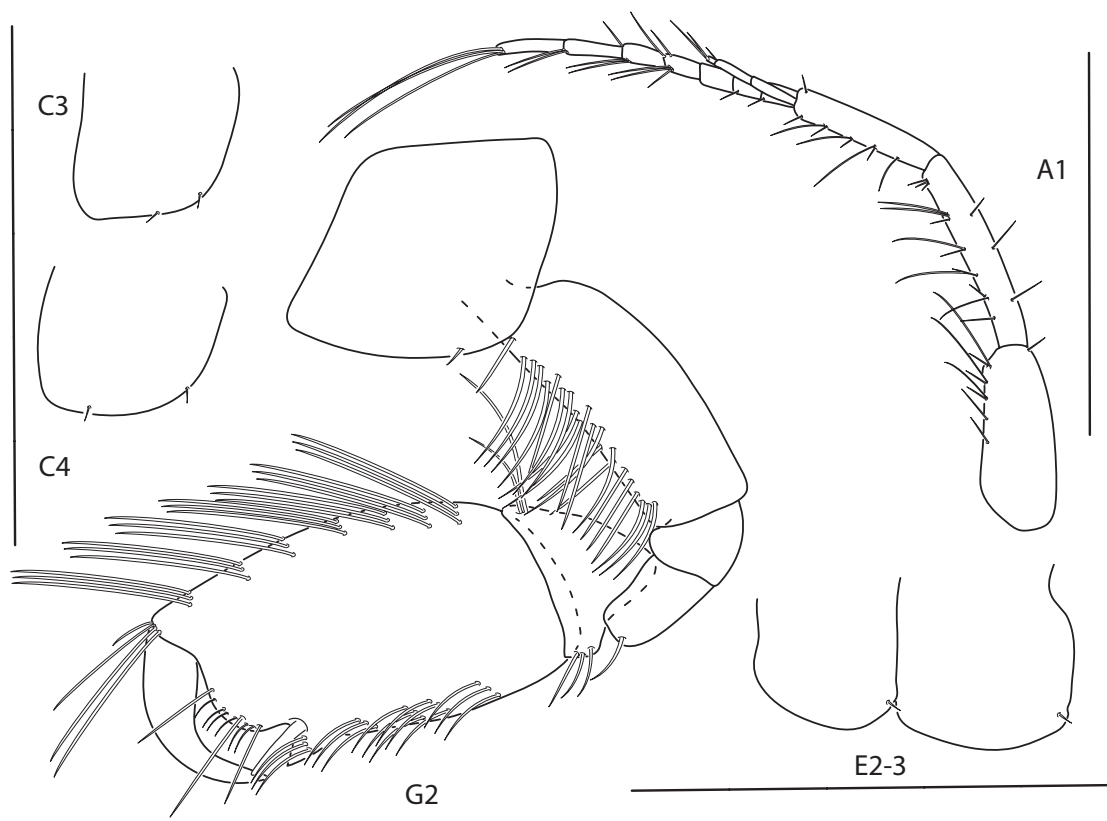


Figure 14. *Latigammaropsis atlantica*, male, 4.9 mm, coxa 3, coxa 4, gnathopod 2 medial, epimera 2 and 3; male, 2.3 mm, antenna 1. Scale bars: 0.5 mm.

Distribution. Cape Verde Islands: Saint Vincent (Stebbing 1888); Sri Lanka (Walker 1904); Maldives: Hulule, Fadifolu, Mahlosmadulu Atoll, Minikoi (Walker 1905); Cape Verde Islands: St. Vincent (Stebbing 1906); Fiji: Momi Bay, Mburelevu, Nananui Ra (Myers 1985); USA: Florida (LeCroy 2000); Panama: Bocas del Toro (present study).

Ecology and remarks. This species occurs among coral rubble and *Halimeda* at depths of 1–15 m. Panamanian specimens agree closely with LeCroy (2000) with the exception of antenna 1, accessory flagellum tri-articulate (vs 5- or 6-articulate). The smaller size of our specimen suggests this character is variable based on size. No females were collected in this study, but LeCroy (2000) reported a convex gnathopod 2 palmar margin of the propodus in females. Ethanol-preserved specimens retained brown coloration on head and pereon. There are many reports of this species worldwide, but they most likely represent a species-group and material from around the world needs to be examined.

Genus *Photis* Krøyer, 1842

Diagnosis. Antenna 1 accessory flagellum vestigial or absent. Coxae 1 and 2 subequal in length with coxae 3 and 4. Gnathopod 2 sexually dimorphic. Male gnathopod 2 subchelate; dactylus slender. Female gnathopod 2 propodus anterior margin sparsely to moderately setose. Female pereopods 3 and 4 oostegites broadly expanded, longer than basis. Urosomites separate. Uropods 1 and 2 inner ramus lanceolate with apical robust setae. Uropod 3 inner ramus minute.

***Photis butalus* sp. nov.**

<https://zoobank.org/2C9CC06A-324D-4E52-A321-E016006F291E>

Figs 15–17, 32E

Type locality. Bocas del Toro, Panama: Swan Cay; 9.4533°N, 82.2983°W, depth 3 m, among brown algae, hydroids, and filamentous algae.

Material examined. *Holotype*: PANAMA • 1 ♂, 2.1 mm; Bocas del Toro, Swan Cay; 9.4533°N, 82.2983°W; depth 3 m, among brown algae, hydroids, and filamentous algae; 4 Aug 2005; T.A. Haney leg.; USNM 1743981. *Paratype*: PANAMA • 1 ♀, 2.3 mm; same station data as for preceding; GCRL 6669. *Other material*: PANAMA • 1 ♂, 1.8 mm; 4 ♀, 2–2.6 mm; 1 juvenile, mm; same station data as for preceding; GCRL 6670.

Diagnosis. Eye well developed, not touching outer margin of ocular lobe. Gnathopod 1 propodus palm entire. Pereopod 6 of adult male greatly enlarged; merus ovate; propodus thick, width $0.4 \times$ length, palmar margin minutely serrate with short setae, one short subtriangular seta present; dactylus apical margin subacute. Pereopod 7 dactylus with posterior and anterior accessory claws.

Description. Male (holotype, 2.1 mm). **Head.** Eye well developed, not touching outer margin of ocular lobe. Antenna 2 flagellum 5-articulate. Maxilliped inner plate lined with setae along inner margin, two rows of apical setae present, outer plate with row of four thick setae, and six sagittate-shaped setae. Lower lip inner lobes rounded, outer lobes with large gape, apically setose, with few thick bifurcate setae; inner plate length $0.8 \times$ length of outer plate, apically setose. Maxilla 1 inner plate small, bare; outer plate with two rows of five apical bifurcated robust setae; palp bi-articulate, article 2 lined with marginal setules, apical margin with three bifurcated robust setae. Maxilla 2 inner lobe with two rows of marginal setae; outer lobe with two rows of apical setae. Mandibles similar, molar small; palp tri-articulate, article 3 lined with fine setules.

Pereon. Coxae sparsely setose. Coxa 1–4 subrectangular, longer than wide. Gnathopod 1 subchelate; basis anterior and posterior margins with few long setae; merus with posterodistal cluster of setae; carpus subequal in length to propodus, densely setose; propodus palm convex, serrate, proximal margin with one large robust seta; dactylus lined with minute stout setae, with one serration at distal end. Gnathopod 2 subchelate; basis anterior and posterior margins each with one long seta and one short distal seta; merus with posterodistal bunch of long setae, posterodistal margin with fine setules; carpus subtriangular, with posterodistal cluster of fine setae; propodus palm with weak excavation, palmar robust seta present; dactylus extending past excavation of propodus palm, lined with minute stout setae, with one distal serration. Pereopods 3 and 4 bases thick, posterodistal margin with few long setae; dactylus apically subacute. Pereopod 3 merus anterodistal margin densely setose. Pereopod 5 basis nearly circular, sparsely setose; propodus with two posterodistal robust setae; dactylus stout with accessory claw. Pereopod 6 of adult male greatly enlarged; merus ovate; propodus thick, width $0.4 \times$ length, palmar margin minutely serrate with short setae, one short subtriangular robust seta present; dactylus apical margin subacute. Pereopod 7 basis narrowing distally; remaining articles slender; propodus distal margin sparsely lined with short setae and one short subtriangular robust seta; dactylus with posterior and anterior accessory claws.

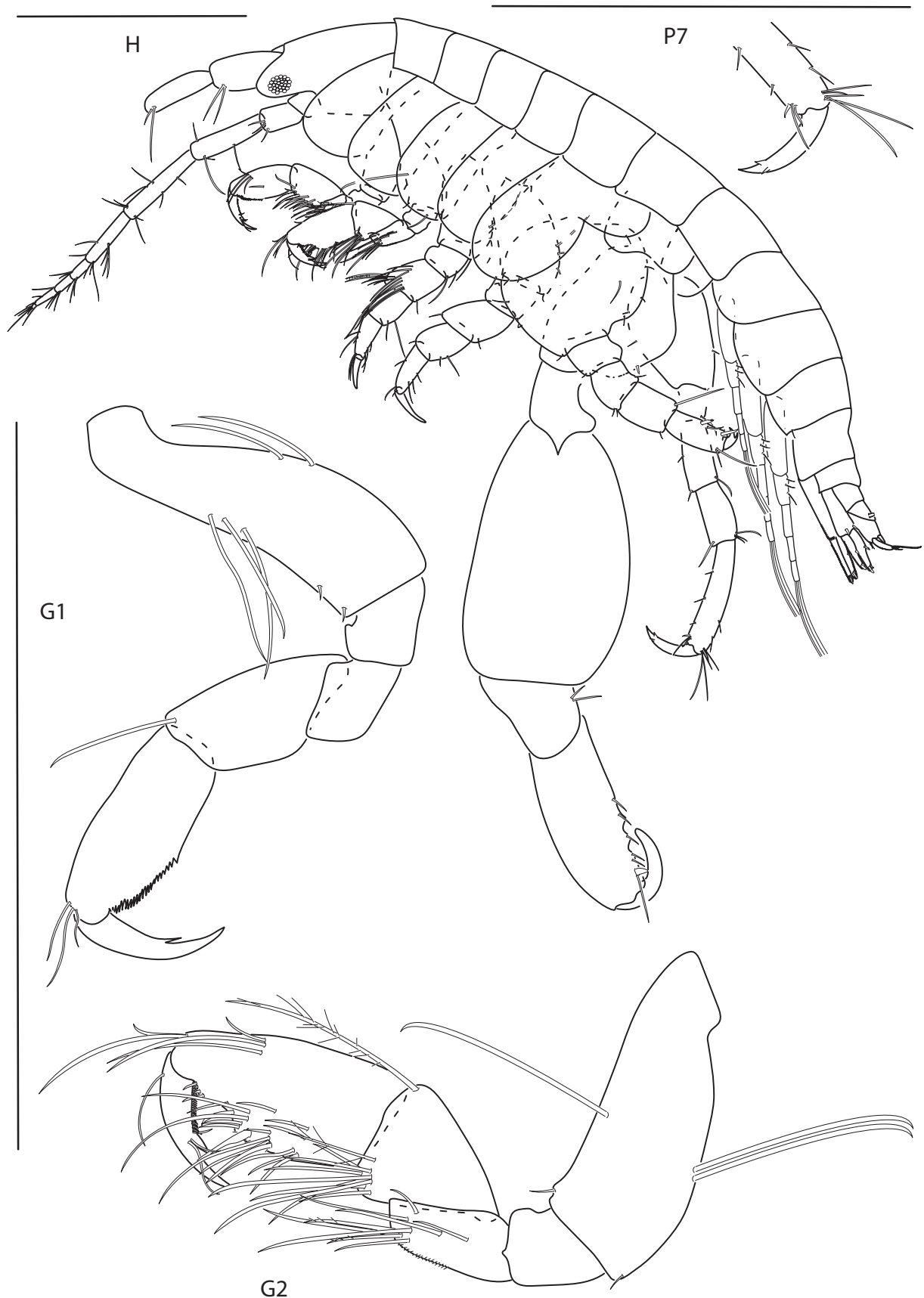


Figure 15. *Photis butalus* sp. nov., male holotype, 2.1 mm, habitus, pereopod 7 dactylus, gnathopod 1 medial, gnathopod 2 medial. Scale bars: 0.5 mm.

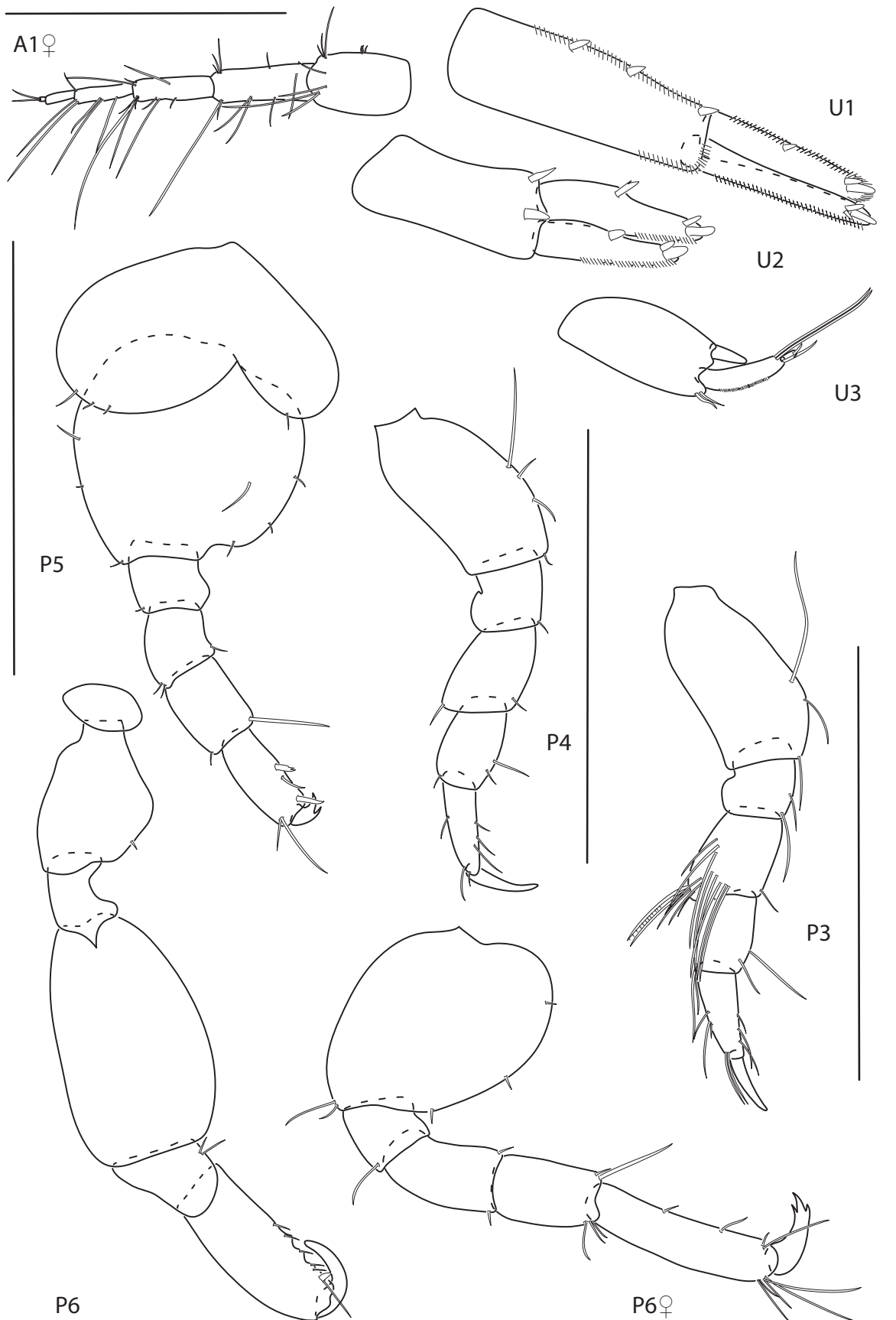


Figure 16. *Photis butalus* sp. nov., female paratype, 2.3 mm, antenna 1, pereopod 6; male holotype, 2.1 mm, uropod 1, uropod 2, uropod 3, pereopod 5, pereopod 4, pereopod 3, pereopod 6. Scale bars: 0.5 mm.

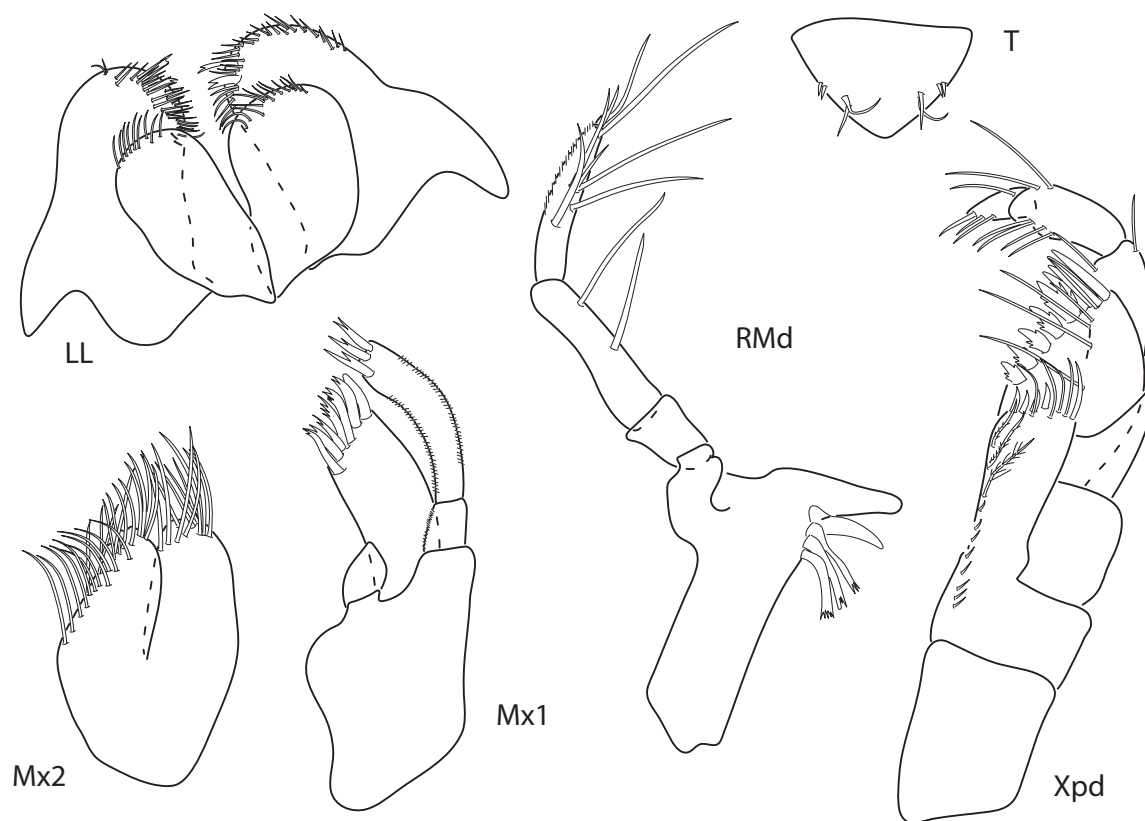


Figure 17. *Photis butalus* sp. nov., male holotype, 2.1 mm, lower lip, maxilla 2, maxilla 1, right mandible, telson, maxilliped. Scale bars: 0.5 mm.

Pleon. Uropod 1 peduncle $1.3 \times$ length of inner ramus, with three marginal robust setae and lined with fine setules; inner ramus $1.1 \times$ length of outer ramus, with one marginal stout seta, lined with marginal setules, apex with two robust setae; lined with marginal setules, apex with three robust setae. Uropod 2 peduncle with two distal robust setae, subequal in length with inner ramus; inner ramus $1.2 \times$ length of outer ramus, one marginal robust setae, inner margin lined with setules, apex with two robust setae; outer ramus outer margin lined with setules, with one marginal robust setae, apex with two robust setae. Uropod 3 peduncle $3.9 \times$ length of inner ramus, with two distal setae; inner ramus $0.4\text{--}0.5 \times$ length of outer ramus, bare; outer ramus bi-articulate, first article outer margin lined with setules, with three long distal setae; second article with one distal seta. Telson narrowing distally, apically rounded with four dorsal setae.

Female (paratype, 2.3 mm). Similar in all aspects to the male with the exception of the following: pereopod 6 merus not enlarged, propodus width $0.2 \times$ length, smooth; dactylus apically acute with accessory claws.

Etymology. After the Latin *bu*, meaning large and *talus*, meaning ankle, heel, die and referring to the greatly enlarged pereopod 6, specifically the thickened propodus, of males of this species.

Distribution. Panama: Bocas del Toro (present study).

Ecology and remarks. This species occurs among brown algae, hydroids, and filamentous algae at a depth of three meters.

Photis butalus sp. nov. is similar to *Photis trapherus* Thomas & Barnard, 1991 and *Photis elephantis* Barnard, 1962 based on the enlarged male pereopod 6.

The new species differs from *P. trapherus* in the following characters: eye not touching outer margin of ocular lobe (vs touching); entire gnathopod 1 propodus palm (vs slightly excavate); male pereopod 6 merus ovate (vs subrectangular), and propodus thick, posterior margin serrate (vs thin, smooth). The new species differs from *P. elephantis* in the following characters: ocular lobe pronounced, rounded (vs small, subquadrate); male pereopod 6 basis posteriorly rounded (vs posterior margin with acute distal point), merus posteriorly rounded (vs posterodistal margin produced into lobe), and propodus posterior margin serrate (vs smooth). This species is also similar to *Photis* sp. E LeCroy, 2000 but differs in the following characters: eye well developed (vs poorly developed); male pereopod 6 greatly enlarged (vs slightly enlarged), merus ovate (vs subrectangular with large posterodistal projection). This species is easily distinguishable from all remaining described *Photis* species based on the enlarged male pereopod 6. Ethanol-preserved specimens retained brown specks of color.

***Photis bulla* sp. nov.**

<https://zoobank.org/E0C60C56-2A5F-402C-B5C5-07CA6F32BF35>

Figs 18–20, 32F

Photis sp. C: LeCroy 2000: 157, fig. 185.

Type locality. Bocas del Toro, Panama: Crawl Caye, 9.2475°N, 82.1290°W, depth 1.5–3 m, among *Halimeda*.

Material examined. Holotype: PANAMA • 1 ♀, 2.4 mm; Bocas del Toro, Crawl Caye; 9.2475°N, 82.1290°W; depth 1.5–3 m, among coral rubble; 11 Aug 2021; K.N. White leg.; USNM 1743963. **Paratype:** PANAMA • 1 ♂, 1.2 mm; Bocas del Toro, Crawl Caye; 9.2376°N, 82.1438°W; depth 5 m, among *Halimeda*; 12 Aug 2021; K.N. White leg.; USNM 1743964. **Other material:** PANAMA • 2 ♀, 1.8–2.2 mm; Bocas del Toro, Crawl Caye; 9.2376°N, 82.1438°W; depth 4.6 m, among coral rubble; 11 Aug 2021; K.N. White leg.; USNM 1743966 • 1 juvenile, 1.2 mm; Bocas del Toro, Crawl Caye; 9.2475°N, 82.1290°W; depth 5 m, among *Halimeda*; 12 Aug 2021; K.N. White leg.; USNM 1743965.

Diagnosis. Head ocular lobe rounded distally. Coxae 1–4 ventral margins lined with long setae; coxa 1 anteroventral margin slightly produced with gap in marginal setae. Gnathopod 1 carpus slightly shorter than propodus in length, anterior margin subquadrate proximally. Gnathopod 2 propodus with stout robust seta at palmar angle, dactyl, flexor margin serrate. Pereopods 5–7 basis anterior margin with row of long submarginal plumose setae. Pereopods 6 and 7 propodus each with posterodistal cluster of setae surpassing length of dactylus. Uropod 3 inner ramus with minute spinule.

Description. (Female 2.4 mm). **Head.** Head, ocular lobe rounded distally. Maxilliped, inner plate apical margin lined with plumose robust setae; outer plate with row of marginal sagittate-shaped robust setae and row of submarginal simple setae; palp 4-articulate, articles 1–3 inner margins lined long thin setae, article 4 with stout setae. Upper lip apically setose. Lower lip inner and outer lobes rounded, apically setose; outer lobe with few thick bifurcate setae. Maxilla 1 outer plate with four apical robust setae and four slender setae; inner plate with nine apical robust setae. Maxilla 2 inner plate outer margin lined with setae, submarginal row

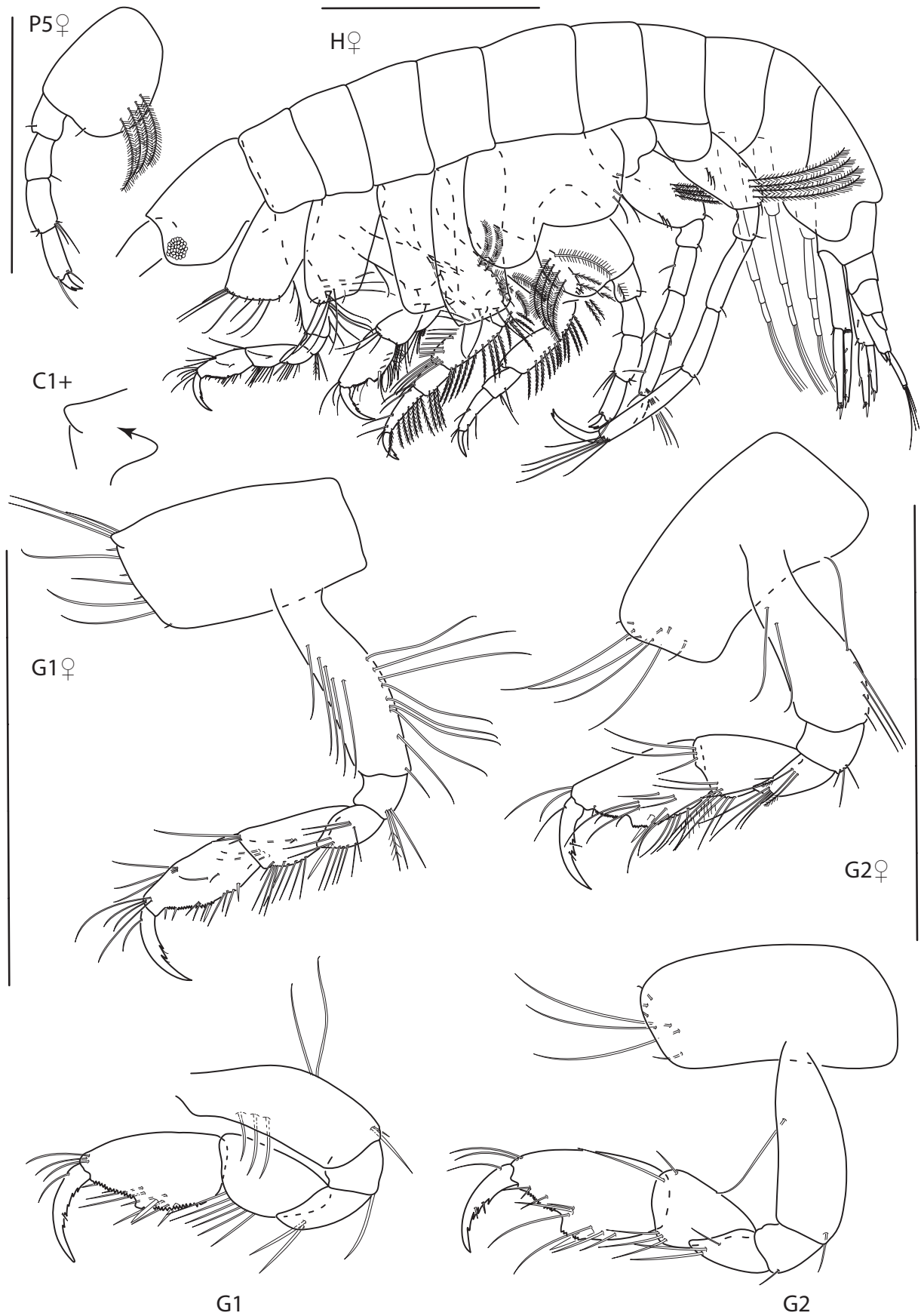


Figure 18. *Photis bulla* sp. nov., female holotype, 2.4 mm, pereopod 5, habitus, gnathopod 1 medial, gnathopod 2 medial; male paratype, 1.2 mm, gnathopod 1 medial, gnathopod 2 medial. Scale bars: 0.5 mm.

of long setae; outer plate apical margin lined with long plumose setae. Mandibles similar, molar small; palp tri-articulate, articles 2 and 3 with plumose setae.

Pereon. Coxae 1–4 lined with long ventral setae; coxa 1 anteroventral margin slightly produced with gap in marginal setae. Gnathopod 1 subchelate; basis unexpanded, margins lined with long setae; carpus slightly shorter than propodus; propodus palm serrate with one robust seta at proximal margin; dactylus serrate. Gnathopod 2 similar to gnathopod 1 with deep palmer excavation just before robust seta at palmar angle. Pereopods 3 and 4 posterior margins of articles 2–4 lined with long plumose setae. Pereopod 5 basis length $1.2 \times$ width; dactylus stout. Pereopods 5–7 basis with row of submarginal plumose setae. Pereopods 6 and 7 propodus each with posterodistal cluster of setae surpassing length of dactylus; dactylus with accessory claw.

Pleon. Epimera 1–3 distal margins rounded. Uropod 1 peduncle subequal in length with inner ramus; inner ramus $1.1 \times$ length of outer ramus, both rami with marginal and apical robust setae. Uropod 2 peduncle $1.1 \times$ length to inner ramus, peduncle with two strong distomedial robust setae; inner ramus $1.3 \times$ length of outer ramus, each ramus with one marginal robust seta and two or three apical robust setae. Uropod 3 peduncle $5.3 \times$ length of inner ramus; inner ramus $0.3 \times$ length of outer ramus, with small apical spinule; outer ramus bi-articulate, terminal article with many long setae. Telson apex rounded, subtriangular.

Male (paratype 1.2 mm). Similar in all aspects to the female with the exception of the following: Gnathopod 1 propodus palm with excavation. Gnathopod 2 with process near insertion of dactylus. Pereopods 3, 5, and 7 missing. Pereopod 4 sparsely setose. Pereopod 6 lacking plumose setae on basis.

Etymology. After the Latin *bulla*, meaning knob, boss, stud, bubble and referring to the anteroventral projection on the anteroventral margin of coxa 1 of this species.

Distribution. U.S.A.: Florida: Hutchinson Island to the Florida Keys, Florida Bay to Perdido Key (LeCroy 2000); Panama: Bocas del Toro (present study).

Ecology and remarks. This species occurs among coral rubble and *Halimeda* at depths of 1.5–3 m. Panamanian specimens agree closely with the description of *Photis* sp. C of LeCroy (2000) with the exception of unequal rami on uropod 1 and a more rounded telson apex. Panamanian specimens have a small spinule on the inner ramus of uropod 3, which LeCroy noted as variable. *Photis bulla* sp. nov. most closely resembles *Photis spinicarpa* Shoemaker, 1942 based on gnathopod 1 carpus subquadrate proximally, gnathopod 2 with stout seta at palmar angle, gnathopod 2 dactyl flexor margin serrate, and pereopod 5 basis anterior margin with plumose setae but can be distinguished based on the absence of robust setae on upper proximal margin of gnathopod 1 carpus, male gnathopod 2 basis and carpus without anterodistal process, and pereopod 3 merus unexpanded. *Photis bulla* sp. nov. differs from *Photis probolion* sp. nov. in the following characters: coxa 1 with setae; male coxae 3 and 4 without stridulating ridges; female pereopod 5 with submarginal plumose setae; uropods 1 and 2 outer ramus with marginal setae. *Photis bulla* sp. nov. differs from all remaining described *Photis* species in having coxa 1 anteroventral margin slightly produced with gap in marginal setae. Additionally, the new species differs from *Photis melanica* and *Photis butalus* sp. nov. in having a posterodistal cluster of setae surpassing length of dactylus on pereopods 6 and 7. Live specimens are a mottled purple-brown color with purple-brown stripes on distal ends of antennae.

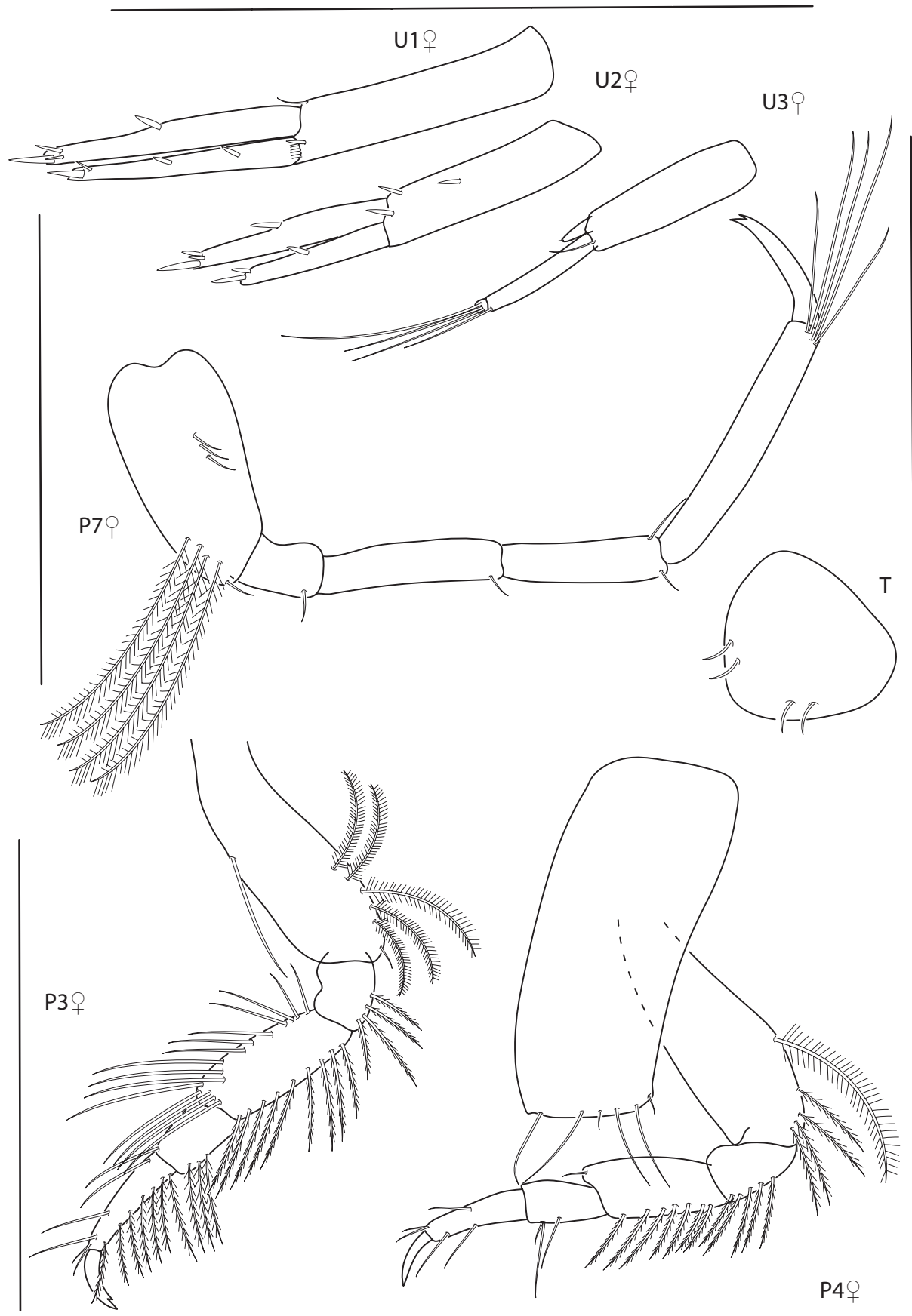


Figure 19. *Photis bulla* sp. nov., female holotype, 2.4 mm, uropod 1, uropod 2, uropod 3, pereopod 7, pereopod 3, pereopod 4; male paratype, 1.2 mm, telson. Scale bars: 0.5 mm.

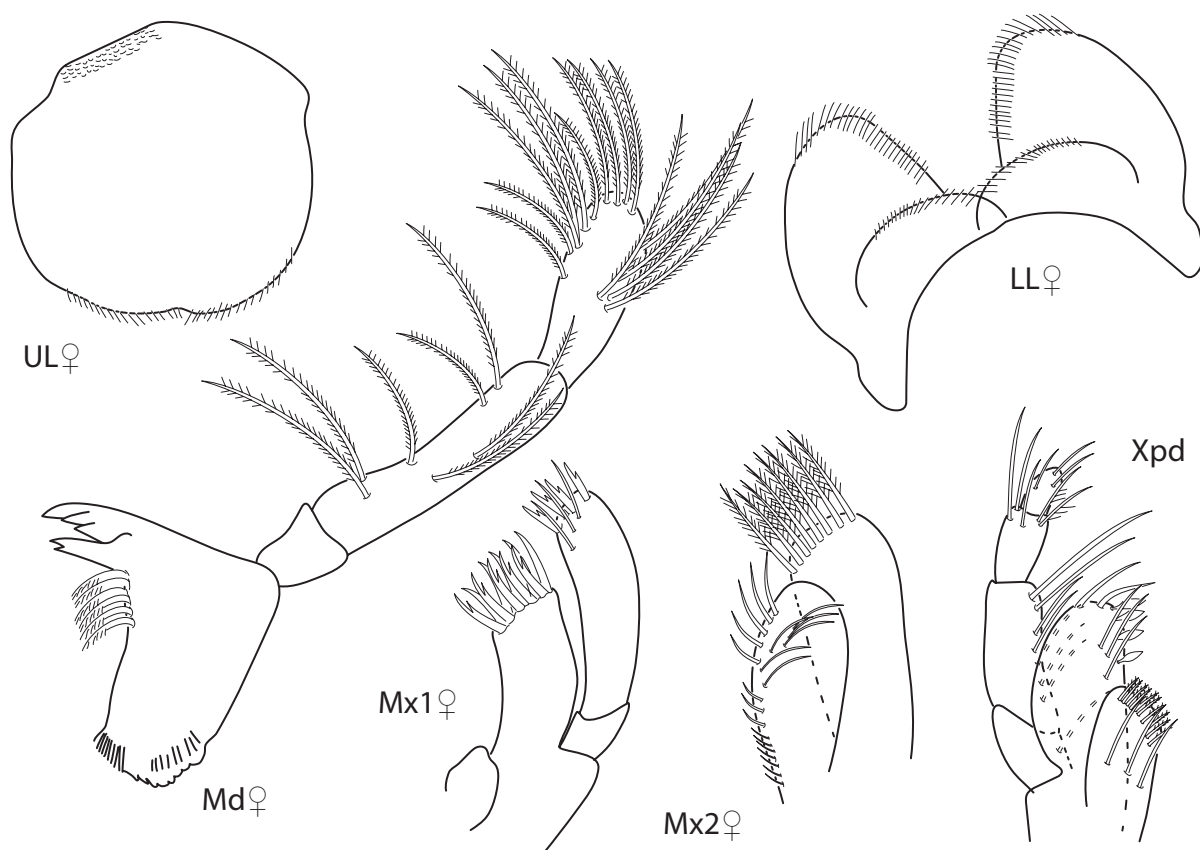


Figure 20. *Photis bulla* sp. nov., female holotype, 2.4 mm, upper lip, lower lip, mandible, maxilla 1, maxilla 2; male paratype, 1.2 mm, maxilliped. Scale bars: 0.5 mm.

***Photis probolion* sp. nov.**

<https://zoobank.org/7428F59B-F31A-49AA-B069-60CEC6B3C3AF>

Figs 21–23, 32G

Photis sp. D: LeCroy 2000: 158, fig. 193.

Type locality. Bocas del Toro, Panama: Crawl Caye, 9.2502°N, 82.1318°W, depth 5–13 m, among coral rubble.

Material examined. **Holotype:** PANAMA • 1 ♂, 1.4 mm; Bocas del Toro, Crawl Caye; 9.2502°N, 82.1318°W; depth 10–13 m, among coral rubble; 29 June 2023; K.N. White leg; USNM 1743967. **Paratypes:** PANAMA • 1 ♂, 1.6 mm; same station data as for preceding; USNM 1743968 • 1 ♀, 1.68 mm; same station data as for preceding; USNM 1743969. **Other material:** PANAMA • 5 ♂, 2 ♀; same station data as for preceding; USNM 1743971 • 2 ♂, 4 ♀; Bocas del Toro, Crawl Caye; 9.2502°N, 82.1318°W; depth 5 m, among coral rubble; 29 June 2023; K.N. White leg; USNM 1743970.

Diagnosis. Male coxa 1 anteroventral angle rounded, without setae. Male gnathopod 2 basis with large anterodistal lobe, lined with stridulating ridges; propodus process at palmar angle long, slender, curved. Male coxae 3 and 4 with stridulating ridges. Uropods 1–3 rami without marginal robust setae. Uropod 3 inner ramus lanceolate, inner ramus 0.2 × length of outer ramus, outer ramus, bi-articulate, article 2 with at least one apical seta.

Description. Male (holotype, 1.7 mm). *Head*. Eyes round, circle of dark ommatidia surrounded by light ommatidia, touching anterior margin of ocular lobe. Antenna 1 broken; peduncle article 2 $2.3 \times$ length of article 1. Antenna 2 flagellum 7-articulate. Maxilliped inner plate apical margin with two rows of plumose setae; outer plate with four robust setae, lined with submarginal setae; palp 4-articulate. Lower lip inner and outer lobes rounded, lined with fine setae. Maxilla 1 inner plate small with one apical seta; outer plate with eight bifurcate robust setae; palp bi-articulate with three apical robust setae and two marginal setae. Maxilla 2 outer plate with eight apical setae; inner plate with five apical and five marginal setae. Mandibles similar, incisors dentate; palp tri-articulate, articles 2 and 3 setose, with some plumose setae. Upper lip rounded with indentation, apically setose on either side of indentation.

Pereon. Coxae sparsely setose, setae short; coxae 1–4 longer than wide; coxae 3–4 with stridulating ridges. Gnathopod 1 subchelate; basis unexpanded, margins with tufts of long setae; carpus $0.1 \times$ length of propodus; propodus palm serrate, lacking robust setae; dactylus minutely serrate. Gnathopod 2 basis with large anterodistal lobe, lined with stridulating ridges; propodus process at palmar angle long, slender, curved. Pereopod 3 merus minutely expanded anteriorly. Pereopod 4 anterodistal margin of carpus with pointed projection, with few setae. Pereopods 5–7 bases rounded, narrowing sequentially. Pereopod 7 significantly longer than pereopods 5 and 6.

Pleon. Epimeron 3 posteroventral corner subquadrate without notch. Uropod 1 peduncle with one distal robust seta, $1.3 \times$ length of inner ramus; inner ramus $1.3 \times$ length of outer ramus, rami lined with minute setules, lacking robust setae. Uropod 2 peduncle $0.8 \times$ length of inner ramus, with one distal robust seta; inner ramus $1.2 \times$ length of outer ramus, lined with minute setules, lacking robust setae. Uropod 3 peduncle $2.0 \times$ length of inner ramus with one apical seta; inner ramus lanceolate, $0.2 \times$ length of outer ramus, bare; outer ramus bi-articulate, article 2 with two apical setae.

Male (paratype, 1.6 mm). *Head*. Antenna 1 shorter than antenna 2, distal margins with sparse, long setae, flagellum tri-articulate, terminal article minute. Antenna 2 flagellum 4-articulate, terminal article minute. *Pleon*. Telson entire, apex subtriangular, with two setae, lateral margins with subacute points.

Female (paratype, 1.7 mm). Similar in all aspects to the male with the exception of the following: antenna 1 5-articulate; antenna 2 8-articulate; coxae without stridulating ridges; coxa 1 ventral margin with few short setae; gnathopod 2 basis anterodistal margin unexpanded, without lobe; propodus with reduced distal thumb, lacking triangular process near insertion of dactylus; pereopod 4 basis anterior and posterior margins with long plumose setae, anterodistal margin of carpus without pointed projection.

Etymology. After the Latin *probolos*, meaning any projecting or jutting object or prominence and referring to large anterodistal lobe on the basis of the gnathopod 2 of males of this species.

Distribution. U.S.A.: Florida: Biscayne Bay, Florida Bay (LeCroy 2000); Panama: Bocas del Toro (present study).

Ecology and remarks. This species occurs among coral rubble at depths of 1.6–13 m. Panamanian specimens closely resemble *Photis* sp. D LeCroy, 2000 with the exception of male gnathopod 2 propodus having a small, rounded process near palmar angle and a smaller thumb at palmar angle, which is most

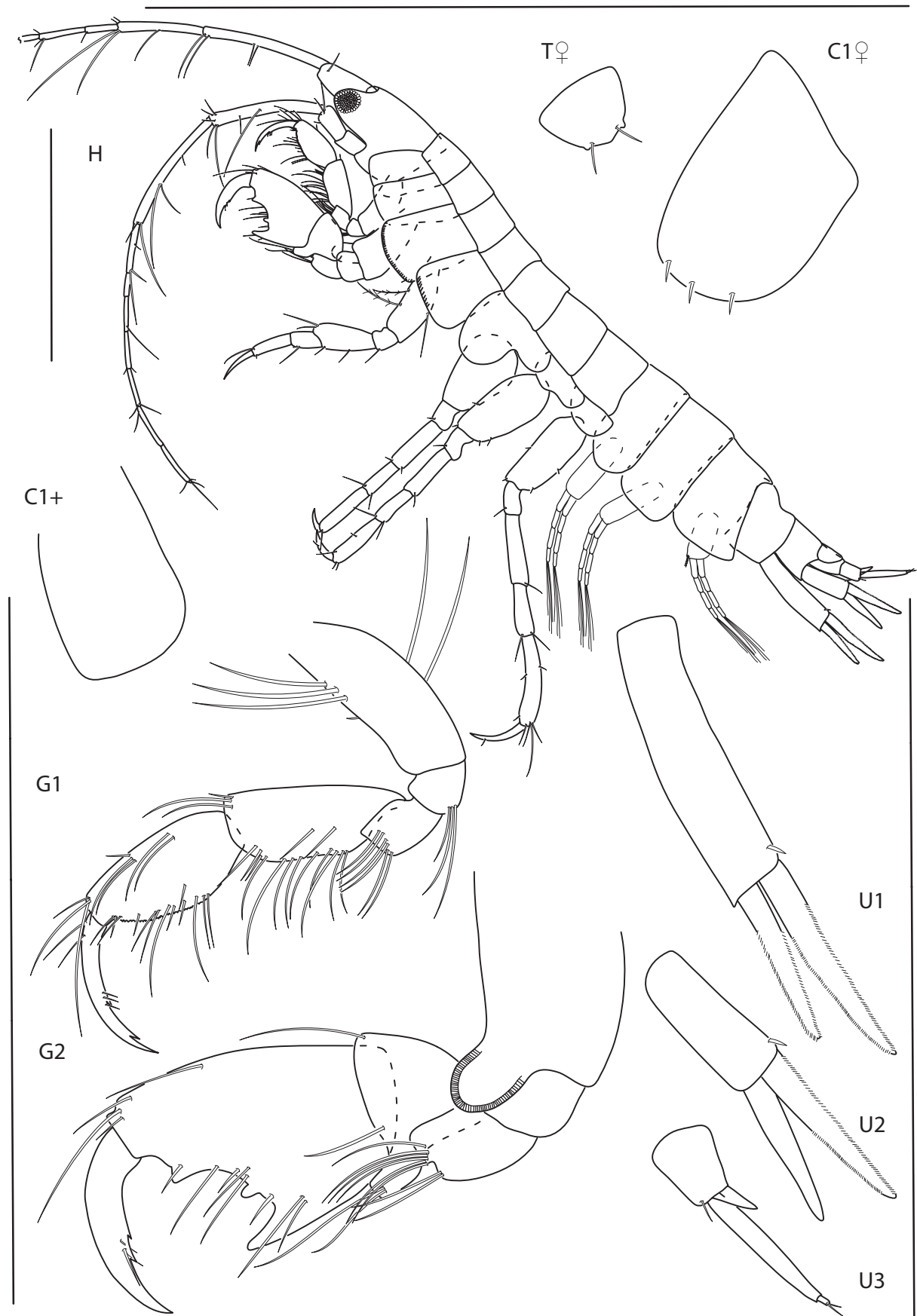


Figure 21. *Photis probolion* sp. nov., male holotype, 1.4 mm, habitus, coxa 1, gnathopod 1 medial, gnathopod 2 medial, uropod 1, uropod 2, uropod 3; female paratype, 1.7 mm, telson, coxa 1. Scale bars: 0.5 mm.

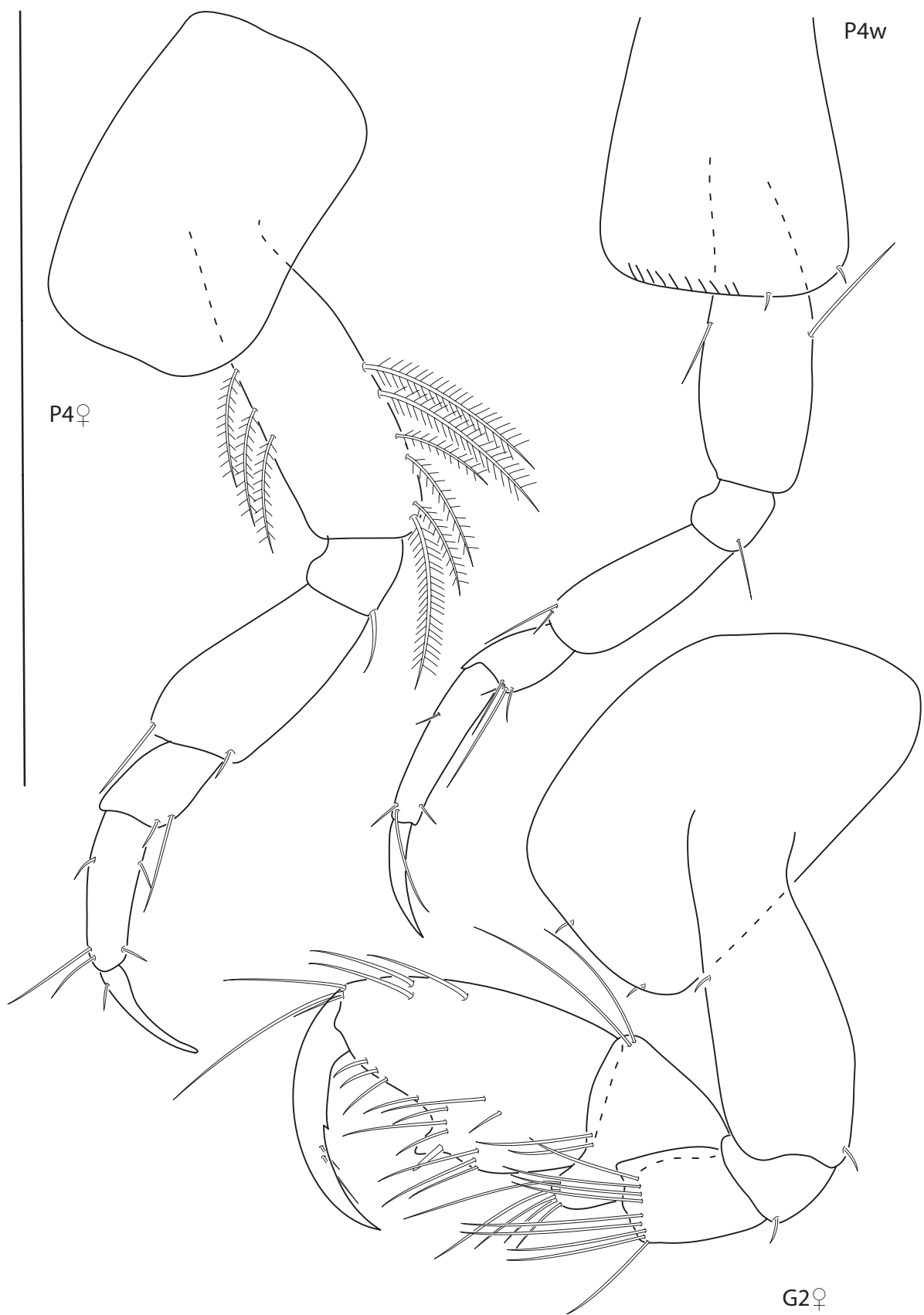


Figure 22. *Photis probolion* sp. nov., female paratype, 1.7 mm, pereopod 4, gnathopod 2 medial; male paratype “w”, 1.6 mm, pereopod 4. Scale bars: 0.5 mm.

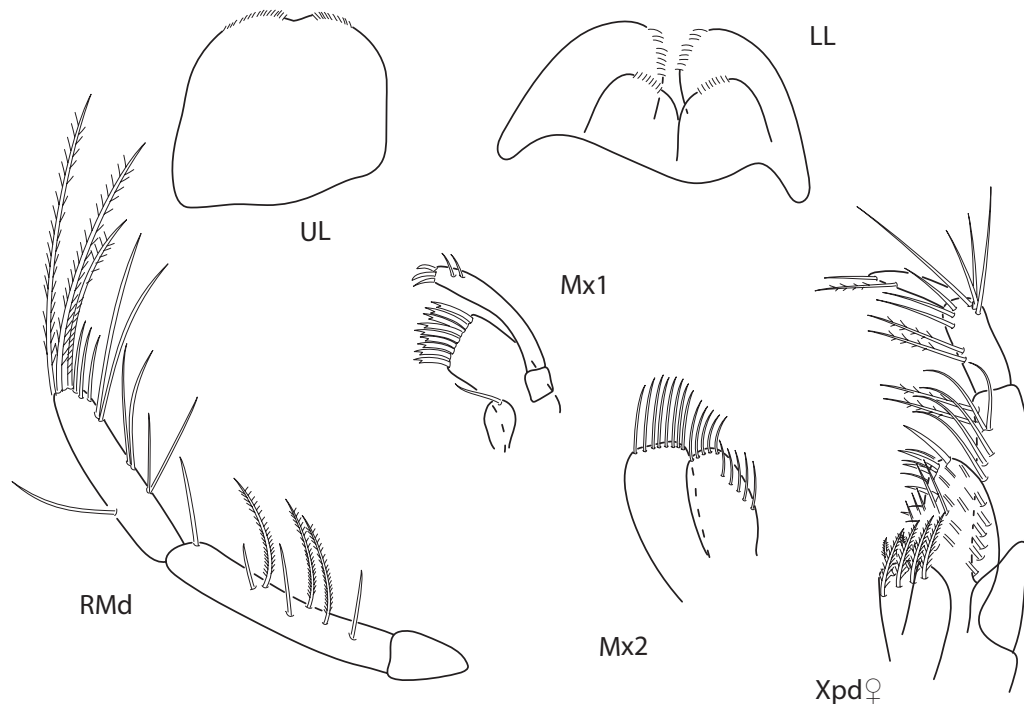


Figure 23. *Photis probolion* sp. nov., male holotype, 1.4 mm, upper lip, lower lip, right mandible, maxilla 1, maxilla 2; female paratype, 1.7 mm, maxilliped. Scale bars: 0.5 mm.

likely due to the small size of the Panamanian specimens. *Photis probolion* sp. nov. most closely resembles *Photis longicaudata* (Bate & Westwood, 1862) and *Photis bronca* Jung et al., 2019 in sharing the rounded anteroventral angle on coxa 1 and the large anterodistal lobe with stridulating ridges on gnathopod 2 basis. The new species differs from *P. longicaudata* in having stridulating ridges on male coxa 4 and in lacking robust setae on uropods 1 and 2 outer rami. The new species differs from *P. bronca* in lacking setae on coxa 1 and in having uropod 3 peduncle shorter than the inner ramus (vs peduncle longer than inner ramus). *Photis probolion* sp. nov. can be easily distinguished from all other described *Photis* species in having a large anterodistal lobe lined with stridulating ridges on the male gnathopod 2 basis, the general shape of the gnathopod 2 propodus, stridulating ridges on male coxae 3 and 4, and in lacking marginal robust setae on uropods 1–3 rami. Live specimens are white, sometimes with faint brown stripes and pink markings, especially on the antennae.

***Photis melanica* McKinney, 1980**

Figs 24, 32H

Photis melanicus McKinney, 1980: 57–61, fig. 1.

Photis melanica: LeCroy 2000: 154, fig. 187; LeCroy et al. 2009: 941–972.

Photis sp. B: McKinney 1977: 112, fig. 19.

Material examined. PANAMA • 1.7 mm • 1 ♀; Bocas del Toro, Laboratory Dock; 9.4159°N, 82.2489°W; depth 14 m, in light trap; 8 Aug 2005; T.A. Haney leg.; GCRL 6671.

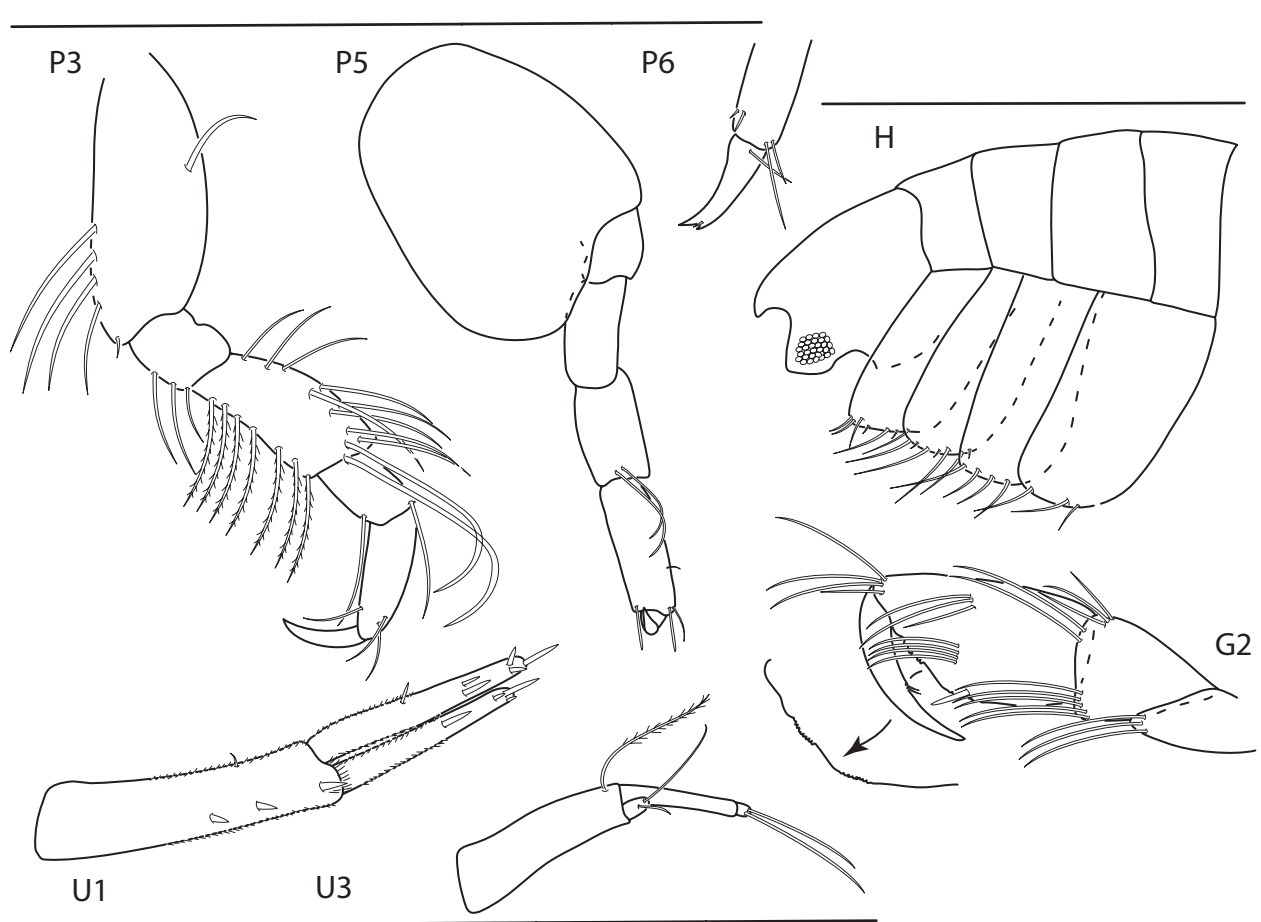


Figure 24. *Photis melanica*, female, 1.7 mm, pereopod 3, pereopod 5, pereopod 6 dactylus, head and coxae 1–4; uropod 1, uropod 3, gnathopod 2 medial. Scale bars: 0.5 mm.

Diagnosis. Ocular lobe distal margin subacute. Coxae 1–4 ventral margins lined with long setae. Coxa 1 anteroventral margin evenly rounded. Female gnathopod 2 propodus palmar margin lacking process. Pereopod 3 merus with long plumose setae. Pereopod 5 basis bare. Pereopods 6 and 7 propodus with few setae shorter than dactylus; dactylus with accessory claw. Uropod 1 inner ramus $1.2 \times$ length of outer ramus. Uropod 3 peduncle with plumose distoventral seta; inner ramus $0.2 \times$ length of outer ramus, apical margin with setae.

Distribution. U.S.A.: Florida Bay, Tampa Bay, Florida (LeCroy 2000), South of Galveston, Texas (McKinney 1977, 1980), Gulf of Mexico (LeCroy et al. 2009); Venezuela: exact location unspecified (Martín and Díaz 2003; LeCroy et al. 2009). Panama: Bocas del Toro (present study).

Ecology and remarks. This species was collected with light traps at a depth of 14 m. Panamanian specimens agree closely with previous descriptions. Ethanol-preserved specimens retained faint brown coloration on most of body.

Genus *Posophotis* Barnard, 1979

Diagnosis. Antenna 1 accessory flagellum 2- or 3-articulate (possibly with tiny additional article). Head cephalic lobe subacute. Coxae elongate, large, and overlapping. Dactylus of maxilliped short, stubby, setose apically. Gnathopod 1 small,

weakly subchelate, carpus slightly longer than propodus. Gnathopod 2 broad, subchelate, posterior margin of propodus broadly lobate, anterior margin of propodus slightly longer than posterior margin, palm oblique, sculptured. Uropod 3 peduncle elongate, rami styliform, slightly shorter than peduncle, one-articulate.

***Posophotis seri* Barnard, 1979**

Figs 25, 33A

Posophotis seri Barnard, 1979: 31–34, figs 11, 12.

Material examined. PANAMA • 2.3–4.7 mm • 2 ♀; Bocas del Toro, Bocas del Drago, 9.4180°N, 82.3375°W, depth 2.4 m, among red algae; 9 Aug 2021; K.N. White leg.; USNM 1743972.

Diagnosis. Eye round. Gnathopod 1 propodus without projections. Female gnathopod 2 propodus with mid-palmar excavation, large robust seta at palmar angle; dactylus longer than palm. Uropod 3 peduncle elongate, rami styliform, lined with minute setae, each ramus with one marginal robust seta.

Distribution. Mexico: Puerto Peñasco (Barnard 1979); Ecuador: Galapagos Islands (Barnard 1979); Panama: unspecified (Barnard 1979), Bocas del Toro (present study).

Ecology and remarks. This species occurs among red algae at a depth of 2.4 m. Panamanian specimens closely resemble specimens described in Barnard, 1979. Ethanol-preserved specimens retained brown coloration on pereon.

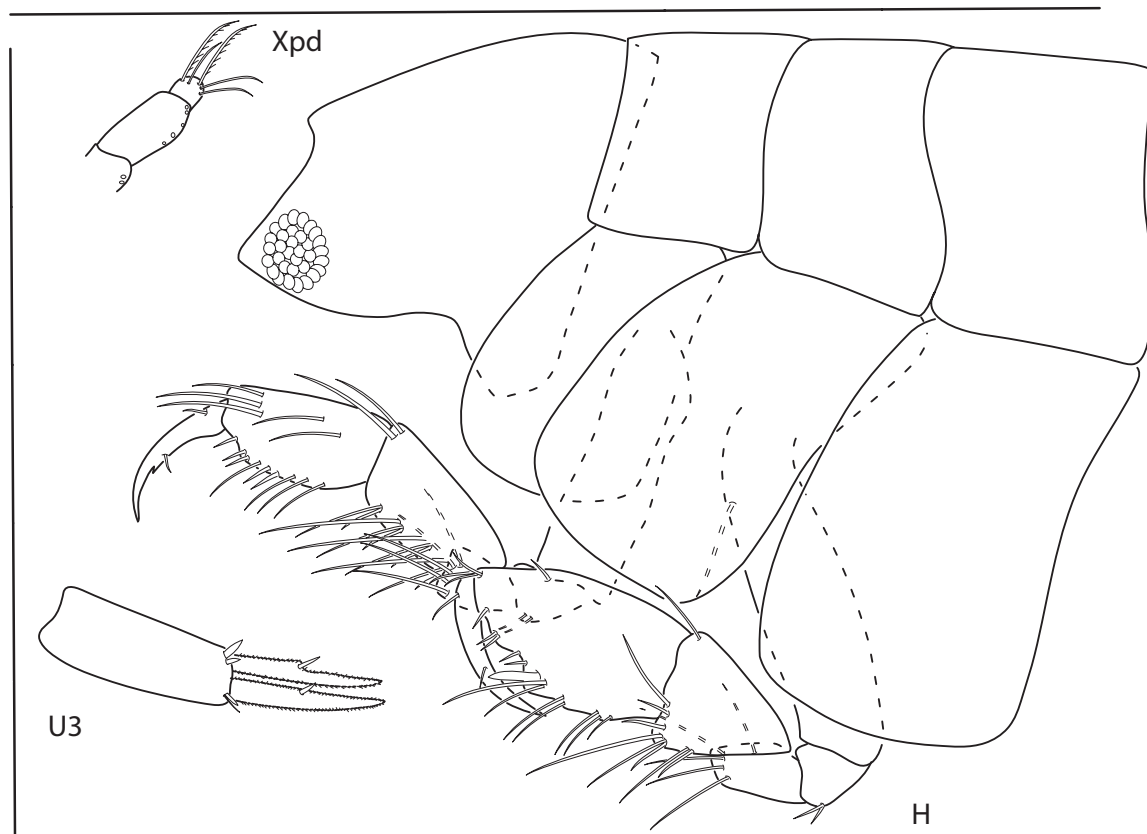


Figure 25. *Posophotis seri*, female, 4.7 mm, maxilliped palp (in part), habitus (in part), uropod 3. Scale bars: 0.5 mm.

Family Podoceridae Leach, 1814

Genus *Podocerus* Leach, 1814

Diagnosis. Body often with dorsal elevations or carinate, pereon segments 2 and 3 fused. Antenna 2 longer than antenna 1, stout. Head not globular, buccal mass similar in size to head. Coxae discontinuous. Urosomites separate, urosomite 1 elongate. Uropods 1–3 dissimilar in structure; uropod 3 greatly reduced.

Podocerus offucia sp. nov.

<https://zoobank.org/B828F2DD-0E9C-49EE-A0E4-580D7F3D6E9E>

Figs 26–28, 33B

Type locality. Bocas del Toro, Panama: Swan Cay, 9.4536°N, 82.3000°W, among coral rubble.

Material examined. Holotype: PANAMA • 2.8 mm • 1 ♂; Bocas del Toro, Panama: Swan Cay, 9.4536°N, 82.3000°W, depth 1–3 m; among coral rubble; 27 June 2023; K.N. White leg; USNM 1743973. **Paratype:** PANAMA • 2.8 mm • 1 ♀; station data same as holotype; USNM 1743974.

Diagnosis. Pereon segments 5–7 dorsally setose. Male antenna 1 flagellum 4-articulate; accessory flagellum uni-articulate. Coxa 1 with four marginal setae. Gnathopod 1 basis slender. Male gnathopod 2 propodus palm serrate with one large, rounded projection, posteriorly concave. Pereopods 3–7 propodus with posterodistal notch. Uropods 1 and 2 each with distoventral interramal spine.

Description. Male (holotype, 2.8 mm). **Head.** Eyes round, bulging. Antenna 1 densely setose, flagellar article 1 shorter than flagellar article 2; accessory flagellum uni-articulate. Antenna 2 densely setose; flagellum 4-articulate. Maxilliped inner plate with seven plumose apical setae, outer plate lined with ten marginal robust setae and many facial setae, palp 4-articulate. Lower lip missing. Maxilla 1 inner plate absent; outer plate with six apical robust setae; palp bi-articulate, apical margin with four bifurcate setae and three slender setae. Maxilla 2 inner and outer plate apical margins lined with setae; outer plate with two rows. Mandibular palp tri-articulate, lined with plumose setae. Upper lip missing.

Pereon. Pereon segments with posterodorsal processes. Pereonites 5–8 with dorsal robust setae. Coxae sparsely setose, discontinuous. Coxa 1 rhomboidal. Gnathopod 1 subchelate; basis slender; ischium posterior margin with two long setae; merus posterior margin with long plumose setae; carpus longer than wide, posterior margin lined with plumose setae, with two plumose facial setae; propodus subequal in length with carpus, posterior margin with many simple and plumose setae, anterolateral margin with facial setae; dactylus inner margin serrate. Gnathopod 2 subchelate, much larger than gnathopod 1; basis expanded anteriorly into rounded process, posterior margin with short setae; ischium posterodistal margin with sparse short setae; merus ventral margin lined with long slender plumose setae and two short, stout setae; carpus reduced, ventral margin lined with long slender plumose setae; propodus palm serrate with one large, rounded projection, posteriorly concave; dactylus closing on concavity. Pereopods 3–6 missing. Pereopod 7 basis ovate; ischium short; merus posteriorly expanded; propodus with posterodistal notch.

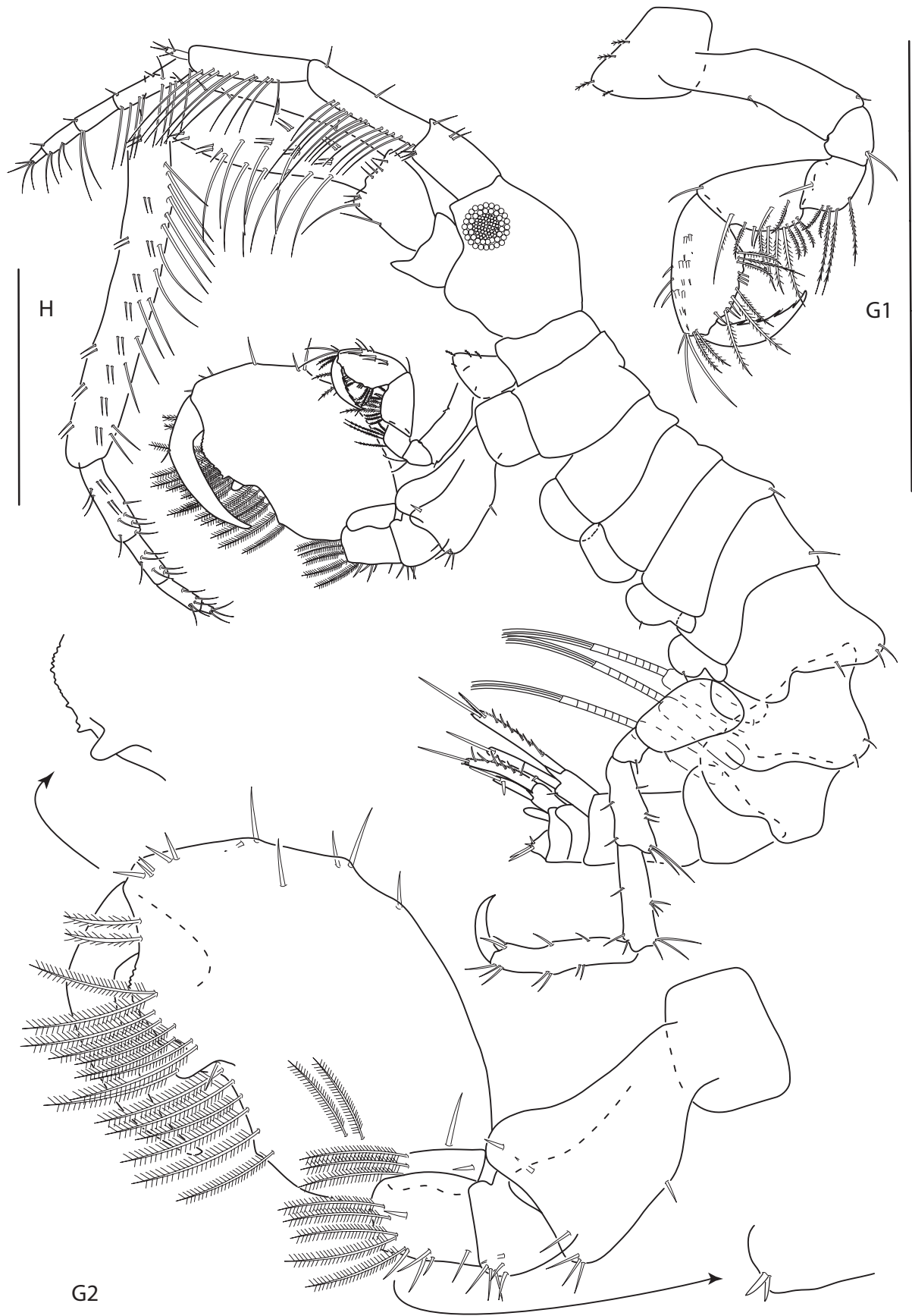


Figure 26. *Podocerus offucia* sp. nov., male holotype, 2.8 mm, habitus, gnathopod 2 medial, gnathopod 2 medial. Scale bars: 0.5 mm.

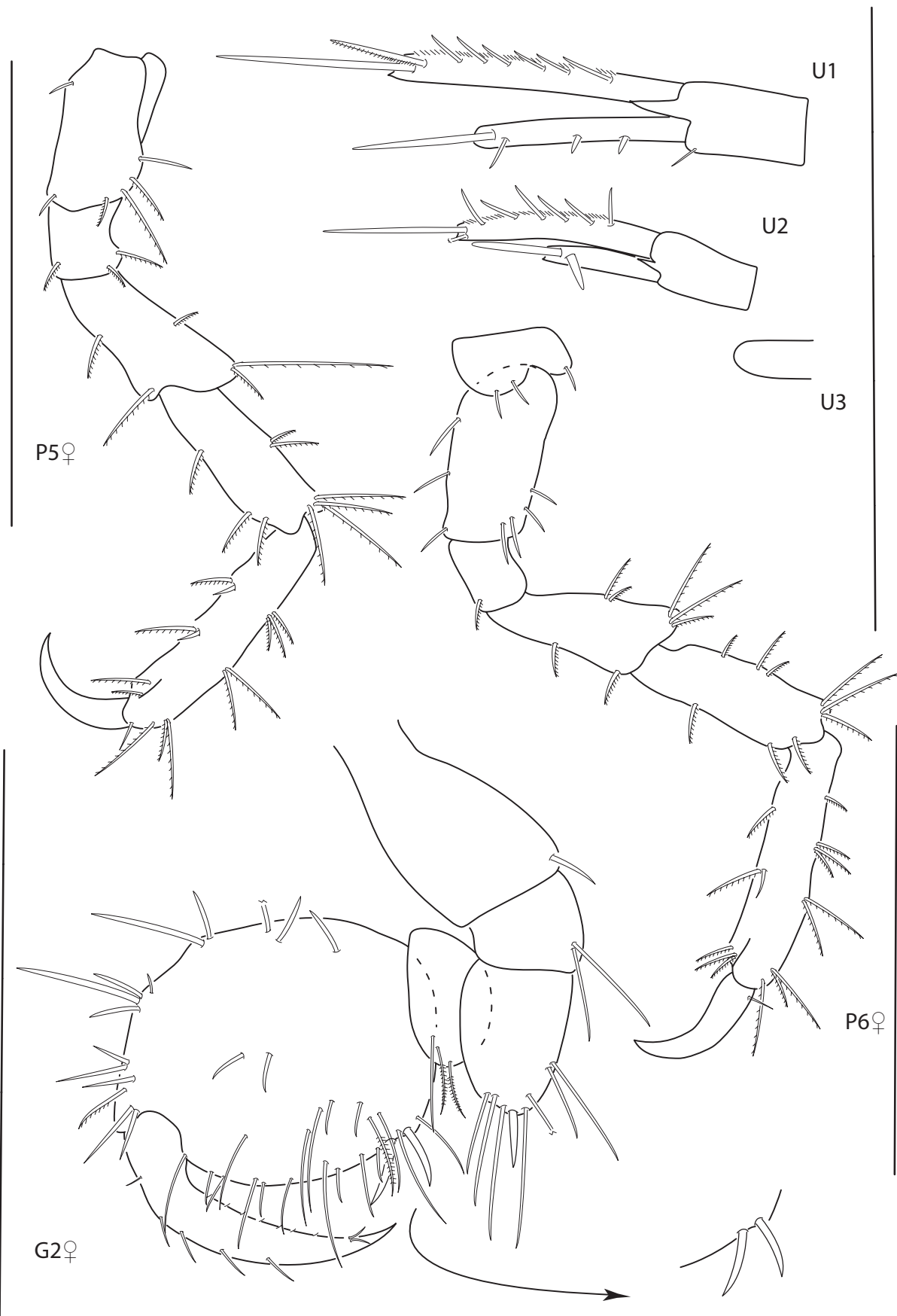


Figure 27. *Podocerus offucia* sp. nov., female paratype, 2.8 mm, pereopod 5, gnathopod 2 medial, pereopod 6; male holotype, 2.8 mm, uropod 1, uropod 2, uropod 3. Scale bars: 0.5 mm.

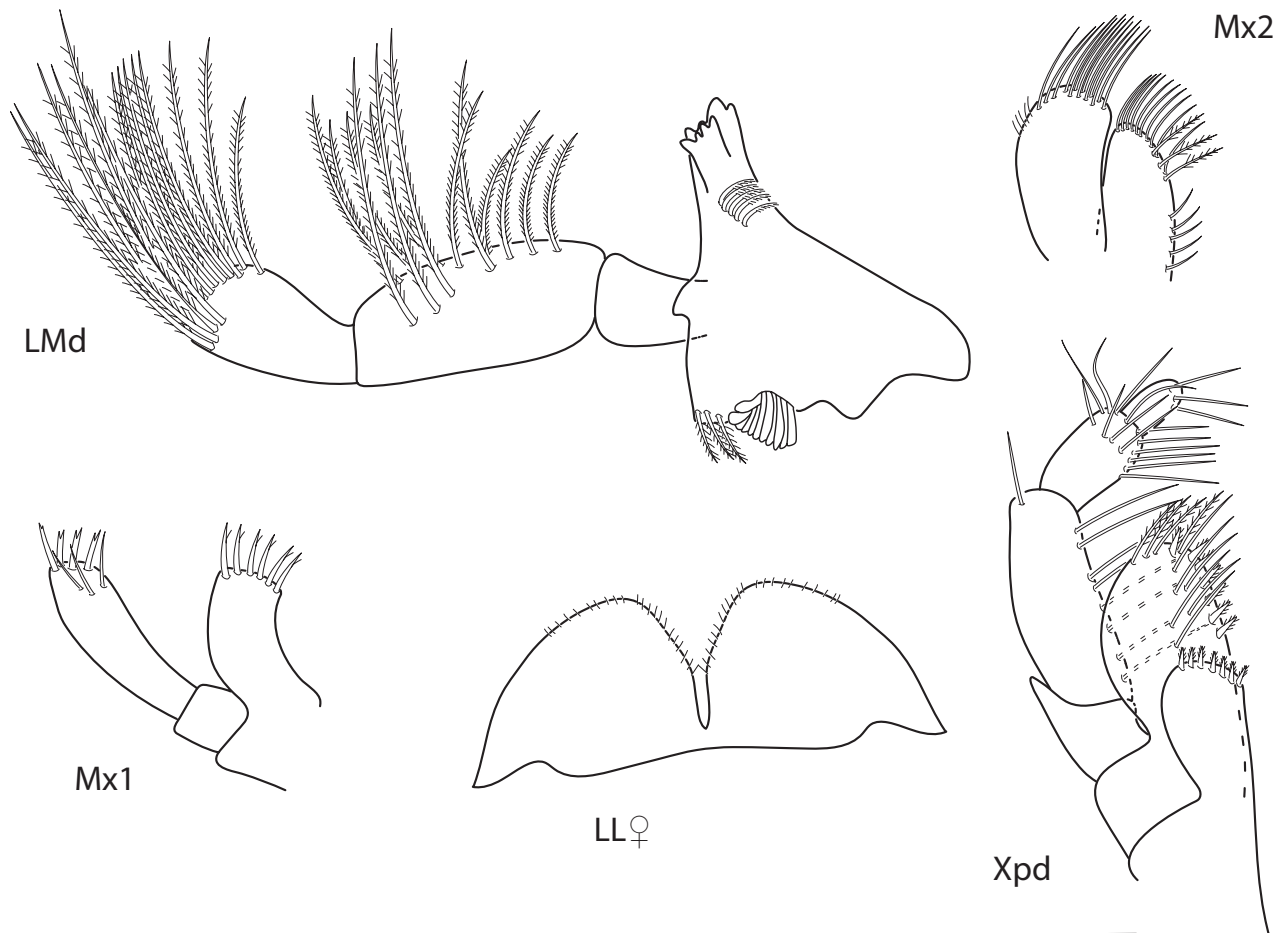


Figure 28. *Podocerus offucia* sp. nov., male holotype, 2.8 mm, left mandible, maxilla 1, maxilla 2, maxilliped; female paratype, 2.8 mm, lower lip. Scale bars: 0.5 mm.

Pleon. Epimera 1–3 with posterodorsal processes; posteroventral margins smooth, rounded. Uropod 1 $1.4 \times$ length of uropod 2; peduncle with distoventral interrampal spine, apical margin with one slender seta; inner ramus $2.3 \times$ length of peduncle, outer margin lined with robust setae and fine setules, apical margin with one long seta; outer ramus outer margin with few robust setae, apical margin with one long seta. Uropod 2 peduncle with distoventral interrampal spine, apical margin with one slender seta; inner ramus $2.9 \times$ length of peduncle, outer margin lined with robust setae and fine setules, apical margin with one long seta; outer ramus outer margin with one robust seta, apical margin with one long seta. Uropod 3 vestigial, rounded. Telson dorsally produced, with two long and two short setae.

Female (paratype, 2.8 mm). Similar in all aspects to the male with the exception of the following: Antenna 1 flagellum tri-articulate. Lower lip outer lobes rounded, setose; mandibular lobes acutely pointed. Gnathopod 2 basis stout, without rounded process, posterodistal margin with one seta; merus rounded posteriorly, with distal robust seta and several slender setae; carpus subtriangular; propodus enlarged, rounded, palmar margin smooth, moderately setose, with two large setae; dactylus inner margin with short setae. Pereopods 5 and 6 anterior and posterior margins of most articles with plumose setae; propodus posterodistal margin with notch.

Etymology. After the Latin *offucia*, meaning paint or wash for face and referring to dark pigment on the head of this species.

Distribution. Panama: Bocas del Toro (present study).

Ecology and remarks. These amphipods occur among coral rubble, occurring with other *Podocerus* species at depths of 1–3 m. *Podocerus offucia* sp. nov. is most similar to *Podocerus lazowaemi* Baldinger & Gable, 1994 in sharing the following characters: male antenna 1 flagellum 4-articulate, accessory flagellum uni-articulate; gnathopod 1 basis slender; and uropods 1–2 each with distoventral interramal spine. The new species differs in the following characters: antenna 2 flagellum 4-articulate (vs 5-articulate), coxae 1 with four setae (vs 1 robust seta), coxa 2 bare (vs 1 robust seta), pereopods 3–7 propodus with posterodistal notch (vs lacking). *Podocerus offucia* sp. nov. is also similar to *Podocerus kleidus* Thomas & Barnard, 1992 in the presence of interramal spines on uropod 1 and 2 but differs in the following characters: antenna 1 flagellum 3 or 4-articulate (vs 6-articulate), coxa 1 entire (vs cleft), and four robust setae on telson (vs 9 robust setae). *Podocerus offucia* sp. nov. can be easily distinguished from all remaining described *Podocerus* species based on having dorsal setae only on pereon segments 5–7, the shape of male gnathopod 2 propodus, and having uropods 1 and 2 each with distoventral interramal spine. Ethanol-preserved specimens of the new species retained purple-brown coloration on the head with faint coloration on the pereon.

***Podocerus fissipes* Serejo, 1995**

Figs 29, 33C

Podocerus fissipes Serejo, 1995[1996]: 49–55, figs 1–3; Baldinger and Gable 2002: 11–19, figs 6–12; LeCroy 2011: 702, fig. 560.

Material examined. PANAMA • 3–5.1 mm • 2 ♂, 5 ♀; Bocas del Toro, Hospital Bight, 9.3044°N, 82.1316°W, depth 1.5 m, among coral rubble; 7 Aug 2005; S. LeCroy leg.; GCRL 6672 • 3 ♂, 8 ♀, 2 juveniles; Bocas del Toro, Hospital Point, 9.3333°N, 82.2185°W, depth 11 m, from buoy scrapings; 26 June 2023; K.N. White leg.; USNM 1743975 • 9 ♂, 7 ♀, 1 juvenile; Bocas del Toro, Crawl Caye, 9.2475°N, 82.1290°W, depth 0–1 m, from buoy scrapings; 28 June 2023; K.N. White leg.; USNM 1743976.

Diagnosis. Maxilla 2 inner and outer plates each with two rows of apical setae. Gnathopod 2 merus without robust setae; propodus with two robust setae at palmar angle. Uropods 1 and 2 without interramal spines. Telson apex truncate with two long and two short setae.

Distribution. Brazil: Prainha in Arraial do Cabo, Rio de Janeiro; Santo Aleixo Island, Serinhaém, Pernambuco (Serejo 1995); British Virgin Islands: Guana (Baldinger and Gable 2002); U.S.A.: Biscayne Bay, Florida (LeCroy 2011); Bocas del Toro (present study).

Ecology and remarks. Panamanian specimens agree with previous descriptions of *Podocerus fissipes* with the following exceptions: variation in dorsal carinae; gnathopod 2 with two robust setae (vs one robust seta in Serejo 1995 and LeCroy 2011). Baldinger and Gable (2002), however, also describe two robust setae on the gnathopod 2 propodus. The variation may be due to the size difference (Panama = 4.6 mm, B.V.I. = 3.0 mm, Brazil = 2.3 mm) or due to regional variation. Live specimens have orange coloration lining pereonites and are covered with orange speckles.

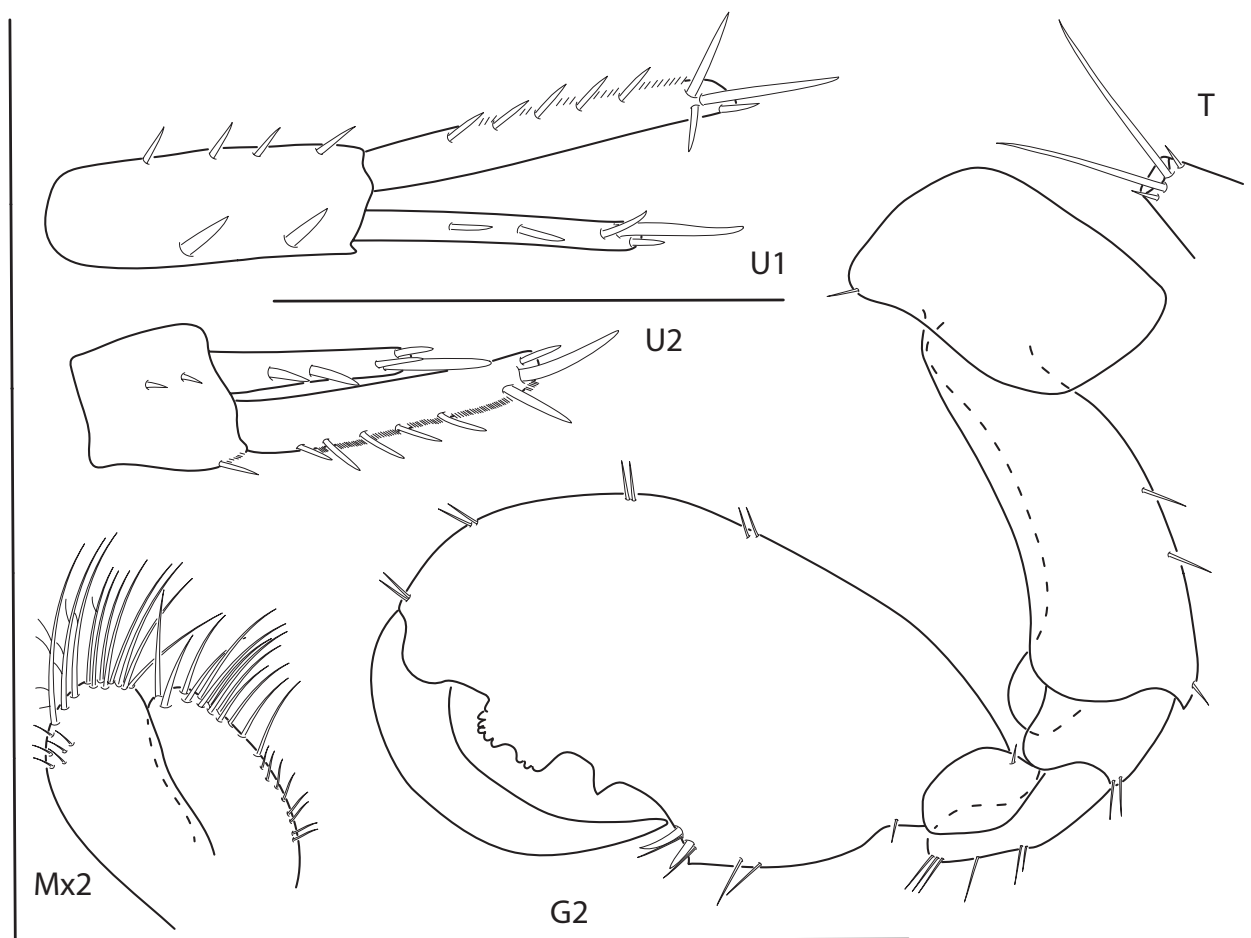


Figure 29. *Podocerus fissipes*, male, 4.6 mm, uropod 1, uropod 2, maxilla 2, gnathopod 2 lateral, telson apex. Scale bars: 0.5 mm.

***Podocerus jareckii* Baldinger & Gable, 2002**

Figs 30, 33D

Podocerus jareckii Baldinger & Gable, 2002: 3–11, figs 1–5.

Material examined. PANAMA • 2.4 mm • 1 ♂, 1 ♀; Bocas del Toro, Swan Cay, 9.4536°N, 82.3000°W, among coral rubble; 27 June 2023; K.N. White leg; USNM 1743977.

Diagnosis. Maxilla 2 inner and outer plates each with one row of apical setae. Gnathopod 2 propodus with proximal robust seta, dactylus bent at angle. Uropod 1 interramal spine present. Uropod 2 interramal spine absent.

Distribution. British Virgin Islands: Guana Island (Baldinger and Gable 2002); Panama: Bocas del Toro (present study).

Ecology and remarks. This species occurs among coral rubble at a depth of 2.3–2.4 m. Panamanian specimens closely resemble the original description with the following exceptions: male dorsal robust setae starting on pereonite 5–7 (vs pereonite 2–7); gnathopod 2 merus with two robust setae (vs 1); telson with four apical setae (vs 5). Live specimens are orange, purple-red, and white in color.

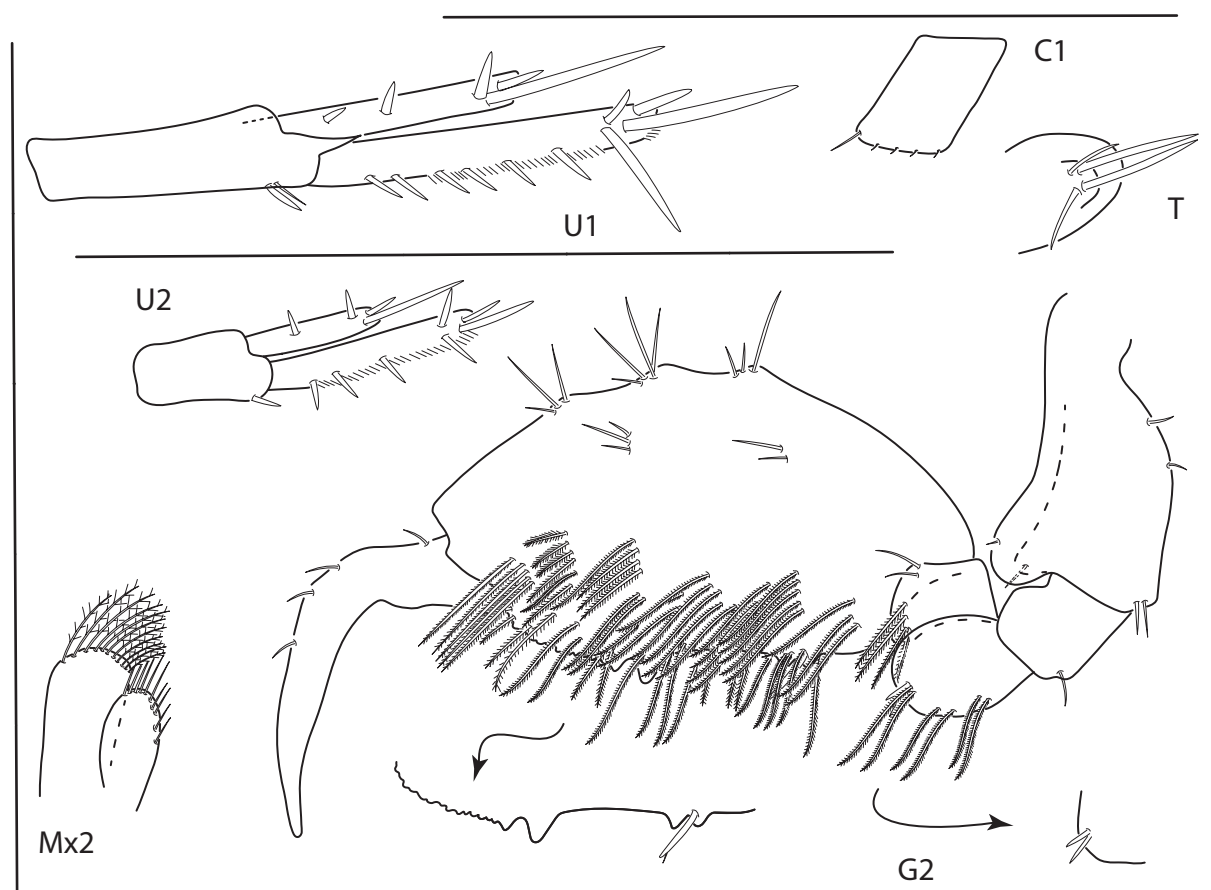


Figure 30. *Podocerus jareckii*, male, 2.4 mm, uropod 1, uropod 2, maxilla 2, coxa 1, telson, gnathopod 2 medial. Scale bars: 0.5 mm.

Identification Key to the Caribbean Caprellidira of Panama

- 1 Head anteroventral margin entire, rounded; pereonite 1 fused to head; body skeletal, segments tubular; gills not exceeding 3 pairs; oostegites not exceeding 2 pairs; abdomen vestigial (Fig. 1).....**2**
- Head anteroventral margin recessed, excavate; head free from pereonite 1; body compressed or flattened; gills exceeding 3 pairs; oostegites exceeding 2 pairs; abdomen well developed (Figs 26, 27).....**4**
- 2 Body without dorsal projections; male pereonite 2 with sharp projection on anteroventral margin; male gnathopod 2 basis posterior margin with proximal bump (Fig. 3).....***Paracaprella pusilla***
- Body with dorsal projections; male pereonite 2 without projection on anteroventral margin; male gnathopod 2 basis posterior margin smooth (Fig. 1) ... **3**
- 3 Pereopods 3 and 4 are bi-articulate (Fig. 2)***Deutella cf. pseudoincerta***
- Pereopods 3 and 4 are uni-articulate (Fig. 1)***Deutella caribensis***
- 4 Antenna 2 distinctly longer than antenna 1, antenna 1 not reaching past antenna 2 peduncle (Fig. 26); urosome segment 1 longer than deep, distinctly longer than segment 2 (Fig. 26).....**5**
- Antenna 2 slightly longer than antenna 1, antenna 1 usually reaching past antenna 2 peduncle (Fig. 5); urosome segment 1 at least as deep as long, not distinctly longer than segment 2 (Fig. 9).....**7**

- 5 Maxilla 2 inner and outer plates each with one row of apical setae (Fig. 28); gnathopod 2 merus with robust setae; uropod 1 interrampal spine present (Fig. 27) **6**
- Maxilla 2 inner and outer plates each with two rows of apical setae; gnathopod 2 merus without robust setae; uropod 1 interrampal spine absent (Fig. 29) ***Podocerus fissipes***
- 6 Male gnathopod 2 propodus posterior margin straight; dactylus bent at angle; uropod 2 without interrampal spine (Fig. 30) ***Podocerus jareckii***
- Male gnathopod 2 propodus posterior margin concave; dactylus evenly curved (Fig. 26); uropod 2 with interrampal spine (Fig. 27) ***Podocerus offucia* sp. nov.**
- 7 Gnathopod 1 subequal or larger than gnathopod 2, carpus longer than or subequal to propodus (Fig. 9) **8**
- Gnathopod 1 smaller than gnathopod 2, carpus shorter than or subequal to propodus (Fig. 8) **9**
- 8 Male coxa 1 subquadrate, not significantly larger than coxa 2; male gnathopod 1 chelate, carpus and propodus fused, dactylus with elongate tooth along posteroproximal margin; male pereopod 5 basis length 1.4 × width; telson apex convex (Fig. 12) ***Varohios topianus***
- Male coxa 1 subovate, significantly larger than coxa 2; male gnathopod 1 carpocheate, 7-articulate, dactylus lacking elongate tooth along posteroproximal margin; male pereopod 5 basis length 2.6 × width; telson apex concave (Figs 9, 10) ***Konatopus tridens* sp. nov.**
- 9 Coxae not overlapping (Fig. 8); pereopods 3 and 4 distinctly expanded (Figs 4, 8); uropod 3 uniramous (Fig. 8) or lacking rami (Fig. 4) **10**
- Coxae overlapping; pereopods 3 and 4 bases slightly or not expanded; uropod 3 biramous (one ramus may be much smaller than other) (Fig. 21) **14**
- 10 Gnathopod 1 simple; gnathopod 2 propodus palm lined with stout setae; uropod 2 absent; uropod 3 lacking rami (Fig. 4) ***Caribboecetes intermedius***
- Gnathopod 1 subchelate; gnathopod 2 propodus palm not lined with stout setae; uropod 2 present; uropod 3 uniramous or biramous (Fig. 8) **11**
- 11 Uropod 1 inner ramus subequal in length with outer ramus; pereopod 5 not geniculate; uropod 2 biramous; telson entire (Fig. 8) ***Ericthonius brasiliensis***
- Uropod 1 inner ramus shorter than outer ramus; pereopod 5 geniculate (Fig. 5); uropod 2 uniramous (Fig. 7); telson cleft (Figs 5, 7) **12**
- 12 Female pereopod 3 basis at right angle posteriorly; telson partially cleft (Fig. 7) ***Cerapus thomasi***
- Female pereopod 3 basis not at right angle posteriorly; telson entirely cleft (Fig. 5) **13**
- 13 Antennae 1 and 2 with > 3 flagellar segments; uropod 1 inner ramus with apical robust seta, distal margin of seta narrowing unevenly (Fig. 5) ***Cerapus benthophilus***
- Antennae 1 and 2 with 3 flagellar segments; uropod 1 inner ramus with apical robust seta, distal margin of seta narrowing evenly (Fig. 6) ***Cerapus slayeri***
- 14 Male antenna 2 flagellum dorsoventrally flattened; female gnathopod 1 merus and carpus with ventral setae, all setae plumose; female gnathopod

- 2 propodus anterior margin with dense rows of setae; male uropod 3 rami subequal in length (Fig. 13) ***Audulla chelifera***
- Male antenna 2 flagellum not dorsoventrally flattened; female gnathopod 1 merus and carpus with or without ventral setae, if present none or few setae plumose; female gnathopod 2 propodus anterior margin without dense rows of setae; male uropod 3 rami unequal in length (Fig. 6) **15**
- 15 Antenna 1, accessory flagellum vestigial or absent; uropod 3, inner ramus minute (Fig. 21) **16**
- Antenna 1, accessory flagellum present, composed of > 1 article; uropod 3, inner ramus not minute (Fig. 6) **17**
- 16 Eye touching margin of ocular lobe; pereopod 5 basis length $1.5 \times$ width; uropods 1 and 2 outer ramus without marginal robust setae (Fig. 21) ***Photis probolion* sp. nov.**
- Eye not touching margin of ocular lobe; pereopod 5 basis length $< 1.5 \times$ width (Fig. 18); uropods 1 and 2 outer ramus with marginal robust setae (Fig. 19) **18**
- 17 Coxa 1 anteroventral margin slightly produced with gap in marginal setae (Fig. 18); pereopods 6 and 7 propodus each with posterodistal cluster of setae surpassing length of dactylus (Fig. 19) ***Photis bulla* sp. nov.**
- Coxa 1 anteroventral margin not produced without gap in marginal setae; pereopods 6 and 7 propodus posterodistal cluster of setae, if present, no longer than length of dactylus (Fig. 24) **19**
- 18 Ocular lobe distal margin subacute; pereopod 3 merus posterior margin with several long, plumose setae; male pereopod 6 normal (based on literature); uropod 1 rami unequal in length; uropod 3 peduncle with plumose distoventral seta (Fig. 24) ***Photis melanica***
- Ocular lobe distal margin rounded; pereopod 3 merus posterior margin without plumose setae; male pereopod 6 greatly enlarged; uropod 1 rami subequal in length; uropod 3 peduncle without plumose distoventral seta (Fig. 11) ***Photis butalus* sp. nov.**
- 19 Head cephalic lobe subacute; coxa 2 length $1.5 \times$ width (Fig. 25) ***Posophotis seri***
- Head cephalic lobe rounded; coxa 2 length subequal to width (Fig. 14) ***Latigammaropsis atlantica***

Discussion

This study describes five new species and includes a range extension for 15 caprellidiran amphipods to include the Caribbean waters of Panama. Five species have a distribution pattern including the Pacific and Caribbean (*Audulla chelifera*, *Erichthonius brasiliensis*, *Latigammaropsis atlantica*, *Paracaprella pusilla*, *Posophotis seri*). These distribution patterns indicate that these five species were likely established before the isthmus of Panama closed, more than three million years ago. Examination of specimens has clarified that several characters vary and should not be used for species determination. Body spination should not be used as a diagnostic character among species of *Deutella* based on McCain (1968), Guerra-García et al. (2006), and Winfield and Guerra-García (2021). The number of antennae segments is also

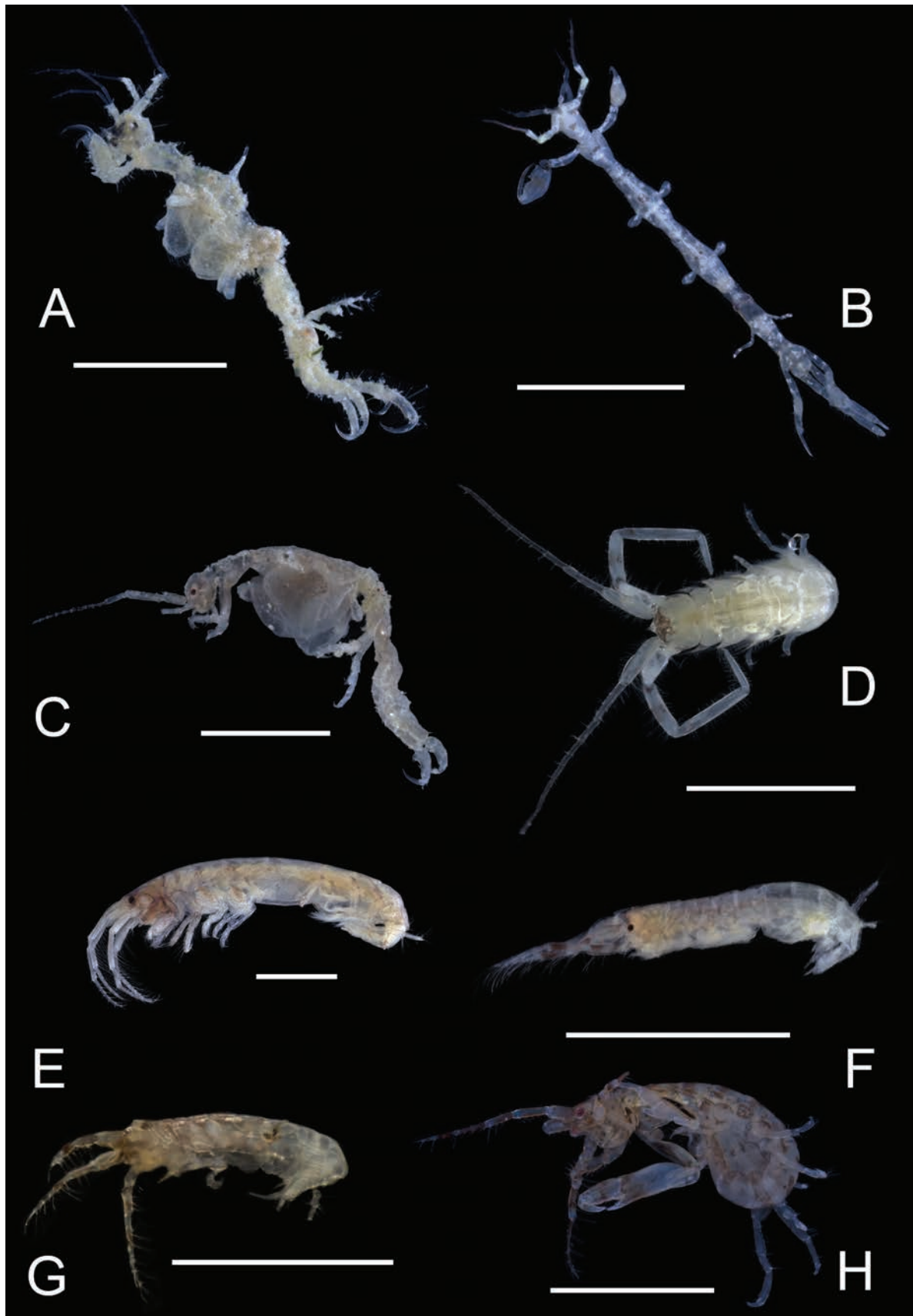


Figure 31. Photographs of live specimens unless noted. **A** *Deutella caribensis* **B** *Deutella* cf. *pseudoincerta* **C** *Paracaprella pusilla* **D** *Caribboecetes intermedius* **E** *Cerapus benthophilus* (ethanol-preserved specimen) **F** *Cerapus slayeri* (ethanol-preserved specimen) **G** *Cerapus thomasi* (ethanol-preserved specimen) **H** *Ericthonius brasiliensis*. Scale bars: 1.0 mm.

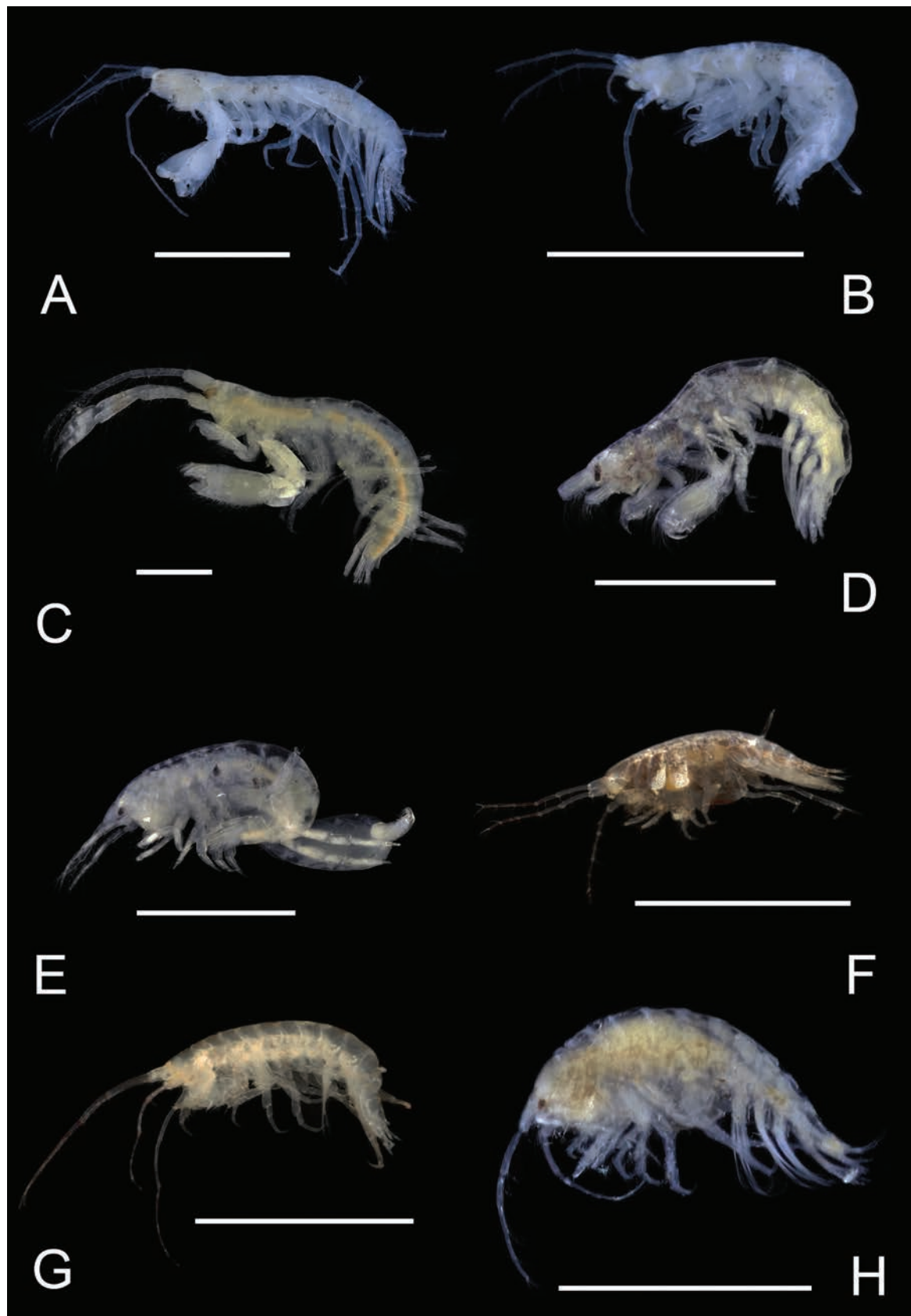


Figure 32. Photographs of live specimens unless noted. **A** *Konatopus tridens* sp. nov. **B** *Variohos topianus* **C** *Audulla chelifera* (ethanol-preserved specimen) **D** *Latigammaropsis atlantica* (ethanol-preserved specimen) **E** *Photis butalus* sp. nov. (ethanol-preserved specimen) **F** *Photis bulla* sp. nov. **G** *Photis probolion* sp. nov. **H** *Photis melanica* (ethanol-preserved specimen). Scale bars: 1.0 mm.



Figure 33. Photographs of live specimens unless noted. **A** *Posophotis seri* (ethanol-preserved specimen) **B** *Podocerus offucia* sp. nov. (ethanol-preserved specimen) **C** *Podocerus fissipes* **D** *Podocerus jareckii*. Scale bars: 1.0 mm.

variable based on comparison of Panama material to original descriptions in the literature for *Deutella* cf. *pseudoincerta*, *Cerapus benthophilus*, *Cerapus thomasi*, and *Latigammaropsis atlantica*. This study increases the known number of caprellidiran amphipods from Caribbean Panama from one to 21 species. The Caribbean Amphipoda of Panama identification key is available online (<https://www.invertebase.org/portal/ident/key.php?clid=58&pid=4&dynclid=0&taxon=All+Species>).

Acknowledgments

Logistical support and facilities were provided by Georgia College & State University Department of Biological and Environmental Sciences and the Smithsonian Tropical Research Institute (STRI). Special thanks to Carolina Cesar and Valentina Cardona for assistance with diving and collecting in Bocas del Toro. The authors also wish to thank Dr. Lauren Hughes and the Amphipod Taxonomy Course members for collecting assistance in 2023. Special thanks go to Sara LeCroy for her loan of specimens collected in 2005 and to Abby Dugger and Madison Oliver for assistance with imaging specimens.

Additional information

Conflict of interest

The authors have declared that no competing interests exist.

Ethical statement

No ethical statement was reported.

Funding

Funding for this study was provided by a National Science Foundation grant: Collaborative Research: ARTS: Understanding Tropical Invertebrate Diversity Through Integrative Revisionary Systematics and Training (1856421).

Author contributions

Conceptualization: KNW. Data curation: SJS, KNW. Formal analysis: SJS, KNW. Funding acquisition: KNW. Investigation: SJS, KNW. Methodology: KNW. Project administration: KNW. Supervision: KNW. Writing – original draft: KNW, SJS. Writing – review and editing: SJS, KNW.

Author ORCIDs

Sally J. Sir  <https://orcid.org/0000-0002-1270-1192>

Kristine N. White  <https://orcid.org/0000-0002-5203-1656>

Data availability

All of the data that support the findings of this study are available in the main text or Supplementary Information.

References

- Ariyama H, Hoshino O (2019) A new superfamily, family, genus and species of marine amphipod, *Protodulichia scandens*, from Japan (Crustacea: Amphipoda: Senticaudata: Corophiida). *Journal of Natural History* 53(39–40): 2467–2477. <https://doi.org/10.1080/00222933.2019.1704588>
- Baldinger AJ, Gable MF (1994) Two new species of *Podocerus* Leach (Crustacea: Amphipoda: Podoceridae) from Bermuda. *Proceedings of the Biological Society of Washington* 107(4): 707–720.
- Baldinger AJ, Gable MF (2002) The genus *Podocerus* (Crustacea: Amphipoda: Podoceridae) from Guana Island, British Virgin Islands. *Postilla* 226: 1–21. https://elischolar.library.yale.edu/cgi/viewcontent.cgi?article=1225&context=peabody_museum_natural_history_postilla
- Barnard KH (1957) Additions to the fauna-list of South African Crustacea. *The Annals and Magazine of Natural History*, series 12 109: 1–12. <https://doi.org/10.1080/00222935708655919>
- Barnard JL (1962) Benthic Marine Amphipoda of Southern California: Families Aoridae, Photidae, Ischyroceridae, Corophiidae, Podoceridae. *Pacific Naturalist* 3(1): 1–72.
- Barnard JL (1970) Sublittoral Gammaridea (Amphipoda) of the Hawaiian Islands. *Smithsonian Contributions to Zoology* (34): 1–286. <https://doi.org/10.5479/si.00810282.34>

- Barnard JL (1979) Littoral Gammaridean Amphipoda from the Gulf of California and the Galapagos Islands. *Smithsonian Contributions to Zoology* 271: 1–149. <https://doi.org/10.5479/si.00810282.271>
- Barnard JL, Karaman GS (1991) The families and genera of marine gammaridean Amphipoda (Except marine Gammaroidea). *Records of the Australian Museum Supplement* 13 (Part 2): 419–866. <https://doi.org/10.3853/j.0812-7387.13.1991.367>
- Bate CS, Westwood JO (1862) *A History of the British Sessile-eyed Crustacea* Vol. 1. John Van Voorst, London, 507 pp. <https://doi.org/10.5962/bhl.title.1936>
- Boeck A (1871) *Crustacea Amphipoda borealia et arctica*. *Forhandlinger i Videnskabs-Selskabet i Christiania* 1870: 83–280. <https://doi.org/10.5962/bhl.title.2056>
- Bousfield EL (1973) *Shallow-Water Gammaridean Amphipoda of New England*. Cornell University Press, Ithaca, N.Y., 312 pp. <https://archive.org/details/shallowwatergammm0000bous>
- Camp DK (1998) Checklist of shallow-water marine Malacostracan Crustacea of Florida. In: Camp K, Lyons WG, Perkins TH (Eds) *Checklists of Selected Shallow-water Marine Invertebrates of Florida*. Florida Marine Research Institute Technical Report TR-3, 123–189. <https://palmm.digital.flvc.org/islandora/object/uf%3A56604#page/124/mode/1up>
- Caribbean Amphipoda of Panama (2025) Occurrence dataset. <https://www.invertebase.org/portal/ident/key.php?clid=58&pid=4&dynclid=0&taxon=All+Species>
- Chevreaux E (1901) *Crustacés Amphipodes*. Mission scientifique de M. Ch. Alluaud aux Iles Séchelles (Mars, Avril, Mai 1892). *Mémoires de La Société Zoologique de France* 14: 388–438.
- Coleman CO (2003) “Digital inking”: How to make perfect line drawings on computers. *Organisms Diversity & Evolution* 3(14): 1–14. <https://doi.org/10.1078/1439-6092-00081>
- Dana JD (1849) Synopsis of the genera of Gammaracea. *American Journal of Science and Arts Series 2* 8: 135–140.
- Dana JD (1852) On the classification of the Crustacea Choristopoda or Tetradecapoda. *The American Journal of Science and Arts Second Series* 14(41): 297–316.
- Dana JD (1853) *Crustacea*. Part II. United States Exploring Expedition. During the years 1838, 1839, 1840, 1841, 1842 under the command of Charles Wilkes. U.S.N. 14: 689–1618.
- Díaz YJ, Guerra-García JM, Martínez A (2005) Caprellids (Crustacea: Amphipoda: Caprellidae) from shallow waters of the Caribbean coast of Venezuela. *Organisms Diversity and Evolution* 5(Electronic Supplement 10): 1–25. <https://doi.org/10.1016/j.ode.2004.11.010>
- Drumm DT (2018) Two new species of *Cerapus* (Crustacea: Amphipoda: Ischyroceridae) from the Northwest Atlantic and Gulf of Mexico. *Zootaxa* 4441(3): 495–510. <https://doi.org/10.11646/zootaxa.4441.3.4>
- Guerra-García JM, Thiel M (2001) La fauna de caprellidos (Crustacea: Amphipoda: Caprellidca) de la costa de Coquimbo, centro-norte de Chile, con una clave taxonomica para la identificacion de las especies. *Revista Chilena de Historia Natural* 74(4): 873–883. <https://doi.org/10.4067/S0716-078X2001000400014>
- Guerra-García JM, Krapp-Schickel T, Müller HG (2006) Caprellids from the Caribbean coast of Colombia, with description of three new species and a key for species identification. *Bulletin of Marine and Coastal Research* 35: 149–194. <https://doi.org/10.25268/bimc.invemar.2006.35.0.222>
- Hirayama A (1988) Taxonomic Studies on the Shallow Water Gammaridean Amphipoda of West Kyushu, Japan. VIII. Pleustidae, Podoceridae, Priscomilitaridae, Stenothoidae, Synopiidae, and Urothoidae. *Publications of the Seto Marine Biological Laboratory* 33(1–3): 39–77. <https://doi.org/10.5134/176149>

- Horton T, Lowry J, De Broyer C, Bellan-Santini D, Copilaş-Ciocianu D, Corbari, L, Costello MJ, Daneliya M, Dauvin JC, Fišer C, Gasca R, Grabowski M, Guerra-García JM, Hendrycks E, Hughes L, Jaume D, Jazdzewski K, Kim YH, King R, Krapp-Schickel T, LeCroy S, Lörz AN, Mamos T, Senna AR, Serejo C, Souza-Filho JF, Tandberg AH, Thomas JD, Thurston M, Vader W, Väinölä R, Valls Domedel G, Vonk R, White K, Zeidler W (2024) World Amphipoda Database. <https://doi.org/10.14284/368>
- Jung TW, Coleman CO, Yoon SM (2019) Taxonomic study on the photid amphipods (Senticaudata, Corophiida, Photoidea, Photidae) from Korean waters, with descriptions of a new genus and seven new species. *ZooKeys* 886: 1–59. <https://doi.org/10.3897/zookeys.886.38511>
- Just J (1983) Siphonoecetinae subfam.n. (Crustacea, Amphipoda, Corophiidae) 1: Classification. *Steenstrupia* 9(6): 117–135.
- Just J (1984) Siphonoecetinae (Crustacea, Amphipoda, Corophiidae) 2: *Caribboecetes* Just, 1983, with description of six new species. *Steenstrupia* 10(2): 37–64. <https://doi.org/10.3853/j.0067-1975.37.1985.330>
- Krøyer HN (1842) Nye nordiske Slaegter og Arter af Amfipodernes Orden, henherrende til Familien Gammarina. *Naturhistorisk Tidsskrift* 4: 141–166.
- Kudrjaschov VA, Vassilenko SV (1966) A New Family Caprogammaridae (Amphipoda, Gammaridea) Found in the North-West Pacific. *Crustaceana* 10(2): 192–198. <https://doi.org/10.1163/156854066X00711>
- Kunkel BW (1910) The Amphipoda of Bermuda. *Transactions of the Connecticut Academy of Arts and Sciences* 16: 1–116.
- Lazo-Wasem EA, Gable MF (1987) A review of recently discovered type specimens of Bermuda Amphipoda (Crustacea: Peracarida) described by B. W. Kunkel (1882–1969). *Proceedings of the Biological Society of Washington* 100(2): 321–336. <https://www.biodiversitylibrary.org/page/34570725>
- Leach, WE (1814) Crustaceology. In: Brewster D (Ed.) *The Edinburgh Encyclopedia*. Balfour, Edinburgh 7(2): 385–437, 765–766. <https://www.biodiversitylibrary.org/page/37187640>
- LeCroy SE (2000) An Illustrated Identification Guide to The Nearshore Marine and Estuarine Gammaridean Amphipoda of Florida Volume 1: Families Gammaridae, Hadziidae, Isaeidae, Melitidae, and Oedicerotidae. Florida Department of Environmental Protection Annual Report Contract No. WM724 1: 1–195.
- LeCroy SE (2007) An Illustrated Identification Guide to The Nearshore Marine and Estuarine Gammaridean Amphipoda of Florida Volume 4: Families Anamixidae, Eusiridae, Hyalellidae, Hyalidae, Iphimediidae, Ischyroceridae, Lysianassidae, Megaluropidae, and Melphidippidae. Florida Department of Environmental Protection Annual Report Contract No. WM880 4: 503–614.
- LeCroy SE (2011) An Illustrated Identification Guide to The Nearshore Marine and Estuarine Gammaridean Amphipoda of Florida Volume 5: Families Leucothoidae, Liljeboriidae, Neomegamphopidae, Ochlesidae, Phliantidae, Phoxocephalidae, Platyschnopidae, Pleustidae, Podoceridae, Pontoporeiidae, Sebidae, Stenothoidae, Synopiidae, and Talitridae. Florida Department of Environmental Protection Annual Report Contract No. WM949 5: 615–816.
- LeCroy SE, Gasca R, Winfield I, Ortiz M, Escobar-Briones E (2009) Amphipoda (Crustacea) of the Gulf of Mexico. In: Felder DL, Camp DK (Eds) *Gulf of Mexico: Origin, Waters, and Biota*. Texas A&M University Press, Texas, 941–972. <https://www.scopus.com/record/display.uri?eid=2-s2.0-84894972887&origin=inward&txGid=e29d13fc15a0acc24d283fbc3588f6f4>

- Ledoyer M (1979) Les Gammariens de la pente externe du Grand Récif de Tuléar (Madagascar) (Crustacea Amphipoda). *Memorie del Museo Civico di Storia Naturale, Verona*, (ser 2) 2: 1–149.
- Ledoyer M (1982) Crustacés Amphipodes Gammariens. Familles des Acanthonotozomatidae à Gammaridae. *Faune de Madagascar* 59(1): 1–598.
- Ledoyer M (1986) Faune mobile des herbiers de phanérogames marines (Halodule et Thalassia) de la Laguna de Términos (Mexique, Campêche). I. Les Caridea (Crustacea Decapoda) et aperçu sur la faune globale. *Anales del Instituto de Ciencias del Mar y Limnología. Universidad Nacional Autónoma de México* 13(3): 147–170.
- Lowry J K, Myers AA (2009) Benthic Amphipoda (Crustacea: Peracarida) of the Great Barrier Reef. *Zootaxa* 2260: 1–16. <https://doi.org/10.11646/zootaxa.2260.1.2>
- Lowry JK, Myers AA (2013) A Phylogeny and Classification of the Senticaudata subord. nov. (Crustacea: Amphipoda). *Zootaxa* 3610(1): 1–80. <https://doi.org/10.11646/zootaxa.3610.1.1>
- Lowry JK, Thomas JD (1991) A new species of *Cerapus* from Cudjoe Channel, Lower Florida Keys, USA, with notes on male behaviour (Crustacea: Amphipoda: Corophioidea). *Journal of Natural History* 25(6): 1461–1467. <https://doi.org/10.1080/00222939100770931>
- Martín A, Díaz YJ (2003) La fauna de anfípodos (Crustacea: Amphipoda) de las aguas costeras de la region oriental de Venezuela. *Boletín Instituto Espanol de Oceanografía* 19(1–4): 327–344.
- Martín A, Díaz Y, Miloslavich P, Escobar-Briones E, Guerra-García JM, Ortiz M, Valencia B, Giraldo A, Klein E (2013) Regional diversity of Amphipoda in the Caribbean Sea. *Revisita de Biología Tropical* 61(4): 1681–1720. <https://doi.org/10.15517/rbt.v61i4.12816>
- Mayer P (1890) Die Caprelliden des Golfes von Neapel und der angrenzenden meeres-abschnitte. Nachtrag zur Monographie derselben. *Fauna und Flora des Golfes von Neapel und der angrenzenden Meeres-Abschnitte* 17: 1–157. <https://doi.org/10.5962/bhl.title.7084>
- Mayer P (1903) Die Caprellidae der Siboga-Expedition. *Siboga-Expeditie. Uitkomsten op zoologisch, botanisch, oceanographisch en geologisch gebied verzameld in Nederlandsch Oost-Indie 1899–1900 aan boord H.M. Siboga* 34: 1–160. <https://doi.org/10.5962/bhl.title.53742>
- McCain JC (1967) *Paracaprella barnardi*, A New Species of Caprellid (Crustacea; Amphipoda) from the West Coast of Panama. *Proceedings of the Biological Society of Washington* 80: 219–222.
- McCain JC (1968) The Caprellidae (Crustacea: Amphipoda) of the western North Atlantic. *Bulletin of the National Science Museum* 278: 1–47. <https://doi.org/10.5962/bhl.part.8960>
- McKinney LD (1977) The origin and distribution of shallow water gammaridean Amphipoda in the Gulf of Mexico and Caribbean Sea with notes on their ecology. PhD Thesis, Texas A&M University, College Station, Texas, U.S.A.
- McKinney LD (1980) The Genus *Photis* (Crustacea: Amphipoda) from the Texas Coast with the description of a new species, *Photis melanicus*. *Contributions in Marine Science* 23: 57–61.
- Milne Edwards H (1830) Extrait de recherches pour servir à l'histoire naturelle des crustacés amphipodes. *Annales des Sciences Naturelles* 20: 353–399. <https://doi.org/10.5962/bhl.part.12300>
- Miloslavich P, Díaz JM, Klein E, Alvarado JJ, Díaz C, Gobin J, Escobar-Briones E, Cruz-Motta JJ, Weil E, Cortés J, Bastidas AC, Robertson R, Zapata F, Martín A, Castillo J, Ka-

- zandjian A, Ortiz M (2010) Marine Biodiversity in the Caribbean: Regional Estimates and Distribution Patterns. PLOS ONE 5(8): e11916. <https://doi.org/10.1371/journal.pone.0011916>
- Myers AA (1981) Amphipod Crustacea. I. Family Aoridae. Memoirs of the Hourglass Cruises 5(5): 1–75.
- Myers AA (1982) Family Corophiidae. In: Ruffo S (Ed.) The Amphipoda of the Mediterranean. Mémoires de l'Institut Océanographique, Monaco 13: 185–208.
- Myers AA (1985) Shallow-water, coral reef and mangrove Amphipoda (Gammaridea) of Fiji. Records of the Australian Museum Supplement 5: 1–143. <https://doi.org/10.3853/j.0812-7387.5.1985.99>
- Myers AA (2002) Marine amphipods of the families Aoridae and Neomegamphopidae from Phuket, Thailand. Phuket Marine Biological Center Special Publication 23(1): 213–228.
- Myers AA (2009) Photidae. In: Lowry JK, Myers AA (Eds) Benthic Amphipoda (Crustacea: Peracarida) of the Great Barrier Reef, Australia. Zootaxa 2260: 771–799. <https://doi.org/10.11646/zootaxa.2260.1.43>
- Myers AA, Lowry JK (2003) A phylogeny and a new classification of the Corophiidea Leach, 1814 (Amphipoda). Journal of Crustacean Biology 23: 443–485. <https://doi.org/10.1163/20021975-99990353>
- Myers AA, McGrath D (1984) A revision of the North-east Atlantic species of *Ericthonius* (Crustacea: Amphipoda). Journal of the Marine Biological Association of the United Kingdom 64(2): 379–400. <https://doi.org/10.1017/S002531540003006X>
- Myers AA, Lowry JK, Billingham Z (2016) A new family, genus and species of freshwater amphipod *Australomicroprotopus megacoxa* gen. nov. sp. nov. (Senticaudata, Corophiidea, Microprotopoidea, Australomicroprotopidae fam. nov.) from Australia. Zootaxa 4161(3): 412–418. <https://doi.org/10.11646/zootaxa.4161.3.8>
- Nelson WG (1995) Amphipod crustaceans of the Indian River Lagoon: current status and threats to biodiversity. Bulletin of Marine Science 57(1): 143–152.
- Ortiz M, Lemaitre R (1994) Crustaceos Anfipodos (Gammaridea) Colectados en Las Costas del Caribe Colombiano, al sur de Cartagena. Anales del Instituto de Investigaciones Marinas de Punta de Betin 23: 119–127. <https://doi.org/10.25268/bimc.invenmar.1994.23.0.391>
- Ortiz M, Lemaitre R (1997) Seven new amphipods (Crustacea: Peracarida: Gammaridea) from the Caribbean coast of South America. Boletín de Investigaciones Marinas y Costeras 26: 71–104. <https://doi.org/10.25268/bimc.invenmar.1997.26.0.365>
- Rafinesque CS (1815) Analyse de la nature ou Tableau de l'univers et des corps organisés. Palermo: 1–224. <https://doi.org/10.5962/bhl.title.106607>
- Reid DM (1951) Report on the Amphipoda (Gammaridea and Caprellidea) of the coast of tropical West Africa Atlantide Report. Scientific results of the Danish expedition to the coasts of tropical West Africa 1945–1946(2): 189–291.
- Ros M, Guerra-García JM (2012) On the occurrence of the tropical caprellid *Paracaprella pusilla* Mayer, 1890 (Crustacea: Amphipoda) in Europe. Mediterranean Marine Science 13(1): 134–139. <https://doi.org/10.12681/mms.30>
- Ros M, Vázquez-Luis M, Guerra-García JM (2013) The tropical caprellid amphipod *Paracaprella pusilla*: a new alien crustacean in the Mediterranean Sea. Helgoland Marine Research 67: 675–685. <https://doi.org/10.1007/s10152-013-0353-4>
- Say T (1817) An account of the Crustacea of the United States (continued). Journal of the Academy of Natural Sciences at Philadelphia 1(1): 155–169.

- Serejo CS (1995) *Podocerus fissipes* n. sp., a new species of sponge-dwelling amphipod (Amphipoda, Podoceridae) from the Brazilian Coast. *Nauplius Revista de Sociedade Brasileira de Carcinologia* 3: 49–57.
- Shoemaker CR (1942) Amphipod crustaceans collected on the Presidential Cruise of 1938. *Smithsonian Miscellaneous Collections* 101(11): 1–52.
- Stebbing TRR (1888) Report on the Amphipoda collected by H.M.S. Challenger during the years 1873–1876. *Zoology* 29: 1–1737.
- Stebbing TRR (1899) Revision of Amphipoda. *Annals and Magazine of Natural History Series* 7(4): 205–211. <https://doi.org/10.1080/00222939908678185>
- Stebbing TRR (1906) Das Tierreich. Eine Zusammenstellung und Kennzeichnung der rezenten Tierformen. Amphipoda. *Königlichen Preussische Akademie des Wissenschaften zu Berlin* 21: 1–806.
- Steinberg JE, Dougherty EC (1957) The skeleton shrimps (Crustacea, Caprellidae) of the Gulf of Mexico. *Tulane Studies in Zoology and Botany* 5(11): 267–288.
- Thomas JD (1976) A survey of gammarid amphipods of the Barataria Bay, Louisiana region. *Contributions in Marine Science* 20: 87–100.
- Thomas JD (1993) Identification manual for marine Amphipoda (Gammaridea): I. Common coral reef and rocky bottom amphipods of South Florida. Florida Department of Environmental Protection Final Report Contract No. SP290: 1–83.
- Thomas JD, Barnard JL (1987) The Indo-Pacific *Audulla chelifera* reported from the Caribbean Sea (Crustacea: Amphipoda). *Proceedings of the Biological Society of Washington* 100(2): 364–370. <https://archive.org/details/biostor-74915>
- Thomas JD, Barnard JL (1991) *Photis trapherus*, a new elephantine species from the Caribbean Sea (Crustacea: Amphipoda). *Proceedings of the Biological Society of Washington* 104(1): 96–100. https://www.academia.edu/90046996/Photis_trapherus_a_new_elephantine_species_from_the_Caribbean_Sea_Crustacea_Amphipoda
- Thomas JD, Barnard JL (1992) *Podocerus kleidus*, a new species from the Florida Keys (Crustacea, Amphipoda, Dulichiidae). *Bulletin of Marine Science* 51(3): 309–314.
- Thomas JD, Heard RW (1979) A new species of *Cerapus* Say, 1817 (Crustacea: Amphipoda) from the northern Gulf of Mexico with notes on its ecology. *Proceedings of the Biological Society of Washington* 92(1): 98–105.
- Wakabara Y, Tararam AS, Valrio-Berardo MT, Duleba W, Leite FPP (1991) Gammaridean and Caprellidean fauna from Brazil. *Hydrobiologia* 223: 69–77. <https://doi.org/10.1007/BF00047629>
- Walker AO (1904) Report on the Amphipoda collected by Professor Herdman, at Ceylon, in 1902. Report to the Government of Ceylon on the Pearl Oyster Fisheries of the Gulf of Manaar, with supplementary reports upon the marine biology of Ceylon. Part II. The Royal Society, London, 229–300.
- Walker AO (1905) Marine crustaceans. XVI. Amphipoda. *Fauna and Geography of the Maldive and Laccadive Archipelagoes* 2 Supplement 1: 923–932.
- Winfield AI, Guerra-García JM (2021) A new species of *Deutella* (Amphipoda: Caprellidae) from the Gulf of Mexico. *Revista Mexicana de Biodiversidad* 92: e923403. <https://doi.org/10.22201/ib.20078706e.2021.92.3403>
- Winfield I, Ortiz M, Franco J, Bedia C (1997) Distribución y diversidad del superorden Paracarida asociado a pastos marinos de Alvarado, Veracruz. *Cuadernos Mexicanos de Zoología* 3(1): 1–8.
- Winfield I, Escobar-Briones E, Álvarez F (2001) Crustáceos peracáridos asociados a praderas de *Ruppia maritima* (Ruppiaceae) en la laguna de Alvarado,

México. Anales del Instituto de Biología, Universidad Nacional Autónoma de México 72: 29–41. <https://anales.ib.unam.mx/index.php?journal=SerZool&page=article&op=view&path%5B%5D=2628>

Winfield I, Escobar-Briones E, Morrone JJ (2006) Updated checklist and identification of areas of endemism of benthic amphipods (Caprellidea and Gammaridea) from offshore habitats on the SW Gulf of Mexico. *Scientia Marina* 70(1): 99–108. <https://doi.org/10.3989/scimar.2006.70n199>

Supplementary material 1

Locality table Panama Caprellidira


Authors: Sally J. Sir, Kristine N. White

Data type: xlsx

Copyright notice: This dataset is made available under the Open Database License (<http://opendatacommons.org/licenses/odbl/1.0/>). The Open Database License (ODbL) is a license agreement intended to allow users to freely share, modify, and use this Dataset while maintaining this same freedom for others, provided that the original source and author(s) are credited.

Link: <https://doi.org/10.3897/zookeys.1234.145826.suppl1>

Advances in the taxonomy and distribution of *Scolomus* (Hymenoptera, Ichneumonidae), including the description of a new Andean species and an updated identification key

Rodrigo O. Araujo¹, Isamara Silva-Santos², Andrés Moreira-Muñoz³, Cristian Montalva⁴,
Diego G. Pádua¹

1 Laboratorio de Entomología General y Aplicada, Centro de Investigación de Estudios Avanzados del Maule, Universidad Católica del Maule, Avenida San Miguel, 3605, Talca, Chile

2 Programa de Pós-Graduação em Entomologia, Instituto Nacional de Pesquisas da Amazônia, Manaus, Amazonas, Brazil

3 Instituto de Geografía, Pontificia Universidad Católica de Valparaíso, Avenida Brasil, 2241, Valparaíso 2340025, Chile

4 Laboratorio de Salud de Bosques, Instituto de Conservación, Biodiversidad y Territorio, Facultad de Ciencias Forestales y Recursos Naturales, Universidad Austral de Chile, Valdivia, Chile

Corresponding author: Diego G. Pádua (paduadg@gmail.com)



Academic editor:

Francisco Javier Peris Felipo

Received: 27 December 2024

Accepted: 19 March 2025

Published: 10 April 2025

ZooBank: <https://zoobank.org/5FDE2F7B-CA29-4E54-847D-A0CD6A5CA396>

Citation: Araujo RO, Silva-Santos I, Moreira-Muñoz A, Montalva C, Pádua DG (2025) Advances in the taxonomy and distribution of *Scolomus* (Hymenoptera, Ichneumonidae), including the description of a new Andean species and an updated identification key. ZooKeys 1234: 207–219. <https://doi.org/10.3897/zookeys.1234.145472>

Copyright: © Rodrigo O. Araujo et al.
This is an open access article distributed under terms of the Creative Commons Attribution License (Attribution 4.0 International – CC BY 4.0).

Abstract

Scolomus Townes & Townes, 1950 is a genus in Ichneumonidae, with six species occurring in the Holarctic and Neotropical regions. In this study, a new species is described from Chile, *Scolomus valenzuelai* Araujo, Pádua & Silva-Santos, **sp. nov.** Also, the female of *S. magellanicus* Walkley, 1962 is described for the first time and new occurrences of *S. maculatus* Araujo & Vivallo, 2018, and *S. magellanicus* are reported from Chile, including the northernmost record of this genus in South America. Additionally, we provide an updated identification key for all known species of the genus.

Key words: Andean Region, Chile, Darwin wasps, Maulean Coastal Forest, parasitoid wasps, South America

Introduction

Metopiinae Förster, 1869 is widely distributed and comprises 26 genera and more than 860 species (Yu et al. 2016; Ranjith and Priyadarsanan 2022). Members of this subfamily are koinobiont endoparasitoids that oviposit in lepidopteran larvae and emerge from the host pupa as adults (Broad and Shaw 2005; Bennett 2008). They can be distinguished by their strongly convex face, broad pronotum, relatively thick antennae, and shortened tarsal segments, which are adaptations believed to facilitate movement through semi-resistant substrates, such as partially silken host retreats or rolled-up leaves (Broad and Shaw 2005).

Scolomus Townes & Townes, 1950, is a small, widely distributed genus within Metopiinae, comprising six species: *S. borealis* (Townes, 1971), *S. clypeatus* Araujo & Santos, 2018, *S. maculatus* Araujo & Vivallo, 2018, *S. magellanicus* Walkley, 1962, *S. talamanca* (Gauld & Sithole, 2002), and *S. viridis* Townes & Townes, 1950. Little is known about the biology of this genus, except for a record of

S. borealis as a parasitoid of the immature stages of *Schreckensteinia festaliella* (Hübner, 1819) (Lepidoptera, Schreckensteiniidae) (Broad and Shaw 2005).

The genus was initially described in Tryphoninae (Townes and Townes 1949) but was later transferred to Pionini (Ctenopelmatinae) without justification (Townes and Townes 1966). Subsequently, Gauld and Wahl (2006) synonymized *Apolophus* Townes, 1917 under *Scolomus* based on morphological similarities. *Apolophus* and *Scolomus* exhibit several shared apomorphic features, including an elongated head with an extended malar space, a flat face with a weak supraclypeal suture, and a hind wing with a strongly curved basal abscissa of vein M+Cu1, where the distal abscissa of vein Cu1 joins vein cu-a closer to vein 1A than to vein M. Based on these characteristics, *Scolomus* was placed in Metopiinae, although its definitive position requires a detailed phylogenetic analysis of the Ophioniformes clade (sensu Wahl 1991, 1993) (Broad and Shaw 2005; Bennett et al. 2019).

In this study, we describe a new species of *Scolomus* from Chile and provide the first taxonomic description of the female of *S. magellanicus*. Additionally, we expand the knowledge about distribution range of both *S. magellanicus* and *S. maculatus*. As the new species rendered the initial steps of the identification key proposed by Araujo et al. (2018) unfeasible, we provide an adapted identification key for all known species of the genus.

Materials and methods

The specimens were studied from the following institutions (curators in parentheses): **LEGA-UCM**: Laboratorio de Entomología General y Aplicada, Universidad Católica del Maule, Chile (Rodrigo Araujo); **MNNC**: Museo Nacional de Historia Natural, Chile (Mario Elgueta); **NMNH**: National Museum of Natural History, USA (Sean Brady); **UACH**: Colección de Insectos Ernesto Krahmer, Universidad Austral de Chile, Chile (Cristian Montalva).

The holotype of *Scolomus maculatus* (MNNC) was examined, while the following holotypes were studied through high-resolution photographs: *S. magellanicus* (NMNH), *S. viridis* (NMNH), and *S. clypeatus* (lost). Regarding the last species, the holotype was destroyed in the fire that consumed the Museu Nacional do Rio de Janeiro, Brazil, and we relied on the photographs provided by Araujo et al. (2018), which we consider sufficiently detailed for study. The holotype of *S. valenzuelai* Araujo, Pádua & Silva-Santos, sp. nov. is deposited in the MNNC.

The type specimen of the new species was recently collected within remnants of the coastal Maulino forest (Escobedo et al. 2024), an endemic vegetation formation dominated by deciduous species such as *Nothofagus glauca* (Phil.) Krasser (Nothofagaceae). This forest type is highly threatened due to the historical replacement of native vegetation with *Pinus radiata* (D. Don) and *Eucalyptus globulus* Labill plantations. The most hygrophilous remnants are characterized by the presence of Myrtaceae species, like *Luma apiculata* (DC.) Burret and *Myrceugenia exsucca* (DC.) O. Berg., alongside iconic Chilean trees such as *Drimys winteri* J.R. Forst. & G. Forst. and *Persea lingue* Nees. The understory is rich in native ferns and shrubs, notably *Blechnum chilense* (Kaulf.) Mett. (Doll et al. 2024).

General morphological terminology follows Broad et al. (2018) and proportions follow Araujo et al. (2018). The topics “type material” and “examined ma-

terial” include the details provided on the label. The use of an asterisk (*) indicates a new distribution record.

Images were captured with a Leica S9i stereomicroscope with an LED illumination dome (Kawada and Buffington 2016). Measurements and image stacking were done using the Leica Application Suite X extended-focus software, followed by editing in Adobe Photoshop 2020. All measurements were rounded to the nearest 0.05 mm.

Distribution data for *Scolomus* spp. were extracted directly from specimen labels and plotted on a map using SimpleMappr (Shorthouse 2010).

Results

Taxonomy

Scolomus Townes & Townes, 1950

Scolomus Townes and Townes 1950: 420. Type species: *Scolomus viridis* Townes & Townes, 1950, by original designation.

Apolophus Townes 1971: 111. Type species: *Apolophus borealis* Townes, 1971, by original designation.

Diagnosis. The head is elongate, with an exceptionally long malar space measuring 1.20–1.80× the basal mandibular width. The clypeus is large, subquadrate, and with the clypeal sulcus weakly impressed or absent, which results in the face and clypeus forming a nearly uniform, smooth plane in most species. The occipital carina is ventrally incomplete. The mandible is slender, with the lower tooth 0.50–1.00× the length of the upper tooth. The fore wing features a rhomboid to pentagonal areolet (areolet lightly petiolate in *S. valenzuelai* sp. nov.), and the pterostigma is broad and triangular, with a maximum length 2.30–3.00× its maximum width. In the hind wing, the basal abscissa of vein M+Cu1 is strongly arched, and the distal abscissa of vein Cu1 connects to vein cu-a much closer to vein 1A than to vein M. The first metasomal tergite exhibits an anterior median depression bordered laterally by raised edges. The glymma is deep, converging at the midline, and often separated only by a translucent partition. In females, the hypopygium is large and arched but not folded medioventrally. The ovipositor is slender, slightly upcurved, and lacks a dorsal subapical notch.

Distribution. The genus is distributed in the Holarctic region (Austria, England, Germany, Poland, Russia, Ukraine, and the United States of America) and Neotropical region (Argentina, Chile, and Costa Rica), which includes the Andean biogeographic zone (sensu Morrone 2015).

Included species. *S. borealis* (Townes, 1971) (Nearctic, West Palearctic); *S. clypeatus* Araujo & Santos, 2018 (Andean); *S. maculatus* Araujo & Vivallo, 2018 (Andean); *S. magellanicus* Walkley, 1962 (Andean); *S. talamanca* (Gauld & Sithole, 2002) (Neotropical); *S. viridis* Townes & Townes, 1950 (Andean).

Key to the world species of *Scolomus*

- 1 Mandible stout, 3.00–4.00× as long as basal width. Labrum apex always visible, even with mandibles closed. Subtegular ridge produced as a sharp,

- curved spine (Figs 1–4). Deep groove between the propodeum and metanotum **2**
- Mandible slender, 5.50–6.50× as long as basal width; labrum more or less concealed when mandibles closed (Araujo et al. 2018: figs 1, 3, 5). Subtegular ridge not produced into a sharp spine. Superficial groove between the propodeum and metanotum **4**
- 2(1) Wings with a lightly petiolate areolet, rhombic, with vein 2rs-m joining 3rs-m shortly before touching RS (Fig. 3). Postscutellum rounded posteriorly (Fig. 2). Lateromedian longitudinal carina slightly sinuous, lateromedian longitudinal carinae almost parallel. Area basalis trapezoidal (Fig. 2). Wings strongly and entirely infusate, pterostigma and all veins dark brown (Fig. 3) ***Scolomus valenzuelai* Araujo, Pádua & Silva-Santos, sp. nov.**
- Wings with a pentagonal areolet, with vein 2rs-m complete and 3rs-m partially complete or faintly impressed, both touching RS independently (Fig. 6). Postscutellum straight posteriorly (Fig. 5). Lateromedian longitudinal carina oblique until the intersection with anterior transverse carina, converging or not. Area basalis triangular (Fig. 5). Wings hyaline to lightly infusate, pterostigma and all veins brown (Fig. 6) **3**
- 3(2) Propodeum with lateromedian longitudinal carina defined until the intersection with anterior transverse carina and faintly impressed posteriorly. Area superomedia absent (Fig. 5). Lateral longitudinal carina sharper and more distinct near propodeal spiracle. Vein 3rs-m partially complete (faintly impressed only when touching vein M) ***S. magellanicus* Walkley, 1962**
- Propodeum with posterior transverse carina strong and complete. Area superomedia present (although open posteriorly). Lateral longitudinal carina uniform throughout its entire length. Vein 3rs-m faintly impressed ***S. viridis* Townes & Townes, 1950**
- 4(1) Propodeum with no trace of lateromedian longitudinal carina. Head and mesoscutum with reddish-brown marks, fore leg orange-brown. Central America ***S. talamanca* (Gauld & Sithole, 2002)**
- Propodeum with lateromedian longitudinal carina discernible. Head and mesoscutum without reddish-brown marks, fore legs brown or green **5**
- 5(4) Propodeum with lateral longitudinal carina incomplete. Clypeus with simple, uniformly distributed setae in female. Body mostly blackish, without extensive green areas; Holarctic ***S. borealis* (Townes, 1971)**
- Propodeum with lateral longitudinal carina complete. Clypeus with clusters of seemingly bifurcate setae in female. Body with extensive green areas. Chile **6**
- 6(5) Clypeus width 3.00× its height (Araujo et al. 2018: fig. 1). Distance between eye and lateral ocellus 1.50× diameter of lateral ocellus. Areolet 0.80× as wide as long. Hypopygium 1.55× as long as wide, in lateral view. Ovipositor 12.50× as long as basal width. Head, mesoscutum, postscutellum, and pronotum entirely brownish yellow ***S. clypeatus* Araujo & Santos, 2018**
- Clypeus width 1.55–2.30× its height (Araujo et al. 2018: figs 3, 5). Distance between eye and lateral ocellus 0.90–1.00× diameter of lateral ocellus. Areolet 1.00× as wide as long; hypopygium 1.90× as long as wide, in lateral view. Ovipositor 5.30× as long as basal width. Head and pronotum greenish, mesoscutum yellow with dark brown spots on lateral lobes and around scutellum ***S. maculatus* Araujo & Vivallo, 2018**

***Scolomus valenzuelai* Araujo, Pádua & Silva-Santos, sp. nov.**

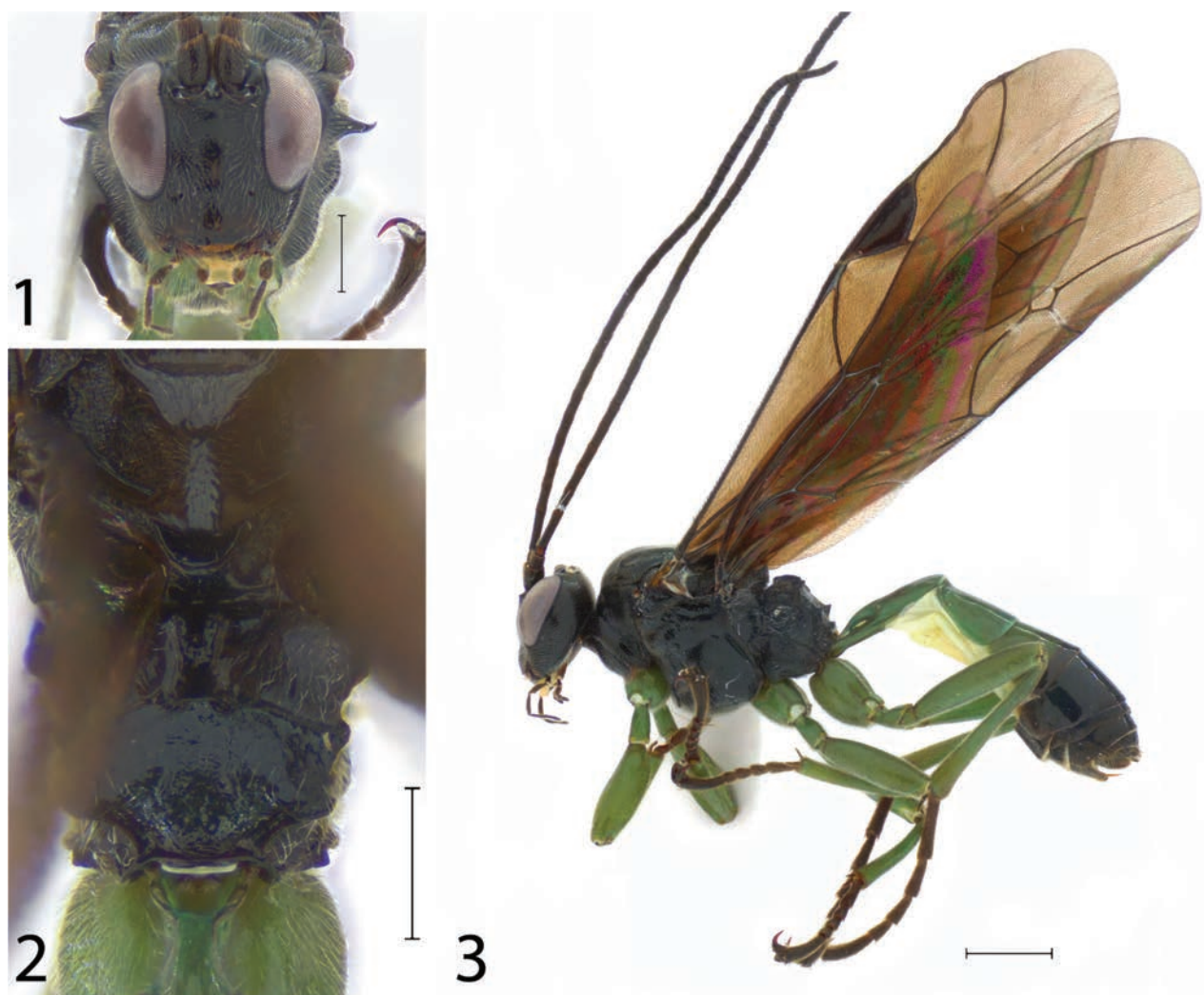
<https://zoobank.org/E88548D2-D19F-4C81-9DD9-37471ACF849B>

Figs 1–3

Type material. Holotype. CHILE • 1♀; Región del Maule, Cauquenes, El Secreto de Pilén; 35°59'1"S, 72°28'21"W; 1, 370 m alt.; 09 Sep–09 Oct 2024; Malaise trap; R.O. Araujo, D.G. Pádua & B. Cortés-Rivas leg.; (MNNC).

Type locality. Chile: Región del Maule, Cauquenes, El Secreto de Pilén; 35°59'1"S, 72°28'21"W; 1, 370 m alt.

Diagnosis. *Scolomus valenzuelai* sp. nov. can be distinguished from the other species of the genus by the combination of the following characteristics: 1) clypeus lightly punctate with setae, flat in profile, weakly impressed; 2) postscutellum rounded posteriorly; 3) metapleuron strongly strigose near its ventral margin; 4) lateromedian longitudinal carina elevated, strong until the intersection with the anterior transverse carina, and faintly impressed posteriorly, lateromedian longitudinal carina parallel; 5) area basalis present, well delimited, trapezoidal and smooth; 6) lateral longitudinal carina slightly curved in apical third; 7) fore wing with a lightly petiolate areolet,



Figures 1–3. *Scolomus valenzuelai* Araujo, Pádua & Silva-Santos, sp. nov., holotype female. **1** Head in frontal view **2** propodeum in dorsal view **3** habitus in lateral view. Scale bars: 0.50 mm (**1**, **2**); 1.00 mm (**3**).

rhomboidal; 8) wings strongly and entirely infusate, and pterostigma and all veins dark brown.

Description. Holotype female (Figs 1–3). Body length (without ovipositor): 7.85 mm; antenna length: 6.70 mm; fore wing length: 6.75 mm.

Head. Head polished, with sparse short pubescence. Face narrowly elongate, densely punctate, with setae laterally and dorsally but sparse centrally. Maximum face width about 1.20× as high (measured from base of antennae to base of clypeus) as wide. Anterior tentorial pits visible. Clypeus lightly punctate with setae, flat in profile, weakly impressed, its apical margin truncated, sinuous, 1.40× as wide as high. Labrum slightly visible even with mandibles closed. Malar space 1.25× as long as basal mandibular width; mandible relatively stout, mandible basally and centrally punctate, with setae. Mandible bidentate, teeth smooth, upper tooth longer than lower tooth. Upper tooth 3.35× as long as basally wide. Frons without distinct punctures. Inner orbits almost parallel, very slightly indented opposite antennal socket. Stemmaticum slightly convex. Posterior ocellus separated from eye about 0.95× its maximum diameter. Distance between posterior ocelli 1.15× the maximum diameter of posterior ocellus. Vertex shiny, without punctures. Temple shiny with setiferous punctures; temples almost parallel behind eye. Antenna with 36 flagellomeres; first flagellomere 3.85× as long as apically wide.

Mesosoma. Mesosoma polished, with very short whitish setae, longer on propodeum. Pronotum with very small punctures with setae, smoother laterally. Mesoscutum slightly convex dorsally, strongly carinate, especially posteriorly; notaulus faintly impressed anteriorly. Mesoscutum polished, with very small, dense, and evenly distributed punctures. Scuto-scutellar groove very deep. Scutellum convex in profile, with strong anterolateral carinae. Postscutellum rounded posteriorly. Scutellum and postscutellum polished, elevated, with very small and dense punctures. Subtegular ridge produced into a sharp, curved spine. Mesopleuron polished, with small, dense punctures with setae on dorsal half anterior to speculum and on ventral half; speculum polished and entirely smooth. Epicnemial carina complete, strong, elevated, reaching anteroventral margin of mesopleuron. Sternaulus indistinct. Posterior transverse carina of mesosternum complete, medially strongly excised. Posterior margin of mesosternum expanded and upcurved, producing into a small lobe. Metapleuron polished, with many small punctures, strongly strigose and convex near its ventral margin, about 1.15× as long as height. Submetapleural carina complete, strong, produced anteriorly and posteriorly into a small lobe. Propodeal spiracle circular, almost connected to laterolongitudinal carina. Propodeum shiny, in dorsal view about 1.10× as medially wide as long. Anterior transverse carina complete, medially lightly excised. Laterolongitudinal carina complete, strong, explanate above spiracles, elevated at intersection with anterior transverse carina and with posterior transverse carinae, forming apophyses just after the last-mentioned intersection. Posterior transverse carinae absent medially, between apophyses; lateromedian longitudinal carina elevated, strong until the intersection with the anterior transverse carina, and faintly impressed posteriorly; lateromedian longitudinal carinae parallel. Area basalis present, well delimited, trapezoidal, and smooth. Area externa shiny and smooth. Lateral longitudinal carina slightly curved in apical third. Coxae shiny, punctate with setae well distributed throughout. Hind femur about 5.35× as long as its maximum height and about 0.90× as long as hind tibia. Tarsal claws large, longer than arolium.

Fore wing with large pterostigma and a lightly petiolate areolet, rhomboidal. Vein 1 cu -a inclivous, lightly postfurcal relative to M&RS. Distal abscissa of Rs very slightly sinuate. Abscissa of CU present and touching wing posterior margin. CU strongly inclivous, cu-a reclivous.

Metasoma. Metasoma polished, with very short and relatively sparse setae. Tergite I about 1.20× as long as posteriorly wide. Spiracle near its center, smooth, with isolated setiferous punctures. Dorsolateral carina of tergite I absent. Postpetiole 4.35× as long as maximum width. Glymma deep, seemingly with thin membrane between both sides. Tergal-sternal suture of first metasomal segment complete and strong. Tergite II 2.00× as long as its height (lateral view). Thyridium not discernible. Tergites III–VII similarly sculptured. Hypopygium large and triangular in lateral view, 2.85× as long as wide. Ovipositor short, needle-shaped, 5.00× as long as basal width.

Color. Predominantly black and turquoise-green. Head black; antenna, basal half of mandible, and palpi brownish black. Mesosoma entirely black. Tegula black; legs with all coxae, trochanters, femurs, and tibia turquoise-green; all trochantelli brownish black. Wings strongly and entirely infusate; pterostigma and all veins dark brown. Metasoma turquoise green, with posterior margin of tergites III, T-shaped mark extending from the apical margin to the center of tergite III; tergites VI onwards black. Ovipositor sheath black, ovipositor yellowish red. Body covered by silvery pubescence.

Male. Unknown.

Etymology. *Scolomus valenzuelai* is named in honor of Pablo Valenzuela, a distinguished Chilean biochemist whose pioneering contributions to biotechnology and molecular biology have been profound in both scientific research and public health. Dr Valenzuela's crucial role in the development of the hepatitis B vaccine, the identification of the hepatitis C virus, and Chile's genomic research advancement has significantly shaped the country's biomedical innovation. His work fosters a legacy of scientific excellence and technological progress. By dedicating this species to him, we recognize science's debt to his invaluable contributions and his enduring influence on future generations' research. The species epithet, *valenzuelai*, is to be treated as a noun in genitive case.

Distribution. Known only from the type locality (Fig. 7).

Biology. Unknown.

Comments. *Scolomus valenzuelai* sp. nov. is most similar to the South American *S. magellanicus* and *S. viridis* by the stout mandible; the subtegular ridge produced into a sharp, curved spine; a deep groove between the propodeum and metanotum; and predominantly green coloration. The new species can be differentiated from these species by (1) the lateromedian longitudinal carina, which is strong and elevated until the intersection with the anterior transverse carina, then becoming faintly impressed posteriorly; the parallel lateromedian longitudinal carina (vs. lateromedian longitudinal carina converging posteriorly, generating a reduced, triangular area basalis in *S. magellanicus*; and lateromedian longitudinal carina strongly impressed posteriorly in *S. viridis*); (2) fore wing with a lightly petiolate areolet, rhomboidal (vs. a pentagonal areolet, with vein 2 rs -m complete and 3 rs -m partially complete and both independently touching RS); (3) the strongly and entirely infusate wings, with the pterostigma and all veins dark brown (vs. wings with pterostigma and all veins brown, hyaline to lightly infusate in *S. magellanicus* and lightly infusate in *S. viridis*); (4) the posteriorly rounded postscutellum (vs.

posteriorly straight in *S. magellanicus* and *S. viridis*). Additionally, *S. valenzuelai* sp. nov. differs from *S. magellanicus* by having the lateral longitudinal carina slightly curved in its apical third (vs. straight in its apical third); the hypopygium large, 2.85× as long as wide (vs. hypopygium 1.70× as long as wide); and differs from *S. viridis* due the absence of the superomedia area (vs. present, although open posteriorly).

***Scolomus magellanicus* Walkley, 1962**

Figs 4–6

Examined material. CHILE • **Holotype:** ♀; Magallanes, El Ganso; 14 Feb 1952; Maria Etcheverry C. leg.; NMNH 001 (digital images examined) • 1 ♀; Magallanes, El Canelo; 8 Mar 1969; L. Peña leg.; MNNC • 1 ♀; Magallanes, Punta Arenas; 15 Mar 1969; L. Peña leg.; MNNC • 1 ♀; Nuble Prov., Refugio Las Cabras, Cord. Chillan; 1500 m alt.; L.E. Peña leg.; MNNC • 1 ♀; Chiloé Prov., Dalcahue; 1–30 Jan 2022; G. Barriga leg.; Malaise trap; LEGA-UCM 001.

Diagnosis. *Scolomus magellanicus* can be distinguished from the other species of the genus by the combination of the following characteristics: 1) clypeus lightly punctate with setae, uniformly distributed, moderately impressed and convex in profile; 2) postscutellum straight posteriorly; 3) metapleuron moderately strigose near its ventral margin; 4) lateromedian longitudinal carina posteriorly converging, generating a reduced and triangular area basalis, and faintly impressed posteriorly to the anterior transverse carina; 5) lateral longitudinal carina straight in apical third; 6) fore wing with a pentagonal areolet, with vein 2rs-m complete and 3rs-m partially complete (faintly touching vein M), and both touching RS independently; 7) wings hyaline or lightly infusate, pterostigma and all veins brown.

Description. Female (Figs 4–6). Approximate body length (without ovipositor): 7.80 mm; antenna length: 7.00 mm; fore wing length: 7.60 mm.

Head. Head polished, with sparse, short pubescence. Face narrowly elongate, densely punctate, with small, uniformly distributed setiferous punctures. Maximum width of face about 1.40× width (measured from base of antennae to base of clypeus). Anterior tentorial pits visible. Clypeus lightly punctate, evenly covered with setae, moderately impressed, convex in profile, its apical margin truncate and sinuous, 1.20× as wide as high. Labrum slightly visible with mandibles closed. Malar space 1.45× as long as basal mandibular width. Mandible relatively stout, basally and centrally punctate with setae. Mandible bidentate, with teeth smooth; upper tooth 3.00× as long as its width at base, and slightly longer than lower tooth. Frons without distinct punctures. Inner orbits almost parallel, very slightly indented opposite antennal socket. Stemmaticum slightly convex. Posterior ocellus separated from eye about 0.95× its maximum diameter. Distance between posterior ocelli 1.15× maximum diameter of posterior ocellus. Vertex shiny, without punctures. Temple shiny with setiferous punctures; temples almost parallel behind eye. Antenna with 37 flagellomeres, first flagellomere 3.80× as long as width at apex.

Mesosoma. Mesosoma polished, with very short setae, longer in propodeum. Pronotum with very small, setiferous punctures but laterally smoother. Mesoscutum slightly convex dorsally, strongly carinate, especially posteriorly; notaulus faintly impressed anteriorly; mesoscutum polished, with very small, dense, evenly distributed punctures. Scuto-scutellar groove very deep. Scutellum convex in profile, with strong anterolateral carinae. Postscutellum straight posteriorly. Scute-



Figures 4–6. *Scolomus magellanicus* Walkley, 1962, female. 4 Head in frontal view 5 propodeum in dorsal view 6 habitus in lateral view. Scale bars: 0.50 mm (4, 5); 1.00 mm (6).

Illum and postscutellum polished, elevated, with very small, dense punctures. Subtegular ridge produced into a sharp, curved spine. Mesopleuron polished, with small, dense punctures with setae on dorsal half anterior to speculum and on ventral half. Speculum polished and entirely smooth. Epicnemial carina complete, strong, elevated, reaching anteroventral margin of mesopleuron. Sternaulus indistinct. Posterior transverse carina of mesosternum complete and medially, strongly excised. Posterior margin of mesosternum expanded and upcurved, produced into a small lobe. Metapleuron polished, moderately strigose and convex near its ventral margin, about 1.30× as long as height; metapleuron with many small punctures with long setae. Submetapleural carina complete, strong, produced anteriorly and posteriorly into a small lobe. Propodeal spiracle circular, almost connected to laterolongitudinal carina. Propodeum shiny, in dorsal view about 1.20× as medially wide as long. Anterior transverse carina complete, medially lightly excised. Laterolongitudinal carina complete, strong, explanate above spiracles, elevated at intersection with anterior transverse carina and with posterior transverse carina, forming apophyses just after this intersection. Posterior transverse carina absent medially, between apophyses. Lateromedian longitudinal carina elevated until the intersection with the anterior transverse carina and faintly impressed posteriorly. Lateromedian longitudinal carina converging posteriorly, generating a reduced and triangular shaped area basalis. Area externa shiny and smooth. Lateral longitudinal carina straight in apical third. Coxae shiny, punctate with well-distributed setae throughout. Hind femur about 5.50× as long as its maximum height and about 0.75× as long as hind tibia. Tarsal claws large, longer than arolium. Fore wing with large pterostigma and a pentagonal areolet,

with vein 2rs-m complete and 3rs-m partially complete (faintly touching vein M), both touching RS independently. Vein 1cu-a inclivous, lightly postfurcal relative to M&RS. Distal abscissa of Rs very slightly sinuate. Abscissa of CU present and touching wing posterior margin. CU strongly inclivous; cu-a reclivous.

Metasoma. Metasoma polished, with very short and relatively sparse setae. Tergite I about 1.80× as long as posteriorly wide. Spiracle near its center, smooth, with isolated setiferous punctures. Dorsoleateral carina of tergite I absent. Postpetiole 3.60× as long as maximum width. Glymma deep, seemingly with thin membrane between both sides. Tergal-sternal suture of first metasomal segment complete and strong. Tergite II 2.90× as long as its height (lateral view). Thyridium not discernible. Tergites III–VII similarly sculptured. Hypopygium triangular in lateral view, 1.70× as long as wide. Ovipositor short, needle-shaped, 5.90× as long as basal width.

Color. Predominantly black and pale green. Head black; antenna, clypeus, basal half of mandible, and palpi dark brown. Mesosoma entirely black; tegula black; legs with all coxae, trochanters, femurs, and tibiae pale green; all trochantelli brown. Wings lightly infusate; pterostigma and all veins brown. Metasoma pale green, with tergites VI onwards black; Ovipositor sheath black; ovipositor yellowish red. Body covered by silvery pubescence.

Variation. Approximate body length (without ovipositor): 7.80–9.45 mm; fore wing length 7.60–9.50 mm. Antenna with 37–39 flagellomeres. Clypeus dark brown to reddish brown. Wings hyaline to lightly infusate.

Distribution. Chile: Región de Los Lagos: Chiloé (Dalcachue*); Región del Ñuble: Pinto (Refugio Las Cabras*); Región Magallanes y la Antártica Chilena: Magallanes (El Canelo*, El Ganso, and Punta Arenas*) (Fig. 7).

***Scolomus maculatus* Araujo & Vivallo, 2018**

Examined material. CHILE • **Holotype:** ♀; Región Los Ríos, Valdivia, Parque Oncol, Cordillera de la Costa, Bosque Siempreverde; 39°42'10"S, 73°18'31"W; 2, 493 m alt.; 06–20 Mar 2007; Cecilia Ruiz et al. leg.; Malaise trap; MNNC (digital images examined) • 1♀; Curicó, 20km E Potrero Grande • 1♂; Región Los Ríos, Valdivia, Parque Oncol, Cordillera de la Costa, Bosque Siempreverde; 39°42'0.48"S, 73°19'36.54"W; 1, 569 m alt.; 20 Mar–04 Apr 2007; Cecilia Ruiz et al. leg.; Malaise trap; UACH 002 • 1♂; Región Los Ríos, Valdivia, Reserva Privada Punta Curiñanco, Ecorregión Valdiviana, Bosque Siempreverde; 5602646N, 636889E; 06–20 Mar 2007; Cecilia Ruiz et al. leg.; Malaise trap (trampa A, curi–3(?)); UACH 003 • 2♀, 2♂; Región Los Ríos, Valdivia, Reserva Privada Punta Curiñanco, Ecorregión Valdiviana, Bosque Siempreverde; 5602646N, 636889E; 18 Apr–02 May 2007; Cecilia Ruiz et al. leg.; Malaise trap (trampa A, curi–3(?)); UACH 004 • 1♀; Región Los Ríos, Valdivia, Parque Oncol, Cordillera de la Costa, Bosque Siempreverde; 39°42'0.48"S, 73°19'36.54"W; 1, 569 m alt.; 01–20 Feb 2007; Cecilia Ruiz et al. leg.; Malaise trap; UACH 005 • 1♀, 1♂; Región Los Ríos, Valdivia, Parque Oncol, Cordillera de la Costa, Bosque Siempreverde; 39°42'0.48"S, 73°19'36.54"W; 1, 569 m alt.; 05–19 Jan 2007; Cecilia Ruiz et al. leg.; Malaise trap; UACH 006.

Diagnosis. See Araujo et. al. (2018).

Distribution. Chile: Región de Los Ríos, Valdivia, (Parque Oncol and Reserva Punta Curiñanco). Región del Maule: Talca (Altos de Vilches and Curicó*) (Fig. 7).

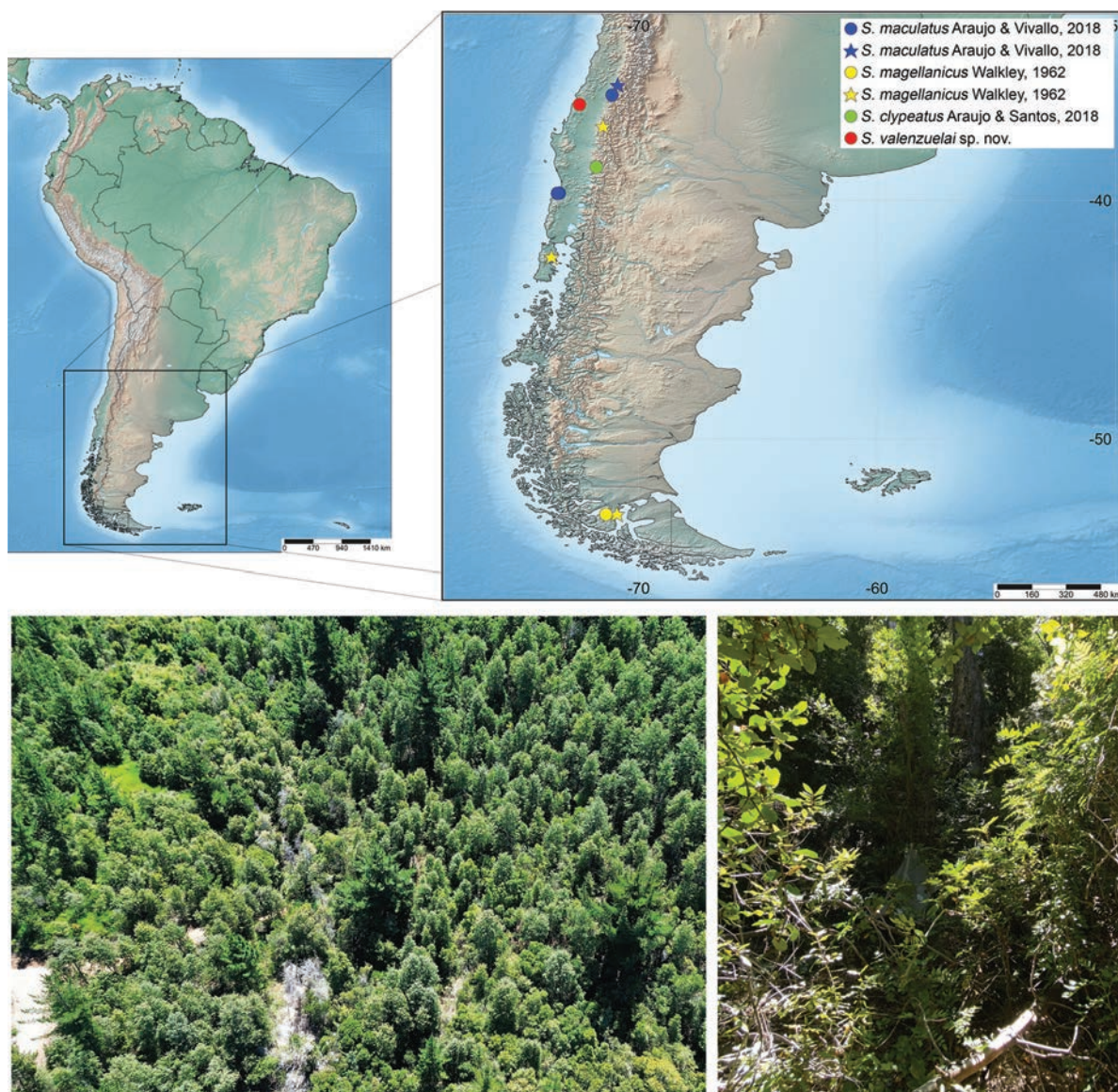


Figure 7. Distribution of *Scolomus* in Chile. Blue circle: previous distribution of *S. maculatus* Araujo & Vivallo, 2018; blue star: new distribution record of *S. maculatus*; yellow circle: previous distribution of *S. magellanicus* Walkley, 1962; yellow star: new distribution record of *S. magellanicus*; green circle: distribution of *S. clypeatus* Araujo & Vivallo, 2018; red circle: distribution of *S. valenzuelai* Araujo, Pádua & Silva-Santos, sp. nov. Images below showing the vegetation and the Malaise trap in the field.

Discussion

The known Argentine and Chilean *Scolomus* species have been described based on a single specimen or only a few specimens (e.g., Townes and Townes 1950; Walkley 1962; Araujo et al. 2018). In this study, approximately 25,000 Chilean Darwin wasp specimens were examined in the LEGA-UCM, MNNC, and UACH collections. Among these, only 15 specimens were identified as belonging to *Scolomus*: 10 specimens of *S. maculatus*, four *S. magellanicus*, and one specimen, which is described here as a new species. The scarcity of specimens underscores the rarity of this genus in entomological collections. This limited representation suggests that *Scolomus* may have a restricted distribution in the Andean biogeographic zone (sensu Morrone 2015), low population densities, or specific ecological requirements that hinder its collection and study.

Acknowledgements

We thank the staff at El Secreto de Pilén, Chile, for their logistical support during the expeditions.

Additional information

Conflict of interest

The authors have declared that no competing interests exist.

Ethical statement

No ethical statement was reported.

Funding

This study was financed by the Agencia Nacional de Investigación y Desarrollo (ANID), Chile, through the FONDECYT Regular no. 1221879 project. Additional support was provided in part by the Fundação de Amparo à Pesquisa do Estado do Amazonas (FAPEAM) – POSGRAD and by the Coordenação de Aperfeiçoamento de Pessoal de Nível Superior - Brasil (CAPES) - Finance Code 001.

Author contributions

ROA, ISS, and DGP conceptualized the research, gathered the data, described the parasitoid wasps, and prepared the initial draft. ROA also developed the taxonomic key. All authors contributed to reviewing and editing the manuscript and approved the final submitted version.


Author ORCIDs

Rodrigo O. Araujo  <https://orcid.org/0000-0002-9438-3238>

Isamara Silva-Santos  <https://orcid.org/0000-0001-8802-6720>

Andrés Moreira-Muñoz  <https://orcid.org/0000-0002-9136-1391>

Cristian Montalva  <https://orcid.org/0000-0002-8357-774X>

Diego G. Pádua  <https://orcid.org/0000-0001-5061-2978>

Data availability


All of the data that support the findings of this study are available in the main text.

References

- Araujo RO, Vivallo F, Santos BF (2018) Discovery of two new Andean species of *Scolomus* (Townes & Townes), with a key to all known species (Hymenoptera: Ichneumonidae: Metopiinae). *Zootaxa* 4429: 189–194. <https://doi.org/10.11646/zootaxa.4429.1.12>
- Bennett AMR (2008) Review and identification keys to the ichneumonid parasitoids (Hymenoptera: Ichneumonidae) of Nearctic *Choristoneura* species (Lepidoptera: Tortricidae). *The Canadian Entomologist* 140: 1–47. <https://doi.org/10.4039/n07-011>
- Bennett AMR, Cardinal S, Gauld ID, Wahl DB (2019) Phylogeny of the subfamilies of Ichneumonidae (Hymenoptera). *Journal of Hymenoptera Research* 71: 1–156. <https://doi.org/10.3897/jhr.71.32375>
- Broad GR, Shaw MR (2005) The species of four genera of Metopiinae (Hymenoptera: Ichneumonidae) in Britain, with new host records and descriptions

- of four new species. *Journal of Natural History* 39: 2389–2407. <https://doi.org/10.1080/00222930500102074>
- Broad GR, Shaw MR, Fitton MG (2018) Ichneumonid Wasps (Hymenoptera: Ichneumonidae): Their Classification and Biology. *RES Handbooks for the Identification of British Insects* 7(12). Field Studies Council, Shrewsbury, 418 pp. <https://doi.org/10.1079/9781800625471.0000>
- Doll U, Soto-Cerda L, Rebolledo J, Peña F, Valdés-Reyes C, Acuña C, Cabrera M (2024) Ravine forests of the Maule Coast: spatial and vegetational evaluation in a context of anthropic impacts. *Bosque* 45(1):125–138. <https://doi.org/10.4067/s0717-92002024000100125>
- Escobedo VM, Gómez P, Molina-Montenegro MA, Acuña-Rodríguez IS (2024) Post-fire negative relationship between a native tree and an invasive pine at the Coastal Maulino Forest in Central Chile. *Frontiers in Ecology and Evolution* 12: 1494548. <https://doi.org/10.3389/fevo.2024.1494548>
- Förster A (1869) Synopsis der Familien und Gattungen der Ichneumonen. *Verhandlungen des Naturhistorischen Vereins der Preussischen Rheinlande und Westfalens* 25(1868): 135–221.
- Gauld ID, Whal DB (2006) The relationship and taxonomic position of the genera *Apolophus* and *Scolomus* (Hymenoptera: Ichneumonidae). *Zootaxa* 1130: 35–41. <https://doi.org/10.11646/zootaxa.1130.1.2>
- Kawada R, Buffington ML (2016) A scalable and modular dome illumination system for scientific microphotography on a budget. *PLoS ONE* 11: e0153426. <https://doi.org/10.1371/journal.pone.0153426>
- Morrone JJ (2015) Biogeographical regionalization of the Andean region. *Zootaxa* 3936: 207–236. <https://doi.org/10.11646/zootaxa.3936.2.3>
- Ranjith A, Priyadarsanan DR (2022) A new Darwin wasp genus, *Soliga* (Hymenoptera: Ichneumonidae: Metopiinae), from India. *European Journal of Taxonomy* 852: 57–76. <https://doi.org/10.5852/ejt.2022.852.2009>
- Shorthouse DP (2010) SimpleMappr, an online tool to produce publication-quality point maps. <https://www.simplemappr.net> [Accessed on 2024-12-27]
- Townes HK (1971) The genera of Ichneumonidae, Part 4. *Memoirs of the American Entomological Institute* 17: 1–372.
- Townes HK, Townes M (1949) A revision of the genera and of the American species of Tryphoninae Part II. *Annals of the Entomological Society of America* 42: 397–447. <https://doi.org/10.1093/aesa/42.4.397>
- Townes HK, Townes M (1966) A catalogue and reclassification of the Neotropical Ichneumonidae. *Memoirs of the American Entomological Institute* 8: 1–367.
- Walkley LM (1962) A second species of Ichneumonidae belonging to *Scolomus* Townes (Hymenoptera). *Proceedings of the Entomological Society of Washington* 64: 231–233.
- Yu DS, van Achterberg C, Horstmann K (2016) Taxapad 2016. Ichneumonoidea 2015. Database on flash-drive. [Nepean, Ottawa, Canada] www.taxapad.com

Description of two new species of the genus *Pteromalus* Swederus (Hymenoptera, Pteromalidae, Pteromalinae) from Xinjiang, China

Qin Li^{1,2}, Ya-Lin Liu^{1,2}, Guo-Hua Yan^{1,2}, Tong-You Zhang^{1,2}, Hui Xiao³, Hong-ying Hu^{1,2}

¹ College of Life Science and Technology, Xinjiang University, 666 Shengli Road, Tianshan District, Urumqi, Xinjiang, 830046, China

² Xinjiang Key Laboratory of Biological Resources and Genetic Engineering, 666 Shengli Road, Tianshan District, Urumqi, Xinjiang, 830046, China

³ Key Laboratory of Zoological Systematics and Evolution, Institute of Zoology, Chinese Academy of Sciences, Beijing, 100101, China

Corresponding author: Hong-ying Hu (hooHY-69@163.com)

Abstract

Two new species of *Pteromalus* Swederus (Hymenoptera, Pteromalidae, Pteromalinae), *Pteromalus steppensis* Li & Hu, **sp. nov.** and *Pteromalus xiaomoheensis* Yan & Li, **sp. nov.**, are described and illustrated for the first time. *Pteromalus steppensis* Li & Hu, **sp. nov.** was reared as a primary, solitary ectoparasitoid of the larval and pupal stages of *Orchestes steppensis* Korotyaev, 2016 (Coleoptera, Curculionidae). Figures of its development and its host damage are also provided.

Key words: Key, morphological characters, new taxa, *Orchestes steppensis*



Academic editor: Zachary Lahey

Received: 27 December 2024

Accepted: 6 March 2025

Published: 11 April 2025

ZooBank: <https://zoobank.org/1557F207-4C10-48BE-88A6-D1FD7412963A>

Citation: Li Q, Liu Y-L, Yan G-H, Zhang T-Y, Xiao H, Hu H (2025) Description of two new species of the genus *Pteromalus* Swederus (Hymenoptera, Pteromalidae, Pteromalinae) from Xinjiang, China. ZooKeys 1234: 221–237. <https://doi.org/10.3897/zookeys.1234.145429>

Copyright: © Qin Li et al.
This is an open access article distributed under terms of the Creative Commons Attribution License (Attribution 4.0 International – CC BY 4.0).

Introduction

The genus *Pteromalus* Swederus, 1795 (type species *Ichneumon puparum* (Linnaeus, 1795)) belongs to the family Pteromalidae, subfamily Pteromalinae, and is distributed in the all the zoogeographical regions of the world (UCD 2024). This genus includes about 500 described species, with 375 in Europe alone (Gibson et al. 2024). It is the most speciose genus of the family Pteromalidae and has been taxonomically studied since the 19th century (Maletti et al. 2021). The genus can be recognized by the following combination of characters (Graham 1969; Bouček and Rasplus 1991; Bouček and Heydon 1997; Baur 2015): clypeus striate, its anterior margin truncate or weakly to strongly emarginate, always without a median tooth; flagellum with two anelli and six funicular segments; clava in females symmetrical; prepectus with relatively small upper triangular area; paraspiracular sulci rather deep and usually with some transverse costulae. Most taxonomic or faunistic studies of *Pteromalus* concern the Palaearctic fauna (Graham 1969, 1984; Bouček and Rasplus 1991; Dzhaokmen 1998, 2001; Gijswijt 1999; Mitroiu 2008; Baur 2015; Klimmek and Baur 2018; Maletti et al. 2021; Haas et al. 2021; Yan et al. 2023).

All species of *Pteromalus* with known biology are parasitoids of larvae and pupae of various holometabolous insects, such as Lepidoptera, Coleoptera, gall-forming Hymenoptera (Cynipidae, Tenthredinidae), and Diptera (Tephritidae) (Mitroiu 2008; Baur 2015). They play a crucial role in nature as regulating agents of these phytophagous insects (Bouček and Rasplus 1991; Ishizaki and Ishikawa 2010; Mahdavi and Madjdzadeh 2013; Li et al. 2018; Mbata and Warsi 2019; Haas et al. 2021). Despite their ecological and economic importance, *Pteromalus* species are often difficult to identify because of their diversity and sometimes subtle morphological characters that are used to separate species (Burks et al. 2022). Until now, the genus *Pteromalus* comprised 494 valid species, with only 19 species being recorded from China, including *P. albipennis* Walker, 1835; *P. astragali* (Liao, 1987); *P. bifoveolatus* Förster, 1861; *P. chrysos* Walker, 1836; *P. coleophorae* Yang & Yao, 2015; *P. elevatus* (Walker, 1834); *P. miyunensis* Yao & Yang, 2008; *P. orgyiae* Yang & Yao, 2015; *P. procerus* Graham, 1969; *P. puparum* (Linnaeus, 1758); *P. qinghaiensis* Liao, 1987; *P. sanjiangyuanicus* Yang, 2020; *P. semotus* (Walker, 1834); *P. sequester* Walker, 1835; *P. shanxiensis* Huang, 1987; *P. smaragdus* Graham, 1969; *P. temporalis* (Graham, 1969); *P. varians* (Spinola, 1808); and *P. xizangensis* (Liao, 1982) (Liao 1982; Sheng 1985; Liao et al. 1987; Huang et al. 1987; Huang et al. 2003; Yao and Yang 2008; Ye et al. 2012; Yang et al. 2015; Li et al. 2018; Yang et al. 2020; Yan et al. 2023).

The Chinese *Pteromalus* fauna has been poorly studied until now, and many new species, as well as newly recorded species, may be found in China. During a biodiversity expedition of the pteromalid wasps in northern Xinjiang, China, between 2014 and 2022 (funded by the first author's projects), most *Pteromalus* individuals belonged to species not previously known from Xinjiang. The aim of this work is to review the genus *Pteromalus* from China based on this collected material and data from the literature data (1982–2023), to describe two new species, and to provide the key to the two new species and their similar species.

Materials and methods

Collected material

All specimens of *Pteromalus xiaomoheensis* Yan & Li, sp. nov. and partial specimens of *Pteromalus steppensis* Li & Hu, sp. nov. were collected with a sweeping net from Xinjiang, China during 2020–2022. Some specimens of *Pteromalus steppensis* Li & Hu, sp. nov. were reared from their hosts during 2014–2016, the rearing process of *Pteromalus steppensis* Li & Hu, sp. nov. and *P. varians* (Spinola, 1808) follows Li et al. (2018). All specimens were mounted, labeled, and examined under a Nikon SMZ 745T stereomicroscope. Images except for *P. tripolii* Graham were taken with a Nikon DS-Fi3 connected to a Nikon SMZ 25 stereomicroscope and the images of *P. tripolii* were downloaded from the interactive key <http://pteromalus.identification-key.fr/mkey.html> in Klimmek and Baur (2018). All images were stacked with NIS-Elements software and arranged in figures using Adobe Photoshop. All specimens from Xinjiang, China, including the types of the new species

are deposited in the Insect Collection of the College of Life Science and Technology, Urumqi, Xinjiang, China (**ICXU**), and all specimens from the other provinces in China are deposited in the Institute of Zoology, Chinese Academy of Sciences, Beijing, China (**IZCAS**).

Morphological description

Morphological terms follow Bouček (1988), Gibson et al. (1997), and Burks et al. (2022). Body length excludes the protruding parts of ovipositor sheaths and was measured in millimeters (mm); other measurements are given as ratios. Abbreviations of morphological terms used are: Fu_n = antennal funicular 1, 2...; Gt_n = gastral tergite 1, 2...; OOL = shortest distance between eye margin and a posterior ocellus; POL = shortest distance between posterior ocelli.

Results

Taxonomy

Twenty-one species of *Pteromalus* from China are summarized in Table 1, including 19 species previously reported from China. Among them, there are six species from Xinjiang, including four species reported by Li et al. (2018) (*P. varians* (Spinola, 1808)) and Yan et al. (2023) (*P. elevatus* (Walker, 1834), *P. albipennis* Walker, 1835, *P. temporalis* (Graham, 1969)) and the two new species, *P. steppensis* Li & Hu, sp. nov. and *P. xiaomoheensis* Yan & Li, sp. nov.

The number of teeth on each mandible (both mandibles with four teeth, or left mandible with three teeth and right mandible with four) was not considered a good key character because of the lack of visibility (Gibson et al. 2024), but it is an important differentiating feature for species recognition. Thus, characterize our specimens by reporting the number of mandibular teeth, including the two new species: *P. steppensis* Li & Hu, sp. nov. (both mandibles with four teeth), and *P. xiaomoheensis* Yan & Li, sp. nov. (left mandible with three teeth and right mandible with four). According to Gibson et al. (2024), at present there are 22 species of *Pteromalus* with a 4:4 mandibular formula worldwide, including eight species reported by Graham (1969) (*P. apum* (Retzius, 1783)) (as *P. venustus* Statz, 1938), *P. bifoveolatus* Förster, 1861, *P. procerus*, *P. proprius* Walker, 1874, *P. puparum* (Linnaeus, 1758) (type species of *Pteromalus*), *P. smaragdus* Graham, 1969, *P. squamifer* Thomson, 1878 and *P. vopiscus* Walker, 1839, six species described from Europe since 1969 (*P. bottnicus* Vikberg, 1979, *P. briani* Baur, 2015, *P. discors* Graham, 1992, *P. osmia* Hedqvist, 1979, *P. paludicola* Bouček, 1972, and *P. sylveni* Hedqvist, 1979), three species from Kazakhstan (*P. melitaeae* Dzhanokmen, 1998, *P. maculatus* Dzhanokmen, 1998, and *P. transiliensis* Dzhanokmen, 1998), four species from China (*P. miyunensis* Yao & Yang, 2008, *P. orgyiae* Yang & Yao, 2015, *P. qinghaiensis* Liao, 1987, and *P. sanjiangyuanicus* Yang, 2020), and one species from North America (*P. quadridentatus* Gibson, 2024). *Pteromalus steppensis* Li & Hu, sp. nov. is different from the above 22 species and thus is newly described herein. The other new species, *P. xiaomoheensis* Yan & Li, sp. nov. is identified as belonging to the *P. albipennis* group of species and is separated from the existing species of that group based on Dzhanokmen (2001), Baur (2015), Klimmek and Baur (2018), and Maletti et al. (2021).

Table 1. Twenty-one Chinese species of *Pteromalus* and their citation in the Chinese literature between 1982 and 2023.

| Num. | Species | Detailed (re) description in Chinese | Distribution in China | Citation | Deposition of type material |
|------|---|--------------------------------------|--|---|-------------------------------------|
| 1 | <i>P. albipennis</i> Walker, 1835 | Yes | Xinjiang | Yan et al. 2023 | ICXU |
| 2 | <i>P. astragali</i> (Liao, 1987) | Yes | Beijing | Liao et al. 1987 | IZCAS |
| 3 | <i>P. bifoveolatus</i> Förster, 1861 | Yes | Jiangxi, Shandong | Sheng 1985; Huang et al. 1987; Yao and Yang 2008 | IZCAS |
| 4 | <i>P. chrysos</i> Walker, 1836 | Yes | Fujian | Huang et al. 2003 | IZCAS |
| 5 | <i>P. coleophorae</i> Yang & Yao, 2015 | Yes | Heilongjiang | Yang et al. 2015 | IZCAS |
| 6 | <i>P. elevatus</i> (Walker, 1834) | Yes | Xinjiang | Yan et al. 2023 | ICXU |
| 7 | <i>P. miyunensis</i> Yao & Yang, 2008 | Yes | Beijing | Yao and Yang 2008 | IZCAS |
| 8 | <i>P. orgyiae</i> Yang & Yao, 2015 | Yes | Ningxia | Yang et al. 2015 | IZCAS |
| 9 | <i>P. procetus</i> Graham, 1969 | Yes | Beijing | Yao and Yang 2008 | IZCAS |
| 10 | <i>P. puparum</i> (Linnaeus, 1758) | No | Jiangsu, Xinjiang, Xizang, Sichuan, Yunnan, Zhejiang | Liao 1982; Liao et al. 1987 | ICXU, IZCAS; new record in Xinjiang |
| 11 | <i>P. qinghaiensis</i> Liao, 1987 | Yes | Qinghai | Liao et al. 1987 | IZCAS |
| 12 | <i>P. sanjiangyuanicus</i> Yang, 2020 | Yes | Qinghai | Yang et al. 2020 | IZCAS |
| 13 | <i>P. semotus</i> (Walker, 1834) | Yes | Beijing, Fujian, Jilin, Xinjiang | Huang et al. 1987; Huang et al. 2003; Yao and Yang 2008 | ICXU, IZCAS; new record in Xinjiang |
| 14 | <i>P. sequester</i> Walker, 1835 | Yes | Inner Mongolia | Ye et al. 2012 | IZCAS |
| 15 | <i>P. shanxiensis</i> Huang, 1987 | Yes | Shanxi | Huang et al. 1987 | IZCAS |
| 16 | <i>P. smaragdus</i> Graham, 1969 | Yes | Fujian, Xinjiang | Huang et al. 2003 | ICXU, IZCAS; new record in Xinjiang |
| 17 | <i>P. steppensis</i> Li & Hu, sp. nov. | Yes | Xinjiang | This study | ICXU |
| 18 | <i>P. temporalis</i> (Graham, 1969) | Yes | Xinjiang | Yan et al. 2023 | ICXU |
| 19 | <i>P. varians</i> (Spinola, 1808) | No | Xinjiang | Li et al. 2018 | ICXU |
| 20 | <i>P. xiaomoheensis</i> Yan & Li, sp. nov. | Yes | Xinjiang | In this study | ICXU |
| 21 | <i>P. xizangensis</i> (Liao, 1982) | Yes | Taiwan, Xizang | Liao 1982 | IZCAS |

Description two new species of *Pteromalus* from Xinjiang, China.

Key to the two new species and their similar species (Female)

- 1 Both mandibles with four 4:4 (Fig. 1C)2
- Left mandible with three teeth and right mandible with four (Fig. 5D)3
- 2 POL 1.10–1.14× OOL (Fig. 1F); distance between upper margin of antennal toruli and lower margin of median ocellus 1.00–1.42× as long as distance between lower margin of antennal toruli and lower margin of clypeus (Fig. 1B); antennae with scape reaching lower margin of anterior ocellus (Fig. 1F); combined length of pedicellus and flagellum shorter than breadth of head (0.73–0.84×) (Fig. 1B); medial area of propodeum smooth and shiny (Fig. 1G)..... ***Pteromalus steppensis* Li & Hu, sp. nov.**
- POL 1.20–1.25× OOL; toruli about equidistant from the median ocellus and the lower margin of clypeus; antennae with scape reaching to level of vertex or slightly above it; combined length of pedicellus and flagellum almost equal to breadth of head; propodeum panels almost uniformly reticulate and not shiny***P. procerus* Graham, 1969**

- 3 Body length 3.0–3.4 mm (Fig. 5A); lower margin of clypeus deeply incised medially, hence appearing almost bidentate (Fig. 5C); POL 1.50–1.86× OOL (Fig. 5G); the basal fovea of propodeum are relatively large (Fig. 5I); marginal vein length 1.09–1.13× longer than stigmal vein (Fig. 5J); gaster long-oval (Fig. 5L), 1.57–1.85× as long as broad, 1.06–1.30× as long as mesosoma ***Pteromalus xiaomoheensis* Yan & Li, sp. nov.**
- Body length 2.7–3.1 mm (Fig. 6A); lower margin of clypeus moderately incised medially, hence without appearing bidentate (Fig. 6B); POL 1.40–1.50× OOL (Fig. 6C); the basal fovea of the propodeum are small (Fig. 6D); marginal vein 1.2–1.6× as long as the stigmal vein (Fig. 6E); gaster (Fig. 6F) short-oval, 1.2 to 1.6 times as long as broad, slightly shorter than to at most as long as the mesosoma ***P. tripolii* (Graham, 1969)**

***Pteromalus steppensis* Li & Hu, sp. nov.**

<https://zoobank.org/B206A28A-E5AA-4ECB-9B1B-73037259EDC4>

Fig. 1A–K

Type material. Holotype. • 1 ♀ (ICXU 20240801), Xinjiang, China, swept by Qin Li research group from *Ulmus pumila* L. (Ulmaceae) in People's park of Changji City; 44°01'33.38"N, 87°18'42.67"E; 567 m; 24 May 2022 and deposited in ICXU. **Paratypes:** • 26 ♀ (ICXU 20240802–20240827), and 68 ♂ (ICXU 20240828–20240895), same collection site as holotype; China, Xinjiang, Urumqi, campus of Xinjiang University, Qin Li reared from the larva and pupa of *Orchestes steppensis* Korotyaev, 2016: • 5 ♀ (ICXU 20240896–20240900) 2 ♂ (ICXU 20240901–20240902), 30 May 2014; • 1 ♂ (ICXU 20240903), 31 May 2015; • 2 ♀ (ICXU 20240904–20240905), 2 Jun 2015; • 1 ♀ (ICXU 20240906), 3 Jun 2015; • 1 ♂ (ICXU 20240907), 4 Jun 2015; • 2 ♀ (ICXU 20240908–20240909), 7 Jun 2015; • 26 ♀ (ICXU 20240910–20240935), 8 Jun 2015; • 9 ♀ (ICXU 20240936–20240944), 9 Jun 2015; • 8 ♀ (ICXU 20240945–20240952), 12 Jun 2015; • 1 ♀ (ICXU 20240953), 15 Jun 2015; • 18 ♀ (ICXU 20240954–20240971) 14 ♂ (ICXU 20240972–20240985), 29.V.2016; • 5 ♀ (ICXU 20240986–20240990) 13 ♂ (ICXU 20240991–20241003), 31 May 2016; • 2 ♀ (ICXU 20241004–20241005) 2 ♂ (ICXU 20241006–20241007), 3 Jun 2016; • 2 ♀ (ICXU 20241008–20241009), 8 Jun 2016; • 3 ♀ (ICXU 20241010–20241012) 1 ♂ (ICXU 20241013), 13 Jun 2016; • 2 ♀ (ICXU 20241014–20241015) 2 ♂ (ICXU 20241016–20241017), 23 Jun 2016.

Description. Female. Body (Fig. 1A) length 2.5–3.2 mm ($n = 24$). Head and mesosoma dark green, propodeum with bluish-green metallic reflections, metasoma dark green with shine, hind margin of Gt_1 , Gt_5 and Gt_6 , mid-part of Gt_2 , Gt_3 and Gt_4 black. Antenna with yellowish-brown scape; dorsal side of pedicel and flagellum dark chocolate-brown; ventral side yellowish brown. Mandibles brown, with dark-brown teeth. Legs with all coxae dark, metallic green; femora dark-chocolate-brown, tibiae and tarsi yellowish brown except last segment black-brown. Wings hyaline, forewing with venation brown.

Head in frontal view (Fig. 1B) 1.26–1.35× as broad as high, face with metallic reflections and regular raised-reticulation; clypeus (Fig. 1B) with longitudinal striations; lower margin moderately emarginate, without teeth; both

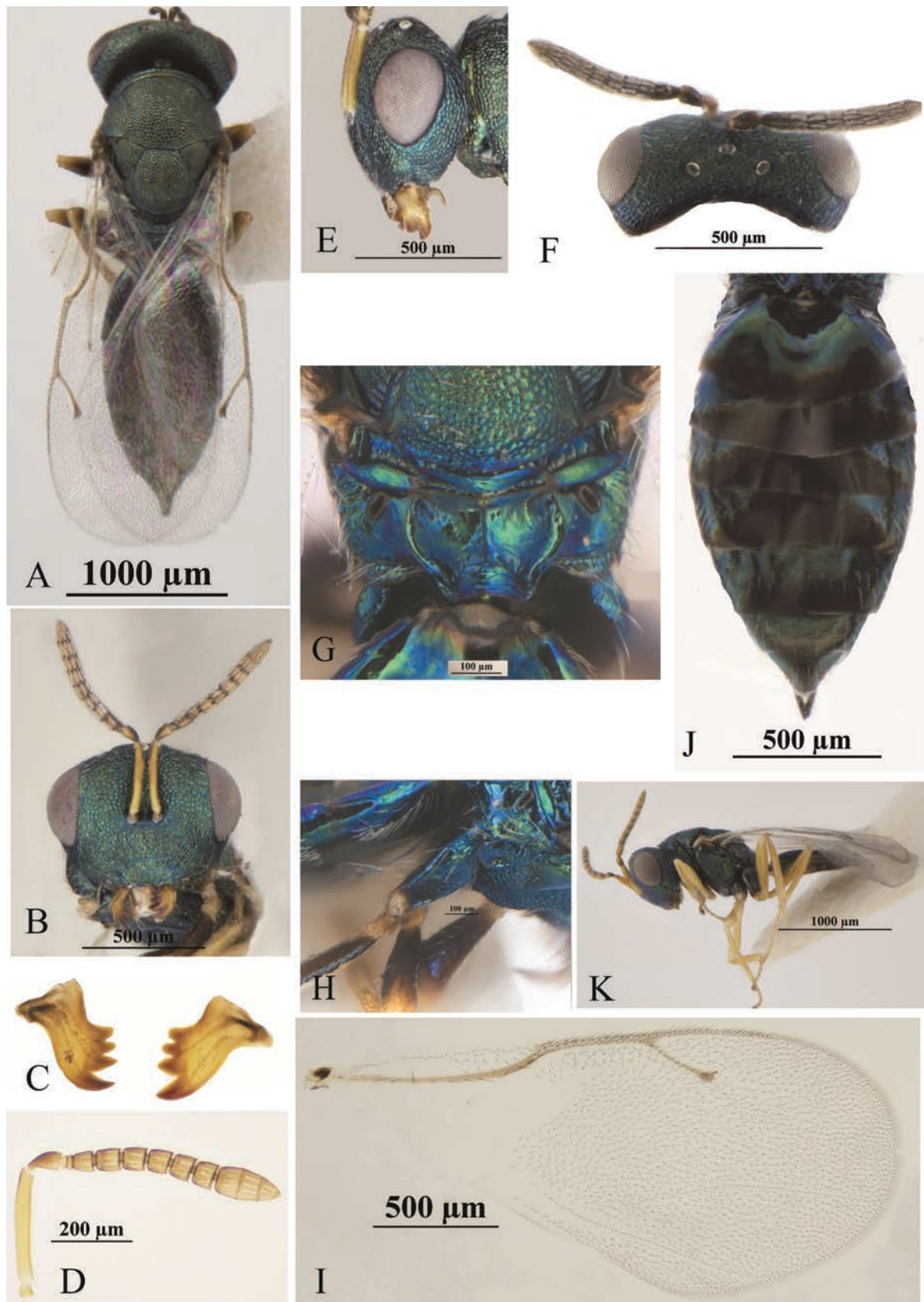


Figure 1. *P. steppensis* Li & Hu, sp. nov. **A–J** female **A** habitus, dorsal view **B** head, frontal view **C** mandible **D** antenna **E** head, lateral view **F** head, dorsal view **G** propodeum, dorsal view **H** hind coxa **I** forewing **J** metasoma, dorsal view **K** male, lateral view.

mandibles (Fig. 1C) 4-toothed. Antennae (Fig. 1B, D) inserted at centre of face, higher than the lower margin of eyes; distance between upper margin of antennal toruli and lower margin of median ocellus $1.00\text{--}1.42\times$ as long as distance between lower margin of antennal toruli and lower margin of clypeus; antennae with scape reaching lower margin of anterior ocellus, $7.25\text{--}7.63\times$ as long as broad; pedicel $1.33\text{--}1.67\times$ as long as broad in dorsal view, $1.71\text{--}1.98\times$ as long as fu_1 ; two anelli annular; funicular segments connected tightly to each other and each with one row of sensilla; fu_1 and fu_2 $1.00\text{--}1.20\times$ as long as broad each, fu_3 quadrate, fu_4 and fu_5 $0.79\text{--}0.87$ as long as broad each, fu_6 $0.64\text{--}0.69\times$ as long as broad; clava $2.13\text{--}2.67\times$ as long as broad; pedicel and flagellum combined $0.73\text{--}0.84\times$ head width. Head in lateral view as in Fig. 1E; eye height $1.24\text{--}1.46\times$ eye width; malar sulcus linear and complete; malar space $0.35\text{--}0.50\times$ eye height. Head in dorsal view (Fig. 1F) about $2.13\text{--}2.45\times$ as broad as long; POL $1.10\text{--}1.14\times$ OOL (Fig. 1F).

Mesosoma in dorsal view $0.84\text{--}0.87\times$ head width; pronotum collar margined with carina, $0.71\text{--}0.85\times$ as wide as mesoscutum, medially $1/9\text{--}1/7\times$ as long as mesoscutum; mesoscutum $0.51\text{--}0.63\times$ as long as broad; scutellum $0.90\text{--}1.00\times$ as long as width, frenal line absent. Propodeum (Fig. 1G) $0.50\text{--}0.55\times$ as long as scutellum, with medial area smooth; median carina and plica complete and sharp; nucha with fine transverse striations. Mesosoma in lateral view with prepectus smooth, $0.75\text{--}0.86\times$ as long as tegula; entire thoracic pleura regularly reticulate, except upper mesepimeron smooth and shiny-metallic. Forewing (Fig. 1I) with apex exceeding apex of gaster, $2.01\text{--}2.24\times$ as long as broad; upper surface of costal cell bare, lower surface of costal cell with 2–3 rows of setae interrupted medially; basal setal line incomplete and basal cell bare; speculum large and open posteriorly. Marginal vein length $0.96\text{--}1.00\times$ postmarginal vein length and $1.43\text{--}1.68\times$ stigmal vein length; postmarginal vein length $1.50\text{--}1.71\times$ stigmal vein length. Metacoxa in dorsal view bare, with several long setae (Fig. 1H), metafeumur $4.29\text{--}4.71\times$ as long as broad.

Gaster (Fig. 1J) long-oval, $1.98\text{--}2.38\times$ as long as broad, $1.43\text{--}1.88\times$ as long as mesosoma, $1.13\text{--}1.21\times$ as long as head plus mesosoma; Gt1 $0.20\text{--}0.25\times$ as long as gaster and sides of Gt1 with some sparse long setae; Gt7 $0.62\text{--}0.73\times$ as long as broad; ovipositor sheaths slightly exerted; hypopygium extending about $0.38\text{--}0.45\times$ the length of gaster.

Male (Fig. 1K). Body length: 3.0–3.2 mm. Body color: head, mesosoma, and metasoma the same color as the female; antenna yellowish brown; legs yellow, except all coxae dark green with metallic reflections and apical tarsi black-brown. Wings hyaline, forewing with venation brown.

Head in frontal view $1.25\text{--}1.35\times$ as broad as high; distance between upper margin of antennal toruli and lower margin of median ocellus $0.92\text{--}1.16\times$ as long as distance between lower margin of antennal toruli and lower margin of clypeus; pedicel and flagellum combined $0.89\text{--}0.96\times$ head width. Head in dorsal view $2.08\text{--}2.29\times$ as broad as long; POL $1.19\text{--}1.29\times$ OOL.

Mesosoma in dorsal view $0.79\text{--}0.81\times$ as head width; pronotum $0.81\text{--}0.85\times$ as wide as mesoscutum; mesoscutum $0.66\text{--}0.67\times$ as long as broad. Propodeum $0.49\text{--}0.54\times$ as long as scutellum. Forewing with marginal vein length $1.03\text{--}1.19\times$ postmarginal vein length and $1.48\text{--}1.88\times$ stigmal vein length; postmarginal vein length $1.44\text{--}1.60\times$ stigmal vein length.

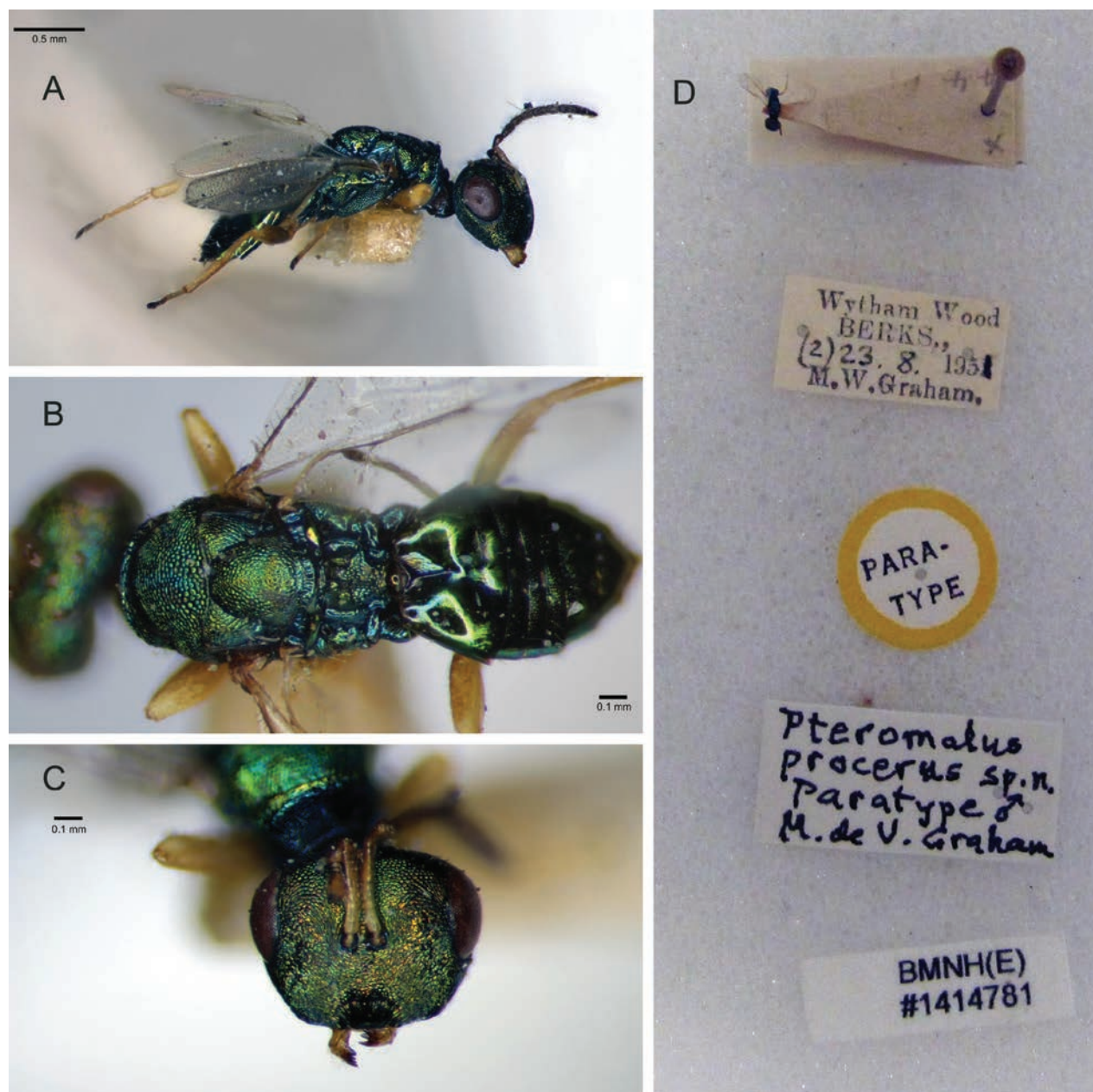


Figure 2. *P. procerus* Graham, 1969 **A–C** male **A** body, lateral view **B** mesosoma and metasoma, dorsal view **C** head, frontal view **D** paratype information.

Gaster long-oval, 1.89–2.18× as long as broad, 0.77–0.84× as long as head plus mesosoma; Gt1 about 0.35–0.39× as long as gaster.

Etymology. The species is named after its host species *Orchestes steppensis* Korotyaev, 2016 (Coleoptera, Curculionidae) (used as a noun in apposition).

Biology. This species was reared as a primary, solitary ectoparasitoid of the larval and pupal stage of *O. steppensis* Korotyaev, 2016. Figures of the development and its damage on the host are provided in Figs 3, 4.

Distribution. Changji and Urumqi, Xinjiang, China.

Comments. This species is similar to *P. procerus*. In females of that species: both mandibles with four teeth; anterior margin of clypeus shallowly emarginate, hardly impressed in the middle; clypeus strigose, the striae hardly extending on to the face and genae; pronotal collar distinctly less wide than the

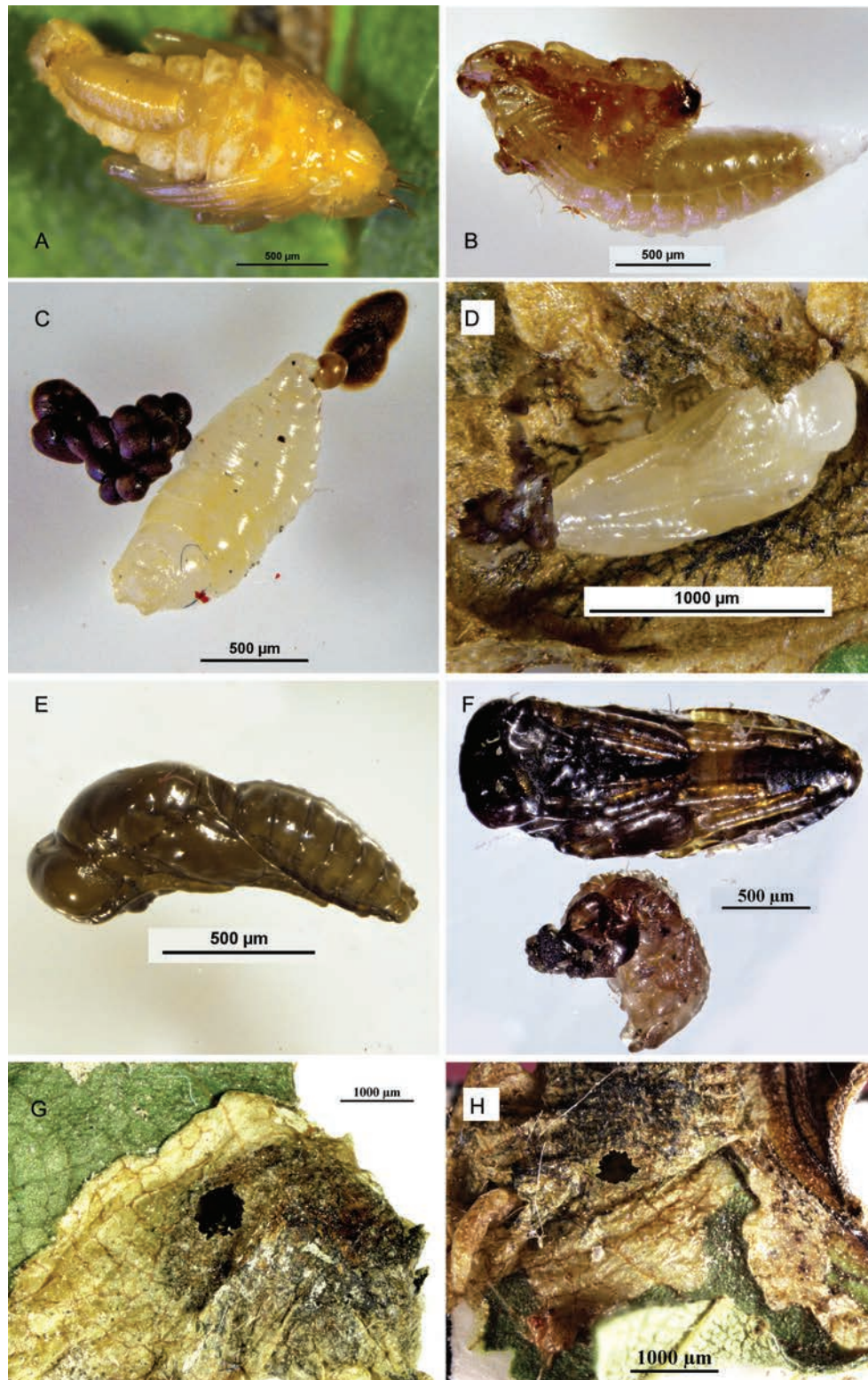


Figure 3. Development stages of *P. steppensis* Li & Hu, sp. nov. and their emergence holes, **A–H**. **A, B** the parasitoid larva feeding on the third larva of the host **C** prepupa **D–F** pupa **G, H** emergence holes.

mesoscutum, shorter medially than at the sides, medially from slightly more than 1/8–1/7 as long as the mesoscutum, finely reticulate with a narrow shiny strip along its hind edge, slightly to distinctly margined anteriorly; propodeum somewhat more than half as long as the mesoscutellum (Graham 1969:

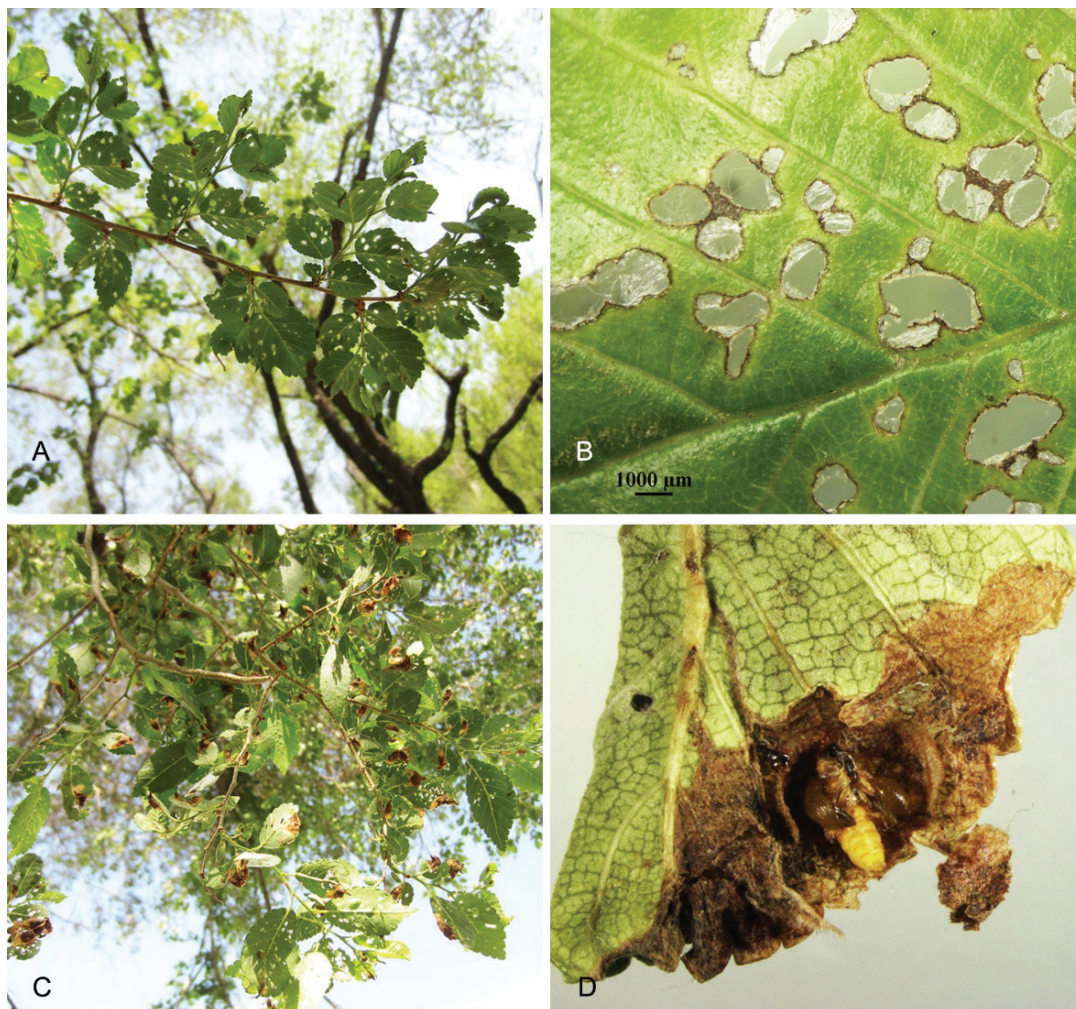


Figure 4. Damage on *Ulmus pumila* leaves made by the adults as well as the larvae of *O. steppensis* Korotyaev, 2016 **A–D**. **A, B** holes on *U. pumila* leaves made by the adults **C, D** *U. pumila* leaves.

fig. 389); gaster lanceolate or sublanceolate, usually as long as or slightly longer than the head plus thorax, occasionally slightly shorter, 1.8–2.3 times as long as broad. However, the new species can be distinguished from *P. procerus* by the following: POL 1.10–1.14× OOL; distance between upper margin of antennal toruli and lower margin of median ocellus 1.00–1.42× as long as distance between lower margin of antennal toruli and lower margin of clypeus; antennae with scape reaching lower margin of anterior ocellus; combined length of pedicellus and flagellum shorter than breadth of head (0.73–0.84×); medial area of propodeum smooth and shiny. In *P. procerus*: POL 1.20–1.25× OOL; toruli about equidistant from the median ocellus and the lower margin of clypeus; antennae with scape reaching to level of vertex or slightly above it; combined length of pedicellus and flagellum almost equal to breadth of head; propodeum panels almost uniformly reticulate and not shiny.

In males of *P. steppensis* Li & Hu, sp. nov. (Fig. 1K): antenna yellowish brown; legs yellow, except all coxae dark green with metallic reflections, and apical tarsi black-brown; propodeum smooth and shiny, 0.49–0.54× as long as scutellum. In contrast, in *P. procerus* (Fig. 2A–D): antenna dark brown to black; pale parts of the legs yellowish, hind femora lightly infusate at the base only and the fore and mid femora yellowish; propodeum reticulated, about 2/3× as long as scutellum.

***Pteromalus xiaomoheensis* Yan & Li, sp. nov.**

<https://zoobank.org/A52C92F0-6305-431B-B59C-AC9BAF665E4C>

Fig. 5A–L

Type material. Holotype. • 1 ♀ (ICXU 20246442), Xinjiang, China, Gongliu County of Yili Prefecture; 43°10'52.04"N, 82°44'9.49"E; 1377 m; 10 Jul 2021, coll. Liqin research group. **Paratypes.** • 8 ♀ (ICXU 20246443–20246450), same collection information as holotype; • 2 ♀ (ICXU 20246451–20246452), Qinghe County of Altay Prefecture; 46°26'5.83"N, 90°2'45.15"E; 600 m; 9 Jul 2020, coll. Liqin research group; • 1 ♀ (ICXU 20246453), Altai City of Altay Prefecture; 47°39'26.97"N, 88°17'20.22"E; 624 m; 24 Jun 2021, coll. Liqin research group; • 1 ♀ (ICXU 20246454), Fuyun County of Altay Prefecture; 47°17'7.69"N, 89°45'24.35"E; 830 m; 11 Jul 2020, coll. Liqin research group; • 6 ♀ (ICXU 20246455–20246460), Zhaosu County of Yili Prefecture; 43°9'10.43"N, 81°26'38.83"E; 1556 m; 9 Jul 2021, coll. Liqin research group; • 1 ♀ (ICXU 20246461), Xinyuan County of Yili Prefecture; 43°22'38"N, 83°36'18"E; 1279 m; 28 Jul 2018, Coll. Hongying Hu research group; • 1 ♀ (ICXU 20246462), Tekes County of Yili Prefecture; 43°13'19.12"N, 81°48'31.80"E; 1200 m; 8 Jul 2021, coll. Liqin research group; • 33 ♀, Tekes County of Yili Prefecture; 43°9'19.98"N, 88°47'23.76"E; 1184 m; 9 Jul 2021, coll. Liqin research group; • 1 ♀ (ICXU 20246463), Gongliu County of Yili Prefecture; 43°20'22.85"N, 82°31'4.19"E; 881 m; 10 Jul 2021, coll. Liqin research group; • 1 ♀ (ICXU 20246464), Urumqi County of Urumqi; 43°27'25.02"N, 87°22'37.20"E; 1757 m; 5 Jul 2022, Coll. Hongying research Hu.

Description. Female. Body (Fig. 5A, B) length 3.0–3.4 mm ($n = 5$). Head and mesosoma dark metallic-green, metasoma dark green with reflections. Antenna with yellowish-brown scape; pedicel and flagellum dark-chocolate-brown. Legs (Fig. 5K) with all coxae dark metallic-green, femora dark green, except for apical part brown, tibiae yellowish brown to brown and tarsi pale yellow, except last segment brown. Wings hyaline; forewing with venation brown.

Head in frontal view (Fig. 5C) 1.19–1.28× as broad as high, face with metallic reflections and regular raised-reticulations; clypeus (Fig. 5C) with longitudinal striations, with lower margin deeply incised medially, hence appearing almost bidentate; left mandible 3-toothed and right mandible 4-toothed (Fig. 5D). Antennae (Fig. 5C) inserted at centre of face, higher than the lower margin of eyes; distance between upper margin of antennal toruli and lower margin of median ocellus 0.91–1.11× as long as distance between lower margin of antennal toruli and lower margin of clypeus; antennae with scape reaching lower margin of anterior ocellus; pedicel 1.55–1.59× as long as broad in dorsal view; two anelli annular; funicular segments (Fig. 5E, G) connected tightly to each other and each with two rows of sensilla; fu_1 to fu_4 each about 1.10–1.30× as long as broad each; fu_5 0.95–1.12× as long as broad; fu_6 0.73–0.77× as long as broad; clava 2.52–2.68× as long as broad; pedicel and flagellum combined 0.75–0.90× head width. Head in lateral view (Fig. 5F), eye height 1.42–1.70× as eye width; malar sulcus linear and complete, and malar space 0.46–0.48× eye height. Head in dorsal view (Fig. 5G), 2.19–2.44× as broad as long; POL 1.50–1.86× OOL.

Mesosoma in dorsal view (Fig. 5A) 0.86–0.96× as head width; pronotum collar (Fig. 5H) margined with carina, 0.88–0.91× as wide as mesoscutum, medially one quarter as long as mesoscutum; mesoscutum 0.62–0.72× as long as broad; scutellum 0.95–1.00× as long as width, frenal line absent. Propodeum

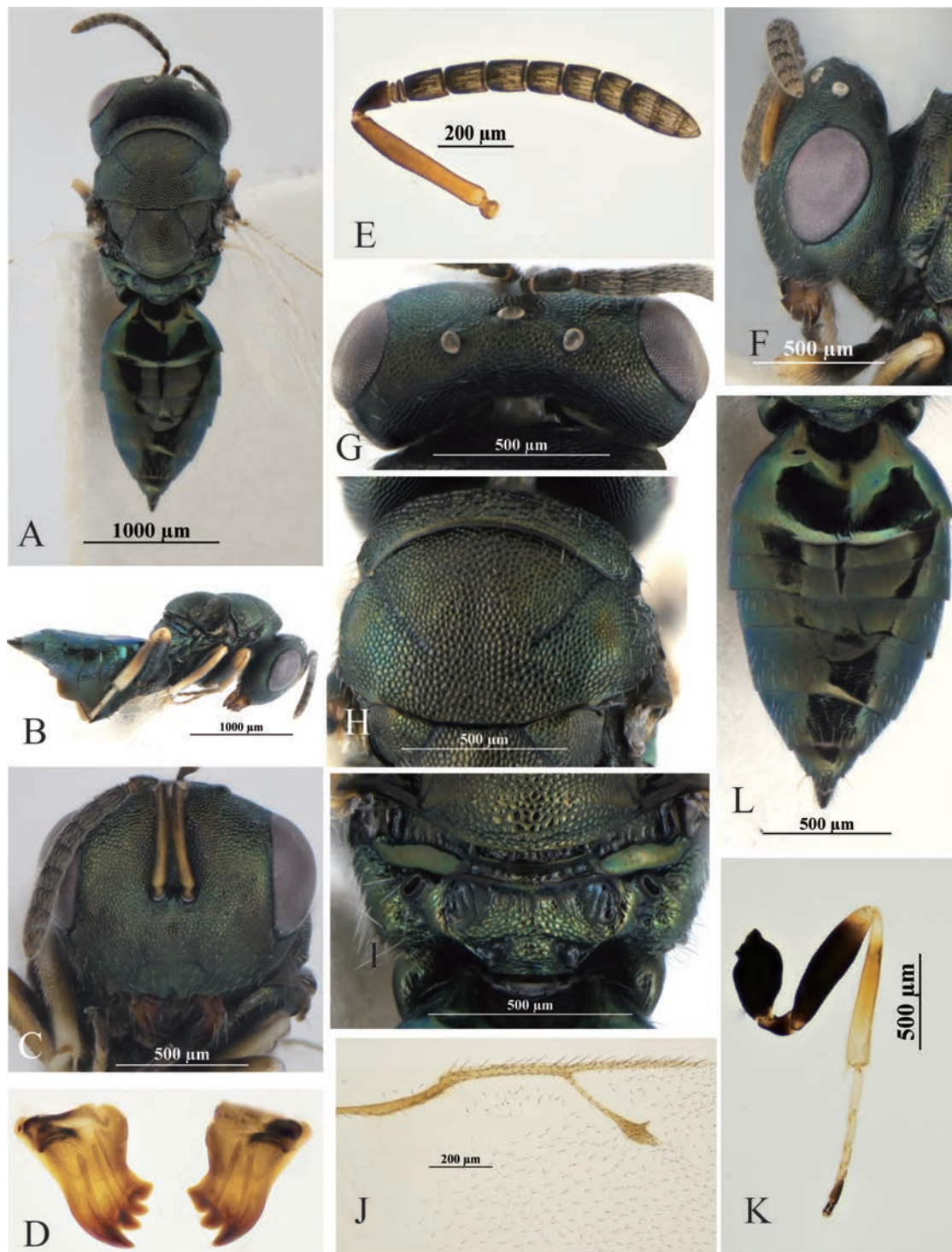


Figure 5. *P. xiaomoheensis* Yan & Li, sp. nov. holotype **A–L** female **A** habitus, dorsal view **B** body, lateral view **C** head, frontal view **D** mandible **E** antenna **F** head, lateral view **G** head, dorsal view **H** mesoscutum, dorsal view **I** propodeum, dorsal view **J** forewing **K** hind leg **L** metasoma, dorsal view.

(Fig. 5I) 0.35–0.47× as long as scutellum, medial area reticulated; median carina and plica complete and sharp; nucha large and reticulate. Mesosoma in lateral view with prepectus smooth, 0.62–0.80× as long as tegula; entire thoracic pleura regularly reticulate, except the upper mesepimeron smooth and shiny metallic. Forewing (Fig. 5J) apex exceeding apex of gaster, 2.05–2.14× as long

as broad; lower surface of costal cell with one row of hairs interrupted medially; basal setal line and basal cell bare; speculum large and open posteriorly. Marginal vein length $0.96\text{--}1.04\times$ postmarginal vein length and $1.09\text{--}1.13\times$ longer than stigmal vein length; postmarginal vein $1.10\text{--}1.14\times$ as long as stigmal vein. Metacoxa in dorsal view bare, metafemur (Fig. 5K) $3.87\text{--}4.16\times$ as long as broad.

Gaster long-oval (Fig. 5L), $1.57\text{--}1.85\times$ as long as broad, $1.06\text{--}1.30\times$ as long as mesosoma, $0.81\text{--}0.97\times$ as long as head plus mesosoma; Gt_1 about $0.31\text{--}0.35\times$ as long as gaster; Gt_7 $0.63\text{--}1.14\times$ as long as broad; ovipositor sheaths exerted, length of extend part $0.5\text{--}1.25\times$ as long as Gt_7 length; hypopygium extending about $0.51\text{--}0.67\times$ the length of gaster.

Male. Unknown.

Etymology. The species is named after the collection locality of its holotype.

Biology. Unknown.

Distribution. Xinjiang, China: Yili Prefecture (Gongliu County; Zhaosu County; Xinyuan County; Tekes County; Gongliu County), Altay Prefecture (Qinghe County; Altai City) and Urumqi.

Comments. This species is similar to *P. tripolii* (Fig. 6A–F); both species belong to the *albipennis* species group, both have with left mandible with three teeth and right mandible with four; head and thorax brightly metallic, green to blue, brassy, or coppery; antenna with sensilla usually numerous and in two irregular rows on at least the proximal segments of the funicle; fu_1 longer than broad and fu_6 quadrate or transverse; combined length of pedicellus and flagellum distinctly less than the breadth of the head; propodeum medially a little less than half as long as the scutellum (Graham 1969: fig. 377); gaster ovate, basal tergite occupying $1/3\text{--}2/5$ of the total length. However the new species is distinguished from *P. tripolii* by the following characters: body color dark blue; body length $3.0\text{--}3.4$ mm; gaster long-oval (Fig. 5L), $1.57\text{--}1.85\times$ as long as broad, $1.06\text{--}1.30\times$ as long as mesosoma. In *P. tripolii*: body color usually bright green to blue (Fig. 6A); body length $2.7\text{--}3.1$ mm (Fig. 6A); gaster (Fig. 6F) short-oval, about as long as, or slightly shorter than, the mesosoma, about as broad as the latter, 1.2 to 1.6 times as long as broad, acute but not acuminate apically (Fig. 6A).

Discussion

This study adds significant knowledge on the faunal composition and distribution of *Pteromalus* species in China. With the description of two new species from western China (Eastern Palaearctic Region), the genus now includes 496 valid species worldwide, with 21 of these in China and six species in Xinjiang. As reported by Gibson et al. (2024: p202) “Described species of *Pteromalus* with a 4:4 mandibular formula appear to be far fewer in number than those with a 3:4 formula. For example, of the 67 species Graham (1969) treated from northwestern Europe, eight named species were reported under *Pteromalus* and 59 named species under *Habroclytus* (12%)”. We had similar results, with only nine Chinese species of *Pteromalus* having four teeth on both mandibles, and 12 species with three teeth on the left mandible and four teeth on the right mandible.

Pteromalus steppensis Li & Hu, sp. nov. is described from both sexes and was reared as a primary, solitary ectoparasitoid of larval and pupal stages of

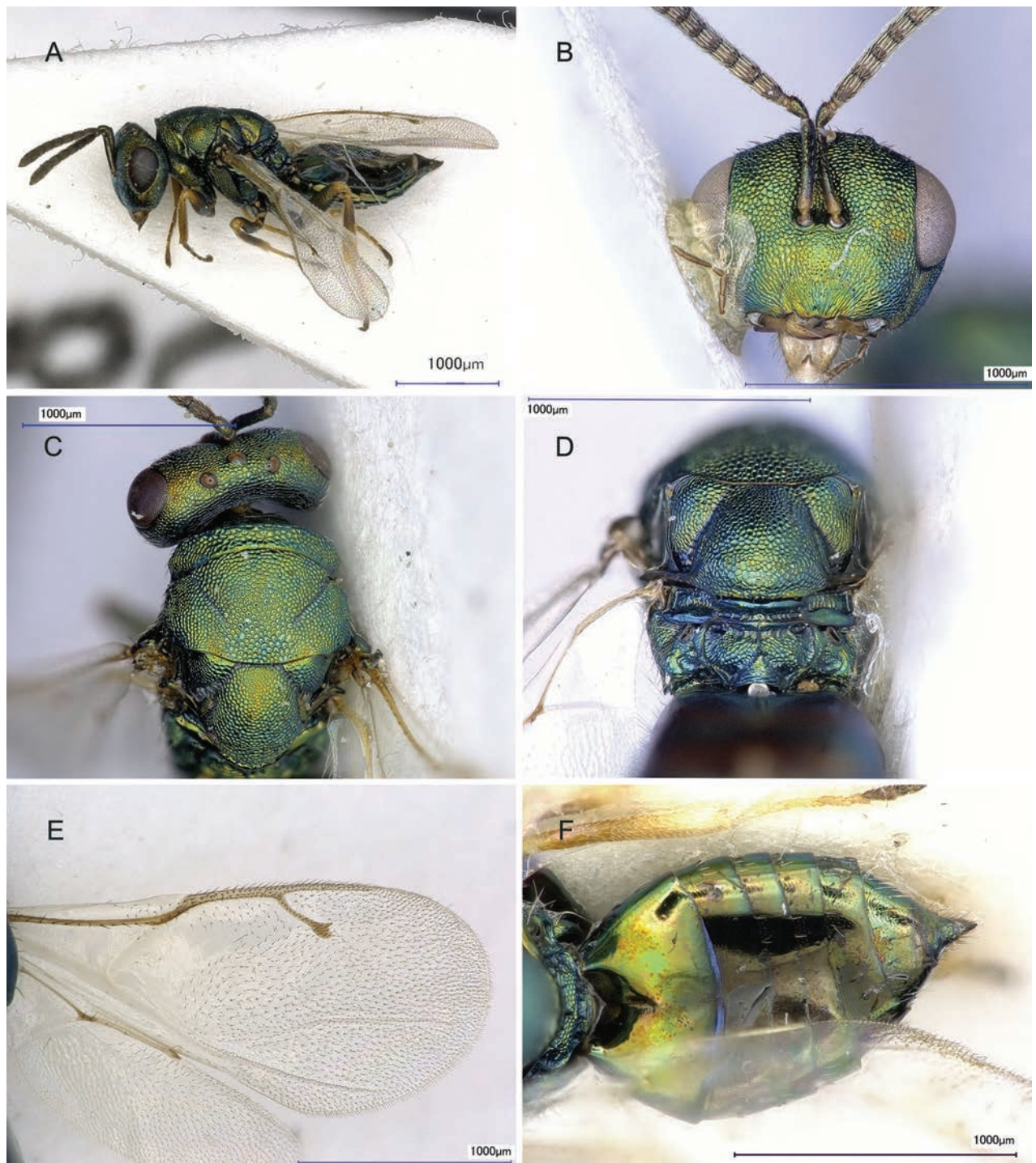


Figure 6. *P. tripolii* (Graham, 1969) **A–F** female **A** body, lateral view **B** head, frontal view **C** head and mesosoma, dorsal view **D** propodeum, dorsal view **E** forewing **F** gaster, dorsal view.

Orchestes. Steppensis. Detailed information on its life history and phenology of its host in Xinjiang, images of its larval and pupal stages, as well as of its host's life habits can be found in the publication by Li et al. (2018). Almost 10 years have passed since the first author (Qin Li) reared 558 (340 ♀, 218 ♂) specimens of this new species from its host *O. steppensis*. Li et al. (2018) reported this new species as *Pteromalus* sp. 2. Guohua Yan studied the integrated taxonomy of *Pteromalus* from Xinjiang based on three methods, including morphological

taxonomy, comparative morphology, and DNA Barcoding (28S rDNA and ITS2 genes) (Li et al. 2018). She collected 95 specimens (27 ♀, 68 ♂) of this new species by sweep netting on *Ulmus pumila* L. (Ulmaceae) heavily infested by the pest, *O. steppensis* in People's park of Changji City, Urumqi, Xinjiang, China. She compared her specimens with the specimens reared by Qin Li from the elm pest, *O. steppensis* and based on its morphological characters, and confirmed they are the same species, *P. steppensis* Li & Hu, sp. nov. These results indicate that many more investigations are necessary to have a complete overview of the *Pteromalus* fauna from China.

Acknowledgements

We are very thankful to Andrew Polaszek (Natural History Museum, London, United Kingdom) for his great help with photographing paratypes of *P. procerus* in the Natural History Museum, London; Zhulidezi Aishan research group of Xinjiang University, China for providing some of our specimens; Mircea Dan Mitroiu (Faculty of Biology, Alexandru Ioan Cuza University, Iasi, Romania) for reviewing the manuscript prior to its submission; Gary A.P. Gibson (Agriculture and Agri-Food Canada, Canadian National Collection of Insects, Arachnids and Nematodes, Ottawa, Canada) for sending his new paper to us.

Additional information

Conflict of interest

The authors have declared that no competing interests exist.

Ethical statement

No ethical statement was reported.

Funding

This work was funded by the Natural Science Foundation of Xinjiang Autonomous Region (2023D01C14), the National Natural Science Foundation of China (grant no. 31900349), the Third Xinjiang Scientific Expedition Program (grant no. 2022xjkk1505), the Postdoctoral program of Beet pest survey project (grant no. 202206140011, TCT-JSYF-20221122) to Qin Li and the Youth Talent Promotion Project of Autonomous Region Association for Science and Technology of Xinjiang (grant no. RCTJ60).

Author contributions

Investigation and specimen collection, Q.L., G.-H.Y. and T.-Y.Z.; writing original draft preparation, Q.L. and Y.-L. L.; writing review and editing, Q.L., H.X. and H.-Y.H.; supervision project administration, Q.L.; funding acquisition, Q.L., H.-Y.H. All authors have read and agreed to the published version of the manuscript.

Author ORCIDs

Qin Li  <https://orcid.org/0000-0002-1780-7332>

Hong-ying Hu  <https://orcid.org/0000-0002-2295-1072>

Data availability

All of the data that support the findings of this study are available in the main text.

References

- Baur H (2015) Pushing the limits—two new species of *Pteromalus* (Hymenoptera, Chalcidoidea, Pteromalidae) from Central Europe with remarkable morphology. *ZooKeys* 514: 43–72. <https://doi.org/10.3897/zookeys.514.9910>
- Bouček Z, Heydon SL (1997) Pteromalidae. In: Gibson GAP, Huber JT, Woolley JB (Eds) *Annotated Keys to the Genera of Nearctic Chalcidoidea* (Hymenoptera). NRC Research Press, Ottawa, 541–692. <https://doi.org/10.1093/aesa/91.3.359>
- Bouček Z, Rasplus J-Y (1991) Illustrated key to West-Palearctic genera of Pteromalidae (Hymenoptera: Chalcidoidea). Institut National de la Recherche Agronomique Paris, 140 pp.
- Burks R, Mitroiu MD, Fusu L, Heraty JM, Janšta P, Heydon S, Papilloud NDS, Peters RS, Tselikh EV, Woolley JB, van Noort S, Baur H, Cruaud A, Darling C, Haas M, Hanson P, Krogmann L, Rasplus JY (2022) From hell's heart, I stab at thee! A determined approach towards a monophyletic Pteromalidae and reclassification of Chalcidoidea (Hymenoptera). *Journal of Hymenoptera Research* 94: 13–88. <https://doi.org/10.3897/jhr.94.94263>
- Dzhanokmen KA (1998) Review of pteromalids of the genus *Pteromalus* Swederus (Hymenoptera, Pteromalidae) from Kazakhstan: I. *Entomological Review* 78: 706–717. [Translated from *Entomologicheskoe Obozrenie* 77: 483–496.]
- Dzhanokmen KA (2001) Review of pteromalids of the genus *Pteromalus* Swederus (Hymenoptera, Pteromalidae) from Kazakhstan: II. *Entomological Review* 81: 75–97. [Translated from *Entomologicheskoe Obozrenie* 80: 472–496.]
- Gibson GAP, Yonathan U, Jade S, Paul KA, Tara DG, Zhang YM, Baur H, Gates M, Franklin MT (2024) The species of *Pteromalus* Swederus in America north of Mexico with a 4:4 mandibular formula, and description of a potential biocontrol agent of the introduced pest *Anthonomus rubi* (Herbst) (Coleoptera: Curculionidae). *Zootaxa* 5501(2): 201–236. <https://doi.org/10.11646/zootaxa.5501.2.1>
- Gijswijt MJ (1999) Four new species of *Pteromalus* Swederus (Hymenoptera: Chalcidoidea: Pteromalidae) and redescrptions of three other species. *Zoologische Mededelingen Leiden* 72(7): 167–170.
- Graham MWR, de V (1969) The Pteromalidae of north-western Europe (Hymenoptera: Chalcidoidea). *Bulletin of the British Museum (Natural History) (Entomology)*, Supplement 16: 1–908. <https://doi.org/10.5962/p.258046>
- Huang DW, Liao DX, Niu YZ (1987) Studies on pteromalids from insect pests of poplar from Shuoxian County, Shanxi Province. *Sinozoologica* 5: 155–160. [In Chinese]
- Huang BK, Huang DW, Xiao H (2003) *Fauna of Insects in Fujian Province of China* (VII). Fujian Science and Technology Press, Fuzhou, 501–502. [In Chinese]
- Ishizaki T and Ishikawa T (2010) Pteromalid parasitoids (Hymenoptera) of *Oulema oryzae* (Kuwayama) (Coleoptera: Chrysomelidae) from Japan, with notes on *Pteromalus bifoveolatusens*. *Entomological Science* 13: 144–149. <https://doi.org/10.1111/j.1479-8298.2010.00369.x>
- Klimmek F, Baur H (2018) An interactive key to Central European species of the *Pteromalus albipennis* species group and other species of the genus (Hymenoptera: Chalcidoidea: Pteromalidae), with the description of a new species. *Biodiversity Data Journal* 6: e27722. <https://doi.org/10.3897/BDJ.6.e27722>
- Li Q, Triapitsyn SV, Wang C, Zhong W, Hu HY (2018) Biological traits and the complex of parasitoids of the elm pest *Orchestes steppensis* (Coleoptera: Curculionidae)

- in Xinjiang, China. *Bulletin of Entomological Research* 108(1): 48–57. <https://doi.org/10.1017/S0007485317000499>
- Liao DX (1982) Hymenoptera: Chalcidoidea. *Insects of Xizang* 2: 355–370. [In Chinese]
- Liao DX, Li XL, Pang XF, Chen TL (1987) Hymenoptera: Chalcidoidea (1). *Economic Insect Fauna of China*, 34, i–x+ 1–241. [In Chinese]
- Mahdavi M, Madjazadeh SM (2013) Contribution to the knowledge of Chalcidoidea (Pteromalidae and Eupelmidae) of Iran. *North-Western Journal of Zoology* 9: 94–98.
- Maletti S, Niehuis O, Mayer C, Sann M, Klopstein S, Nottebrock G, Baur H, Peters RS (2021) Phylogeny, taxonomics, and ovipositor length variation of the *Pteromalus albipennis* species group (Hymenoptera: Chalcidoidea: Pteromalidae: Pteromalinae). *Journal of Zoological Systematics and Evolutionary Research* 59: 349–358. <https://doi.org/10.1111/jzs.12433>
- Mbata GN, Warsi S (2019) *Habrobracon hebetor* and *Pteromalus cerealellae* as tools in post-harvest integrated pest management. *Insects* 10: 1–12. <https://doi.org/10.3390/insects10040085>
- Marziyeh M, Seyed MM (2013) Contribution to the knowledge of Chalcidoidea (Pteromalidae and Eupelmidae) of Iran. *North-Western Journal of Zoology* 9(1): 94–98.
- Mbata W (2019) *Habrobracon hebetor* and *Pteromalus cerealellae* as tools in post-harvest integrated pest management. *Insects* 10(85): 1–12. <https://doi.org/10.3390/insects10040085>
- Haas M, Baur H, Schweizer T, Monje JC, Moser M, Bigalk S, Krogmann L (2021) Tiny wasps, huge diversity—a review of German Pteromalidae with new generic and species records (Hymenoptera: Chalcidoidea). *Biodiversity Data Journal* 9: e77092. <https://doi.org/10.3897/BDJ.9.e77092>
- Mitroiu MD (2008) Checklist of the Romanian species of Pteromalidae (Hymenoptera: Chalcidoidea). *Analele Științifice ale Universității “Al. I. Cuza”, Iași, s. Biologie Animală* 54: 7–23. http://www.bio.uaic.ro/publicatii/anale_zoologie/issue/2008/02Mitroiu1.pdf
- Sheng JK (1985) One newly recorded species of Pteromalidae (Hymenoptera, Chalcidoidea). *Acta Agriculturae Universitatis Jiangxis* 23(2): 42.
- UCD (2024) Community. Universal Chalcidoidea Database Website. 2024. <https://ucd.chalcid.org> [Accessed on: 2024-04-18]
- Yan GH, Li Y, Hu HY, Li Q (2023) Three new record species of *Pteromalus* (Hymenoptera: Pteromalidae) from China, *Sichuan Journal of Zoology* 42(4): 446–461. <https://doi.org/10.11984/j.issn.1000-7083.20220304> [In Chinese]
- Yang ZQ, Yao YX, Cao LM (2015) Chalcidoidea parasitizing forest defoliators (Hymenoptera). Science Press, Beijing, vii + 283 pp. [21 pls] [In Chinese]
- Yang ZQ, Wang XY, Zhong X, Liu X, Cao LM, Wang HZ (2020) A new species of *Pteromalus* parasitizing pupa of *Gynaephora qinghaiensis* (Lepidoptera: Lymantriidae) from Qinghai-Tibet-Plateau 56: 99–105. [In Chinese]
- Yao YX, Yang ZQ (2008) Three species of genus *Pteromalus* (Hymenoptera: Pteromalidae) parasitizing *Rhynchaenus empoulifolis* (Coleoptera: Curculionidae), with description of a new species from China. *Scientia Silvae Sinicae* 44: 90–94. [In Chinese]
- Ye HZ, Hu HY, Xiao H (2012) Three newly recorded species of *Pteromalus* (Chalcidoidea, Pteromalidae) from China. *Acta Zootaxonomica Sinica* 37(3): 676–680.

Review of the genus *Isca* (Ephemeroptera, Leptophlebiidae) from China with a new species and a new species record

De-Wen Gong¹, Chang-Fa Zhou¹

¹ College of Life Sciences, Nanjing Normal University, Nanjing 210023, China

Corresponding author: Chang-Fa Zhou (zhouchangfa@njnu.edu.cn)

Abstract

Previously, only one *Isca* species (*Isca purpurea* Gillies, 1951) was recorded in China. In this review, three *Isca* species are presented and photographed. Among them, *I. acutata* sp. nov. is a new species with an acute male penal apex, a uniform brown abdomen of the imago, and a bilamellate gill VII of the nymph. Another species, *I. fascia*, previously reported from Vietnam, is found in China for the first time. The nymphs of *I. fascia* exhibit a banded body and a convex apex of the penes. The structure of the third species *I. purpurea*, shown graphically, has separated penes and a paler nymphal body than the other two species. The diverse morphology of the penes, wings, venation, and gills show that *Isca* has diverse species and evolutionary directions, suggesting that the previous subgeneric classification may not adequately represent some species. Biologically, their nymphs were observed living in tiny pits on substrate surfaces, where their ventral gills may facilitate respiration while they hide.

Key words: Barcode gene, China, COI, mayfly, morphology, new species, subgenus, taxonomy



Academic editor: Ben Price
Received: 11 November 2024
Accepted: 14 March 2025
Published: 11 April 2025

ZooBank: <https://zoobank.org/70EE2B15-6E8A-4740-897B-BDCE44D02A27>

Citation: Gong D-W, Zhou C-F (2025) Review of the genus *Isca* (Ephemeroptera, Leptophlebiidae) from China with a new species and a new species record. ZooKeys 1234: 239–258. <https://doi.org/10.3897/zookeys.1234.140905>

Copyright: © De-Wen Gong & Chang-Fa Zhou. This is an open access article distributed under terms of the Creative Commons Attribution License (Attribution 4.0 International – CC BY 4.0).

Introduction

The genus *Isca* was first established by Gillies in 1951, based on imaginal specimens of *Isca purpurea* Gillies, 1951, collected from southern China (Hong Kong) and India. Later, Peters and Edmunds (1970) associated the nymphs with the imago of this genus. In the same paper, they also established two subgenera for two additional species: *I. (Minyphlebia) janiceae* Peters & Edmunds, 1970 from Thailand and *I. (Tanycola) serendiba* Peters & Edmunds, 1970 from Ceylon, based on wing characteristics (such as the presence or absence of wing cilia, the fusion or unfusion of MP2 with MP1, and whether MA forks were more or less than halfway from the base to the margin). Nguyen and Bae (2003) named the fourth species *I. fascia* from Vietnam with both nymphal and imaginal stages. The fifth species *I. lea*, described by Sartori and Derleth (2010) from Indonesia (East Kalimantan) based on the nymphal stage, was the only one with a bilamellate gill VII. Despite being one of the first countries noted for the presence of *Isca*, further research on the Chinese species has not been conducted.

Both adults and nymphs of the known *Isca* species show high morphological diversity. Their wings can be transparent (*I. janiceae*) or translucent (*I. purpurea*,

I. serendiba, *I. fascia*), with marginal cilia (*I. purpurea*, *I. serendiba*, *I. fascia*) or without (*I. janiceae*), nymphs with bilamellate gills VII (*I. lea*) or unilamellate gills VII (*I. purpurea*, *I. serendiba*, *I. fascia*, *I. janiceae*). The increasing number of reported species suggests a broader variety of potential evolutionary trends within the genus.

Both nymphs and imagoes of *Isca* have remarkable characters. Besides their tiny bodies, the imagoes have forewings only, and the nymphs have ventral gills. To our knowledge, only psammophilous nymphs in the genera *Paradolania* Zhou, 2024, *Dolania* Edmunds & Traver, 1959, and *Behingia* Lestage, 1930 exhibit similar ventral gills (Zheng et al. 2024), while some species in the family Oligoneuriidae possess either ventral gill I or gills I–II (Bauernfeind and Soldán 2012). However, *Isca* nymphs have been reported living on stony substrates (Peters and Edmunds 1970). Further biological observations of these species will unveil the function of their morphological characters.

In recent years, we conducted extensive collection efforts across South China to uncover more leptophlebiids in this region. As a result, three *Isca* species were found, including the known one *I. purpurea*, the newly recorded *I. fascia* and a new species *I. acutata* sp. nov. These findings highlight the diversity of the *Isca* genus in China.

Material and methods

Collecting

The nymphs were collected by hand net in a little stream near the road, some of the adults were caught under the leaves or on the spider webs nearby, and the rest of them were reared indoors from mature nymphs. All materials were stored in ethanol (more than 80%).

Observing

Digital photos were taken using a Sony A7RIV Interchangeable Lens Digital Camera with a Laowa FF 25 mm F2.8 Ultra Macro (macro lens), and a Nikon Eclipse 50i microscope with an Mshot MDX10 Image System. Final plates were prepared and polished using Adobe Photoshop 2022.

SEM

Eggs were dissected from the female adult (*I. acutata* sp. nov.) and mature female nymphs (*I. purpurea*). All SEM (scanning electronic microscope) samples were prepared with a standard protocol: fixed in 4% glutaraldehyde for 5–8 h, rinsed with PBS (physiological saline) 2 or 3 times (10–15 min each), dehydrated in concentration gradient acetone (30%, 50%, 70%, 80%, 90%, 100%, 10 to 15 min each), and coated with gold film in a vacuum.

COI sequencing

In order to associate our nymphs and adults of selected species and differentiate species of *Isca*, we sequenced five Chinese individuals. Morphologically, three of them were *Isca purpurea*, and two were *I. acutata* sp. nov. Additionally,

we downloaded three Indian *I. purpurea* sequences from GenBank and used the species *Habrophlebiodes zijinensis* as the outgroup (Table 1).

The DNA extraction and amplification followed the process by Zheng and Zhou (2021). The COI sequence data of these species was uploaded to GenBank, and its GenBank accession number is listed in Table 1. The sequences were aligned with the software ClustalW.

All specimens used in this study are deposited in the Mayfly Collection, College of Life Sciences, Nanjing Normal University (NNU).

Nymph-adult associating

The association between nymph and imago of *I. acutata* sp. nov. and *I. purpurea* was established using COI sequences (see Tables 1, 2). At the same time, one male of *I. acutata* sp. nov. was reared from nymphs, and both imaginal and mature nymphal genitalia were compared and associated with three species in this study. Furthermore, the color pattern of their nymphs and adults, especially those of *I. fascia*, were good characters in our association.

To reconstruct the molecular tree, Bayesian inference (BI) and maximum likelihood (ML) analyses were performed. The partition model was selected by ModelFinder based on BIC (Bayesian information criterion) and AICc (standard correction to Akaike information criterion) (Kalyaanamoorthy et al. 2017). BI phylogenies were reconstructed using MrBayes v. 3.2.6 through the online CIPRES Science Gateway (Miller et al. 2011; Ronquist et al. 2012), with the following settings: two

Table 1. The species and their COI sequences used in this research.

| Species | GenBank accession number | Remarks |
|-----------------------------------|--------------------------|--------------------------------|
| <i>I. purpurea</i> (1) | PQ558934 | China (Fujian), Male |
| <i>I. purpurea</i> (2) | PQ558935 | China (Fujian), Female |
| <i>I. purpurea</i> (3) | PQ558936 | China (Guangdong) |
| <i>I. acutata</i> sp. nov. (1) | PQ558937 | China (Hainan) Nymph |
| <i>I. acutata</i> sp. nov. (2) | PQ558938 | China (Hainan) Male |
| <i>I. purpurea</i> (4) | ON557588 | India |
| <i>I. purpurea</i> (5) | MW160191 | India |
| <i>I. purpurea</i> (6) | LC061468 | India (Selvakumar et al. 2016) |
| <i>Habrophlebiodes zijinensis</i> | OP908297 | – |

Table 2. K2P genetic distance among the COI sequences.

| | <i>I. purpurea</i> (1) | <i>I. purpurea</i> (2) | <i>I. purpurea</i> (3) | <i>I. acutata</i> sp. nov. (1) | <i>I. acutata</i> sp. nov. (2) | <i>I. purpurea</i> (4) | <i>I. purpurea</i> (5) |
|--------------------------------|------------------------|------------------------|------------------------|--------------------------------|--------------------------------|------------------------|------------------------|
| <i>I. purpurea</i> (2) | 0.29% | | | | | | |
| <i>I. purpurea</i> (3) | 1.63% | 1.94% | | | | | |
| <i>I. acutata</i> sp. nov. (1) | 20.01% | 20.11% | 20.39% | | | | |
| <i>I. acutata</i> sp. nov. (2) | 20.79% | 20.57% | 20.79% | 0.48% | | | |
| <i>I. purpurea</i> (4) | 19.61% | 20.12% | 19.42% | 17.61% | 18.13% | | |
| <i>I. purpurea</i> (5) | 19.07% | 19.57% | 18.88% | 17.07% | 17.56% | 1.05% | |
| <i>I. purpurea</i> (6) | 16.68% | 16.78% | 16.47% | 18.71% | 18.44% | 12.63% | 11.81% |

parallel runs with four Markov chains were run for 10 million generations (with a sampling frequency of 1000), with a burn-in of 25% trees. RAXML v. 8.2.0 was used for ML analyses, with the model GTRGAMMAI and 1000 bootstrap replicates (Stamatakis 2014). FigTree v. 1.4.2 (<http://tree.bio.ed.ac.uk/software/figtree/>; accessed on 5 July 2021) was used for the editing of phylogenetic trees.

Results

Taxonomy

Genus *Isca* Gillies, 1951

Figs 1–6, 8–15

Isca acutata sp. nov.

<https://zoobank.org/13349861-975E-460C-917E-CEC50D0F32F3>

Figs 1–5, 6A

Material examined. *Holotype* • 1 male imago, Shuiman Village, Wuzhishan City, Hainan Province, CHINA, 730m a.s.l., 18.907855°N, 109.679361°E, 2024-I-8-10, Dewen Gong, Xuhongyi Zheng leg. *Paratypes* • 1 male imago (reared from nymph) and 10 nymphs, same data as holotype.

Other material. • 3 female subimagos (reared from nymphs), 21 nymphs, Limu Mountain, Wuzhishan City, Hainan Province, CHINA, 627m a.s.l., 19.169685°N, 109.746047°E, 2023-IV-29, Dewen GONG, Xiaofang Chen, Xinhe Qiang leg. • 4 nymphs, Jianfengling Mountain, Ledong County, Hainan Province, CHINA, 850 m a.s.l., 18.743911°N, 108.854413°E, 2022-VI-29, Dewen Gong, Manqing Ding, Xinhe QIANG leg. • 1 nymph, Nandao Farm, Sanya City, Hainan Province, CHINA, 231 m a.s.l., 18.394447°N, 109.388103°E, 2022-VII-6, Dewen Gong, Manqing Ding, Xinhe Qiang leg. • 2 male imagos, 5 nymphs, Qixianling Mountain, Baoting County, Hainan Province, CHINA, 280 m a.s.l., 18.702331°N, 109.692115°E, 2024-I-11, Dewen Gong, Xuhongyi Zheng leg.

Description. *Nymph (in alcohol)*: Body length 4.2–4.4 mm, cerci subequal to body length, terminal filament 6.4–7.2 mm (Fig. 1A–C). General coloration brown, head and thorax washed light brown, abdominal terga I–VIII brown, terga IX–X light brownish, without any specific pattern, sterna much lighter than terga. Wingpad dark brown, legs uniformly yellowish to amber (Fig. 1A–C).

Head: prognathous, area between three ocelli darker than others (Fig. 1A, C).

Labrum: ca. 1.8 times wider than long, anterior margin concave in the middle, forming a wide V-shape, lateral-anterior angle rounded, lateral-posterior margin shrunken inward; dorsal surface with two rows of setae sub-marginally, setae in the anterior row slender, denser and longer than those in the posterior row, ventral surface with scattered setae near anterolateral angles and a tuft of hair-like setae sub-medially (Fig. 2A).

Mandible: outer margin smoothly convex, with ca. 16 setae at median surface; outer and inner incisors of left mandible divided into three teeth respectively, prosthema with a spur and a tuft of spines; outer incisor of right mandible with 3 teeth (2 tiny denticles on inner tooth), inner incisor with 2 teeth, each of them with additional two acute denticles on both sides; prosthema with a tuft of spines, one bigger than others; four long mesal setae under the molar (Fig. 2B). Hypopharynx: superlinguae with concave lateral



Figure 1. Nymphal structures of *I. acutata* sp. nov.: **A** female nymph (dorsal view) **B** female nymph (ventral view) **C** male nymph (dorsal view) **D** foreleg **E** midleg **F** hindleg **G** claw **H** gill IV **I** gill VII.

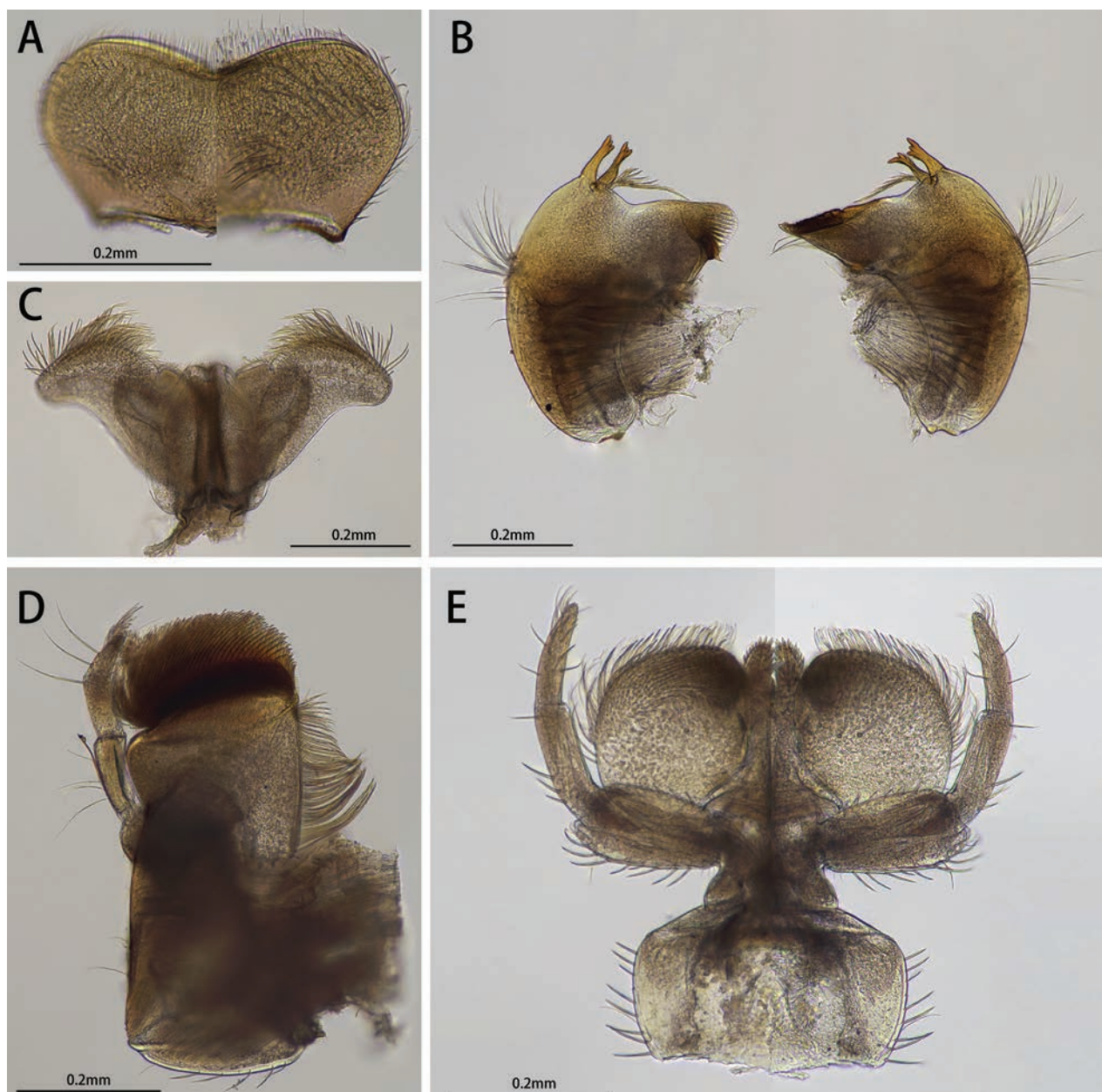


Figure 2. Mouth part of *I. acutata* sp. nov.: **A** labrum (left: dorsal view, right: ventral view) **B** mandible (left: left mandible / right: right mandible) **C** hypopharynx **D** maxilla (ventral view) **E** labium (left: dorsal view / right: ventral view).

margins, two apices extended into oval lobes; apical margin with hair-like setae; two arms of lingua subequal to median oval lobe (Fig. 2C). Maxilla: crown covered with dense of setae, galea-lacinia with row of setae, inner apex with a comb-like setae; maxillary palp three-segmented, length ratio of them from I to III = 1.6: 1.0: 1.0, outer margin of segment I with six setae, segment II with a seta, segment III with two setae, tip of segment III with tuft of relatively short setae; outer margin of stipes with very sparse hair-like setae, outer margin of cardo with six long setae (Fig. 2D). Labium: length ratio of 3 segments of labial palp from I to III = 1.4: 1.1: 1.0; two apical segments slimmer than basal one (Fig. 2E).

Thorax: Setae on outer margin of femur strong, relatively longer than that on inner margin; inner margin of tibiae and tarsi with stout setae; outer mar-

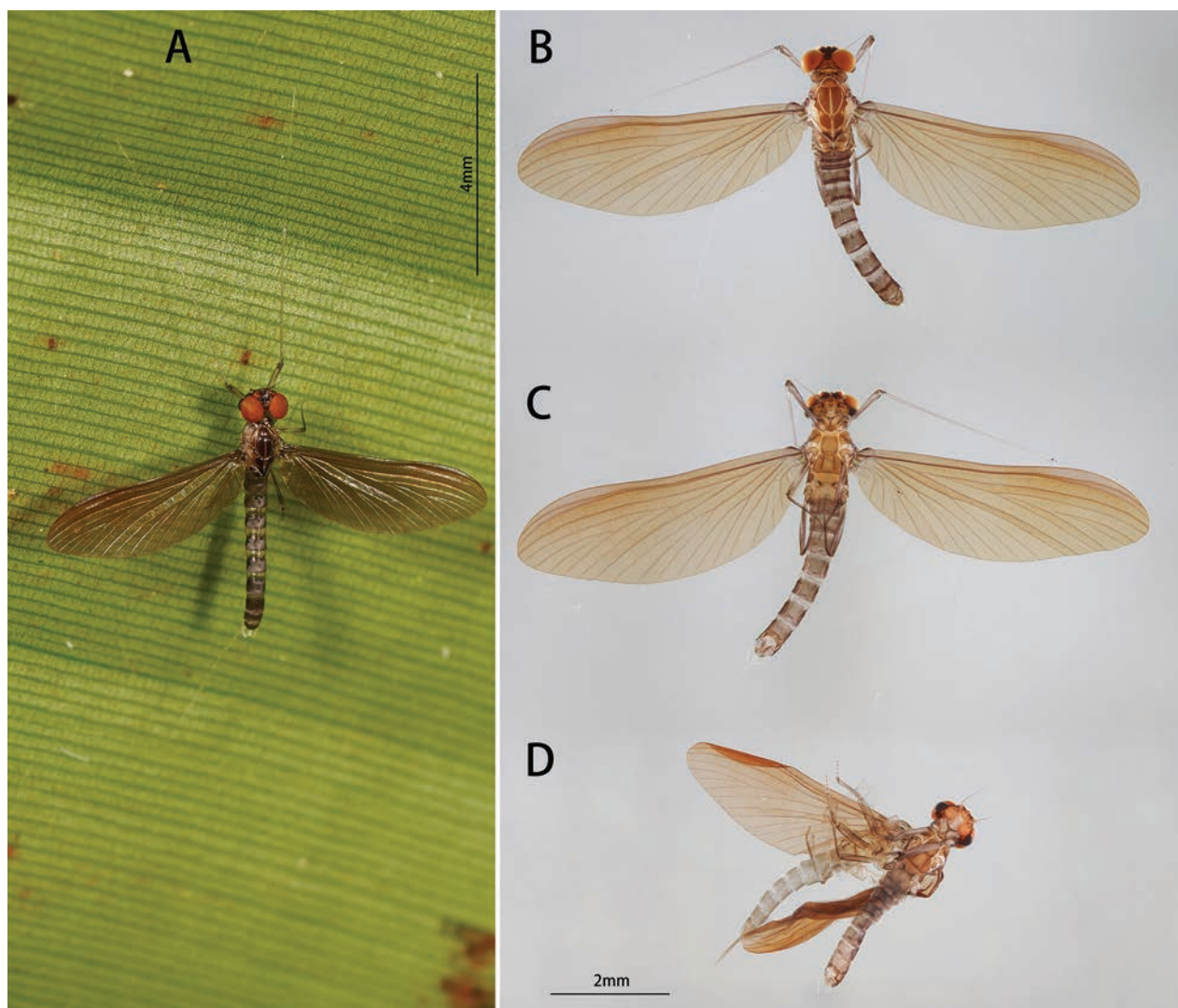


Figure 3. Male of *I. acutata* sp. nov.: **A** imago (dorsal view, living specimen in the field) **B** imago (dorsal view) **C** imago (ventral view) **D** imago with exuviate of subimago.

gin of tibiae and tarsi with hair-like setae, those on tibia of hindleg with extra stout setae (Fig. 1D–F). Length ratio of femora: tibiae: tarsi of forelegs = 2.3: 1.8: 1.0, that of midlegs = 2.4: 2.0: 1.0, and hindlegs = 2.5: 2.3: 1.0 (Fig. 1D–F). Claw with 14 denticles, distal one larger than others, proximal four denticles smaller (Fig. 1G).

Abdomen: posterior margin of each tergite with contiguous acute spines, posterolateral projections on segment IX only (Fig. 1A–C). Gills present on segments II to VII of ventral side of abdomen (Fig. 1B). Gills similar morphologically, consist of two slender and unbranched lamellae, gills progressively smaller from anterior to posterior (Fig. 1H–I). Caudal filaments brown, terminal filament slightly darker than cerci; posterior margin of each segment with spines, every second segment from segment II with an encircling row of hair-like setae around posteriorly (Fig. 1A–C).

Male imago (in alcohol): Body length 4.4 mm, generally amber to brownish, wings deep brown (Fig. 3).

Head: Width between two compound eyes about half of one eye width; upper half of it orange, lower half black (Fig. 4A).

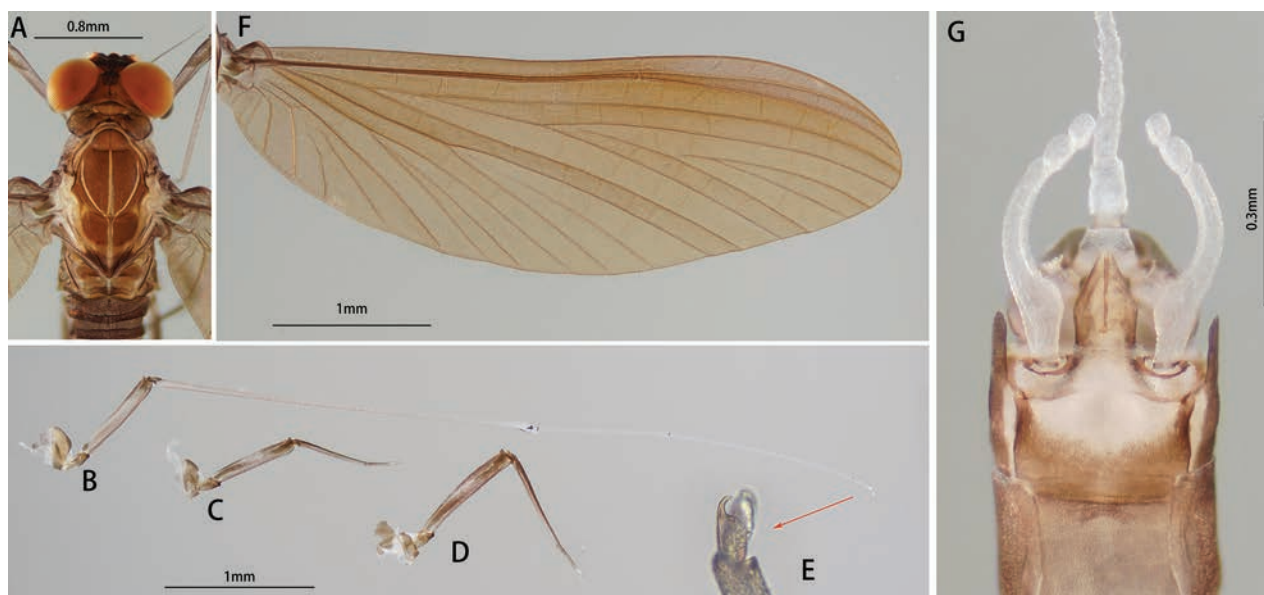


Figure 4. Male structures of *I. acutata* sp. nov.: **A** head (dorsal view) **B** foreleg **C** midleg **D** hindleg **E** claw **F** wing **G** genitalia (ventral view).

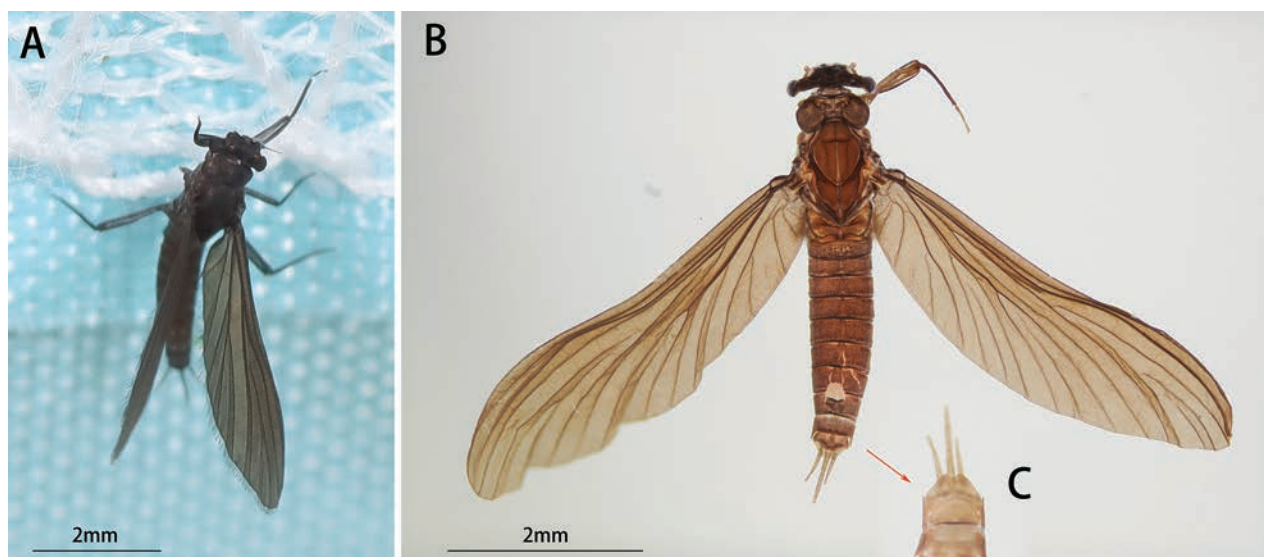


Figure 5. Female structures of *I. acutata* sp. nov.: **A** female subimago (living specimen) **B** female subimago (dorsal view) **C** sternum IX (ventral view).

Thorax: Legs: Foretarsus and tip of tibia pale, other portion brown, ratio of femur: tibia: tarsus = 1.0: 3.8: 3.5, ratio of foretarsal segments from I to V = 1.0: 14.0: 11.9: 8.6: 2.5. Midleg and hindleg dark brown, ratios of femur: tibia: tarsus = 2.9: 2.4: 1.0 and 2.9: 2.5: 1.0 (Fig. 4B–D). Claw dissimilar, one hooked, one blunt (Fig. 4E).

Wing opaque, brown; veins clear, posterior margin with cilia, vein MA forked slightly less than 1/2 of distance from base to margin (Fig. 4F).

Abdomen: color of terga I to IX alike, anterior 1/3 pale and semi-transparent, posterior 2/3 brown, sterna lighter than terga; tergite X brown (Fig. 3). Genitalia: forceps pale; segment I with a mesal expansion at 2/5 point; segments II and III subequal, nearly sphere; penes brown, two penes situated together, forming a pen-point like structure, margin of basal half straight, apical half straightly

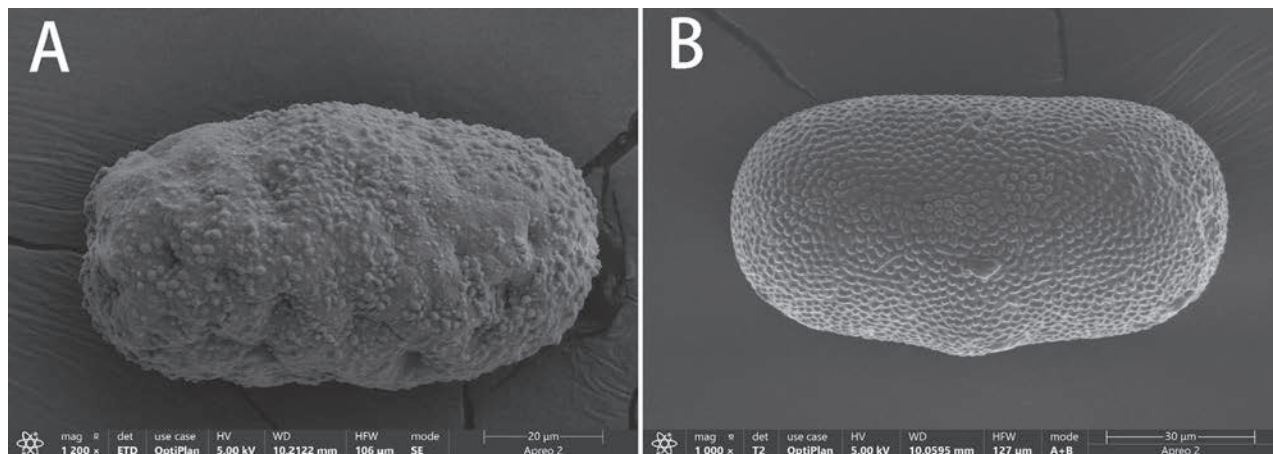


Figure 6. SEM photos: **A** egg from female subimago of *I. acutata* sp. nov. **B** egg from female nymph of *Isca purpurea*.

oblique; length of penes about 2/5× of forceps (Fig. 4G). Caudal filaments pale (Figs 3A, 4G).

Female: body length 4.1 mm, caudal filaments brown with spine-like setae. Coloration similar to male, sternum IX slightly concave apically (Fig. 5).

Egg. Egg oval, length about 85 μm, width about 45 μm, surface scattered with protuberances and cavities; their size and location irregular (Fig. 6A).

Biology. Nymphs found under stones with coarse surfaces in slow water currents of a montane stream about 1–2 m, without direct sunlight (Fig. 7). Adults emerged in the late afternoon. Some male imagoes were found under leaves above the stream.

Etymology. *acutata* comes from the Latin adjective *acutatus*, indicating the shape of sharp penal apex of the new species.

Diagnosis. The nymph of *Isca acutata* sp. nov. can be distinguished from other *Isca* species by the following characters: abdominal terga I–VIII brown, terga IX–X light brown (Fig. 1A, C); abdominal sterna light brown (Fig. 1B); gill VII with dorsal and ventral lamella (Fig. 1I); posterolateral projection on segment IX (Fig. 1B). The male imago of *I. acutata* sp. nov. can be distinguished by: wings translucent with cilia along posterior margin; anterior 1/3 of each abdominal tergum, and sterna I–VIII pale and semi-transparent; posterior 2/3 brown, sterna slightly lighter than terga (Fig. 3); forceps pale; penes brown, fused basally, nib-like (Fig. 4G).

Comparison. Among six known species, only two species (*I. lea* and *I. acutata* sp. nov.) have bilamellate gills VII in their nymphal stage. Those two nymphs can be differentiated by: (1) ventral setae on labrum of *Isca acutata* sp. nov. is less than *Isca lea* because it has two setal tufts (Fig. 2A), and (2) more setae on the tip of the maxillary palpal segment III of *Isca acutata* than *Isca lea* (Fig. 2D).

In males, the new species *Isca acutata* sp. nov. is unique in penal shape: penes fused basally (Fig. 4G) while those of *I. purpurea*, *I. serendiba*, *I. janiceae* are separated; its apical margin is straight (Fig. 4G) while that of *I. fascia* is convex (Fig. 15C); vein MA is forked less than 1/2 of distance from base to margin (Fig. 4F) while vein MA of *I. janiceae* and *I. purpurea* forked more than 1/2 of distance from base to margin; cilia present on posterior margin of wings (Fig. 4F) while absent in *I. janiceae*; sternum IX of female *Isca acutata* sp. nov. cleft (Fig. 5C) but not as deeply as *I. purpurea* (Fig. 12B), while that of *I. janiceae* is entire.

Distribution. China (Hainan Island).



Figure 7. Habitat of *I. acutata* sp. nov.

***Isca purpurea* Gillies, 1951**

Figs 6B, 8–12

Isca purpurea Gillies, 1951: 21–130, figs 15–22 (male, female). Type: male, from China (Hong Kong) and India (Mirik).

Isca purpurea: Peters and Edmunds 1970: 159–240, figs 71, 106, 330, 350–357 (nymph, male).

Material examined. • 55 nymphs, Chebaling Mountain, Shaoguan City, Guangdong Province, CHINA, 460 m a.s.l., 24.701644°N, 114.190687°E, 2024-IV-2-14, Dewen Gong, Xuhongyi Zheng leg. • 10 male imagoes, 3 female subimagoes, 3 nymphs, Laipoli, Jinan District, Fuzhou City, Fujian Province, CHINA, 390 m a.s.l., 26.251947°N, 119.283899°E, 2024-IV-25, Xuhongyi Zheng leg. • 5 nymphs, Jiulian Mountain, Ganzhou City, Jiangxi Province, CHINA, 24.539800°N, 114.467900°E, 2020-IX-14, Zhengxing MA leg.

Description. Nymph (in alcohol, first formal description): Body length 4.0–4.5 mm (Fig. 8A, B).

General coloration brownish, thorax light brown, abdomen brownish, without any specific pattern, ventral surface much lighter. Wingpad dark brown, legs uniformly yellowish (Fig. 8A, B).

Head: prognathous (Fig. 8A, B). Labrum ca. 1.8 times wider than long, anterior margin concaved in the middle, lateral-anterior angle rounded, lateral-posterior margin shrunk inward; dorsal side with two rows of setae anteriorly, anterior row denser than posterior row but length of them subequal (Fig. 9A).

Mandible with rounded outer margin, with 14 setae in the middle; outer incisor of left mandible with 3 apical teeth, inner incisor with 3 teeth, prostheca with a spur and a tuft of spines; outer incisor of right mandible with 3 teeth, inner incisor with 2 teeth and a denticle aside, prostheca with a relatively small spur and a tuft of spines, 4 long setae under the molar (Fig. 9B).

Hypopharynx: superlinguae with concave lateral margins, apex with setal tufts, lateral angles rounded (Fig. 9C).



Figure 8. Nymphal structures of *I. purpurea*: **A** male nymph (dorsal view) **B** male nymph (ventral view) **C** foreleg **D** midleg **E** hindleg **F** claw **G** gill IV **H** gill VII.

Maxilla covered with dense crown of setae, galea-lacinia with row of setae, margin of cardo with 5 long setae; maxillary palp 3-segmented, length ratio of 3 segments from I to III = 1.6: 1.0: 1.2, outer margin of segment I with 5 setae, segment II with a seta on the tip, segment III with 2 setae, tip of segment III with tuft of relatively short setae (Fig. 9D).

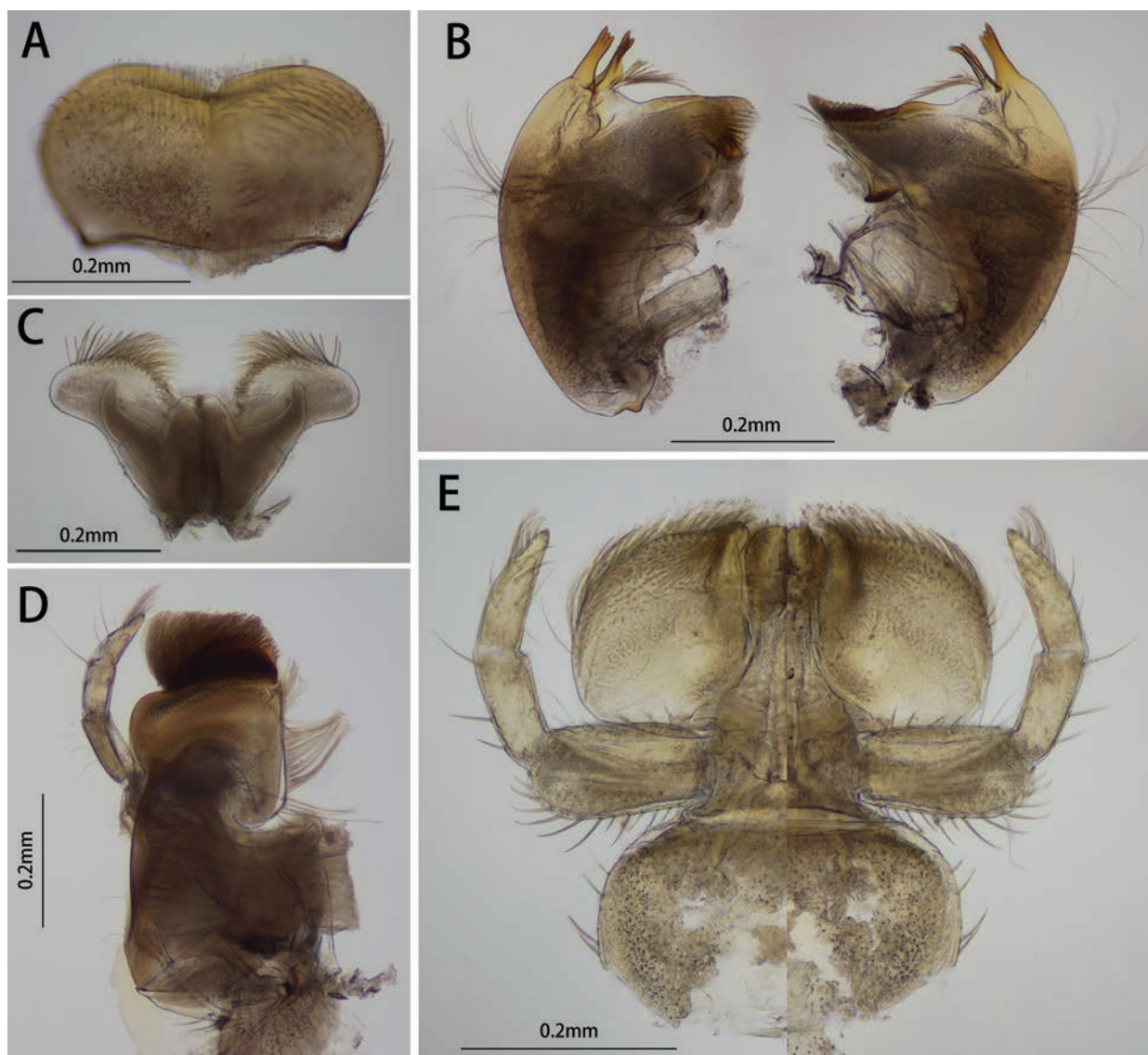


Figure 9. Mouth part of *I. purpurea*: **A** labrum (dorsal view) **B** mandible (left: left mandible / right: right mandible) **C** hypopharynx **D** maxilla (ventral view) **E** labium (left: dorsal view / right: ventral view).

Labium like other *Isca* species, the ratio of 3 segments of labial palp from I to III = 1.3: 0.9: 1.0 (Fig. 9E).

Thorax: Setae on outer margin of femur strong, relatively longer than that on inner margin; inner margin of tibiae and tarsi with stout setae; outer margin of tibiae and tarsi with hair-like setae, those on tibia of hindleg with extra stout setae (Fig. 8C–E). Claw with 11 denticles 4 on inner side small, 1 on outer side biggest (Fig. 8F). Ratio of femora: tibiae: tarsi of forelegs = 2.0: 1.8: 1.0, that of midlegs is 2.3: 1.9: 1.0, and hindlegs = 2.5: 2.2: 1.0 (Fig. 8C–E).

Abdomen: posterior surface of each tergite with contiguous acute spines, posterolateral projection on segment IX only (Fig. 8A, B). Gills present on segments II to VII of ventral abdomen (Fig. 8B). Gills II to VI similar morphologically, consisted of two slender and unbranched lamella, gill VII with single slender lamella (Fig. 8G, H).

Male imago (in alcohol; also see Gillies 1951 and Peters and Edmunds 1970):

Body length 4.5 mm, generally brownish (Fig. 10). Head: Compound eyes contiguous basally, upper part separated with dark stripes around facets (Fig. 11A).

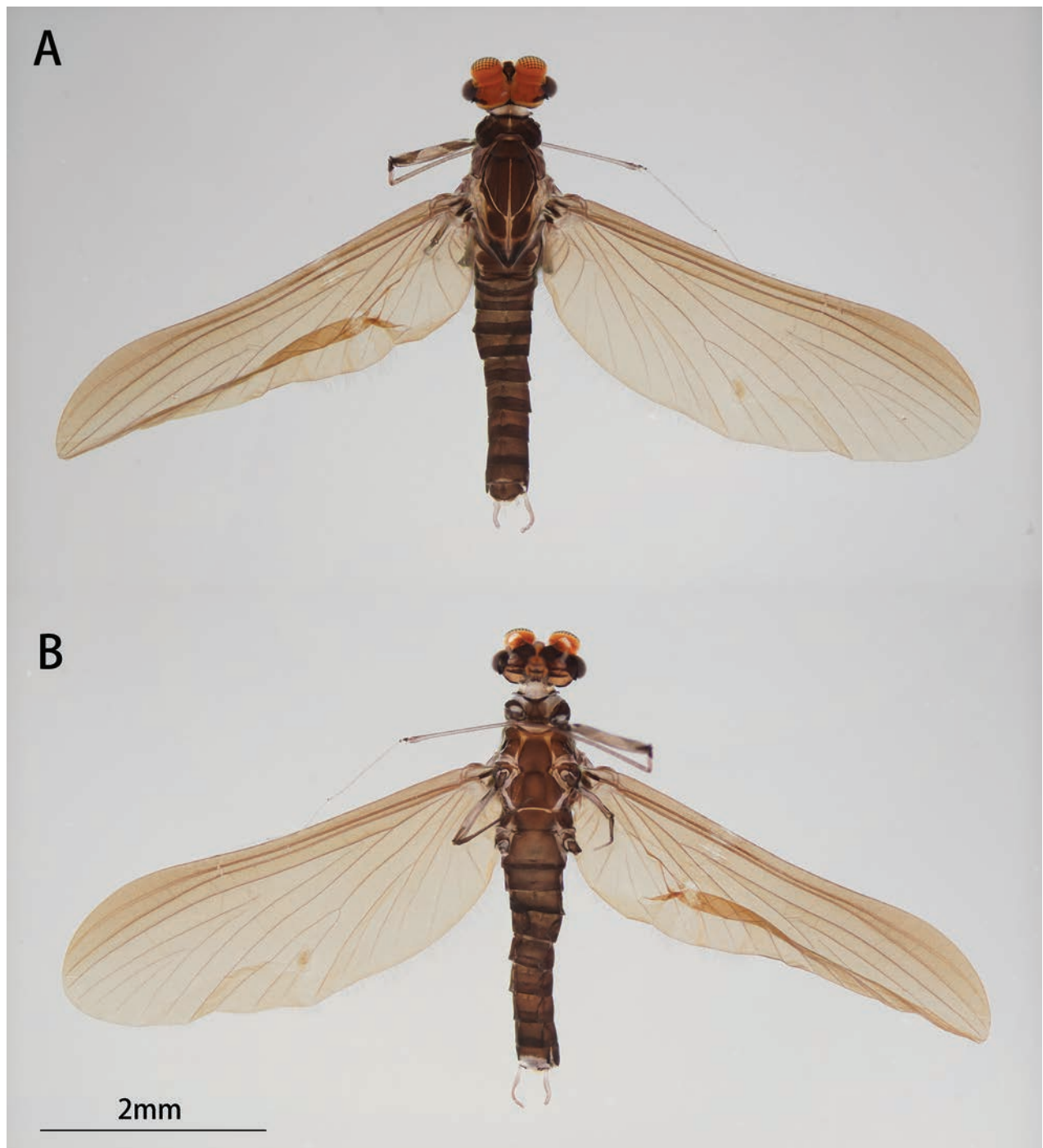


Figure 10. Male imago of *I. purpurea*: **A** dorsal view **B** ventral view.

Legs generally dark brown, mid part of femora slightly lighter than both ends, tarsus of foreleg brownish from base to tip (Fig. 11C). Ratio of femur: tibia: tarsus of foreleg = 1.0: 3.1: 3.1, those of midleg and hind leg = 2.9: 2.2: 1.0 and 3.2: 2.5: 1.0, ratio of foretarsal segments from I to V = 1.0: 13.7: 12.5: 8.0: 3.0 (Fig. 11C–E). Claw dissimilar, one hooked and acute, one blunt (Fig. 11F).

Wing brown, transparent; veins clear, posterior margin with cilia, vein MA forked slightly more than 1/2 of distance from base to margin (Fig. 11B).

Abdomen: tergites of both dorsal and ventral view dark brown; tergite IX with posterolateral projection (Fig. 10). Genitalia: forceps brownish, segment I

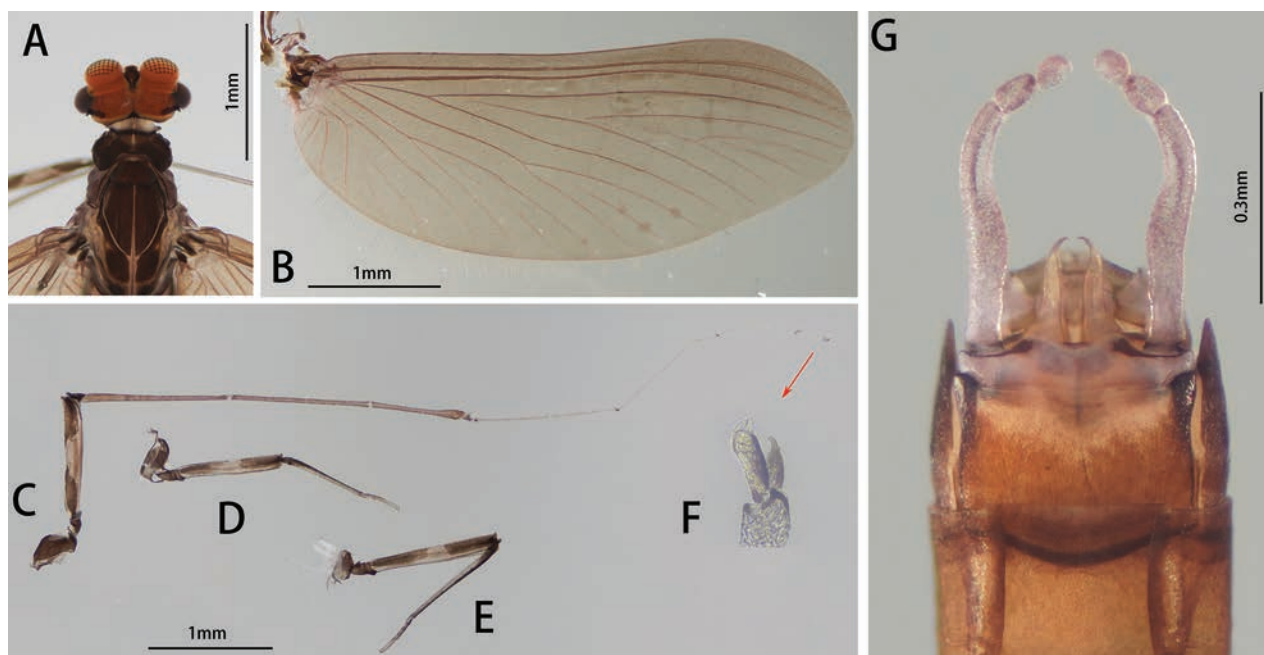


Figure 11. Male structures of *I. purpurea*: **A** head (dorsal view) **B** wing **C** foreleg **D** midleg **E** hindleg **F** claw **G** genitalia (ventral view).

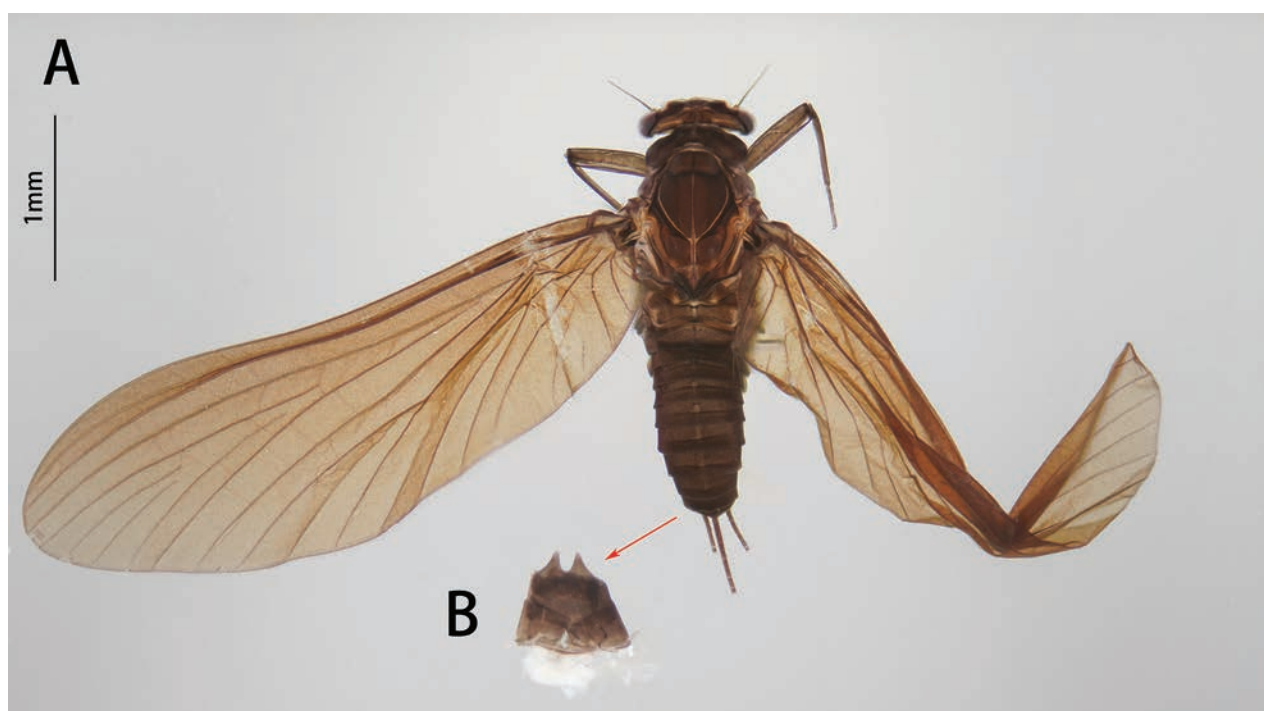


Figure 12. Female structures of *I. purpurea*: **A** female subimago (dorsal view) **B** sternum IX (ventral view).

longest, midpart slightly protuberant inward; segment II slightly longer than III. Penes brownish; broad at base, gradually narrowing to tip; base separated; tips sharp, bend inward; length of penes about 2/5 of forceps (Fig. 11G).

Female (in alcohol): Body length 4.2 mm, terminal filaments brown with spine-like setae. Coloration like male, apex of sternum IX deeply concave (Fig. 12).

Egg. Egg oval, length about 100 μ m, width about 50 μ m, surface covered with subequal small protuberances (Fig. 6B).



Figure 13. Habitat of *I. purpurea*.

Biology. Like *I. acutata*, nymphs of *I. purpurea* were found under stones with coarse surfaces in slow flowing mountain stream; the stream was about 2 m wide with good shade (Fig. 13).

Diagnosis. The nymph of *I. purpurea* can be distinguished from other *Isca* species by the following characters: abdominal terga brown, and abdominal sterna light brown. The male imago of *I. purpurea* can be distinguished by vein MA forked slightly more than 1/2 of the distance from base to margin (Fig. 11B); cilia present on the posterior margin of the wings (Fig. 11B); abdominal terga and sterna dark brown (Fig. 10); forceps and penes brown (Fig. 11G); and penes separated widely at base, tip hook-like, curved inward (Fig. 11G).

Distribution. China (Hong Kong, Guangdong, Fujian, Jiangxi); India.

***Isca fascia* Nguyen & Bae, 2003**

Figs 14, 15

(first record from China)

Isca fascia Nguyen & Bae, 2003: 453–466, figs 20–24 (nymph, male). Type: female nymph, from Vietnam.

Material examined. • 1 male imago 11 nymphs, Ailao Mountain, Yuxi City, Yunnan Province, CHINA, 2200 m a.s.l., 23.970333°N, 101.527147°E, 2022-II-7, Xuhongyi Zheng leg.

Description. (see Nguyen and Bae 2003).

Diagnosis. The nymph of *I. fascia* can be distinguished from other *Isca* species by the following characters: abdominal terga I–II and VII–IX dark brown, terga III–VI light brown (Fig. 14A); abdominal sterna I–VI and X light brown, sterna VII–IX dark brown (Fig. 14B). The male imago of *I. fascia* can be distinguished by: wings translucent, vein MA forked slightly more than 1/2 of distance from base to margin; cilia present on posterior margin of wings (Fig. 15A); abdominal terga I–II and VII–IX dark brown, terga III–VI pale (Fig. 15A); forceps pale (Fig. 15C); penes yellow, large, lateral margin round, fused basally (Fig. 15C).

Distribution. China (Yunnan Prov.); northern Vietnam.

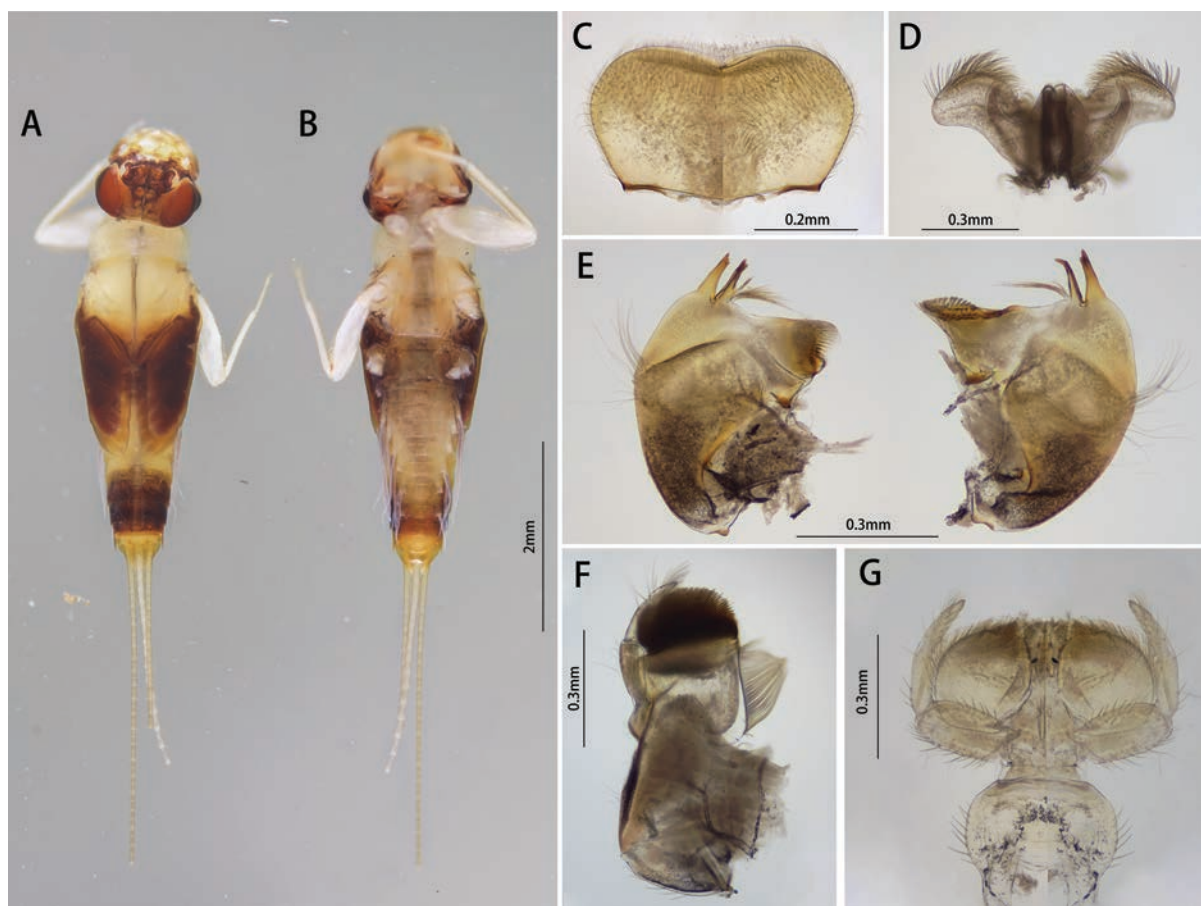


Figure 14. Nymphal structures of *I. fascia*: **A** male nymph (dorsal view) **B** male nymph (ventral view) **C** labrum (left: dorsal view, right: ventral view) **D** hypopharynx **E** mandible (left: left mandible, right: right mandible) **F** maxilla (ventral view) **G** labium (left: dorsal view, right: ventral view).

Genetic distance

Both materials of Chinese *I. purpurea* and *I. acutata* sp. nov. have very close genetic distance. The COI K2P distance of *I. purpurea* is from 0.29% to 1.94%, while that of *I. acutata* sp. nov. is 0.48% (Table 2). So, our morphological identification is supported by genetic distance.

Similarly, three Indian *I. purpurea* populations have short COI sequence distances, which are 1.05% and 11.81% respectively. However, the Chinese *I. purpurea* and Indian *I. purpurea* have relatively large genetic distances: the K2P distance is from 16.47% to 20.12% (Table 2).

Discussion

Gillies (1951) designated the specimens from Hong Kong as types and mentioned there are differences between Indian and Chinese material of *I. purpurea*, stating the Bengal specimen has rather darker eyes. Here we compared the COI sequences of Indian specimens (GenBank: MW160191, ON557588, LC061468, Table 1) and our specimens. The K2P distance of those two populations is from 16.47% to 20.12% (Table 2). This point is reflected in the BI and MP tree (Fig. 16), in which the Chinese *Isca purpurea* and Indian *Isca purpurea* are clustered into two different clades. So, the Indian "*Isca purpurea*" needs more work to confirm its real status.

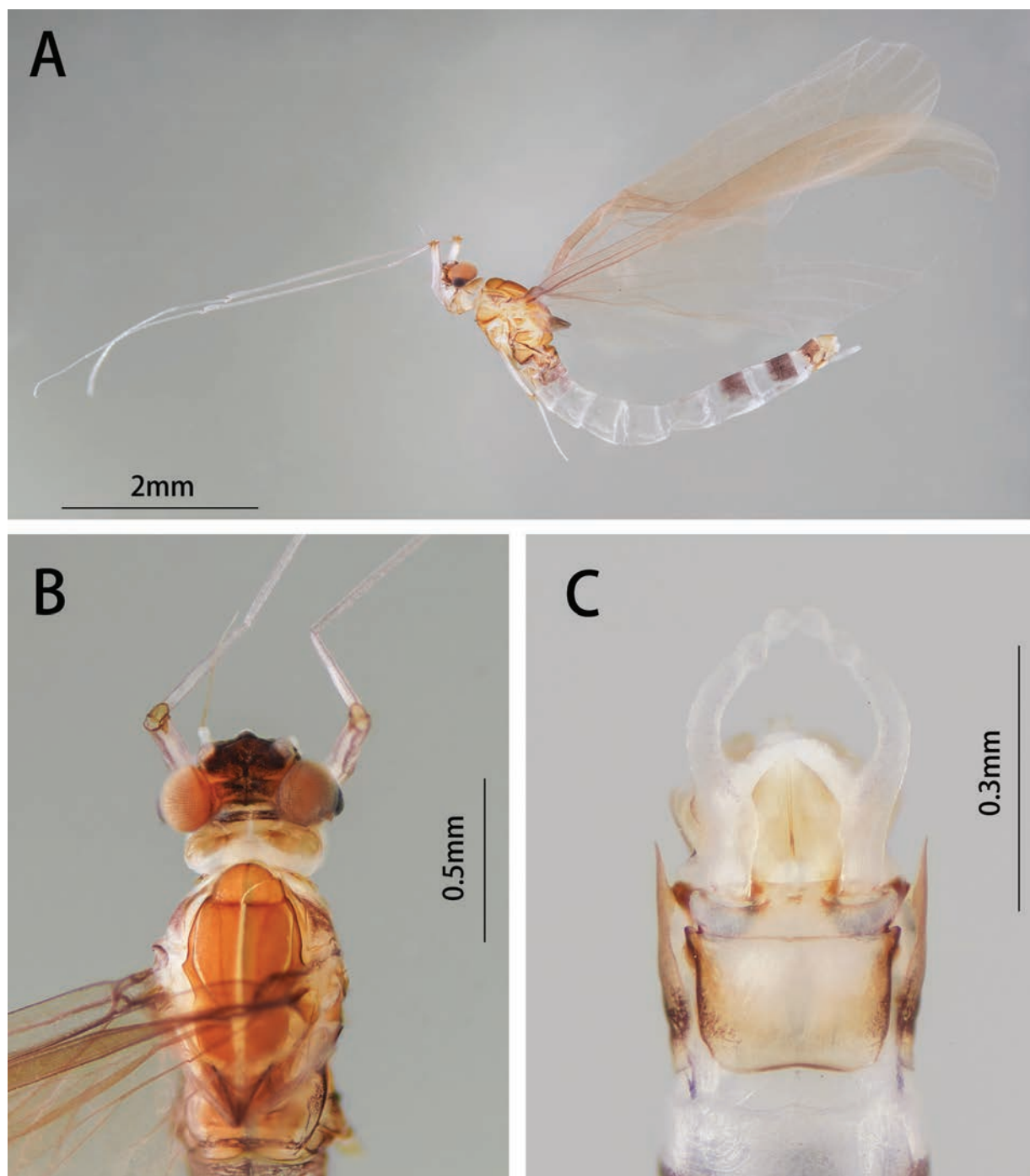


Figure 15. Male structures of *I. fascia*: **A** male imago (lateral view) **B** head (dorsal view) **C** genitalia (ventral view).

Considering these above, together with the huge distance between India and China, we propose that the Indian and Chinese species of *Isca purpurea* could be classified as separate species. Despite certain similarities, further studies are needed to clarify their distinctions (Gillies 1951).

Based on previous research and our study, the distribution of *Isca* spp. is now given (Fig. 17). It is shown that South China has a relatively rich species diversity of genus *Isca*, and we believe South Asia and Southeast Asia contain many more *Isca* species.

Gillies (1951) referred to “subimago” and “subimagines” but did not specify their sexes. Peters and Edmunds (1970) and Nguyen and Bae (2003) did not

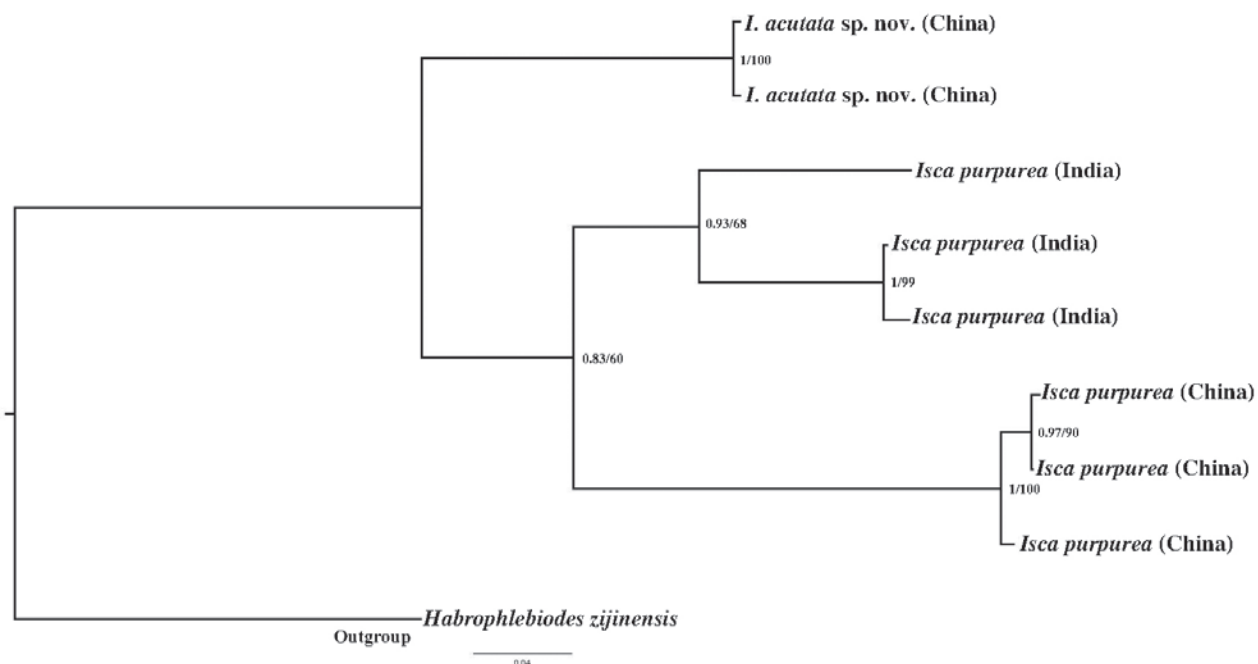


Figure 16. the BI and MP tree upon COI sequences of Indian and Chinese *Isca purpurea*.

mention or describe the subimago stage at all. Kluge (2014) noted that “the *Isca* female subimago does not molt to imago.” In our observations, male adults exhibit both subimaginal and imaginal stages, whereas the female’s subimago represents its final stage. During our rearing process, three female subimagos of the new species, *I. acutata* sp. nov., successfully emerged from nymphs without undergoing any further molts. In contrast, one male individual was able to molt twice from nymph to imago, with the final molt occurring 2–3 hours after it reached the subimago stage. Additionally, the morphology of the female adult, particularly their cerci, is similar to that of the male subimago. Moreover, the female adults of *I. purpurea*, collected from cobwebs and exhibiting empty or nearly empty abdomens, resemble the females of *I. acutata* sp. nov.

The new species, *I. acutata* sp. nov., found in Hainan, is notable as the second species to possess two lamellae on gill VII. Apart from this characteristic, there are no other obvious differences in the nymphs or adults when compared to other known species. Furthermore, the reduction or loss of gills has occurred multiple times across various lineages within Ephemeroptera. Therefore, we consider the presence of bilamellate gills to be a useful diagnostic character, albeit not an essential synapomorphy.

Peters and Edmunds (1970) divided the genus *Isca* into three subgenera (*Isca*, *Minyphlebia*, *Tanycola*) upon imaginal characteristics. However, *I. fascia* has mixed characteristics of those subgenera: 1) like *Minyphlebia*, vein MA forked less than 1/2 of distance from base to margin (Fig. 15A); 2) like *Isca* and *Tanycola*, cilia are present on the posterior margin of the wings (Fig. 15A); and 3) penes are fused basally (Fig. 15C), a unique character, not reported in any subgenera. Under this circumstance, Nguyen and Bae (2003) and Sartori and Derleth (2010) did not place their species *I. fascia* or *I. lea* into any subgenus. Here, the new species *I. acutata* sp. nov. also has the same imaginal characteristics as *I. fascia* and remarkable bilamellate gills VII. So, at this moment, we have not placed our three species into any subgenus here.

Acknowledgements

Additional information

Conflict of interest

Ethical statement

Funding

Author contributions

Author ORCIDs

De-Wen Gong <https://orcid.org/0000-0002-3740-7125>

Chang-Fa Zhou <https://orcid.org/0000-0001-8785-5228>




Data availability

All of the data that support the findings of this study are available in the main text.

References

- Bauernfeind E, Soldán T (2012) The Mayflies of Europe (Ephemeroptera). Apollo Books, Ollerup, 781 pp.
- Edmunds GF, Traver JR (1959) The classification of Ephemeroptera. I. Ephemeroidea: Behningiidae. Annals of the Entomological Society of America 52(1): 43–51. <https://doi.org/10.1093/aesa/52.1.43>
- Gillies MT (1951) Further notes on Ephemeroptera from India and South East Asia. Proceedings of the Royal Society of London (B) 20: 121–130. <https://doi.org/10.1111/j.1365-3113.1951.tb01009.x>
- Kalyaanamoorthy S, Minh BQ, Wong TKF, von Haeseler A, Jermiin LS (2017) ModelFinder: fast model selection for accurate phylogenetic estimates. Nature Methods 14: 587–589. <https://doi.org/10.1038/nmeth.4285>
- Kluge NJ (2014) New Oriental tribe Iscini, new non-dilatognathan species of *Notophlebia* Peters & Edmunds 1970 and independent origin of *Dilatognathus*-type mouth apparatus in Atalophlebiinae (Ephemeroptera: Leptophlebiidae). Zootaxa 3760(4): 522–538. <https://doi.org/10.11646/zootaxa.3760.4.2>
- Lestage JA (1930) Contribution à l'étude des larves des Ephéméroptères. V. – Les larves à trachéo-branchies ventrales. Bulletin et Annales de la Société Entomologique de Belgique 69: 433–440.
- Miller MA, Wayne P, Terri S (2011) The CIPRES science gateway: A community resource for phylogenetic analyses. In: Towns J (Ed.) Proceedings of the 2011 TeraGrid Conference: Extreme Digital Discovery. Association for Computing Machinery, New York, 41: 1–8. <https://doi.org/10.1145/2016741.2016785>
- Nguyen VV, Bae YJ (2003) The mayfly family Leptophlebiidae (Ephemeroptera) from Vietnam. Insecta Koreana 20(3–4): 453–466.
- Peters WL, Edmunds Jr GF (1970) Revision of the generic classification of the Eastern Hemisphere Leptophlebiidae (Ephemeroptera). Pacific Insects 12: 157–240.
- Ronquist F, Teslenko M, Mark PVD, Ayres DL, Darling A, Höhna S, Larget B, Liu L, Suchard MA, Huelsenbeck JP (2012) MrBayes 3.2: Efficient Bayesian phylogenetic inference and model choice across a large model space. Systematic Biology 61(3): 539–542. <https://doi.org/10.1093/sysbio/sys029>
- Sartori M, Derleth P (2010) The dipterous Leptophlebiidae of Borneo (Insecta, Ephemeroptera). Zootaxa 2490: 33–39. <https://doi.org/10.11646/zootaxa.2490.1.3>
- Selvakumar C, Sivaramakrishnan KG, Janarthanan S (2016) DNA barcoding of mayflies (Insecta: Ephemeroptera) from South India. Mitochondrial DNA Part B 1(1): 651–655. <https://doi.org/10.1080/23802359.2016.1219623>
- Stamatakis A (2014) RAxML version 8: A tool for phylogenetic analysis and post-analysis of large phylogenies. Bioinformatics 30(9): 1312–1313. <https://doi.org/10.1093/bioinformatics/btu033>
- Zheng XHY, Zhou CF (2021) First detailed description of adults and nymph of *Cincticostella femorata* (Tshernova, 1972) (Ephemeroptera: Ephemerellidae). Aquatic Insects 42: 23–36. <https://doi.org/10.1080/01650424.2020.1871026>
- Zheng X, Gong D, Qiang X, Zhou C (2024) A new genus and a new species of Behningiidae from China contributing new insights to the evolution of the family (Insecta: Ephemeroptera). Oriental Insects 58(3): 536–567. <https://doi.org/10.1080/00305316.2024.2312271>

Intruders in beehives? New bee-associated *Ellingsenius* species (Pseudoscorpiones, Cheliferidae) from China based on morphological data and molecular analyses, with comments on pseudoscorpion-bee relationships

Zhizhong Gao¹, Jianzhou Sun², Feng Zhang²

¹ Department of Biology, Xinzhou Normal University, Xinzhou, Shanxi 034000, China

² The Key Laboratory of Zoological Systematics and Application, Institute of Life Science and Green Development, Hebei University, Baoding, Hebei 071002, China

Corresponding authors: Zhizhong Gao (gaozhizhong1987@126.com); Feng Zhang (dudu06042001@163.com)

Abstract

Ellingsenius renae sp. nov., encountered in Guizhou, southern China and the eighth species of the genus, is described and illustrated. An analysis of the *COI* mitochondrial gene (LC01490/HC02198) confirms the identity of the new species. An identification key to all *Ellingsenius* species is provided, and comments on the pseudoscorpion-bee relationships are included.

Key words: China, *COI* gene, phoresy, pseudoscorpions



Academic editor: Jana Christophoryová

Received: 12 December 2024

Accepted: 19 March 2025

Published: 11 April 2025

ZooBank: <https://zoobank.org/EF5F6B2A-6FD2-4761-94E8-3E7A5C44F25C>

Citation: Gao Z, Sun J, Zhang F (2025) Intruders in beehives? New bee-associated *Ellingsenius* species (Pseudoscorpiones, Cheliferidae) from China based on morphological data and molecular analyses, with comments on pseudoscorpion-bee relationships. ZooKeys 1234: 259–274. <https://doi.org/10.3897/zookeys.1234.144259>

Copyright: © Zhizhong Gao et al.
This is an open access article distributed under terms of the Creative Commons Attribution License (Attribution 4.0 International – CC BY 4.0).

Introduction

The pseudoscorpion family Cheliferidae Risso, 1827 is nearly cosmopolitan in distribution, occurring on all land masses and many oceanic islands. Although cheliferids are mostly found in leaf litter and under tree bark, some are phoretic on tree-dwelling insects (Harvey 1985) or occur in the nests of vertebrates. Cheliferidae is divided into two subfamilies, Cheliferinae and Philomaoriinae (Harvey 1992; WPC 2025) and currently includes 312 taxa, including 282 species, nine subspecies, eight nominotypical subspecies, and 12 fossil species, assigned to 64 genera, including five fossil genera (WPC 2025). Only 10 species in six genera have been reported from China (Schawaller 1995; Gao and Zhang 2012; Zang and Zhang 2019; WPC 2025).

The genus *Ellingsenius* Chamberlin, 1932, a member of the subfamily Cheliferinae, was established by Chamberlin (1932) and is widely distributed in the Afrotropical, Indo-Malayan, and Mediterranean regions. There is a single suspect occurrence in the Nearctic. The genus differs from all other genera of the family Cheliferidae in having three galeal setae on the chelicerae (Murthy and Ananthakrishnan 1977). *Ellingsenius* currently includes only seven valid species (Judson 1990; WPC 2025), which are all associated with beehives (Gonzalez et al. 2008).

Pseudoscorpions have been recently reported in colonies of the eastern honey bee (*Apis cerana cerana* Fabricius, 1793) in China (Lin et al. 2020); they were assigned to *Ellingsenius* based on a bioinformatics analysis where the sequences were compared to the NCBI GenBank database using the BLAST tool with the MegaBlast algorithm. Although Lin et al. (2020) did not present any morphological data, their phylogenetic study showed that the pseudoscorpions might represent a new species of *Ellingsenius*.

We recently received some pseudoscorpion specimens collected from beehives from Guizhou province, China, which were easily attributed to the genus *Ellingsenius* using morphological criteria. However, we found characters that differed from all known species, and these specimens are here described as *E. renae* sp. nov. Molecular analyses were also performed to clarify the status of the new species. This allows us to describe the *Ellingsenius* species morphologically from China for the first time, which expands the distributional range of the genus.

Materials and methods

Morphology

The specimens examined for this study are preserved in 75% alcohol and deposited in the Museum of Hebei University (**MHBU**) (Baoding, China). Photographs, drawings and measurements were taken using a Leica M205A stereomicroscope equipped with a Leica DFC550 Camera. Detailed examination was carried out with an Olympus BX53 general optical microscope. Temporary slide mounts were prepared in compliance with the method outlined by Gao et al. (2017). Images were edited and formatted using Adobe Photoshop 2022.

Terminology and measurements follow Chamberlin (1931) with some minor modifications to the terminology of trichobothria (Harvey 1992; Judson 2007) and chelicera (Judson 2007). The chela and chelal hand are measured in lateral view and others taken in dorsal view. All measurements are given in mm unless noted otherwise. Proportions and measurements of pedipalps and carapace correspond to length/width, those of legs to length/depth.

The following abbreviations are used for the trichobothria: *b* = basal; *sb* = subbasal; *st* = subterminal; *t* = terminal; *ib* = interior basal; *isb* = interior subbasal; *ist* = interior subterminal; *it* = interior terminal; *eb* = exterior basal; *esb* = exterior subbasal; *est* = exterior subterminal; *et* = exterior terminal. Cheliceral setae: *gs* = galeal; *es* = exterior; *is* = interior; *sb* = subbasal; *b* = basal.

Molecular methods

We extracted total genomic DNA from pseudoscorpion chela and legs using the QIAGEN DNeasy Blood & Tissue Kit (Qiagen Inc., Valencia, CA), following the manufacturer's protocols with the elution buffer volume used is 60 µl. We used the primer pair LCO1490/HCO2198 (Folmer et al. 1994) to amplify *COI* sequences under the following PCR reaction protocol: initial denaturation at 94 °C for 5 min; 35 cycles of denaturation at 94 °C for 30 s, annealing at 45 °C for 40 s, and elongation at 72 °C for 1 min; and final extension at 72 °C for 7 min.

The 25 µl PCR reactions included 12.5 µl of 2×Tag Master Mix (KangWei Biotech, Beijing, China), 0.8 µl of each forward and reverse 10 µM primer, 4 µl of genomic DNA, and 6.9 µl of double-distilled H₂O. The PCR products were visualized by agarose gel electrophoresis (1% agarose). All PCR products were purified and sequenced at Sangon Biotech (Shanghai, China) Co., Ltd.

Sequence alignments were carried out using MAFFT v. 7.313 (Kato and Standley 2013) with the L-INS-I strategy, and checked for the presence of stop codons of *COI* by translating them into amino acid sequence using Geneious Prime (Kearse et al. 2012). Ambiguously aligned positions were culled using trimAl v. 1.2 (Capella-Gutiérrez et al. 2009) with default parameters. The final alignment as Suppl. materials 1, 2. The pairwise genetic distances (Kimura 2-parameter K2P) were calculated using MEGA v. 11 (Tamura et al. 2021) to assess the genetic differences (with pairwise deletion option).

Phylogenetic analyses were performed under the assumptions of maximum likelihood (ML) with GTR+I model and Bayesian inference (BI) with GTR model, respectively. The best-fit nucleotide substitution model was tested using ModelFinder (Kalyaanamoorthy et al. 2017) in PhyloSuite v. 1.2.3 software (Zhang et al. 2020). The ML analysis was conducted using IQ-TREE v. 1.6.8 (Nguyen et al. 2015) in PhyloSuite. The robustness was evaluated by 5000 bootstrap pseudo replicates. BI analysis was performed using MrBayes v. 3.2.6 (Ronquist et al. 2012) (2×10^6 generations) in PhyloSuite, in which the initial 25% of the sampled data was discarded as burn-in. The remaining trees were used to assess posterior probabilities for nodal support. The resulting trees were visualized and edited using FigTree v. 1.4.4 (Rambaut 2018).

Results

Taxonomy

Family Cheliferidae Risso, 1827

Subfamily Cheliferinae Risso, 1827

Ellingsenius Chamberlin, 1932

Type species. *Chelifer sculpturatus* Lewis, 1903, by original designation.

Ellingsenius renae Gao & Zhang, sp. nov.

<https://zoobank.org/3FEDC5B9-6643-46ED-BFA8-6CBD91171D6C>

Figs 1–5

Chinese name: 任氏蜂伪蝎

Type material. Holotype: CHINA • ♂; Ps.-MHBU-HBUARA#GZ23122701, Huohua Town, Ziyun Miao and Buyei Autonomous County, Anshun City, Guizhou Province; 25°37'46"N, 105°59'12"E; 27 November 2023, Xiaoxiao Ren leg.; collected in bee hives of *Apis cerana cerana*. **Paratype:** • 6 ♂♂ Ps.-MHBU-HBUARA#GZ23122702–07; same data as holotype • 5 ♀♀, Ps.-MHBU-HBUARA#GZ23122708–12, same data as holotype.



Figure 1. *Ellingsenius renae* sp. nov., a bee-associate pseudoscorpion, found in bee hives of *Apis cerana cerana* in southern China. Photographs by Dr Xiaoxiao Ren.

Diagnosis. The new species is distinguished from other members of the genus *Ellingsenius* by the following combination of characters: posterior disc of carapace and tergites I–X with wrinkled surface and lateral keels; both transverse furrows on carapace prominent; carapace, pedipalpal trochanter, femur and retrolateral surface of petella with developed tubercles; middle teeth of both pedipalpal fingers concave outwards, forming a large gap; *gs* of cheliceral movable finger tripled; coxal sac and atrium absent; tarsi with dorsal projection; tarsus IV without tactile seta.

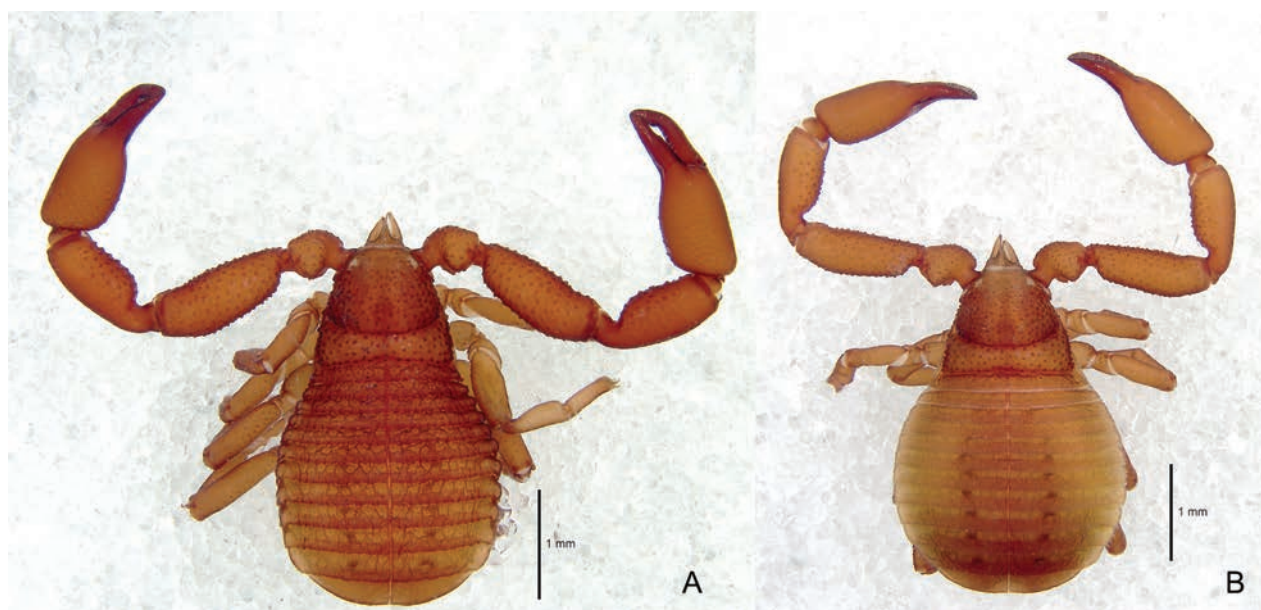


Figure 2. *Ellingsenius renae* sp. nov. **A** holotype male, dorsal view **B** paratype female, dorsal view.

Etymology. The specific epithet is a patronym in honor of Dr Xiaoxiao Ren, who collected the specimens. It is a noun in the genitive.

Description. Adult male (Fig. 2A)

Color: Carapace, pedipalps, and tergites reddish brown; remaining parts (legs, sternites, and pleural membranes) yellowish brown.

Cephalothorax (Fig. 3A): carapace barely longer than wide ($0.91\text{--}0.95\times$), with a pair of eyespots; both transverse furrows prominent, distance between posterior furrow and posterior margin slightly shorter than that between posterior furrow and anterior furrow; carapace strongly granulate and with scattered larger setiferous tubercles; anterior margin with 10, posterior margin with 7–8 setae; anterior disc with c. 140, median with 75–76 and with 28–30 (243–246 in total) dentate setae, and those of anterior and median discs set on large tubercles; posterior disc with wrinkled modification; setae of carapace and tergites short and denticulate; posterior margin of carapace and tergites I–X with sclerotic lateral keels.

Chelicera (Fig. 5B): chelicera small, with two acuminate setae and two lyri-fissures on hand, $1.43\text{--}1.46\times$ as long as broad, movable finger with three short, curved subdistal seta, *b* and *sb* dentate, *gs* of movable finger tripled; fixed finger with 3–4 continuous, pointed teeth; apex of movable finger with one developed tooth; serrula exterior with 27–29 lamellae; lamina exterior present; rallum (Fig. 5C) composed of three blades, distalmost blade slightly dentate; galea (Fig. 5D) relatively long and simple, with 7–8 small, distal rami.

Pedipalp (Figs 3B, C, 5A, E, F): stout; all segments evenly granulated, except for smooth chelal fingers; trochanter, femur (dorsal and ventral), ventral side of patella, and hand adorned with scattered, setiferous tubercles; all setae denticulate. Apex of pedipalpal coxa with 3–4 setae, including one long seta. Chelal fingers stout; movable finger with 26–28 teeth; fixed finger with 29–32 teeth; distal ones larger, middle teeth of both fingers concave outwards, forming a large gap; venom apparatus present in both fingers; nodus ramosus (Fig. 5E): close to *st* on movable finger and to *est* on fixed finger. Trichobothrial patterns

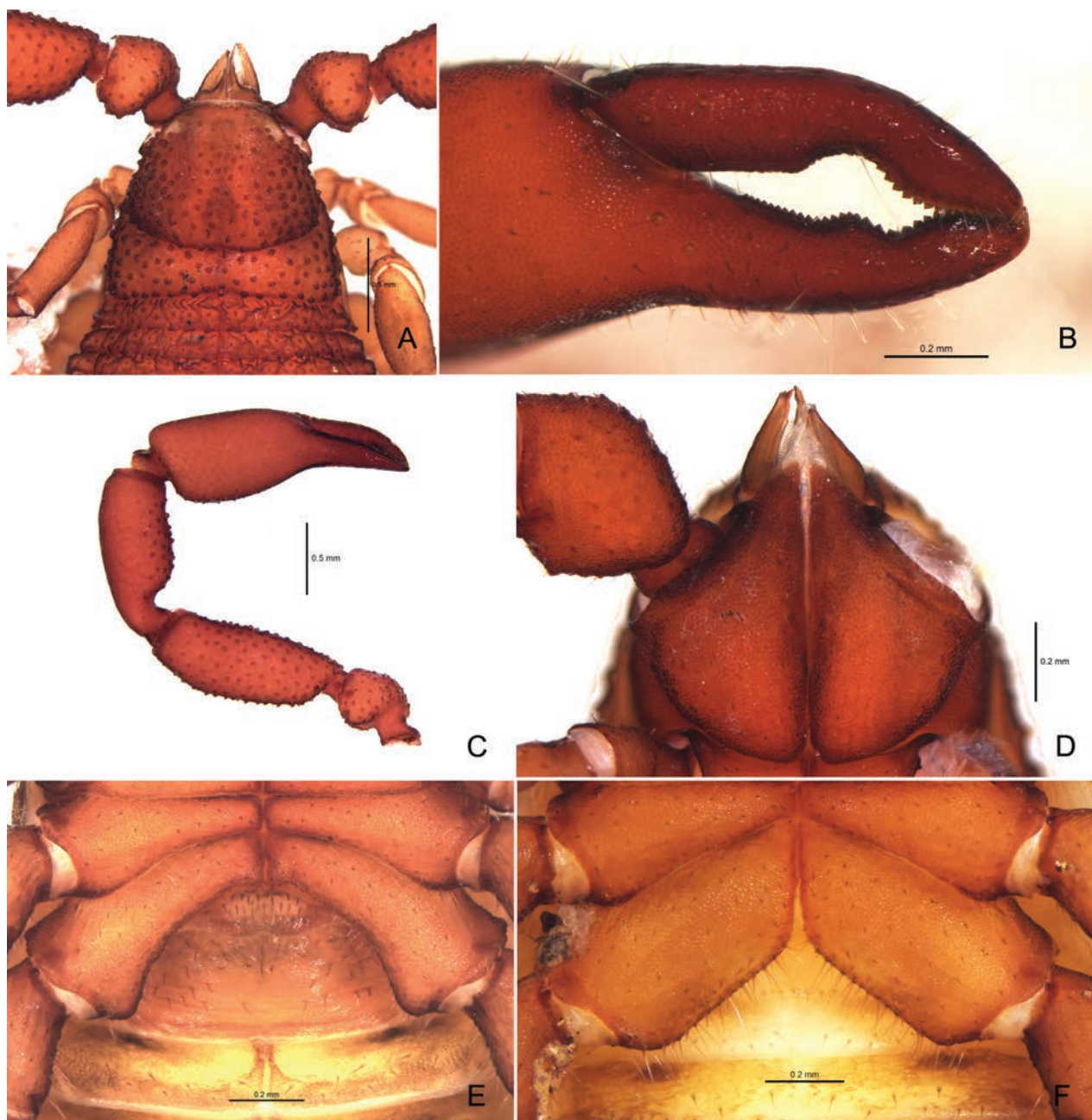


Figure 3. *Ellingsenius renae* sp. nov. **A–E** holotype male **A** carapace, dorsal view **B** left chelal fingers, lateral view **C** left pedipalp, dorsal view **D** pedipalpal coxa, ventral view **E** genital region, ventral view **F** paratype female, genital region, ventral view.

(Fig. 5E): *eb* and *esb* basally situated; *est* and *ist* medially situated; *t* far from apex of movable finger; *st* closer to *t* than to *sb*; distance between *sb* and *b* somewhat longer than distance between *esb* and *eb*. Proportions (length to breadth): trochanter 1.41–1.49×; femur 2.55–2.80×; patella 2.47–2.51×; chela with pedicel 3.20–3.39×, without pedicel 2.90–3.10×; hand with pedicel 1.80–2.00×, without pedicel 1.52–1.69×. Proportion of movable finger 0.75–0.78× as long as hand with pedicel, and 0.89–0.92× without pedicel.

Opisthosoma: all tergites divided by narrow, obvious median line; each half of tergites with 1–4 lyrifissures and 9–14 short, dentate setae on posterior margin, with finely granulated and wrinkled surface; tergite XI without pseudotactile seta and wrinkled modification. Coxa I with 18–21, II 19–20, III 30–32, IV with

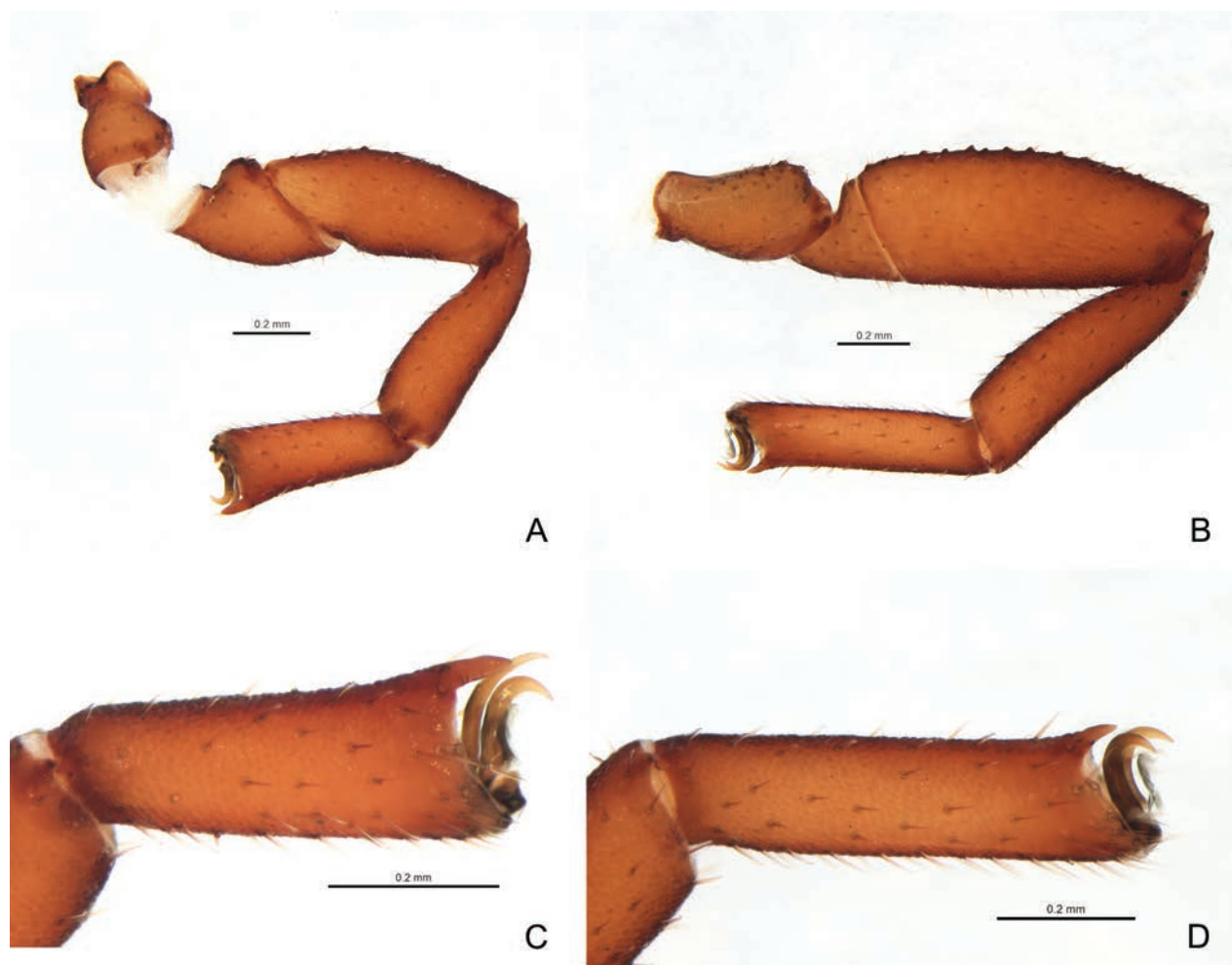


Figure 4. *Ellingsenius renae* sp. nov., holotype male **A** left leg I, lateral view **B** left leg IV, lateral view **C** left tarsus I, lateral view **D** left tarsus IV, lateral view.

45–50 setae. Coxal sacs of male vestigial; atrium absent. Sternites narrowly divided, with fine granulation, each half-sternites with 1–5 lyrifissures and 7–12 setae, all setae short and denticulate. Pleural membrane with irregular longitudinal grooves. Posterior margin of anterior genital operculum with 17–19 setae; posterior genital operculum with 29–34 forwardly projecting setae.

Legs (Figs 4A–D, 5G–J): legs generally typical, stout. Legs I–IV covered with coarse granulation. Setae of leg I short and denticulate. Leg I: trochanter 1.33–1.74×, femur 1.74×, patella 2.58–2.70×, tibia 2.59–3.26×, tarsus 2.58–2.84× longer than deep. Tarsi with dorsal projection; tarsus I modified terminally, claws asymmetrical: anterior claw almost rectangular-curved; posterior claw slender and acute. Leg IV with short and denticulate setae. Tarsus IV without tactile setae, claws symmetrical, arolium slightly shorter than claws; subterminal setae long and simple. Trochanter 1.52–1.96×, femur + patella 2.95–3.24×, tibia 3.83–4.23×, tarsus 3.76–4.56× longer than deep.

Dimensions (length/width or, in the case of the legs, length/depth in mm; ratios in parentheses). Body length 3.21–3.57. Chelicera 0.33–0.35/0.23–0.24. Carapace 1.21–1.27/1.28–1.39. Pedipalp: trochanter 0.62–0.64/0.43–0.44; femur 1.30–1.43/0.51; patella 1.21–1.23/0.49; chela with pedicel 1.92–2.00/0.59–0.60; length of chela without pedicel 1.74–1.83; length of hand

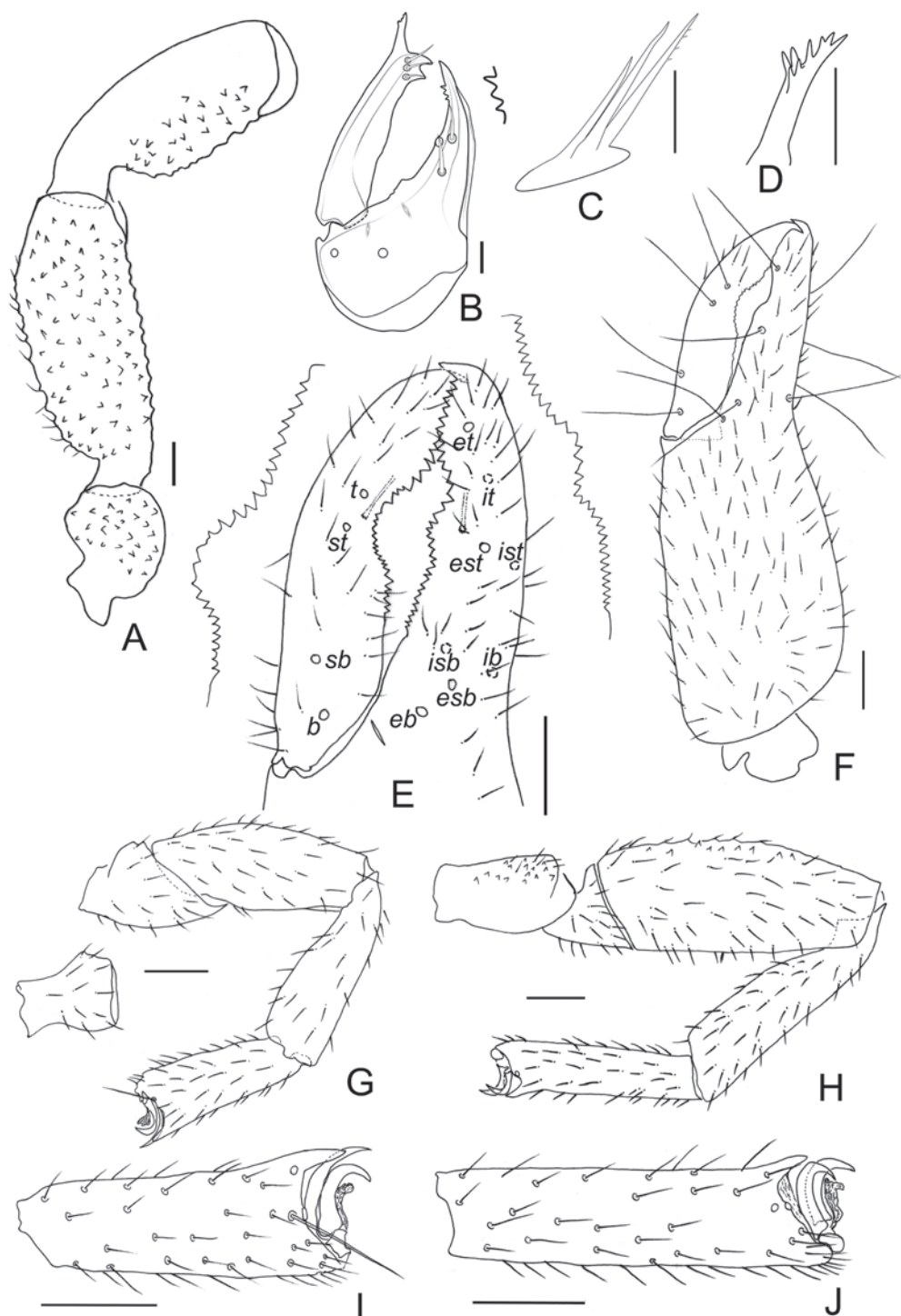


Figure 5. *Ellingsenius renae* sp. nov., holotype male **A** left pedipalp, minus chela, dorsal view **B** left chelicera, dorsal view **C** rallum **D** galea **E** left chelal fingers, lateral view, showing trichobothrial pattern and teeth **F** left chela, lateral view **G** left leg I, lateral view **H** left leg IV, lateral view **I** tarsus I, lateral view **J** tarsus IV, lateral view. Scale bars: 0.05 mm (**B–D**); 0.2 mm (**A, E–J**).

with pedicel 1.08–1.18, without pedicel 0.91–1.00; length of movable finger 0.84–0.89. Leg I: trochanter 0.32–0.47/0.24–0.27; femur 0.47/0.27; patella 0.67–0.73/0.26–0.27; tibia 0.62–0.70/0.19–0.27; tarsus 0.49–0.54/0.19. Leg IV: trochanter 0.50–0.51/0.26–0.33; femur + patella 1.12–1.23/0.38; tibia 0.88–0.93/0.22–0.23; tarsus 0.64–0.73/0.16–0.17.

Female paratype (Figs 2B, 3F). Color slightly lighter than males. Chelicera 1.43–1.48× as long as broad. Carapace slightly longer than wide (0.80–0.93×); chaetotaxy of carapace: anterior margin with 10, posterior margin with 7–8 denticulate setae; a total of c. 260 setae. Posterior margin of carapace and tergites I–IX with vestigial lateral keels, all tergites and sternites IV–XI narrowly divided; each half tergites with 1–3 lyrifissures and 10–15 short and dentate setae on posterior margin, with fine granulation and wrinkled skin; tergite XI without pseudotactile seta and wrinkled modification; each half–sternites with 2–3 lyrifissures and 6–11 setae, all setae short and denticulate, all galea broken.

Proportions of pedipalp: trochanter 1.27–1.28×; femur 2.77–2.93×; patella 2.64–2.67×; chela with pedicel 3.50–3.51×, without pedicel 3.20–3.25× as long as broad. Hand with pedicel 1.91–1.93×, without pedicel 1.63–1.65× as long as broad. Movable finger 0.84× as long as hand with pedicel, 0.97–0.99× without pedicel. Leg I: trochanter 1.21–1.24×; femur 1.57–1.59×; patella 2.54–2.67×; tibia 3.05×; tarsus 3.13–3.43× longer than deep. Leg IV: trochanter 1.42–1.47× longer than deep; femur + patella 3.37–3.39× longer than deep; tibia 4.05–4.09× longer than deep; tarsus 4.06–4.24× longer than deep.

Body length 3.34–3.36. Chelicera 0.33–0.34/0.23. Carapace 1.23–1.24/1.32–1.55. Pedipalp: trochanter 0.57–0.64/0.45–0.50; femur 1.30–1.32/0.45–0.47; patella 1.19–1.23/0.45–0.46; chela with pedicel 1.89–1.93/0.54–0.55; length of chela without pedicel 1.73–1.79; length of hand with pedicel 1.04–1.05; length of hand without pedicel 0.88–0.91; length of movable finger 0.87–0.88. Leg I: trochanter 0.29–0.31/0.24–0.25; femur 0.44–0.46/0.28–0.29; patella 0.71–0.72/0.27–0.28; tibia 0.61–0.64/0.20–0.21; tarsus 0.48–0.50/0.14–0.16. Leg IV: trochanter 0.53–0.54/0.36–0.38; femur + patella 1.28–1.29/0.38; tibia 0.89–0.90/0.22; tarsus 0.69–0.72/0.17.

Distribution. Known only from the type locality.

Remarks. *Ellingsenius renae* sp. nov. is morphologically most similar to *E. indicus* Chamberlin, 1932, as they share the following characters: tarsi with dorsal projection, coxal sacs of male vestigial, atrium absent, and similar trichobothrial pattern. The new species can be distinguished in having tergites I–IX with lateral keels in *E. indicus*, while they are with sclerotic lateral keels in *E. renae*. Pedipalps are slender in *E. renae* (femur 2.55–2.80× vs 2.30–2.40× in *E. indicus*), the carapace has a distinct longitudinal furrow in *E. indicus* (absent in *E. renae*), and the pedipalpal fingers have a larger gap in the new species (Fig. 3B; Chamberlin 1932, 1949). Furthermore, the phylogenetic analyses indicated that our samples belong to a distinct species.

Molecular analyses

All sequences have been deposited in GenBank, with the accession numbers of the DNA barcodes provided in Table 1. The K2P genetic distance of intraspecific and interspecific nucleotide divergences of eight sequences of *Ellingsenius* are shown in Table 2.

Although the specimens of *Ellingsenius renae* (ZZG001, ZZG002) were collected at localities > 1100 km away from the specimens reported by Lin et al. (2020) (MK722156, MK722157), they have a relatively low genetic distance (0.3–0.8%), which was much lower than the interspecific genetic distance in

Table 1. Voucher specimen and sequences information.

| Species | Voucher code | Sex | GenBank accession number | Collection localities | Source |
|--------------------------------------|--------------|--------|--------------------------|-----------------------|-----------------------|
| <i>Ellingsenius renae</i> sp. nov. | ZZG001 | Female | PQ730040 | China, Guizhou | This study |
| <i>E. renae</i> sp. nov. | ZZG002 | Male | PQ730041 | China, Guizhou | This study |
| <i>E. sp.</i> | – | – | MK722157 | China, Anhui | Lin et al. (2020) |
| <i>E. sp.</i> | – | – | MK722156 | China, Anhui | Lin et al. (2020) |
| <i>E. ugandanus</i> | – | – | KU755526 | Kenya | Fombong et al. (2016) |
| <i>E. indicus</i> | – | – | KT354340 | Nepal | Harvey et al. (2015) |
| <i>E. ugandanus</i> | – | – | KU755528 | Kenya | Fombong et al. (2016) |
| <i>E. ugandanus</i> | – | – | KU755527 | Kenya | Fombong et al. (2016) |
| <i>Chelifera cancroides</i> | – | – | OR601911 | Greece | Just et al. (2023) |
| <i>Hysterochelifera tuberculatus</i> | – | – | OR601885 | France | Just et al. (2023) |

Table 2. Intraspecific and interspecific nucleotide divergences for eight sequences of *Ellingsenius*, using Kimura 2-parameter model.

| Species | MK722157 | MK722156 | KU755526 | KT354340 | KU755528 | KU755527 | PQ730040 | PQ730041 |
|-----------------------------------|----------|----------|----------|----------|----------|----------|----------|----------|
| MK722157 <i>E. sp.</i> | | | | | | | | |
| MK722156 <i>E. sp.</i> | 0.008 | | | | | | | |
| KU755526 <i>E. ugandanus</i> | 0.172 | 0.179 | | | | | | |
| KT354340 <i>E. indicus</i> | 0.148 | 0.148 | 0.152 | | | | | |
| KU755528 <i>E. ugandanus</i> | 0.172 | 0.179 | 0.000 | 0.152 | | | | |
| KU755527 <i>E. ugandanus</i> | 0.172 | 0.179 | 0.000 | 0.152 | 0.000 | | | |
| PQ730040 <i>E. renae</i> sp. nov. | 0.005 | 0.003 | 0.158 | 0.124 | 0.158 | 0.158 | | |
| PQ730041 <i>E. renae</i> sp. nov. | 0.008 | 0.005 | 0.156 | 0.126 | 0.156 | 0.156 | 0.002 | |

other species (12.4–17.9%) (Table 2) in the dataset. Consequently, we consider *E. renae* and Lin et al.'s (2020) undescribed species to be conspecific.

The intraspecific genetic distance ranged from 0–0.8%, and the interspecific genetic distance ranged from 12.4–17.9%. All maximum intraspecific distances were much lower than minimum interspecific distances for all species in this study and the optimal identification threshold of 4.7% for Chthoniidae and 3.6% for Neobisiidae (Hlebec et al. 2023). The results of Kimura 2-parameter genetic distances confirm the associated matching of male and female in our dataset.

The ML and BI analyses result in the same relationships for the *Ellingsenius* clade (Fig. 6). The topology of the ML tree (Fig. 6), equivalent to that of the BI phylogram, showed three clades representing three *Ellingsenius* species. The monophyly of *E. indicus* and *E. renae* were strongly supported (uBV = 87%, pp = 0.99; uBV = 100%, pp = 1) and *E. ugandanus* was the sister group to *E. indicus* and *E. renae* (uBV = 98%, pp = 1). The present phylogenetic analyses result also support *E. renae* and *E. sp.* (MK722156, MK722157) as being conspecific.

Key to species of *Ellingsenius*

- 1 Chelal hand with many well-developed tubercles **2**
- Chelal hand with few vestigial tubercles or without tubercles **3**
- 2 Tergites smooth, carapace with vestigial transverse furrows ***E. perpustulatus***
- Tergites strongly granulate and sculptured, carapace with prominent transverse furrows ***E. hendrickxi***

- 3 Pedipalps stout, femur < 2.5× and patella < 2.0× longer than broad.....**4**
- Pedipalp slender, femur > 2.5× and patella > 2.0× longer than broad.....**5**
- 4 Chelal fingers longer than hand..... ***E. globosus***
- Chelal fingers clearly shorter than hand***E. indicus***
- 5 Tarsus of legs with well-developed dorsal projections..... ***E. renae***
- Tarsus of legs with vestigial or without dorsal projections**6**
- 6 All surfaces of pedipalpal femur and patella with tubercles***E. sculpturatus***
- Only prolateral surface of pedipalpal femur and patella with tubercles**7**
- 7 Pedipalpal femur and patella with few well- developed tubercles
..... ***E. ugandanus***
- Pedipalpal femur and patella with a larger number of vestigial tubercles ..
..... ***E. fulleri***

Discussion

Fifteen pseudoscorpion species, belonging to six genera in three families, have been reported from colonies of three stingless bee species and two honeybee species, and all *Ellingsenius* species occur as commensals in beehives (Gonzalez et al. 2008). *Ellingsenius renae* sp. nov. was found in the beehives of *Apis cerana cerana* from southern China (Fig. 7), similar to *E. indicus*, which is also associated with *A. c. cerana* (Gonzalez et al. 2008).

Pseudoscorpions are considered beneficial to bees because they eat *Varroa* mites and other pests of bees (Donovan and Paul 2005, 2006; van Toor et al. 2015). However, *E. hendrickxi* Vachon, 1954 preys on the host bees (Vachon 1954), negating their usefulness to apiarists. Based on the observations of apiarists from

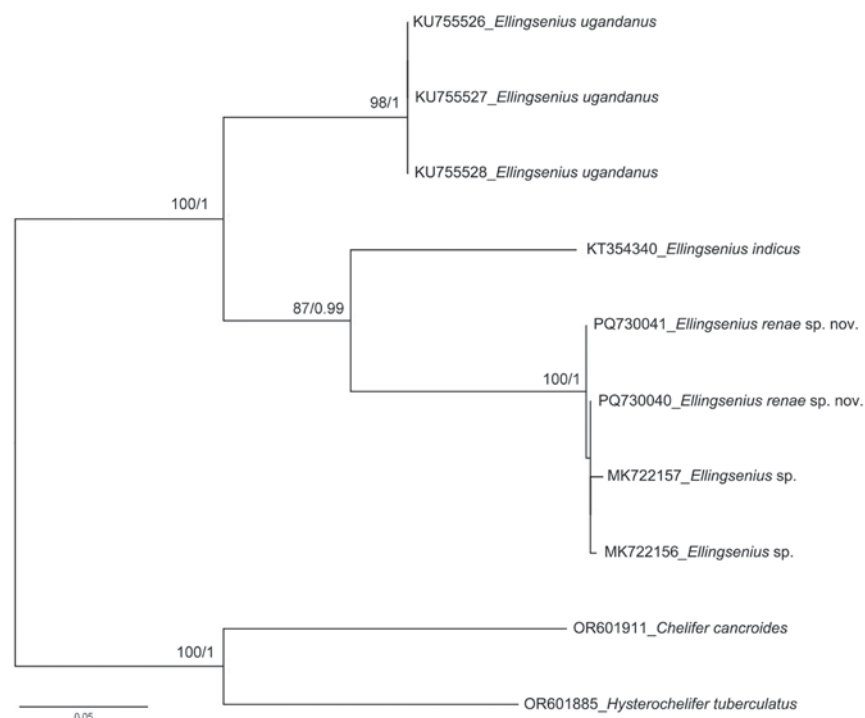


Figure 6. ML phylogram based on *COI* sequence data. The topology is equivalent in both the ML and BI analyses. Support for each node is represented by ultrafast bootstrap values (uBV, %) and posterior probability (pp).

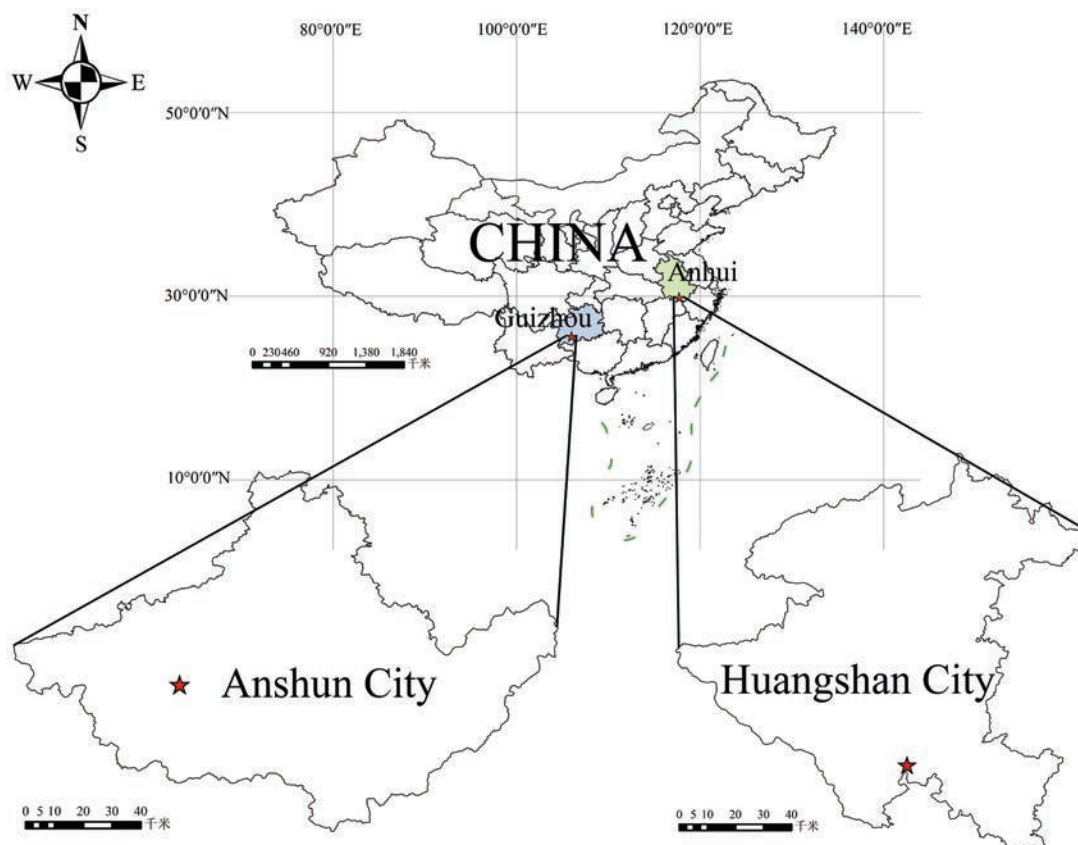


Figure 7. Known distribution areas of *Ellingsenius renae* sp. nov. (Lin et al. 2020).

Guizhou, China, *E. renae* in beehives are usually harmless to the bees; on the contrary, they prey on bee mites that parasitize the beehive. Once *E. renae* individuals appear in a beehive, they are usually found in relatively low numbers, and bees do not attack them. Subsequently, the number of *E. renae* will gradually form a certain population size, and if the number of *E. renae* is too high in a hive, it may affect the activity of the bees. The bees may attempt to drive *E. renae* away, and in this case, *E. renae* will disperse to other hives through phoresy on the bees.

Phoretic behavior is commonly found in pseudoscorpions (Muchmore 1971; Poinar et al. 1998), especially in the Cheliferidae. The characteristic gap in the middle of the chelal fingers in both males and females of *E. renae* sp. nov. (Figs 3B, 5E) may be evidence of phoretic behavior on bees, as pseudoscorpions in the beehive will grasp the legs of bees for phoresy, with the gap allowing a firmer grip.

The ecology of pseudoscorpions in beehives suggests that they have potential as biological control agents of bee pests, especially in controlling bee mites. If pseudoscorpions can effectively control these pests, beekeepers would not need to use chemical agents, which would avoid chemical residues in honey or wax, benefit the environment, and may also avoid the mites' resistance to evolution.

Acknowledgements

We are grateful to Dr Xiaoxiao Ren (Sericulture Institute, Guizhou Academy of Agricultural Sciences, China) for providing the valuable specimens, to Dr Zhao Pan (Hebei University, China) and Dr Zhaoyi Li (Hebei University, China) for their

assistance in the molecular analysis, to Dr Mark S. Harvey (Western Australian Museum, Australia) for his valuable comments on the manuscript, to subject editor Dr Jana Christophoryová and two anonymous reviewers for their helpful suggestions that greatly improved this paper.

Additional information

Conflict of interest

The authors have declared that no competing interests exist.

Ethical statement

No ethical statement was reported.

Funding

Financial support was granted by a Program of Ministry of Science and Technology of the People's Republic of China (2015FY210300) to Feng Zhang, by the Fundamental Research Program of Shanxi Province (202403021211040), the Special Project of "1331 Project" to Wutai Mountain Cultural Ecological Collaborative Innovation Center in 2022, and Xinzhou Science and Technology Plan Project (20230214) to Zhizhong Gao.

Author contributions

Conceptualization and Writing – original draft: ZG. DNA extraction: JS. Phylogenetic analyses: ZG. Writing – review and editing: FZ.

Author ORCIDs

Zhizhong Gao  <https://orcid.org/0000-0002-6666-8746>

Jianzhou Sun  <https://orcid.org/0009-0001-4940-7130>

Feng Zhang  <https://orcid.org/0000-0002-3347-1031>

Data availability

All genetic data have been deposited in GenBank. The final alignment are provided on-line as supplementary files.

References

- Capella-Gutiérrez S, Silla-Martínez JM, Gabaldón T (2009) trimAl: a tool for automated alignment trimming in large-scale phylogenetic analyses. *Bioinformatics* 25: 1972–1973. <https://doi.org/10.1093/bioinformatics/btp348>
- Chamberlin JC (1931) The arachnid order Chelonethida. *Stanford University Publications, Biological Sciences* 7: 1–284.
- Chamberlin JC (1932) A synoptic revision of the generic classification of the chelonethid family Cheliferidae Simon (Arachnida) (continued). *Canadian Entomologist* 64: 35–39. <https://doi.org/10.4039/Ent6435-2>
- Chamberlin JC (1949) New and little-known false scorpions from various parts of the world (Arachnida, Chelonethida), with notes on structural abnormalities in two species. *American Museum Novitates* 1430: 1–57.
- Donovan BJ, Paul F (2005) Pseudoscorpions: the forgotten beneficials inside beehives and their potential for management for control of varroa and other arthropod pests. *Bee World* 8: 83–87. <https://doi.org/10.1080/0005772X.2005.11417322>

- Donovan BJ, Paul F (2006) Pseudoscorpions to the rescue. *American Bee Journal*, October 2006: 867–869.
- Folmer O, Black M, Hoeh W, Lutz R, Vrijenhoek R (1994) DNA primers for amplification of mitochondrial cytochrome c oxidase subunit I from diverse metazoan invertebrates. *Molecular Marine Biology and Biotechnology* 3(5): 294–299.
- Fombong AT, Cham DT, Nkoba K, Neethling JA, Raina SK (2016) Occurrence of the pseudoscorpions *Ellingsenius ugandanus* and *Paratemnoides pallidus* in honey bee colonies in Cameroon. *Journal of Apicultural Research* 55(3): 247–250. <https://doi.org/10.1080/00218839.2016.1227553>
- Gao Z, Zhang F (2012) A new species of the genus *Dactylochelifer* Beier from Shanxi, China (Pseudoscorpiones: Cheliferidae). *International Scholarly Research Network Zoology* 2012: 583830. <https://doi.org/10.5402/2012/583830>
- Gao Z, Zhang F, Harvey MS (2017) A modified definition of the genus *Haplochernes* (Pseudoscorpiones: Chernetidae), with a new species from Hainan Island. *Journal of Arachnology* 45: 112–122. <https://doi.org/10.1636/JoA-S-16-042.1>
- Gonzalez VH, Mantilla B, Mahnert V (2008) A new host record for *Dasychernes Inquilinus* (Arachnida, Pseudoscorpiones, Chernetidae), with an overview of Pseudoscorpion-Bee relationships. *The Journal of Arachnology* 35: 470–474. <https://doi.org/10.1636/H06-62.1>
- Harvey MS (1992) The phylogeny and classification of the Pseudoscorpionida (Chelicerata: Arachnida). *Invertebrate Taxonomy* 6: 1373–1435. <https://doi.org/10.1071/IT9921373>
- Harvey MS, Lopes PC, Goldsmith GR, Halajian A, Hillyer MJ, Huey JA (2015) A novel symbiotic relationship between sociable weaver birds (*Philetairus socius*) and a new cheliferid pseudoscorpion (Pseudoscorpiones: Cheliferidae) in southern Africa. *Invertebrate Systematics* 29: 444–456. <https://doi.org/10.1071/IS15027>
- Harvey MS (1985) Zoological catalogue of Australia. In: Walton DW (Ed.) 3: 126–155. Australian Government Publishing Service, Canberra.
- Hlebec D, Podnar M, Kučinić M, Harms D (2023) Molecular analyses of pseudoscorpions in a subterranean biodiversity hotspot reveal cryptic diversity and microendemism. *Scientific Reports* 13: 430. <https://doi.org/10.1038/s41598-022-26298-5>
- Judson MLI (1990) Redescription of the bee-associate *Ellingsenius fulleri* (Hewitt and Godfrey) (Arachnida, Chelonethi, Cheliferidae) with new records from Africa, Europe and the Middle East. *Journal of Natural History* 24: 1303–1310. <https://doi.org/10.1080/00222939000770771>
- Judson MLI (2007) A new and endangered species of the pseudoscorpion genus *Lagynochthonius* from a cave in Vietnam, with notes on chelal morphology and the composition of the Tyrannochthoniini (Arachnida, Chelonethi, Chthoniidae). *Zootaxa* 1627: 53–68. <https://doi.org/10.11646/zootaxa.1627.1.4>
- Just P, Šťáhlavský F, Bogusch P, Astapenková A, Opatova V (2023) Dispersal capabilities do not parallel ecology and cryptic speciation in European Cheliferidae pseudoscorpions (Pseudoscorpiones: Cheliferidae). *Diversity* 15: 1040. <https://doi.org/10.3390/d15101040>
- Kalyaanamoorthy S, Minh BQ, Wong TKF, von Haeseler A, Jermini LS (2017) ModelFinder: fast model selection for accurate phylogenetic estimates. *Nature Methods* 14: 587–589. <https://doi.org/10.1038/nmeth.4285>
- Katoh K, Standley DM (2013) MAFFT multiple sequence alignment software version 7: improvements in performance and usability. *Molecular Biology and Evolution* 30: 772–780. <https://doi.org/10.1093/molbev/mst010>

- Kearse M, Moir R, Wilson AC, Stones-Havas S, Cheung M, Sturrock S, Buxton, S, Cooper A, Markowitz S, Duran, C, Thierer T, Ashton B, Meintjes P, Drummond AJ (2012) Geneious Basic: an integrated and extendable desktop software platform for the organization and analysis of sequence data. *Bioinformatics* 28(12): 1647–1649. <https://doi.org/10.1093/bioinformatics/bts199>
- Lin Z, Chen H, Page P, Wang K, Ji T, Chen G (2020) First record of pseudoscorpions in the Eastern honey bee colonies in China. *Journal of Apicultural Research* 59(4): 515–518. <https://doi.org/10.1080/00218839.2019.1673577>
- Muchmore WB (1971) On phoresy in pseudoscorpions. *Bulletin of the British Arachnological Society* 2: 38.
- Murthy VA, Ananthakrishnan TN (1977) Indian Chelonethi. *Oriental Insects Monograph* 4: 1–210.
- Nguyen LT, Schmidt HA, von Haeseler A, Minh BQ (2015) IQ-TREE: a fast and effective stochastic algorithm for estimating maximum-likelihood phylogenies. *Molecular Biology and Evolution* 32(1): 268–274. <https://doi.org/10.1093/molbev/msu300>
- Poinar Jr GO, Ćurčić BPM, Cokendolpher JC (1998) Arthropod phoresy involving pseudoscorpions in the past and present. *Acta Arachnologica* 47(2):79–96 <https://doi.org/10.2476/asjaa.47.79>
- Rambaut A (2018) FigTree v1.4.4, a graphical viewer of phylogenetic trees. <http://tree.bio.ed.ac.uk/software/figtree/>
- Ronquist F, Teslenko M, van der Mark P, Ayres DL, Darling A, Höhna S, Larget B, Liu L, Suchard MA, Huelsenbeck JP (2012) MrBayes 3.2: efficient Bayesian phylogenetic inference and model choice across a large model space. *Systematic Biology* 61(3): 539–542. <https://doi.org/10.1093/sysbio/sys029>
- Schawaller W (1995) Review of the pseudoscorpion fauna of China (Arachnida: Pseudoscorpionida). *Revue Suisse de Zoologie* 102(4): 1045–1063. <https://doi.org/10.5962/bhl.part.80489>
- Tamura K, Stecher G, Kumar S (2021) MEGA 11: Molecular Evolutionary Genetics Analysis version 11. *Molecular Biology and Evolution* 38(7): 3022–3027. <https://doi.org/10.1093/molbev/msab120>
- Vachon M (1954) Remarques sur un pseudoscorpion vivant dans les ruches d'Abeilles au Congo Belge, *Ellingsenius hendrickxi* n. sp. *Annales du Musée du Congo Belge, Sciences Zoologiques* 1: 284–287.
- van Toor RF, Thompson SE, Gibson DM, Smith GR (2015) Ingestion of *Varroa destructor* by pseudoscorpions in honey bee hives confirmed by PCR analysis. *Journal of Apicultural Research* 54(5): 555–562. <https://doi.org/10.1080/00218839.2016.1184845>
- WPC (2025) World Pseudoscorpiones Catalog. Natural History Museum Bern. <https://wac.nmbe.ch/order/pseudoscorpiones/3> [Accessed on: 2025-3-18]
- Zang X, Zhang F (2019) Newly recorded species of the genus *Dactylochelifer* (Pseudoscorpiones: Cheliferidae) from China. *Acta Arachnologica Sinica* 28(1): 1–6.
- Zhang D, Gao F, Jakovlić I, Zou H, Zhang J, Li WX, Wang GT (2020) PhyloSuite: An integrated and scalable desktop platform for streamlined molecular sequence data management and evolutionary phylogenetics studies. *Molecular Ecology Resources* 20(1): 348–355. <https://doi.org/10.1111/1755-0998.13096>

Supplementary material 1

Sequence alignment

Authors: Zhizhong Gao, Jianzhou Sun, Feng Zhang

Data type: fas

Copyright notice: This dataset is made available under the Open Database License (<http://opendatacommons.org/licenses/odbl/1.0/>). The Open Database License (ODbL) is a license agreement intended to allow users to freely share, modify, and use this Dataset while maintaining this same freedom for others, provided that the original source and author(s) are credited.

Link: <https://doi.org/10.3897/zookeys.1234.144259.suppl1>

Supplementary material 2

Sequence alignment

Authors: Zhizhong Gao, Jianzhou Sun, Feng Zhang

Data type: fas

Copyright notice: This dataset is made available under the Open Database License (<http://opendatacommons.org/licenses/odbl/1.0/>). The Open Database License (ODbL) is a license agreement intended to allow users to freely share, modify, and use this Dataset while maintaining this same freedom for others, provided that the original source and author(s) are credited.

Link: <https://doi.org/10.3897/zookeys.1234.144259.suppl2>

Copulatory mechanism and genital coupling of the longhorn beetle *Moechotypa diphysis* (Coleoptera, Cerambycidae)

Dan-Wen Long¹, Xin Tong¹ 

¹ Guangxi Key Laboratory of Agro-environment and Agric-products Safety, National Demonstration Center for Experimental Plant Science Education, College of Agriculture, Guangxi University, Nanning 530004, Guangxi, China

Corresponding author: Xin Tong (tongxin@gxu.edu.cn)

Abstract

The function of insect external genitalia has played a significant role in exploring insect mating mechanisms and male fertilization strategies. However, due to the privacy of genital coupling, insect copulatory mechanisms have only been investigated in a few insect groups. In this study, we observed the mating behavior using freeze-fixated pairs in copula to reveal the copulatory mechanism of the longhorn beetle *Moechotypa diphysis* (Pascoe, 1871). At the beginning stage of mating, the male *M. diphysis* usually takes 30 min to control the female and then extends its median lobe and endophallus. Approximately 80% of males (19/24) of *M. diphysis* exhibit multiple expansions (the membranous endophallus expands and enters into the female genital tract), ranging from two to five times. There are two types of expansions: short ones lasting for 1.4 to 49 s and long ones ranging from 1.03 to 7.23 min. During copulation, male tarsi continuously grasped the female elytra, thorax, and abdomen to help the male to initiate and maintain copulation. Male genital structures are closely connected to female genital structures: the apical phallomere and flagellum on the male endophallus contacting the bursa copulatrix duct and the spermathecal duct of the female, and the abundant microstructures on the surface of the everted male endophallus directly anchoring the female genital tract. Finally, we discuss the possible reasons for the evolution of their complex mating-related structures. Our research will help to explore the evolutionary mechanisms of insect genital structures.

Key words: Copulation, copulatory mechanism, endophallus, functional morphology, genital structure, insemination, mating behaviour



Academic editor: Francesco Vitali

Received: 29 October 2024

Accepted: 27 February 2025

Published: 17 April 2025

ZooBank: <https://zoobank.org/6C49332C-60C6-4BD4-B8A0-DCC1E9CE946A>

Citation: Long D-W, Tong X (2025) Copulatory mechanism and genital coupling of the longhorn beetle *Moechotypa diphysis* (Coleoptera, Cerambycidae). ZooKeys 1234: 275–290. <https://doi.org/10.3897/zookeys.1234.140491>

Copyright: © Dan-Wen Long & Xin Tong.
This is an open access article distributed under terms of the Creative Commons Attribution License (Attribution 4.0 International – CC BY 4.0).

Introduction

Firm coupling of male and female genitalia during copulation is critical to the success of sperm transfer for insects (Stutt and Siva-Jothy 2001; Chapman 2013; Matthews and Matthews 2010). Therefore, in order to guarantee the stability of genital coupling, males usually evolve diverse reproductive and non-reproductive structures to serve to manipulate and stimulate females, such as claws, hooks, and spines (Arnqvist and Nilsson 2000; Arnqvist and Rowe 2002a, b, 2005; Chapman et al. 2003; Wilson and Crans-ton 2010, 2014; Simmons 2014; Woller and Song 2017; Wulff et al. 2017).

Understanding the roles of mating-related structures in copulation is important for revealing the functional morphology of insect genitalia (Wulff et al. 2017; Kelly and Moore 2016; Woller and Song 2017; Tong and Hua 2019). However, due to the difficulty of observing internal genital structures during copulation, relevant research is very limited.

In recent years, an effective method of freeze-fixation of copulating pairs has been proposed to examine the internal coupling of male and female genitalia (Grieshop and Polak 2012; Dougherty et al. 2015; Zhong et al. 2015; Tong et al. 2017; Woller and Song 2017; Lyu et al. 2018). However, this method has not been applied to the vast majority of insects, including Cerambycidae.

Many studies have delved into the structural functions associated with the mating behavior of longhorn beetles (Galford 1977; Hughes 1981; Akutsu and Kuboki 1983a, b; Iwabuchi 1985; Kuboki et al. 1985; Bianchi et al. 1988; Wang et al. 1990, 1991). Notably, Hubweber and Schmitt (2010) have explored the morphological diversity and functions of specific external genital structures within Cerambycidae. Bi et al. (2022, 2024) have also reported the enormous diversity of male endophallus in morphological structures. However, due to technological limitations, the examination of how the internal genital structures of male and female longhorn beetles interacted during mating remains limited. The application of freeze-fixated technology may gain insights into the internal coupling of male and female genitalia and unravel the functional morphology of Cerambycidae.

Moechotypa diphysis (Pascoe, 1871) (Cerambycidae, Lamiinae, Crossotini) is a common species in China, Russia, Japan and Korea, where it has been identified as an economically significant pest species. Investigating the mating behavior and the genital coupling of *M. diphysis* is crucial for understanding the functional morphology of the genital structures of Cerambycidae.

In this study, we observed the mating process of *M. diphysis* by dissecting the male and female genital systems in genital copula to analyze the functional morphology of male and female genital structures, to shed light on their mating behavior characteristics and elucidate the mode of male sperm transfer. Our research will help to explore the evolutionary mechanisms of insect genital structures.

Material and methods

Insect collection and rearing

The egg-infested wood (tree segments of oak trees *Quercus dentata* Thunb.) were cut down and stored in a temporary laboratory at Huabo Mountain in Kuandian County, Liaoning Province in northeastern China from 2020 to 2022. In the peak period of adult emergence of the second year (May to June and October to November of 2021–2023), the newly emerged adults were collected every day, and their emergence times were recorded. These adults were then individually placed in plastic boxes and promptly transferred to the Entomology Institute of Guangxi University (China) for separate rearing to sexual maturity. Then, twenty females or males of similar age were maintained separately in cages (40 × 30 × 30 cm) containing fresh chestnut branches (*Castanea mollissima*

Blume) to simulate the habitat. A small amount of water was provided to maintain humidity in the cage. The rearing temperature was maintained at 25 ± 1 °C and humidity $75 \pm 5\%$ under a 14:10 h (L:D).

Mating behavior observation

In the preliminary experiment, the adults were observed 24 h per day by people who took shifts for a week to check the circadian rhythms of mating activities. Then, five virgin females and five virgin males (7–10 days old) were randomly selected and placed in a transparent box to observe their mating. After the mating behavior of a pair of couples was recorded, they were removed to the new box immediately, and a new virgin male and female were added to the transparent box to maintain five virgin females and five virgin males. Their courtship behavior, mating process, copulation duration, and the activities of the mating-related structures were observed from noon to midnight. The mating processes were recorded using a Nikon D7100 digital camera. The duration of mounting, the duration of single expansion, and the duration of total expansion were recorded in detail. The duration of one single expansion of less than one minute was defined as a short expansion, and more than one minute was defined as a long expansion (Tong et al. 2024). At the end of the observation, males and females were separated and reared in different cages.

Freeze-fixation of copulating pairs

The *M. diphysis* pairs in copula were frozen through carbon dioxide aerosol spray compressed in hydraulic cans and were immediately fixed in Carnoy's solution at room temperature for 24–48 h to stabilize the interactions of their genital structures and preserved in 75% ethanol.

Microscopic observations

The male and female genital systems of *M. diphysis* adults were dissected under a stereomicroscope (Nikon, SMZ800N). Photographs were taken with a Keyence VHX 6000 digital microscope. For scanning electron microscopy, the endophallus (internal sac) was dissected and then dried for 20 minutes on a glass slide. After that, the samples were coated with a film of gold in a sputter coater (Cressington, 108auto) and finally observed by the scanning electron microscope (FEI, Quattro S) at 5 kV.

Statistical analyses

The length and width of the male and female genital structures were measured three times using Image-J ver. 1.8.0 ($N = 5$ each for males and females). Multi Timer ver. 2.12.1 was used to record the total duration of mating, the total duration of expansion, the duration of a single long expansion, and the duration of a single short expansion for each pair of beetles (a total of 24 pairs were observed). The number of expansions during mating was also recorded. All the data were subjected to statistical analysis using SPSS 20.0, and means and standard errors were calculated.

Results

Mating process

The mating behavior of *M. diphysis* mainly occurs in the afternoon. The complete mating process can be divided into three stages: meeting and mounting, expansion and ejaculation, and guarding after copulation. The detailed process of each stage is described as follows.

In the stage of meeting and mounting, the males exhibit a higher level of activity to search for a suitable mate. Upon approaching a female, the male mounts her back rapidly, and then the female shakes her body. Subsequently, the male flexes his abdomen, extending the lateral lobes to make contact with the female copulatory pore.

This process lasts for 29.31 ± 5.74 min (mean \pm SE, $N = 24$) (Table 1), ranging from 9 s to 2 h. The male then extends the median lobe and expands the endophallus into the copulatory pore at the end of the female abdomen.

In the stage of expansion and ejaculation (Fig. 1A), approximately 20% of males (5/24) expand only once; however, 80% of males (19/24) exhibit multiple expansions. The expansion can be divided into short and long expansions. The duration of short expansions ranges from 1.4 to 49 s, and the duration of long expansions ranges from 1.03 to 7.23 min. Among the males with multiple-expansions behaviors, about 15% of males (3/19) engage in multiple short expansions, and 85% of males (16/19) engage in multiple long expansions. Notably, the duration of the first expansion is usually the longest. During the process of endophallus expansion, the male rubs the base of the female elytra with his forelegs quickly, wiggles his antennae and touches the female with his maxillary palps (Fig. 1B). The average durations of a single expansion, total expansion and total mating for males are 2.39 ± 0.27 min, 6.56 ± 0.57 min, and 70.81 ± 11.15 min (mean \pm SE, $N = 24$), respectively (Table 1).

After mating, the male pulls out the endophallus and mounts the female back to prevent other males from approaching the female (Fig. 1C). During the post-copulatory guarding stage, the female can carve grooves on the branch with her mandibles and lay eggs, completing the mating process.

Table 1. Duration of the mating process of *Moechotypa diphysis* (mean \pm SE, $N = 24$).

| Mounting duration (min) | Short expansion duration (s) | Long expansion duration (min) | Total expansion duration (min) | Expansion times (min) | Total mating duration (min) |
|-------------------------|------------------------------|-------------------------------|--------------------------------|-----------------------|-----------------------------|
| 29.31 ± 5.74 | 3.85 ± 2.12 | 4.29 ± 0.35 | 6.56 ± 0.57 | 2.39 ± 0.27 | 70.81 ± 11.15 |

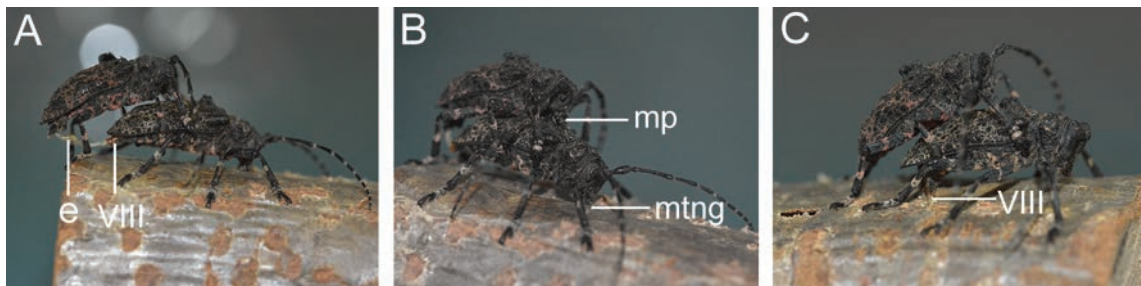


Figure 1. Mating process of *Moechotypa diphysis* **A** male expands the endophallus into the female ovipositor **B** male uses the maxillary palps to lick the female back, and the female carves grooves on branch **C** after copulation, the female lays eggs. Abbreviations: e, endophallus; mp, maxillary palps; mtng, manufacture the notch grooves; VIII, the eighth abdominal segment.

Genital structures of the two sexes

The male and female abdomen of *M. diphysis* adults differ on sternite VII and tergite VII. The male sternite VII and tergite VII are wider and straighter (Fig. 2A), while the female sternite VII and tergite VII are narrower and they have a noticeable indentation at the apex (Fig. 2B).

The aedeagus (Fig. 2C) is formed by the combination of the median lobe with the tegmen, which consists of the paired parameres (lateral lobes) connected to the tegminal struts by the tegminal ring. The tegmen is $432.74 \pm 63.59 \mu\text{m}$ (mean \pm SE, $N = 5$) long and $1036 \pm 26.36 \mu\text{m}$ (mean \pm SE, $N = 5$) wide, and the paramere is $1176.78 \pm 37.06 \mu\text{m}$ (mean \pm SE, $N = 5$) long and $227.20 \pm 16.18 \mu\text{m}$ (mean \pm SE, $N = 5$) wide. The parameres of *M. diphysis* are longer and straighter, compared with those of the cerambycidae *Psacothoe hilaris* (Pascoe, 1871) and *Glenea cantor* (Fabricius, 1787) (Fukaya and Honda 1992; Lu 2007), and equipped with sensory hairs of different lengths (Fig. 2B). The median lobe is $4737.48 \pm 310.15 \mu\text{m}$ (mean \pm SE, $N = 5$) long and $937.25 \pm 111.52 \mu\text{m}$ (mean \pm SE, $N = 5$) wide, and is sclerotized and curved (Fig. 2C).

The female genitalia consist of segment VIII and the ovipositor enclosed within it (Fig. 2D). Segment VIII is trapezoidal, $1961.63 \pm 113.90 \mu\text{m}$ (mean \pm SE, $N = 5$) long and $1604.64 \pm 128.83 \mu\text{m}$ (mean \pm SE, $N = 5$) wide.

Reproductive systems of both sexes and the internal coupling of genitalia

The female reproductive system is composed of ovaries, lateral oviducts, middle oviduct, genital chamber, ovipositor, bursa copulatrix duct, bursa copulatrix, spermathecal duct, spermatheca, and spermathecal glands (Fig. 3A). The paired lateral oviducts of *M. diphysis* converge towards the middle to form a middle oviduct. The middle oviduct, the genital chamber and the ovipositor are three structures connected from top to bottom. There is also a bursa copulatrix duct at the junction of the middle oviduct and the genital chamber, and the bursa copulatrix duct is connected with the bursa copulatrix. The base part of the bursa copulatrix duct branched out into a spermathecal duct, which is successively connected with the spermatheca and the spermathecal glands. The bursa copulatrix is spherical-shaped, significantly enlarged, with a clearly

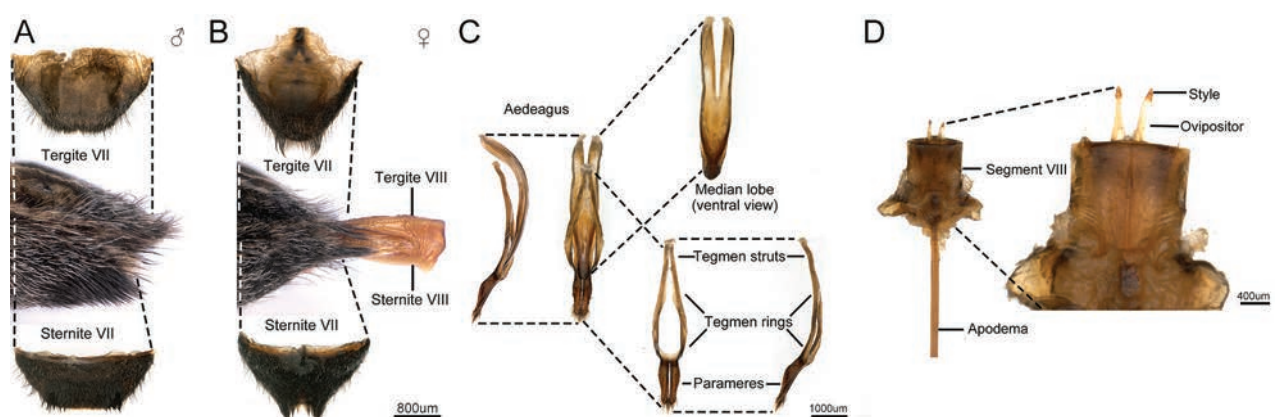


Figure 2. Abdominal apex and genital structures of the male and female *Moechotypa diphysis* adults **A** male **B** female **C** median lobe and tegmen **D** segment VIII and ovipositor (ventral view).

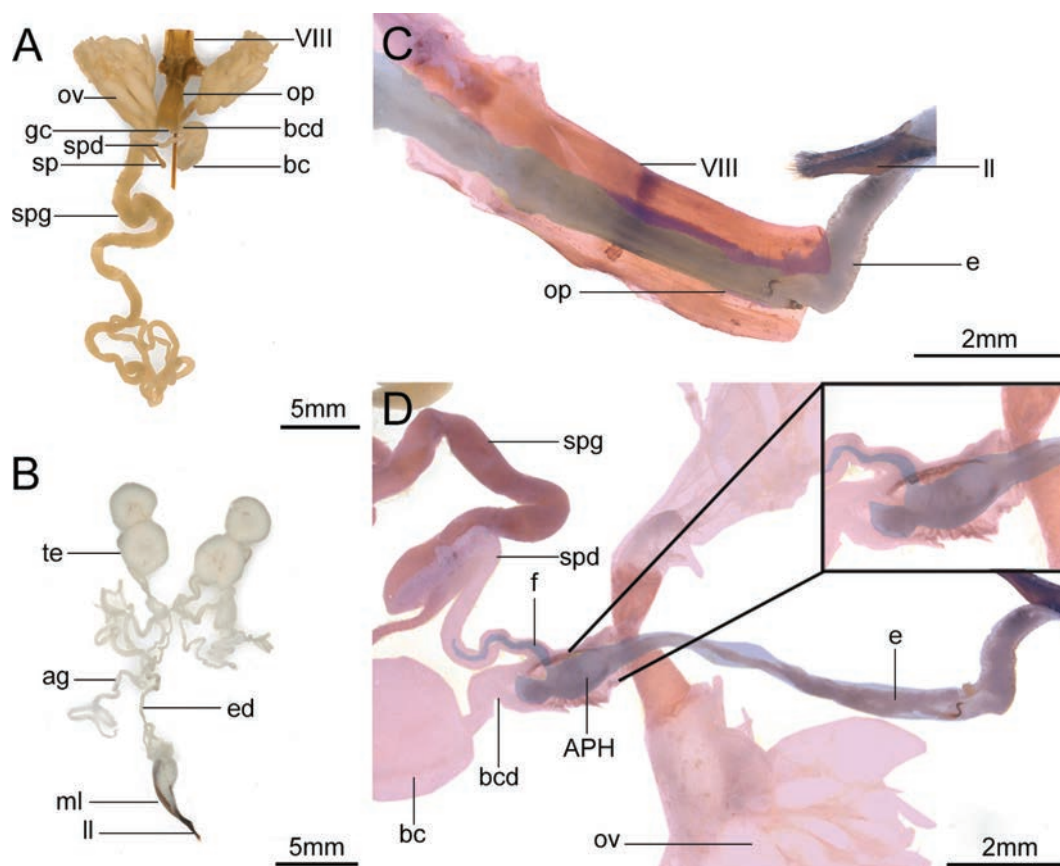


Figure 3. Reproductive system and the genitalia internal connection of *Moechotypa diphysis* **A** reproductive system of the female **B** reproductive system of the male **C** endophallus expands into segment VIII, and the ovipositor **D** apical phallomere enters into the bursa copulatrix duct and flagellum enters into the spermathecal duct. Abbreviations: ag, accessory gland; APH, apical phallomere; bc, bursa copulatrix; bcd, bursa copulatrix duct; e, endophallus; ed, ejaculatory duct; f, flagellum; ll, lateral lobe; ml, median lobe; op, ovipositor; ov, ovary; sp, spermatheca; spd, spermathecal duct; spg, spermathecal gland; te, testis; VIII, the segment VIII.

curved base. The spermatheca is brown, rod-shaped and has 18 hardened rings that resemble springs (Fig. 3A).

The male reproductive system is composed of the testes, one pair of vasa deferentia, two pairs of accessory glands, and one ejaculatory duct (Fig. 3B). The two pairs of testes are white, well-developed and spherical-shaped. After each pair of testes are connected, they enter into the lateral vas deferens. Two pairs of accessory glands of similar length are fused at the base of the lateral vasa deferentia in *M. diphysis*. Two lateral vasa deferentia merge into the ejaculatory duct. The ejaculatory duct is connected to the endophallus. The endophallus is folded inside the middle lobe when unmated (Fig. 3B).

Initially, the mechanical connection of male and female genitalia is established through the median ventral leaf and the median dorsal leaf of the median lobe (Fig. 4B). At the beginning of mating, the male touches the end of the female abdominal copulatory pore with the parameres and then expands the median ventral leaf of the median lobe into the female segment VII. When the male genitalia are fully coupled to the female genitalia, the endophallus is closely pressed against the inner wall of the female genitalia. Specifically, the endophallus is sequentially expanded into segment VIII, the ovipositor (Fig. 3C), the bursa copulatrix duct and the spermathecal duct (Fig. 3D). Finally, the apical phallomere of the endophallus

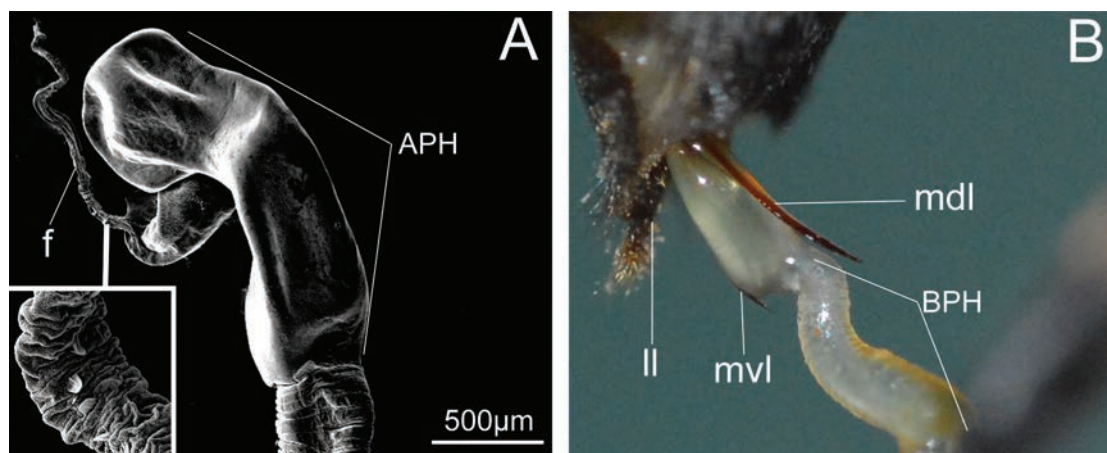


Figure 4. Morphology of a part of endophallus in *Moechotypa diphysis* **A** flagellum and apical phallomere of the endophallus **B** the base of the endophallus is located between the median ventral leaf and median dorsal leaf. Abbreviations: APH, apical phallomere; BPH, basal phallomere; f, flagellum; ll, lateral lobes; mvl, median ventral leaf; mdl, median dorsal leaf.

is expanded into the bursa copulatrix duct to form a stable connection. The flagellum is located just at the opening of the spermathecal duct and enters the vicinity of the spermatheca by expanding the spermathecal duct (Fig. 3D).

Male endophallus in mating

The endophallus is a membranous and tubular structure. Its apical region is composed of an apical phallomere and a flagellum (Fig. 4A). The endophallus is located inside the median lobe of the aedeagus when in repose. It is turned outward from the median lobe (Fig. 4B) and moves to the bursa copulatrix duct and the spermathecal duct during copulation. The endophallus is covered with various microstructures except for the flagellum (Fig. 5). The apical and the basal areas of the phallomere are without spines, while the median phallomere is the area with spines. There are elongated spines, short spines and broad spines in the upper, middle and lower parts of median phallomere (Fig. 5A).

If the median ventral leaf and median dorsal leaf of the median lobe are accidentally disconnected before complete eversion of the endophallus, the endophallus will fail to fully enter the genital chamber, leading to the separation of genitalia and the failure of mating. In such instances, the male needs to reinitiate the process. After the complete eversion of the endophallus, the microstructures of the endophallus contact different areas of the female genital tract.

The surface of the apical phallomere is covered with two different types of leaf-like microstructures (Fig. 5B, C), which are in close contact with the female bursa copulatrix duct. The short spines (Fig. 5D) and elongated spines (Fig. 5E) are in close contact with the female genital chamber. The broad spines (Fig. 5F) and a few sensilla basiconica (Fig. 5G) get in contact with the female ovipositor. However, none of the microstructures penetrate the female genital tissues.

Clamping function and morphological characteristics of male leg

The legs serve as a crucial control structure in male longhorn beetles, facilitating their ability to grasp and secure the female during mating. The forelegs adeptly hold the base of the female elytra. The middle legs firmly secure

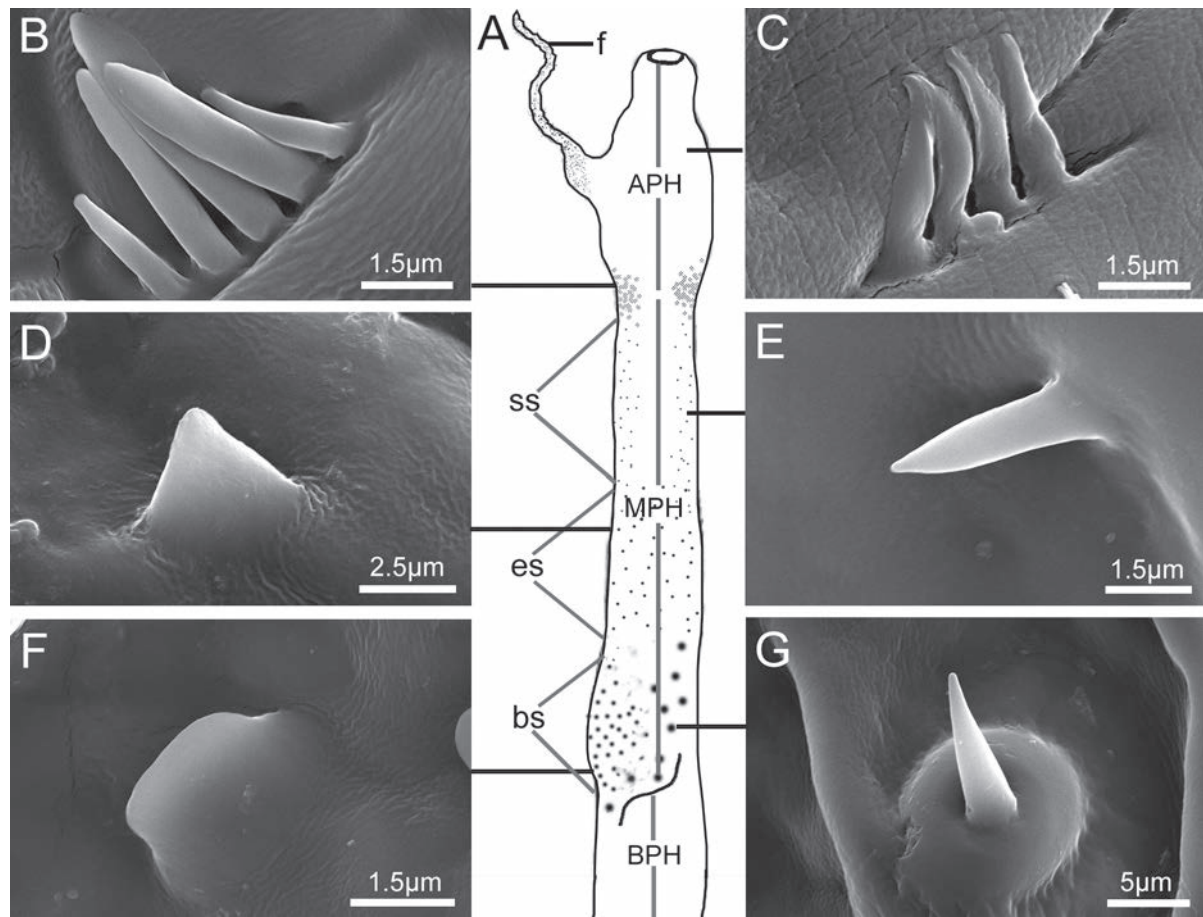


Figure 5. The diverse microstructures on the endophallus surface in *Moechotypa diphysis* **A** surface of the endophallus showing the areas of apical and basal phallomere without spines, and the area of median phallomere with spines **B, C** apical phallomere covered with two different types of leaf-like microstructures **D** middle part of the median phallomere covered with short spines **E** upper part of the median phallomere covered with elongated spines **F** lower part of the median phallomere covered with broad spines **G** region of broad spines on the median phallomere surrounded by sensilla basiconica. Abbreviations: APH, apical phallomere; BPH, basal phallomere; bs, broad spines; es, elongated spines; f, flagellum; MPH, median phallomere; ss, short spines.

the midsection of the female body. The hind legs typically provide support on two sides. No matter how the female shakes, the male can utilize the three pairs of legs to firmly grasp the female during mating.

There is no difference in the structure of the protarsus of the *M. diphysis* between males and females. However, males and females have differences in the shape of the setae and the setules on the surface of the plates. The male protarsus is wider (Fig. 6A) than the female protarsus (Fig. 6C), the setae are spoon-like and the setules are blunter (Fig. 6D).

Discussion

In this study, we investigated the copulation process, genital structures, and the freeze-fixated pairs in the copula of *M. diphysis*. There were multiple endophallus expansions (the membranous endophallus expands and enters into the female genital tract) of various durations during *M. diphysis* mating. The short expansion ranges from 1.4 to 49 s, and the long expansion ranges from 1.03 to 7.23 min. During copulation, male tarsi continuously grasped

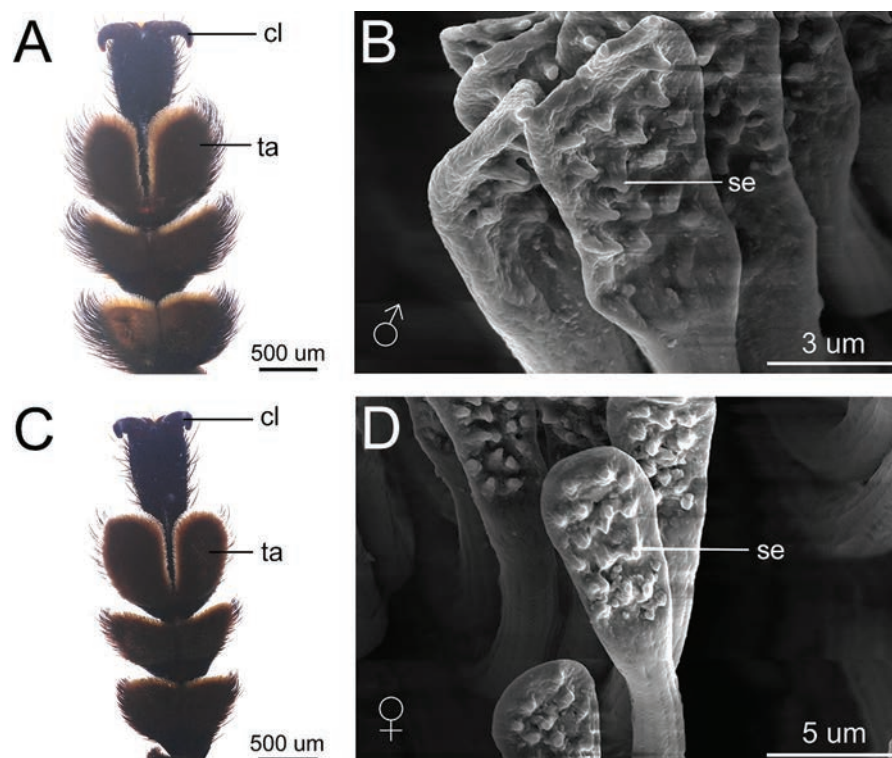


Figure 6. Protarsi and setae of male and female in *Moechotypa diphysis* **A** male protarsus **B** male setae **C** female protarsus **D** female setae. Abbreviations: cl, claws; se, setule; ta, tarsus.

female elytra, thorax, and abdomen to help the male to initiate and maintain copulation. The apical phallomere of the endophallus are in contact with the female bursa copulatrix duct. The microspicules on the surface of the everted male endophallus directly contact the female genital tract. This appears to secure the connection between the male and female genitalia.

The mating processes of Cerambycidae are basically similar, however, there are differences in expansion times and copulation durations among different species (Kim et al. 2006; Fonseca and Zarbin 2009; Luo et al. 2011). For instance, most males of *Monochamus alternatus* (Hope, 1842) and *Psacotheta hilaris* (Pascoe, 1871) perform multiple expansions in a single mating. Each expansion can transfer sperm. The copulation duration can range from seconds to minutes (Fukaya and Honda 1992; Kobayashi et al. 2003). In contrast, *Glenea cantor* (Fabricius, 1787) males expand only once during mating, and their copulation can last several hours (Li et al. 2015). The males of *M. diphysis* frequently exhibit multiple expansions. There are two possible reasons for their multiple expansions: First, it may be attributed to reproductive stress resulting from sperm competition, which has led males to evolve multiple strategies to counteract this stress (Cordero-Rivera 2017). We hypothesize that the multiple expansions could increase male fertilization success by enhancing sperm transfer, thereby potentially producing more offspring. Second, the extension of the male median ventral leaf appears to be unstable. Observations of the mating process reveal that the initial seconds of endophallus expansion coincide with the extension of the male median ventral leaf. The short expansion events are likely indicative of the failed mating, without or with only a small amount of sperm transferred. Therefore, the male needs multiple expansions in order to successfully transfer sperm. We need more experiments to test these hypotheses in the future.

Some structures of the male genital can control females during mating, for example, the grasping apparatus (Arnqvist and Rowe 2005; Edvardsson and Canal 2006; Maroni et al. 2023), achieving rapid fertilization (Eberhard and Huber 1998) or removing the sperm of the competitor (Córdoba-Aguilar 1999; Simmons 2001). In the bruchid beetle *Callosobruchus maculatus* (Fabricius, 1775), the spines of the endophallus penetrate the bursa copulatrix (Crudgington and Siva-Jothy 2000; Blanckenhorn et al. 2002). In other species, such spines can reinforce the mechanical coupling of the female and male genitalia (Düngelhoef and Schmitt 2006; Rönn and Hotzy 2012; Shcherbakov 2023). The surface microstructures (such as spines) of the endophallus of Cerambycidae vary greatly in morphology (Kasatkin 2006; Lu et al. 2007; Hubweber and Schmitt 2010). In *Psacotha hilaris*, the spines are believed to function to remove sperm from competitors (Yokoi 1990). At present, we find that the spines may function to stabilize fertilization due to their contact with the female genital tract. This finding is similar to other research on longhorn beetles, including *Prionoplus reticularis* (White, 1843) (Edwards 1961) and *Dorysthenes granulatus* (Thomson, 1861) (Tong et al. 2024). In addition, there are some sensilla basiconica on the endophallus of *M. diphysis*. These sensilla basiconica have a smooth surface without pores and a ring-shaped base. Based on their morphological characteristic, we believe that these sensilla basiconica are more likely to play a role in mechanical perception (Kerkut and Gilbert 1985; Keil 1997; Zhuge et al. 2010; Zhou et al. 2015). They may serve to locate the female genital tract or receive stimulation from the genital tract.

Besides controlling females, the evolution of the male genitalia may also be related to female oviposition. For example, the males of Cerambycidae Trachyderini or Torneutini have a short endophallus that matches the smaller ovipositor in females (Kasatkin 2006). Compared with other longhorn beetles of genera *Echinovelleda* Breuning, 1936, *Meges* Pascoe, 1866 and *Pseudomeges* Breuning, 1944 (Bi et al. 2022, 2024), the endophallus of *M. diphysis* is significantly different. The flagellum of *M. diphysis* is located on the side of apical phallomere, which is physically more compatible with the spermathecal duct of a female. In *M. diphysis*, the shape of the endophallus of the male and the ovipositor of the female are identical. Therefore, our results support the idea that the morphology of the endophallus of the male and the ovipositor of the female have evolved in mutual adaptation.

The female reproductive fluid (FRF) can generate paternity biases by affecting key traits in sperm competition (Higginson et al. 2012; Pinzoni et al. 2024). The secretions from the spermathecal glands of the honeybee *Apis mellifera* (Linnaeus, 1758) and the cotton boll weevil *Anthonomus grandis* (Boheman, 1843) have been shown to contribute to the activation and sustained movement of sperm (Koeniger 1970; Ruttner and Koeniger 1971; Villavaso 1975). In *M. diphysis*, the sperm is transported to the spermatheca through the flagellum of the endophallus. The spermatheca is connected to the well-developed spermathecal glands. The spermathecal glands of *M. diphysis* are significantly more developed than those of *Monochamus alternatus* (Hope, 1842) and *P. hilaris*. Therefore, we hypothesize that the *M. diphysis* spermatheca may participate in improving sperm vitality or selecting sperm by some secretions of the spermathecal glands.

Generally, the protarsus of male insects is used to grasp the female (Bergsten et al. 2001; Bergsten and Miller 2007; Green et al. 2013), and the setae on the protarsus have the effect of increasing adhesion (Zhang and Liang 2012; Xiong et

al. 2014). The morphological structure of the setae in the protarsus of *M. diphysis* males is similar to that of the *Philonthus cognatus* (Stephens, 1832) males. The most unusual feature of these setae both in *M. diphysis* and *P. cognatus* is the presence of setules on the surface of the plates. Stork (1980) proposed that these structures may act as antimatting devices. Therefore, we believe that the setae of the *M. diphysis* belongs to a kind of adherent seta, and males have a wider protarsus, and their greater number of setae may be better for holding the female.

Our study has unveiled the mating behavior and how males use their genital structures for sperm transfer in *M. diphysis*. We also found that males have a multiple-expansions mating pattern, and we suspect that this reproductive strategy is aimed at reducing the difficulty of sperm competition. Finally, we briefly discuss the possible reason why the spermathecal glands of the *M. diphysis* female are so much better developed than other longhorns with multiple expansion patterns. This is likely related to female choice. It will be necessary to add more cerambycid beetles to increase the rigor and quality of similar studies of insect genitalia and utilize some of the newer methods of investigation, such as laser ablation, X-ray cineradiography, and micro-CT, to investigate the function of the internal and external genitalia in more detail (Schmitt and Uhl 2015).

Acknowledgements

We are grateful to Wen Lu, Xia-Lin Zheng, Qiong-Hua Gao, Le-Yun Wang, Xiao-Yun Wang, and Lu Liu for help in the whole experiment process. We are indebted to Chang-Tai Liu for assistance in the observation of scanning electron microscopy. We also appreciate the assistance of the scientific instrument platform of the State Key Laboratory for Conservation and Utilization of Subtropical Agro-bioresources (Guangxi University) for performing the SEM analysis in this study.

Additional information

Conflict of interest

The authors have declared that no competing interests exist.

Ethical statement

No ethical statement was reported.

Funding

This research is supported by the National Natural Science Foundation of China (Grant No. 32200361), Natural Science Foundation of Guangxi Province (Grant No. 2024GXNS-FBA010440), and the Specific Research Project of Guangxi for Research Bases and Talents (Grant No. AD23026233).

Author contributions

Conceptualization: XT. Data curation: DWL. Funding acquisition: XT. Investigation: DWL. Methodology: XT. Project administration: XT. Resources: XT. Supervision: XT. Validation: DWL. Visualization: DWL. Writing - original draft: DWL. Writing - review and editing: XT.

Author ORCIDs

Xin Tong  <https://orcid.org/0000-0003-1926-0024>

Data availability

The data supporting the findings of this study are available from the corresponding author upon reasonable request.

References

- Akutsu K, Kuboki M (1983a) Mating behavior of the udo longicorn beetle, *Acalolepta luxuriosa* Bates (Coleoptera: Cerambycidae). Japanese Journal of Applied Entomology and Zoology 27(3): 189–196. <https://doi.org/10.1303/jjaez.27.189>
- Akutsu K, Kuboki M (1983b) Analysis of mating behavior of udo longicorn beetle, *Acalolepta luxuriosa* Bates (Coleoptera: Cerambycidae). Japanese Journal of Applied Entomology and Zoology 27(4): 247–251. <https://doi.org/10.1303/jjaez.27.247>
- Arnqvist G, Nilsson T (2000) The evolution of polyandry: multiple mating and female fitness in insects. Animal Behaviour 60(2): 145–164. <https://doi.org/10.1006/anbe.2000.1446>
- Arnqvist G, Rowe L (2002a) Antagonistic coevolution between the sexes in a group of insects. Nature 415(6873): 787–789. <https://doi.org/10.1038/415787a>
- Arnqvist G, Rowe L (2002b) Correlated evolution of male and female morphologies in water striders. Evolution 56(5): 936–947. <https://doi.org/10.1111/j.0014-3820.2002.tb01406.x>
- Arnqvist G, Rowe L (2005) Sexual Conflict. Princeton University Press, Princeton, New Jersey, 29–40. <https://doi.org/10.1515/9781400850600>
- Bergsten J, Miller KB (2007) Phylogeny of diving beetles reveals a coevolutionary arms race between the sexes. PLoS ONE 2(6): e522. <https://doi.org/10.1371/journal.pone.0000522>
- Bergsten J, Toyra A, Nilsson AN (2001) Intraspecific variation and intersexual correlation in secondary sexual characters of three diving beetles (Coleoptera: Dytiscidae). Biological Journal of the Linnean Society 73(2): 221–232. <https://doi.org/10.1111/j.1095-8312.2001.tb01359.x>
- Bi WX, Chen CC, Lin MY (2022) Taxonomic studies on the genera *Meges* Pascoe, 1866 and *Pseudomeges* Breuning, 1944 from China (Coleoptera, Cerambycidae, Lamiinae, Lamiini). Zootaxa 5120(2): 242–250. <https://doi.org/10.11646/zootaxa.5120.2.4>
- Bi WX, Mu C, Lin MY (2024) Taxonomic studies on the genera *Echinovelleda* Breuning, 1936 and *Propedicellus* Huang, Huang & Liu, 2020 (Coleoptera, Cerambycidae, Lamiinae, Lamiini). Zootaxa 5399(1): 65–78. <https://doi.org/10.11646/zootaxa.5399.1.5>
- Bianchi A, Cirio U, DeBellis E (1988) Mating behaviour of *Saperda carcharias* L. (Coleoptera: Cerambycidae). I. Partner localization and copulation. Proceedings of the 15th Italian National Entomology Congress 825–832.
- Blanckenhorn WU, Hosken DJ, Martin OY, Reim C, Teuschl Y, Ward PI (2002) The costs of copulating in the dung fly *Sepsis cynipsea*. Behavioral Ecology 13(3): 353–358. <https://doi.org/10.1093/beheco/13.3.353>
- Chapman RF (2013) The Insects: Structure and Function (5th edn.). Cambridge University Press, Cambridge, 282–312.
- Chapman T, Arnqvist G, Bangham J, Rowe L (2003) Sexual conflict. Trends in Ecology and Evolution 18(1): 41–47. [https://doi.org/10.1016/S0169-5347\(02\)00004-6](https://doi.org/10.1016/S0169-5347(02)00004-6)
- Cordero-Rivera A (2017) Sexual conflict and the evolution of genitalia: male damselflies remove more sperm when mating with a heterospecific female. Scientific Reports 7(1): 7844. <https://doi.org/10.1038/s41598-017-08390-3>
- Córdoba-Aguilar A (1999) Male copulatory sensory stimulation induces female ejection of rival sperm in a damselfly. Proceedings of the Royal Society B-Biological Sciences 266(1421): 779–784. <https://doi.org/10.1098/rspb.1999.0705>

- Crudgington HS, Siva-Jothy MT (2000) Genital damage, kicking and early death. *Nature* 407(6806): 855–856. <https://doi.org/10.1038/35038154>
- Dougherty LR, Rahman IA, Burdfield-Steel ER, Greenway EV, Shuker DM (2015) Experimental reduction of intromittent organ length reduces male reproductive success in a bug. *Proceedings of the Royal Society B-Biological Sciences* 280(1808): 20150724. <https://doi.org/10.1098/rspb.2015.0724>
- Düngelhoef S, Schmitt M (2006) Functional morphology of copulation in Chrysomelidae—Criocerinae and Bruchidae (Insecta: Coleoptera). *Bonner Zoologische Beiträge* 1(4): 201–208.
- Eberhard WG, Huber BA (1998) Copulation and sperm transfer in *Archiseopsis* flies (Diptera, Sepsidae) and the evolution of their intromittent genitalia. *Studia Dipterologica* 5: 217–248.
- Edvardsson M, Canal D (2006) The effects of copulation duration in the bruchid beetle *Callosobruchus maculatus*. *Behavioral Ecology* 17(3): 430–434. <https://doi.org/10.1093/beheco/arj045>
- Edwards JS (1961) Anomalous development of ovaries in *Prionoplus reticularis* White (Coleoptera: Cerambycidae). *New Zealand Entomologist* 2(6): 47–48. <https://doi.org/10.1080/00779962.1961.9722802>
- Fonseca MG, Zarbin PHG (2009) Mating behaviour and evidence for sex-specific pheromones in *Hedypathes betulinus* (Coleoptera: Cerambycidae: Lamiinae). *Journal of Applied Entomology* 133(9–10): 695–701. <https://doi.org/10.1111/j.1439-0418.2009.01424.x>
- Fukaya M, Honda H (1992) Reproductive biology of the yellow-spotted longicorn beetle, *Psacotha hilaris* (Pascoe) (Coleoptera: Cerambycidae). I. Male mating behaviors and female sex pheromones. *Applied Entomology and Zoology* 27(1): 89–97. <https://doi.org/10.1303/aez.27.89>
- Galford JR (1977) Evidence for a Pheromone in the Locust Borer (Coleoptera: Cerambycidae). USDA Forest Service-Research Note, WA-Washington, 240 pp.
- Green KK, Kovalev A, Svensson EI, Gorb SN (2013) Male clasping ability, female polymorphism and sexual conflict: fine-scale elytral morphology as a sexually antagonistic adaptation in female diving beetles. *Journal of The Royal Society Interface* 10(86): 20130409. <https://doi.org/10.1098/rsif.2013.0409>
- Grieshop K, Polak M (2012) The precopulatory function of male genital spines in *Drosophila ananassae* [Doleschall] (Diptera: Drosophilidae) revealed by laser surgery. *Evolution* 66(8): 2637–2645. <https://doi.org/10.1111/j.1558-5646.2012.01638.x>
- Higginson DM, Miller KB, Segraves KA, Pitnick S (2012) Female reproductive tract form drives the evolution of complex sperm morphology. *Proceedings of the National Academy of Sciences of the United States of America* 109: 4538–4543. <https://doi.org/10.1073/pnas.1111474109>
- Hubweber L, Schmitt M (2010) Differences in genitalia structure and function between subfamilies of longhorn beetles (Coleoptera: Cerambycidae). *Genetica* 138(1): 37–43. <https://doi.org/10.1007/s10709-009-9403-x>
- Hughes AL (1981) Differential male mating success in the white spotted sawyer *Monochamus scutellatus* (Say) (Coleoptera: Cerambycidae). *Annals of the Entomological Society of America* 74(2): 180–184. <https://doi.org/10.1093/aesa/74.2.180>
- Iwabuchi K (1985) Mating behavior of *Xylotrechus pyrrhoderus* Bates (Coleoptera: Cerambycidae). II. Female recognition by male and the existence of a female sex pheromone. *Applied Entomology and Zoology* 20(4): 416–423. <https://doi.org/10.1303/aez.20.416>

- Kasatkin DG (2006) Vnutrenniy meshok edeagusa zhukov - drovosekov (Coleoptera: Cerambycidae): morfologiya, nomenklatura struktur, taksonomicheskoye znachenie [Internal sac of aedeagus of longhorn beetles (Coleoptera: Cerambycidae): morphology, nomenclature of structures, taxonomic significance]. Kavkazskiy entomologicheskii byulleten [Caucasian Entomological Bulletin] 2(1): 83–104. [in russian]
- Keil TA (1997) Functional morphology of insect mechanoreceptors. Microscopy Research and Technique 39(6): 506–531. [https://doi.org/10.1002/\(SICI\)1097-0029\(19971215\)39:6<506::AID-JEMT5>3.0.CO;2-B](https://doi.org/10.1002/(SICI)1097-0029(19971215)39:6<506::AID-JEMT5>3.0.CO;2-B)
- Kelly DA, Moore BC (2016) The morphological diversity of intromittent organs. Integrative and Comparative Biology 56(4): 630–634. <https://doi.org/10.1093/icb/icw103>
- Kerkut GA, Gilbert LI (1985) Comprehensive Insect Physiology, Biochemistry and Pharmacology. Pergamon Press, Oxford, 71–132.
- Kim MK, Kim JS, Han JH, Kim YJ, Yoon C, Kim GH (2006) Mating behavior of pine sawyer, *Monochamus saltuarius* Gebler (Coleoptera: Cerambycidae). Journal of Asia-Pacific Entomology 9(3): 275–280. [https://doi.org/10.1016/S1226-8615\(08\)60303-9](https://doi.org/10.1016/S1226-8615(08)60303-9)
- Kobayashi H, Yamane A, Iwata R (2003) Mating behavior of the pine sawyer, *Monochamus saltuarius* (Coleoptera: Cerambycidae). Applied Entomology and Zoology 38(1): 141–148. <https://doi.org/10.1303/aez.2003.141>
- Koeniger G (1970) Die Bedeutung der Tracheenhülle und der Anhangsdrüse der Spermatheka für die Befruchtungsfähigkeit der Spermatozoen in der Bienenkönigin. Apidologie 1: 55–71. <https://doi.org/10.1051/apido:19700103>
- Kuboki M, Akutsu K, Sakai A (1985) Bioassay of the sex pheromone of the sex pheromone of the udo longicorn beetle, *Acalolepta luxuriosa* Bates (Coleoptera: Cerambycidae). Applied Entomology and Zoology 20(1): 88–89. <https://doi.org/10.1303/aez.20.88>
- Li YS, Li CF, Zhang YJ, Wang YL, Zheng XL, Lu W (2015) Evaluation on effect of a new rearing method for *Glenea cantor* Fabricius larvae. Journal of Southern Agriculture 46(8): 1420–1424.
- Lu W, Wang Q, Tian MY, He XZ, Zeng XL, Zhong YX (2007) Mate location and recognition in *Glenea cantor* (Fabr.) (Coleoptera: Cerambycidae: Lamiinae): roles of host plant health, female sex pheromone, and vision. Environmental Entomology 36(4): 864–870. <https://doi.org/10.1093/ee/36.4.864>
- Luo SL, Zhong PP, Wang MQ (2011) Mating behavior and contact pheromones of *Battus horsfieldi* (Hope) (Coleoptera: Cerambycidae). Entomological Science 14(3): 359–363. <https://doi.org/10.1111/j.1479-8298.2011.00442.x>
- Lyu QH, Zhang BB, Hua BZ (2018) Ultrastructure and function of the seminal vesicle of Bittacidae (Insecta: Mecoptera). Arthropod Structure and Development 47(2): 173–179. <https://doi.org/10.1016/j.asd.2018.02.001>
- Maroni PJ, Bryant KA, Tataric NJ (2023) Female genital concealment and a corresponding male clasping apparatus in Australian ripple bugs (Hemiptera: Veliidae). Arthropod Structure and Development 74: 101254. <https://doi.org/10.1016/j.asd.2023.101254>
- Matthews RW, Matthews JR (2010) Insect Behavior (2nd edn.). Springer, London, 341–388. https://doi.org/10.1007/978-90-481-2389-6_9
- Pinzoni L, Rasotto MB, Gasparini C (2024) Sperm performance in the race for fertilization, the influence of female reproductive fluid. Royal Society Open Science 11(7): 11240156. <https://doi.org/10.1098/rsos.240156>
- Rönn JL, Hotzy C (2012) Do longer genital spines in male seed beetles function as better anchors during mating? Animal Behaviour 83(1): 75–79. <https://doi.org/10.1016/j.anbehav.2011.10.007>

- Ruttner F, Koeniger G (1971) Die Füllung der Spermatheka der Bienenkönigin-aktive Wanderung oder passiver Transport der Spermatozoen? Zeitschrift für Vergleichende Physiologie 72: 411–422. <https://doi.org/10.1007/BF00300712>
- Schmitt M, Uhl G (2015) Functional morphology of the copulatory organs of a reed beetle and a shining leaf beetle (Coleoptera: Chrysomelidae: *Donaciinae*, *Criocerinae*) using X-ray micro-computed tomography. ZooKeys 547(547): 193–203. <https://doi.org/10.3897/zookeys.547.7143>
- Shcherbakov E (2023) Functional morphology of the praying mantis male genitalia (Insecta: Mantodea). Arthropod Structure and Development 74: 101267. <https://doi.org/10.1016/j.asd.2023.101267>
- Simmons LW (2001) *Sperm Competition and its Evolutionary Consequences in the Insects*. Princeton University Press, Princeton, New Jersey, 2001, 448 pp. <https://doi.org/10.2307/j.ctvs32sr2>
- Simmons LW (2014) Sexual selection and genital evolution. Austral Entomology 53(1): 1–17. <https://doi.org/10.1111/aen.12053>
- Stork NE (1980) A scanning electron microscope study of tarsal adhesive setae in the Coleoptera. Zoological Journal of the Linnean Society 68: 173–306. <https://doi.org/10.1111/j.1096-3642.1980.tb01121.x>
- Stutt AD, Siva-Jothy MT (2001) Traumatic insemination and sexual conflict in the bed bug. Proceedings of the National Academy of Sciences of the United States of America 98(10): 5683–5687. <https://doi.org/10.1073/pnas.101440698>
- Tong X, Hua BZ (2019) The sperm pump and genital coupling of *Panorpodes kuandianensis* (Mecoptera: Panorpididae). Arthropod Structure and Development 50: 15–23. <https://doi.org/10.1016/j.asd.2019.03.002>
- Tong X, Jiang L, Hua BZ (2017) A unique mating pattern of *Panorpodes kuandianensis* (Mecoptera: Panorpididae). Contributions to Zoology 86(3): 229–237. <https://doi.org/10.1163/18759866-08603003>
- Tong X, Huang ZY, Huang Q (2024) Mating behavior and functional morphology of genitalia in longhorn beetle *Dorysthenes granulatus* (Coleoptera: Cerambycidae: Prioninae). Applied Entomology and Zoology 59(2): 163–171. <https://doi.org/10.1007/s13355-024-00866-9>
- Villavaso EJ (1975) The role of the spermathecal gland of the boll weevil, *Anthonomus grandis*. Journal of Insect Physiology 21: 1457–1462. [https://doi.org/10.1016/0022-1910\(75\)90208-5](https://doi.org/10.1016/0022-1910(75)90208-5)
- Wang Q, Zeng WY, Li JS (1990) Reproductive behavior of *Paraglenea fortunei* (Coleoptera: Cerambycidae). Annals of the Entomological Society of America 83(4): 860–866. <https://doi.org/10.1093/aesa/83.4.860>
- Wang Q, Li JS, Zeng WY (1991) Sex recognition by males and evidence for a female sex pheromone in *Paraglenea fortunei* (Coleoptera: Cerambycidae). Annals of the Entomological Society of America 84(1): 107–110. <https://doi.org/10.1093/aesa/84.1.107>
- Wilson PJ, Cranston PS (2010) The insects: an outline of entomology. Journal of Insect Conservation 14(6): 745–746. <https://doi.org/10.1007/s10841-010-9351-x>
- Wilson PJ, Cranston PS (2014) *The Insects: An Outline of Entomology* (5th edn.). Wiley-Blackwell, 400 pp.
- Woller DA, Song H (2017) Investigating the functional morphology of genitalia during copulation in the grasshopper *Melanoplus rotundipennis* (Scudder, 1878) via correlative microscopy. Journal of Morphology 278(3): 334–359. <https://doi.org/10.1002/jmor.20642>

- Wulff NC, van de Kamp T, Dos Santos Rolo T, Baumbach T, Lehmann GU (2017) Copulatory courtship by internal genitalia in bushcrickets. *Scientific Reports* 7(1): 42345. <https://doi.org/10.1038/srep42345>
- Xiong S, He S, Li Z, Chen L, Zhang QX (2014) Observation of sensilla on the cephalic appendages of *Nadezhdiella cantori* using a scanning electron microscope. *Journal of the Southwest University* 36(5): 36–45. <https://doi.org/doi:10.13718/j.cnki.xdzk.2014.05.006>
- Yokoi N (1990) The sperm removal behavior of the yellow spotted longicorn beetle *Psacothaea hilaris* (Coleoptera: Cerambycidae). *Applied Entomology and Zoology* 25(3): 383–388. <https://doi.org/10.1303/aez.25.383>
- Zhang XS, Liang AP (2012) Ultrastructural morphology of the pulvilli in *Musca domestica*, *BercAea cruentata* and *Chrysomya pinguis* (Diptera). *Acta Zootaxonomica Sinica* 37(4): 694–700.
- Zhong W, Qi ZY, Hua BZ (2015) Atypical mating in a scorpionfly without a notal organ. *Contributions to Zoology* 84(4): 305–315. <https://doi.org/10.1163/18759866-08404003>
- Zhou P, Zhao PP, Cao X, Gao J, Ju YW (2015) Observation of sensilla on the larval head of *Sphecodoptera sheni* by using scanning electron microscopy. *Plant Protection* 41(4): 63–67. <https://doi.org/10.3969/j.issn.0529-1542.2015.04.011>
- Zhuge PP, Luo SL, Wang MQ, Zhang GA (2010) Observation of sensilla on the cephalic appendages of *Batocera horsfieldi* with scanning electron microscope. *Scientia Silvae Sinicae* 46(5): 116–121. <https://doi.org/10.11707/j.1001-7488.20100519>

Genomic and ecological divergence support recognition of a new species of endangered *Satyrrium* butterfly (Lepidoptera, Lycaenidae)

Zachary G. MacDonald^{1,2,3*}, Julian R. Dupuis^{4*}, James R. N. Glasier⁵, Robert Sissons⁶, Axel Moehrenschrager^{7,8}, H. Bradley Shaffer^{1,2}, Felix A. H. Sperling³

1 UCLA La Kretz Center for California Conservation Science, Institute of the Environment and Sustainability, University of California, Los Angeles, California, USA

2 Department of Ecology and Evolutionary Biology, University of California Los Angeles, Los Angeles, California, USA

3 Department of Biological Sciences, University of Alberta, Edmonton, Alberta, Canada

4 Department of Entomology, University of Kentucky, Lexington, Kentucky, USA

5 Wilder Institute/Calgary Zoo, Calgary, Alberta, Canada

6 Resource Conservation, Waterton Lakes National Park, Waterton Park, Alberta, Canada

7 IUCN SSC Conservation Translocation Specialist Group, Calgary, Alberta, Canada

8 Panthera, New York, New York, USA

Corresponding authors: Zachary G. MacDonald (zmacdonald@ioes.ucla.edu); Julian R. Dupuis (julian.dupuis@uky.edu)



Academic editor: Shinichi Nakahara

Received: 9 December 2024

Accepted: 11 March 2025

Published: 17 April 2025

ZooBank: <https://zoobank.org/3CFC1AF4-F94A-45B7-ABB3-01078B9CB1F4>

Citation: MacDonald ZG, Dupuis JR, Glasier JRN, Sissons R, Moehrenschrager A, Shaffer HB, Sperling FAH (2025) Genomic and ecological divergence support recognition of a new species of endangered *Satyrrium* butterfly (Lepidoptera, Lycaenidae). ZooKeys 1234: 291–307. <https://doi.org/10.3897/zookeys.1234.143893>

Copyright: This is an open access article distributed under the terms of the CC0 Public Domain Dedication.

Abstract

We describe a highly isolated population of hairstreak butterfly from Waterton Lakes National Park, Alberta, Canada, as a new species, *Satyrrium curiosolus* sp. nov., previously recognized as *Satyrrium semiluna* (Half-moon Hairstreak). We propose “Curiously Isolated Hairstreak” as the common name due to its disjunct and unusual distribution. Previous whole-genome analyses revealed *S. curiosolus* has extremely low genomic diversity and is highly divergent from the nearest *S. semiluna* populations in British Columbia and Montana, more than 400 km distant. Further analysis suggested prolonged inbreeding and isolation for up to ~40,000 years BP. Ecological niche modeling indicated that *S. curiosolus* occupies environmental conditions that are distinct from *S. semiluna*, suggesting niche divergence driven by long-term geographical and ecological separation. While host plant and ant associations have not been definitively resolved, they likely differ between *S. curiosolus* and *S. semiluna*. As part of this description, we provide whole-genome consensus sequences for each individual of the type series and identify 21,985 single nucleotide polymorphisms (SNPs) that are divergently fixed between *S. curiosolus* and *S. semiluna*, including 117 unlinked SNPs distributed across the genome as putative diagnostic markers. Previously listed as Endangered in Canada as the Waterton population of *S. semiluna*, *S. curiosolus* should retain this conservation status due to its extreme isolation, small population size, and flatlined genomic diversity. We propose species recognition as a testable hypothesis under the General Lineage Concept and recommend further research to explore the taxonomy, ecological relationships, and conservation of the greater species complex, including *S. curiosolus*, *S. semiluna*, and *S. fuliginosa*.

Key words: Butterfly, Curiously Isolated Hairstreak, endangered species, genomics, Half-moon Hairstreak, niche divergence, Sagebrush Sooty Hairstreak

* These authors contributed equally.

Introduction

The northernmost populations of a North American butterfly, the Half-moon Hairstreak (*Satyrrium semiluna* Klots; sometimes called “Sagebrush Sooty Hairstreak”), have received recent study by MacDonald et al. (2025), but their taxonomic status remains in question. Although *S. semiluna* is “apparently secure” across its range in the USA (COSEWIC 2006, 2022; ECCC 2016; NatureServe 2024), the species’ northern range limit extends into Canada, where it is listed as Endangered under the “Species at Risk Act”. All but one Canadian population occur in south-central British Columbia, with an estimated aggregate abundance of 5,000–15,000 individuals. Based on continuity of both suitable habitat and the species’ occurrence records, British Columbia populations are presumably well connected to others south of the USA–Canada border and likely represent an example of political boundaries dictating protection rather than range-wide conservation concern. British Columbia populations have been recommended for downlisting to Threatened (COSEWIC 2022). The single other Canadian population persists on a ~300 ha alluvial fan (Blakiston Fan) in Waterton Lakes National Park, Alberta, where it is isolated from all other *S. semiluna* populations by a distributional gap of more than 400 km. This population was recently recommended for uplisting to Critically Endangered based on its uniqueness, small size, and considerable isolation (COSEWIC 2022).

The Alberta population is small, with genomically based estimates of contemporary effective population size (N_e) around 500 individuals and surveys suggesting that between 1,000 and 10,000 adults fly annually (COSEWIC 2022; MacDonald et al. 2025). Aside from enigmatic island insect populations, such as the Lord Howe Island stick insect (*Dryococelus australis* (Montrouzier)) (Priddel et al. 2003) and some Hawaiian drosophilids (O’Grady and DeSalle 2018), few if any other insects have been documented with such a small population size and high degree of long-term isolation. The Alberta population’s environmental and ecological associations are also unique, adding to its scientific interest. Blakiston Fan receives an average summer precipitation of ~200 mm, while the locations of all other *S. semiluna* populations in the central-northern portion of the species’ range receive between 32 and 154 mm (mean = 71 mm) (MacDonald et al. 2025). This difference in precipitation manifests in different habitat characteristics—Populations throughout British Columbia and the USA inhabit steppe-like habitats dominated by big sagebrush (*Artemisia tridentata* Nutt.). In contrast, occupied habitat at Blakiston Fan is best described as prairie/grassland dominated by sedges, grasses, and herbaceous plant species.

Another possible axis of niche divergence is larval host-plant association. Populations throughout British Columbia and the USA Pacific Northwest feed on silky lupine (*Lupinus sericeus* Pursh) and possibly Pacific lupine (*Lupinus lepidus* Lindl.) (James and Nunnallee 2011), while the Alberta population feeds only on silvery lupine (*Lupinus argenteus* Pursh), even though *L. sericeus* is common at the site. Host associations of most other populations east of the continental divide in the USA are unknown and require investigation. Myrmecophily presents a third possible axis of niche divergence (MacDonald et al. 2025). Larvae of the Alberta population exhibit a mutualistic relationship with *Lasius ponderosae* Schär, Talavera, Rana, Espadaler, Cover, Shattuck & Vila. In British Columbia, *L. ponderosae* is absent in *S. semiluna* habitat, and larvae

associate with *Formica* and *Camponotus* species. Similar associations with *Formica* and *Camponotus* have been observed in California (Runquist 2012).

Given the Alberta population's small size and considerable isolation, inbreeding depression and loss of adaptive potential were identified by Parks Canada and the Half-moon Hairstreak Conservation Committee as likely threats to its long-term persistence. In these situations, genetic rescue is often assumed to be an effective conservation strategy (Storfer 1999; Weeks et al. 2011; Frankham et al. 2017; Ralls et al. 2020; Clarke et al. 2024). To assess whether genetic rescue is indeed appropriate for the Alberta population, MacDonald et al. (2025) generated the first chromosome-level genome assembly for the species and whole-genome resequencing data for the Alberta population, British Columbia populations, and the nearest USA population in Montana. Based on genetic divergence, environmental and ecological differences and a very long inferred history of isolation with no evidence of contemporary or recent gene flow, we, together with Parks Canada and the Half-moon Hairstreak Conservation Committee, determined that the Alberta population satisfies requirements of a distinct species that has long been on an independent evolutionary trajectory. Species-level recognition highlights the unique ecology and evolution of this butterfly, demonstrates a clear need for continued consideration under the "Species at Risk Act" and International Union for the Conservation of Nature, and provides an important case study on the utility of genomics in taxonomy. Genomics has an increasingly important role in taxonomic descriptions (Fennessy et al. 2016; Nater et al. 2017; Zhou et al. 2018; Stanton et al. 2019). However, chromosome-level genome assemblies for new species, along with whole-genome consensus sequences for the type series, remain rare (see Brandão-Dias et al. 2022).

Methods

All types (Fig. 2) are deposited in the University of Alberta E.H. Strickland Entomological Museum (UASM).

Here we summarize the taxonomically relevant methods of MacDonald et al. (2025). Eight individuals were collected from Blakiston Fan, Alberta, four from Richter Pass, British Columbia, three from Anarchist Mountain, British Columbia, and four near Red Lodge, Montana (Parks Canada Agency Research and Collection Permit WL-2021-39,020, Nature Conservancy Canada Research Permit NCC_BC_2021_SS001, and Nature Trust of British Columbia Permit #3461). Four Alberta individuals were used to generate a chromosome-level reference genome assembly using PacBio HiFi long-read sequencing (Pacific BioSciences, Menlo Park, California, USA) and Omni-C proximity ligation (Dovetail Genomics, Scotts Valley, California, USA).

Whole-genome resequencing of individuals from Blakiston Fan ($n = 4$) and the geographically nearest populations from Richter Pass ($n = 4$), Anarchist Mountain ($n = 3$), and near Red Lodge ($n = 4$) was performed on an Illumina NovaSeq S1 platform, with a target coverage of $\sim 20\times$. Reads were aligned to our reference genome assembly and used to identify millions of single nucleotide polymorphisms (SNPs). Population structure and degree of admixture was assessed using PCA and the program "structure" (Pritchard et al. 2000) and genetic divergence among inferred genomic clusters was estimated using F_{ST} (Weir and Cockerham 1984). Genetic diversity was estimated using individual-based heterozygosity and nucleotide

diversity (π), while the proportion of an individual's genome within runs of homozygosity over 0.1 Mb (F_{ROH}) served as an index of inbreeding. Historical effective population size (N_e) was inferred from each individual's genome sequence using the pairwise sequentially Markovian coalescent (PSMC) (Li and Durbin 2011).

Nuclear whole-genome consensus sequences (fastq format) were generated for each individual using individual-level BAM files (produced in genotype calling) and the mpileup command (-C 50, -Q 30, and -q 30) in samtools (Danecek et al. 2021). This was piped into the vcf2fq command from vcfutils.pl using our genome assembly as the reference. Filtering included sites with inferred consensus quality < 20 and a read depth less than 8× or greater than two times each individual sample's mean coverage, calculated from BAM files using samtools "depth".

A series of MaxEnt models (Phillips et al. 2006) were generated to assess environmental and ecological associations of *S. semiluna* across the central and northern extent of the species' range. To assess niche divergence of the Alberta population relative to others within this modelling extent, a MaxEnt model was trained excluding Alberta occurrences and used to predict habitat suitability for all *S. semiluna* occurrences, including Alberta. If the predicted suitability of Blakiston Fan was substantially lower than the locations of all other occurrences, niche divergence was inferred (Campbell et al. 2022).

Results

Our reference genome assembly was highly contiguous, spanning 1.25 Gb across 86 scaffolds, with an N50 of 56.2 Mb. Whole-genome resequencing of 15 individuals produced > 1.4 billion high-quality reads, yielding a dataset of 41,083,914 variants, with 23,889,641 SNPs retained after filtering. PCA and "structure" cleanly split all individuals into three populations with no evidence of admixture (Fig. 1a, b). F_{ST} values indicated substantial genetic divergence between Alberta and British Columbia (0.424), Alberta and Montana (0.292), and British Columbia and Montana (0.322). The two British Columbia sites showed no divergence, suggesting a high degree of gene flow ($F_{\text{ST}} = -0.004$). Mean heterozygosity was lowest in Alberta (0.083), compared to British Columbia (0.216) and Montana (0.154), and nucleotide diversity (π) was also lower in Alberta (0.003) than in British Columbia (0.008) and Montana (0.005) (Fig. 1b). This suggests much larger population sizes and broad-scale population connectivity in British Columbia and Montana compared to Alberta. Runs of homozygosity were 5–70 times more abundant in Alberta individuals, with individual F_{ROH} values averaging 0.192 in Alberta, 0.006 in British Columbia, and 0.033 in Montana (Fig. 1b). PSMC indicated that the Alberta population has been very small, isolated, and stable from 40 to 5 kya, with effective population size (N_e) estimated between 1,000 and 5,000 individuals (Fig. 1c). In contrast, British Columbia and Montana populations experienced large expansions toward the end of this time period, suggesting broad-scale connectivity. MaxEnt models predicted habitat suitability with high accuracy ($\text{AUC}_{\text{ROC}} = 0.94$) and identified mean summer precipitation as the most important environmental variable predicting *S. semiluna* occurrences (Fig. 1d). When Alberta occurrences were excluded from model training, predictive accuracy increased ($\text{AUC}_{\text{ROC}} = 0.97$). Using this model to predict habitat suitability at Blakiston Fan resulted in an estimate of 0.003, much lower than the locations of all other *S. semiluna* occurrences. This was interpreted as evidence of niche divergence.

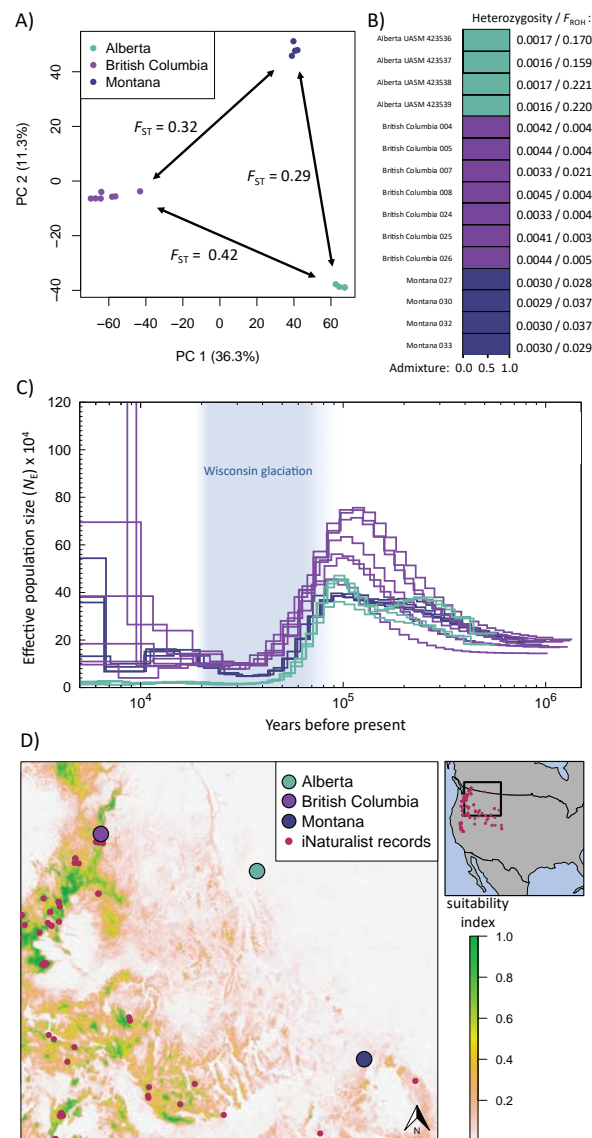


Figure 1. Summary of genomic and niche analyses from MacDonald et al. (2025) **A** principal component analysis (PCA) using a dataset of 108,283 physically unlinked single nucleotide polymorphisms (SNPs) separated sequenced individuals into three discrete clusters. Weir and Cockerham's (1984) F_{ST} values are shown between the three clusters **B** clustering analyses using the program *structure* (Pritchard et al. 2000) of all individuals found an optimal K value of 2, splitting Alberta and Montana from British Columbia; hierarchical runs excluding British Columbia identified an optimal K value of 2 with virtually no admixture between Alberta and Montana. Here, we combine hierarchical runs into a single admixture plot. Average heterozygosity and an estimate of inbreeding (F_{ROH}) for each individual is shown to the left of the admixture plot. Analyses of runs of homozygosity (ROH) and the proportion of each individual's genome contained in ROH > 0.1 MB (F_{ROH}) suggested that historical inbreeding has been much more prevalent in the Alberta population (mean F_{ROH} = 0.192) than in British Columbia (F_{ROH} = 0.006) or Montana (F_{ROH} = 0.033) populations, suggesting a long history of isolation **C** the pairwise sequentially Markovian coalescent (PSMC) from 2.5 mya until 5 kya of the three identified clusters, with each individual's genome serving as an independent sample. Years before present is shown on the x-axis and estimated effective population size (N_e) on the y-axis. The Alberta population flatlined between 1,000 and 5,000 individuals from 40 to 5 kya, indicating complete isolation. British Columbia and Montana both experienced substantial increases in N_e , suggesting broad-scale connectivity. The approximate duration of the Wisconsin glaciation is shown in blue (Clayton and Moran 1982; Bischoff and Cummins 2001) **D** Predicted *S. semiluna* habitat suitability, predicted using 17 environmental variables, landcover data, and various terrain indices. "Research-grade" iNaturalist occurrences and the collection locations of sequenced individuals, excluding the Alberta population, were used to parameterize the model. Blakiston Fan had suitability value of 0.003, while other *S. semiluna* populations inhabited areas of much higher suitability. Environmental conditions at Blakiston Fan are therefore atypical for the species, indicating niche divergence.

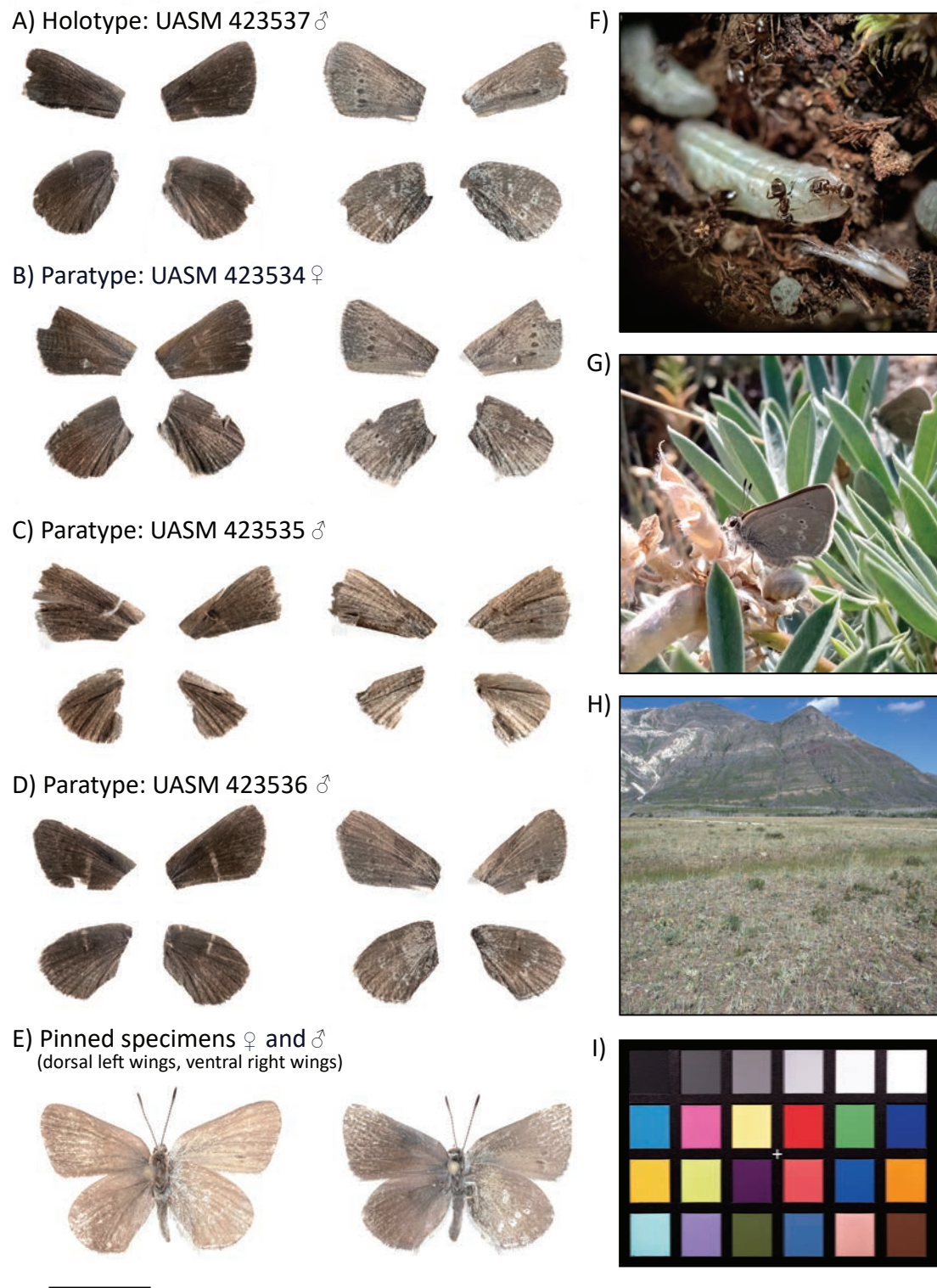


Figure 2. A–D dorsal and ventral wing surfaces of the *Satyrium curiosolus* type series. Bodies of these specimens were used in genomic DNA extractions. Sequence data were used to generate a whole-genome consensus sequence for each specimen. Metadata for each specimen are given under “Type material” E composite photographs of pinned specimens (female left, male right), showing the dorsal wing surface on the left forewing and hindwing and the ventral wing surface on the right forewing and hindwing F *S. curiosolus* larvae being attended to by *Lasius ponderosae* ants G a freshly eclosed *S. curiosolus* on silvery lupine (*Lupinus argenteus*); H) Photograph of Blakiston Fan, Alberta, Canada I) Calibrite ColorChecker Classic, photographed with the same setup and settings used to photograph the type series. The scale bar (bottom left) is 1 cm, against which A–E are scaled.

Genetic divergence, environmental and ecological divergence, and a very long history of isolation with no evidence of contemporary or recent gene flow are sufficient to recognize the Alberta population as a distinct taxonomic entity. We propose its recognition as a new species.

***Satyrrium curiosolus* MacDonald, Dupuis, Glasier, Sissons, Moehrensclager, Shaffer & Sperling, sp. nov.**

<https://zoobank.org/92A9AB4C-2C9B-47CD-AB08-F248D92A078D>

Type locality. Canada: Alberta, Waterton Lakes National Park, Blakiston Fan, 49.068, -113.877.

Type material examined. Holotype. 1 ♂ [white label] "CANADA: Alberta, Waterton Lakes National Park, Blakiston Fan (Marquis), 49.068, -113.877 (WGS84), 14-Jul-2021, J. Glasier; 14008, *Satyrrium curiosolus*_016"; [white label] "UASM 423537"; [red label] "Holotype *Satyrrium curiosolus*". BioSample: SAMN45172752.

Paratypes. 1 ♂ [white label] "CANADA: Alberta, Waterton Lakes National Park, Blakiston Fan (Hay Barn), 49.079, -113.866 (WGS84), 14-Jul-2021, J. Glasier; 14002, *Satyrrium curiosolus*_009"; [white label] "UASM 423534". BioSample: SAMN45172749 • 1 ♂ [white label] "CANADA: Alberta, Waterton Lakes National Park, Blakiston Fan (Hay Barn), 49.078, -113.869 (WGS84), 14-Jul-2021, J. Glasier; 14003, *Satyrrium curiosolus*_010"; [white label] "UASM 423535". BioSample: SAMN45172750 • 1 ♂ [white label] "CANADA: Alberta, Waterton Lakes National Park, Blakiston Fan (Hay Barn), 49.076, -113.869 (WGS84), 14-Jul-2021, J. Glasier; 14006, *Satyrrium curiosolus*_012"; [white label] "UASM 423536". BioSample: SAMN45172751.

Description. The morphological description follows Mattoon and Austin's (1998: 685) description of *Satyrrium fuliginosum semiluna* Klotz, which is now recognized as *Satyrrium semiluna semiluna* Klotz (Warren 2005).

A small, drab butterfly. As with many *Satyrrium*, wings predominately brownish or dark brown dorsally (fading to light brown with age), lacking any hint of blue, and lacking tails. Males with strong dorsal scent pad of androconial scales, shared with *S. semiluna*, but lacking in *S. fuliginosa* (W.H. Edwards) (Warren 2005). Ventral wing surface light brown with grey overscaling along margins, and large black postmedial spots slightly outlined in white (reduced in hindwings). Females slightly larger and paler ventrally.

Diagnosis. Males with small wingspan (<25 mm vs > 30 mm) and less conspicuous ventral spotting than *S. semiluna* (Kondla 2004). Due to the cryptic nature of the species, identification without reference to source locality is most reliably achieved by DNA as follows, with representative (see Remarks section) diagnostic single nucleotide polymorphisms (SNPs) that are fixed for *S. curiosolus* (formatted as scaffold: position[*S. curiosolus* allele/*S. semiluna* allele]: ScvBUXZ_1.HRSCAF10: 1568673[C/A], 12071375[C/A], 22597556[G/C], 33128087[T/G], 43633436[G/C], 54341325[T/A]; ScvBUXZ_11.HRSCAF312: 939246[C/T], 11508752[A/T], 23223489[T/C], 34114361[T/C]; ScvBUXZ_12.HRSCAF324: 2725346[G/T], 13277889[C/A], 23561701[T/A], 34983585[G/A]; ScvBUXZ_15.HRSCAF369: 604178[A/G], 10688359[A/G], 22742875[A/G], 33306760[T/C], 43372888[A/C]; ScvBUXZ_16.

HRSCAF394: 1798098[A/G], 13584119[G/C], 24134185[G/A], 36106687[A/G]; ScvBUXZ_18.HRSCAF419: 1271585[C/T], 12498609[T/A], 22674145[A/C], 32848269[A/G], 43126131[A/G], 53221485[G/A], 63907163[T/A]; ScvBUXZ_20. HRSCAF485: 1278399[C/A], 11291064[A/G], 22201816[G/T], 34957432[C/T], 45290319[A/G], 56419490[G/A], 70868124[T/C], 82626599[G/C]; ScvBUXZ_21. HRSCAF503: 3759737[G/A], 14004891[T/C], 24159643[A/T], 34796558[A/G], 46064578[A/C]; ScvBUXZ_22.HRSCAF557: 1241910[T/C], 11429001[A/G], 22696299[A/G], 32721285[T/C], 43059425[T/G], 53074410[A/G], 63089033[T/G], 74842831[G/T]; ScvBUXZ_23.HRSCAF563: 1626681[A/G], 12005836[C/A], 22106743[T/G], 32206731[A/C], 42322988[A/C]; ScvBUXZ_27. HRSCAF638: 617786[A/G], 10908292[T/G], 20909876[T/C], 31703436[A/C], 42607435[A/G], 52716659[T/C], 63015994[A/G]; ScvBUXZ_3.HRSCAF45: 40925[T/C], 10620232[A/C], 20622161[A/C]; ScvBUXZ_33.HRSCAF736: 1025752[C/T], 11845689[T/C], 21926431[A/G], 33073314[T/C], 43525185[C/A]; ScvBUXZ_36.HRSCAF762: 496718[G/T], 12599380[T/C], 22623129[A/C], 32789532[T/G], 43886779[C/T], 53941324[T/C]; ScvBUXZ_37.HRSCAF777: 1137238[A/C], 11176395[C/T], 21849140[A/G], 36719032[G/T], 46746341[A/C], 57389780[G/A]; ScvBUXZ_4.HRSCAF59: 2539048[A/C], 15455375[T/G], 25460453[T/C], 35798787[C/A], 46323982[A/C], 59292711[A/G]; ScvBUXZ_41. HRSCAF810: 342264[A/G], 10823670[C/T], 21337909[T/C], 31863338[G/C], 41915594[A/T], 52015696[T/G]; ScvBUXZ_48.HRSCAF855: 2065895[T/C], 12340828[G/C], 22489657[A/G], 33211401[A/G], 43237667[T/A]; ScvBUXZ_5. HRSCAF87: 653322[A/G], 11521727[C/G], 22249471[A/G], 32408138[T/A], 42462727[T/G], 52471692[A/G]; ScvBUXZ_54.HRSCAF883: 1953965[C/A], 12005082[A/G], 22185366[C/T], 32223581[C/T]; ScvBUXZ_6.HRSCAF109: 2728984[T/C], 14807116[G/A], 25931083[T/C]; ScvBUXZ_9.HRSCAF216: 1632867[C/G], 14935276[A/G], 26523755[C/G], 37425842[T/A]

Genomic sequence of the holotype. BioSample: SAMN45172752; whole-genome consensus sequence available on Dryad: <https://doi.org/10.5061/dryad.sf7m0cgj2>.

Distribution. Currently known only from Blakiston Fan, Alberta, Canada, approximately 300 ha in area.

Seasonality. Eggs overwinter before hatching in early spring in late April or early May. Larvae can first be found in early May, develop through four instars, pupate in July (at the base of *L. argenteus*, often under the previous year's stems in ant galleries), and then emerge after about two weeks of pupation in July to mid-August.

Ecology. Restricted to Blakiston Fan, a 300-ha area of course-textured alluvial fan at an elevation of ~1,300 m. The habitat of *S. curiosolus* is short-grass prairie with abundant *L. argenteus*, *L. sericeus*, and yellow buckwheat (*Eriogonum flavum* Nutt.). This habitat differs from that of *S. semiluna*, in that it is lacking big sagebrush (*A. tridentata*). *Satyrium semiluna* is associated with *A. tridentata* to the point that, in the USA, the butterfly's common name is the Sagebrush Sooty Hairstreak. Another notable difference is that *S. semiluna* populations generally inhabit hillsides or mountainsides, while *S. curiosolus* inhabits an alluvial fan in the middle of a montane valley.

Unlike previous reports stating that that *S. curiosolus* uses both local lupine species as plant hosts (COSEWIC 2006, 2022; ECCC 2016), our surveys found that they only use *L. argenteus*. Out of ~500 larvae detected in repeated surveys throughout 2020–2024, all were on *L. argenteus*. *Satyrium semiluna* populations on the west

side of the Rocky Mountains, and presumably those throughout the central USA, feed on *L. sericeus*. These populations may also feed on *L. lepidus* (James and Nunnallee 2011), but in extensive surveys throughout British Columbia in 2021–2024, we have not observed any such association (Glasier pers. obs.). *Satyrrium curiosolus* larvae feed on new buds and stems at the base of lupines and commonly hide under the woody stems from the previous year when not feeding.

At Blakiston Fan, all *S. curiosolus* larvae observed in 2021–2024 surveys were closely associated with *Lasius ponderosae* ant colonies (identified using Glasier et al. 2013 and Schär et al. 2022). Ants groomed and protected the larvae, and larvae were observed to retreat into ant colonies when threatened. Other ant species seen interacting with larvae at Blakiston Fan include *Formica argentea* and *Formica lasioides* (ants identified using Glasier et al. 2013). However, these interactions appeared to be more opportunistic, as these larvae observed were still primarily associated with a *L. ponderosae* colony. We have also observed *S. curiosolus* larvae pupating in the galleries of *L. ponderosae* colonies at the base of *Lupinus argenteus* plants. During our butterfly surveys in 2021–2024 in British Columbia, no *Lasius* species were found attending *S. semiluna* larvae. Instead, *Camponotus vicinus*, *Formica obscuripes*, and *Formica argentea* were observed interacting with larvae, and several pupae were found in a *Camponotus vicinus* nest at the base of a *L. sericeus*. In California, *Camponotus* and *Formica* attendants were also reported (Runquist 2012).

Satyrrium curiosolus fluctuates in abundance from year to year, with genomically based estimates of contemporary effective population size (N_e) around 500 (MacDonald et al. 2025) and surveys suggesting that between 1,000 and 10,000 adults fly annually (COSEWIC 2006, 2022; unpublished data). Based on our observations from 2020–2024, the *S. curiosolus* flight period occurs during July to mid-August and lasts about two weeks. Adults are most frequently observed as they perch, sunning themselves on buckwheats, lupines, and shrubby cinquefoil (*Dasiphora fruticosa*). Males tend to spend more time on alpine buckwheat, while females tend to spend more time on lupines. Mating occurs at any time of day and may last several hours. Females lay an unknown total number of eggs but have been observed laying eggs singly or in small clusters, in the soil around the base of *L. argenteus* and/or near the entrance of *L. ponderosae* nests.

Etymology. The specific epithet *curiosolus* derives from the Latin “*curiosus*” meaning curious and “*solus*” meaning to be alone or isolated, and it is to be treated as a noun in apposition. We suggest the common name “Curiously Isolated Hairstreak”.

Remarks. Using our reference genome assembly (NCBI JASDAZ000000000) and whole-genome resequencing data for 15 individuals, we identified 21,985 SNPs across 22 scaffolds that were fixed for alternate nucleotides between individuals from Alberta and those from Montana and British Columbia. The 117 SNPs included in this description result from thinning to one SNP per 10 Mb (using `--thin` option in `vcftools` v0.1.16, Danecek et al. 2011) to ensure that they are evenly spaced across the genome and likely physically unlinked. DNA barcodes (mitochondrial gene cytochrome oxidase subunit I) have been shown to be identical between populations of *S. semiluna* from Alberta, British Columbia, and Washington (COSEWIC 2006), and haplotype sharing (in cytochrome oxidase subunit II) has been observed more broadly between *S. semiluna* and *S. fuliginosa* (Runquist 2012); both observations suggest that mitochondrial/

nuclear discordance exists within the genus. Taken together with other systematic studies with broader taxonomic sampling (Robbins et al. 2022), these data also provide support for the inclusion of *S. curiosolus* within *Satyrium*. Nuclear whole-genome consensus sequences for each individual of the type series are available at: <https://doi.org/10.5061/dryad.sf7m0cgj2>.

Discussion

Satyrium curiosolus warrants recognition as a distinct taxonomic entity. We evaluated whether to describe it as a subspecies or a species based on two main criteria. Braby et al. (2012) defined subspecies by the combination of partial isolation of allopatric lineages, phenotypic distinctiveness, and at least one fixed, diagnosable character. This definition is rooted in the General Lineage Concept (GLC), which considers species as independently evolving lineages supported by multiple lines of evidence including criteria often associated with various species concepts (De Queiroz 1998, 2007). To ensure an objective comparison, we assess explicit criteria from these concepts (Table 1), taking them at face value as described in their original publications. While one interpretation of the GLC is that it lacks any specific criteria, like intrinsic reproductive isolating mechanisms or fixed morphological characters (De Queiroz 1998), practical application necessitates that we identify and score multiple criteria in making a species/subspecies determination. Thus, we focus on criteria used by alternative species concepts relevant to the “grey zone” of speciation (De Queiroz 2007).

Allopatry and isolation are critical properties for many subspecies and species concepts. Here, all evidence indicates that divergence between *S. curiosolus* and the geographically nearest *S. semiluna* populations is non-clinal, with no evidence of contemporary or recent gene flow. *Satyrium curiosolus* is completely isolated today, and coalescent-based analyses suggest this isolation may extend up to 40,000 years BP. Given this considerable isolation, traditional considerations of potential or actual reproductive isolation (Mayr 1942) are difficult to apply, and secondary contact with *S. semiluna* is improbable given both species’ relatively low vagility and the magnitude of range shift required (MacDonald et al. 2024). From a geographical standpoint, there is no possibility of hybridization and gene flow. This is a hypothesis that could be falsified by the discovery of genetic and environmental/ecological intermediates between *S. curiosolus* and *S. semiluna*. We consider this unlikely, given the prominent butterfly survey effort in the region. Nonetheless, we and others will continue to search for undiscovered populations. *Satyrium curiosolus* exhibits ecological distinctiveness, including unique environmental, host plant, and ant associations. Morphological distinctiveness was not extensively investigated but has been suggested by other species experts—Kondla (2004) noted that males from Blakiston Fan (*S. curiosolus*) have a smaller wingspan than other *S. semiluna* populations investigated (<25 mm vs > 30 mm) and less conspicuous ventral spotting. Beyond size and wing pattern, our most concrete diagnosable characters include 21,985 SNPs that are divergently fixed for alternate nucleotides between *S. curiosolus* and the nearest *S. semiluna* populations. For simplicity, we identified a subset of 117 SNPs evenly spaced across the genome. Future resequencing of additional *S. curiosolus* and *S. semiluna* individuals may

Table 1. Criteria and properties used to define subspecies following Braby et al. (2012) and species following concepts unified under the General Lineage Concept (De Queiroz 1998, 2007, and references therein for various properties of alternative species concepts). “This study” represents whether a criterion/property is satisfied in this system (“1”), not satisfied (“0”), or unknown with the data at hand (“?”).

| Concept/definition | Criteria/property | This study |
|--|--|------------|
| Subspecies, Braby et al. (2012) | Partially isolated lineages | 0 |
| | Allopatric | 1 |
| | Phenotypically distinct | ?* |
| | ≥1 fixed, diagnosable character state (assumed correlation to evolutionary independence) | 1 |
| Species, General Lineage Concept (De Queiroz 1998, 2007) | | |
| | Reproductive incompatibility/character displacement | ?** |
| | entirely allopatric | 1 |
| | Mate recognition systems | ? |
| | Ecologically distinct | 1 |
| | Monophyly | 1 |
| | Lack of gene flow | 1 |
| | Morphologically diagnosable | ?* |
| | Genetically diagnosable | 1 |
| | Ecologically diagnosable | 1 |

*Morphological diagnosability is generally possible with many specimens in series, but confident morphological delimitation of single specimens of *S. curiosolus* from *S. semiluna* may be difficult without other data (collection locality, DNA data).

**MacDonald et al. (2025) inferred that the Alberta *Satyrrium* population in question (described here as *S. curiosolus*) would likely experience outbreeding depression if it mated with other populations, which may be interpreted as a form of reproductive isolation; experimental crosses are needed to further assess this inference.

reveal some of these SNPs to be “near fixed” even though they are fixed in our sample set—this would not invalidate them as diagnostic characters, but simply suggest that they have not evolved to complete fixation. As with any set of diagnostic characters, our evaluation of genomic diagnostic characters may change as new information becomes available.

Complete absence of gene flow, and a long history of isolation combined with genomic, environmental, and ecological differentiation, satisfies many of the criteria associated with alternate species concepts and unified under the GLC, notably those originating from the phylogenetic species concept (including variants introduced by Rosen 1979; Baum and Shaw 1995; Nelson and Platnick 1981; Cracraft 1983), the ecological species concept (Van Valen 1976), and the evolutionary species concept (Simpson 1951; Wiley 1978). The alternative—retaining *S. curiosolus* as a subspecies—would imply ongoing or potential gene flow, which is demonstrably absent, making species recognition the most taxonomically defensible classification (Braby et al. 2012). Still, we extensively debated the appropriate classification, initially considering subspecies as a more prudent and conservative option, anticipating that further evidence and analyses may substantiate species-level recognition. However, assuming that subspecies rank is the more prudent or conservative classification was potentially problematic. This assumption treats subspecies as an intermediate stage rather than objectively evaluating evolutionary independence based on multiple lines of evidence. Subspecies status often reflects structured intraspecific variation with some degree of contemporary or recent gene flow, not clear lineage separation (Mayr 1963; Braby et al. 2012). Under our view of the GLC, species

recognition is a testable hypothesis, not a permanent designation, and should be based on the strength of evidence rather than a default bias toward subspecies as a sort of evolutionary null. Treating subspecies as a holding category creates an asymmetrical burden of proof, requiring disproportionately strong evidence for species recognition while subspecies designations persist under weaker criteria. This bias could obscure evolutionary significance and delay the recognition of independent lineages by misrepresenting biodiversity.

Future taxonomy and conservation

Further taxonomic and phylogenomic research on this species complex should incorporate *S. fuliginosa*, which is currently thought to be restricted to California and southern Oregon, where it is sympatric and may hybridize with *S. semiluna* (Runquist 2012). These putative sister species were historically distinguished by the presence of a male forewing scent patch in *S. semiluna* (a synapomorphy of *Satyrium*; see Martins et al. 2019), which is entirely absent in *S. fuliginosa* (Warren 2005), as well as the generally browner wing coloration of *S. fuliginosa* compared to the greyer *S. semiluna*. However, the validity of these distinct taxa has been questioned (Runquist 2012), and morphological outlier populations—greyer *S. fuliginosa* and browner *S. semiluna*—have been identified in western California (Warren 2005; Runquist 2012). Despite this complexity, the male scent patch of the Blakiston Fan population aligns it with the *semiluna* group *sensu* Matton and Austin (1998), rather than the *fuliginosa* group. This distinction, along with the fact that *S. fuliginosa* is more geographically distant from *S. curiosolus*, suggests that only comparisons between *S. curiosolus* and northern *S. semiluna* populations are pertinent to the taxonomic revision proposed here. However, to understand the full extent of differentiation and diversity between and within related groups of species within this genus, we recommend that future research include the full geographical extent of known populations of all three taxa as well as other *Satyrium* species to provide phylogenetic context (e.g. *S. calanus* Hübner, *S. californica* W.H. Edwards, and *S. sylvinus* Boisduval; Runquist 2012). We also recommend further sequencing to confirm the reported identical mitochondrial haplotypes observed between *S. curiosolus* and *S. semiluna* (COSEWIC 2006) and shared haplotypes between *S. semiluna* and *S. fuliginosa* (Runquist 2012). When such comparative data are available, the second component of the species concept of Sperling (2003) can be applied, which uses the extent of divergence between recognized sister species in parapatry or sympatry to calibrate the threshold for species recognition of allopatric populations.

We note that *S. fuliginosa* is frequently referred to as “*S. fuliginosum*” in species status assessments of *S. semiluna* (e.g. COSEWIC 2006, 2022, with inconsistent usage within single documents), survey reports (e.g. Kondla 2003), and the original *S. semiluna* description (Matton and Austin 1998). Originally described as *Lycaena fuliginosa* (W.H. Edwards), the species was later reclassified into *Satyrium* and the use of “*S. fuliginosum*” stems from the inference that *Satyrium* is a neuter genus name, requiring gender agreement of species epithets (Scudder 1876). However, global lepidopterists’ societies have maintained original orthography, even in cases of gender incongruence (Sommerer 2002; van Nieukerken et al. 2019). We have chosen to use the name *S. fuliginosa*, as reflected in Pelham’s (2023) catalogue of butterflies of the United States and Canada.

Based on genomic and ecological divergences, MacDonald et al. (2025) recommended that genetic rescue, involving the translocation of individuals from other *S. semiluna* populations to Blakiston Fan, is more likely to be harmful than helpful at present. Parks Canada has accepted this recommendation and is managing *S. curiosolus* in isolation. The taxonomic distinctiveness of *S. curiosolus* suggests substantial risk of outbreeding depression or reproductive incompatibility if genetic rescue involving *S. semiluna* were attempted. However, the low genetic diversity that characterizes *S. curiosolus* may hinder adaptation under accelerating climate change. In the future, the trade-off between a lack of adaptive capacity and outbreeding depression may shift in favor of managed introgression with *S. semiluna* populations, should they be found to be reproductively compatible. Genetic rescue can introduce beneficial genomic variation that is integral to rapid adaptation (Edelman and Mallet 2021) and hybrid vigor (“heterosis”) has long been recognized as a possible benefit of hybridization, even between distinct species (Darwin 1859; Birchler et al. 2003; Lippman and Zamir 2007; Parmesan et al. 2023). Hybridization is common between species, and should not always be viewed as undermining species-level recognition (Mallet 1995; Sperling 2003; Taylor et al. 2015). The possibility of genetic rescue—should be regularly revisited as local climatic and habitat conditions at Blakiston Fan continue to change.

Acknowledgements

We acknowledge John Acorn for preparation and photography of pinned specimens, Lacey Hébert and Llewellyn Haines for fieldwork support, Steve Kohler for providing Montana specimens, Natasha Lloyd for logistical and permit support, Janet Sperling for assistance with lab work, including DNA barcoding of specimens to confirm species-level identifications, Eric Runquist for consultation, members of the UCLA Shaffer lab for analysis comments and critiques, the Waterton Lakes National Park Ecological Restoration Team for leading habitat restoration programs and assisting population monitoring, and the Half-moon Hairstreak Conservation Committee for discussions on impacts of this research. We also wish to acknowledge two anonymous reviewers whose comments greatly improved the quality of the manuscript.

Additional information

Conflict of interest

The authors have declared that no competing interests exist.

Ethical statement

No ethical statement was reported.

Funding

Funding was provided by the Calgary Zoo Foundation, Parks Canada (GC-1341), Shell Canada, a Natural Sciences and Engineering Research Council (NSERC) Discovery Grant awarded to FAHS (RGPIN-2018–04920), a USDA-NIFA HATCH grants to JRD (Project KY008091), and a La Kretz Center for California Conservation Science Postdoctoral Fellowship (2021/22) and an NSERC Postdoctoral Fellowship (PDF - 578319 – 2023), both awarded to ZGM.

Author contributions

All authors collectively conceived of this taxonomic revision. ZGM and JRD led analyses and writing with assistance from all authors. Field work and observations were led by JRNG and RS with assistance from ZGM.

Author ORCIDs

Zachary G. MacDonald  <https://orcid.org/0000-0002-7966-5712>

Julian R. Dupuis  <https://orcid.org/0000-0002-6989-9179>

James R. N. Glasier  <https://orcid.org/0000-0002-3449-9183>

Axel Moehrenschrager  <https://orcid.org/0000-0003-2789-0376>

H. Bradley Shaffer  <https://orcid.org/0000-0002-5795-9242>

Felix A. H. Sperling  <https://orcid.org/0000-0001-5148-4226>

Data availability

All of the data that support the findings of this study are available in the main text.

References



- Baum DA, Shaw KL (1995) Genealogical perspectives on the species problem. In: Hoch PC, Stephenson AG (Eds) *Experimental and Molecular Approaches to Plant Biosystematics*. Monographs in Systematic Botany 53. Missouri Botanical Garden, St. Louis, 289–303.
- Birchler JA, Auger DL, Riddle NC (2003) In search of the molecular basis of heterosis. *The Plant Cell* 15(10): 2236–2239. <https://doi.org/10.1105/tpc.151030>
- Bischoff JL, Cummins K (2001) Wisconsin glaciation of the Sierra Nevada (79,000–15,000 yr BP) as recorded by rock flour in sediments of Owens Lake, California. *Quaternary Research* 55(1): 14–24. <https://doi.org/10.1006/qres.2000.2183>
- Braby MF, Eastwood R, Murray N (2012) The subspecies concept in butterflies: Has its application in taxonomy and conservation biology outlived its usefulness? *Biological Journal of the Linnean Society* 106(4): 699–716. <https://doi.org/10.1111/j.1095-8312.2012.01909.x>
- Brandão-Dias PF, Zhang YM, Pirro S, Vinson CC, Weinersmith KL, Ward AK, Egan SP (2022) Describing biodiversity in the genomics era: a new species of Nearctic Cynipidae gall wasp and its genome. *Systematic Entomology* 47(1): 94–112. <https://doi.org/10.1111/syen.12521>
- Campbell EO, MacDonald ZG, Gage EV, Gage RV, Sperling FA (2022) Genomics and ecological modelling clarify species integrity in a confusing group of butterflies. *Molecular Ecology* 31(8): 2400–2417. <https://doi.org/10.1111/mec.16407>
- Clarke JG, Smith AC, Cullingham CI (2024) Genetic rescue often leads to higher fitness as a result of increased heterozygosity across animal taxa. *Molecular Ecology* 33: e17532. <https://doi.org/10.1111/mec.17532>
- Clayton L, Moran SR (1982) Chronology of late Wisconsinan glaciation in middle North America. *Quaternary Science Reviews* 1(1): 55–82. [https://doi.org/10.1016/0277-3791\(82\)90019-1](https://doi.org/10.1016/0277-3791(82)90019-1)
- COSEWIC (Committee on the Status of Endangered Wildlife in Canada) (2006) COSEWIC assessment and status report of Half-moon Hairstreak *Satyrium semiluna* in Canada. COSEWIC, Ottawa, vi + 26 pp. www.sararegistry.gc.ca/status_e.cfm. Accessed on: 2025-01-10.
- COSEWIC (Committee on the Status of Endangered Wildlife in Canada) (2022) COSEWIC assessment and status report on the Half-moon Hairstreak *Satyrium semiluna* Okanagan-Similkameen and population Waterton Lakes population in Canada. COSE-

- WIC, Ottawa, xvi + 66 pp. <https://www.canada.ca/en/environment-climate-change/services/species-risk-public-registry.html> [Accessed on: 2025-01-10]
- Cracraft J (1983) Species concepts and speciation analysis. *Current Ornithology* 1: 159–187. https://doi.org/10.1007/978-1-4615-6781-3_6
- Danecek P, Auton A, Abecasis G, Albers CA, Banks E, DePristo MA, Durbin R (2011) The variant call format and VCFtools. *Bioinformatics* 27(15): 2156–2158. <https://doi.org/10.1093/bioinformatics/btr330>
- Danecek P, Bonfield JK, Liddle J, Marshall J, Ohan V, Pollard MO, Li H (2021) Twelve years of SAMtools and BCFtools. *Gigascience* 10(2): giab008. <https://doi.org/10.1093/gigascience/giab008>
- Darwin C (1859) *On the Origin of Species by Means of Natural Selection*. John Murray, London, 502 pp.
- De Queiroz K (1998) The general lineage concept of species, species criteria, and the process of speciation. In: Howard DJ, Berlocher SH (Eds) *Endless Forms: Species and Speciation*. Oxford University Press, New York, 57–75.
- De Queiroz K (2007) Species concepts and species delimitation. *Systematic Biology* 56(6): 879–886. <https://doi.org/10.1080/10635150701701083>
- Edelman NB, Mallet J (2021) Prevalence and adaptive impact of introgression. *Annual Review of Genetics* 55: 265–283. <https://doi.org/10.1146/annurev-genet-021821-020805>
- Edwards WH (1861) Descriptions of certain species of diurnal Lepidoptera, found within the United States and British America. *Proceedings of Academy of Natural Sciences* 13: 160–164.
- Environment and Climate Change Canada (ECCC) (2016) *Recovery Strategy for the Half-moon Hairstreak (Satyrium semiluna) in Canada*. Species at Risk Act Recovery Strategy Series. ECCC, Ottawa, 24 + 33 pp.
- Fennessy J, Bidon T, Reuss F, Kumar V, Elkan P, Nilsson MA, Janke A (2016) Multi-locus analyses reveal four giraffe species instead of one. *Current Biology* 26(18): 2543–2549. <https://doi.org/10.1016/j.cub.2016.07.036>
- Frankham R, Ballou JD, Ralls K, Eldridge MDB, Dudash MR, Fenster CB, Lacy RC, Sunnucks P (2017) *Genetic Management of Fragmented Animal and Plant Populations*. Oxford University Press, Oxford, 432 pp. <https://doi.org/10.1093/oso/9780198783398.001.0001>
- Glasier JRN, Acorn JH, Nielsen SE, Proctor H (2013) Ants (Hymenoptera: Formicidae) of Alberta: a key to species based primarily on the worker caste. *Canadian Journal of Arthropod Identification* 22: 1–104. <https://doi.org/10.3752/cjai.2013.22>
- James DG, Nunnallee D (2011) *Life Histories of Cascadia Butterflies*. Oregon State University Press, Corvallis, 448 pp. <https://doi.org/10.1353/book12706>
- Kondla NG (2003) The Sooty Hairstreak in British Columbia. *Boreus* 23: 10–12.
- Kondla NG (2004) Waterton Lakes National Park Sooty Hairstreak survey, 2004. Unpublished report prepared for Parks Canada Agency, 24 pp.
- Li H, Durbin R (2011) Inference of human population history from individual whole-genome sequences. *Nature* 475(7357): 493–496. <https://doi.org/10.1038/nature10231>
- Lippman ZB, Zamir D (2007) Heterosis: revisiting the magic. *Trends in Genetics* 23(2): 60–66. <https://doi.org/10.1016/j.tig.2006.12.006>
- MacDonald ZG, Shaffer HB, Sperling FAH (2024) Impacts of land use and climate change on natural populations: the butterfly perspective. In: Cork S, Whiteside D (Eds) *Case Studies in Eco Health*. 5m Books, Great Easton, UK, 109–131. <https://doi.org/10.52517/9781789183313.008>

- MacDonald ZG, Dupuis JR, Glasier JR, Sissons R, Moehrensclager A, Shaffer HB, Sperling FA (2025) Whole-genome evaluation of genetic rescue: the case of a curiously isolated and endangered butterfly. *Molecular Ecology* 34(4): e17657. <https://doi.org/10.1111/mec.17657>
- Mallet J (1995) A species definition for the modern synthesis. *Trends in Ecology & Evolution* 10(7): 294–299. [https://doi.org/10.1016/0169-5347\(95\)90031-4](https://doi.org/10.1016/0169-5347(95)90031-4)
- Martins ARP, Duarte M, Robbins RK (2019) Hairstreak butterflies (Lepidoptera: Lycaenidae) and evolution of their male secondary sexual organs. *Cladistics* 35(2): 173–197. <https://doi.org/10.1111/cla.12355>
- Mattoon SO, Austin GT (1998) Review of *Satyrrium fuliginosum* (W. H. Edwards) with the description of three new subspecies (Lepidoptera: Lycaenidae). In: Emmel TC (Ed.) *Systematics of Western North American butterflies*. Mariposa Press, Gainesville, 681–690.
- Mayr E (1942) *Systematics and the Origin of Species*. Columbia University Press, New York, 334 pp.
- Mayr E (1963) *Animal Species and Evolution*. Harvard University Press, Cambridge, 797 pp. <https://doi.org/10.4159/harvard.9780674865327>
- Nater A, Mattle-Greminger MP, Nurcahyo A, Nowak MG, De Manuel M, Desai T, Krützen M (2017) Morphometric, behavioral, and genomic evidence for a new orangutan species. *Current Biology* 27(22): 3487–3498. <https://doi.org/10.1016/j.cub.2017.09.047>
- NatureServe (2024) NatureServe. <https://explorer.natureserve.org/> [Accessed on: 2025-01-10]
- Nelson G, Platnick NI (1981) *Systematics and Biogeography*. Columbia University Press, New York, 567 pp.
- O’Grady P, DeSalle R (2018) Hawaiian *Drosophila* as an evolutionary model clade: days of future past. *BioEssays* 40(5): 1700246. <https://doi.org/10.1002/bies.201700246>
- Parmesan C, Singer MC, Wee B, Mikheyev S (2023) The case for prioritizing ecology/behavior and hybridization over genomics/taxonomy and species’ integrity in conservation under climate change. *Biological Conservation* 281: 109967. <https://doi.org/10.1016/j.biocon.2023.109967>
- Pelham JP (2023) *A catalogue of the butterflies of the United States and Canada* (Rev. ed.). McGuire Center for Lepidoptera and Biodiversity, Florida Museum of Natural History. <https://butterfliesofamerica.com/US-Can-Cat.htm> [Accessed on: 2025-03-01]
- Phillips SJ, Anderson RP, Schapire RE (2006) Maximum entropy modeling of species geographic distributions. *Ecological Modelling* 190(3–4): 231–259. <https://doi.org/10.1016/j.ecolmodel.2005.03.026>
- Priddel D, Carlile N, Humphrey M, Fellenberg S, Hiscox D (2003) Rediscovery of the ‘extinct’ Lord Howe Island stick-insect (*Dryococelus australis* (Montrouzier)) (Phasmatodea) and recommendations for its conservation. *Biodiversity & Conservation* 12: 1391–1403. <https://doi.org/10.1023/A:1023625710011>
- Pritchard JK, Stephens M, Donnelly P (2000) Inference of population structure using multilocus genotype data. *Genetics* 155(2): 945–959. <https://doi.org/10.1093/genetics/155.2.945>
- Ralls K, Sunnucks P, Lacy RC, Frankham R (2020) Genetic rescue: a critique of the evidence supports maximizing genetic diversity rather than minimizing the introduction of putatively harmful genetic variation. *Biological Conservation* 251: 108784. <https://doi.org/10.1016/j.biocon.2020.108784>
- Robbins RK, Cong Q, Zhang J, Shen J, Busby RC, Faynel C, Duarte M, Martins ARP, Prieto C, Lamas G, Grishin NV (2022) Genomics-based higher classification of the spe-

- cies-rich hairstreaks (Lepidoptera: Lycaenidae: Eumaini). *Systematic Entomology* 47: 445–469. <https://doi.org/10.1111/syen.12541>
- Rosen DE (1979) Fishes from the uplands and intermontane basins of Guatemala: revisionary studies and comparative geography. *Bulletin of the American Museum of Natural History* 162(5): 267–376.
- Runquist EB (2012) Patterns and mechanisms of divergence in butterflies across spatial scales. PhD thesis, University of California, Davis, 125 pp.
- Schär S, Talavera G, Rana JD, Espadaler X, Cover SP, Shattuck SO, Vila R (2022) Integrative taxonomy reveals cryptic diversity in North American *Lasius* ants, and an overlooked introduced species. *Scientific Reports* 12: 5970. <https://doi.org/10.1038/s41598-022-10047-9>
- Scudder SH (1876) Synonymic list of the butterflies of North America, north of Mexico. Part ii. Rurales. *Bulletin of the Buffalo Society of Natural Sciences* 3: 98–129.
- Simpson GG (1951) The species concept. *Evolution* 5(4): 285–298. <https://doi.org/10.2307/2405675>
- Sommerer MD (2002) To agree or not to agree: the question of gender agreement in the International Code of Zoological Nomenclature. *Nota Lepidopterologica* 25(2/3): 191–204.
- Sperling FAH (2003) Butterfly molecular systematics: from species definitions to higher level phylogenies. In: Boggs C, Ehrlich P, Watt W (Eds) *Ecology and Evolution Taking Flight: Butterflies as Model Study Systems*. University of Chicago Press, Chicago, 431–458.
- Stanton DW, Frandsen P, Waples RK, Heller R, Russo IRM, Orozco-terWengel PA, Bruford MW (2019) More grist for the mill? Species delimitation in the genomic era and its implications for conservation. *Conservation Genetics* 20: 101–113. <https://doi.org/10.1007/s10592-019-01149-5>
- Storfer A (1999) Gene flow and endangered species translocations: a topic revisited. *Biological Conservation* 87(2): 173–180. [https://doi.org/10.1016/S0006-3207\(98\)00066-4](https://doi.org/10.1016/S0006-3207(98)00066-4)
- Taylor SA, Larson EL, Harrison RG (2015) Hybrid zones: windows on climate change. *Trends in Ecology & Evolution* 30(7): 398–406. <https://doi.org/10.1016/j.tree.2015.04.010>
- van Nieukerken EJ, Karsholt O, Hausmann A, Holloway J D, Huemer P, Kitching IJ, Nuss M, Pohl GR, Rajaei H, Rennland E, Rodeland J, Rougerie R, Scoble MJ, Sinev SYu, Sommerer M (2019) Stability in Lepidoptera names is not served by reversal to gender agreement: a response to Wiemers et al. (2018). *Nota Lepidopterologica* 42(1): 101–111. <https://doi.org/10.3897/nl.42.34187>
- Van Valen L (1976) Ecological species, multispecies, and oaks. *Taxon* 25: 233–239. <https://doi.org/10.2307/1219444>
- Warren AD (2005) *Lepidoptera of North America 6. Butterflies of Oregon: Their Taxonomy, Distribution, and Biology*. C.P. Gillette Museum of Arthropod Diversity, Colorado State University, Fort Collins, 408 pp.
- Weeks AR, Sgro CM, Young AG, Frankham R, Mitchell NJ, Miller KA, Hoffmann AA (2011) Assessing the benefits and risks of translocations in changing environments: a genetic perspective. *Evolutionary Applications* 4(6): 709–725. <https://doi.org/10.1111/j.1752-4571.2011.00192.x>
- Weir BS, Cockerham CC (1984) Estimating *F*-statistics for the analysis of population structure. *Evolution* 38(6): 1358–1370. <https://doi.org/10.2307/2408641>
- Wiley EO (1978) The evolutionary species concept reconsidered. *Systematic Biology* 27(1): 17–26. <https://doi.org/10.2307/2412809>
- Zhou X, Guang X, Sun D, Xu S, Li M, Seim I, Yang G (2018) Population genomics of finless porpoises reveal an incipient cetacean species adapted to freshwater. *Nature Communications* 9(1): 1276. <https://doi.org/10.1038/s41467-018-03722-x>

Delineation of species of the *Tetramorium caespitum* complex (Hymenoptera, Formicidae) in Anatolia with a diagnosis of related species-complexes

Herbert C. Wagner^{1,2}, Marion Cordonnier³, Bernard Kaufmann⁴, Kadri Kiran⁵, Celal Karaman⁵, Roland Schultz⁶, Bernhard Seifert⁶, Sándor Csősz^{7,8}

¹ Centre for Ecological Research, Institute of Ecology and Botany, 2163 Vácrátót, Alkotmány u. 2-4, Hungary

² Institute of Biology, 8010 Graz, Universitätsplatz 2/I, Austria

³ Lehrstuhl für Zoologie/Evolutionsbiologie, Universität Regensburg, Universitätsstraße 31, D-93053 Regensburg, Germany

⁴ Université Claude Bernard Lyon 1, LEHNA UMR 5023, CNRS, ENTPE, F-69622, Villeurbanne, France

⁵ Department of Biology, Faculty of Sciences, Trakya University, 22030, Edirne, Türkiye

⁶ Section Pterygota, Senckenberg Museum of Natural History, Am Museum 1, D-02826 Görlitz, Germany

⁷ HUN-REN-ELTE-MTM Integrative Ecology Research Group, Pázmány Péter ave 1/C, Budapest 1117, Hungary

⁸ Department of Systematic Zoology and Ecology, Institute of Biology, ELTE-Eötvös Loránd University, Pázmány Péter ave 1/C, Budapest 1117, Hungary

Corresponding author: Sándor Csősz (csosz.sandor@ttk.elte.hu)



Academic editor: Sebastian Salata

Received: 29 November 2024

Accepted: 20 February 2025

Published: 22 April 2025

ZooBank: <https://zoobank.org/AFAAF015-A1EC-4789-8862-46554AFA3D34>

Citation: Wagner HC, Cordonnier M, Kaufmann B, Kiran K, Karaman C, Schultz R, Seifert B, Csősz S (2025) Delineation of species of the *Tetramorium caespitum* complex (Hymenoptera, Formicidae) in Anatolia with a diagnosis of related species-complexes. ZooKeys 1234: 309–339. <https://doi.org/10.3897/zookeys.1234.142963>

Abstract

The high level of morphological crypsis of the hyper-diverse Palearctic *Tetramorium caespitum* group have challenged taxonomists for decades. Within this group, Wagner et al. (2017) offered a multidisciplinary solution for the delimitation of ten European species of the *Tetramorium caespitum* complex. Anatolia, harboring a high level of endemism in ants, has never been subject of focus research within this genus. In this study, the *Tetramorium caespitum* complex diversity in Anatolia and the Caucasus region was investigated by examining 191 nest-samples using an in-depth integrative-taxonomic approach. Quantitative morphometric and microsatellite data of 505 and 133 workers, respectively, and genital-morphology data of 33 nests were collected. Unsupervised analyses provided independent species-hypotheses based on the morphological and molecular disciplines. Based on the final species-hypotheses, we confirm *T. caespitum* (Linnaeus, 1758), *T. hungaricum* Rösler, 1935, *T. indocile* Santschi, 1927, *T. caucasicum* Wagner et al., 2017, *T. impurum* (Foerster, 1850), *T. immigrans* Santschi, 1927, and *T. flavidulum* Santschi, 1910 as valid species of the *T. caespitum* complex occurring in Anatolia. A lectotype of *T. flavidulum* was designated. The host of the temporary social-parasitic species *Tetramorium aspina* Wagner et al., 2018 is *T. caucasicum* instead of *T. immigrans* – as it was suggested before. An identification key to species complexes of the *T. caespitum* group and to workers of the species of the *T. caespitum* complex in Anatolia is provided. Every cluster we identified could be linked to described species and the region's species-composition is similar to those of the Balkans and Central Europe.

Key words: Morphometrics, nest centroid clustering, microsatellites, pavement ants, *Tetramorium flavidulum*, Türkiye

Copyright: © Herbert C. Wagner et al.

This is an open access article distributed under terms of the Creative Commons Attribution License (Attribution 4.0 International – CC BY 4.0).

Introduction

The genus *Tetramorium*, a diverse and ancient lineage with fossil records up to 37 million years old (Radchenko and Dlussky 2015), has diverged especially in the last 20 million years (Ward et al. 2015; Cicconardi et al. 2020). All native European and Anatolian *Tetramorium* species belong to the *Tetramorium caespitum* group (Bolton 1979; Kiran and Karaman 2012). However, within this group, the task of identifying not only species but even species complexes poses formidable challenges to taxonomists (Csősz and Schulz 2010; Wagner et al. 2017). Seven West-Palearctic species complexes have been outlined, each with its unique characteristics and intricacies: the *T. ferox* complex, the *T. chefketi* complex, the *T. caespitum* complex, the *T. semilaeve* complex (Csősz and Schulz 2010), the *T. striativentre* complex [as “*striativentre* species group”] (Radchenko and Scupola 2015), the *T. biskrense* complex [as “*biskrense* group”] (Lebas et al. 2016), and the *T. meridionale* complex [as “*Tetramorium meridionale* species-group”] (Salata et al. 2024). One further complex is briefly introduced in the frame of this study: the well-defined *T. inerme* complex with at least five species (*T. inerme* Mayr, 1877; *T. armatum* Santschi, 1927; *T. sulcinode* Santschi, 1927; *T. goniommoide* Poldi, 1979; *T. taueret* Bolton, 1995). In summary, we consider eight West Palearctic similar species-complexes within the *T. caespitum* group, each requiring a unique set of morphometric characters for delimitation.

The target complex of this study, the *Tetramorium caespitum* complex, has an age of approximately 6.78 million years (95% confidence interval: 8.66–2.23 million years) (Cicconardi et al. 2020). Of all complexes of the *T. caespitum* group, it goes farthest to the north, highest in altitude, and deepest into Siberia, so it includes the most oligothermic, frost resistant, and thus most widespread species in Central and North Europe (Steiner et al. 2010; Wagner et al. 2017; Seifert 2021). In Southern Europe and Anatolia, most species occur at high altitudes. The unexpected cryptic diversity in the *T. caespitum* complex was detected in the early 2000s (Steiner et al. 2002; Csősz and Markó 2004; Schlick-Steiner et al. 2006). The *T. caespitum* complex is monophyletic and cryptic is explained by morphological stasis (Wagner et al. 2018b). The in-depth taxonomic revision of Wagner et al. (2017) delimited ten European species, of which some hybridize (Cordonnier et al. 2019, 2020): *Tetramorium alpestre* Steiner et al., 2010; *T. caespitum* (Linnaeus, 1758); *T. hungaricum* Rösler, 1935; *T. breviscapus* Wagner et al., 2017; *T. indocile* Santschi, 1927; *T. caucasicum* Wagner et al., 2017; *T. fusciclava* Consani & Zangheri, 1952; *T. staercke* Kratochvíl, 1944; *T. impurum* (Foerster, 1850); and *T. immigrans* Santschi, 1927. In Siberia and East Asia, there are at least two further species: *Tetramorium tsushimae* Emery, 1925 and *T. sibiricum* Seifert, 2021 (Steiner et al. 2006b; Seifert 2021). The taxonomic revision mentioned above (Wagner et al. 2017) mainly considered European but only very little Anatolian material because the predicted high number of cryptic species had discouraged the authors. Thus, a taxonomically unsatisfyingly solved situation in the diversity-hotspot Anatolia (cf. Kiran and Karaman 2012) remained.

The current study aims to delimit the Anatolian species of the *Tetramorium caespitum* complex based on an integrative-taxonomy approach. Morphological and molecular-genetic data are used as independent methods for establishing species hypotheses. Distribution and ecology data, and an identification key are provided.

Materials and methods

Integrative-taxonomy workflow

Species hypotheses given in Wagner et al. (2017), based on integrative taxonomy, were used as the starting hypotheses for the present study. With new specimens from Anatolia, we seek to untangle the intricate situation in the *T. caespitum* species complex. To this aim, our protocol for integrative taxonomy (Schlick-Steiner et al. 2010) is based on three methods, two of them quantitative and analyzed unsupervised (i.e., morphometrics and microsatellites) and one qualitative (i.e., male genital morphology). Mitochondrial DNA was not analyzed in this study, as it is of little value for species delimitation in the *Tetramorium caespitum* complex (Wagner et al. 2017) as well as in ants generally (Seifert 2018, 2024).

Artificial intelligence (AI) was not used in this study, but we will likely see large-scale deployment of this technology soon. The fact that morphometric data can separate the species of the *T. caespitum* complex makes them interesting candidates for testing some next-generation AI identification-techniques.

A workflow to assign new samples based on results of different disciplines was implemented as follows: A Nest-Centroid cluster, including all morphometric data of Anatolia and the Caucasus region, was established. Morphometric clusters were compared with male genital morphology and microsatellite data. Samples with discordant results between any disciplines were treated as wild cards in linear discriminant analyses (LDA) using morphometric data on the level of workers, performed with the software package SPSS Statistics v16 (IBM, USA) and the method “stepwise selection”, to fix species affiliation.

The Gene and Gene expression (GAGE) Species Concept (Seifert 2020, 1033) was employed in a conservative manner. It defines species as “... separable clusters that have passed a threshold of evolutionary divergence and are exclusively defined by nuclear DNA sequences and/or their expression products ...”. This conservative use of the species concept was a deliberate choice, aimed at reducing the risk of over-splitting in this highly cryptic complex. Only species with at least two independent disciplines resulting in the same species-hypotheses were accepted (Schlick-Steiner et al. 2010), further ensuring the validity of our conclusions.

Sampling

The study utilized material from 191 nest samples in Anatolia and the Caucasus region south of Russia. Among these, 168 samples were newly collected, while 23 were obtained from existing literature (Wagner et al. 2017; see Suppl. material 2). Since all available material was included, the distribution of investigated samples per species reflects their relative abundance in the field. The collected material was preserved in 96% ethanol. Additionally, material outside the *Tetramorium caespitum* complex was used to define the species complex within the *T. caespitum* group, following the taxonomic framework proposed by Bolton (1995). Distribution maps were created using QGIS Development Team (2019) based on our own data and relevant literature (Wagner et al. 2017).

Morphometrics of workers

One worker per sample was used for DNA extraction. Three further individuals, if available, were mounted. If males were available, two workers and one male were prepared. In samples without males, three workers were prepared. If two workers were prepared, the largest and the smallest worker (evaluated by eye-estimation) of the sample were chosen. If three workers were prepared, the largest, the smallest, and one further worker of any size were prepared. This procedure aimed to cover extreme sizes to present a robust calibration set for discriminant analyses. Measurements were made using a Leica MZ16 A high-performance stereomicroscope with magnifications of $\times 80$ –296. Workers were positioned on a pin-holding stage permitting spatial adjustment in all directions. Measurements always referred to cuticula and not pubescence surface. An ocular micrometer with 120 graduation marks was used. Its measuring line was kept vertically to avoid the parallax error (Seifert 2002). A combination of a Fiberoptic L 150 light, equipped with two flexible light ducts, and a Leica KL 1500 LCD coaxial polarized light was used. All bilateral characters except PnHL (see definition) were measured from both sides and an arithmetic mean was calculated. Morphometric data of 505 workers from 191 nest samples were used (on average, 2.6 workers per sample). The used 31 characters were nearly identical as in Wagner et al. (2017); 26 of them originally go back to Csősz et al. (2014), Seifert (2007), or Steiner et al. (2006a). Ppss was modified to sqPpss, the square route of Ppss (used to transform data to normal distribution (as done for, e.g., PDCL in Seifert 2018)). Twenty-nine characters were collected morphometrically, MC1TG and POTCos meristically. The head index CS is a proxy measure for the size of individuals.

Analyses of morphometric data

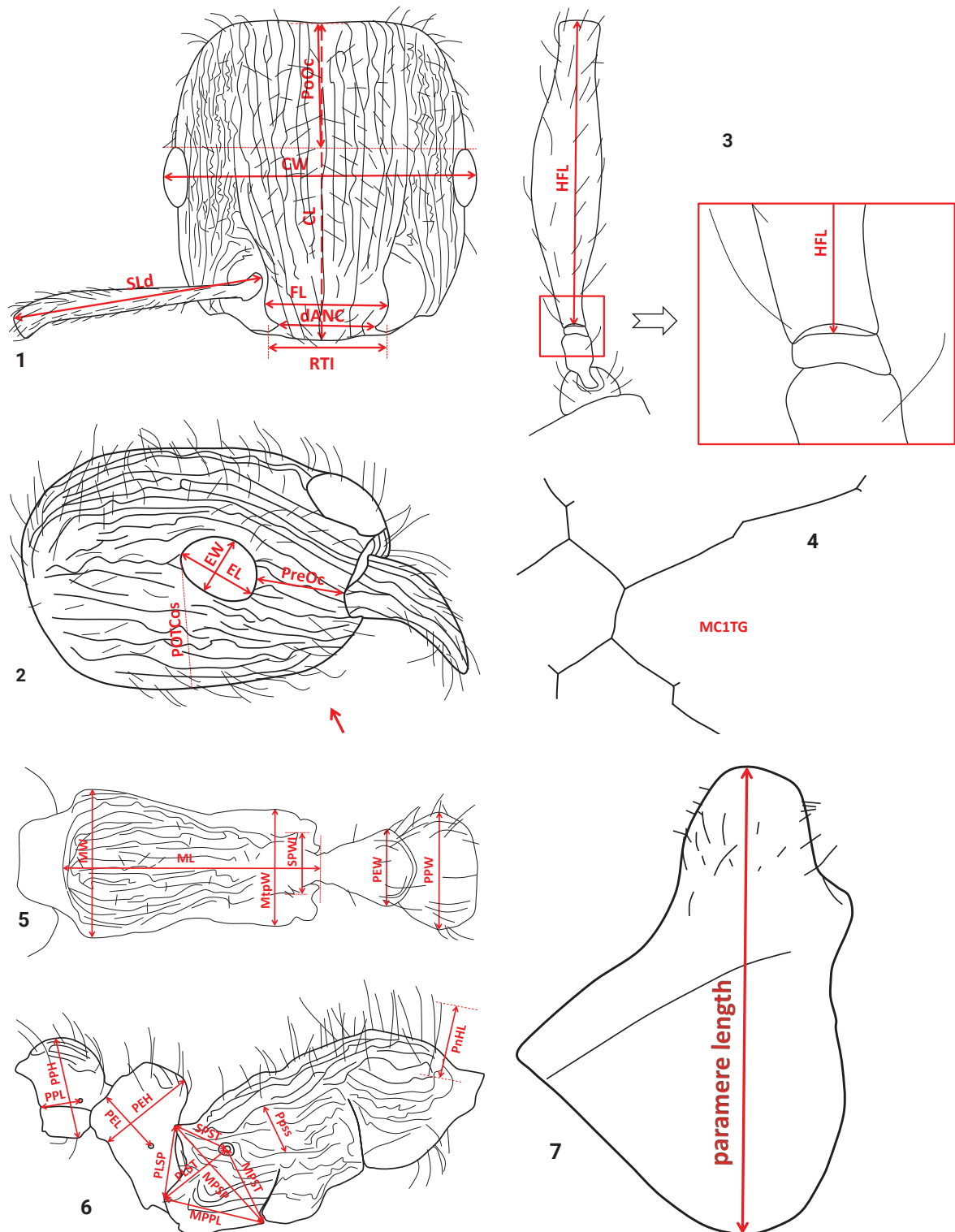
Nest-Centroid clustering (Seifert et al. 2014; Csősz and Fisher 2015) was used as unsupervised approach to establish morphological species-hypotheses independent from genetic data using R v3.0.1 and the packages MASS, ecodist, cluster, plyr, stringr, and scatterplot3d (Ligges and Maechler 2003; Goslee and Urban 2007; Wickham 2009, 2011; R Development core team 2012; Maechler et al. 2013; Ripley et al. 2013). Additionally, we employed a partitioning algorithm, Partitioning Based on Recursive Thresholding (Nilsen et al. 2013), using two distance metrics “part.kmeans” and “part.hclust” to estimate the ideal cluster-number and assign cases into partitions (clusters). The protocol was published by Csősz and Fisher (2016). NC clustering does often not allow for detecting species with only very few samples in the dataset but places them into the cluster of the next similar species. Thus, an alternative strategy was applied to detect rare species: In addition to the standard analyses, every sample was used as wild-card with available comparison data (Wagner et al. 2017) to detect putative samples of species known from the Balkans but not from Anatolia, for example, *T. staerckei*.

Male genital morphology

Genital morphology of 33 males from 33 nests was qualitatively investigated. Mounted genitals of interest were used for z-stack imaging with a Keyence VHX-7000 digital microscope. All male genitals used for pictures are stored at

Table 1. Acronyms and definitions of the worker traditional morphometric characters and male paramere length slightly modified from Wagner et al. (2017). For illustrations, see Figs 1–6.

| Acronym | Definition |
|-----------------|---|
| CL | Maximum cephalic length in median line (Fig. 1); head is carefully tilted to position with true maximum; excavations of occiput and / or clypeus reduce CL. Peaks due to sculpture are ignored and only valleys are considered. |
| CS | Arithmetic mean of CL and CW. |
| CW | Maximum cephalic width across eyes (Fig. 1). |
| dANC | Minimum distance between antennal fossae (Fig. 1); measured in dorsofrontal view. |
| EL | Maximum diameter of one eye. All structurally defined ommatidia, pigmented or not, are included (Fig. 2). |
| EW | Minimum diameter of one eye. All structurally defined ommatidia, pigmented or not, are included (Fig. 2). |
| EYE | Arithmetic mean of EL and EW. |
| FL | Maximum distance between external margins of frontal lobes (Fig. 1). If this distance is not defined because frontal carinae constantly converge frontad, FL is measured at FRS level (definition of FRS see Seifert (2003)) as distance between the outer margins of frontal carinae. |
| HFL | Length of hind femur in dorsal view (Fig. 3). Second trochanter, which could appear to be portion of femur, must not be mistakenly included. |
| MC1TG | Quantification of stickman-like or reticulate microsculpture units on 1 st gastral tergite (use > 150× magnification; Fig. 4): Number of connected lines building units and being separated by line intersections and by flexions angled > 10° is counted. Also very short lines are full counts. Straight lines twice as long as the typical length of one line, that is > 20 µm, are counted as 2. Arithmetic means of at least five units per worker are taken. |
| ML | Mesosoma length measured in dorsal view from caudalmost portion of propodeum to dorsofrontal corner of pronotal slope (i.e., where coarsely structured dorsum of pronotum meets finely structured pronotal neck; Fig. 5); equivalent measuring also possible in lateral view. |
| MPPL | Distance between most anteroventral point of metapleuron and most dorsocaudal point of propodeal lobe in lateral view (Fig. 6). If there are two points coming into question to be most dorsocaudal point on propodeal lobe, the one which is provided with a carina is taken. |
| MPSP | Distance between most anteroventral point of lateral metapleuron and distalmost point of propodeal spine (it does not need to be uppermost point of spine; Fig. 6). |
| MPST | Distance between most anteroventral point of metapleuron and center of propodeal stigma (Fig. 6). |
| MtpW | Maximum metapleuron width measured in dorsal view (Fig. 5). (In most cases, maximum is at caudal and in few cases at central or frontal region of metapleuron.) |
| MW | Maximum mesosoma width (Fig. 5). |
| paramere length | Maximum length of male genital paramere-structure in lateral view (Fig. 7). |
| PEH | Petiole height. Measured from uppermost point of concave ventral margin to node top (Fig. 6). |
| PEL | Petiole length. Measured in lateral view from center of petiolar stigma to caudal margin of petiole (both measuring points on same focal level; Fig. 6). |
| PEW | Maximum petiole width (Fig. 5). |
| PLSP | Distance between most dorsocaudal point of propodeal lobe (if there are two points coming into question to be most dorsocaudal point of propodeal lobe, the one which is provided with a carina is taken) and distalmost point of propodeal spine (it does not need to be uppermost point of spine; Fig. 6). |
| PLST | Distance between most dorsocaudal point of propodeal lobe and center of propodeal stigma (Fig. 6). |
| PnHL | Length of hair at frontolateral corner of pronotum (Fig. 6). Take longest hair of both sides. |
| PoOc | Postocular distance. Using cross-scaled ocular micrometer, head is adjusted to measuring position of CL; caudal measuring point: median posterior margin of head, microsculpture peaks are ignored and valleys are considered; frontal measuring point: median head crossing line between posterior eye margins (Fig. 1). |
| POTCos | Number of postoculo-temporal costae and costulae (Fig. 2). With head in lateral view and longitudinal axis of head adjusted horizontally, counted by focusing along perpendicular line from caudalmost point of eye down to underside of head. Costae / costulae just touching measuring line are counted as 0.5, those positioned just at ventral margin of head silhouette are not counted. |
| PPH | Maximum postpetiole height (Fig. 6). |
| PPL | Postpetiole length; distance from center of postpetiolar stigma to caudalmost intersection point of tergite and sternite (both measuring points at same focal level; Fig. 6). |
| Ppss | Maximum height of smooth and shiny area on lateral side of propodeum (Fig. 6). This area is brought into visual plane; a line is positioned perpendicular to main costae on propodeum and maximum height of smooth and shiny area without any costulae and costae is measured. |
| sqPpss | Square root of Ppss. |
| PPW | Maximum postpetiole width (Fig. 5). |
| PreOc | Preocular distance in lateral view. Measured as minimum distance between anterior eye margin and sharp frontal margin of gena (Fig. 2). |
| RTI | Distance between tops of ridges between antennal fossae and clypeus (Fig. 1). Tops are defined as most dorsofrontal points of ridges, provided with a costa on clypeus. Measured in dorso-anterior view. |
| SLd | Maximum scape length, including scape lobe, excluding articular condyle (Fig. 1). |
| SPST | Distance between distalmost point of propodeal spine (it does not need to be uppermost point of spine) and center of propodeal stigma (Fig. 6). |
| SPWI | Maximum distance between outer margins of propodeal spines (Fig. 5). Measured in dorso-anterior view. |



Figures 1–7. Measurement lines for the morphometric characters **1** CL, CW, dANC, FL, PoOc, RTI, and SLd **2** EL, EW, and PreOc; including an artificial line for the meristic character POTCos; in this example, POTCos = 7 **3** HFL **4** meristic character MC1TG. In this example, MC1TG = 18 **5** ML, MtpW, MW, PEW, PPW, and SPWI **6** MPPL, MPSP, MPST, PEH, PEL, PLSP, PLST, PnHL, PPH, PPL, Ppss, and SPST **7** paramere length (for abbreviations, see Table 1).

the Senckenberg Museum of Natural History Görlitz. Representative images were used to draw anatomical figures. Interspecific differences of male genital morphology allowed a qualitative assessment in many cases.

Microsatellite genotyping

DNA extraction from 170 whole individuals and the following microsatellite-genotyping protocols followed Cordonnier et al. (2018). For each microsatellite marker we computed the observed and expected heterozygosity, the number of alleles, and the effective alleles (GENALEX v. 6; Peakall and Smouse 2006) (Suppl. material 4). The identification of microsatellite clusters followed largely the procedure described in Cordonnier et al. (2018).

Identification of microsatellite clusters

To determine the number of genetic clusters, we used the admixture model with correlated allele frequencies and with a number of a priori unknown clusters (K) varying from $K = 1$ to $K = 20$, running ten iterations for each K -value in the software STRUCTURE v. 2.3.1 (Pritchard et al. 2000). The dataset used included the 133 genotypes from Anatolia plus the genotypes of 12 individuals collected in France and Belgium (4 *Tetramorium caespitum*, 4 *T. immigrans*, and 4 *T. impurum*).

Following the procedure described in Cordonnier et al. (2018), each run of STRUCTURE consisted of 500,000 replicates of the MCMC after a burn-in of 500,000 replicates. The ten independent runs were analyzed with CLUMPAK (Kopelman et al. 2015) and the sets of similar runs grouped to generate a consensus solution for each distinct group. For each K , the different runs were either consensual, one single group of runs, or resulting in both a majority mode (larger part of the iterations) and minority mode(s) (remaining iterations). The software CLUMPAK allowed to identify the optimal K -value based on the median values of $\text{Ln}(\text{Pr Data})$ (Earl and von Holdt 2012). The membership coefficient of each individual at each of the K clusters corresponding to the consensus solution of the majority mode was selected as Q -value. Individuals were then assigned to a cluster based on their higher Q -value across the different clusters. Individuals having no Q -value higher than 0.6 were not assigned to any cluster.

Reanalyzed linear discriminant-analysis (LDA) of morphometric data

After development of final species-hypotheses by the integrative-taxonomy approach, all nests were reanalyzed in a supervised approach using the same data as for Nest-Centroid clustering of morphometrics. SPSS Statistics v21 was used to perform the LDAs. To avoid overfitting, the number of individuals of each group had to be at least three times larger than the number of characters (Moder et al. 2007 and references therein).

Thermal niches

Standard air-temperature (TAS) in °C, a rough approximation of the ecological niche (Seifert and Pannier 2007), was calculated as in Steiner et al. (2010). Only locality data from Wagner et al. (2017) and the current study were considered, all in all 165 species-locality combinations. TAS was used to explore ecological differences in re-analyses. TAS values were tested for species-specific differences using SPSS Statistics v. 16.0. Species-specific pairwise differences of TAS were calculated in SPSS 16.0 as 2-side independent-sample t-tests. Since

in all cases Levene’s Test of Equality of Variances was > 0.05, *p* values for t-test type of line 1 (“variances are equal”) were accepted for Table 2. An α -level of 0.05 was used; in cases of multiple comparisons with single-character morphological distances, Bonferroni-Holm correction was applied (Holm 1979).

Type material

Type material of *Tetramorium flavidulum* Santschi, 1910 belongs to the *Tetramorium caespitum* complex based on quantitative and qualitative evaluation of morphological data (details in Taxonomy).

Results and discussion

Morphometry

The Nest-Centroid cluster showed seven separated large clusters (C1-7) including eleven to 50 nest samples each (Fig. 8; for morphometric data, see Suppl. material 2): C1: 46 samples of *T. immigrans*, 2 *T. caucasicum*, 1 *T. impurum*; C2: 37 *T. caucasicum*, 4 *T. impurum*, 1 *T. flavidulum*; C3: 18 *T. impurum*, 1 *T. caucasicum*; C4: 13 *T. caespitum*; 1 *T. indocile*; C5: 18 *T. indocile*, 1 *T. caucasicum*; C6: 23 *T. flavidulum*, 1 *T. caucasicum*; C7: 11 *T. hungaricum*. In C2, three samples of *T. impurum* build a subcluster within those of *T. caucasicum*. There are two smaller clusters: each with four samples, one with two of *T. caucasicum* and two of *T. impurum*, and one with three of *T. caespitum* and one of *T. caucasicum*. Moreover, there are four samples building clusters of their own, two of *T. caucasicum*, one of *T. immigrans*, and one of *T. caespitum*.

Male genital morphology

We detected seven different male genital morphologies. Of them, six were already known (Wagner et al. 2017): Male genitals of *T. alpestre* sensu drawings in Wagner et al. (2017): detected in 3 samples of *T. caucasicum*

Table 2. Separation of species based on different methods: from left to right: NC clustering of morphometrics, male genital-morphology, and microsatellite analyses. Significant separations are signed with a checkmark, non-significant ones with a cross.

| | caespitum | | | hungaricum | | | indocile | | | caucasicum | | | impurum | | | immigrans | | | flavidulum | | |
|------------|------------|-------------------------|-------------------------|------------|-------------------------|-------------------------|------------|-------------------------|-------------------------|------------|-------------------------|-------------------------|------------|-------------------------|-------------------------|------------|-------------------------|-------------------------|------------|-------------------------|-------------------------|
| | NC cluster | male genital-morphology | microsatellite analysis | NC cluster | male genital-morphology | microsatellite analysis | NC cluster | male genital-morphology | microsatellite analysis | NC cluster | male genital-morphology | microsatellite analysis | NC cluster | male genital-morphology | microsatellite analysis | NC cluster | male genital-morphology | microsatellite analysis | NC cluster | male genital-morphology | microsatellite analysis |
| nests | 17 | 2 | 11 | 11 | 3 | 7 | 19 | 4 | 9 | 47 | 14 | 23 | 25 | 3 | 17 | 48 | 1 | 32 | 24 | 5 | 17 |
| caespitum | | | | | | | | | | | | | | | | | | | | | |
| hungaricum | ✓ | ✗ | ✗ | | | | | | | | | | | | | | | | | | |
| indocile | ✓ | ✓ | ✗ | ✓ | ✓ | ✓ | | | | | | | | | | | | | | | |
| caucasicum | ✓ | ✓ | ✗ | ✓ | ✓ | ✓ | ✓ | ✓ | ✗ | | | | | | | | | | | | |
| impurum | ✓ | ✓ | ✓ | ✓ | ✓ | ✓ | ✓ | ✓ | ✓ | ✗ | ✓ | ✓ | | | | | | | | | |
| immigrans | ✓ | ✓ | ✓ | ✓ | ✓ | ✓ | ✓ | ✓ | ✓ | ✓ | ✓ | ✓ | ✓ | ✓ | ✓ | | | | | | |
| flavidulum | ✓ | ✓ | ✓ | ✓ | ✓ | ✓ | ✓ | ✓ | ✓ | ✓ | ✓ | ✓ | ✓ | ✓ | ✓ | ✓ | ✓ | ✓ | | | |

(Suppl. material 1: fig. S1); *T. caespitum/hungaricum*: 4 *T. caespitum*, 3 *T. hungaricum*; *T. indocile*: 3 *T. indocile*; *T. caucasicum*: 11 *T. caucasicum*; *T. impurum*: 3 *T. impurum* (from east of 35° E); *T. immigrans*: 1 *T. immigrans*. Males of *T. indocile*, *T. impurum*, *T. immigrans*, and normal form of *T. caucasicum*, as already described in Wagner et al. (2017), can be delimited at the species level with genital morphology. *Tetramorium caespitum* and *T. hungaricum* are the only species having identical male-genital-morphology. In addition to Wagner et al. (2017), we detected one new type of male genital morphology: The paramere structure of *T. flavidulum* (n = males of 5 nests) was very homogenous within the four samples of this species including males (Suppl. material 1: fig. S2). It belongs to the *impurum*-like form sensu Wagner et al. (2017) and is most similar with the normal form of *T. caucasicum* (Details under Treatment of species). The male genital morphology of western *T. caucasicum* samples (n = males of 3 nests from 3 sites), newly described here, is similar to those of *T. alpestre* but different from all Anatolian species as well as clearly different from eastern Anatolian and Caucasian *T. caucasicum*. The new *T. caucasicum* paramere structure belongs to the *T. impurum*-like form sensu Wagner et al. (2017): It has a rounded ventral paramere lobe without any corner in dorsal or ventral view but with clear division of ventral and dorsal paramere lobes, visible by deep emargination between lobes in posterior view. There is no sharp corner at the end of the ventral lobe visible in posterior view. The dorsal paramere lobe is relatively long and sharp-ended, visible in posterior and dorsal view. The ventral paramere lobe is slender than in *T. impurum*, visible in posterior view (Suppl. material 1: fig. S1). The paramere length of 3 males in lateral view was 956 ± 24 (928, 973) μm and thus below the range of *T. impurum*. Overall, there is no difference to *T. alpestre* but to all other species of the complex. Based on results of other disciplines, we consider western samples of *T. caucasicum* as conspecific but we cannot exclude that they might turn out to be a good species in future.

Microsatellites

Bayesian clustering analysis based on microsatellite genetic data at 17 loci suggested either eight or ten distinct genetic clusters ($K = 8$: LnProb mean = -14410.237; $K = 10$: LnProb mean = -14462.500), but the mean similarity score between the runs of the major mode was higher for $K = 8$ (0.98 against 0.87 for $K = 10$). In view of parsimony, we therefore retained the simplest and more robust solution and considered 8 genetic clusters (Suppl. material 3).

Of 145 individuals, 116 Anatolian had Q -values > 0.6 and were considered for the analyses. The eight suggested clusters included samples of the following species (Fig. 8): Q1: 32 *T. immigrans*; Q2: 10 *T. caespitum*, 7 *T. indocile*, 2 *T. caucasicum*, and 1 *T. hungaricum*; Q3: 10 *T. caucasicum*, 1 *T. indocile*, and 1 *T. flavidulum*; Q4: 16 *T. flavidulum*; Q5: 12 *T. caucasicum* and 1 *T. impurum*; Q6: 7 *T. impurum* from west of 35° E; Q7: 10 *T. impurum* from east of 35° E; Q8: 6 *T. hungaricum*.

Tetramorium caespitum and *T. indocile* were not separated by this method while *T. caucasicum* and *T. impurum* were each split into two clusters. There were six further disagreements to morphological clustering.

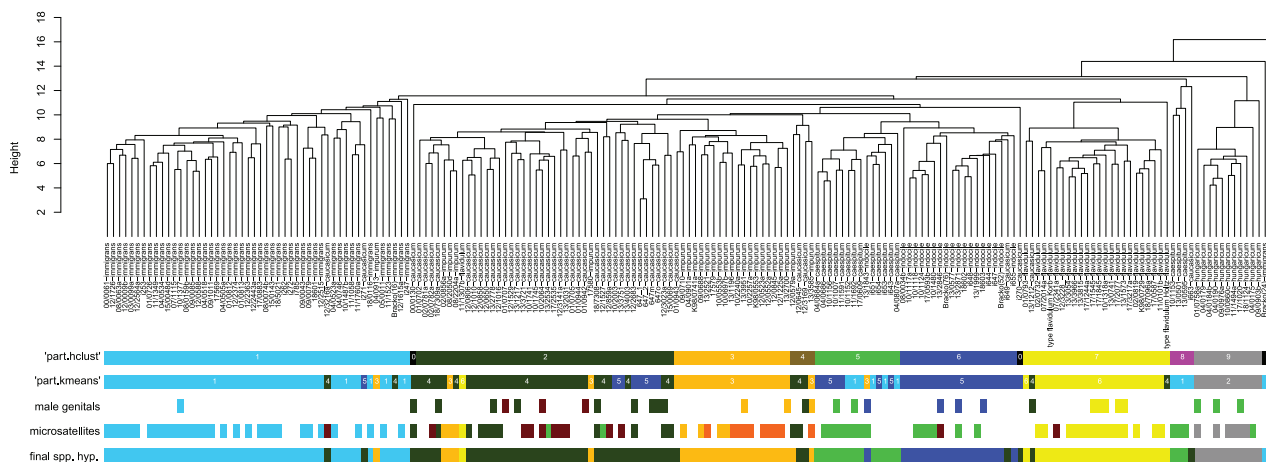


Figure 8. Nest-Centroid clustering of species occurring in Anatolia and Caucasus region. Results of both NC clustering algorithms “part.hclust” and “part.kmeans”, male genital morphology, microsatellites, and final species hypothesis are given in bars below the NC cluster.

Integrative-taxonomy approach

Results of morphometrics, male genital morphology, and microsatellites largely concord (Fig. 8). Two samples of *T. caucasicum* are nested within the NC cluster of *T. immigrans*, which we explain by morphological crypsis. Several misclassifications occur in *T. caucasicum* and *T. impurum*. While these species are clearly separated from each other by male genital morphology and microsatellites, morphological similarity led to affiliation errors of four *T. impurum* samples nesting in the *T. caucasicum* cluster and one *T. caucasicum* nesting in the *T. impurum* cluster. Moreover, both species each include two microsatellite clusters, which we consider to represent intra-specific populations. In *T. caucasicum*, of seven samples with male genital plus microsatellite data available, the only one with genitals of the western form of *T. caucasicum* is also the only one of the microsatellite cluster Q3. The relation, however, is not significant (Fisher’s exact test, $p = 0.1429$). Hence, we consider the described differences as intraspecific variability. It has been already suggested that *Tetramorium* species of higher altitudes – due to the fragmented profile of mountains – are more difficult to identify because they might form local morphologically and genetically distinct populations (Wagner et al. 2017). The new data of *T. caucasicum* are in line with this idea.

While eastern Anatolian males have an identical genital morphology as drawn in Wagner et al. (2017; $n = 9$ newly analyzed nests), western samples ($n = 3$) have male genitalia clearly different from the eastern but similar with the European species *T. alpestre* (Suppl. material 1: fig. S1). Conspecificity of western *T. caucasicum* samples with *T. alpestre*, however, can be rejected by worker morphometrics with the discriminant $D_{alp} = 0.0269 \cdot SPWI + 0.0447 \cdot MtpW + 0.0727 \cdot dANC - 0.0266 \cdot SLd - 0.0170 \cdot PnHL + 0.2220 \cdot sqPpss - 0.0534 \cdot MPSP + 0.0600 \cdot MPPL - 0.1427 \cdot MC1TG - 0.0996 \cdot EYE - 1.9945$. While western Anatolian *T. caucasicum* workers have values < 0 (error 2.9% in 35 workers and 0.0% in 12 nest means), *T. alpestre* workers have values > 0 (error = 0.0% in 142 workers). The geographic position of western Anatolian *T. caucasicum*

between the main population of *T. caasicum* in the Caucasus region and *T. alpestre* in Europe suggests that hybridization between these two alpine species could have occurred.

In *Tetramorium impurum*, we detected two separated lineages: Anatolian samples from west of 35° E and from Central Europe belong to the microsatellite cluster Q6 (Suppl. material 3); this line had been termed “*T. impurum* eastern clade” in the past (Wagner et al. 2017). Samples from east of 35° E belong to the microsatellite clade Q7, which was newly detected in the frame of this study. There is neither an NC-cluster difference (Fig. 8) nor a male-genital-morphology difference between these two lineages. However, the discriminant $D_{imp} = -0.0385 \cdot HFL - 0.0611 \cdot PPW + 0.0601 \cdot PoOc + 0.1046 \cdot FL - 0.0300 \cdot RTI - 0.1036 \cdot PreOc + 0.1795 \cdot PPL + 0.1142 \cdot MPPL - 0.1127 \cdot PLST + 0.1705 \cdot MC1TG - 10.9419$ separates 100% of Anatolian worker individuals ($n = 36$ workers from west of 35° E and 33 workers from east of 35° E). Workers from west of 35° E have values < 0 , those from east of 35° E values > 0 .

The species pair *T. caespitum* and *T. indocile* shows highest similarities in NC clusters with one *T. indocile* sample placed erroneously in the *T. caespitum* cluster. The Bayesian clustering approach we used did not allow separation of these two species based on microsatellites. A larger number of individuals or integration of a hierarchical approach (see, e.g., Balkenhol et al. 2014) could improve the delimitation of individuals from these genetically very similar species.

The NC cluster of *T. flavidulum* includes one sample of *T. caasicum*, while, vice versa, the cluster of *T. caasicum* also includes one sample of *T. flavidulum*.

To summarize, our integrative-taxonomy approach yielded evidence for seven clusters of nest samples for Anatolia: *Tetramorium caespitum* (17 samples), *T. hungaricum* (11), *T. indocile* (19), *T. caasicum* (47), *T. impurum* (25), *T. immigrans* (48), and *T. flavidulum* (24).

Reanalyzed linear discriminant-analysis (LDA) of morphometric data

For the reanalysis, 21 combinations for pairwise species comparisons were available. The mean error-rate of cross-validations of LDAs was 1.0%. Only one species pair had an error-rate higher than 5%: *T. caasicum* and *T. indocile* with 5.7% (Table 3).

Table 3. Worker-individual error-rates of cross-validation LDA results for pairwise species or clade comparisons [%]. n = number of nests, i = number of individuals. Values $< 5\%$ in bold. (The number of individuals per group was at least 3× higher than the number of used characters.).

| | <i>caespitum</i> | <i>hungaricum</i> | <i>indocile</i> | <i>caasicum</i> | <i>impurum</i> | <i>immigrans</i> | <i>flavidulum</i> |
|-------------------|------------------|-------------------|-----------------|-----------------|----------------|------------------|-------------------|
| n / i | 17/42 | 11/30 | 19/43 | 47/132 | 25/69 | 48/113 | 24/76 |
| <i>caespitum</i> | | | | | | | |
| <i>hungaricum</i> | 0.0 | | | | | | |
| <i>indocile</i> | 2.4 | 0.0 | | | | | |
| <i>caasicum</i> | 2.3 | 0.0 | 5.7 | | | | |
| <i>impurum</i> | 0.0 | 0.0 | 0.9 | 5.0 | | | |
| <i>immigrans</i> | 0.0 | 0.0 | 0.0 | 2.0 | 0.5 | | |
| <i>flavidulum</i> | 0.0 | 0.0 | 0.0 | 1.9 | 0.0 | 1.1 | |

Thermal niches

Species-specific ecological differences were significant in 14 of 21 pairwise species comparisons (67%) (Tables 4, 5). *Tetramorium caucasicum* had the lowest TAS values, followed by the three moderately thermophilous species *T. impurum*, *T. indocile*, and *T. caespitum*. Three species were distinctly thermophilous: *T. immigrans*, *T. hungaricum*, and *T. flavidulum* (Table 4).

Type material assignment

Both type samples of *Tetramorium flavidulum* fall into the NC cluster (Fig. 8) of the taxon which had been already considered to be *T. flavidulum* (Kiran and Karaman 2020). For the ten worker syntypes of “*Tetramorium caespitum flavidulum*”, collected by Max Korb between 1886 and 1900 (cf. Arnold 1921, D. 1933), using all morphometric variables the geometric mean was $p = 1.00$ in an 11-class LDA with wild-card run for the taxon (Fig. 9). Two syntype *T. flavidulum* workers, collected by Martin Holtz in 1897, using all morphometric variables, have a geometric mean of $p = 0.96$ for *T. caucasicum* and 0.03 for *T. caespitum*; including geographic coordinates $p = 0.96$ for *T. immigrans*, $p = 0.02$ for *T. flavidulum*, and 0.02 for *T. caespitum*. *Tetramorium flavidulum* is the only species of the complex which can be identified by subjective characters quite well: Postpetiole with strong longitudinal costae, dorsum of petiole mostly strongly rugulose (Fig. 9D). Color often yellowish to light brown. MC1TG is high. Based on subjective investigation of morphology,

Table 4. Standard air-temperature (TAS) comparison as an overview of ecological niches. Given are arithmetic means of localities \pm standard deviation [lower extreme, upper extreme]; n = number of localities, TAS in °C. Only localities in Anatolia and the Caucasus region are considered.

| species | <i>n</i> | TAS |
|-------------------|----------|-----------------------------|
| <i>caespitum</i> | 14 | 16.1 \pm 2.8 [13.0, 23.2] |
| <i>hungaricum</i> | 8 | 18.1 \pm 1.3 [16.2, 20.4] |
| <i>indocile</i> | 16 | 14.8 \pm 1.8 [12.4, 19.6] |
| <i>caucasicum</i> | 33 | 11.7 \pm 2.3 [8.1, 17.5] |
| <i>impurum</i> | 25 | 14.0 \pm 2.2 [9.9, 18.9] |
| <i>immigrans</i> | 46 | 19.2 \pm 2.3 [15.1, 24.6] |
| <i>flavidulum</i> | 23 | 17.1 \pm 2.6 [12.1, 26.5] |

Table 5. Species-specific standard air temperature. Significances at $\alpha = 0.05$. Student's t-test after Bonferroni-Holm correction are labeled with *.

| Species | <i>caespitum</i> | <i>hungaricum</i> | <i>indocile</i> | <i>caucasicum</i> | <i>impurum</i> | <i>immigrans</i> | <i>flavidulum</i> |
|-------------------|------------------|-------------------|-----------------|-------------------|----------------|------------------|-------------------|
| <i>caespitum</i> | | | | | | | |
| <i>hungaricum</i> | 0.075 | | | | | | |
| <i>indocile</i> | 0.127 | < 0.001* | | | | | |
| <i>caucasicum</i> | < 0.001* | < 0.001* | < 0.001* | | | | |
| <i>impurum</i> | 0.010 | < 0.001* | 0.217 | < 0.001* | | | |
| <i>immigrans</i> | < 0.001* | 0.182 | < 0.001* | < 0.001* | < 0.001* | | |
| <i>flavidulum</i> | 0.280 | 0.317 | 0.004* | < 0.001* | < 0.001* | 0.001* | |

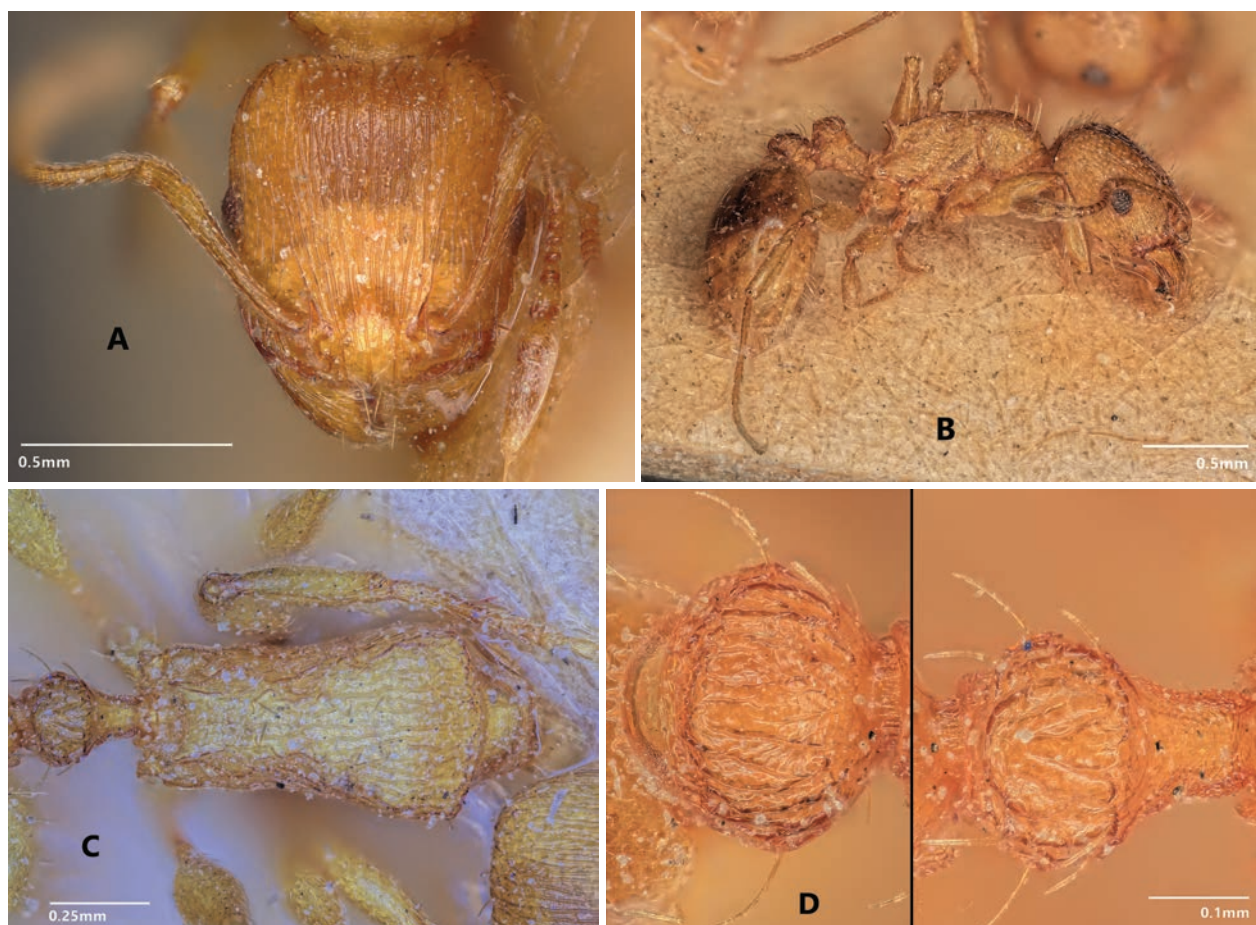


Figure 9. Lectotype of *Tetramorium flavidulum* in (A) full face (B) lateral view. Paralectotype of *T. flavidulum* in dorsal view (C mesosoma, D petiole and postpetiole) (photographer RS).

types of both Korb and Holtz do not belong to any alternative species suggested by LDAs (*T. caespitum*, *T. caucasicum*, or *T. immigrans*). The ambiguous affiliation of the two type workers from Holtz, however, is unsatisfactory. We suggest that these types are untypical individuals of *T. flavidulum* but, since they are the only workers of the Anatolian south-coast used in this study, cannot fully exclude that they will turn out to belong to a cryptic species unknown to us and putatively with more southern distribution than the similar *T. flavidulum*. Thus, we have designated a worker of a card with 2 syntype workers, collected by Korb, as lectotype.

The host of *Tetramorium aspina* Wagner et al., 2018 is *T. caucasicum*

Three host workers of the type material of *T. aspina* (12/0859) in an 8-class LDA (including all Anatolian species and *T. staerckei*) using all morphometric variables belong to *T. caucasicum* with a geometric mean of $p = 0.92$, $p = 0.04$ to *T. immigrans*, and $p = 0.04$ for *T. flavidulum*. Including the three geographic variables they belong to *T. caucasicum* with a geometric mean of $p = 0.99$ and to *T. flavidulum* with $p = 0.01$. We found three further nests of *T. caucasicum* (including 2 nests with males showing the typical species-specific paramere-structure) and one of *T. impurum*, but none of *T. immigrans* syntopically. The TAS value of the site is 11.7, which is outside of

the range of *T. immigrans* with 19.2 ± 2.3 [15.1, 24.6]. We conclude that this sample belongs to *T. caucasicum*. The misidentification of *T. caucasicum* as *T. immigrans* in Wagner et al. (2018a), detected in the frame of this study, resulted from an underestimation of the area of *T. caucasicum* into southwest and a lack of morphometric data from the southern part of its area (e.g., MC1TG was 21.4 and thus much higher than the species' mean known at this time with 14.47 ± 1.81). In other words, it resulted from using an identification key for outside of the region for which it was designed. We can learn from this mistake that a large morphometric calibration background is needed before taxonomic conclusions can be drawn.

Zoogeography

We demonstrated the occurrence of seven species of the *T. caespitum* complex in Anatolia (*T. caespitum*, *T. hungaricum*, *T. indocile*, *T. caucasicum*, *T. impurum*, *T. immigrans*, and *T. flavidulum*, Figs 10–13). Herewith, species diversity turned out to be lower than the authors had inferred before the results were available. Interestingly, the species composition in Anatolia is very similar as in Central Europe (with *T. alpestre*, *T. caespitum*, *T. hungaricum*, *T. indocile*, *T. staerckei*, *T. impurum*, and *T. immigrans*). Of Central European species, only *T. alpestre* and some COI clades of *T. caespitum* had (also) Western European or Apennine refugia; COI haplotypes of *T. caespitum* in eastern Central Europe, however, are more similar to those of the Caucasus than to those of the Apennine peninsula or western Europe (Wagner et al. 2017). *Tetramorium hungaricum*, which is missing in Iberia and the Apennine peninsula, has a southeastern origin. *Tetramorium indocile*, rare in Iberia and probably missing in the Apennine peninsula, might have originated in the Caucasus. *Tetramorium impurum* is absent from the Apennine peninsula and occurs in three genetically clearly different lineages (two of them

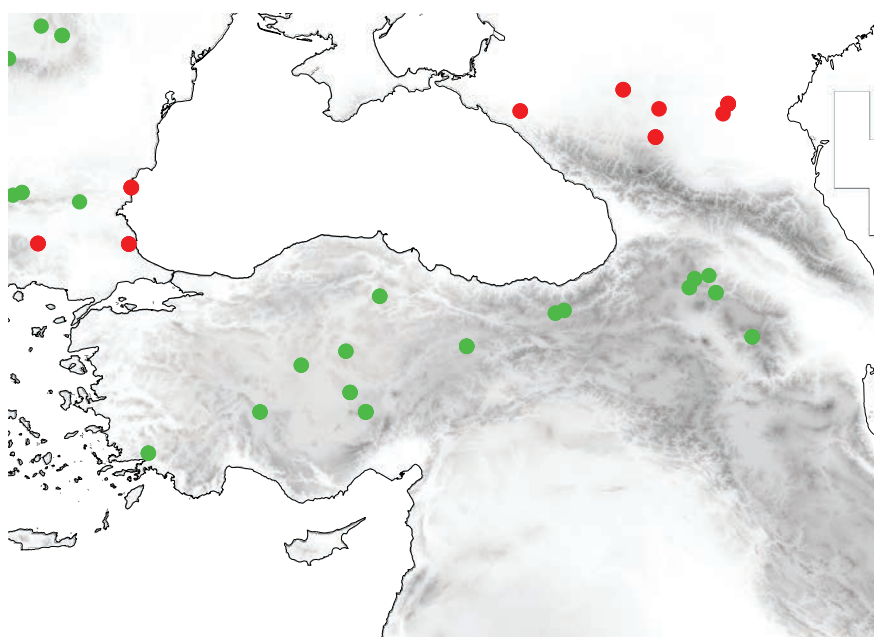


Figure 10. Distribution of *Tetramorium caespitum* (light green) and *T. staerckei* (red) in Anatolia and surrounding regions.

described in Wagner et al. 2017). Its western clade occurs in Iberia and western Europe (Wagner et al. 2017; Attewell and Wagner 2019), the “eastern” clade in Central Europe, the Balkans, and western Anatolia; the latter has a southeastern origin and migrated from the Balkans or western Anatolia to Central Europe. A third clade, detected in the frame of this study, occurs in Anatolia east of 35° E. *Tetramorium staerckei*, a steppe species with an origin in southern Russia north of the Caucasus or Central Asia, migrated north of the Black Sea to the Balkans and Central Europe but not to Anatolia.

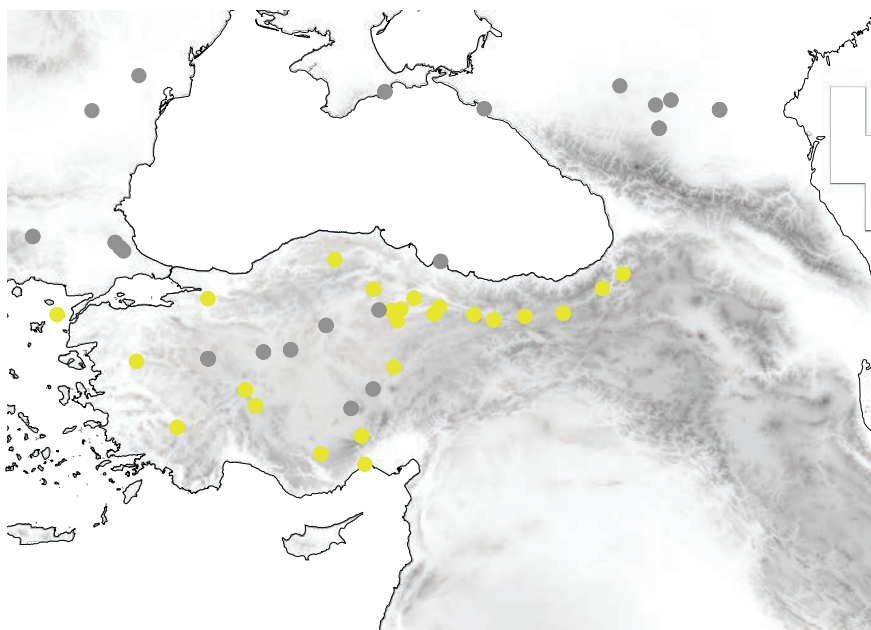


Figure 11. Distribution of *Tetramorium hungaricum* (grey) and *T. flavidulum* (pale yellow) in Anatolia and surrounding regions.

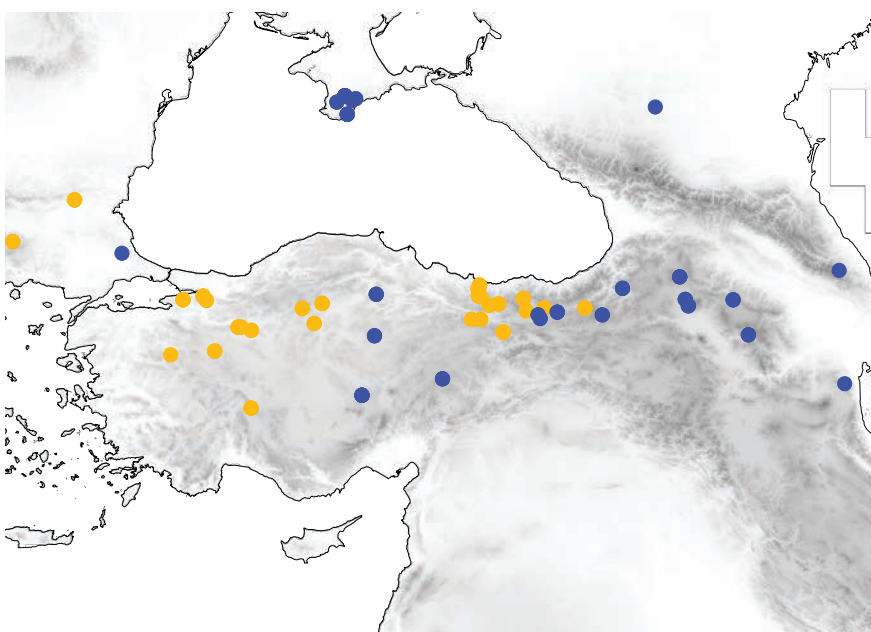


Figure 12. Distribution of *Tetramorium indocile* (dark blue) and *T. impurum* (dark yellow) in Anatolia and surrounding regions.

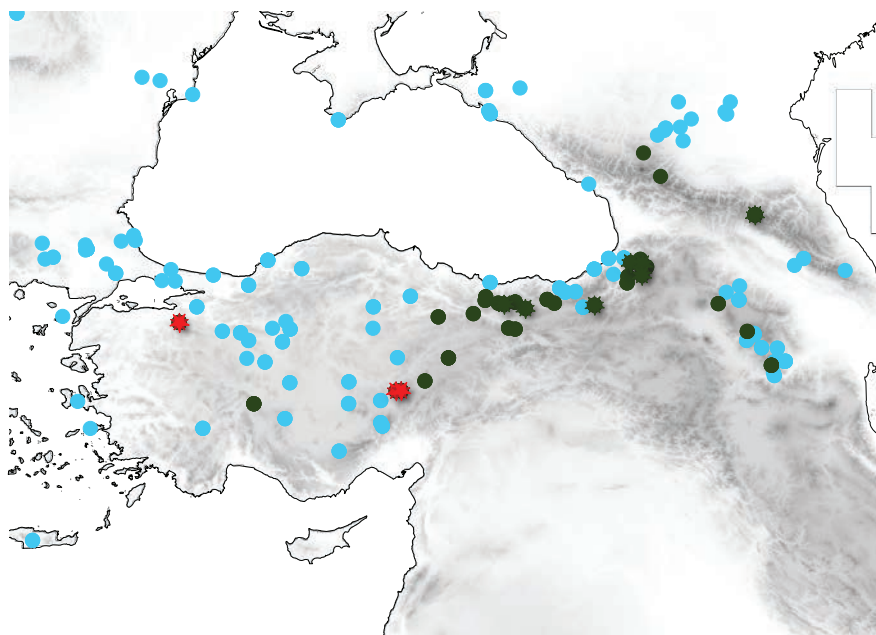


Figure 13. Distribution of *Tetramorium caucasicum* (dark green) and *T. immigrans* (cyan) in Anatolia and surrounding regions. Stars are records of *T. caucasicum* with males. Red stars show records with western (*alpestre*-like) and dark-green stars records with normal male genital morphology.

In *Tetramorium immigrans*, a neozoon in Western and Central Europe (Gipet et al. 2017; Borowiec and Salata 2018; Seifert 2018; Castracani et al. 2020; Cordonnier et al. 2020; Sheard et al. 2020), high haplotype-diversity in mitochondrial DNA suggested Anatolia and the Caucasus region are the most likely geographic origin of *T. immigrans* (Wagner et al. 2017). *Tetramorium flavidulum*, also of Anatolian or Caucasian origin, migrated northwest at least to Turkish Thrace (Bračko et al. 2016) and Greece (Finzi et al. 1928); Bulgarian records are doubtful (pers. comm. Albena Lapeva-Gjonova). We conclude that most Anatolian or Caucasian species migrated to Central Europe after the last ice age. Anatolia and the Caucasus region could also be the evolutionary origin of the species complex.

Taxonomy

Diagnosis of the *Tetramorium caespitum* complex

- 1) Sexualls are larger than in most species outside the *Tetramorium caespitum* complex, MW of gynes > 1198 µm, CS > 1129 µm (but see, e.g., *T. moravicum*).
- 2) Gyne with high mesosoma in contrast to most species outside the *T. caespitum* complex.
- 3) Gyne with normal waist width and not with widened waist as species of the *T. ferox* complex or *T. meridionale* complex.
- 4) Male genital structure larger (paramere length > 843 µm) and with more species-specific features than in other complexes.
- 5) Males with ten antennal segments (not nine as in *T. biskrense* complex).
- 6) Some workers at underside of head with long c-shaped, crinkly, or sinuous hairs arising just behind buccal cavity (which are absent in most

species outside the *T. caespitum* complex, but also present in *T. pelagium* Mei, 1995, *T. goniommoide* Poldi, 1979, and *T. feroxoides* Dlussky & Zabelin, 1985).

- 7) Workers without dense and distinct longitudinal striato-punctated sculpture on 1st gastral tergite (as in the *T. striativentre* complex) but only stickman-like or reticulate microstructure with varying from few, scattered stickman-like to complex reticulate structures (Fig. 4), MC1TG < 33 (but not > 34 as in the *T. chefketi* complex).
- 8) Worker head, dorsum, and occiput with longitudinal costae and costulae, but occiput not with transversal or arching posterolaterally costae and costulae as in the *T. meridionale* complex.
- 9) Eye shorter than preocular distance, EL < PreOc (not as in most species of the *T. inerme* complex and partly in the *T. biskrense* complex where EL often > PreOc).
- 10) Metanotal groove shallow (not missing as in the *T. inerme* complex).
- 11) Propodeal spines short to medium but not reduced to small corners as in several species of the *T. ferox* (e.g., *T. aspina*) and the *T. inerme* complexes (e.g., *T. taueret*).
- 12) Worker head, mesosoma, petiole, and postpetiole surface partly smooth (as in *T. hungaricum* or *T. indocile*) to coarsely sculptured (as in *T. staerckei* or *T. flavidulum*) but not very coarsely sculptured as in the *T. chefketi* complex.
- 13) Color of most species brownish to blackish; in the Benelux, Central Europe, and Balkan mountain-areas sometimes light brown (*T. impurum*), in Anatolia even often yellowish (*T. flavidulum*).

The morphology of sexuals displays the most characteristic characters to define species complexes. Based on gyne morphology, we consider *Tetramorium flavidulum* Santschi, 1910 as member of the *T. caespitum* complex. Gynes of the *T. ferox* complex differ from them by their wide waist (Csősz and Schulz 2010), those of the *T. chefketi* complex by the dense polygonal striation of the 1st gaster tergite (Csősz et al. 2007), gynes of the *T. semilaeve* complex and the *T. inerme* complex are distinct smaller (Salata and Borowiec 2017).

Taxonomic treatment by species

All Palearctic *Tetramorium caespitum* group names listed by Bolton (2014) have been evaluated recently concerning their possible affiliation to the *T. caespitum* complex (Wagner et al. 2017). Since then, no further West Palearctic species of the *T. caespitum* complex have been described (Bolton 2024). In addition to type material investigated by Wagner & al. (2017), it was necessary to investigate types of *T. flavidulum* Santschi, 1910:

Tetramorium flavidulum Santschi, 1910 (12 workers of 2 samples) [Turkey]: 10 workers labeled as: “anatolia Korb” [–] MUSEO GENOVA coll. C. Emery (dono 1925) [–] SYNTYPUS „*Tetramorium caespitum flavidulum*” [thereof we have chosen the lectotype worker]. 2 workers labeled as: “Tet. caespitum [sic!] v. flavidula [sic!] Em” [–] Asia minor Mersina 1897. Holtz [–] “Lectotype *Tetramorium flavidulum* Emery, 1922” [–] “% designated by CSŐSZ, 2005” [–] MUSEO GENOVA coll. C. Emery (dono 1925) [–] ANTWEB CASENT0904803.

***Tetramorium flavidulum* Santschi, 1910**

Note. Based on morphological criteria (Csősz et al. 2007; Csősz and Schulz 2010; Radchenko and Scupola 2015; Wagner et al. 2017; 2021) we place this species into the *Tetramorium caespitum* complex; however, we are unsure of its phylogenetic position. Future studies should investigate whether it is more closely related to species of the *T. caespitum* or the *T. chefketi* complex.

Tetramorium caespitum caespitum var. *flavidula* Emery, 1909: 702 (unavailable name); first available use: *Tetramorium caespitum* var. *flavidula* Santschi, 1910; raised to species rank: Borowiec 2014: 198. Morphology of type material investigated.

Type locality. Lectotype: Anatolia, leg. M. Korb, 1886–1900.

Lectotype designation. Worker with non-decapitated body (of two syntype workers on one card; the other worker is decapitated with head fixed separately), labeled “anatolia Korb” [–] MUSEO GENOVA coll. C. Emery (dono 1925) [–] SYNTYPUS “*Tetramorium caespitum flavidulum*”. Lectotype worker and nine paralectotype workers in Museo Civico di Storia Naturale, Genova (Italy). Morphometric data of lectotype in μm : CL = 760, CW = 731, dANC = 199, EL = 152, EW = 110, FL = 285, HFL = 596, MC1TG = 29.6, ML = 845, MPPL = 250, MPSP = 331, MPST = 182, MtpW = 346, MW = 459, PEH = 256, PEL = 166, PEW = 240, PLSP = 160, PLST = 165, PnHL = 182, PoOc = 301, POTCos = 8.0, PPH = 253, PPL = 111, Ppss = 9, PPW = 283, PreOc = 197, RTI = 285, SLd = 595, SPST = 156, SPWI = 213.

Redescription of worker. Medium size, CS = 734 ± 53 [614, 855]. 76% of workers with yellowish head and mesosoma and an often brownish gaster (which does usually not occur in other species of the complex), 21% of workers light to medium brownish, 3% dark brownish ($n = 76$ workers of 24 nests).

Head strongly elongate, CL / CW = 1.031 ± 0.018 [0.990, 1.088]. Eye medium-sized, EYE / CS = 0.176 ± 0.005 [0.167, 0.191]. Scape long, SLd / CS = 0.787 ± 0.015 [0.722, 0.815]. Mesosoma short and narrow, ML / CS = 1.110 ± 0.022 [1.057, 1.179], MW / CS = 0.619 ± 0.014 [0.580, 0.667].

Promesonotal dorsum convex, metanotal groove shallow. Head, dorsum, and occiput with longitudinal costae and costulae. Postoculo-temporal area of head with rather many costae and costulae, POTCos = 9.35 ± 2.47 [4.00, 15.50]. Mesosoma dorsum longitudinally rugulose, lateral side of propodeum with strongest sculpture of complex, Ppss = 15.7 ± 10.9 [6.0, 63.7]. Dorsum of petiolar node with strong reticulate costae, dorsum of postpetiole node with strong mostly longitudinal, sometimes reticulate costae. General surface appearance dull. Connected stickman-like or reticulate microsculpture: very large units scattered over 1st gastral tergite, MC1TG = 25.93 ± 3.45 [16.30, 32.60]. Most workers with long c-shaped hairs on ventral head just posterior to buccal cavity, sinuous or crinkly hairs only in 13% of workers.

Description of male. Yellowish. Ten antennal segments. Paramere structure belongs to the *impurum*-like form sensu Wagner et al. (2017). Ventral paramere lobe with one sharp corner visible in posterior view. Clear division of ventral and dorsal paramere lobes, visible by emargination between lobes in posterior view. Relatively short dorsal paramere lobe, visible in posterior and dorsal view. Maximal paramere structure length in lateral view of four males 912 ± 27 (885, 949) μm . No corner on ventral paramere lobe between lobe top and emargination with dorsal lobe in dorsal and posterior view. Distinct different from all other species.

Distribution. Known from 22 localities in Anatolia and Gökçeada Island (Fig. 11; more localities given in Kiran and Karaman 2020).

Ecology. Rather thermophilic, TAS of 23 sites 17.1 ± 2.6 [12.1, 26.5]. More thermophilic than *T. indocile*, *T. caasicum*, and *T. impurum*, less thermophilic than *T. immigrans*. 17 of 22 sites inhabiting woodland: *Quercus* forests (6), *Pinus nigra* forests (4), *Pinus sylvestris* forest (1), *Pinus sylvestris-Quercus* forests (2), other types of mixed forests (2), *Olea* stands (1), and scrublands (1). The rest in meadows (2), barren areas (1), river banks (1), and city centers (1).

Phenology. Adult sexuals in nests on 2 July ± 12 [9 June, 13 July] ($n = 7$).

Identification key to the complexes of the *Tetramorium caespitum* group

Data for this key have been taken from material investigated in the frame of this study and from the literature (Csősz and Schulz 2010; Borowiec et al. 2015; Radchenko and Scupola 2015; Lebas et al. 2016; Salata and Borowiec 2017; Wagner et al. 2017, 2018a, 2021).

- 1 First gastral tergite, or at least its anterior half, with dense and distinct longitudinal striato-punctated sculpture. Asia only
..striativentre complex [see Dietrich 2004; Radchenko and Scupola 2015]
- First gastral tergite without longitudinal striato-punctated sculpture but only stickman-like or reticulate microstructure.....**2**
- 2 Occiput with transversal or arching posterolaterally costae and costulae. Mediterranean and Iran..... **meridionale complex** [Salata et al. 2024]
- Occiput without transversal costae and costulae.....**3**
- 3 Eye often longer than or with same length as preocular distance. No metanotal groove, propodeal spines short, and petiolar node dorsocaudally extended (Fig. 14). $D_{ine}: 0.0439*PPW+0.0105*FL+0.0409*SPST+0.0544*PreOc-0.0053*ML-0.0312*PEW-0.0221*MW-0.0663*EL+1.9998 < 0$ (error 0.0% in 92 workers). Gynes smaller and with lower mesosoma than in *caespitum* complex. In Europe, only southern Russia and Caucasus; northern Africa and Asia**innerme complex**
- Eye often shorter than preocular distance. $D_{ine} > 0$ (under exclusion of the three large-eyed western Mediterranean species *T. biskrense*, *T. pelagium*, and *T. fusciclava* error 2.3% in 1638 workers and 1.6% in 693 nest means; most errors in *T. semilaeve* complex and *T. hungaricum*).....**4**
- 4 Very complex stickman-like or reticulate microstructure on 1st gastral tergite, MC1TG in 55 workers of species occurring in Europe > 34 . If number of connected lines building units of stickman-like or reticulate microstructure smaller (*T. anatolicum* with MC1TG < 34), units are so dense that nearly connected with each other (but then not yellowish as *T. flavidulum*). All species except *T. anatolicum* very coarsely sculptured.....
.....chefketi complex [see Csősz et al. 2007]
- Microstructure on 1st gastral tergite varying from few, scattered stickman-like to complex reticulate structures (Fig. 4), MC1TG < 33**5**
- 5 Eye larger and/or distance between most anteroventral point of metapleuron and most dorsocaudal point of propodeal lobe larger, hind femur shorter and/or postpetiole lower. Discriminant $D_{bis}: 0.1210*EL+0.0726*MPPL-0.0357*HFL-0.0396*PPH-6.5356 > 0$ (error 0.0% in 6 workers of *pelagium*,

- 5 of *brevicorne*, and 1 of *biskrense*). Males with only 9 antennal segments. Gynes smaller and with lower mesosoma than in *caespitum* complex. In Europe southern Spain, Corsica, Sardinia, Sicily, Lampedusa, and Linosa; common in North Africa **biskrense complex** [see Lebas et al. 2016]
- Eye smaller and/or distance between most anteroventral point of metapleuron and most dorsocaudal point of propodeal lobe smaller, hind femur longer and/or postpetiole higher. $D_{bis} < 0$ (error 1.6% in 1648 workers and 0.5% in 733 nest means of *caespitum*, *ferox*, and *semilaeve* complex). Males with ten antennal segments **6**
 - 6 Discriminant $D_{fer} : 0.0157 \cdot CW - 0.052 \cdot FL - 0.069 \cdot PEW + 0.074 \cdot PPH + 1.4815 < 0$ (error 2.6% in 461 workers and 1.1% in 93 nest means, Fig. 15). CS of gynes $< 1113 \mu m$ ($n = 78$). Gynes with wide petiole and postpetiole, $PEW / CS = 0.6115 \pm 0.034$, $PPW / CS = 0.785 \pm 0.040$ ($n = 22$). Males small, paramere length $< 843 \mu m$. In Europe, Italy, Pannonia, and Balkans; Anatolia and Caucasus region ... **ferox complex** [see Csősz and Schulz 2010; Wagner et al. 2021]
 - $D_{fer} > 0$ (error 5.4% in 1990 workers and 2.3% in 794 nest means). Gynes with narrow or normal petiole and postpetiole (*semilaeve* complex: $PEW / CS = 0.371 \pm 0.014$, $PPW / CS = 0.492 \pm 0.028$, $n = 26$; *caespitum* complex: $PEW / CS = 0.414 \pm 0.032$, $PPW / CS = 0.607 \pm 0.033$, $n = 54$ **7**
 - 7 Some workers at underside of head with long c-shaped, crinkly, or sinuous hairs arising just behind buccal cavity. Discriminant $D_{sem} : 0.03096 \cdot CL - 0.08355 \cdot FL + 0.09060 \cdot PEW - 0.07793 \cdot PPH - 1.598 < 0$ (error 6.4% in 1877 workers and 3.7% in 761 nest means, Fig. 16). Gynes large, $CS > 1129 \mu m$ ($n = 63$). Gynes with high mesosoma. Males large, paramere length $> 843 \mu m$. Nearly whole Palearctic **caespitum complex** [see 'Identification key to workers of the *Tetramorium caespitum* complex' below]
 - C-shaped, crinkly, or sinuous hairs on underside of head absent. Discriminant $D_{sem} > 0$ (error 8.1% in 99 workers and 3.0% in 33 nest means). Gynes with low mesosoma. Males small, paramere length $< 843 \mu m$. Mediterranean **semilaeve complex** [see Csősz and Schulz 2010; Borowiec et al. 2015; Salata and Borowiec 2017]

Identification key to workers of the *Tetramorium caespitum* complex in Anatolia and the Caucasus

Data for this key have been taken from material investigated in the frame of this study and from the literature (Wagner et al. 2017); only data from Anatolia and the Caucasus region are included.

- 1 Postpetiole with strong longitudinal costae (Fig. 9). Dorsum of petiole strongly rugulose. Stickman-like or reticulate microsculpture on first gastral strongly pronounced: $MC1TG = 25.93 \pm 3.45$. Color often light: 76% of workers head and mesosoma yellowish and gaster yellowish to medium brownish, 21% of workers light to medium brownish, 3% dark brownish ($n = 76$ of 24 nests). Postpetiole narrow, short, and low: $PPW / CS = 0.375 \pm 0.014$, $PPL / CS = 0.145 \pm 0.008$, $PPH / CS = 0.336 \pm 0.013$. Distances between center of propodeal stigma and most anteroventral point of metapleuron as well as most dorsocaudal point of propodeal lobe small: $MPST / CS = 0.242 \pm 0.007$, $PLST / CS = 0.239 \pm 0.008$. Discriminant

- D11: $0.0167 \cdot \text{HFL} + 0.0118 \cdot \text{ML} + 0.0149 \cdot \text{MtpW} - 0.0356 \cdot \text{PoOc} - 0.0436 \cdot \text{FL} + 0.0301 \cdot \text{dANC} - 0.0861 \cdot \text{EL} - 0.0391 \cdot \text{PreOc} + 0.0234 \cdot \text{PEH} + 0.0289 \cdot \text{PPH} + 0.0127 \cdot \text{PnHL} + 0.1725 \cdot \text{sqPpss} - 0.0521 \cdot \text{MPSP} + 0.0922 \cdot \text{MPST} + 0.0432 \cdot \text{SPST} - 0.0503 \cdot \text{MPPL} - 0.0241 \cdot \text{PLSP} - 0.0897 \cdot \text{MC1TG} + 6.8364 < 0$ (error 3.9% of 76 workers and 4.2% of 24 nest means)..... **flavidulum**
- Postpetiole without strong longitudinal costae. Median dorsum of petiole fully smooth to strongly rugulose. Stickman-like or reticulate microsculpture on first gastral often less strongly pronounced. Usually, dark brown to blackish. Postpetiole often wider, longer, and higher: $\text{PPW} / \text{CS} = 0.399 \pm 0.018$, $\text{PPL} / \text{CS} = 0.155 \pm 0.010$, $\text{PPH} / \text{CS} = 0.358 \pm 0.014$. Distances between center of propodeal stigma and most anteroventral point of metapleuron as well as most dorsocaudal point of propodeal lobe larger: $\text{MPST} / \text{CS} = 0.259 \pm 0.010$, $\text{PLST} / \text{CS} = 0.253 \pm 0.011$. $\text{D11} > 0$ (error 1.9% in 429 workers and 0.0% of 166 nest means; most errors in *caucasicum*) **2**
- 2 Sculpture on head and mesosoma reduced and large parts smooth and shiny. Very few postoculo-temporal costae and costulae: $\text{POTCos} = 2.30 \pm 1.77$. Lateral face of propodeum anterior propodealstigma often smooth: $\text{Ppss} = 88.01 \pm 26.63$. Petiole and postpetiole narrow, low, and short: $\text{PEW} / \text{CS} = 0.296 \pm 0.013$, $\text{PEH} / \text{CS} = 0.329 \pm 0.008$, $\text{PEL} / \text{CS} = 0.220 \pm 0.007$, $\text{PPW} / \text{CS} = 0.370 \pm 0.013$, $\text{PPH} / \text{CS} = 0.337 \pm 0.012$, $\text{PPL} / \text{CS} = 0.148 \pm 0.011$. Eye longer: $\text{EL} / \text{CS} = 0.216 \pm 0.008$. Mesosoma short: $\text{ML} / \text{CS} = 1.101 \pm 0.022$. Spines short: $\text{MPSP} / \text{CS} = 0.401 \pm 0.017$, $\text{SPST} / \text{CS} = 0.179 \pm 0.011$. Distance between most anteroventral point of lateral metapleuron and dorsocaudal point of propodeal lobe small: $\text{MPPL} / \text{CS} = 0.327 \pm 0.011$. Small size: $\text{CS} = 630 \pm 51 \mu\text{m}$. Discriminant D12: $0.0275 \cdot \text{HFL} + 0.0291 \cdot \text{SPWI} - 0.0307 \cdot \text{SLd} - 0.119 \cdot \text{POTCos} + 0.0818 \cdot \text{EL} - 0.0356 \cdot \text{PEL} - 0.0417 \cdot \text{PPH} + 0.027 \cdot \text{Ppss} - 0.0294 \cdot \text{SPST} + 0.0524 \cdot \text{MC1TG} + 1.7633 > 0$ (error 0.0% of 30 workers) **hungaricum**
- Sculpture on head often more developed, extending over most parts of dorsal head surface. Number of postoculo-temporal costae and costulae higher: $\text{POTCos} = 9.39 \pm 3.08$. Lateral face of propodeum anterior propodealstigma often not smooth: $\text{Ppss} = 26.77 \pm 18.82$. Petiole and postpetiole wider, higher, and longer: $\text{PEW} / \text{CS} = 0.321 \pm 0.014$, $\text{PEH} / \text{CS} = 0.347 \pm 0.011$, $\text{PEL} / \text{CS} = 0.231 \pm 0.009$, $\text{PPW} / \text{CS} = 0.402 \pm 0.016$, $\text{PPH} / \text{CS} = 0.359 \pm 0.013$, $\text{PPL} / \text{CS} = 0.156 \pm 0.010$. Eye shorter: $\text{EL} / \text{CS} = 0.196 \pm 0.008$. Mesosoma longer: $\text{ML} / \text{CS} = 1.154 \pm 0.031$. Spines longer: $\text{MPSP} / \text{CS} = 0.430 \pm 0.020$, $\text{SPST} / \text{CS} = 0.197 \pm 0.015$. Distance between most anteroventral point of lateral metapleuron and dorsocaudal point of propodeal lobe larger: $\text{MPPL} / \text{CS} = 0.342 \pm 0.012$. Often larger: $\text{CS} = 748 \pm 82 \mu\text{m}$. $\text{D12} < 0$ (error 0.3% of 399 workers and 0.0% of 155 nest means) **3**
- 3 Sculpture well developed, number of postoculotemporal costae and costulae large, smooth area on lateral face of propodeum anterior propodeal stigma small: $\text{POTCos} = 12.29 \pm 2.16$, $\text{Ppss} = 21.3 \pm 12.6$. Eye wider: $\text{EW} / \text{CS} = 0.153 \pm 0.005$. Distance between propodeal stigma and dorsocaudal end of propodeal lobe larger: $\text{PLST} / \text{CS} = 0.262 \pm 0.009$. Hind femur longer: $\text{HFL} / \text{CS} = 0.837 \pm 0.023$. D13: $-0.0256 \cdot \text{SPWI} + 0.0147 \cdot \text{MtpW} - 0.0252 \cdot \text{MW} - 0.0217 \cdot \text{CL} + 0.0320 \cdot \text{dANC} + 0.1281 \cdot \text{POTCos} + 0.1427 \cdot \text{EW} - 0.0428 \cdot \text{EL} + 0.0492 \cdot \text{PreOc} + 0.0202 \cdot \text{PEH} + 0.0164 \cdot \text{PPH} + 0.0133 \cdot \text{PnHL} - 0.0954 \cdot \text{MPSP} + 0.0216 \cdot \text{PLST} + 0.0660 \cdot \text{MPST} + 0.0725 \cdot \text{SPST} + 0.120$

- 3*MC1TG-10.7343 > 0 (error 2.7% of 113 workers and 0.0% of 48 nest means) **immigrans**
- Sculpture strongly reduced to well developed. Eye narrower: EW / CS = 0.147 ± 0.006 . Distance between propodeal stigma and dorsocaudal end of propodeal lobe smaller: PLST / CS = 0.251 ± 0.010 . Hind femur shorter: HFL / CS = 0.795 ± 0.028 . D13 < 0 (error 1.0% of 286 workers and 0.0% of 108 nest means) **4**
 - 4 Hind femur longer: HFL / CS = 0.829 ± 0.026 . Mesosoma longer and wider: ML / CS = 1.189 ± 0.028 , MtpW / CS = 0.502 ± 0.017 , MW / CS = 0.647 ± 0.017 . Postocular distance smaller: PoOc / CS = 0.389 ± 0.008 . Often larger: CS = 782 ± 69 . Stickman-like or reticulate microsculpture on first gastral tergite reduced: MC1TG = 10.88 ± 3.01 . Distance between most anterioventral point of metapleuron and most dorsocaudal point of propodeal lobe larger: MPPL / CS = 0.353 ± 0.010 . Distance between frontal carinae and ridges of frontal antennal fossae larger: FL / CS = 0.395 ± 0.008 , RTI / CS = 0.407 ± 0.011 . Postpetiole longer: PPL / CS = 0.165 ± 0.007 . D14: $-0.0256*HFL-0.0209*ML+0.0581*PEW-0.0482*MtpW+0.0685*PoOc+0.0869*EW-0.0374*PPL-0.0284*PPH-0.0111*PnHL+0.0563*MPST+0.1100*MC1TG+0.0228*MW-1.1852 < 0$ (error 0.0% in 42 workers) **caespitum**
 - Hind femur shorter: HFL / CS = 0.789 ± 0.024 . Mesosoma shorter and narrower: ML / CS = 1.142 ± 0.027 , MtpW / CS = 0.483 ± 0.014 , MW / CS = 0.633 ± 0.014 . Postocular distance larger: PoOc / CS = 0.408 ± 0.013 . Often smaller: CS = 705 ± 55 . Stickman-like or reticulate microsculpture on first gastral tergite moderate or pronounced: MC1TG = 16.61 ± 4.31 . Distance between most anterioventral point of metapleuron and most dorsocaudal point of propodeal lobe smaller: MPPL / CS = 0.338 ± 0.012 . Distance between frontal carinae and ridges of frontal antennal fossae smaller: FL / CS = 0.384 ± 0.011 , RTI / CS = 0.391 ± 0.015 . Postpetiole shorter: PPL / CS = 0.155 ± 0.010 . D 14 > 0 (error 1.2% in 244 workers and 0.0% in 91 nest means) **5**
 - 5 Distance between antennae fossae larger: dANC / CS = 0.288 ± 0.008 . Postocular distance smaller: PoOc / CS = 0.396 ± 0.010 . Number of postoculo-temporal costae and costulae often smaller, POTCos = 5.82 ± 2.22 . Stickman-like or reticulate microsculpture on first gastral tergite moderate: MC1TG = 13.11 ± 2.34 . D15: $0.0182*SPWI+0.0429*MtpW+0.0511*PoOc-0.0819*dANC+0.0175*SLd+0.1641*POTCos+0.0407*PPL-0.0460*PPH-0.0610*SPST-0.0403*MPPL+0.0790*MC1TG+0.0335*PEH-0.0323*PEL-5.6482 < 0$ (error 2.3% in 43 workers and 0.0% in 19 nest means) **indocile**
 - Distance between antennae fossae smaller: dANC / CS = 0.277 ± 0.009 . Postocular distance larger: PoOc / CS = 0.410 ± 0.012 . Number of postoculo-temporal costae and costulae often larger, POTCos = 8.30 ± 2.16 . Stickman-like or reticulate microsculpture on first gastral tergite pronounced: MC1TG = 17.37 ± 4.27 . D15 > 0 (error 3.0% in 201 workers and 1.1% in 91 nest means) **6**
 - 6 Distance between dorsocaudal end of propodeal lobe and propodeal spine as well as propodeal stigma larger: PLSP / CS = 0.233 ± 0.015 , PLST / CS = 0.256 ± 0.009 . Longest hair on

- frontolateral corner of pronotum longer: $PnHL = 0.287 \pm 0.028$. D16: $-0.0352*HFL+0.0257*ML-0.0554*MtpW+0.0327*MW+0.0296*SLd-0.1006*POTCos+0.0426*EL+0.0440*PreOc+0.0481*PPH-0.0210*PnHL-0.0389*SPST-0.0351*PLST-0.0296*PLSP+0.0739*MC1TG-0.0391*PEL < 0$ (error 5.8% in 69 workers and 4.0% in 25 nest means).....***impurum***
- Distance between dorsocaudal end of propodeal lobe and propodeal spine as well as propodeal stigma smaller: $PLSP / CS = 0.215 \pm 0.015$, $PLST / CS = 0.245 \pm 0.010$. Longest hair on frontolateral corner of pronotum shorter: $PnHL = 0.260 \pm 0.029$. D16 > 0 (error 3.0% in 132 workers and 0.0% in 47 nest means).....***caucasicum***

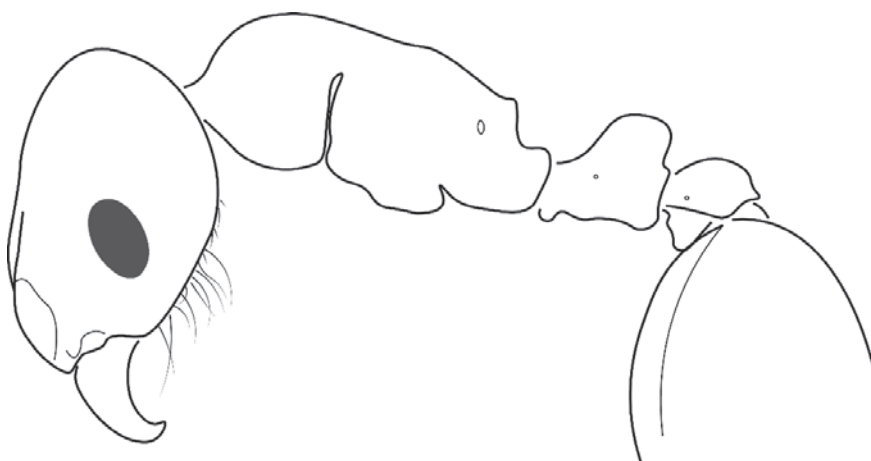


Figure 14. Schematic view of a *T. inerme* complex worker.

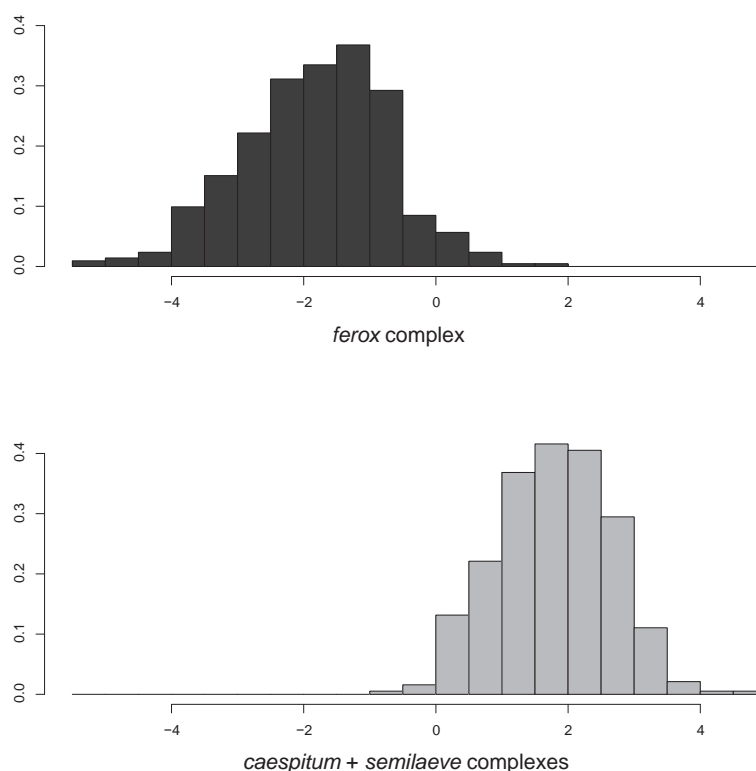


Figure 15. A linear discriminant-analysis separating workers of the *Tetramorium ferox* complex from those of the *T. caespitum* and *T. semilaeve* complexes.

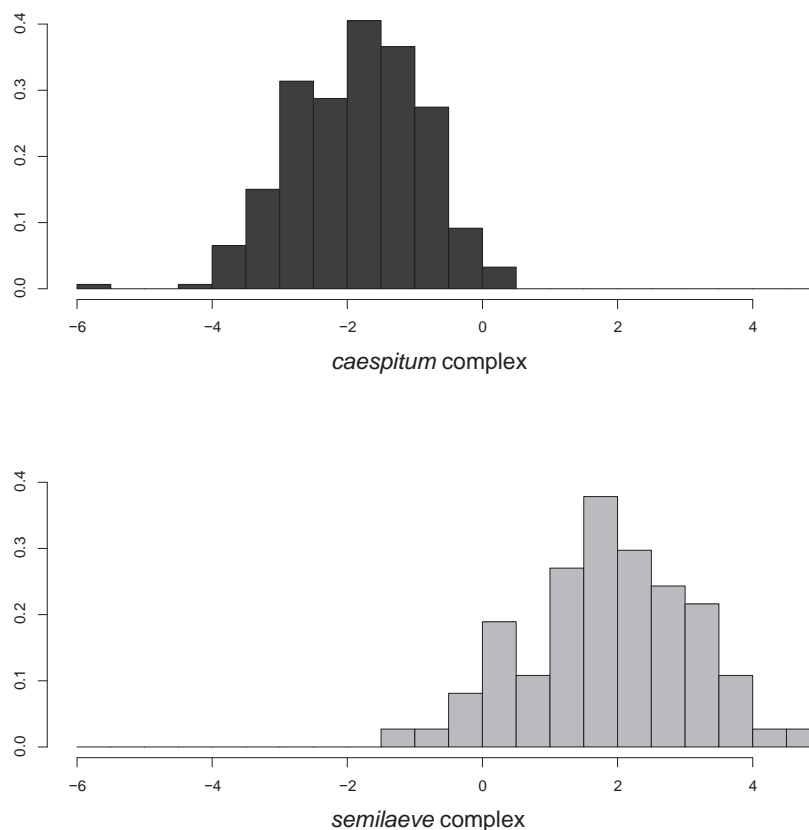


Figure 16. A linear discriminant-analysis separating workers of the *Tetramorium caespitum* complex from those of the *T. semilaeve* complex.

Acknowledgements

Christian Komposch (Graz) provided lab material (ethanol, needles, etc.). Maria Tavano (Museo Civico di Storia Naturale, Genova, Italy) sent types of *Tetramorium flavidulum* and pictures of *Tetramorium brevicorne* type males.

Additional information

Conflict of interest

The authors have declared that no competing interests exist.

Ethical statement

No ethical statement was reported.

Funding

HCW was supported by the Hungarian Academy of Sciences in the frame of the “MTA Distinguished Guest Scientist Fellowship Programme VK-11/2022”. This project has received funding from the HUN-REN Hungarian Research Network. This research was co-financed by the National Research, Development, and innovation Fund (Hungary) under Grant No. K 147781 (on behalf of SC). The Turkish material used in this project was provided with the support of the projects numbered 109T088 and 111T811 supported by the Scientific and Technological Research Council of Türkiye (TÜBİTAK), and the projects numbered 2016-248, 2018-135 and 2019-179 of the Trakya University Scientific Research Unit (on behalf of KK and CK). The Keyence VHX-7000 digital microscope

was co-funded with tax money on the basis of the state budget passed by the Sächsischer Landtag (Saxon state parliament, Germany) according to the Antragsnummer 100590787 of the Sächsische Aufbaubank issued 3 August 2021. MC was funded by an Alexander von Humboldt Foundation postdoctoral fellowship.

Author contributions

Herbert C. Wagner: conceptualization; data curation; formal analysis; funding acquisition; investigation; methodology; project administration; resources; validation; visualization; writing – original draft; writing – review and editing. Marion Cordonnier: conceptualization; data curation; formal analysis; funding acquisition; investigation; methodology; resources; validation; writing – original draft; writing – review and editing. Bernard Kaufmann: conceptualization; data curation; funding acquisition; investigation; methodology; project administration; resources; validation; writing – original draft; writing – review and editing. Kadri Kiran: data curation; funding acquisition; resources; writing – review and editing. Celal Karaman: data curation; funding acquisition; resources; writing – review and editing. Roland Schultz: data curation; resources; visualization; writing – review and editing. Bernhard Seifert: conceptualization; data curation; methodology; resources; validation; writing – review and editing. Sándor Csősz: conceptualization; data curation; formal analysis; funding acquisition; investigation; methodology; project administration; resources; validation; visualization; writing – original draft; writing – review and editing.

Author ORCIDs

Herbert C. Wagner  <https://orcid.org/0000-0002-5453-9357>

Kadri Kiran  <https://orcid.org/0000-0001-7983-0194>

Celal Karaman  <https://orcid.org/0000-0002-2158-5592>

Bernhard Seifert  <https://orcid.org/0000-0003-3850-8048>

Sándor Csősz  <https://orcid.org/0000-0002-5422-5120>

Data availability

All data generated or analyzed during this study are included in this published article and its supplementary information files.

References

- Arnold E (1921) Festnummer zu Ehren des 70. Geburtstages von Max Korb. Mitteilungen der Münchner Entomologischen Gesellschaft 9: 45–49.
- Arnold E (1933) Max Korb zum Gedächtnis. Mitteilungen der Münchner Entomologischen Gesellschaft 23: 103–107.
- Attewell PJ, Wagner HC (2019) *Tetramorium impurum* Foerster, 1850 (Hym.: Formicidae), first record for Guernsey and the Channel Islands. British Journal of Entomological and Natural History 32: 287–295.
- Balkenhol N, Holbrook JD, Onorato D, Zager P, White C, Waits LP (2014) A multi-method approach for analyzing hierarchical genetic structures: a case study with cougars *Puma concolor*. Ecography 37: 552–563. <https://doi.org/10.1111/j.1600-0587.2013.00462.x>
- Bolton B (1979) The ant tribe Tetramoriini (Hymenoptera: Formicidae). The genus *Tetramorium* Mayr in the Malagasy region and in the New World. Bulletin of the British Museum (Natural History), Entomology 38: 129–181.

- Bolton B (1995) A new general catalogue of the ants of the world. Harvard University Press, Cambridge, 504 pp.
- Bolton B (2014) New general catalogue of the ants of the world, and synopsis of taxonomic publications on Formicidae.
- Bolton B (2024) An online catalog of the ants of the world. AntCat. <http://antcat.org> [accesses 5 July 2024]
- Borowiec L, Salata S (2018) *Tetramorium immigrans* Santschi, 1927 (Hymenoptera: Formicidae) nowy gatunek potencjalnie inwazyjnej mrówki w Polsce. Acta entomologica silesiana 26: 1–5.
- Borowiec L, Galkowski C, Salata S (2015) What is *Tetramorium semilaeve* André, 1883? (Hymenoptera, Formicidae). ZooKeys 512: 39–62. <https://doi.org/10.3897/zookeys.512.10006>
- Bračko G, Kiran K, Karaman C, Salata S, Borowiec L (2016) Survey of the ants (Hymenoptera: Formicidae) of the Greek Thrace. Biodiversity Data Journal 4: e7945. <https://doi.org/10.3897/BDJ.4.e7945>
- Castracani C, Spotti FA, Schifani E, Giannetti D, Ghizzoni M, Grasso DA, Mori A (2020) Public engagement provides first insights on Po Plain ant communities and reveals the ubiquity of the cryptic species *Tetramorium immigrans* (Hymenoptera, Formicidae). Insects 11: 678. <https://doi.org/10.3390/insects11100678>
- Cicconardi F, Krapf P, D'Annessa I, Gamisch A, Wagner HC, Nguyen AD, Economo EP, Mikheyev AS, Guénard B, Grabherr R, Andesner P, Wolfgang A, di Marino D, Steiner FM, Schlick-Steiner BC (2020) Genomic signature of shifts in selection in a sub-alpine ant and its physiological adaptations. In: Su B (Ed.) Molecular Biology and Evolution 37: msaa076. <https://doi.org/10.1101/696948>
- Cordonnier M, Bellec A, Dumet A, Escarguel G, Kaufmann B (2018) Range limits in sympatric cryptic species: a case study in *Tetramorium* pavement ants (Hymenoptera: Formicidae) across a biogeographical boundary. Insect Conservation and Diversity 12: 109–120. <https://doi.org/10.1111/icad.12316>
- Cordonnier M, Escarguel G, Dumet A, Kaufmann B (2020) Multiple mating in the context of interspecific hybridization between two *Tetramorium* ant species. Heredity 124: 675–684. <https://doi.org/10.1038/s41437-020-0310-3>
- Cordonnier M, Gayet T, Escarguel G, Kaufmann B (2019) From hybridization to introgression between two closely related sympatric ant species. Journal of Zoological Systematics and Evolutionary Research. <https://doi.org/10.1111/jzs.12297>
- Csősz S, Fisher B (2015) Diagnostic survey of Malagasy *Nesomyrmex* species-groups and revision of *hafahafa* group species via morphology-based cluster delimitation protocol. ZooKeys 526: 19–59. <https://doi.org/10.3897/zookeys.526.6037>
- Csősz S, Fisher BL (2016) Taxonomic revision of the Malagasy members of the *Nesomyrmex angulatus* species group using the automated morphological species delineation protocol NC-PART-clustering. PeerJ 4: e1796. <https://doi.org/10.7717/peerj.1796>
- Csősz S, Markó B (2004) Redescription of *Tetramorium hungaricum* Rösler, 1935, a related species of *T. caespitum* (Linnaeus, 1758) (Hymenoptera: Formicidae). Myrmecologische Nachrichten 6: 49–59.
- Csősz S, Schulz A (2010) A taxonomic review of the Palaearctic *Tetramorium ferox* species-complex (Hymenoptera, Formicidae). Zootaxa 2401: 1–29. <https://doi.org/10.11646/zootaxa.2401.1.1>
- Csősz S, Radchenko AG, Schulz A (2007) Taxonomic revision of the Palaearctic *Tetramorium chefketi* species complex (Hymenoptera: Formicidae). Zootaxa 1405: 1–38. <https://doi.org/10.11646/zootaxa.1405.1.1>

- Csősz S, Wagner HC, Bozsó M, Seifert B, Arthofer W, Schlick-Steiner BC, Steiner FM, Péntes Z (2014) *Tetramorium indocile* Santschi, 1927 stat. rev. is the proposed scientific name for *Tetramorium* sp. C sensu Schlick-Steiner et al. (2006) based on combined molecular and morphological evidence (Hymenoptera: Formicidae). *Zoologischer Anzeiger* 253: 469–481. <https://doi.org/10.1016/j.jcz.2014.06.002>
- D H (1933) Max Korb † Lebensbild eines deutschen Entomologen. *Entomologische Rundschau* 18: 229–233.
- Dietrich CO (2004) Taxonomische Beiträge zur Myrmekofauna Jordaniens (Hymenoptera: Formicidae). *Denisia* 14: 319–344.
- Earl DA, von Holdt BM (2012) STRUCTURE HARVESTER: a website and program for visualizing STRUCTURE output and implementing the Evanno method. *Conservation Genetics Resources* 4: 359–361. <https://doi.org/10.1007/s12686-011-9548-7>
- Finzi B, Adensamer W, Käufel F, Strouhal H, Priesner H (1928) Weitere Beiträge zur Kenntnis der Fauna Griechenlands und der Inseln des Aegäischen Meeres. 1. Ameisen aus Griechenland und von den Aegäischen Inseln. *Sitzungsberichte der Akademie der Wissenschaften in Wien. Mathematisch-Naturwissenschaftlichen Klasse Abteilung I* 137: 787–792.
- Gippet JMW, Mondy N, Diallo-Dudek J, Bellec A, Dumet A, Mistler L, Kaufmann B (2017) I'm not like everybody else: urbanization factors shaping spatial distribution of native and invasive ants are species-specific. *Urban Ecosystems* 20: 157–169. <https://doi.org/10.1007/s11252-016-0576-7>
- Goslee SC, Urban DL (2007) The ecodist package for dissimilarity-based analysis of ecological data. *Journal of Statistical Software* 22: 1–19. <https://doi.org/10.18637/jss.v022.i07>
- Holm S (1979) A simple sequentially rejective multiple test procedure. *Scandinavian Journal of Statistics* 6: 65–70.
- Kiran K, Karaman C (2012) First annotated checklist of the ant fauna of Turkey (Hymenoptera: Formicidae). *Zootaxa* 3548: 1–38. <https://doi.org/10.11646/zootaxa.3548.1.1>
- Kiran K, Karaman C (2020) Additions to the ant fauna of Turkey (Hymenoptera, Formicidae). *Zoosystema* 42: 285–329. <https://doi.org/10.5252/zoosystema2020v42a18>
- Kopelman NM, Mayzel J, Jakobsson M, Rosenberg NA, Mayrose I (2015) Clumpak: a program for identifying clustering modes and packaging population structure inferences across K. *Molecular Ecology Resources* 15: 1179–1191. <https://doi.org/10.1111/1755-0998.12387>
- Lebas C, Galkowski C, Blatrix R, Wegnez P (2016) *Fourmis d'Europe occidentale*. Delachaux et Niestlé, Paris, 415 pp.
- Ligges U, Maechler M (2003) Scatterplot3d - an R package for visualizing multivariate data. *Journal of Statistical Software* 11: 1–20. <https://doi.org/10.18637/jss.v008.i11>
- Maechler M, Rousseeuw P, Struyf A, Hubert M, Hornik K, Studer M, Roudier P, Gonzalez J (2013) Package 'cluster.' *Dosegljivo na*: 980.
- Moder K, Schlick-Steiner BC, Steiner FM, Cremer S, Christian E, Seifert B (2007) Optimal species distinction by discriminant analysis: comparing established methods of character selection with a combination procedure using ant morphometrics as a case study. *Journal of Zoological Systematics and Evolutionary Research* 45: 82–87. <https://doi.org/10.1111/j.1439-0469.2006.00372.x>
- Nilsen G, Borgan Ø, Liestøl K, Lingjærde OC (2013) Identifying clusters in genomics data by recursive partitioning. *Statistical Applications in Genetics and Molecular Biology* 12: 637–652. <https://doi.org/10.1515/sagmb-2013-0016>

- Peakall R, Smouse PE (2006) GenAlEx 6: genetic analysis in Excel. Population genetic software for teaching and research. *Molecular Ecology Resources* 6: 288–295. <https://doi.org/10.1111/j.1471-8286.2005.01155.x>
- Pritchard JK, Stephens M, Rosenberg NA, Donnelly P (2000) Association mapping in structured populations. *The American Journal of Human Genetics* 67: 170–181. <https://doi.org/10.1086/302959>
- QGIS Development Team (2019) QGIS Geographic Information System. Open Source Geospatial Foundation Project. <http://qgis.osgeo.org>
- R Development core team (2012) R: a language and environment for statistical computing.
- Radchenko AG, Dlussky GM (2015) First record of fossil species of the genus *Tetramorium* (Hymenoptera, Formicidae). *Vestnik Zoologii* 49: 311–316. <https://doi.org/10.1515/vzoo-2015-0033>
- Radchenko AG, Scupola A (2015) Taxonomic revision of the *striativentre* species group of the genus *Tetramorium* (Hymenoptera, Formicidae). *Vestnik Zoologii* 49: 219–244. <https://doi.org/10.1515/vzoo-2015-0024>
- Ripley B, Venables B, Bates DM, Hornik K, Gebhardt A, Firth D, Ripley MB (2013) Package ‘mass.’ *Cran R* 538: 113–120.
- Salata S, Borowiec L (2017) Species of *Tetramorium semilaeve* complex from Balkans and western Turkey, with description of two new species of (Hymenoptera: Formicidae: Myrmicinae). *Annales Zoologici* 67: 279–313. <https://doi.org/10.3161/00034541ANZ2017.67.2.008>
- Salata S, Khalili-Moghadam A, Borowiec L (2024) A new species of the *Tetramorium meridionale* species-group (Hymenoptera: Formicidae) from Iran. *Zoology in the Middle East*. <https://doi.org/10.1080/09397140.2024.2359167>
- Schlick-Steiner BC, Steiner FM, Moder K, Seifert B, Sanetra M, Dyreson E, Stauffer C, Christian E (2006) A multidisciplinary approach reveals cryptic diversity in Western Palearctic *Tetramorium* ants (Hymenoptera: Formicidae). *Molecular Phylogenetics and Evolution* 40: 259–273. <https://doi.org/10.1016/j.ympev.2006.03.005>
- Schlick-Steiner BC, Steiner FM, Seifert B, Stauffer C, Christian E, Crozier RH (2010) Integrative Taxonomy: a multisource approach to exploring biodiversity. *Annual Review of Entomology* 55: 421–438. <https://doi.org/10.1146/annurev-ento-112408-085432>
- Seifert B (2002) How to distinguish most similar insect species – improving the stereomicroscopic and mathematical evaluation of external characters by example of ants. *Journal of Applied Entomology* 126: 445–454. <https://doi.org/10.1046/j.1439-0418.2002.00693.x>
- Seifert B (2003) The ant genus *Cardiocondyla* (Insecta: Hymenoptera: Formicidae) – a taxonomic revision of the *C. elegans*, *C. bulgarica*, *C. batesii*, *C. nuda*, *C. shuckardi*, *C. stambuloffii*, *C. wroughtonii*, *C. emeryi*, and *C. minutior* species groups. *Annalen des Naturhistorischen Museums Wien, Serie B* 104: 203–338.
- Seifert B (2007) Die Ameisen Mittel- und Nordeuropas. Iutra Verlags- und Vertriebsgesellschaft, Görlitz und Tauer, 368 pp.
- Seifert B (2018) The ants of Central and North Europe. Iutra Verlags- und Vertriebsgesellschaft, Tauer, 408 pp.
- Seifert B (2020) The gene and gene expression (GAGE) species concept: an universal approach for all eukaryotic organisms. *Systematic Biology*: syaa032. <https://doi.org/10.1093/sysbio/syaa032>
- Seifert B (2021) Surviving the winter: *Tetramorium sibiricum* n. sp., a new Central Siberian ant species (Hymenoptera: Formicidae). *Osmia* 9: 15–24. https://doi.org/10.25849/myrmecol.news_025:095

- Seifert B (2024) Frequent misclassification by mtDNA barcoding as revealed by nuDNA and/or testable analysis of its expression products. *Biodiversity Journal* 15: 129–133. <https://doi.org/10.31396/Biodiv.Jour.2024.15.2.129.133>
- Seifert B, Pannier L (2007) A method for standardized description of soil temperatures in terrestrial ecosystems. *Abhandlungen und Berichte des Naturkundemuseums Görlitz* 78: 151–182.
- Seifert B, Csősz S, Schulz A (2014) NC-Clustering demonstrates heterospecificity of the cryptic ant species *Temnothorax luteus* (Forel, 1874) and *T. racovitzai* (Bondroit, 1918) (Hymenoptera: Formicidae). *Contributions to Entomology* 64: 47–57. <https://doi.org/10.21248/contrib.entomol.64.1.47-57>
- Sheard JK, Sanders NJ, Gundlach C, Schär S, Larsen RS (2020) Monitoring the influx of new species through citizen science: the first introduced ant in Denmark. *PeerJ* 8: e8850. <https://doi.org/10.7717/peerj.8850>
- Steiner FM, Schlick-Steiner BC, Nikiforov A, Kalb R, Mistrik R (2002) Cuticular hydrocarbons of *Tetramorium* ants from central Europe: analysis of GC-MS data with self-organizing maps (SOM) and implications for systematics. *Journal of Chemical Ecology* 28: 2569–2584. <https://doi.org/10.1023/A:1021496305308>
- Steiner FM, Schlick-Steiner BC, Moder K (2006a) Morphology-based cyber identification engine to identify ants of the *Tetramorium caespitum/impurum* complex (Hymenoptera: Formicidae). *Myrmecological News* 8: 175–180.
- Steiner FM, Schlick-Steiner BC, Trager JC, Moder K, Sanetra M, Christian E, Stauffer C (2006b) *Tetramorium tsushimae*, a new invasive ant in North America. *Biological Invasions* 8: 117–123. <https://doi.org/10.1007/s10530-004-1249-7>
- Steiner FM, Seifert B, Moder K, Schlick-Steiner BC (2010) A multisource solution for a complex problem in biodiversity research: Description of the cryptic ant species *Tetramorium alpestre* sp.n. (Hymenoptera: Formicidae). *Zoologischer Anzeiger* 249: 223–254. <https://doi.org/10.1016/j.jcz.2010.09.003>
- Wagner HC, Arthofer W, Seifert B, Muster C, Steiner FM, Schlick-Steiner BC (2017) Light at the end of the tunnel: integrative taxonomy delimits cryptic species in the *Tetramorium caespitum* complex (Hymenoptera: Formicidae). *Myrmecological News* 25: 95–130.
- Wagner HC, Karaman C, Aksoy V, Kiran K (2018a) A mixed colony of *Tetramorium immigrans* Santschi, 1927 and the putative social parasite *Tetramorium aspina* sp.n. (Hymenoptera: Formicidae). *Myrmecological News* 28: 25–33.
- Wagner HC, Gamisch A, Arthofer W, Moder K, Steiner FM, Schlick-Steiner BC (2018b) Evolution of morphological crypsis in the *Tetramorium caespitum* ant species complex (Hymenoptera: Formicidae). *Scientific Reports* 8: preprint 12547. <https://doi.org/10.1038/s41598-018-30890-z>
- Wagner HC, Steiner FM, Schlick-Steiner BC, Csősz S (2021) Mixed-colony records together with nest densities and gyne morphology suggest temporary social parasitism in *Tetramorium* (Hymenoptera: Formicidae). *Zoologischer Anzeiger* 293: 190–201. <https://doi.org/10.1016/j.jcz.2021.06.003>
- Ward PS, Brady SG, Fisher BL, Schultz TR (2015) The evolution of myrmicine ants: phylogeny and biogeography of a hyperdiverse ant clade (Hymenoptera: Formicidae). *Systematic Entomology* 40: 61–81. <https://doi.org/10.1111/syen.12090>
- Wickham H (2009) stringr: Simple, Consistent Wrappers for Common String Operations.: 1.5.1. <https://doi.org/10.32614/CRAN.package.stringr>
- Wickham H (2011) The split-apply-combine strategy for data analysis. *Journal of Statistical Software* 40: 1–29. <https://doi.org/10.18637/jss.v040.i01>

Supplementary material 1

Male genital morphology of species of the *Tetramorium caespitum* complex

Authors: Herbert C. Wagner, Marion Cordonnier, Bernard Kaufmann, Kadri Kiran, Celal Karaman, Roland Schultz, Bernhard Seifert, Sándor Csősz

Data type: docx

Explanation note: **fig. S1.** Male genital morphology of three males of *Tetramorium caucasicum* of western Anatolia in dorsal, ventral, lateral, and posterior view (photographer RS, drawing by HCW). The genitals are very similar to those of *T. alpestre*. **fig. S2.** Male genital morphology of two males of *Tetramorium flavidulum* of western Anatolia in dorsal, ventral, lateral, and posterior view (photographer RS, drawing by HCW). **fig. S3.** Male genital morphology of 3 males of *Tetramorium alpestre* in dorsal, ventral, lateral, and posterior view (ex Wagner et al. 2017). **fig. S4.** Male genital morphology of 4 males of *Tetramorium caespitum* in dorsal, ventral, lateral, and posterior view (ex Wagner et al. 2017). **fig. S5.** Male genital morphology of 2 males of *Tetramorium hungaricum* in dorsal, ventral, lateral, and posterior view (ex Wagner et al. 2017). **fig. S6.** Male genital morphology of 3 males of *Tetramorium indocile* in dorsal, ventral, lateral, and posterior view (ex Wagner et al. 2017). **fig. S7.** Male genital morphology of 2 males of *Tetramorium caucasicum* in dorsal, ventral, lateral, and posterior view (ex Wagner et al. 2017). **fig. S8.** Male genital morphology of 2 males of *Tetramorium staerckei* in dorsal, ventral, lateral, and posterior view (ex Wagner et al. 2017). **fig. S9.** Male genital morphology of males of *Tetramorium impurum* in dorsal, ventral, lateral, and posterior view (ex Wagner et al. 2017).

Copyright notice: This dataset is made available under the Open Database License (<http://opendatacommons.org/licenses/odbl/1.0/>). The Open Database License (ODbL) is a license agreement intended to allow users to freely share, modify, and use this Dataset while maintaining this same freedom for others, provided that the original source and author(s) are credited.

Link: <https://doi.org/10.3897/zookeys.1234.142963.suppl1>

Supplementary material 2

Morphometric data of workers of the *Tetramorium caespitum* complex in Anatolia and adjacent regions

Authors: Herbert C. Wagner, Marion Cordonnier, Bernard Kaufmann, Kadri Kiran, Celal Karaman, Roland Schultz, Bernhard Seifert, Sándor Csősz

Data type: xls

Copyright notice: This dataset is made available under the Open Database License (<http://opendatacommons.org/licenses/odbl/1.0/>). The Open Database License (ODbL) is a license agreement intended to allow users to freely share, modify, and use this Dataset while maintaining this same freedom for others, provided that the original source and author(s) are credited.

Link: <https://doi.org/10.3897/zookeys.1234.142963.suppl2>

Supplementary material 3

Microsatellite Q-values of *Tetramorium caespitum* complex workers

Authors: Herbert C. Wagner, Marion Cordonnier, Bernard Kaufmann, Kadri Kiran, Celal Karaman, Roland Schultz, Bernhard Seifert, Sándor Csősz

Data type: xlsx

Copyright notice: This dataset is made available under the Open Database License (<http://opendatacommons.org/licenses/odbl/1.0/>). The Open Database License (ODbL) is a license agreement intended to allow users to freely share, modify, and use this Dataset while maintaining this same freedom for others, provided that the original source and author(s) are credited.

Link: <https://doi.org/10.3897/zookeys.1234.142963.suppl3>

Supplementary material 4

Observed and expected heterozygosity, the number of alleles, and the effective alleles of microsatellite data

Authors: Herbert C. Wagner, Marion Cordonnier, Bernard Kaufmann, Kadri Kiran, Celal Karaman, Roland Schultz, Bernhard Seifert, Sándor Csősz

Data type: docx

Copyright notice: This dataset is made available under the Open Database License (<http://opendatacommons.org/licenses/odbl/1.0/>). The Open Database License (ODbL) is a license agreement intended to allow users to freely share, modify, and use this Dataset while maintaining this same freedom for others, provided that the original source and author(s) are credited.

Link: <https://doi.org/10.3897/zookeys.1234.142963.suppl4>

Spotlighting Darwin wasps (Hymenoptera, Ichneumonidae) in Zambia: a new species and the urgent need for further exploration

Noah Meier^{1,2*}, Alexandra Viertler^{1*}, Meekness Kapaale³, Cyprian Katongo³, Tamara Spasojevic^{1,4}

1 Natural History Museum Basel, Augustinerstrasse 2, 4051 Basel, Switzerland

2 University of Bern, Institute of Ecology and Evolution, Baltzerstrasse 6, 3012 Bern, Switzerland

3 Department of Biosciences and Biotechnology, University of Zambia, Great East Road Campus, Lusaka, Zambia

4 Natural History Museum Vienna, Burgring 7, 1010 Wien, Austria

Corresponding author: Noah Meier (noah.meier@bs.ch)

Abstract

The parasitoid Darwin wasps (Ichneumonidae) are one of the most species-rich families of insects, with a crucial role in ecosystem functioning while many species are known as potential biological control agents. However, the group is poorly studied, especially in the Afrotropical realm, where for several countries only a handful of species have been recorded. Zambia is one of the countries with the fewest records for Darwin wasps with only 26 species reported in the largest Ichneumonidae database, “Taxapad”, from 2016 and subsequent publications. In this study, the species of Darwin wasps recorded from Zambia were reviewed and complemented with newly collected species in the Northern Province, to provide a first preliminary checklist of Darwin wasps in Zambia. Our findings increased the number of species known for Zambia to 44, which might still represent as little as 1.7% of the true diversity of the group. Despite the limited scale of the study, one new species of Afrotropical Cremastinae, *Pristomerus roussei* Meier, Viertler & Spasojevic, **sp. nov.**, is described. The study thus highlights both the substantial potential for discovery of new taxa and significant gaps in our knowledge about the Darwin wasp diversity in Zambia. To tackle these shortcomings, comprehensive collecting efforts considering the various ecotypes found in Zambia are recommended, as well as studies of natural history collections, collaborative effort by taxonomic experts, and enhancing local capacities for taxonomic research by involving students and enlarging local natural history collections.

Key words: Afrotropical region, biodiversity, Lake Tanganyika, parasitoids, *Pristomerus*, taxonomy

Introduction

Darwin wasps (Ichneumonidae) are parasitoids of holometabolous insects and spiders, playing a crucial role in natural ecosystems and as biological control agents in agriculture (Mates et al. 2012). Despite their ecological importance, the hyperdiverse Darwin wasps remain one of the most understudied insect families, with more than 25,000 species formally described (Yu et al. 2016)



Academic editor: Bernardo Santos

Received: 17 December 2024

Accepted: 27 February 2025

Published: 22 April 2025

ZooBank: <https://zoobank.org/A0726655-4738-4135-A6F0-1BF89364C845>

Citation: Meier N, Viertler A, Kapaale M, Katongo C, Spasojevic T (2025) Spotlighting Darwin wasps (Hymenoptera, Ichneumonidae) in Zambia: a new species and the urgent need for further exploration. ZooKeys 1234: 341–367. <https://doi.org/10.3897/zookeys.1234.144751>

Copyright: © Noah Meier et al.
This is an open access article distributed under terms of the Creative Commons Attribution License (Attribution 4.0 International – CC BY 4.0).

* These authors contributed equally.

and as many as 60,000 species estimated worldwide (Townes 1969). The vast disparity between known and estimated species richness is particularly pronounced in certain biogeographical regions.

One of the largest gaps in species documentation is found within the Afrotropical realm, where only 2,322 species of Darwin wasps have been recorded but 9,200–15,500 species are currently expected (Townes 1969; Meier et al. 2024). Notably, the descriptions of the majority of Afrotropical species date back to the early and mid-20th century, with half of the species described by a small group of entomologists, including G. Heinrich, A. Seyrig, P. Benoit, and C. Morley (Morley 1912; Benoit 1951b, 1952, 1953d, 1953c, 1953b, 1953a, 1955, 1956, 1957; Heinrich 1967a, 1967b, 1968a, 1968b, 1968c). Spatial focus of these early works was on the Democratic Republic of Congo (Benoit 1951a, 1953c, 1953d), and Madagascar (Seyrig 1932, 1934, 1952), while taxonomically only Ichneumoninae (Heinrich 1967b, 1967a, 1968b, 1968a, 1968c), and Ophioninae (Gauld and Mitchell 1978) have been more comprehensively treated. And although some countries, such as the Republic of South Africa (Rousse and van Noort 2013, 2014a; Reynolds Berry and van Noort 2016; Rousse et al. 2016), Gabon (van Noort 2004), Namibia (van Noort et al. 2000), Uganda (Hopkins et al. 2018, 2019), Central African Republic (Rousse and van Noort 2014a; Azevedo et al. 2015), and Tanzania (Russel-Smith et al. 1999) have been later systematically sampled, less than a quarter of their actual species richness of Darwin wasps seems to be recorded up to now (Meier et al. 2024). Several other Afrotropical countries have barely any faunistic records of Darwin wasps. For example, Zambia has only 26 recorded species according to the “Catalogue of world Ichneumonidae” (Yu and Horstmann 1997; Yu et al. 2016), implying a vast, untapped biodiversity awaiting exploration and formal description.

There has never been any Darwin wasp research focused on Zambia and most of the available records are simply a byproduct of studies with broader taxonomic and geographic focus. The two main catalogues dealing with Afrotropical ichneumonids, the first a catalogue of Ethiopian (= Afrotropical) Ichneumonidae by Townes and Townes (1973) and the second a revision of the subfamily Ophioninae by Gauld and Mitchell (1978), the latter updated by Rousse and van Noort (2014b), listed in sum only 13 species of ichneumonids for Zambia. Besides a few additional records from the 20th Century, the record of Darwin wasps in Zambia is supplemented by recent revisionary works on Darwin wasp genera in the Afrotropical region and by a few faunistic studies (e.g., Rousse and van Noort 2015; Riedel 2016; Khalaim 2019; Giovanni and Varga 2021). Finally, with the present day studies about diversity and distribution of insects in Zambia being skewed towards economically important species, such as edible caterpillars (Kusia et al. 2023), agricultural pests (Sohati et al. 2001; Durocher-Granger et al. 2021), pollinators (Mayes and Petrillo 2017), and disease vectors (Lobo et al. 2015; Nyirenda et al. 2020; Kallu et al. 2023), there are some new species records for Darwin wasps, and parasitoids in general, coming from studies focusing on biological control (Midingoyi et al. 2016; Durocher-Granger et al. 2021). While such studies are beneficial, they alone cannot provide a comprehensive species list of Zambian Darwin wasps and a map of their distribution.

As a fundamental step towards a more complete checklist of Darwin wasps in Zambia, we provide here a first preliminary checklist, which is based on thorough literature research and a small-scale collecting effort in the Northern Province of

Zambia. The goal of this preliminary checklist is to record the status quo of our knowledge about the Zambian fauna, provide a basis for future research, and highlight the gap between the known and expected species richness in Zambia.

Materials and methods

Abbreviations of depositories

| | |
|--------------|---|
| NHMUK | Natural History Museum, London, UK (Gavin Broad) |
| CABI | CAB International, Delémont, Switzerland (Marc Kenis) |
| LKG | Oberösterreichische Landes-Kultur GmbH, Linz (Esther Ockermüller) |
| LMNH | Livingstone Museum, Zambia (Martha Imakando) |
| MNHN | Muséum national d'Histoire naturelle, Paris, France (Claire Villemant) |
| MZH | Finnish Museum of Natural History, Helsinki (Juho Paukkunen) |
| NHMZ | Natural History Museum of Zimbabwe |
| NMBS | Naturhistorisches Museum, Basel (Seraina Klopstein) |
| RMNH | Naturalis, Leiden, The Netherlands (Frederique Bakker) |
| SAMC | Iziko South African Museum, Cape Town, South Africa (Simon van Noort) |
| TC | Townes Collection, Ann Arbor, Michigan, USA (now in Logan, Utah) (David Wahl) |
| UNZA | University of Zambia, Lusaka, Natural history collection (Philip Nkunika) |
| ZSM | Zoologische Staatssammlung München |

Sampling locality and material

Zambia is a landlocked country located in the Sub-Equatorial Afrotropics (Burkart 2023). It covers an area of 752,612 square kilometres and lies between latitudes 8° and 18° south and longitudes 22° and 34° east. Based on the amount of rainfall received but also to a limited extent according to soils and other climatic characteristics, Zambia is divided into three agro-ecological regions (Zones I, II, and III). Our study site belongs to the agro-ecological Zone III, which covers northern and north-western parts of the country, and it is classified as a high rainfall region, receiving more than 1000 mm rainfall per annum on average (Dautu et al. 2012). Based on the dominant vegetation type, our study sites belong to the Central Zambezian Miombo woodlands ecoregion, which covers circa 50% of Zambian territory (Malambo and Syampungani 2008). This ecoregion is characterised by a long dry season, up to seven months, and a rainy season from approximately November to March. It is a part of the Zambezian regional centre of endemism, and it is home to dozens of endemic plant species.

We collected specimens in the Northern Province of Zambia in the region of Lake Tanganyika around Mpulungu for two weeks, from the end of August to the beginning of September 2023 (Fig. 1). This fieldwork was conducted at the end of the dry season, following a couple of months without rain. Most of the sampling occurred in well-watered areas, such as those near lodges, streams, and the shores of Lake Tanganyika. Specimens were collected using sweep nets at all collection sites, and at Kalambo falls lodge additionally with Malaise traps, pitfall traps and light traps. All samples were stored in 80% ethanol on site and subsequently sorted and dry-mounted at the NMBS in Switzerland.



Figure 1. Maps of the sampling locality **a** map of Zambia, where Lusaka (black dot) and our sampling area (orange rectangle) are marked **b** sampling sites: **1** Kalambo River delta **2** Kalambo falls lodge **3** Chitili, with a nearby stream **4** Isanga Bay lodge **5** Kalambo River above Kalambo waterfall (yellow dot).

Collected ichneumonids are currently at the NMBS but they will be divided between the NMBS and LMNH, where ichneumonid holotypes will be deposited in the NMBS, and paratypes in the LMNH and NMBS. For this study, we obtained all necessary collection and export permits, issued by the National Health Research Authority (NHRA) of Zambia. The permits are in accordance with the principles and regulations of the Nagoya protocol as confirmed by the Ministry of Lands and Natural Resources in Zambia.

Species descriptions

Morphological terminology follows Broad et al. (2018). The dimensions of the face (excluding the clypeus) are measured from the antennal sockets to the tentorial pits and from the inner margin of one eye to the inner margin of the other eye at level of the antennal sockets. The dimensions of the clypeus are measured between the mandibular bases and from the apical margin of clypeus to the height of the tentorial pits (largest distance). Images of the collected samples were taken with a Keyence VHX-6000 using stacking and stitching techniques.

Lab work

We sequenced the barcoding portion of cytochrome oxidase subunit 1 (COI) gene as a reference for a newly described species. One leg with coxa from a female and a male paratype was used to extract DNA. DNA extracts and the voucher specimens are stored at the NMBS. Extractions were done with the DNeasy blood and tissue kit from Qiagen according to the standard protocol, but with a prolonged digestion step over night at 56 °C and two elution steps with only 50 µl each. We used previously published primers for COI (Folmer et al. 1994) for PCR with annealing temperatures of 50 °C. The quality of the PCR products was then checked on a 2% agarose electrophoresis gel and successful amplification were sent for cleanup and sequencing to Macrogen Europe in the Netherlands. Sequence editing was done with the CodonCode Aligner software version 9.0.1.3 (CodonCode Corporation, Dedham, MA, USA), while sequence alignment was done with MEGAX (Kumar et al. 2018) using the MUSCLE alignment algorithm with default settings. No gaps or stop codons were detected. Uncorrected p-distances for COI were calculated in MEGAX, using pairwise deletions (Kumar et al. 2018). The newly generated sequences are deposited in GenBank, with accession numbers provided in the respective species descriptions.

Results

Species description

We here describe one Cremastinae species new to science.

Pristomerus Curtis, 1836

Pristomerus roussei Meier, Viertler & Spasojevic, sp. nov.

<https://zoobank.org/615E6352-F991-4C94-AD8B-DCB9A85D0B5E>

Fig. 2

Material examined. Holotype. • 1 ♀, ZM Northern Province, Mbala, Kalambo Falls (above waterfall), sweep net, 1170 m, -8.5961/31.2478, 21.viii–2.ix.2023, leg. N. Meier, T. Spasojevic, A. Viertler (NMBS). **Paratypes.** • 1 ♂, ZM Northern Province, Mbala, Kalambo Falls (above waterfall), sweep net, 1170 m, -8.5961/31.2478, 21.viii–2.ix.2023, leg. N. Meier, T. Spasojevic, A. Viertler (NMBS). • 1 ♂, ZM Mpulungu, Chitili stream, sweep net, -8.6390/31.2035, 21.viii–2.ix.2023, leg. N. Meier, T. Spasojevic, A. Viertler, voucher: 20-538 (NMBS). • 2 ♂, ZM Mpulungu, Kalambo delta, sweep net, 777 m, -8.5964, 31.1844, 21.viii–2.ix.2023, leg. N. Meier, T. Spasojevic, A. Viertler (LMNH). • 1 ♀, ZM Mpulungu, Mpulungu town, sweep net, 777 m, -8.7621, 31.1138, 21.viii–2.ix.2023, leg. N. Meier, T. Spasojevic, A. Viertler, voucher: 20-537 (NMBS). • 1 ♀, ZM Mpulungu, Kalambo Falls Lodge, sweep net, 786 m, -8.6241/31.2011, 21.viii–2.ix.2023, leg. N. Meier, T. Spasojevic, A. Viertler (LMNH). • 1 ♀, ZM Northern Western Province, 150 km W Solwezi, Ntambu, 12°18'S, 25°10'E; 11.11.2005; leg. M. Halada (LKG).

Diagnosis. Moderate size; pale yellow with black spots on tergites 1–3 antero-dorsally; femora apically white-dotted; pterostigma anteriorly white; occiput without dark spots; face densely and very shallowly punctate; clypeus transverse

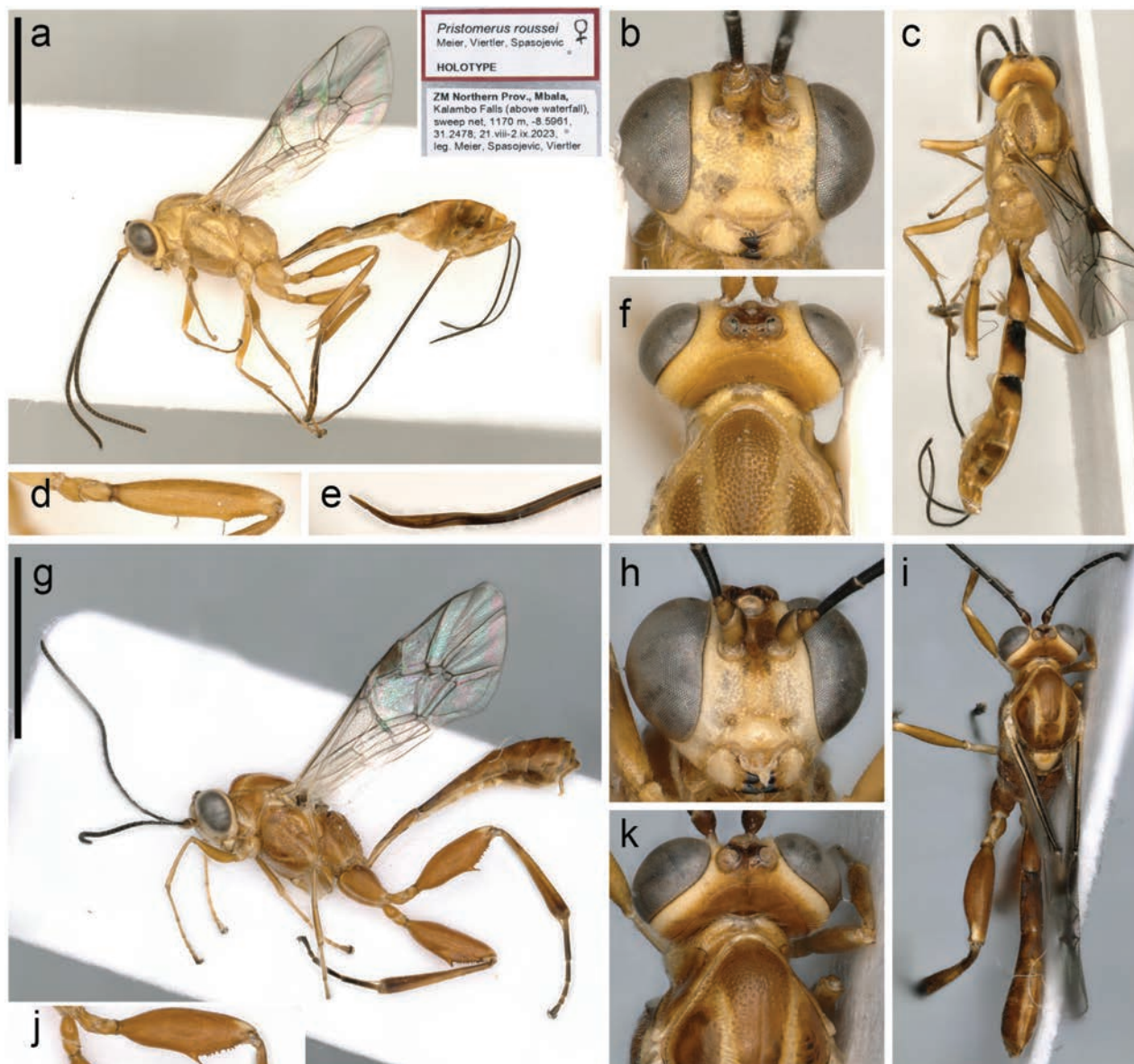


Figure 2. *Pristomerus roussei* sp. nov. Meier, Viertler & Spasojevic. **a–f** holotype (female) **a** habitus, lateral view, with labels **b** face, frontal view **c** habitus, dorsal view **d** hind femur **e** ovipositor tip **f** mesoscutum and occiput, dorsal view. **g–k** paratype (male, with the same collection data as the holotype) **g** habitus, lateral view **h** face, frontal view **i** habitus, dorsal view **j** hind femur **k** mesoscutum and occiput dorsal view. Scale bars: 3 mm.

with dispersed punctures dorsally and almost smooth ventrally; remainder of head coriaceous; malar space shorter than base of mandible; antenna with 30–33 flagellomeres, penultimate flagellomere quadrate; distance between posterior ocelli approx. as wide as one posterior ocellus; mesosoma densely punctate with pronotum and speculum nearly smooth; female femoral tooth distinct but clearly wider than high, followed by a row of minute denticles; ovipositor moderately long, apically weakly sinuous. Male with ocelli enlarged, inner margins of eyes slightly diverging ventrally, femur and femoral tooth stouter with femoral tooth long and acute, area superomedia much more slender than in female.

Differential diagnosis. *Pristomerus roussei* sp. nov. is morphologically very close to *Pristomerus masai* Rousse & van Noort, 2015, which is suspected to represent a species-complex (Rousse and van Noort 2015). In the dichotomous key

of Rousse and van Noort (2015), *P. roussei* ends at couplet #36. It can be differentiated from *P. masai* by a wider distance between the posterior ocelli, a quadrate penultimate flagellomere (females and males) and the lack of dark marks on the occiput (females). *Pristomerus roussei* can be differentiated from *P. wolof* Rousse & van Noort, 2015 by the more strongly developed femoral tooth (females and males), the quadrate penultimate flagellomere rather than elongate (females and males), and by its more extensive dark metasomal colour (females).

Description. Female: 4 specimens (measurements of the holotype in brackets). **Colour.** Pale yellow. Scape, pedicel, frons, stemmaticum and occiput pale brown; mandibular teeth and flagellum black; mesoscutum apart from notauli and posterior parts orange; wings hyaline, venation brown, pterostigma black, proximal corner translucent; legs orange, femur apically with a white spot, hind tibia basally and apically slightly infuscate, hind tarsus except basal 0.2 of first tarsal segment black; tergites 1–3 on the anterior half black; ovipositor sheath black; ovipositor dark brown, basally and apically testaceous.

Head. Face $2.5\times$ ($2.5\times$) wider than high, densely and very shallowly punctate; inner margins of eyes subparallel, distance between posterior ocelli $\sim 1.0\times$ ($1.0\times$) as wide as diameter of one posterior ocellus, distance between posterior ocelli and margin of compound eye $1.1\times$ ($1.1\times$) wider than diameter of one posterior ocellus; clypeus $2.0\times$ ($2.0\times$) wider than high and moderately convex, with dispersed punctures dorsally, almost smooth ventrally; malar space $\sim 0.7\text{--}0.75\times$ ($0.75\times$) base of mandible; frons, vertex and temple coriaceous; occipital carina joining hypostomal carina distinctly above mandible base; antenna with 31–33 (33) flagellomeres, penultimate flagellomere $\sim 1.0\times$ ($1.0\times$) as long as wide.

Mesosoma. Moderately elongate; pronotum nearly smooth posteriorly, with longitudinal striations in its impression and punctures ventrally; mesopleuron and metapleuron with space between punctures less than maximum diameter of punctures, between punctures smooth and shining, mesopleuron with a shallow oblique and transversely strigose furrow below speculum, speculum smooth; mesoscutum densely punctate, between punctures smooth and shiny, notaulus distinct on anterior third of mesoscutum; scutellum densely punctate; propodeum densely punctate, propodeal carination complete, superomedial area $\sim 2.3\text{--}2.5\times$ ($2.3\times$) as long as its maximum width.

Wings. Fore wing $\sim 4.5\text{--}4.9$ mm (4.9 mm) with M between 2rs-m and 2m-cu $\sim 1.25\text{--}1.5\times$ ($1.25\times$) as long as 2rs-m, 2m-cu with a small bulla covering anterior 0.2–0.4 of 2m-cu; hind wing with nervellus intercepted at lower 0.7 (0.7), second abscissa of CU not pigmented.

Legs. Tooth on hind femur distinct, clearly wider than high, followed by a row of minute denticles. Hind tibia with dispersed spines between normal setation. Tarsal claws pectinate with two distinct denticles.

Metasoma. Posterior half of tergite 1, tergite 2, and anterior of tergite 3 longitudinally aciculate, following tergites coriaceous; thyridium elongate, elliptic; ovipositor sheath $\sim 1.5\times$ as long as hind tibia, apically weakly to moderately sinuous; ovipositor notch rather weak, its distance from ovipositor tip $\sim 1.5\times$ basal width of first tarsal segment of hind leg.

Male: 4 specimens. Similar to female; stemmaticum with ocelli slightly raised and ocelli enlarged, distance between posterior ocelli approx. as wide as diameter of one posterior ocellus, distance between posterior ocelli and margin of compound eye less than half diameter of one posterior ocellus; inner margins

of eyes distinctly diverging ventrally; antenna with 29–31 flagellomeres; mesoscutum laterally almost smooth, impunctate; femur swollen, femoral tooth stronger, long and acute, apically with a distinct row of denticles; dark marks on metasoma sometimes absent or reduced.

Etymology. Dedicated to Pascal Rousse, who contributed greatly to our current understanding of Afrotropical *Pristomerus* species.

Molecular data

Sequences of the COI barcode for the female and male paratype are given below. The pairwise distance (p-distance) between these two sequences is 0.3%. The best match according to the NCBI standard nucleotide BLAST search belongs to the Afrotropical *Pristomerus pallidus* (Kriechbaumer, 1884) (GenBank: MF673618.1) with a p-distance of 5.6–6.0%.

GenBank Accession ID: PV176400, NMBS:20-537, female paratype; 645 bp.

ATTTTGGTATATGATCTGGGATAATTGGATCTTCTATAAGATTAATTATTCGATT-
AGAATTAGGGAATCCGGGGTCTTTAATTAATAATGATCAAATTTATAATTCTATAAT-
TACAATACATGCTTTTATTATAATTTTTTTTATAGTTATACCAGTTATAATTGGAGG-
GTTTGGAAATTGATTAATTCCTCTAATATTAGGAGCTCCAGATATAGCTTTTCCTC-
GAATAAATAATTTAAGATTTTGATTATTAATTCCTTCGTTAATGATATTAATTAT-
GAGATCAATTACTAATCAAGGAGTGGGTACAGGATGAACAATATATCCTCCTTTAT-
CATTAAATTTAAATCAAGAAGGTATATCAATAGATTTATCTATTTTTCTTTA-
CATTTAGCAGGTATATCTTCAATTTTAGGATCTATTAATTTTATTTCTACTATTATA-
AATATAAAAATTTTTGATTCAAAATTAGATCAATTAACCTTTATTTCTTGATCAAT-
TAATATTACTACAATTTTATTATTATTAGCTGTTCCAGTATTAGCAGGAGCAATTAC-
TATAATTTTAACAGATCGAAATTTAAATACTTCTTTTTTTGATCCAAGTGGAGGAG-
GAGATCCAATTTTATTTCAACATTTATTT.

GenBank Accession ID: PV176401, NMBS:20-538, male paratype; 645 bp.

ATTTTGGTATATGATCTGGGATAATTGGATCTTCTATAAGATTAATTATTCGATT-
AGAATTAGGGAATCCGGGGTCTTTAATTAATAATGATCAAATTTATAATTCTATAAT-
TACAATACATGCTTTTATTATAATTTTTTTTATAGTTATACCAGTTATAATTGGAGG-
GTTTGGAAATTGATTAATTCCTCTAATATTAGGAGCTCCAGATATAGCTTTTCCTC-
GAATAAATAATTTAAGATTTTGATTATTAATTCCTTCGTTAATAATATTAATTAT-
GAGATCAATTACTAATCAAGGAGTGGGTACAGGATGAACAATATATCCTCCTTTAT-
CATTAAATTTAAATCAAGAAGGTATATCAATAGATTTATCTATTTTTCTTTA-
CATTTAGCAGGTATATCTTCAATTTTAGGATCTATTAATTTTATTTCTACTATTATA-
AATATAAAAATTTTTGATTCAAAATTAGATCAATTAACCTTTATTTCTTGATCAAT-
TAATATTACTACAATTTTATTATTATTAGCTGTTCCAGTATTAGCAGGAGCAATTAC-
TATAATTTTAACAGATCGAAATTTAAATACTTCTTTTTTTGATCCAAGTGGGGGAG-
GAGATCCAATTTTATTTCAACATTTATTT.

Preliminary checklist

By combining published species records from literature and the new material collected in this study, we provide a first preliminary checklist for Darwin wasps in Zambia with 44 species (Table 1). Except for the cosmopolitan *Diplazon laetatorius* (Fabricius, 1781) and widely distributed *Xanthopimpla romani* Krieger, 1915, all other newly collected and identified species ($n = 14$) were previously unrecorded for Zambia (*). We also found literature records of four additional species in

Table 1. Preliminary checklist of species recorded for Zambia based on literature records and our field study in the Northern Province of Zambia, Mpulungu district. In total, 44 species are recorded, one of which is described as new to science in this publication. * Previously unrecorded species; # missing from Yu and Horstmann (1997, 2016) catalogue; [?] no repository mentioned in the reference.

| Subfamily | Species | Literature | Our study | Repository | Reference |
|----------------|---|------------|-----------|--------------------|---|
| Brachycyrtinae | <i>Brachycyrtus lucchii</i> Di Giovanni & Varga, 2021 | x | | NHMMUK | Di Giovanni and Varga (2021) |
| Campopleginae | <i>Diadegma mollipla</i> (Holmgren, 1868) | x | | [?] | Cruickshank and Ahmad (1973) |
| | * <i>Charops electrinus</i> Vas, 2020 | | x | NMBS, LMNH | |
| | * <i>Venturia aquila</i> Vas, 2019 | | x | NMBS | |
| | * <i>Xanthocampoplex oneili</i> (Cameron, 1905) | | x | NMBS | |
| Cremastinae | <i>Pristomerus bamba</i> Rouse & van Noort, 2015 | x | | SAMC | Rouse and van Noort (2015) |
| | <i>Pristomerus bullis</i> Fitton in Polaszek et al. 1994 | x | | SAMC | Rouse and van Noort (2015) |
| | * <i>Pristomerus rousei</i> sp. nov. | | x | NMBS, LMNH | |
| | * <i>Temelucha basiornata</i> (Cameron, 1911) | | x | NMBS, LMNH | |
| | * <i>Trathala annulicornis</i> (Tosquinet, 1896) | | x | NMBS, LMNH | |
| Cryptinae | <i>Coccygodes subquadratus</i> (Waterston, 1927) | x | | [?] | Benoit (1951a); Waterston (1927) |
| | * <i>Ospyrinchotus gigas</i> Kriechbaumer, 1894 | | x | NMBS, LMNH | |
| | <i>Zonocryptus formosus</i> (Brullé, 1846) | x | | [?] | Waterston (1927) |
| Diplazontinae | <i>Diplazon laetatorius</i> (Fabricius, 1781) | x | x | NMBS | |
| Ichneumoninae | # <i>Ctenochares rufithorax</i> (Kriechbaumer, 1894) | x | | NHMMUK | Morley (1915) |
| | # <i>Ischnojoppa luteator</i> (Fabricius, 1798) | x | | NHMMUK | Morley (1915) |
| | # <i>Leptophatnus crococephalus rubricaput</i> (Morley, 1919) | x | | ZSM | Heinrich (1967) |
| Metopiinae | <i>Metopius albipictus</i> Tosquinet, 1896 | x | | LKG | Riedel (2016) |
| | <i>Metopius clathratus</i> Benoit, 1965 | x | | NHMMUK | Riedel (2016) |
| | <i>Metopius discolor</i> Tosquinet, 1896 | x | | NHMMUK | Durocher-Granger et al. (2021); Riedel (2016); Townes and Townes (1973) |
| | <i>Metopius rufigaster zambiensis</i> Riedel, 2016 | x | | LKG | Riedel (2016) |
| | <i>Metopius zuluani</i> Benoit, 1965 | x | | LKG | Riedel (2016) |
| Ophioninae | <i>Enicospilus albiger</i> (Kriechbaumer, 1894) | x | | SAMC | Rouse and van Noort (2014b) |
| | <i>Enicospilus antefurcalis</i> (Szépligeti, 1908) | x | | NHMMUK | Gauld and Mitchell (1978) |
| | <i>Enicospilus biimpressus</i> (Brullé, 1846) | x | | NHMMUK | Gauld and Mitchell (1978) |
| | <i>Enicospilus capensis</i> (Thunberg, 1822) | x | | CABI | Durocher-Granger et al. (2021) |
| | <i>Enicospilus fenestralis</i> (Szépligeti, 1906) | x | | NHMMUK | Gauld and Mitchell (1978) |
| | <i>Enicospilus helvolus</i> Gauld & Mitchell, 1978 | x | | TC | Gauld and Mitchell (1978) |
| | <i>Enicospilus laquaetus</i> (Enderlein, 1921) | x | | NHMMUK | Gauld (1982) |
| | <i>Enicospilus mauritii</i> (Saussure, 1892) | x | | NHMMUK | Morley (1912) |
| | <i>Enicospilus nefarius</i> Gauld & Mitchell, 1978 | x | | TC | Gauld and Mitchell (1978) |
| | <i>Enicospilus nops</i> Gauld & Mitchell, 1978 | x | | NHMMUK | Gauld and Mitchell (1978) |
| | # <i>Enicospilus transvaalensis</i> Cameron, 1911 | x | | TC | Gauld and Mitchell (1978) |
| | <i>Enicospilus watshami</i> Gauld, 1982 | x | | NHMMUK | Gauld (1982) |
| | <i>Euryophion latipennis</i> (Kirby, 1896) | x | | SAMC | Rouse and van Noort (2014b) |
| | * <i>Euryophion nigripennis</i> Cameron, 1906 | | x | NMBS | |
| | <i>Lepiscelus distans</i> (Seyrig, 1935) | x | | TC | Gauld and Mitchell (1978) |
| Pimplinae | * <i>Theronia lurida</i> Tosquinet, 1896 | | x | NMBS | |
| | <i>Xanthopimpla romani</i> Krieger, 1915 | x | x | NHMMZM, NMBS, LMNH | Benoit (1953b) |
| | <i>Xanthopimpla stemmator</i> (Thunberg, 1822) | x | | [?] | Midingoyi et al. (2016) |
| Tersilochinae | <i>Diaparsis interstitialis</i> Khalaim, 2013 | x | | MZH | Khalaim (2019) |
| | <i>Diaparsis mostovskii</i> Khalaim, 2013 | x | | RMNH | Khalaim (2019) |
| | <i>Diaparsis voluptuosa</i> Khalaim, 2013 | x | | MZH | Khalaim (2019) |
| Tryphoninae | <i>Zambion monodon</i> Kasparyan, 1993 | x | | MZH | Kasparyan (1993) |

Zambia (#) that were not included in the Yu and Horstmann (1997) catalogue nor its electronic version (Yu et al. 2016). Moreover, the subfamilies Anomaloninae, Banchinae, Orthocentrinae, and Phygadeuontinae and 17 genera (*Anomalon*, *Spilopimpla*, *Syzeuctus*, *Venturia*, *Porizon*, *Xanthocampoplex*, *Temelucha*, *Trathala*, *Cryptus*, *Goryphus*, *Stenarella*, *Osprynchotus*, *Afromevesia*, *Triclistus*, *Megastylus*, *Paraphylax*, *Theronia*) are recorded from Zambia for the first time (*). Outstandingly, the record of the genus *Porizon* is also the first for the Afrotropical realm. In the list of records below, verbatim data are given in square brackets.

Anomaloninae

**Anomalon cf. flavomaculatum* (Cameron, 1905)

Records. 2 ♂♂, ZM Northern Province, Mpulungu, Mbala, Kalambo falls, (above waterfall), 1170 m, -8.5961/31.2478, 29.viii.2023, leg. N. Meier, T. Spasojevic, A. Viertler (NMBS).

Remarks. There are five additional *Anomalon* specimens, probably belonging to two or three new species, which are currently being treated in the genus revision of Heinz Schnee (H. Schnee, pers. comm.).

Banchinae

**Spilopimpla cf. chappuisi* (Seyrig, 1935)

Records. 1 ♀, ZM Northern Province, Mpulungu, Kalambo River Delta, sweep-net, -8.5965/31.1844, 21.viii–2.ix.2023, leg. N. Meier, T. Spasojevic, A. Viertler (NMBS).

**Syzeuctus* sp.

Records. 1 ♀, ZM Northern Province, Mpulungu, Kalambo River Delta, sweep-net, -8.5965/31.1844, 21.viii–2.ix.2023, leg. N. Meier, T. Spasojevic, A. Viertler (NMBS).

Brachycyrtinae

Brachycyrtus lucchii Di Giovanni & Varga, 2021

Records. 1 ♀, ZM Lusaka Province, 15 km E. Lusaka, 4–15.xii.1979, R. A. Beaver (NHMUK).

1 ♂, ZM Lusaka Province, 15 km E. Lusaka, 11–21.i.1980, R. A. Beaver (NHMUK).

1 ♂, ZM Lusaka Province, Lusaka, 1–14.iv.1980, R. A. Beaver (NHMUK) (Di Giovanni and Varga 2021).

Campopleginae

Diadegma mollipla (Holmgren, 1868)

Records. Unspecified, ZM (Cruickshank and Ahmad 1973).

****Charops electrinus* Vas, 2020**

Records. 1 ♀, ZM Northern Province, Mpulungu, Kalambo Falls Lodge, sweep net, -8.6241/31.2011, 21.viii–02.ix.2023, leg. N. Meier, T. Spasojevic, A. Viertler (NMBS, LMNH). 1 ♀ same as previous except collected by a Malaise trap.

***Charops* sp.**

Records. 3 ♀/♂, ZM Southern Province, Kuzungula district (Chipabika et al. 2023).

Remarks. These specimens were not identified to species level in the original publication. Future examination of the specimens is needed to clarify whether these belong to *C. electrinus* or another *Charops* species.

****Venturia aquila* Vas, 2019**

Records. 1 ♀, ZM Northern Province, Mpulungu, Kalambo Falls Lodge, light trap, -8.6241/31.2011, 21.viii–2.ix.2023, leg. N. Meier, T. Spasojevic, A. Viertler (NMBS).

Remarks. The species is morphologically very similar to the slightly smaller *Venturia desertorum* Horstmann, 2008 from southern Algeria (Horstmann 2008). Future studies should include larger series and molecular data to test whether these species are distinct or rather variations.

****Porizon* sp.**

Records. 1 ♂, ZM Northern Province, Mpulungu, Kalambo Falls Lodge, sweep net, -8.6241/31.2011, 21.viii–02.ix.2023, leg. N. Meier, T. Spasojevic, A. Viertler (NMBS).

Remarks. This is the first record of this genus for the Afrotropical region.

****Xanthocampoplex oneili* (Cameron, 1905)**

Records. 1 ♂, ZM Northern Province, Mpulungu, Kalambo Falls Lodge, -8.6241/31.2011, 21.viii–02.ix.2023, leg. N. Meier, T. Spasojevic, A. Viertler (NMBS).

Cremastinae

***Pristomerus bemba* Rouse & van Noort, 2015**

Records. 1 ♀, ZM Eastern Province, South Luangwa, nr Mfuwe ca 10 km E. Mfuwe Malimba village vicinities, 12.XII.2011, Gumovsky leg. SAM–HYM–P047391” (holotype, SAMC) (Rouse and van Noort 2015).

***Pristomerus bullis* Fitton in Polaszek et al. 1994**

Records. 1 ♂ ZM Eastern Province, South Luangwa, near Mfuwe sweeping on the dried egg tree 09.XII.2011 Gumovsky; Mopane tree [*Colophospermum mopane*, Fabaceae] SAM–HYM–P049439” (SAMC) (Rouse and van Noort 2015).

****Pristomerus roussei* sp. nov.**

Records. 1 ♀, ZM Northern Province, Mbala, Kalambo Falls (above waterfall), sweep net, 1170 m, -8.5961/31.2478, 21.viii–2.ix.2023, leg. N. Meier, T. Spasojevic, A. Viertler (holotype, NMBS).

1 ♂, ZM Northern Province, Mbala, Kalambo Falls (above waterfall), sweep net, 1170 m, -8.5961/31.2478, 21.viii–2.ix.2023, leg. N. Meier, T. Spasojevic, A. Viertler (paratype, NMBS).

1 ♂, “ZM Northern Province, Mpulungu, Chitili stream, sweep net, -8.6390/31.2035, 21.viii–2.ix.2023, leg. N. Meier, T. Spasojevic, A. Viertler, voucher: 20-538 (paratype, NMBS).

2 ♂♂, “ZM Northern Province, Mpulungu, Kalambo delta, sweep net, 777 m, -8.5964, 31.1844, 21.viii–2.ix.2023, leg. N. Meier, T. Spasojevic, A. Viertler (paratype, LMNH).

1 ♀, “ZM Northern Province, Mpulungu, Mpulungu town, sweep net, 777 m, -8.7621, 31.1138, 21.viii–2.ix.2023, leg. N. Meier, T. Spasojevic, A. Viertler, voucher: 20-537 (paratype, NMBS).

1 ♀, ZM Northern Province, Mpulungu, Kalambo Falls Lodge, sweep net, 786 m, -8.6241/31.2011, 21.viii–2.ix.2023, leg. N. Meier, T. Spasojevic, A. Viertler (paratype, LMNH).

1 ♀, ZM Northern Western Province, 150 km W Solwezi, Ntambu, 12°18'S, 25°10'E; 11.11.2005; leg. M. Halada (paratype, LKG).

****Temelucha basiornata* (Cameron, 1911)**

Records. 2 ♀♀, ZM Northern Province, Mpulungu, Kalambo Falls Lodge, -8.6241/31.2011, 21.viii–02.ix.2023, leg. N. Meier, T. Spasojevic, A. Viertler (LMNH).

1 ♀ 1 ♂, ZM Northern Province, Mpulungu, Tomo Sakalani, Isanga Bay Lodge, sweep-net, -8.6554/31.1947, 21.viii–2.ix.2023, leg. N. Meier, T. Spasojevic, A. Viertler (NMBS).

Remarks. This species is quite variable in colouration, e.g., some specimens have black marks on the vertex and the mesoscutum. It can be differentiated from the similar species *Temelucha picta* (Holmgren, 1868) by the lack of black spots on the mesopleuron (Rousse et al. 2011).

****Trathala annulicornis* (Tosquinet, 1896)**

Records. 1 ♀, ZM Northern Province, Mpulungu, Chitili stream, sweep net, -8.6390/31.2035, 21.viii–2.ix.2023, leg. N. Meier, T. Spasojevic, A. Viertler (NMBS).

2 ♀♀, ZM Northern Province, Mpulungu, Kalambo Falls Lodge, sweep net, -8.6241/31.2011, 21.viii–2.ix.2023, leg. N. Meier, T. Spasojevic, A. Viertler (NMBS, LMNH). 1 ♀ same as previous except collected by a Malaise trap.

Remarks. Currently all *Trathala* specimens with white bands on the flagellum are treated as *T. annulicornis*. However, we have seen various specimens that differ from the holotype of *T. annulicornis* in facial dimensions (from the Malagasy region, Rousse et al. 2011) or relative ovipositor length (in our material). Due to the limited number of specimens in our study, we currently refrain from describing new species within this complex.

Cryptinae

***Coccygodes subquadratus* (Waterston, 1927)**

Records. 1 ♀, ZM Lusaka Province, Chilanga, 4,000 ft, 6.x.1913 (F. V. Bruce Miller) (Waterston 1927).

Unspecified, ZM (Benoit 1951a)

****Cryptus* sp.**

Records. 1 ♂, ZM Northern Province, Mpulungu, Kalambo River Delta, sweep net, -8.6390/31.2035, 21.viii–2.ix.2023, leg. N. Meier, T. Spasojevic, A. Viertler (NMBS).

****Goryphus* sp.**

Records. 1 ♀, ZM Northern Province, Mpulungu, Kalambo Falls Lodge, sweep net, -8.6241/31.2011, 21.viii–2.ix.2023, leg. N. Meier, T. Spasojevic, A. Viertler (NMBS).

1 ♀, ZM Northern Province, Mpulungu, Chitili stream, sweep net, -8.6390/31.2035, 21.viii–2.ix.2023, leg. N. Meier, T. Spasojevic, A. Viertler (NMBS).

****Osprynchotus gigas* Kriechbaumer, 1894**

Records. 1 ♀, ZM Northern Province, Mpulungu, Kalambo Falls Lodge, sweep net, -8.6241/31.2011, 21.viii–2.ix.2023, leg. N. Meier, T. Spasojevic, A. Viertler (LMNH).

1 ♀, ZM Northern Province, Mpulungu, Kalambo Falls Lodge, sweep net, -8.6241/31.2011; 29.ix.2021, leg. F. Ronco, F. Schedel & A. Indermaur (NMBS).

6 ♂♂, ZM Northern Province, Mpulungu, Kalambo Falls Lodge, sweep net, -8.6241/31.2011, 21.viii–2.ix.2023, leg. N. Meier, T. Spasojevic, A. Viertler (NMBS).

2 ♂♂, ZM Northern Province, Mpulungu, Chitili stream, sweep net, -8.6390/31.2035, 21.viii–2.ix.2023, leg. N. Meier, T. Spasojevic, A. Viertler (LMNH).

1 ♂, ZM Northern Province, Mpulungu, Kalambo River Delta, sweep net, -8.5965/31.1844, 21.viii–2.ix.2023, leg. N. Meier, T. Spasojevic, A. Viertler (LMNH).

1 ♂, ZM Northern Province, Mbala, Kalambo Falls (above waterfall), sweep net, 1170 m, -8.5961/31.2478, 21.viii–2.ix.2023, leg. N. Meier, T. Spasojevic, A. Viertler (LMNH).

****Stenarella* sp.**

Records. 1 ♂, ZM Northern Province, Mpulungu, Kalambo Falls Lodge, sweep net, -8.6241/31.2011, 21.viii–2.ix.2023, leg. N. Meier, T. Spasojevic, A. Viertler (NMBS).

***Zonocryptus formosus* (Brullé, 1846)**

Records. 1 ♀, ZM Eastern Province, on road from Chipata [Fort Jameson] to Lundazi [Landazi], 4000ft, 7–14.vi.1910 (S. A. Neave) (Waterston 1927).

***Zonocryptus* sp.**

Records. 1 ♀, ZM Northern Province, Mpulungu, Kalambo Falls Lodge, sweep net, -8.6241/31.2011, 21.viii–2.ix.2023, leg. N. Meier, T. Spasojevic, A. Viertler (NMBS).

Remarks. Due to the lack of reference material, identification of two male Cryptinae was not possible to genus level.

Diplazontinae

***Diplazon laetatorius* (Fabricius, 1781)**

Records. Unspecified, ZM Southern Province, Choma, 17.05.2006 (Klopfstein et al. 2010).

1 ♀, ZM Northern Province, Mpulungu, Kalambo Falls Lodge, sweep net, -8.6241/31.2011, 21.viii–2.ix.2023, leg. N. Meier, T. Spasojevic, A. Viertler (LMNH).

Ichneumoninae

#*Ctenochaes rufithorax* (Kriechbaumer, 1894)

Records. Unspecified, ZM, Upper Luangwa River, viii.1910 (Neave) (NHMUK) (Morley 1915).

#*Ischnojoppa luteator* (Fabricius, 1798)

Records. Unspecified, ZM, Luangwa River, 16–1800ft., September (NHMUK) (Morley 1915).

#*Leptophatnus crococephalus rubricaput* (Morley, 1919)

Records. Unspecified, ZM Northern Province, Mbala [Abercorn] (ZSM) (Heinrich 1967b).

****Afromevesia* cf. *merusilvae* (Heinrich, 1968)**

Records. 1 ♀, ZM Northern Province, Mupulung, Tomo Sakalani, Isanga Bay Lodge, sweep-net, -8.6550/31.1946, 26.viii.2023, leg. N. Meier, T. Spasojevic, A. Viertler (LMNH).

1 ♀, ZM Northern Province, Mupulung, Tomo Sakalani, Isanga Bay Lodge, sweep-net, -8.6550/31.1946, 26.viii.2023, leg. N. Meier, T. Spasojevic, A. Viertler (NMBS).

Remark. Our specimens slightly differ from the holotype description of *Afromevesia merusilvae* (Heinrich 1968c). Our two specimens have almost completely white trochanters (~ 90% white), while the holotype description mentions only the apical part of the trochanters white. Also, our specimens

both have 27 antennal segments, while the holotype of *A. merusilvae* is described as having 30 segments.

Metopiinae

***Metopius albipictus* Tosquinet, 1896**

Records. 1 ♂, ZM Copperbelt Province, 25 km W Chingola 1600 m, 16.i.2006, leg. R. Kneco (LKG) (Riedel 2016).

***Metopius clathratus* Benoit, 1965**

Records. 1 ♂, ZM Lusaka Province, 15 km E. Lusaka, 22–31.i.1980 R.A. Beaver (NHMUK) (Riedel 2016).

***Metopius discolor* Tosquinet, 1896**

Records. Unspecified, ZM (Townes and Townes 1973).

1 ♀, ZM Lusaka Province, Lusaka, iv.1980, leg. R.A. Beaver (NHMUK) (Riedel 2016). 2 ♀♀, ZM Lusaka; IV.1980, leg. R.A. Beaver (NHMUK) (Riedel 2016).

Unspecified, Central Province, Chisamba, Golden Valley Agricultural Research Trust, (14,967,373; 28,097,464, altitude: 1147 m) (Durocher-Granger et al. 2021).

***Metopius rufigaster zambiensis* Riedel, 2016**

Records. 1 ♂, holotype, ZM Copperbelt Province, 45 km SE Kitwe, 12–15.i.2003, leg. J. Halada (LKG), (Riedel 2016).

***Metopius zuluani* Benoit, 1965**

Records. 5 ♂♂, ZM Copperbelt Province, 25 km W Chingola 1600 m, 16.i.2006, leg. R. Kmeco (LKG) (Riedel 2016).

****Triclistus* sp.**

Records. 1 ♂, ZM Northern Province, Mpulungu, Kalambo Falls Lodge, light trap, -8.6241/31.2011, 21.viii–2.ix.2023, leg. N. Meier, T. Spasojevic, A. Vierter (NMBS).

Remarks. Here, we report a new *Triclistus* species, represented by a single male specimen. Typically, species descriptions are based on female specimens. Further specimens, particularly females, are required to provide a complete taxonomic diagnosis and confirm the distinctiveness of this species.

Ophioninae

***Enicospilus albiger* (Kriechbaumer, 1894)**

Records. 1 ♂, ZM Eastern Province, South Luangwa nr Mfuwe, xii.2011, A. Gumovsky coll., SAM-HYM-P049484 (SAMC) (Rousse and van Noort 2014b).

***Enicospilus antefurcalis* (Szépligeti, 1908)**

Records. 1 ♂, ZM, Mid Luangwa Valley, viii.10 (Neave) (NHMUK) (Gauld and Mitchell 1978).

***Enicospilus biimpressus* (Brullé, 1846)**

Records. 1 ♂, ZM, Upper Luangwa River, viii.10 (Neave) (NHMUK) (Gauld and Mitchell 1978).

***Enicospilus capensis* (Thunberg, 1822)**

Records. Unspecified, ZM Central Province, Chisamba, Golden Valley Agricultural Research Trust, (14,967,373; 28,097,464, altitude: 1147 m) (Durocher-Granger et al. 2021).

***Enicospilus fenestralis* (Szépligeti, 1906)**

Records. 1 ♀, ZM, Luangwa Valley, viii.10 (Neave) (NHMUK) (Gauld and Mitchell 1978).

***Enicospilus helvolus* Gauld & Mitchell, 1978**

Records. 1 ♂, ZM Northern Province, Mbala, xii.64 (TC) (Gauld and Mitchell 1978).

***Enicospilus laquaetus* (Enderlein, 1921)**

Records. 1 ♀, ZM Lusaka Province, 15 km E Lusaka, Zambia, 22–31.i.1980, R.A. Beaver leg. (NHMUK) (Shimizu et al. 2020).

2 ♀♀, ZM Lusaka Province, 15 km E. of Lusaka, i.1980, R.A. Beaver leg. (NHMUK) (Gauld 1982).

***Enicospilus mauritii* (Saussure, 1892)**

Records. 1 ♂, ZM, Upper Luangwa River, vi.1910, leg. S. A. Neave (NHMUK) (Morley 1912).

***Enicospilus nefarius* Gauld & Mitchell, 1978**

Records. 1 ♀, ZM Northern Province, Mbala (= Abercorn), xii.64 (TC) (Gauld and Mitchell 1978).

***Enicospilus nops* Gauld & Mitchell, 1978**

Records. 2 ♀♀, ZM Northern / Luapula Province, Lake Bangweulu, xi.46 (Steele) (NHMUK) (Gauld and Mitchell 1978).

#*Enicospilus transvaalensis* Cameron, 1911

Records. 1 ♀, ZM Northern Province, Mbala (= Abercorn), xii.64 (TC) (Gauld and Mitchell 1978).

***Enicospilus watshami* Gauld, 1982**

Records. 1 ♀, ZM Lusaka Province, 15 km E. of Lusaka, i.1980 (R. A. Beaver) (paratype, NHMUK) (Gauld 1982).

***Euryophion latipennis* (Kirby, 1896)**

Records. 1 unspecified, [apex of metasoma lacking], ZM Southern Province, Choma Nansa farm xii.1993, A.J. Gardiner coll., SAM-HYM-P044072 (SAMC) (Rousse and van Noort 2014b)

****Euryophion nigripennis* Cameron, 1906**

Records. 1 ♀, ZM Northern Province, Mpulungu, Kalambo Falls Lodge, sweep net, -8.6241/31.2011, 30.ix.2020, leg. A. Indermaur (NMBS).

***Lepiscelus distans* (Seyrig, 1935)**

Records. 1 ♂, ZM Northern Province, Mbala (= Abercorn), xii.64 (TC) (Gauld and Mitchell 1978).

Orthocentrinae

****Megastylus* sp.**

Records. 1 ♀, ZM Northern Province, Mpulungu, Kalambo River Delta, Malaise trap, 8.5965/31.1844, 21.viii–02.ix.2023, leg. N. Meier, T. Spasojevic, A. Viertler (NMBS).

Remarks. This specimen is likely an undescribed species of *Megastylus* common in the Afrotropical region (Augustijn De Ketelaere pers. comm. 2024). However, two of four known species are described only from males, making specimen comparison difficult. Thus, the description of a new species should await a more comprehensive study of Afrotropical *Megastylus*.

Phygadeuontinae

****Paraphylax* sp.**

Records. 1 ♂, ZM Northern Province, Mpulungu, Kalambo Falls Lodge, sweep net, 21.viii–02.ix.2023, leg. N. Meier, T. Spasojevic, A. Viertler (NMBS).

Remarks. At this point, the identification of most of the collected phygadeuontines was not possible even to genus level, due to the lack of reference material. Several of the specimens might represent undescribed ichneumonid genera.

Pimplinae

****Theronia lurida* Tosquinet, 1896**

Records. 1 ♂, ZM Northern Province, Mpulungu, Kalambo Falls Lodge, sweep net, -8.6241/31.2011, 21.viii–02.ix.2023, leg. N. Meier, T. Spasojevic, A. Viertler (NMBS).

***Xanthopimpla romani* Krieger, 1915**

Records. Unspecified, ZM Northern Province, Mbala [Abercorn], 16.vi.1945 (NHMZ) (Benoit 1953b).

2 ♀♀, ZM Northern Province, Chitili stream, sweep net, -8.6390/31.2035, 21.viii–2.ix.2023; leg. N. Meier, T. Spasojevic, A. Viertler (NMBS, LMNH).

***Xanthopimpla stemmator* (Thunberg, 1822)**

Records. Unspecified, ZM (Midingoyi et al. 2016).

Remarks. Introduced in Zambia as a biocontrol agent in the early 2000s.

****Xanthopimpla* sp. 1**

Records. 1 ♀, ZM Northern Province, Mpulungu, Kalambo Falls Lodge, light trap, -8.6241/31.2011, 21.viii–02.ix.2023, leg. N. Meier, T. Spasojevic, A. Viertler (NMBS).

****Xanthopimpla* sp. 2**

Records. 2 ♀♀, ZM Northern Province, Mpulungu, Kalambo Falls Lodge, sweep net, -8.6241/31.2011, 21.viii–02.ix.2023, leg. N. Meier, T. Spasojevic, A. Viertler (NMBS, LMNH).

****Xanthopimpla* sp. 3**

Records. 1 ♀, ZM Northern Province, Mpulungu, Tomo Sakalani, Isanga Bay Lodge, sweep-net, -8.6554/31.1947, 21.viii–2.ix.2023, leg. N. Meier, T. Spasojevic, A. Viertler (NMBS).

Remarks. This species belongs to the *X. terebratrix* group of Krieger (1914), but it differs from the known species in several characters and thus might represent a new species.

Several specimens of *Xanthopimpla* could not be identified despite the published identification keys covering almost all the Afrotropical species (Krieger 1914; Seyrig 1932). While some of the species might be new to science, we also found that some key characters used in the keys to distinguish species showed intraspecific variation, which hindered the identification. This suggests that the genus and available keys should be revised.

Tersilochinae

***Diaparsis interstitialis* Khalaim, 2013**

Records. 1 ♀, ZM Copperbelt Province, Kitwe, Chati [Forest Reserve ?], 27.xii.1979, coll. K. Löyttyniemi (MZH) (Khalaim 2019).

***Diaparsis mostovskii* Khalaim, 2013**

Records. 1 ♀, ZM Western Province, Kalobelelwa, Malaise trap, 11–18.iii.1988, coll. E.G.N. Dijkstra, (RMNH).

1 ♀, Western Province, near Namibian border, Sesheke Town, 950 m, iii–vi.1991, coll. W. Slobbe (RMNH) (Khalaim 2019).

***Diaparsis voluptuosa* Khalaim, 2013**

Records. 2 ♀♀, ZM Copperbelt Province, Kitwe, Chati [Forest Reserve ?], 8.i, 31.iii.1980, coll. K. Löyttyniemi (MZH); 2 ♀, Copperbelt Province, Chati, 9.ii.1980, coll. K. Löyttyniemi (MZH) (Khalaim 2019).

Tryphoninae

***Zambion monodon* Kasparyan, 1993**

Records. 1 ♀, ZM Copperbelt Province, Kitwe, Chati, 27.3.1979, K. Löyttyniemi leg. Label 2: window trap with *Eucalyptus*. Label 3: Holotypus *Zambion monodon* Kasparyan. Label 4: coll. Dept. Agr. Forest. Zool. Univ. Helsinki, (holotype, MZH). 1 ♂, same data as holotype, except 8.iii.1979, (paratype, MZH). 1 ♀, same data except 15.iii.1979, (paratype, MZH) (Kasparyan 1993).

Discussion

A checklist with many missing check marks

With only 30 species recorded in the literature, including the major catalogues of the Afrotropical Darwin wasps, the fauna of Zambia is more poorly known than almost any country. Four of these species were previously unrecorded for Zambia in the “Catalogue of world Ichneumonidae” (Yu and Horstmann 1997; Yu et al. 2016) and were added based on careful examination of the original publications of distribution records, highlighting the need for double-proofing information in taxon catalogues. However, the four records as well as approximately half of the total literature records were published during the 20th Century and thus require verification by examining relevant specimens in collections and supplementing them with more recent samples. This is especially true for the records published before Townes’s revision of ichneumonid systematics (Townes 1969, 1970b, 1970a, 1971).

We supplemented the literature-based checklist with species obtained through targeted sampling of Darwin wasps in the field. With only small-scale field work assessment, we increased the species count from the initial 30 species to 44. In addition, we described one species new to science and recorded 17 genera new to Zambia, including *Porizon* which is also recorded for the Afrotropical realm for the first time. This demonstrates that a very large proportion of the Zambian Darwin wasps are still unrecorded or undescribed due to the lack of studies. The finding aligns with a recent species richness estimate for Afrotropical Darwin wasps (Meier et al. 2024), which suggested that only 13–22% of diversity is known in the most studied Afrotropical countries. For example, in Zambia's neighbouring country Tanzania, between 2,200 and 3,500 species are expected, compared to the ~ 500 recorded species (Meier et al. 2024). Zambia has $\frac{3}{4}$ of the land mass of Tanzania and lies within the same biogeographic region. This suggests that the current species number of Darwin wasps in Zambia might represent as little as 1.7–2.7% of the actual species richness.

While many faunistic checklists are simply based on literature records, their value can be significantly increased by including specimens available in natural history collections. During our research we discovered a small to medium backlog of unsorted material from Zambia at several European museums of natural history (e.g., NHMUK, LKG) and at the Iziko South African Museum (G. Broad, S. van Noort, M. Schwarz, pers. comm. 2024). This material was not yet included in the present checklist mainly due to two constraints. Firstly, it is not rare that material, including type specimens, from an Afrotropical country is widely distributed across the world. Thus, studying these specimens takes time and substantial funding to visit various collections, which we did not have within the scope of this project. Secondly, the species identification requires a coordinated effort of experts on different subfamilies of Darwin wasps, and many species identifications require generic revisions, which is a long-term process.

When genus revisions must forego species identifications

Based on the material collected around the region of Lake Tanganyika, we describe one new Cremastinae species, belonging to the genus *Pristomerus*. This is the only new species of Darwin wasps described based on material from Zambia in the last three years (Di Giovanni and Varga 2021). The designation of the specimens as new species was only possible because of the more recent revisionary works on this genus (Rousse et al. 2011, 2013; Rousse and van Noort 2015). However, for many specimens that we collected in this study, species and sometimes even genus identification was not as straightforward or even possible. A major obstacle to straightforward identification was the lack of identification keys, which are in general rare for the Afrotropical Darwin wasps. Even when keys are present, most of them are rather outdated, with a few exceptions (e.g., Rousse and van Noort 2014b, 2015; Riedel 2016; Rousse et al. 2016; Dal Pos et al. 2024; also available online at WaspWeb (van Noort 2025)). In the absence of revised keys, an examination of original descriptions and usually type material is necessary. However, original descriptions from the 19th Century often just provide a differential diagnosis between species and some of the originally congeneric species were later moved into different genera, making the original descriptions inadequate for differentiating these

species from their actual congeners. Unfortunately, also the primary types of a considerable number of species have gone missing, e.g., *Osprynchotus gigas* (Kriechbaumer, 1894). Consequently, within many subfamilies of Darwin wasps, species and often even genus identification is currently not possible in the Afro-tropical region. A way forward in species identification involves conducting regional taxonomic revisions of the genera in question, or at least more closely related species, by studying original type material and an adequate number of specimens, and by generating molecular sequences to aid in difficult cases.

(Under-) representation of major ecotypes

The Miombo woodlands, where we conducted our fieldwork, represent the most dominant ecoregion in Zambia (Malambo and Syampungani 2008). Although our work took place in this ecoregion, which covers approximately 50% of Zambia's landmass, we do not consider our sampling to be representative of the actual diversity of Darwin wasps, even within this ecotype. One primary reason is that our sampling was conducted during a brief period in the dry season, while significantly higher activity is reported for many insects during and after the rainy season (Löyttyniemi and Löyttyniemi 1993). Moreover, the previous literature records of Darwin wasps in Zambia are extremely patchy, often based on single specimens and, especially in the older literature, with incomplete locality data. To accurately assess the species diversity of Darwin wasps in Zambia, collecting should be conducted throughout the year (e.g., long-term sampling using Malaise traps) and across various localities, not only covering the central and southern Miombo forests but also extending to other ecotypes. Actually, most of the other major ecoregions of Zambia (Malambo and Syampungani 2008), including the Zambesian flooded grasslands, tropical *Cryptosepalum* dry forests, *Baikiaea* woodlands, and Western Zambezian grasslands, have yet to be sampled. Another factor limiting the representativeness of our sampling, especially when it comes to the species endemic to Zambia, is the proximity of our sampling area to the Tanzanian border, where considerable overlap with the species assemblage of Tanzania is likely.

Outlook

In summary, extensive and collaborative collection efforts across all Zambian ecotypes, involving both local research institutions and international taxonomic specialists, are needed to grasp the species richness of Darwin wasps in Zambia. This observation likely holds true not only for Zambia and Darwin wasps but also for most of the Afrotropical region and insect groups (e.g., Azevedo et al. 2015; van Noort et al. 2015; Salden and Peters 2023). We here present a preliminary step towards developing a comprehensive checklist of Darwin wasps for the country. Despite conducting fieldwork at the end of the dry season and near the border with Tanzania, a country with better-studied Darwin wasp diversity in the Afrotropical region, our findings suggest significant opportunities for further discovery.

Building on the insights gained from this initial study, we suggest several improvements for future fieldwork. These include extending the use of Malaise traps over longer periods and fostering collaborations with local

universities and students. Additionally, the fieldwork should be conducted during or closer to the rainy season to capture a broader range of species. Another important next step is to examine several natural history collections containing already sampled Zambian insects. Studying these collections might yield many additional species records and new species descriptions given the extent of this so far mostly unidentified material.

Finally, recent global awareness of biodiversity loss has pushed initiatives aimed at documenting and monitoring biodiversity in Afrotropical countries, including Zambia. These efforts have highlighted the region's immense yet understudied biological richness. Major collection initiatives, such as the expeditions of the African Natural History Research Trust focusing on Lepidoptera, highlight the value of large-scale, collaborative fieldwork. Similar initiatives targeting hymenopteran diversity, such as the extensive surveys of the Afrotropical Hymenoptera Initiative conducted over the last 33 years by Simon van Noort of the Iziko South African Museum in Cape Town (van Noort 2025) could yield insights and help increase understanding of their diversity in the Afrotropical region, while strengthening the local capacity for taxonomic work through education and enlargement of the local natural history collections.

Acknowledgments

We are deeply grateful to Walter Salzburger and his team for inviting us to join their fieldwork, which greatly reduced our logistical organisation. Special thanks also go to Adrian Indermaur, Hiranya Sudasinghe, Rita Gonzalez Dominguez, and Simon Schwarz, who enthusiastically helped us collect Darwin wasps. We want to thank the Kalambo Falls Lodge team for their warm hospitality and outstanding meals. Extractions and PCR reactions took place at the University of Basel (Evolutionary Biology, Salzburger Lab). We also appreciate the guidance of Caephas Sinyangwe at our fieldtrips, and the expertise of Pascal Rousse on Cremastinae, Davide Dal Pos on Ichneumoninae and Martin Schwarz on Phygadeuontinae. Gavin Broad and Simon van Noort provided many constructive comments that help improve our manuscript. Finally, we want to express our gratitude to the Fritz Sarasin Foundation for funding this fieldwork.

Additional information

Conflict of interest

The authors have declared that no competing interests exist.

Ethical statement

No ethical statement was reported.



Funding

This work was supported by the Fritz Sarasin Foundation.

Author contributions

Conceptualization: NM, AV, MK, CK, TS. Funding acquisition: NM, AV, TS. Investigation: NM, AV, TS. Methodology: NM, AV, TS. Visualization: NM, AV, TS. Writing - original draft: NM, AV, TS. Writing - review and editing: NM, AV, MK, CK, TS.

Author ORCIDs

Noah Meier  <https://orcid.org/0000-0003-2139-4339>
Alexandra Viertler  <https://orcid.org/0000-0001-9729-5439>
Meekness Kapaale  <https://orcid.org/0000-0001-9745-9835>
Cyprian Katongo  <https://orcid.org/0000-0002-5276-3216>
Tamara Spasojevic  <https://orcid.org/0000-0001-5301-5722>

Data availability

All of the data that support the findings of this study are available in the main text.

References

- Azevedo CO, Garcia R, Gobbi FT, van Noort S (2015) Insecta, Hymenoptera, Bethyridae: range extension and filling gaps in Central African Republic. Check List 11: 1606. <https://doi.org/10.15560/11.2.1606>
- Benoit PLG (1951a) Les genres *Oneilella* Cam. et *Osprynchotus* Spin. (Hym.-Ichneum.) au Congo belge. Revue de Zoologie et de Botanique Africaines 44(4): 313–320.
- Benoit PLG (1951b) Sur les genres éthiopiens *Gabunia* Kriechb., *Paracollyria* Cam. et *Hieroceryx* Tosq. (Hym. - Ichneum. - Pimpl.) spécialement au Congo belge. Annales de la Société Zoologique de Belgique 82: 93–106.
- Benoit PLG (1952) Révision des espèces continentales du genre *Phorotrophus* Saussure (Ichneum. - Pimplinae). Revue de Zoologie et de Botanique Africaines 45: 330–352.
- Benoit PLG (1953a) Contribution à la connaissance des Ichneumonides de l'Afrique occidentale (1re note). Bulletin de l'Institut Français d'Afrique Noire 15: 543–548.
- Benoit PLG (1953b) Ichneumonidae - Pimplinae du National Museum of southern Rhodesia. Bulletin et Annales de la Société Entomologique de Belgique 89: 278–281.
- Benoit PLG (1953c) Nouveaux Ichneumonidae du Congo belge. Lambillionea 53: 76–78.
- Benoit PLG (1953d) Sur des Polysphinctini du Congo belge (Ichneum. - Pimpl.). Revue de Zoologie et de Botanique Africaines 47: 137–141.
- Benoit PLG (1955) Contributions à l'étude des Ichneumonidae africains (Hymenoptera). I. Annales du Musée Royal du Congo Belge, Sciences Zoologiques 38: 1–55.
- Benoit PLG (1956) Ichneumonidae nouveaux ou intéressants de l'Afrique du Sud. Annals of the South African Museum 43: 123–135.
- Benoit PLG (1957) Les Ichneumonides des îles Mascareignes. Mémoires de l'institut scientifique de Madagascar 8: 307–316.
- Broad GR, Shaw MR, Fitton MG (2018) Handbooks for the identification of British insects. Ichneumonid Wasps (Hymenoptera: Ichneumonidae): their Classification and Biology. Volume 7, Part 12. Field Studies Council for the Royal Entomological Society, Telford, 418 pp. <https://doi.org/10.1079/9781800625471.0000>
- Burkart K (2023) Bioregion 2023. One Earth. <https://www.oneearth.org/bioregions/>
- Chipabika G, Sohati PH, Khamis FM, Chikoti PC, Copeland R, Ombura L, Kachapulula PW, Tonga TK, Niassy S, Sevgan S (2023) Abundance, diversity and richness of natural enemies of the fall armyworm, *Spodoptera frugiperda* (J.E. Smith) (Lepidoptera: Noctuidae), in Zambia. Frontiers in Insect Science 3: 1091084. <https://doi.org/10.3389/finsc.2023.1091084>
- Dal Pos D, De Ketelaere A, Di Giovanni F (2024) Revision of the Afrotropical genus *Protoleptops* Heinrich, 1967 (Hymenoptera, Ichneumonidae, Ichneumoninae), with description of a new species from Burundi. ZooKeys 1214: 197–216. <https://doi.org/10.3897/zookeys.1214.131071>




- Dautu G, Sindato C, Mweene AS, Samui KL, Roy P, Noad R, Paweska J, Majiwa PAO, Musoke A (2012) Rift Valley fever: Real or perceived threat for Zambia? Onderstepoort Journal of Veterinary Research 79: 6. <https://doi.org/10.4102/ojvr.v79i2.466>
- Di Giovanni F, Varga O (2021) First record of the subfamily Brachycyrtinae (Hymenoptera, Ichneumonidae) from continental Africa, with description of three new species. Zootaxa 4985: 203–218. <https://doi.org/10.11646/zootaxa.4985.2.4>
- Durocher-Granger L, Mfuno T, Musesha M, Lowry A, Reynolds K, Buddie A, Cafà G, Offord L, Chipabika G, Dicke M, Kenis M (2021) Factors influencing the occurrence of fall armyworm parasitoids in Zambia. Journal of Pest Science 94: 1133–1146. <https://doi.org/10.1007/s10340-020-01320-9>
- Folmer O, Black M, Hoeh W, Lutz R, Vrijenhoek R (1994) DNA primers for amplification of mitochondrial cytochrome c oxidase subunit I from diverse metazoan invertebrates. Molecular Marine Biology and Biotechnology 3: 294–299.
- Gauld ID (1982) A revised key of the *Enicospilus antefurcalis* (Szépligeti) (Hymenoptera: Ichneumonidae) species group of the Afrotropical region. Bulletin of Entomological Research 72: 33–38. <https://doi.org/10.1017/S0007485300050264>
- Gauld ID, Mitchell PA (1978) The taxonomy, distribution and host preferences of African parasitic wasps of the subfamily Ophioninae. Commonwealth Agricultural Bureaux, Farnham Royal, Slough.
- Heinrich G (1967a) Synopsis and reclassification of the Ichneumoninae stenopneusticae of Africa south of the Sahara. Farmington State College Press 2: 251–480.
- Heinrich G (1967b) Synopsis and reclassification of the Ichneumoninae stenopneusticae of Africa south of the Sahara. Farmington State College Press 1: 1–250.
- Heinrich G (1968a) Synopsis and reclassification of the Ichneumoninae stenopneusticae of Africa south of the Sahara. Farmington State College Press 4: 693–942.
- Heinrich G (1968b) Synopsis and reclassification of the Ichneumoninae stenopneusticae of Africa south of the Sahara. Farmington State College Press 3: 481–692.
- Heinrich G (1968c) Synopsis and reclassification of the Ichneumoninae stenopneusticae of Africa south of Sahara. Farmington State College Press 5: 943–1258.
- Hopkins T, Roininen H, Sääksjärvi IE (2018) Assessing the species richness of Afrotropical ichneumonid wasps with randomly placed traps provides ecologically informative data. African Entomology 26: 350–358. <https://doi.org/10.4001/003.026.0350>
- Hopkins T, Roininen H, van Noort S, Broad GR, Kaunisto K, Sääksjärvi IE (2019) Extensive sampling and thorough taxonomic assessment of Afrotropical Rhyssinae (Hymenoptera, Ichneumonidae) reveals two new species and demonstrates the limitations of previous sampling efforts. ZooKeys 878: 33–71. <https://doi.org/10.3897/zookeys.878.37845>
- Horstmann K (2008) Neue westpaläarktische Arten der Campopleginae (Hymenoptera: Ichneumonidae). Zeitschrift der Arbeitsgemeinschaft Österreichischer Entomologen 60: 3–27.
- Kallu SA, Ndebe J, Qiu Y, Nakao R, Simuunza MC (2023) Prevalence and Association of Trypanosomes and *Sodalis glossinidius* in Tsetse Flies from the Kafue National Park in Zambia. Tropical Medicine and Infectious Disease 8(80): 15 pp. <https://doi.org/10.3390/tropicalmed8020080>
- Kasparyan DR (1993) Zambion, a new Tryphonine genus from Africa (Hymenoptera: Ichneumonidae). Zoosystematica Rossica 1: 86–88.
- Khalaim AI (2019) New records of Afrotropical Tersilochinae (Hymenoptera: Ichneumonidae). Zoosystematica Rossica 28: 267–276. <https://doi.org/10.31610/zsr/2019.28.2.267>

- Klopfstein S, Kropf C, Quicke DLJ (2010) An Evaluation of Phylogenetic Informativeness Profiles and the Molecular Phylogeny of Diplazontinae (Hymenoptera, Ichneumonidae). *Systematic Biology* 59: 226–241. <https://doi.org/10.1093/sysbio/syp105>
- Krieger R (1914) Über die Ichneumonidengattung *Xanthopimpla* Saussure. *Archiv für Naturgeschichte*. 80: 1–148.
- Kumar S, Stecher G, Li M, Knyaz C, Tamura K (2018) MEGA X: Molecular Evolutionary Genetics Analysis across Computing Platforms. *Battistuzzi FU (Ed.) Molecular Biology and Evolution* 35: 1547–1549. <https://doi.org/10.1093/molbev/msy096>
- Kusia ES, Borgemeister C, Subramanian S (2023) A review of edible saturniidae (Lepidoptera) caterpillars in Africa. *CABI Agriculture and Bioscience* 4(43): 11. <https://doi.org/10.1186/s43170-023-00186-y>
- Lobo NF, Laurent BSt, Sikaala CH, Hamainza B, Chanda J, Chinula D, Krishnankutty SM, Mueller JD, Deason NA, Hoang QT, Boldt HL, Thumlop J, Stevenson J, Seyoum A, Collins FH (2015) Unexpected diversity of *Anopheles* species in Eastern Zambia: implications for evaluating vector behavior and interventions using molecular tools. *Scientific Reports* 5: 17952. <https://doi.org/10.1038/srep17952>
- Löyttyniemi K, Löyttyniemi R (1993) Cleridae (Coleoptera) from miombo woodland in Zambia. *Entomologica Fennica* 4: 223–224. <https://doi.org/10.33338/ef.83773>
- Malambo FM, Syampungani S (2008) Opportunities and challenges for sustainable management of miombo woodlands: the Zambian perspective. *Working Papers of the Finnish Forest Research Institute* 98: 125–130.
- Mates SG, Perfecto I, Badgley C (2012) Parasitoid wasp diversity in apple orchards along a pest-management gradient. *Agriculture, Ecosystems & Environment* 156: 82–88. <https://doi.org/10.1016/j.agee.2012.04.016>
- Mayes DM, Petrillo H (2017) Cotton Flower-visiting Insects in Small-scale Farm Fields in Mwachisompola, Zambia. *Journal of the Kansas Entomological Society* 90: 122–130. <https://doi.org/10.2317/JKES1703.1>
- Meier N, Gordon M, Van Noort S, Reynolds T, Rindos M, Di Giovanni F, Broad GR, Spasojevic T, Bennett A, Dal Pos D, Klopfstein S (2024) Species richness estimation of the Afrotropical Darwin wasps (Hymenoptera, Ichneumonidae). *PLoS ONE* 19: e0307404. <https://doi.org/10.1371/journal.pone.0307404>
- Midingoyi SG, Affognon HD, Macharia I, Ong'amo G, Abonyo E, Ogola G, Groote HD, LeRu B (2016) Assessing the long-term welfare effects of the biological control of cereal stemborer pests in East and Southern Africa: Evidence from Kenya, Mozambique and Zambia. *Agriculture, Ecosystems & Environment* 230: 10–23. <https://doi.org/10.1016/j.agee.2016.05.026>
- Morley C (1912) A revision of the Ichneumonidae based on the collection in the British Museum (Natural History), with descriptions of new genera and species. *British Museum (Natural History), London*. <https://doi.org/10.5962/bhl.title.8761>
- Morley C (1915) A revision of the Ichneumonidae based on the collection in the British Museum (Natural History) with descriptions of new genera and species. Part IV. Tribes Joppides, Banchides and Alomyides. *Trustees of the British Museum, London, UK*, 167 pp.
- Nyirenda SS, Hang'ombe BM, Mulenga E, Machang'u RS, Kilonzo BS, Sianzinda E, Chanda P (2020) Biodiversity and distribution of flea (Siphonaptera), rodent (Rodentia), and Crocidura (Insectivora) species associated with plague epidemiology in eastern Zambia. *Journal of Zoonotic Diseases* 4(4): 21–35. <https://doi.org/10.22034/jzd.2020.11601>

- Reynolds Berry T, van Noort S (2016) Review of Afrotropical *Cryptopimpla* Taschenberg (Hymenoptera, Ichneumonidae, Banchinae), with description of nine new species. ZooKeys 640: 103–137. <https://doi.org/10.3897/zookeys.640.10334>
- Riedel M (2016) Contribution to the genus *Metopius* PANZER (Hymenoptera, Ichneumonidae, Metopiinae) from Africa South of Sahara. Linzer biologische Beiträge 48: 1635–1675.
- Rousse P, van Noort S (2013) Revision of the Afrotropical Lycoriniinae (Ichneumonidae; Hymenoptera) with description of a new species from South Africa. Zootaxa 3666(2): 252–266. <https://doi.org/10.11646/zootaxa.3666.2.8>
- Rousse P, van Noort S (2014a) A review of the Afrotropical Rhyssinae (Hymenoptera: Ichneumonidae) with the descriptions of five new species. European Journal of Taxonomy 92: 42. <https://doi.org/10.5852/ejt.2014.91>
- Rousse P, van Noort S (2014b) Afrotropical Ophioninae (Hymenoptera, Ichneumonidae): an update of Gauld and Mitchell's revision, including two new species and an interactive matrix identification key. ZooKeys 456: 59–73. <https://doi.org/10.3897/zookeys.456.8140>
- Rousse P, van Noort S (2015) Revision of the Afrotropical species of *Pristomerus* (Ichneumonidae: Cremastinae), with descriptions of 31 new species. European Journal of Taxonomy 124: 129. <https://doi.org/10.5852/ejt.2015.124>
- Rousse P, Villemant C, Seyrig A (2011) Ichneumonid wasps from Madagascar. V. Ichneumonidae Cremastinae. Zootaxa 3118(1): 30. <https://doi.org/10.11646/zootaxa.3118.1.1>
- Rousse P, Villemant C, Seyrig A (2013) Ichneumonid wasps from Madagascar. VI. The genus *Pristomerus* (Hymenoptera: Ichneumonidae: Cremastinae). European Journal of Taxonomy 49: 38. <https://doi.org/10.5852/ejt.2013.49>
- Rousse P, Broad GR, van Noort S (2016) Review of the genus *Genaemirum* Heinrich (Hymenoptera, Ichneumonidae, Ichneumoninae) with interactive identification keys to species. ZooKeys 636: 77–105. <https://doi.org/10.3897/zookeys.636.10216>
- Russel-Smith A, Stone GN, van Noort S (1999) Chapter 10: Invertebrate biodiversity of Mkomazi. In: Coe MJ, McWilliam NC, Stone GN, Packer M (Eds) Mkomazi: the ecology, biodiversity and conservation of a Tanzanian Savanna. Royal Geographical Society (with The Institute of British Geographers), London, 171–184.
- Salden T, Peters RS (2023) Afrotropical Ceraphronoidea (Insecta: Hymenoptera) put back on the map with the description of 88 new species. European Journal of Taxonomy 884: 386. <https://doi.org/10.5852/ejt.2023.884.2181>
- Seyrig A (1932) Les Ichneumonides de Madagascar. I Ichneumonidae Pimplinae. Mémoires de l'Académie Malgache 11. Antananarivo, Madagascar, 183 pp.
- Seyrig A (1934) Les Ichneumonides de Madagascar. II Ichneumonidae Tryphoninae et Supplément aux I. Pimplinae. Mémoires de l'Académie Malgache 19. Antananarivo, Madagascar, 111 pp.
- Seyrig A (1952) Les Ichneumonides de Madagascar. 4. Ichneumonidae Cryptinae. Mémoires de l'Académie Malgache 31. Antananarivo, Madagascar, 213 pp.
- Shimizu S, Broad GR, Maeto K (2020) Integrative taxonomy and analysis of species richness patterns of nocturnal Darwin wasps of the genus *Enicospilus* Stephens (Hymenoptera, Ichneumonidae, Ophioninae) in Japan. ZooKeys 990: 1–144. <https://doi.org/10.3897/zookeys.990.55542>
- Sohati PH, Musonda EM, Mukanga M (2001) Distribution of cereal stemborers in Zambia and release of *Cotesia flavipes* Cameron, an exotic natural enemy of *Chilo partellus*

- (Swinhoe). *International Journal of Tropical Insect Science* 21: 311–316. <https://doi.org/10.1017/S1742758400008407>
- Townes H (1969) The Genera of Ichneumonidae, Part 1. *Memoirs of the American Entomological Institute* 11: 1–300.
- Townes H (1970a) The Genera of Ichneumonidae, Part 2. *Memoirs of the American Entomological Institute* 12: 1–537.
- Townes H (1970b) The Genera of Ichneumonidae, Part 3. *Memoirs of the American Entomological Institute* 13: 1–307.
- Townes H (1971) The Genera of Ichneumonidae, Part 4. *Memoirs of the American Entomological Institute* 17: 1–372.
- Townes H, Townes M (1973) A catalogue and reclassification of the Ethiopian Ichneumonidae. *Memoirs of the American Entomological Institute* 19: 1–416.
- van Noort S (2004) Ichneumonid (Hymenoptera: Ichneumonoidea) Diversity Across an Elevational Gradient on Monts Doudou in Southwestern Gabon. *California Academy of Sciences Memoir* 28: 187–216.
- van Noort S (2025) Waspweb: Hymenoptera of the World. <https://www.waspweb.org/Ichneumonoidea/Ichneumonidae/Keys/index.htm> [January 1, 2025]
- van Noort S, Prinsloo GL, Compton SG (2000) Hymenoptera excluding Apoidea (Apiformes) & Formicidae (Insecta). In: Kirk-Spriggs AH, Marais E (Eds) *Dâures - biodiversity of the Brandberg Massif, Namibia*. Cimbebasia Memoir. National Museum of Namibia, Windhoek, 289–364.
- van Noort S, Buffington ML, Forshage M (2015) Afrotropical Cynipoidea (Hymenoptera). *ZooKeys* 494: 1–176. <https://doi.org/10.3897/zookeys.493.6353>
- Waterston J (1927) On the Hedycryptine genus *Oneilella* Cam. (Hym. Ichneumonidae). *Bulletin of Entomological Research* 18: 189–204. <https://doi.org/10.1017/S0007485300019908>
- Yu D, Horstmann K (1997) 58 A catalogue of World Ichneumonidae (Hymenoptera). VI&, 1558 pp.
- Yu DSK, van Achterberg K, Horstmann K (2016) Taxapad 2016, Ichneumonoidea 2015 (Biological and taxonomical information), Taxapad Interactive Catalogue Database on flash-drive. www.taxapad.com

Two new species of riparian hoppers (Amphipoda, Talitridae) from Trat and Samut Prakan provinces, Thailand

Anotai Suklom^{1*}, Tosaphol Saetung Keetapithchayakul^{2*}, Azman Abdul Rahim^{3},
Koraon Wongkamhaeng^{1}

¹ Department of Zoology, Faculty of Science, Kasetsart University, Bangkok 10900, Thailand

² The Center for Entomology and Parasitology Research; College of Medicine and Pharmacy, Duy Tan University, 120 Hoang Minh Thao, Lien Chieu, Da Nang, Vietnam

³ Marine Ecosystem Research Centre (EKOMAR), Department of Earth Sciences and Environment, Faculty of Science and Technology, Universiti Kebangsaan Malaysia, 43600 UKM Bangi, Selangor, Malaysia

Corresponding author: Koraon Wongkamhaeng (koraon@gmail.com)

Abstract

Floresorchestia has been recorded from the South African coast throughout the tropical Indo-Pacific and Caribbean seas. *Platorchestia* exhibits a distribution along the coastlines of the Atlantic Ocean and has been documented in the Baltic and Mediterranean seas, North America, Bermuda, and South Africa; however, it has not been recorded in Southeast Asia. This study presents the discovery of two new species of *Floresorchestia* and *Platorchestia* (Crustacea: Amphipoda) from a small creek bank in Trat and Bang Pu, Samut Prakan Province, respectively. These new species, classified as riparian hoppers, significantly contribute to the existing biodiversity in Southeast Asia. *Floresorchestia trisetosa* **sp. nov.** can be distinguished by left mandible lacinia mobilis 4-dentate; gnathopod 2 palm reaching approximately 34%; telson as broad as long, with three robust setae per lobe. *Platorchestia aquaticus* **sp. nov.** can be distinguished by gnathopod 1 subchelate, cuspidactylate, gnathopod 2 palm reaching approximately 35%; telson with three marginal robust setae, and three apical robust setae per lobe.

Key words: *Floresorchestia*, new species, *Platorchestia*, riparian hopper, Talitridae, Thailand



Academic editor: Jörundur Svavarsson

Received: 30 October 2024

Accepted: 8 February 2025

Published: 22 April 2025

ZooBank: <https://zoobank.org/9188E53A-2459-4879-8F61-2909AC9822A6>

Citation: Suklom A, Keetapithchayakul TS, Rahim AA, Wongkamhaeng K (2025) Two new species of riparian hoppers (Amphipoda, Talitridae) from Trat and Samut Prakan provinces, Thailand. ZooKeys 1234: 369–396. <https://doi.org/10.3897/zookeys.1234.140645>

Copyright: © Anotai Suklom et al.
This is an open access article distributed under terms of the Creative Commons Attribution License (Attribution 4.0 International – CC BY 4.0).

Introduction

The amphipod family Talitridae is diverse and widespread. *Floresorchestia* ranges from warm temperate South Africa across the tropical Indian and Pacific Oceans. *Platorchestia* has been reported on every continent, particularly in temperate zones. These two genera were considered coastal or terrestrial (Bousfield 1984) when all Talitridae were attributed to one of these habitat types and salt marshes. Today, ten distinct ecological hopper types are recognized: marsh, beach, driftwood, sand, field, ground, riparian, forest, moss, and cave (Lowry and Myers 2019). At a generic level, forest hoppers make up the largest group, followed by field hoppers and beach hoppers, but the most specific group is the beach hoppers. *Floresorchestia* is the most ecologically tolerant of the talitrid genera, with members classified as marsh hoppers, beach hoppers, forest hoppers, field hop-

* These authors contributed equally to this work.

pers, or riparian hoppers. The wide variety of habitats implies a high adaptation ability, and many studies presumed that the terrestrial species have a coastal *Floresorchestia* ancestor (Bousfield 1984; Lowry and Springthorpe 2015, 2019). *Platorchestia* species, by contrast, are known primarily as beach hoppers, with only one species (*P. negevensis* Myers & Lowry, 2023) previously known as riparian hoppers. In Thailand, there are five species of *Floresorchestia*: *F. boonyanusithii* Wongkamhaeng, Damrongrojwattana & Pattaratumrong, 2016, *F. buraphana* Wongkamhaeng, Damrongrojwattana & Pattaratumrong, 2016, *F. kongsemae* Suklom, Danaisawadi & Wongkamhaeng, 2021, *F. amphawaensis* Suklom, Keetapithchayakul, Abdul Rahim & Wongkamhaeng, 2022 and *F. pongrati* Suklom, Keetapithchayakul, Abdul Rahim & Wongkamhaeng, 2022 (Azman et al. 2014; Wongkamhaeng et al. 2016; Suklom et al. 2021; Suklom et al. 2022). The latter two species were reported in agricultural and urban areas near the Mae Klong River. Although talitrid amphipods can inhabit the terrestrial environment, they require conditions of high humidity and can detect humidity gradients by the virgula davina, the same as terrestrial isopods (Friend and Richardson 1986; Lowry and Springthorpe 2015). Therefore, the dispersal of *Floresorchestia* in Thailand should correspond with the flood plain and may relate to the river basins. The genus *Platorchestia* Bousfield (1982) was included in the subfamily Platorchestiinae Lowry and Myers (2022). Platorchestiinae is well known for its broad distribution. Currently, *Platorchestia* is present on Atlantic Ocean shores (including the Caribbean, Baltic, Mediterranean, and North seas), the Indian Ocean, the western coast of Australia, the Pacific Ocean, the western US Coast, and the East China Sea (Myers and Lowry 2023). This work is the first record of *Platorchestia* in Southeast Asia and of the first riparian hoppers in the Indo-Pacific. Additionally, the new species of *Platorchestia* are the first records of this genus in Southeast Asia.

Materials and methods

This study is based on material collected from leaf litter in ponds of rice fields and urban locations in Trat Province, including the shore of Klong Mai and Bang Pu, Samut Prakan, Thailand (Fig. 1). Specimens were collected using a pit-fall trap and were then carefully transferred into plastic containers. They were fixed in 70% ethanol and preserved in 95% ethanol. The specimens were examined under a dissecting microscope and later selected for dissection. Appendages of the specimens were examined, and representative figures were produced using a camera lucida attached to an Olympus CH30 light microscope. Pencil drawings were scanned and digitally inked using an iPad via the Procreate application. Final plates were prepared using Adobe Photoshop CC 2017. Distribution maps were plotted using SimpleMappr (Shorthouse 2010).

The palm length was measured as a percentage of the length of the propodus of male gnathopod 2 and was calculated using the formula $100(1 - a/b)\%$ (Fig. 2), where 'a' is the length of the posterior margin measured from the seta at the corner of the palm to the base of the propodus and 'b' is the length of the propodus measured from the base of the dactylus to the base of the propodus (Lowry and Springthorpe (2015: 6)). Terminology for setae and mouthparts follows Zimmer et al. (2009). Abbreviations used in figures are **A**, antenna; **EP**, epimera; **G**, gnathopod; **LL**, lower lip; **MD**, mandible; **MX**, maxilla; **MP**, maxilliped; **P**, pereopod; **PL** pleopod; **T** telson; **U**, uropod; **UL**, upper lip; **R**, right; **L**, left.

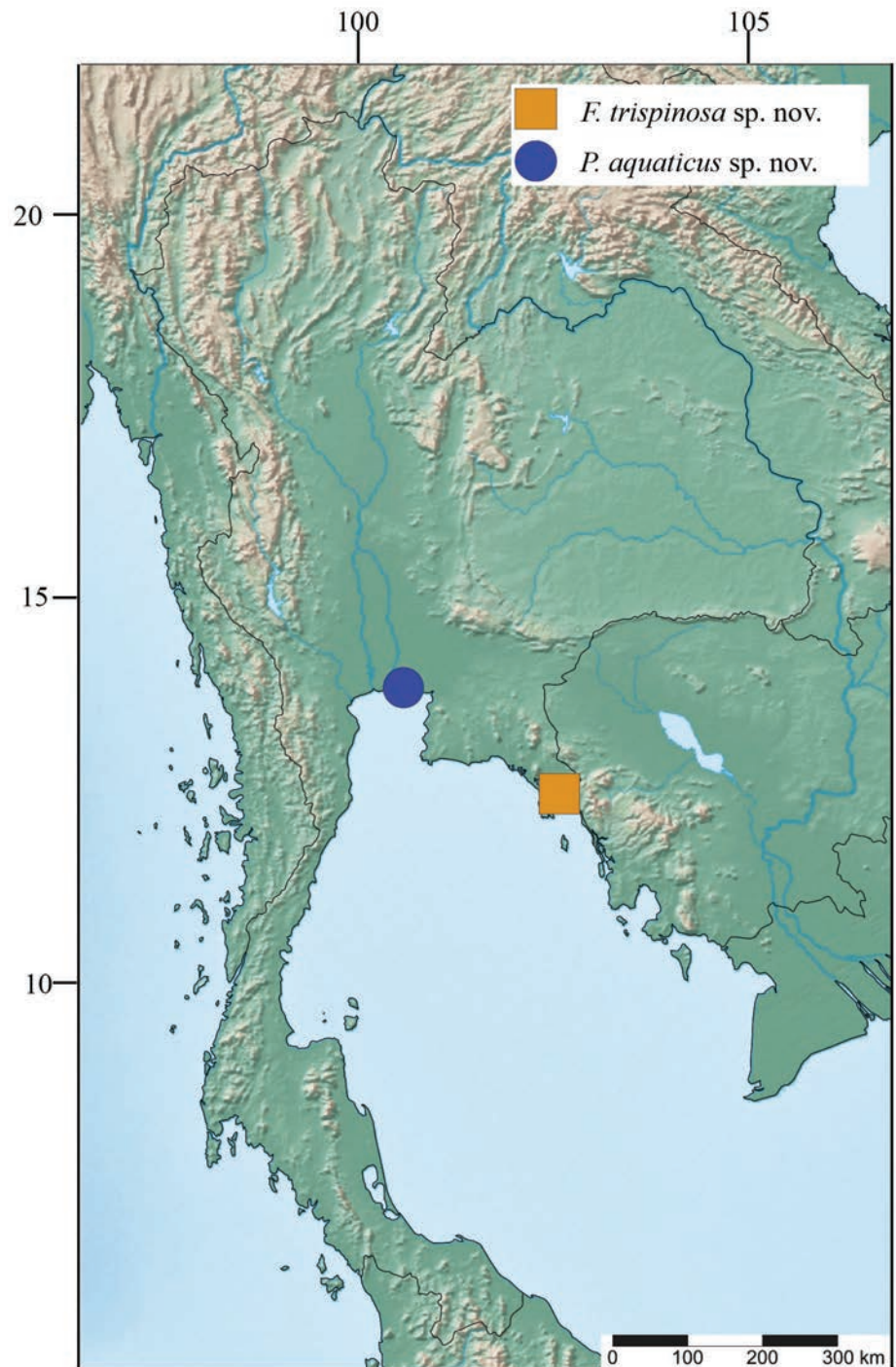


Figure 1. Map showing the sampling area. Orange square represents type locality of *Floresorchestia trispinosa* sp. nov. and blue circle represents type locality of *Platorchestia aquaticus* sp. nov.

Results

Systematics

Superfamily Talitroidea Bulycheva, 1957

Family Talitridae Rafinesque, 1815

Subfamily Floresorchestiinae Myers and Lowry, 2020

***Floresorchestia* Bousfield, 1984**

Orchestia floresiana group: Bousfield 1971: 267.

Floresorchestia Bousfield, 1984: 205. Miyamoto and Morino 2008: 838. Lowry and Springthorpe 2009: 121. Lowry and Springthorpe 2015: 7.

Type species. *Orchestia floresiana* Weber, 1892, original designation.

Diagnostic description. (modified from Lowry and Springthorpe 2009, 2015) *Antenna 1* short, not longer than article 4 of antenna 2 peduncle. *Antenna 2* peduncular articles slender; article 3 without ventral process. *Left mandible* lacinia mobilis 4–5-cuspidate. *Maxilliped* palp article 2 distomedial lobe well developed, article 4 reduced, button-shaped. *Gnathopod 1* sexually dimorphic; subchelate; posterior margin of merus, carpus and propodus each with lobe covered in palmate setae. *Gnathopod 2* sexually dimorphic; subchelate; dactylus distally attenuated (except *Floresorchestia papeari* Lowry & Springthorpe, 2015 and *F. ancheidos* (H.K. Barnard, 1916)). *Pereopods 3–7* cuspidactylate (except *F. odishi* Bhoi, Myers, Kumar & Patro, 2024; pereopods 6 and 7 unidactylate). Pereopods 6 and 7 not sexually dimorphic. *Pleopods* all well developed, biramous. *Epimera 1–3*, 2 and 3, or 2 with slits just above ventral margins, vestigial on epimera 1 (except *F. xueli* Tong, Hoa, Liu, Li & Hou, 2021). *Uropods 1*, 2 not sexually dimorphic. Uropod 1 outer ramus without marginal robust setae. Uropod 2 outer ramus with marginal robust setae. Uropod 3 ramus subequal in length to peduncle. *Telson* with 3–7 robust setae.

Female (sexually dimorphic characters). *Gnathopod 1* posterior margin of merus, carpus and propodus each without lobe covered in palmate setae. *Gnathopod 2* mitten-shaped. *Oostegites* on gnathopod 2 to pereopod 5; setae straight.

Species composition. *Floresorchestia* includes 29 species: *F. amphawaensis* Suklom, Keetapithchayakul, Abdul Rahim & Wongkamhaeng, 2022; *F. andrevo* Lowry & Springthorpe, 2015; *F. anomala* (Chevreux, 1901); *F. anoquesana* (Bousfield, 1971); *F. anpingensis* Miyamoto & Morino, 2008; *F. boonyanusithii* Wongkamhaeng, Dumrongrojwattana & Pattaratumrong, 2016; *F. buraphana* Wongkamhaeng, Dumrongrojwattana & Pattaratumrong, 2016; *F. floresiana* (Weber, 1892); *F. hanoiensis* Hou & Li, 2003; *F. kalili* Lowry & Springthorpe, 2015; *F. kongsemae* Suklom, Danaisawadi & Wongkamhaeng, 2021; *F. laurenae* Lowry & Springthorpe, 2015; *F. malayensis* (Tattersall, 1922); *F. mkomani* Bichang'a & Hou in Bichang'A et al., 2021; *F. odishi* Bhoi, Myers, Kumar & Patro, 2024; *F. oluanpi* Lowry & Springthorpe, 2015; *F. palau* Lowry & Myers, 2013; *F. papeari* Lowry & Springthorpe, 2015; *F. pohnpei* Lowry & Myers, 2013; *F. poorei* Lowry & Springthorpe, 2009; *F. pongratii* Suklom, Keetapithchayakul, Abdul Rahim & Wongkamhaeng, 2022; *F. samoana* (Bousfield, 1971); *F. seringat* Lowry & Springthorpe, 2015; *F. thienemanni* (Schellenberg, 1931); *F. trisetosa* sp. nov.; *F. vitilevana* (J.L. Barnard, 1960); *F. xueli* Tong, Hao, Liu, Li & Hou, 2021; *F. yap* Lowry & Springthorpe, 2015; *F. yehyuensis* Miyamoto & Morino, 2008.

Remarks. The subfamily Floresorchestiinae is comprised of three genera (*Austropacifica*, *Floresorchestia*, and *Gazia*) and is defined by vertical slits on the ventral margin of epimera 1–3, 2 and 3, or only 2. *Floresorchestia* differs from *Gazia* in having a palmate lobe on the merus carpus and propodus of male gnathopod 1, whereas *Gazia* lacks a palmate lobe on the merus of male gnathopod 1. *Floresorchestia* differs from *Austropacifica* in not having the mid-medial robust setae with a modified tip on the outer ramus of uropod 1.

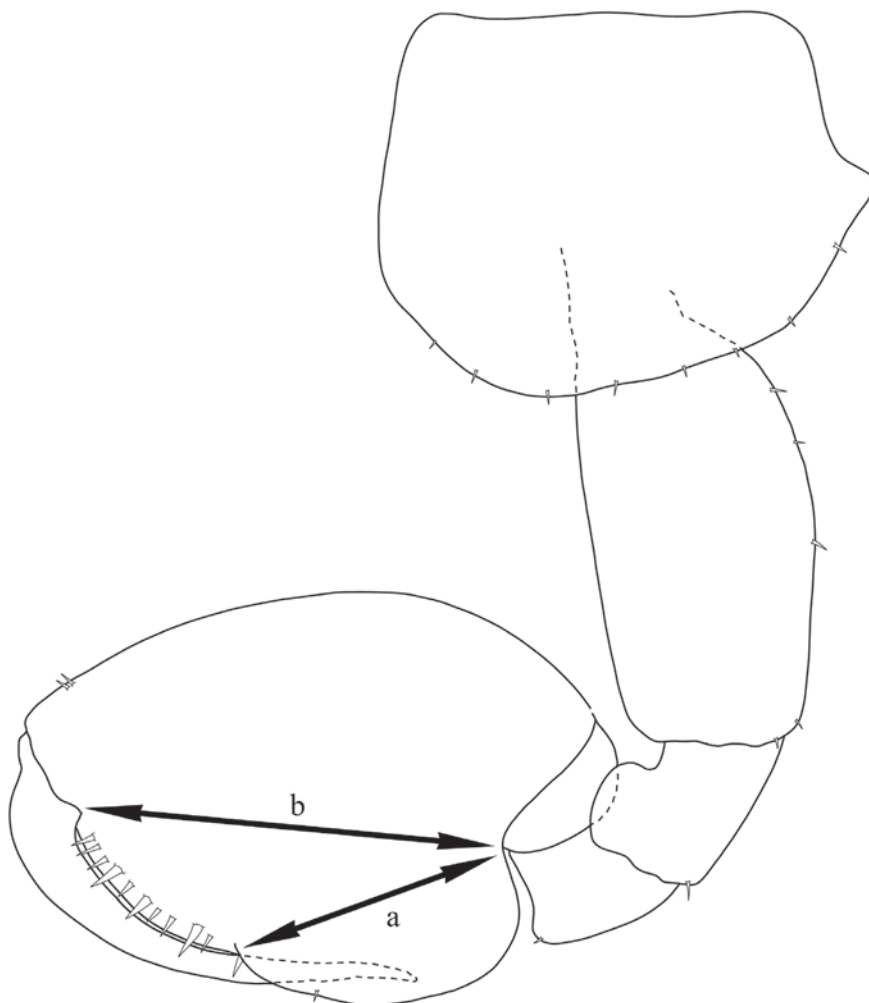


Figure 2. The measurement method for the length of male gnathopod 2 palm and posterior margin of propodus.

***Floresorchestia trisetosa* sp. nov.**

<https://zoobank.org/5C7AA8E3-B49C-4264-80B0-0DBAC71E3FEF>

Figs 3–6

Type material. Holotype • THAILAND, 1 ♂; Muang Trat District, Trat; 12°15'12.9"N, 102°30'31.3"E; 21 February 2021; Anotai Suklom; pit fall trap; THNHM-lv-20866.

Allotype • 1 ♀; collected with holotype; THNHM-lv-20867. **Paratypes** • 2 ♂ and 2 ♀ collected with holotype; THNHM-lv-20868.

Type locality. A small creek near the restaurant, Muang Trat District, Trat, Thailand.

Ecological type. Riparian hoppers (edges of lakes under stones or in very wet vegetation, near or in streams, rivers, creeks, cascades, and waterfalls).

Diagnosis. Mandible lacinia mobilis 4-dentate. Gnathopod 1 with palmate lobes on merus, carpus and propodus; palm acute. Gnathopod 2 propodus palm reaching ~ 33% along posterior margin; dactylus attenuated distally. Pereopod 4 dactylus thickened proximally, with slight notch midway along posterior margin. Epimeron 2 and 3 with slits just above ventral margins. Uropod 1 outer ramus without marginal robust seta, with three marginal robust setae in

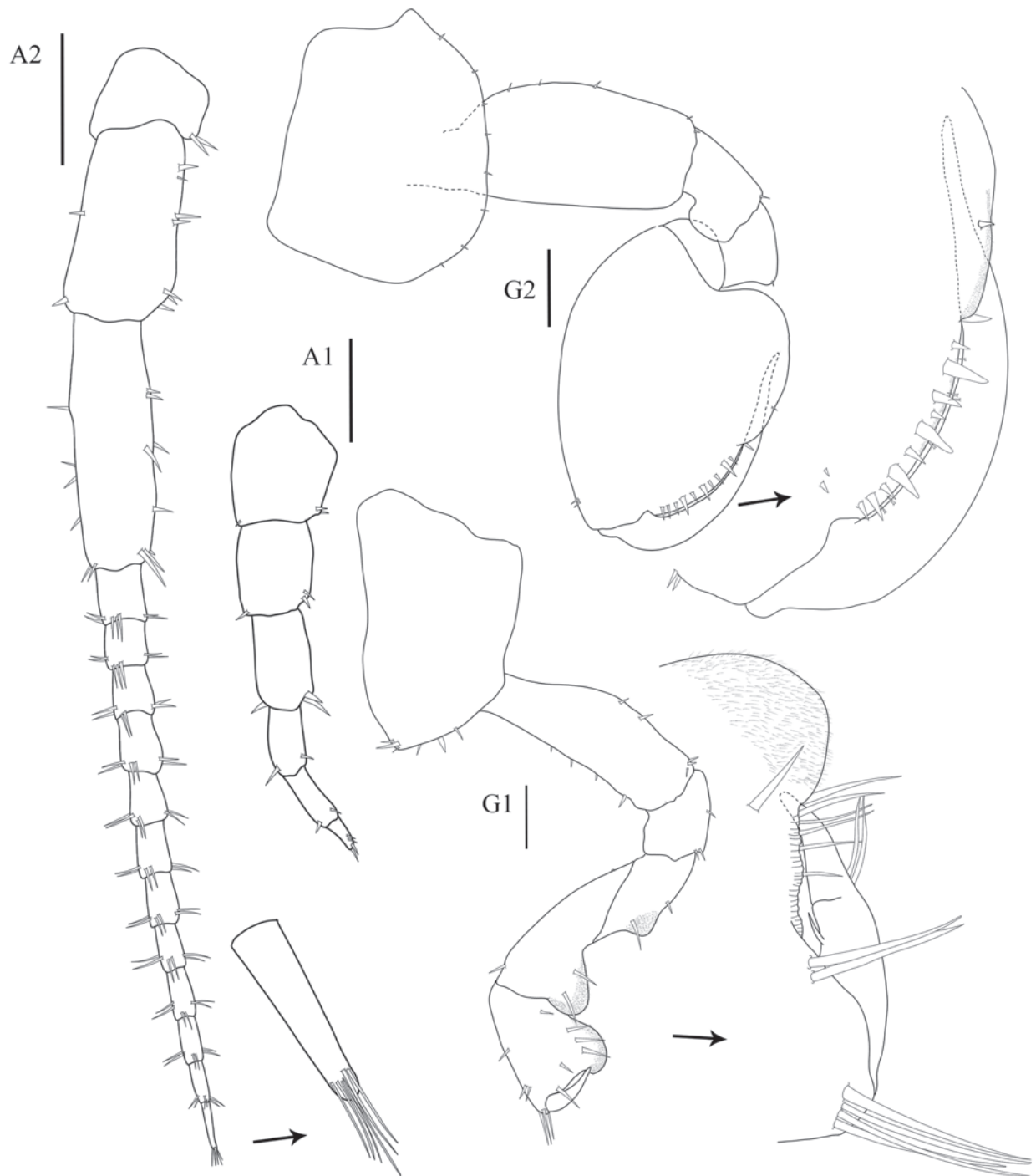


Figure 3. *Floresorchestia trisetosa* sp. nov., holotype, male, 5.5 mm, THNHM-lv-20866. Scale bars: 0.5 mm (**A2**, **G1**, **G2**); 0.2 mm (**A1**).

one row. Uropod 3 peduncle with one robust seta; ramus with two apical robust setae. Telson with one apical robust seta, and two lateral robust seta per lobe.

Description. Based on male holotype 8.7 mm, THNHM-lv-20866.

Head. **Eye** large ($> 1/3$ head length). **Antenna 1** (Fig. 3, A1) short, rarely longer than article 4 of antenna 2 peduncle. **Antenna 2** (Fig. 3, A2) $< 1/2$ body length, peduncular articles slender, article 5 longer than article 4. **Upper lip** (Fig. 4, UL) without robust setae, broad, rounded apex, apical marginal with fine setule.

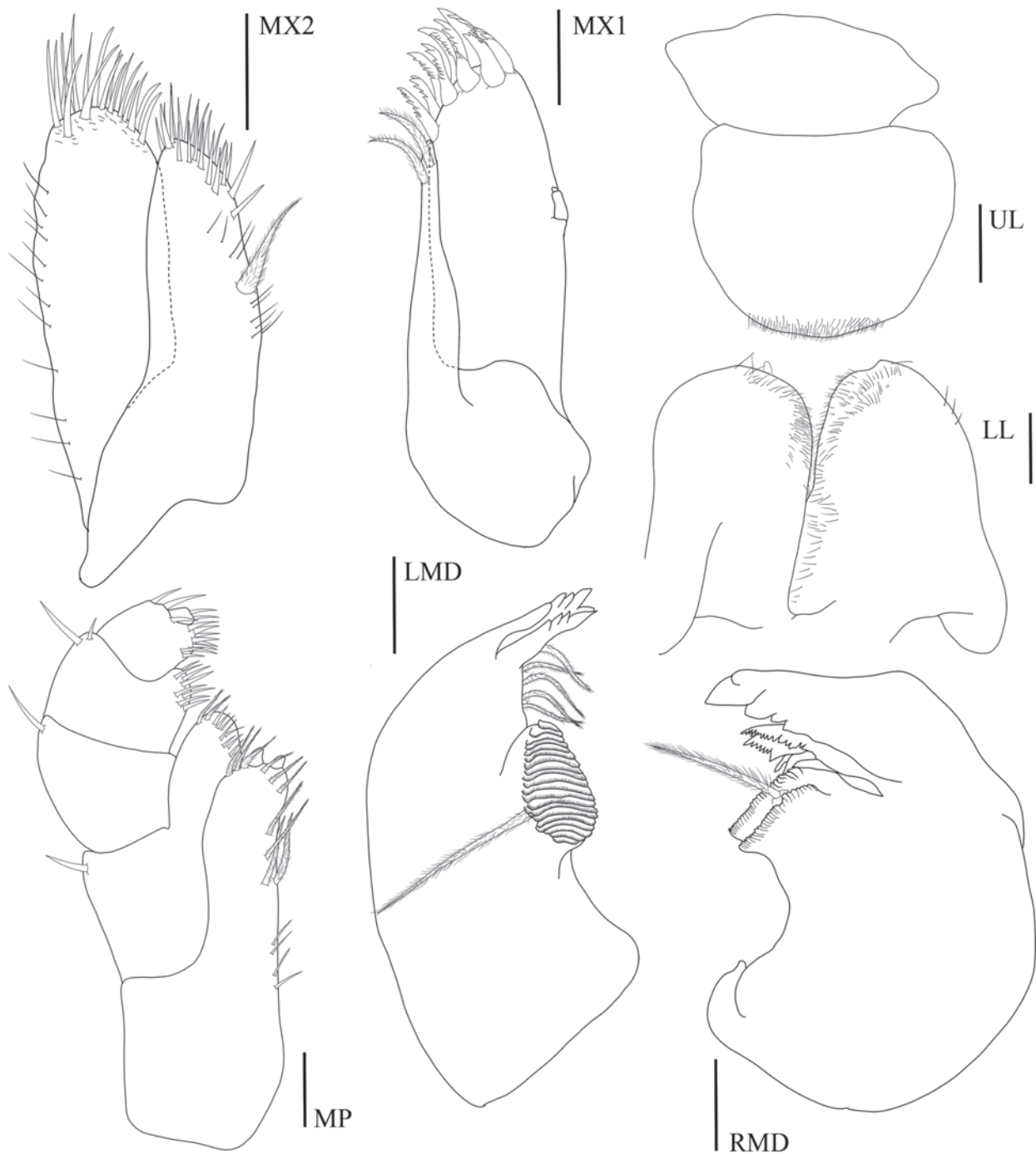


Figure 4. *Floresorchestia trisetosa* sp. nov., holotype, male, 5.5 mm, THNHM-Iv-20866. Scale bars: 0.2 mm (**MX1**, **MX2**, **MP**, **LMD**, **RMD**); 0.1 mm (**UL**, **LL**).

Lower lip (Fig. 4, LL) without inner plate, with fine setule on apex and inner margin. **Left mandible** (Fig. 4, LMD) incisor 5-dentate; left lacinia mobilis 4-dentate and five pappose setae type I in one row; molar strong with 20 striations and one pappose setae type II on the distal of molar. **Right mandible** (Fig. 4, RMD) incisor 5-dentate; lacinia mobilis with numerous cusps; molar strong with 26 striations and 1 distal pappose seta. **Maxilla 1** (Fig. 4, MX1) inner plate slender with 2 apical papposerrate setae type I; outer plate with 9 robust serrate setae type I and small palp 2-articulate on outer lateral margin. **Maxilla 2** (Fig. 4, MX2)

inner plate slightly shorter than outer plate, subapical margin with 19 robust setae, with one mediolateral papposerrate seta type I; outer plate with 18 apical robust setae in two rows. **Maxilliped** (Fig. 4, MP) inner plate apical and subapical margins with papposerrate setae type II, and two large conical robust setae; outer plate subapical margin with robust setae and two pappose setae; palp article 2 distomedial lobe well developed; article 4 reduced, button shaped.

Pereon. Gnathopod 1 (Fig. 3, G1) sexually dimorphic; subchelate; coxa smaller than coxa 2, anterior margin slightly convex distally; basis slightly expanded posteriorly, anterior margin with four robust setae, posterior margin with two marginal robust setae and two terminal robust setae; ischium subquadrate, shortest, anterior lobe slightly rounded; posterior margin of merus, carpus and propodus each with lobe covered in palmate setae; carpus longer than propodus, carpus 1.27× as long as propodus, carpus 1.9× as long as broad; propodus 'subtriangular' with well-developed posterodistal lobe, anterior margin with three groups of robust setae, lateral surface with four cuspidate setae, posterolateral surface with three serrate setae, medial surface with five cuspidate setae, posterior margin without cuspidate setae, with three serrate setae; palm transverse, with five serrate setae; dactylus longer than palm, without spine patch on posterodistal corner. **Gnathopod 2** (Fig. 3, G2) sexually dimorphic; subchelate; coxal gill simple (or slightly lobate); basis slightly expanded; ischium with distally rounded posterodistal lobe on medial surface; posterior margin of merus, carpus and propodus each without lobe covered in palmate setae; carpus reduced, enclosed by merus and propodus, posterior absent, not projecting between merus and propodus; propodus subovate, 1.4× as long as wide; palm acute, reaching ~ 33% along posterior margin, smooth, evenly rounded, lined with robust setae, posteromedial surface of propodus with groove, without cuticular patch at corner of palm; dactylus longer than palm, without anteroproximal bump, posterior margin smooth, attenuate distally; gill lobate.

Pereopods 3–4 (Fig. 5, P3–P7) coxae wider than deep. **Pereopods 3–7** cuspidactylate; dactyli without anterodistal patch of many rows of tiny setae. **Pereopod 3** (Fig. 5, P3) coxa wider than deep, ventral margin with four robust setae, posterior margin with acute process; basis slightly expanded, anterior margin slightly straight and naked, posterior margin with four robust setae; ischium subrectangular, shortest; merus longer than carpus and propodus, distally expanded, anterior margin with four robust setae, posterior margin with four robust setae; carpus as long as propodus, anterior margin with three setae, posterior margin with four robust setae; propodus slender, anterior margin with three robust setae, posterior margin with eight robust setae; dactylus without notch on posterior margin, anterior corner with one robust seta and posterior inner view with two robust setae. **Pereopod 4** (Fig. 5, P4) significantly shorter than pereopod 3; coxa wider than deep, posterior margin with acute process; basis slightly expanded distally, anterior margin distally convex, posterior margin with five robust setae; ischium shortest, subquadrate, distally convex; merus longer than carpus and propodus; carpus significantly shorter than carpus of pereopod 3; propodus slender, anterior margin with three groups of robust setae, posterior margin with three groups of robust setae; dactylus thickened proximally with a notch midway along posterior margin, dactylus without anterodistal setal patch. **Pereopod 5** (Fig. 5, P5) coxa bilobed, anterior lobe distinctly larger than posterior lobe, posterior lobe with setae on ventral margin;

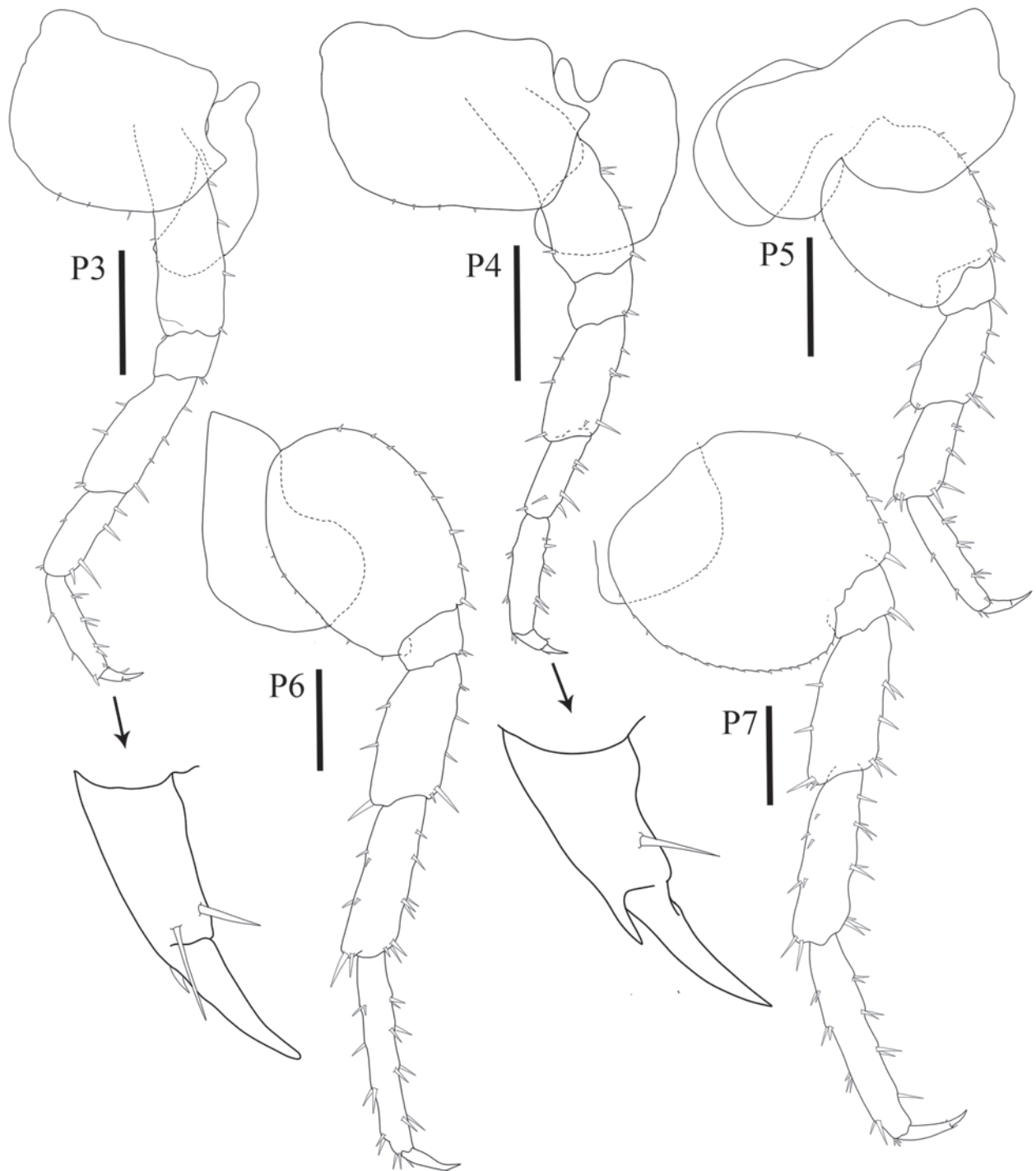


Figure 5. *Floresorchestia trisetosa* sp. nov., holotype, male, 5.5 mm, THNHM-Iv-20866. Scale bars: 0.5 mm.

basis ovate, anterior margin with eight robust setae, posterior margin with five minute setae; ischium shortest, subrectangular, posterior margin distally convex; merus as long as carpus, distally expanded, anterior margin with five robust setae; carpus shorter than propodus, anterior margin with seven robust setae, posterior margin with one marginal robust seta and three robust setae distally; propodus distinctly longer than carpus; dactylus without anterodistal setal patch. **Pereopods 6–7** (Fig. 5, P6 and P7) not sexually dimorphic. **Pereopod 6** (Fig. 5, P6) subequal in length to pereopod 7; coxa posterior lobe larger

than anterior lobe, inner view posteroventral corner rounded, posterior margin perpendicular to ventral margin, posterior lobe without ridge, without marginal setae; basis ovate, anterior margin with eight robust setae, posterior margin with nine or ten minute setae; ischium shortest; merus slightly expanded, anterior margin crenulate with six robust setae, posterior margin convex with three robust setae; carpus as long as merus, anterior margin crenulate with eight robust setae, posterior margin with six robust setae in three groups; propodus longer than carpus, slender, anterior margin with eight robust setae in four groups, posterior margin with nine robust setae; dactylus slender with setae in posterior corner. **Pereopod 7** (Fig. 5, P7) coxa reduced; basis sub ovate, lateral sulcus absent, posterior margin with distinct minute serrations, each with a small seta, posterodistal lobe present, shallow, broadly rounded; ischium shortest, subrectangular with posterior rounded process; merus posterior margin expanded distally, subtriangular; propodus slightly longer than carpus, anterior margin with seven robust setae, posterior margin with eight robust setae and three terminal minute setae; dactylus slender and with subapical setae.

Pleon. Pleopods 1–3 well developed, biramous; peduncle ventral margin without robust setae; rami without ventral robust setae. **Pleopod 1** (Fig. 6, PL1) peduncle longer than rami; inner ramus subequal in length to outer ramus, with eight articles; outer ramus with nine articles. **Pleopod 2** (Fig. 6, PL2) peduncle longer than rami; inner ramus with eight robust setae; outer ramus with eight robust setae. **Pleopod 3** (Fig. 6, PL3) peduncle longer than rami; inner ramus with nine robust setae; outer ramus with seven robust setae. **Epimeron 1** (Fig. 6, EP) posterior corner slightly projecting, and without slits. **Epimera 2 and 3** each with slits above ventral margin; posterior ventral corner and ventral margin smooth. **Uropod 1** (Fig. 6, U1) peduncle slightly longer than ramus with 6 robust setae, distolateral robust seta present, small ($< 1/4$ length of outer ramus), with simple tip; inner ramus subequal in length to outer ramus, inner ramus with three marginal robust setae (1 row), with four apical robust setae; outer ramus without marginal robust setae. **Uropod 2** (Fig. 6, U2) not sexually dimorphic; peduncle shorter than rami with 3 robust setae; inner ramus subequal in length to outer ramus, with marginal robust setae, with one lateral robust seta; outer ramus with marginal robust setae in one row. **Uropod 3** (Fig. 6, U3) peduncle longer than ramus with one robust seta; ramus not fused to peduncle; ramus 1.6× as long as broad. **Telson** (Fig. 6, T) longer than broad, apically incised, dorsal midline less than halfway, with one apical robust seta, and two lateral robust setae.

Female (Fig. 6) (sexually dimorphic characters). Based on allotype, female 4.7 mm. THNHM-lv-20867.

Pereon. Gnathopod 1 (Fig. 6, G1♀) parachelate; coxa anterior margin straight, anteroventral margin with three robust setae; basis slender, anterior margin straight, posterior margin slightly expanded distally with two subterminal robust setae; ischium shortest, subrectangular, anterior margin slightly convex; posterior margin of merus, carpus and propodus without lobe covered in palmate setae; merus triangular with two groups of robust setae on posterior margin; carpus subtriangular, anterior margin curved with four terminal setae, posterior margin slightly convex with three robust setae; propodus slender, anterior margin crenulate with two marginal robust setae and four terminal setae, posterior margin crenulate with three lateromedial robust setae; dactylus

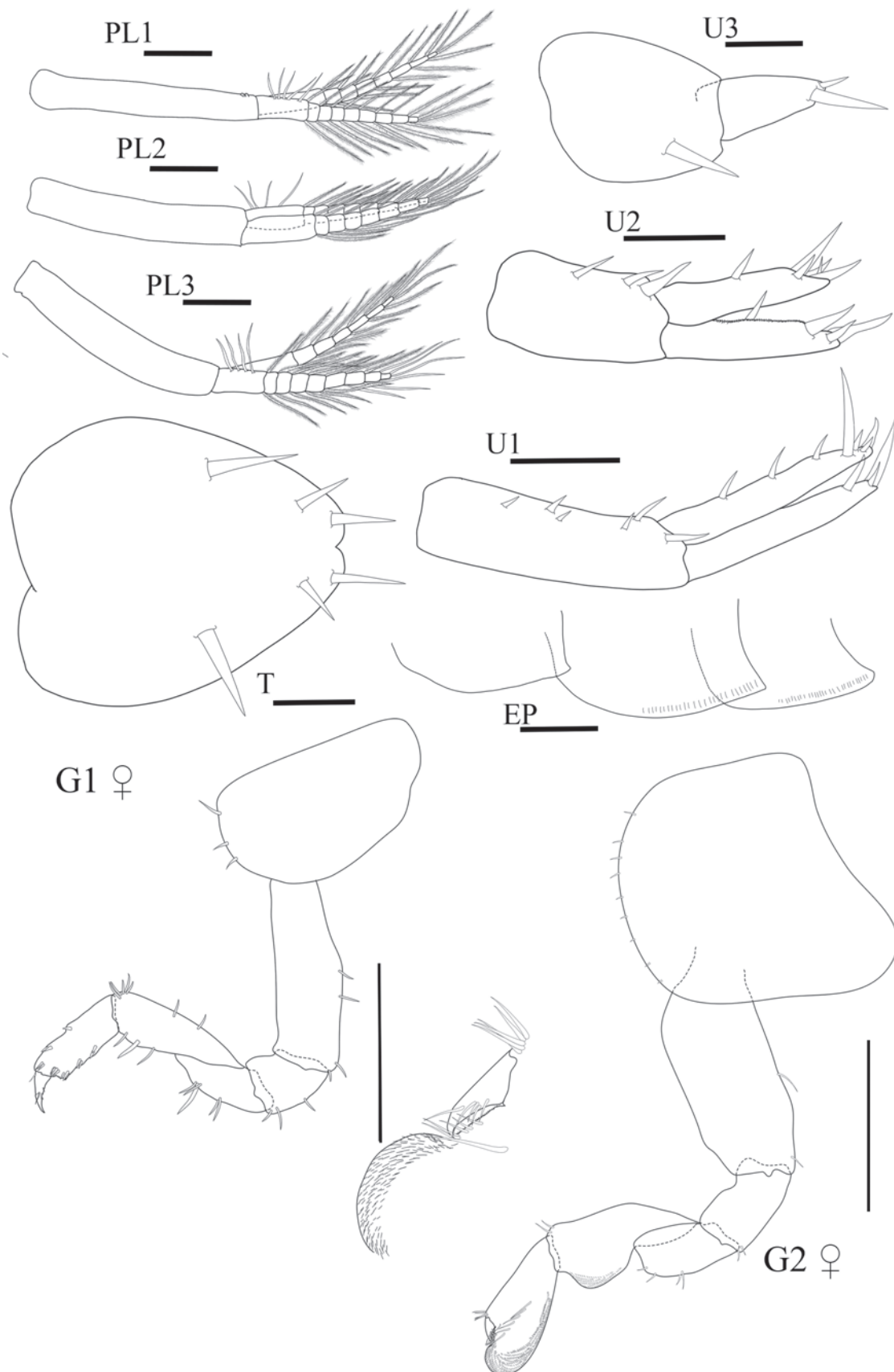


Figure 6. *Floresorchestia trisetosa* sp. nov., holotype, male, 5.5 mm, THNHM-Iv-20866, allotype, female, 4.7 mm, THNHM-Iv-20867. Scale bars: 0.25 mm (PL1–3, EP); 0.2 mm (U1–2, U3); 0.1 mm (T) 0.5 mm (G1♀, G2♀).

slender, anterior corner with one robust seta, posterior margin with one seta and two lateromedial robust setae. **Gnathopod 2** (Fig. 6, G2♀) mitten-shaped; coxa as long as deep, anterior margin straight, posterior margin straight, ventral margin with minute setae; basis expanded, anterior margin naked, posterior margin straight with one seta; ischium as long as merus, anterior margin with rounded lobe, posterior margin straight with one terminal seta; merus shorter than carpus, anterior margin with rounded lobe, posterior margin with rounded lobe; carpus and propodus each with lobe covered in palmate setae; carpus subtriangular, longer than propodus; propodus subovate, lateromedial corner with three robust setae; dactylus slender, shorter than palm, anterior margin with one robust seta, posterior margin with two robust setae.

Distribution. Thailand. Trat town Municipality, Trat.

Etymology. Named for the character of three robust setae on each telsonic lobe.

Remarks. *Floresorchestia trisetosa* sp. nov. is closely related to *F. boonyanusithii* and *F. amphawaensis* by having the gnathopod 2 palm reaching between 31–35%, dactylus posterior margin smooth, proximal tooth absent, and mandible left lacinia mobilis 4-dentate. *F. trisetosa* can be separated from those two species by the combination of characteristics as follows (other species in parentheses): (1) gnathopod 1 carpus 1.2 × propodus (1.4× in *F. boonyanusithii*, 1.5× in *F. amphawaensis*); (2) uropod 1 peduncle with six robust setae (6 in *F. boonyanusithii*; 4 in *F. amphawaensis*); (3) uropod 3 peduncle with two robust setae (4 in *F. amphawaensis* and 2 in *F. boonyanusithii*); (4) telson longer than broad, telsonic lobe with three robust setae (vs 4 robust setae in *F. boonyanusithii*, and *F. amphawaensis*).

Floresorchestia trisetosa is the first riparian hopper to be reported from Thailand (Fig. 7).

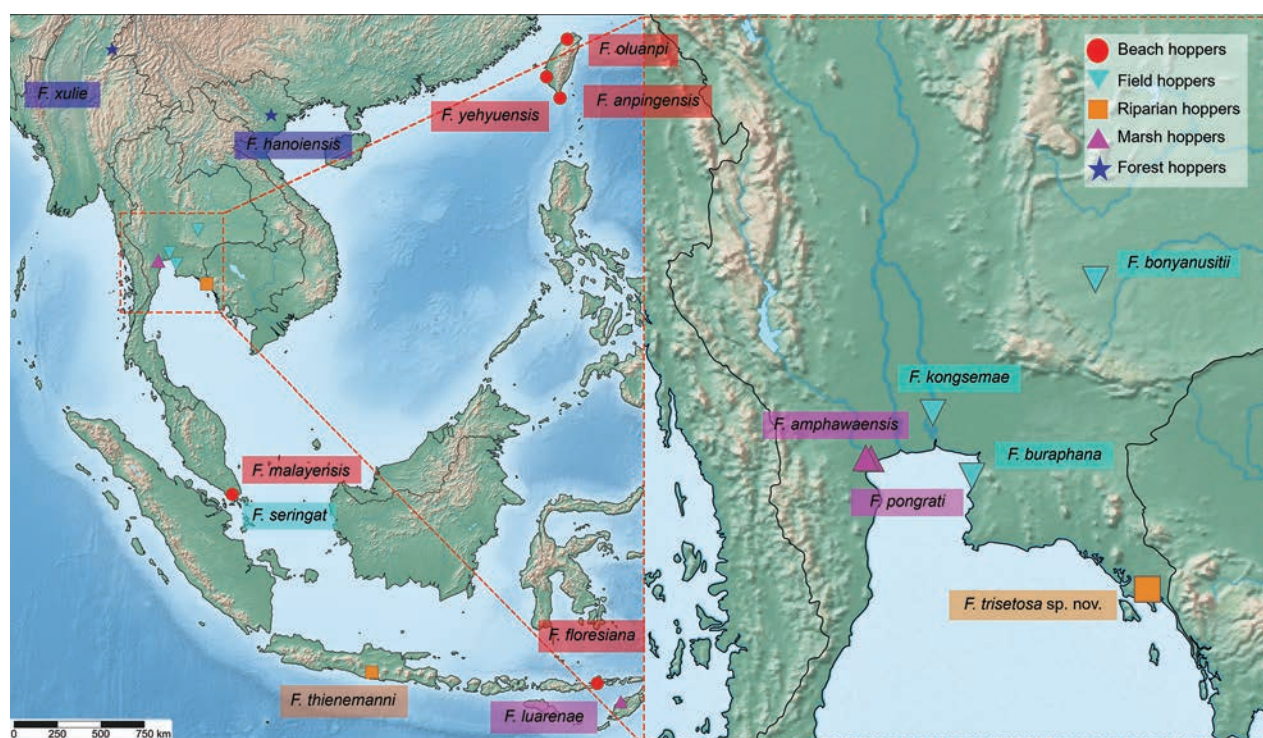


Figure 7. Ecological groups of *Floresorchestia* species in Southeast Asia.

Subfamily Platorchestiinae Lowry & Myers, 2022

Platorchestia Bousfield, 1982

Platorchestia Bousfield, 1982: 26; Jo 1988: 160; Richardson 1991: 186; Morino and Ortal 1995: 825; Miyamoto and Morino 2004: 68; Myers and Lowry 2023: 486.

Type species. *Platorchestia platensis* (Krøyer, 1845), original designation.

Diagnostic description. (modified from Myers and Lowry 2023) **Antenna 1** short, not longer than article 4 of antenna 2 peduncle. **Antenna 2** peduncular article 3 without ventral plate; articles 4 and 5 occasionally incrassate in males. **Maxilliped** palp article 2 with distomedial lobe; article 4 reduced, button-shaped. **Gnathopod 1** sexually dimorphic; subchelate; posterior margin of carpus and propodus each lobe covered in palmate setae; dactylus cuspidactylate. **Gnathopod 2** subchelate in male, mitten-shaped in female; basis narrow or slightly expanded; propodus palm posterodistal corner without protuberance. **Pereopods 3–7** cuspidactylate. Pereopod 7 occasionally incrassate in male. **Uropod 1** outer ramus without marginal robust setae. **Telson** with apical and marginal robust setae.

Species composition. *Platorchestia* contains 13 species: *P. ano* Lowry & Bopiah, 2013; *P. aquaticus* sp. nov.; *P. crassicornis* (Costa, 1867); *P. exte* Myers & Lowry, 2023; *P. griffithsi* Myers & Lowry, 2023; *P. munmui* Jo, 1988; *P. negevensis* Myers & Lowry, 2023; *P. oliveirae* Myers & Lowry, 2023; *P. pachypus* (Derzhavin, 1937); *P. pacifica* Miyamoto & Morino, 2004; *P. parapatensis* Serejo & Lowry, 2008; *P. platensis* (Krøyer, 1845); *P. smithi* Lowry, 2012.

Remarks. Miyamoto and Morino (2004) established three groups of *Platorchestia* based on the presence or absence of sexual dimorphism. Lowry and Myers (2022) established the new subfamily Platorchestiinae, which accommodates 15 genera, including *Platorchestia*. The *Platorchestia* sensu stricto is equivalent to Group 1 of Miyamoto (antenna 2 and pereopods 6 and 7 are strongly sexually dimorphic and represented by supralittoral species). Subsequently, Myers and Lowry (2023) described three new *Platorchestia* species and provided the diagnostic characteristics as antenna 2 sexually dimorphic by articles 4 and 5, which are generally incrassate in males and pereopod 7 often incrassate in male articles 5–7. The combination of antenna 2 and pereopod 7 incrassate was classified into Group 1 and Group 2 by Miyamoto and Morino (2004).

Platorchestia aquaticus sp. nov.

<https://zoobank.org/C7E46D2E-806F-48E8-ACBC-EB8F6322C004>

Figs 8–12

Type material. Holotype • THAILAND, 1 ♂; Bang Pu, Samut Prakan; 13°31.73'N, 100°38.17'E; 21 February 2021; Anotai Suklom; pit fall trap; THNHM-lv-20869.

Allotype • 1 ♀; collected with holotype; THNHM-lv-20870. **Paratypes** • 2 ♂ and 2 ♀ collected with holotype; THNHM-lv-20871.

Type locality. On the shore of Klong Mai, Bang Pu, Samut Prakan, Thailand.

Habitat. Riparian hoppers, living near urban areas in Bang Pu, Samut Prakan.

Ecological type. Riparian hoppers (on the shore of canal under leaf litter or around the fibrous root of aquatic plants).

Diagnosis. Male antenna 2 and pereopod 7 strongly sexually dimorphic. Male gnathopod 1 rudimentary cusp on dactylus. Male gnathopod 2 propodus without notch on palmar margin. Coxa 6 posterior lobe with anterodistal corner subquadrate, with process, one or two marginal setae, posterior margin perpendicular to ventral margin, outer surface with ridge. Pleopod 2 with two marginal robust setae; pleopod 3 with three marginal robust setae. Uropod 1 peduncle with nine or ten robust setae in two rows. Uropod 3 ramus with one marginal robust seta.

Description. Based on holotype, male, 8.72 mm, THNHM-lv-20869. **Head.** **Eye** medium $\sim 1/3$ – $1/5$ of head length. **Antenna 1** (Fig. 8, A1) short, slightly longer than article 4 of antenna 2. **Antenna 2** (Fig. 8, A2) slightly incrassate, shorter than half body length; peduncular articles occasionally expanded, with small setae along the peduncle; article 4 shorter than article 5; flagellum with 15 articles, final article cone-shaped with apical cluster of setae. **Upper lip** (Fig. 9, UL) broad, deep, apex round, without robust setae, apical margin with fine setules. **Lower lip** (Fig. 9, LL) present; without inner plate, with fine setules on the apex and inner margins. **Left mandible** (Fig. 9, LMD) incisor 5-dentate; lacinia mobilis 5-dentate, with six pappose setae type I in one row; molar strong and concave, with 22 striations, with cluster of fine setae on anterior side and one pappose setae type II on the dorsal side of molar. **Right mandible** (Fig. 9, RMD) incisor 5-dentate; lacinia mobilis with numerous cusps and four pappose setae type I in one row; molar strong and convex, with 22 striations, with cluster of fine setae on anterior side and one pappose seta type II on the dorsal side. **Maxilla 1** (Fig. 9, MX1) inner plate slender with two apical papposerrate setae type I; outer plate with seven robust serrate setae type I; outer margin with small 2-articulate palp. **Maxilla 2** (Fig. 9, MX2) inner plate slightly shorter than outer plate; with 25 subapical setae, one papposerrate seta type I and 15 simple slender setae on inner margin; outer plate with 12 simple setae type I and one papposerrate seta type I, inner margin with four robust setae. **Maxilliped** (Fig. 9, MP) inner plate with apical papposerrate setae type II and three large conical robust setae; outer plate with apical papposerrate setae; palp article two distomedial lobe well developed with numerous simple setae; article 4 present, reduced.

Pereon. Gnathopod 1 (Fig. 8, G1) sexually dimorphic; subchelate, coxa smaller than coxa 2, ventral margin with eight robust setae, anterior margin straight; basis expanded posteriorly, anterior margin with six robust setae, posterior margin with four robust setae; posterior margin of carpus and propodus each with lobe covered in palmate setae; ischium shortest; merus and carpus triangular; carpus $1.3\times$ longer than propodus; propodus subtriangular with well-developed posterior lobe, palm straight with four robust setae in one row; dactylus cuspidactylate, shorter than palm. **Gnathopod 2** (Fig. 8, G2) sexually dimorphic; subchelate; coxa as wide as deep without posterior process, ventral margin convex with 13 robust setae; basis expanded, anterior margin straight with six robust setae, posterior margin slightly concave with six robust setae; ischium subrectangular, anterior margin without notch; merus subequal in length to carpus, convex on posterior margin; carpus triangular; reduce; enclosed by merus and propodus, posterior lobe absent; propodus subovate, palm acute and reaching 34.5–35% along posterior margin, $1.5\times$ as long as wide, posteromedial surface of propodus with groove, anterior margin with one distal robust seta, palmar margin slightly convex with 14 robust setae; dactylus longer than palm and fitting in facial groove of propodus, attenuated distally. **Pereopod 3** (Fig. 10, P3) coxa wider than deep without pos-

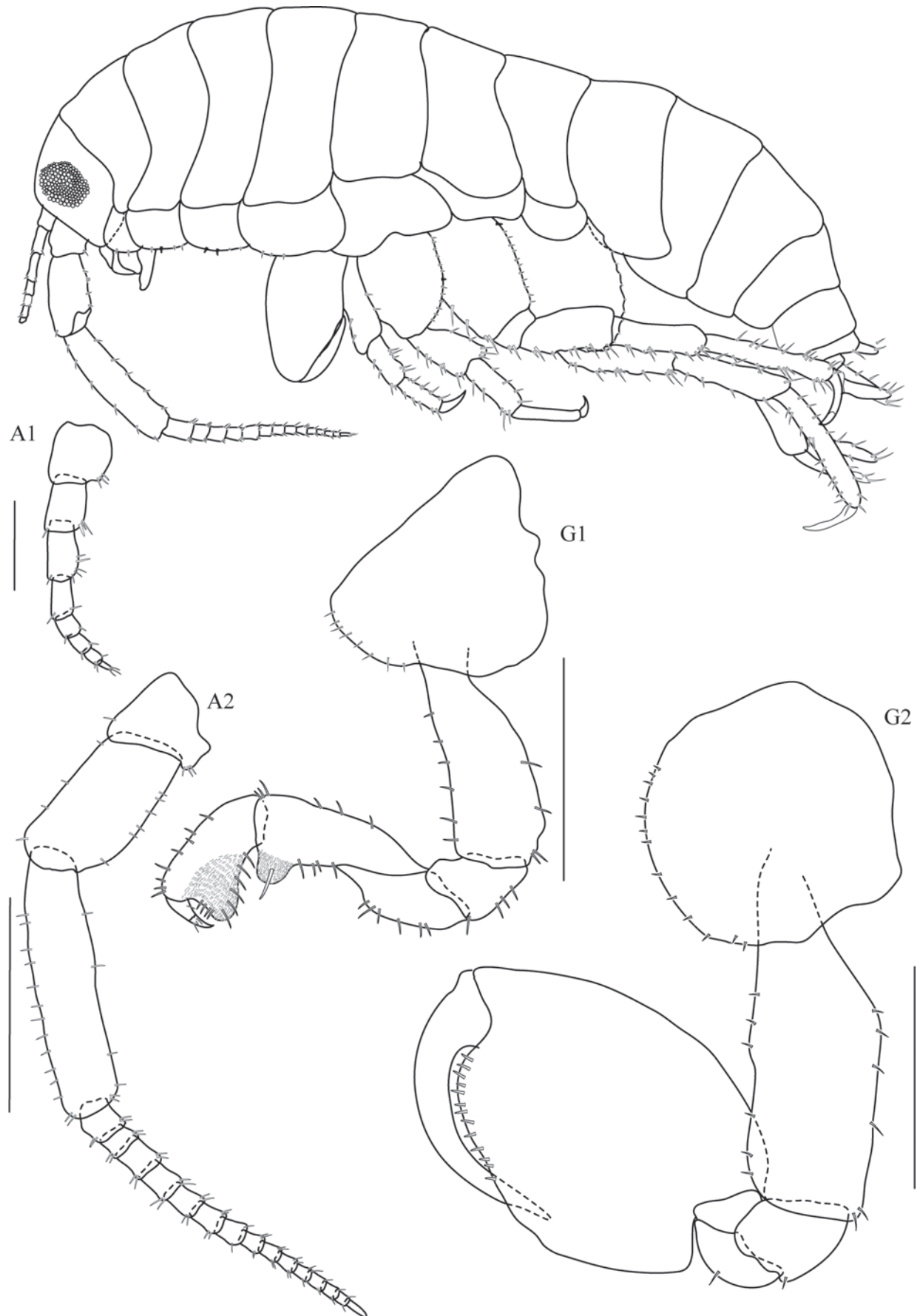


Figure 8. *Platorchestia aquaticus* sp. nov., holotype, male, 8.7 mm, THNHM-iv- 20869. Scale bars: 0.2 mm.

terior process, ventral margin slightly convex and with 15 robust setae, anterior margin straight, anterior and posterior margins naked; basis slightly expanded distally, anterior margin straight with six robust setae, posterior margin slightly crenulate, with four groups of robust setae; ischium shortest, anterior margin with rounded process; merus slightly expanded, longer than carpus and propodus, anterior margin slightly rough and with seven robust setae, posterior margin slightly straight and with ten robust setae; carpus as long as propodus, anterior margin with three robust setae, posterior margin with five robust setae; propodus anterior margin with three groups of two robust setae in each group, posterior margin with three groups of three robust setae in each group, with two distal robust setae; dactylus posterior margin with one seta on anterior margin. **Pereopod 4** (Fig. 10, P4) similar to pereopod 3 but shorter; coxa subrectangular, wider than deep, posterior margin with posterior process, ventral margin with 13 robust setae; basis slightly expanded distally, anterior margin with group of distal robust setae; ischium shortest, anterior margin convex, posterior margin straight with two robust setae; merus slightly expanded, longer than carpus and propodus, anterior margin crenulate with six robust setae, posterior margin crenulate with four groups of robust setae with two robust setae in each group; carpus as long as propodus, anterior margin straight with three robust setae, posterior margin slightly crenulate with seven robust setae; propodus slender, anterior margin with seven robust setae, posterior margin with three groups of robust setae; dactylus slender and longer than pereopod 3, thickened proximally with notch along posterior margin. **Pereopod 5** (Fig. 10, P5) coxa bilobed, anterior lobe distinctly larger than posterior lobe, ventral margin with minute setae; basis ovate, anterior margin with seven robust setae, posterior margin with eight minute setae; ischium subrectangular, shortest, posterior margin notched; merus expanded distally, subequal in length to carpus, anterior margin slightly concave with seven robust setae, posterior margin convex with seven robust setae; carpus anterior margin crenulate with three groups of robust setae with three robust setae in each group, posterior margin slightly straight; propodus slender, longer than merus and carpus, anterior margin with four groups of robust setae with three robust setae in each group, posterior margin crenulate with five robust setae; dactylus with two robust setae on anterior margin. **Pereopod 6** (Fig. 10, P6) coxa bilobed, anterior lobe very small, anterior margin straight, posterior lobe inner view posteroventral corner rounded, posterior margin perpendicular to ventral margin, ventral margin serrate and with minute setae; basis ovate, anterior margin with eight robust setae, posterior margin with six minute setae; ischium shortest; anterior margin straight, posterior margin with rounded process; merus slightly expanded, anterior margin crenulate, with nine robust setae, posterior margin convex and with six robust setae; carpus as long as merus, anterior margin crenulate and with four groups of robust setae, posterior margin crenulate with four groups of robust setae; propodus longer than merus and carpus, anterior margin slightly crenulate with 13 robust setae, posterior margin slightly crenulate with 16 robust setae; dactylus slender with subapical robust setae. **Pereopod 7** (Fig. 10, P7) not sexually dimorphic, coxa reduced, ventral margin with minute setae; basis expanded without lateral sulcus, posterodistal lobe present, anterior margin with ten robust setae, posterior margin serrate with minute setae, ischium shortest with posterior process; merus as long as carpus, anterior margin slightly crenulate with ten robust setae, posterior margin with posteroventral lobe and five robust setae; carpus oblong; anterior

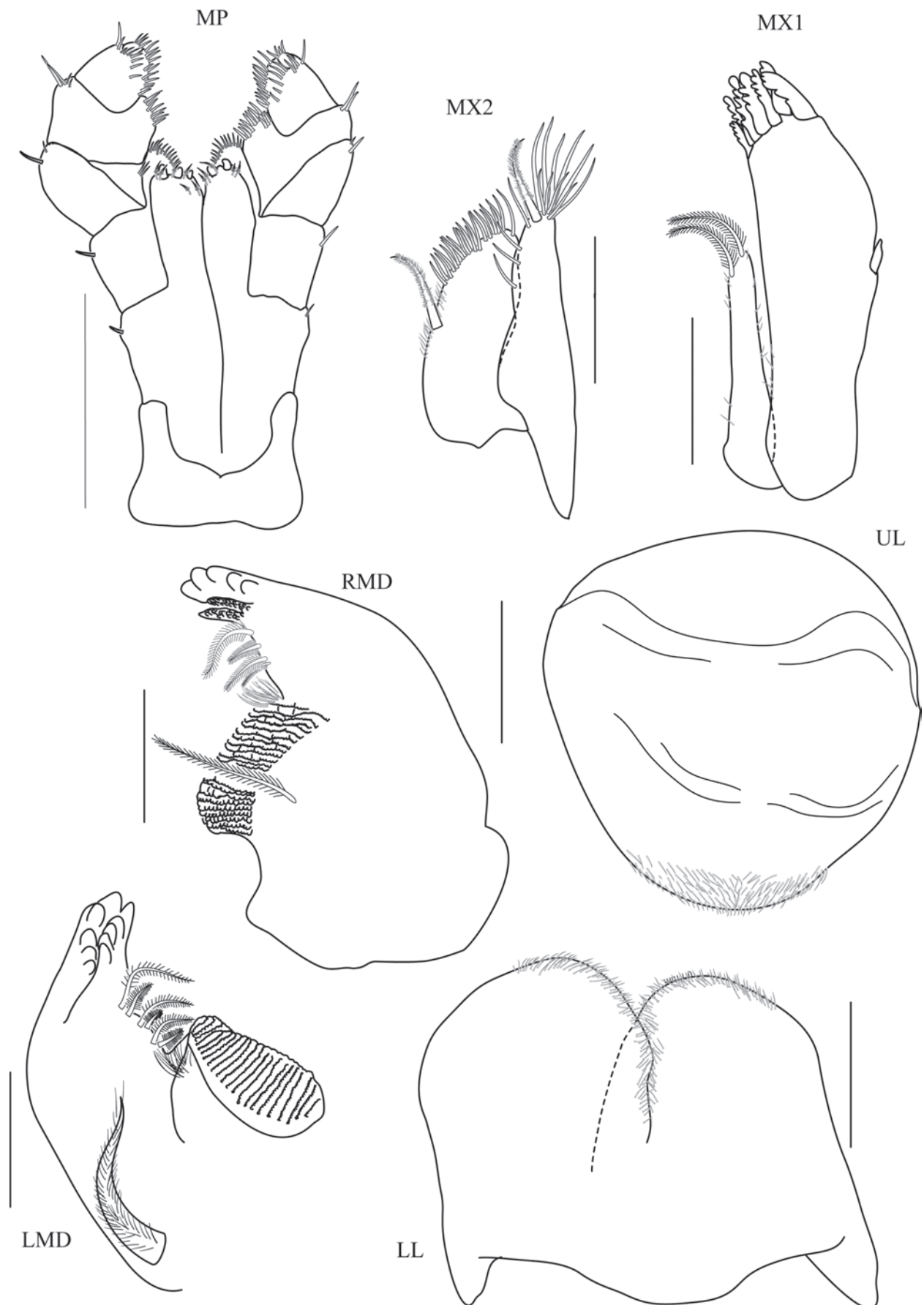


Figure 9. *Platorchestia aquaticus* sp. nov., holotype, male, 8.7 mm, THNHM-lv- 20869. Scale bars 0.2 mm.

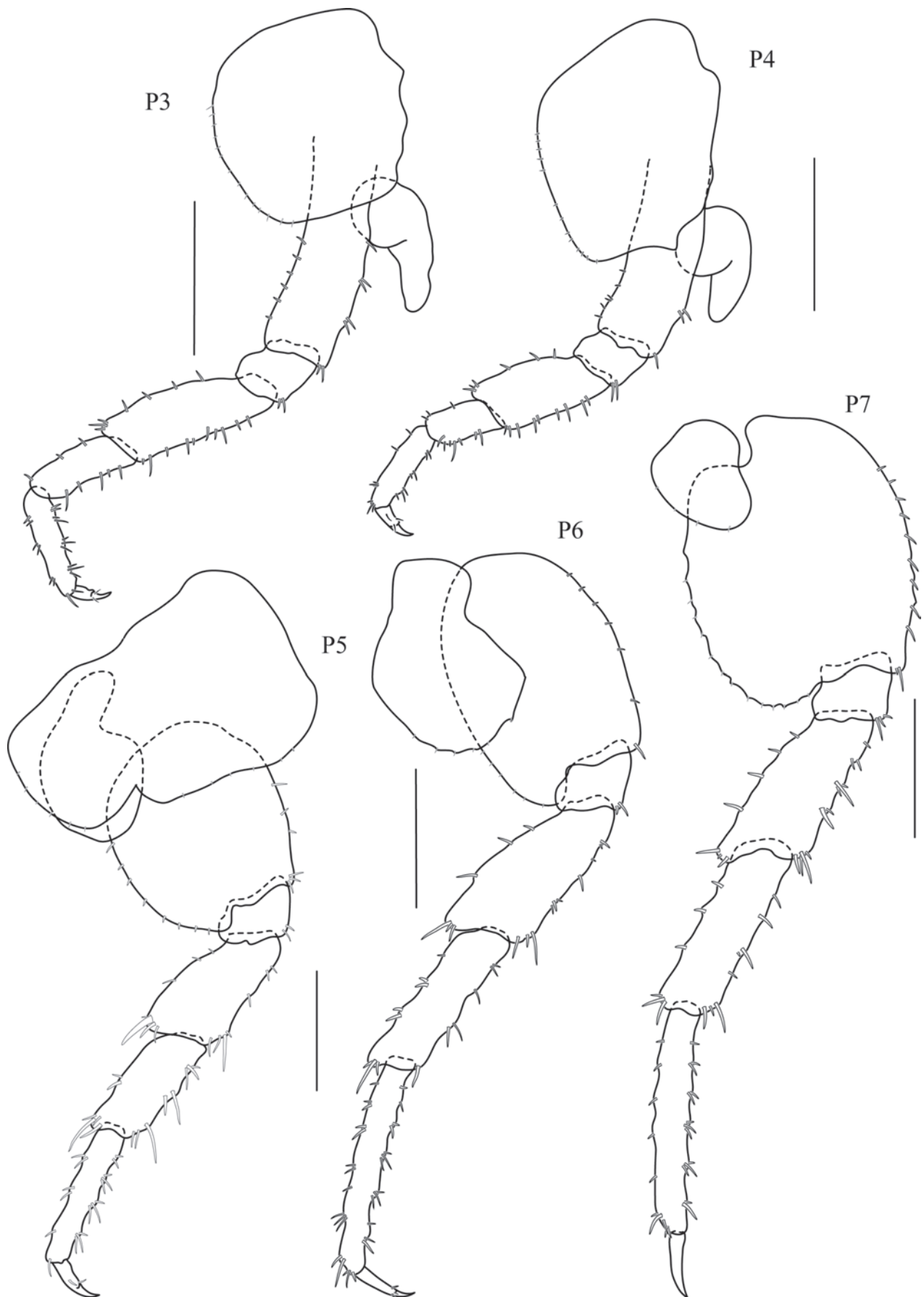


Figure 10. *Platorchestia aquaticus* sp. nov., holotype, male, 8.7 mm, THNHM-lv- 20869. Scale bars: 0.5 mm.

margin slightly crenulate with eight robust setae, posterior margin crenulate with six robust setae; propodus slender, longer than merus and carpus, 1.17× as long as carpus anterior margin with 13 robust setae, posterior margin with eight robust setae; dactylus slender, apically acute without robust setae.

Pleon. Pleopods 1–3 well developed, biramous; **Pleopod 1** (Fig. 11, PL1) peduncle longer than rami, without marginal robust setae; inner ramus as long as outer ramus, with 15 articles; outer ramus with 14 articles. **Pleopod 2** (Fig. 11, PL2) peduncle slightly longer than rami, with marginal robust setae on posterior margin; inner ramus as long as outer ramus, with 12 articles; outer ramus with 12 articles. **Pleopod 3** (Fig. 11, PL3) peduncle longer than rami, posterodistal margin with 3 robust setae; inner ramus longer than outer ramus, with 11 articles; outer ramus with ten articles. **Epimera 1–3** posterior margin slightly serrate, posteroventral corners of epimera 2 and 3 reduced. **Uropod 1** (Fig. 11, U1) peduncle 1.5× longer than rami, with seven robust setae in two rows, without distolateral robust setae; inner ramus subequal in length to outer ramus, with four marginal robust setae and three apical robust setae; outer ramus without marginal robust setae and with three apical robust setae. **Uropod 2** (Fig. 11, U2) peduncle 1.3× longer than rami, with four marginal robust setae; inner ramus with four marginal robust setae and 3 apical robust setae; outer ramus with one or two marginal robust setae and three apical robust setae. **Uropod 3** (Fig. 11, U3) peduncle subequal in length to ramus, with three robust setae; ramus slender, more than 3.5× longer than broad, with one marginal robust seta and four apical robust setae. **Telson** (Fig. 11, T) longer than broad, apically incised, with three marginal robust setae and three apical robust setae per lobe; dorsal midline entire.

Male (minor form). Based on paratype, male 7.9 mm. THNHM-lv-20871.

Head. Antenna 2 (Fig. 12, A2) peduncle not incrassate, peduncle slender.

Pereon. Gnathopod 1 (Fig. 12, G1); basis slightly expanded posteriorly, anterior margin with two robust setae, posterior margin with two robust setae; carpus 1.4× longer than propodus; propodus anterior margin with two groups of robust setae; dactylus subequal to palm. **Gnathopod 2** (Fig. 12, G2) coxa ventral margin with ten robust setae; basis anterior margin slightly concave with two robust setae, posterior margin expanded with four robust setae; ischium subrectangular, anterior margin with lobe; merus longer than carpus, convex on posterior margin; carpus triangular; reduced; enclosed by merus and propodus, posterior lobe absent; propodus subovate, palm acute reaching 45% along posterior margin, 1.4× as long as wide, palmar margin slightly convex with six robust setae; dactylus longer than palm and fitting in facial groove of propodus, attenuated distally.

Female (sexually dimorphic characters) based on allotype type, female 7.8 mm. THNHM-lv-20870.

Pereon. Antenna 2 (Fig. 12, A2♀) peduncle slender. **Gnathopod 1** (Fig. 12, G1♀) parachelate; posterior margin of merus, carpus and propodus without lobe covered in palmate setae; basis slightly expanded with posterodistal rounded process, anterior margin with six robust setae, posterior margin with three robust setae; ischium shortest, anterior margin with rounded lobe; merus triangular, posterior margin with six robust setae; carpus subtriangular, anterior margin straight with four robust setae, posterior margin convex with six robust setae in two groups, propodus subrectangular, palm acute, anterior margin with nine robust setae, posterior margin with 11 robust setae; dactylus much longer than palm, posterior margin with three robust setae. **Gnathopod 2** (Fig. 12, G2♀) mitten-shaped, coxa posterior margin with

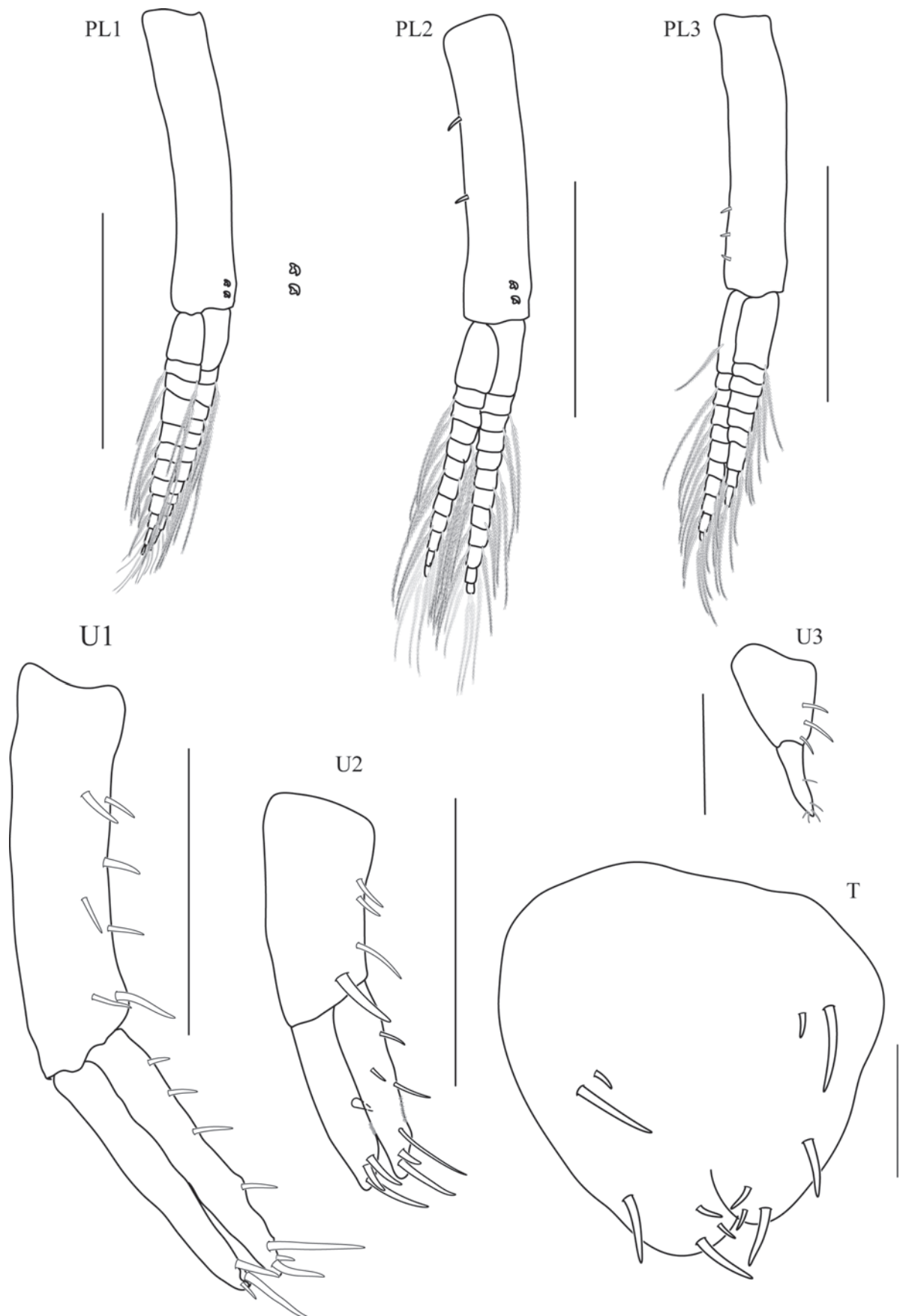


Figure 11. *Platorchestia aquaticus* sp. nov., holotype, male, 8.7 mm, THNHM-Iv- 20869. Scale bars: 0.5 mm (PL1–3); 0.2 mm (U1–2); 0.1 mm (U3, T).

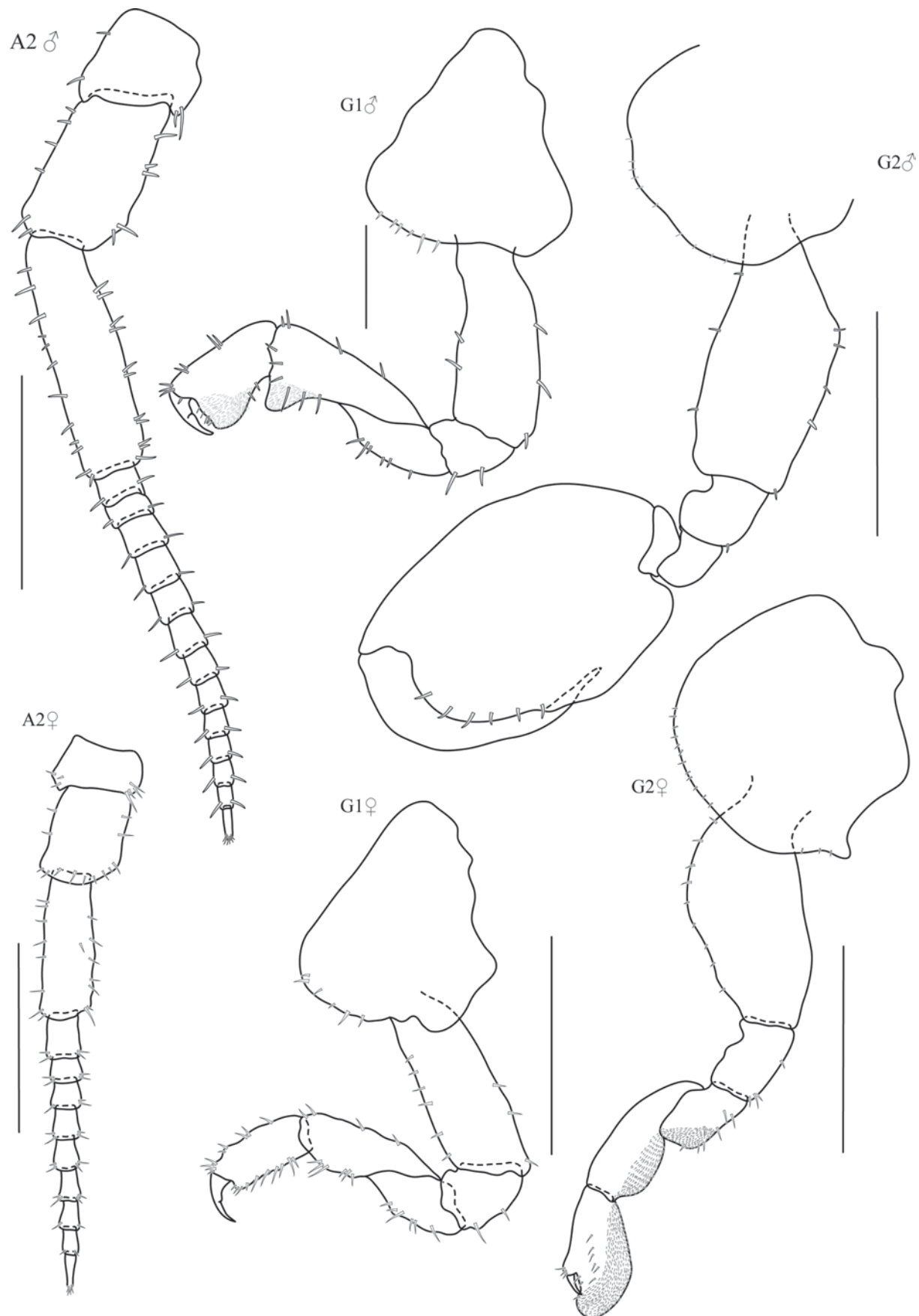


Figure 12. *Platorchestia aquaticus* sp. nov., paratype male 7.9 mm, THNHM-lv- 20871, And allotype female 7.8 mm, THNHM-lv- 20870. Scale bars: 0.5 mm (**A2**, **G2**); 0.2 mm (**G1**).

acute process, ventral margin with minute setae; basis expanded, anterior margin convex with minute setae; ischium subrectangular, anterior margin with round lobe, posterior margin with four robust setae; merus, carpus, and propodus each with lobe covered in palmate setae; merus posterior lobe well developed with seven robust setae; carpus subtriangular; propodus subovate, palm obtuse, laterodistal corner with six robust setae in one line; dactylus slender, not longer than palm.

Distribution. Thailand. Klong Mai, Bang Pu, Samut Prakan.

Etymology. Named for the freshwater habitat where the species was collected.

Remarks. *Platorchestia aquaticus* sp. nov. is the first species of *Platorchestia* recorded from Southeast Asia. The genus *Platorchestia* is classified as supra-littoral and terrestrial and is sexually dimorphic in antenna 2 and gnathopods 1 and 2. Males present two different forms in the population. The major form of *P. aquaticus*, based on the male holotype, appears similar to *P. pacifica* (Miyamoto & Morino, 2004), *P. paraplatis* (Serejo & Lowry, 2008), and *P. smithi* (Lowry, 2012) in the following characteristics: 1) mandible left lacinia mobilis 5 dentate, 2) coxae 3 and 4 as wide as deep, 3) gnathopod 1 dactylus slightly short or subequal to palm, 4) gnathopod 1 propodus subtriangular, palm transverse, 5) Uropod 3 peduncle with two or three robust setae, 6) telson longer than broad. However, *Platorchestia aquaticus* sp. nov. may be distinguished from other closely related species as follows: 1) gnathopod 1 with rudimentary cusps on dactylus (*P. pacifica* and *P. paraplatis* gnathopod 1 with distinct cusp on dactylus), 2) propodus of gnathopod 2 without notch on palmar margin, 3) uropod 1 peduncle with nine or ten robust setae in two rows, 4) uropod 3 ramus with single robust marginal seta, 5) telson with three robust marginal setae and three robust apical setae per lobe.

Key to species of the *Floresorchestia* in Southeast Asia and neighboring regions (modified from Suklom et al. 2022)

- | | | |
|------|--|--|
| 1 | Gnathopod 1 carpus subequal or ? (1.7×) to propodus..... | 2 |
| – | Gnathopod 1 carpus > 1.7× than propodus..... | |
| | <i>F. thienemanni</i> (Schellenberg, 1931) | |
| 2(1) | Gnathopod 1 carpus significantly > 1.2–1.5× than propodus..... | 3 |
| – | Gnathopod 1 carpus subequal in length to propodus | 5 |
| 3(2) | Gnathopod 1 carpus 1.2–1.3× than propodus | 4 |
| – | Gnathopod 1 carpus significantly > 1.5× than propodus..... | 10 |
| 4(2) | Telson approximately as long as broad; antenna 2 longer than head and first 3 pereonites | <i>F. seringat</i> Lowry & Springthorpe, 2015 |
| – | Telson longer than broad; antenna 2 shorter than head and first 3 pereonites | <i>F. kongsemae</i> Suklom et al., 2021 |
| 5(3) | Gnathopod 2 propodus 1.3–1.4× as long as wide..... | 6 |
| – | Gnathopod 2 propodus 1.5–1.8× as long as wide..... | 9 |
| 6(5) | Uropod 1 peduncle without robust setae... <i>F. malayensis</i> (Tattersall, 1922) | |
| – | Uropod 1 peduncle with 4–6 robust setae | 6 |
| 7(5) | Left lacinia mobilis 5-dentate..... <i>F. pongrati</i> Suklom et al., 2022 | |
| – | Left lacinia mobilis 4-dentate..... | 8 |
| 8(7) | Uropod 3 peduncle with 2 robust setae; telsonic lobe with 3 robust setae..... | <i>F. trisetosa</i> sp. nov. |
| – | Uropod 3 peduncle with 4 robust setae; telsonic lobe with 4 robust setae..... | <i>F. amphawaensis</i> Suklom et al., 2022 |

- 9(5) Left lacinia mobilis 5-dentate; uropod 1 peduncle without marginal setae; uropod 3 ramus without marginal robust setae..... ***F. yehyuensis* Miyamoto & Morino, 2008**
- Left lacinia mobilis 4-dentate; uropod 1 peduncle bearing more than 6 robust setae; uropod 3 ramus with 1 marginal seta ***F. buraphana* Wongkamhaeng et al., 2016**
- 10(3) Epimera 2 and 3 with slits **11**
- Epimera 1–3 with slit ***F. laurenae* Lowry & Springthorpe, 2015**
- Epimera 1–3 without slits..... ***F. xueli* Tong & Hou, 2021**
- 11(9) Gnathopod 2 propodus 1.4× as long as wide..... **12**
- Gnathopod 2 propodus 1.5–1.6× as long as wide..... **13**
- 12(11) Telson broader than long; Gnathopod palm without protuberance near dactylar hinge; Uropod 3 ramus without marginal robust setae ***F. hanoiensis* Hou & Li, 2003**
- Telson longer than broad; Gnathopod palm with rounded protuberance near dactylar hinge; Uropod 3 ramus with marginal robust setae ***F. floresiana* (Weber, 1892)**
- 13(11) Gnathopod palm reaching 40–50% of propodus..... **14**
- Gnathopod palm reaching 30–40% of propodus..... ***F. boonyanusithii* Wongkamhaeng et al., 2016**
- 14(13) Uropod 2 outer ramus with 2 marginal setae..... ***F. anpingensis* Miyamoto & Morino, 2008**
- Uropod 2 outer ramus with 2 marginal setae..... ***F. oluanpi* Lowry & Springthorpe, 2015**

Discussion

The genus *Floresorchestia* occupies several ecological types, including marsh hoppers, field hoppers, beach hoppers, riparian hoppers, and forest hoppers (Lowry and Myers 2019). In Thailand, species of *Floresorchestia* are either field hoppers (*F. buraphana*, *F. boonyanusithii*, and *F. kongsemae*) or marsh hoppers (*F. amphawaensis* and *F. pongrati*) (Suklom et al. 2021, 2022). *Floresorchestia trisetosa* sp. nov. is the first record of riparian hopper to be recorded in Thailand. Another riparian hopper reported from Southeast Asia is *F. thienemanni*, which is present near a waterfall among the stand of aroid *Colocasia* in central Java, Indonesia, at 1,400 m altitude. The new species *F. trisetosa* sp. nov. occupies the edge of a small creek in Muang Trat District, Trat at 0 m a.s.l.; therefore, the distribution of *Floresorchestia* is not affected by altitude.

The subfamily Floresorchestiinae is characterized by vertical slits on the ventral margin of epimera 1–3 (Myers and Lowry 2020), but *Floresorchestia xueli* lacks this character. Therefore, the taxonomic status of *F. xueli* should be revised.

Morino (2024) described the variability of certain characteristics of *Platorchestia* and *Dermaorchestia* from the coast of Japan. This variability included 12 characters. The new species *Platorchestia aquaticus* sp. nov. presents variations in the following characters: 1) article 3 of antenna 1 with four marginal robust setae; 2) antenna 2 peduncle slightly incrassate; 3) gnathopod 1 without cusps on dactylus; 4) ratio of propodus to carpus of gnathopod 1 ~ 0.67; 5) gnathopod 2 posterior margin with sharp cusps; 6) gnathopod 2 palm with smooth margins; 7) without robust setae on posterior margin of gnathopod 2; 8) ratio of carpus length to width

Table 1. A summary of the diagnostic characteristics that serve to distinguish closely related *Platorchestia* species (P = peduncle, In = inner ramus, Out = outer ramus, M = marginal, A = apical).

| Species | A2 peduncle | G1 dactylus | G1 carpus | G2 palm margin | G2 posterior notch | Pereopod 6 coxa | Pereopod 7 carpus | Uropod 1 inner ramus | Uropod 2 | Uropod 3 | Telson |
|--|---|--|---------------------------|---------------------------------|--------------------|----------------------|-----------------------|-------------------------|-----------------------------|-------------------------|--------------|
| <i>Platorchestia ano</i> Lowry & Bopiah, 2013 | 5 th longer than 4 th | Subequal in length to palm, cuspidactylate | 2× longer than propodus | rounded | – | Not protruded | slender | 3 robust setae | P 7–8 In 4 Out 2 | P 3 M 2 A 4–5 | 7 per lobe |
| <i>Platorchestia crassicornis</i> (Costa, 1867) | – | Longer than palm, – | 1.5× longer than propodus | 2 strong processes | – | – | Not strong | – | – | – | 8 per lobe |
| <i>Platorchestia exter</i> Myers & Lowry, 2023 | 5 th longer than 4 th | Shorter than palm, cuspidactylate | Less than 3× of width | Slightly mid notch | – | Distinctly protruded | very enlarged | 7 robust setae | P 7–8 In 2 Out 1 | P 1 M 3 A 3–4 | 3–5 per lobe |
| <i>Platorchestia griffithsi</i> Myers & Lowry, 2023 | 5 th longer than 4 th | Much shorter than palm | Over 1.5× of propodus | with subdistal notch | – | Not protruded | incrassate, subovoid | 6 robust setae | P 7–10 In 1 row Out 1 | P 3 M 1 A 3 | 3–5 per lobe |
| <i>Platorchestia munmui</i> Jo, 1988 | 5 th 1.4× as long as 4 th | Shorter than palm | – | Notch near posterior | acute | Not protruded | incrassate | + | – | – | 8 per lobe |
| <i>Platorchestia negevensis</i> Myers & Lowry, 2023 | 5 th longer than 4 th | Shorter than palm, cuspidactylate | – | Nearly straight | – | Not protruded | slender | 8 robust setae | P 8–9 In 6 Out 2 | P 3 M 2 A 3 | 5–7 per lobe |
| <i>Platorchestia oliveirae</i> Myers & Lowry, 2023 | 5 th longer than 4 th | Overlapping palm | – | strong mid palmar notch | – | Not protruded | Weakly expanded | 7 robust setae | P 7–10 In 2 Out – | P 1 M 2–3 A 3–4 | 5–6 per lobe |
| <i>Platorchestia pachypus</i> (Derzhavin, 1937) | – | Shorter than palm, cuspidactylate | – | rounded | – | Not protruded | Distinctly incrassate | 1 subapical 2 apical | – | – | + |
| <i>Platorchestia pacifica</i> Miyamoto & Morino, 2004 | 5 th 1.4× as long as 4 th | Shorter than palm, cuspidactylate | 0.6× as long as propodus | with subdistal notch | acute | Distinctly protruded | weakly incrassate | 7 robust setae | P 6 In 4 Out 1 | P 4 M 3 A 3 | 5 per lobe |
| <i>Platorchestia parapatensis</i> Serejo & Lowry, 2008 | – | Shorter than palm, cuspidactylate | – | Well-developed mid-palmar notch | obtuse | Distinctly protruded | incrassate | 7 robust setae | P 7–10 In 5 Out 3 | P 2–3 M 2 A 4–5 | 3–5 per lobe |
| <i>Platorchestia platensis</i> (Krøyer, 1845) | 5 th 1.4× as long as 4 th | Weakly overlapping palm | – | with subdistal notch | acute | Distinctly protruded | incrassate subovate | 7 robust setae | P 8 In 2 Out 2 | P 2–3 M 0–2 A 3–4 | 3–5 per lobe |
| <i>Platorchestia smithi</i> Lowry, 2012 | 5 subequal than article 4 | subequal in length to palm | – | Weakly notch | smooth | Distinctly protruded | slender | 11 robust setae | P 4 In 1 Out 1 | P 3 M 2 A 5 | 3–6 per lobe |
| <i>Platorchestia aquaticus</i> sp. nov. | 5 th 1.7× as long as 4 th | Shorter than palm, cuspidactylate | 1.3× longer than propodus | rounded | smooth | Not protruded | slender | 4 robust setae | P 6 In 4 Out 1–2 | P 3 M 1 A 4 | 6 per lobe |

~ 1.67; 9) pereopod 6 posterior lobe of coxa without protrusion; 10) pereopod 7 carpus not incrassate; 11) the number of robust setae on the outer margins of pleopods 2 and 3 with three and two robust setae, respectively; 12) six robust setae on the left lobe of telson.

Previously, *Platorchestia* species in the Indo-Pacific were classified as beach hoppers, primarily residing among algal debris on upper marine shores and occasionally found in estuaries and mangrove habitats (Lowry and Myers 2019, 2022; Myers and Lowry 2023). Significantly, *Platorchestia aquaticus* sp. nov. was

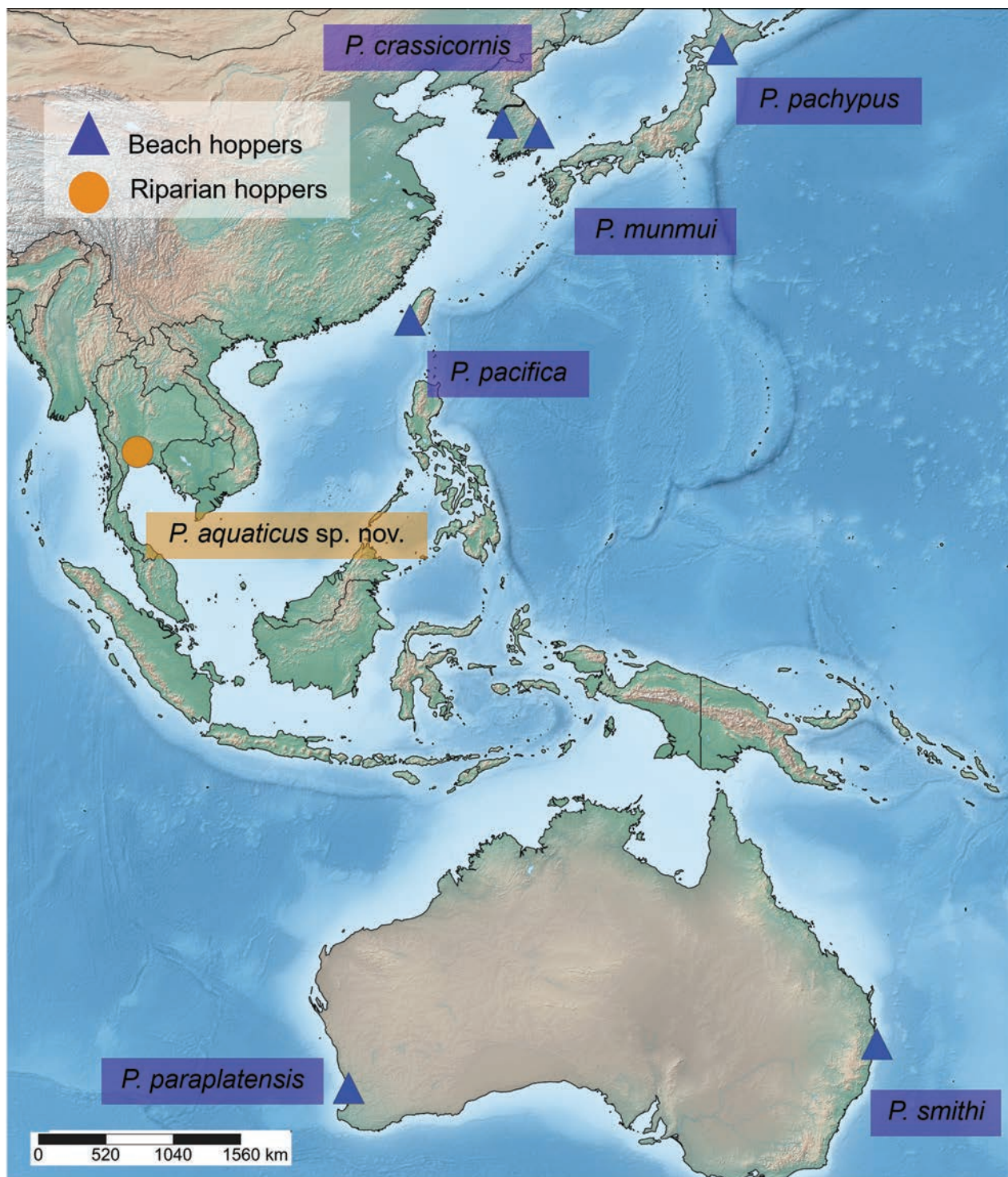


Figure 13. Ecological groups of *Platorchestia* species in the Indo-Pacific region.

found on the edge of the Mai freshwater canal, which runs parallel to Sukhumvit Road and is not directly connected to the coast (Fig. 13).

Platorchestia parapatensis and *P. griffithsi* are two extant species present on the margin of the Swan River, Western Australia and Knysna Lagoon, South Africa, respectively, which are considered to be brackish water. *Platorchestia negevensis* was found near springs and wells in the Negev desert, Israel (Morino and Ortal 1995). Due to their habitat on the edge of water

bodies, *P. negevensis* and *P. aquaticus* sp. nov. are considered to be riparian hoppers. Two hypotheses of amphipod invasion were proposed by Herbst and Dimentman (1983) as follows: the marine origin that penetrated into inland waters and the sea level decreased and left the amphipods along the regression (Herbst and Dimentman 1983). The second hypothesis possibly explains the appearance of *P. aquaticus* sp. nov. and *P. negevensis*, which may have settled down in their (type) localities after the sea level decreased.

Acknowledgments

The authors would like to thank Assoc. Prof. Dr. Supiyanit Maiphae, who discussed and helped us revise our manuscript.

Additional information

Conflict of interest

The authors have declared that no competing interests exist.

Ethical statement

This study was carried out in strict accordance with the recommendations in Animal Care & Use Guidelines of Institutional Animal Care and Use Committee of Burapha University (IACUC BUU) for sampling the amphipod.

Funding

The project was supported in part by the Faculty of Science, Kasetsart University, the capacity building of KU students on internationalization program: KUCSI of the international affairs division, Kasetsart University and Centre of Excellence on Biodiversity (BDC) Office of Higher Education Commission (KUCSI221580M7).

Author contributions

Methodology: TSK. Writing – original draft: AS. Writing – review and editing: AAR, KW.

Author ORCIDs

Tosaphol Saetung Keetapithchayakul  <https://orcid.org/0000-0001-7565-4701>

Azman Abdul Rahim  <https://orcid.org/0000-0002-8964-6638>

Koraon Wongkamhaeng  <https://orcid.org/0000-0001-7671-8869>

Data availability

All of the data that support the findings of this study are available in the main text.

References

- Azman BAR, Wongkamhaeng K, Dumrongrojwattana P (2014) Description of *Floresorchestia samroiiodensis*, a new species of landhopper (Crustacea, Amphipoda, Talitridae) from Thailand. *Zoosystematics and Evolution* 90(1): 7–19. <https://doi.org/10.3897/zse.90.7085>
- Barnard KH (1916) Contributions to the crustacean fauna of South Africa. 5. The Amphipoda. *Annals of the South African Museum* 15: 105–302. <https://doi.org/10.5962/bhl.title.10646>

- Bhoi G, Myers AA, Kumar RK, Patro S (2024) A new species of the genus *Floresorchestia* (Crustacea, Amphipoda, Talitridae) from Chilika Lagoon, east coast of India. *Zootaxa* 5493(5): 590–598. <https://doi.org/10.11646/zootaxa.5493.5.7>
- Bichang'A JS, Kioko EN, Liu H, Li S, Hou Z (2021) Two species of Talitridae (Crustacea, Amphipoda) from Kenya. *Zootaxa* 4927(3): 331–358. <https://doi.org/10.11646/zootaxa.4927.3.2>
- Bousfield EL (1971) Amphipoda of the Bismarck Archipelago and adjacent Indo-Pacific islands (Crustacea). *Steenstrupia* 1: 255–293.
- Bousfield EL (1982) The amphipod superfamily Talitroidea in the northeastern Pacific region. Family Talitridae. Systematics and distributional ecology. National Museum of Natural Science, Publications in Biological Oceanography, 11, [i–vii] 73 pp.
- Bousfield EL (1984) Recent advances in the Systematics and Biogeography of Landhoppers (Amphipoda: Talitridae) of the Indo-Pacific Region. *Bishop Museum Special Publications* 72: 169–205.
- Bulycheva AI (1957) Sea fleas of the seas of the USSR and adjacent waters Amphipoda-Talitroidea. *Opredeliteli po faune SSSR* 65: 1–186.
- Costa A (1867) Saggio della collezione di Crostacei del Mediterraneo del Museo zoologico della Università di Napoli spedito alla Esposizione di Parigi del 1867. *Annuario del Museo zoologico della R. Università di Napoli* 4: 38–46.
- Derzhavin AN (1937) Talitridae of the Soviet coast of the Japan Sea. *Issledovaniya Fauny Morej SSSR* 23: 87–112. [in Russian with English summary]
- Friend JA, Richardson AMM (1986) Biology of Terrestrial Amphipods. *Annual Review of Entomology* 31(1): 25–48. <https://doi.org/10.1146/annurev.en.31.010186.000325>
- Herbst GN, Dimentman C (1983) Distributional patterns and habitat characteristics of Amphipoda (Crustacea) in the inland waters of Israel and Sinai. *Hydrobiologia* 98: 17–24. <https://doi.org/10.1007/BF00019247>
- Jo YW (1988) Talitridae (Crustacea-Amphipoda) of the Korean coasts. *Beaufortia* 38(7): 153–179.
- Krøyer H (1845) Karcinologiske bidrag. *Naturhistorisk tidsskrift* 4: 141–166.
- Lowry JK (2012) Talitrid amphipods from ocean beaches along the New South Wales coast of Australia (Amphipoda, Talitridae). *Zootaxa* 3575(1): 1–26. <https://doi.org/10.11646/zootaxa.3575.1.1>
- Lowry JK, Bopiah A (2013) The talitrid amphipods of Tonga (Crustacea, Amphipoda, Talitridae). *Zootaxa* 3681: 347–370. <https://doi.org/10.11646/zootaxa.3681.4.2>
- Lowry JK, Myers AA (2019) New genera of Talitridae in the revised Superfamily Talitroidea Bulycheva 1957 (Crustacea, Amphipoda, Senticaudata). *Zootaxa* 4553(1): 1–100. <https://doi.org/10.11646/zootaxa.4553.1.1>
- Lowry JK, Myers AA (2022) Platorchestiinae subfam. nov. (Amphipoda, Senticaudata, Talitridae) with the description of three new genera and four new species. *Zootaxa* 5100(1): 1–53. <https://doi.org/10.11646/zootaxa.5100.1.1>
- Lowry JK, Springthorpe RT (2009) The genus *Floresorchestia* (Amphipoda: Talitridae), on Cocos (Keeling) and Christmas Islands. *Memoirs of the Museum of Victoria* 66(1): 117–127. <https://doi.org/10.24199/j.mmv.2009.66.13>
- Lowry JK, Springthorpe RT (2015) The tropical talitrid genus *Floresorchestia* (Crustacea, Amphipoda, Talitridae). *Zootaxa* 3935: 1–68. <https://doi.org/10.11646/zootaxa.3935.1.1>
- Lowry JK, Springthorpe RT (2019) Talitrid amphipods from India, East Africa and the Red Sea (Amphipoda, Senticaudata, Talitroidea, Talitridae). *Zootaxa* 4638(3): 351–378. <https://doi.org/10.11646/zootaxa.4638.3.3>

- Miyamoto H, Morino H (2004) Taxonomic studies on the Talitrid (Crustacea, Amphipoda) from Taiwan. II. The genus *Platorchestia*. Publications of the Seto Marine Biological Laboratory 40: 67–96. <https://doi.org/10.5134/176317>
- Miyamoto H, Morino H (2008) Taxonomic studies on the Talitridae (Amphipoda) From Taiwan, III. The Genus *Floresorchestia* Bousfield, 1984. Crustaceana 81(7): 837–860. <https://doi.org/10.1163/156854008784771667>
- Morino H (2024) Variations in the characters of *Platorchestia pacifica* and *Demaorchestia joi* (Amphipoda, Talitridae, Talitrinae) with revised diagnoses based on specimens from Japan. Diversity 16(1): 31. <https://doi.org/10.3390/d16010031>
- Morino H, Ortal R (1995) Two *Platorchestia* Species (Amphipoda, Talitridae) from Israel. Crustaceana 68(7): 824–832. <https://doi.org/10.1163/156854095X00971>
- Myers AA, Lowry JK (2020) A phylogeny and classification of the Talitroidea (Amphipoda, Senticaudata) based on interpretation of morphological synapomorphies and homoplasies. Zootaxa 4778(2): 281–310. <https://doi.org/10.11646/zootaxa.4778.2.3>
- Myers AA, Lowry JK (2023) The beach-hopper genus *Platorchestia* (Crustacea: Amphipoda: Talitridae) on Atlantic Ocean coasts and on those of associated seas. Records of the Australian Museum 75(4): 485–505. <https://doi.org/10.3853/j.2201-4349.75.2023.1887>
- Rafinesque CS (1815) Analyse de la nature ou Tableau de l'Universitet des corps organises. Aux deipens de l'auteur, Palerme, 224 pp. [in French]. <https://doi.org/10.5962/bhl.title.106607>
- Richardson AMM (1991) Two new species of landhoppers (Crustacea: Talitridae) from O'ahu, Hawaiian Islands, with redescription of *Platorchestia pickeringi* and key to landhoppers of O'ahu. Bishop Museum Occasional Papers 31: 185–201.
- Serejo CS, Lowry JK (2008) The coastal Talitridae (Amphipoda: Talitroidea) of southern and western Australia, with comments on *Platorchestia platensis* (Krøyer, 1845). Records of the Australian Museum 60(2): 161–206. <https://doi.org/10.3853/j.0067-1975.60.2008.1491>
- Shorthouse DP (2010) SimpleMappr, an online tool to produce publication-quality point maps. <http://www.simplemappr.net>
- Suklom A, Danaisawadi P, Wongkamhaeng K (2021) *Floresorchestia kongsemae* sp. n. a new species (Crustacea: Amphipoda: Talitridae) from Kasetsart University, Bangkok, Thailand. Biodiversity Data Journal 9: e63197. <https://doi.org/10.3897/BDJ.9.e63197>
- Suklom A, Keetapithchayakul TS, Azman BAR, Wongkamhaeng K (2022) Two new species of the genus *Floresorchestia* (Crustacea, Amphipoda, Talitridae) from Amphawa Estuary, Samut Songkhram Province, Thailand. Zoosystematics and Evolution 98(2): 285–303. <https://doi.org/10.3897/zse.98.83749>
- Tong Y, Hao J, Liu H, Li S, Hou Z (2021) *Floresorchestia xueli*, a new terrestrial crustacean (Amphipoda, Talitridae) from Yunnan, China. Zootaxa 4991(2): 318–330. <https://doi.org/10.11646/zootaxa.4991.2.5>
- Weber M (1892) Der Susswasser-Crustaceen des Indischen Archipels, nebst bemerkungen uber die Susswasser-Fauna im Allgemeinen. Zoologiscleze Ergebnisse einer Reise nach niederlaizdischen Ost-indien 2: 528–571. https://doi.org/10.1163/9789004599048_009
- Wongkamhaeng K, Dumrongrojwattana P, Pattaratumrong MS (2016) Two new species of *Floresorchestia* (Crustacea, Amphipoda, Talitridae) in Thailand. Zookeys (635): 31–51. <https://doi.org/10.3897/zookeys.635.10454>
- Zimmer A, Araujo PB, Bond-Buckup G (2009) Diversity and arrangement of the cuticular structures of *Hyalella* (Crustacea: Amphipoda: Dogielinotidae) and their use in taxonomy. Zoologia (Curitiba) 26: 127–142. <https://doi.org/10.1590/S1984-46702009000100019>

Novel brood-site pollination mutualism between sympetalous *Heterosmilax* (Smilacaceae, Liliales) and a cecidomyiid gall midge (Cecidomyiidae, Diptera) breeding in fallen male flowers

Makoto Kato¹, Atsushi Kawakita²

¹ Graduate School of Human and Environmental Studies, Kyoto University, Sakyo, Kyoto 606-8501, Japan

² The Botanical Gardens, Graduate School of Science, The University of Tokyo, Tokyo 112-0001, Japan

Corresponding author: Makoto Kato (makotokato1313@gmail.com)

Abstract

Heterosmilax is a unique dioecious genus of Smilacaceae (Liliales, Monocotyledon) in that both male and female flowers are sympetalous, ellipsoid, and almost closed. Our field observations in the Ryukyu Islands of Japan showed that *H. japonica* flowers are visited and pollinated exclusively by females of one cecidomyiid gall midge species, whose larvae breed in fallen male flowers and feed initially on pollen and later on floral tissue. This is the first example of obligate gall midge-associated brood-site pollination mutualism in which the pollinator brood site is fallen male flowers. The pollinator gall midge is described as *Dasineura heterosmilacicola* **sp. nov.** (tribe Dasineurini, supertribe Lasiopteridi). A molecular phylogenetic analysis reveals that it derived from a flower parasite or flower-bud galler. The sympetalous ellipsoid male flowers are thought to have adapted to allow pollen dusting on the post-abdomen of the pollinator midge, in addition to protecting and incubating internal pollinator larvae in the fallen flowers.

Key words: *Dasineura*, dioecy, obligate pollination mutualism, sympetaly



Academic editor: Netta Dorchin

Received: 10 January 2025

Accepted: 20 March 2025

Published: 22 April 2025

ZooBank: <https://zoobank.org/EAED3361-791D-4D66-A28F-BEEBDA942F11>

Citation: Kato M, Kawakita A (2025) Novel brood-site pollination mutualism between sympetalous *Heterosmilax* (Smilacaceae, Liliales) and a cecidomyiid gall midge (Cecidomyiidae, Diptera) breeding in fallen male flowers. ZooKeys 1234: 397–416. <https://doi.org/10.3897/zookeys.1234.146453>

Copyright: © Makoto Kato & Atsushi Kawakita. This is an open access article distributed under terms of the Creative Commons Attribution License (Attribution 4.0 International – CC BY 4.0).

Introduction

In plant–insect pollination mutualism, pollinators visit flowers to seek floral rewards, whether portable, such as nectar and pollen, or non-portable, such as floral tissue and seeds. In the typical, widespread form of pollination mutualism, pollinators collect portable rewards. However, there are also unique, always female pollinators that visit flowers and oviposit on them, such that their larvae utilize non-portable rewards. In this interaction, called brood-site pollination mutualism (Sakai 2002a), the partners are usually highly specific to each other. Especially when seeds are the reward, coevolution between the plant and the seed-parasitic pollinator under conditions of a plant–herbivore chemical arms race causes a highly specific obligate mutualism (Riley 1892; Kato and Kawakita 2017).

The insect groups identified that take part in brood-site pollination mutualism thus far include Curculionidae (Coleoptera) in *Zamia* (Zamiaceae: Tang 1987), *Eupomatia* (Eupomatiaceae: Armstrong and Irving 1990) and

various genera of Arecaceae (Henderson 1986), thrips (Thysanoptera) in *Chloranthus* (Chloranthaceae: Luo and Li 1999), Phoridae (Diptera) in *Aristolochia* (Aristolochiaceae: Sakai 2002b), and Drosophilidae (Diptera) in *Nypa* (Arecaceae: Essig 1973) and several genera of Araceae (Carson and Okada 1980; Takenaka et al. 2006; Takano et al. 2012).

The gall midges (Cecidomyiidae, Nematocera, Diptera) are the smallest, but they represent the most diverse insect clade participating in brood-site pollination mutualism. Gall midges typically lay eggs in the young tissues of plants, inducing plant tissue overgrowth that provides a food source for their larvae, which grow by feeding on the induced galls (Gagné 1989). However, some species of midges oviposit on flowers without inducing plant galls; these species contribute to the pollination of the host flower, which in turn supports larval growth. This type of brood-site pollination mutualism of gall midges occurs in *Kadsura* (Schisandraceae: Luo et al. 2017, 2018), *Illicium* (Schisandraceae: Luo et al. 2010), *Siparuna* (Monimiaceae: Feil 1992), *Aspidistra* (Asparagaceae: Vislobokov et al. 2014), *Artocarpus* (Moraceae: Sakai et al. 2000; Gardner et al. 2018), and *Phyllanthus* (Phyllanthaceae: Kawakita et al. 2022; Elsayed and Kawakita 2022) (Table 1). However, in addition to brood-site pollination mutualism, gall midges contribute to pollination, such as in *Amborella* (Amborellaceae: Thien et al. 2003), *Kadsura* (Schisandraceae: Yuan et al. 2008), *Schisandra* (Schisandraceae: Yuan et al. 2007) and *Anthurium* (Araceae: Etl et al. 2022). Why various types of gall midge pollination systems have evolved several times in basal angiosperm clades (Luo et al. 2018) is unclear.

Molecular phylogenetic studies have revealed that most of the diversity of Cecidomyiidae followed the diversification of angiosperms, and that transitions from mycophagy to phytophagy occurred only once or twice in the evolution of the subfamily (Dorchin et al. 2019). The diversification of Cecidomyiidae is reflected in the high host specificity of its genera (Carneiro et al. 2009). Among the diverse clades of gall midges, three genera of one supertribe, Cecidomyiidi (*Resseliella*, *Asphondylia* and *Clinodiplosis*), have been shown to take part in brood-site pollination (Table 1).

Recently, we found a further example of gall-midge-associated pollination mutualism, in a monocot clade growing on the islands of the Ryukyu Archipelago, Japan. Smilacaceae is a monocot family of Liliales characterized by tuberous or stoloniferous rhizomes, reticulate leaf venation, paired petiolar tendrils, radial dioecious flowers, umbellate inflorescences, fleshy berries, and a mostly woody, climbing habit (Qi et al. 2013). This family of ~210 species is widely distributed in the tropics and subtropics, but it has diversified especially in Asia and the Americas (Qi et al. 2013). Smilacaceae has been classified into two genera, *Smilax* and *Heterosmilax*, differentiated, respectively, by their schizopetalous and sympetalous ellipsoid flowers (Koyama 1984). Recent morphological and molecular phylogenetic studies, however, have shown that *Heterosmilax* is a monophyletic group within the genus *Smilax* and should be synonymized under *Smilax* (Qi et al. 2013). Schizopetalous flowers of some *Smilax* species emit a carrion-like odor and are visited and pollinated by pollen-seeking insects such as bees, beetles, and flies (Sawyer and Anderson 1998). By contrast, the pollination system of sympetalous ellipsoid flowers of *Heterosmilax* was unknown.

Table 1. A list of plants taking part in brood-site pollination mutualism with gall midges.

| Plant | | | | | Pollinator cecidomyiid midge | | | References |
|------------------|----------------|------------------------------|----------------|------------------------------------|------------------------------|---------------|---|---|
| Order | Family | Genus | Sex expression | Brood site | Supertribe | Tribe | Genus | |
| Austrobaileyales | Schisandraceae | <i>Kadsura</i> (in part) | monoecious | resin chamber of male flower | Cecidomyiidi | ? | <i>Resseliella</i> | Fan et al. 2011; Luo et al. 2017 |
| Austrobaileyales | Schisandraceae | <i>Illicium</i> (in part) | hermaphrodite | heated brood chamber | Cecidomyiidi | ? | <i>Clinodiplosis</i> | Luo et al. 2010 |
| Laurales | Monimiaceae | <i>Siparuna</i> | monoecious | male flower | Cecidomyiidi | Asphondyliini | <i>Asphondylia</i> (= <i>Asynapta</i>) | Feil 1992 |
| Asparagales | Asparagaceae | <i>Aspidistra</i> (in part) | hermaphrodite | anther | Cecidomyiidi | | not identified | Vislobokov et al. 2014 |
| Liliales | Smilacaceae | <i>Heterosmilax</i> | dioecious | fallen male flower | Lasiopteridi | Dasineurini | <i>Dasineura</i> | This study |
| Rosales | Moraceae | <i>Artocarpus</i> (in part) | monoecious | fungus-infected male inflorescence | Cecidomyiidi | ? | <i>Clinodiplosis</i> | Gardner et al. 2018 |
| Malpighiales | Phyllanthaceae | <i>Phyllanthus</i> (in part) | monoecious | galled male flower bud | Cecidomyiidi | ? | <i>Clinodiplosis</i> | Kawakita et al. 2022; Elsayed and Kawakita (2022) |

Our preliminary observations suggest that the *Heterosmilax* flowers are visited exclusively by cecidomyiid midges of the genus *Dasineura* and that the midge larvae breed in male flowers. *Dasineura* is a species-rich genus of Cecidomyiidae (tribe Oligotrophini, supertribe Lasiopteridi, subfamily Cecidomyiidae) comprising 476 species (Gagné and Jaschhof 2021) and generally associated with the flowers of diverse angiosperms (Gagné 1989). Thus, the newly identified interaction between *Heterosmilax* and *Dasineura* gall midges provides novel insights into how a flower parasite became a mutualistic pollinator, and how brood-site pollination mutualism has evolved in a monocot clade. In the following, we describe the pollination system of *Heterosmilax japonica* and report the pollinator gall midge as a new species. The phylogenetic position of the pollinator based on a molecular phylogenetic study and the evolution of pollination mutualism are discussed.

Materials and methods

Studied plants and field sites

Heterosmilax japonica grows along the fringes of evergreen forests in the Ryukyu Archipelago and bears flowers from March to August. Insect visits to the flowers were observed directly at Amami-Ōshima Island (Higashi-nakama: 28.2856°N, 129.4355°E, altitude 120 m), Iriomote Island (Funaura: 24.3987°N, 123.8040°E, altitude 20 m, and Komi: 24.2929°N, 123.8964°E, altitude 140 m) and Yonaguni Island (Mt Kubura: 24.4572°N, 122.9586°E, altitude 90 m) and photographed using time-lapse and video cameras. Insect behavior was also observed directly. Samples of female flowers were obtained and examined for pollen attachment on stigmas and insect herbivory on flowers. Male flowers were sampled and examined for pollen production in anthers and insect infestation of pollen and petals. Because preliminary observation suggested that male flowers fall 1 day after they bloom, fallen male flowers were collected and examined for insect infestation on floral tissue.

Observation of floral visitors

Insect visitors to male and female flowers were observed using a time-lapse camera on 4–5 June 2018 on Yonaguni Island, on 14–16 June on Amami Island, on 15–16 April 2023 at Funaura, Iriomote Island, and on 5–6 April 2024 at Komi, Iriomote Island. Some of the visitors were collected directly into killing jars for later identification and determination of pollen attachment.

After each observation, 60–200 female flowers visited by insects were collected and examined for pollen attachment on the stigmas and for deposited eggs. In addition, 200–300 male flowers visited by the insects were collected and examined for eggs/larvae of the insects. The male flowers were placed in plastic cases filled with vermiculite and kept moist in an incubator at 25 °C for about a month.

The gall midges collected on the flowers, having emerged in the rearing cases, were either pinned using micropins (stainless steel pins A1, Watkins & Doncaster Co.) and freeze-dried in a refrigerator or preserved in 99% and 70% ethanol. Some of these specimens were later dissected according to the method outlined by Gagné (1989) and then mounted on permanent microscopic slides using Euparal (Waldeck GmbH & Co. KG). Gall-midge larvae collected from male flowers were also preserved in 99% and 70% ethanol. The pupa is unknown. The specimens and slides were examined under a microscope (VHS-7000; Keyence). The terminology used to describe adult morphology followed that of McAlpine et al. (1981). The type specimens are deposited at the National Museum of Nature and Science, Tokyo (NSMT), and other specimens at Kyoto University Museum, Japan.

Phylogeny of the pollinator gall midge

As *Dasineura* is a species-rich, polyphyletic genus (Dorchin et al. 2019), the approximate phylogenetic position of the gall midge associated with *Heterosmilax japonica* was investigated by sequencing the nuclear 28S ribosomal RNA gene and the mitochondrial cytochrome c oxidase subunit I (COI) gene of one adult gall midge collected on a flower at Funaura, Iriomote Island. The obtained sequences were analyzed using the 28S rRNA and COI gene dataset of Dorchin et al. (2019), who studied the phylogenetic relationships of all Cecidomyiinae (the largest subfamily of Cecidomyiidae). Two additional adults and 10 larvae collected on the flowers at Funaura were further sequenced for the mitochondrial COI gene to confirm that the adults and larvae belonged to the same species.

Genomic DNA was extracted using the NucleoSpin Tissue DNA extraction kit (Macherey-Nagel, Germany). The primers used for the PCR were D2 and D3R (Belshaw et al. 2001) and LCO and HCO (Folmer et al. 1994) for the 28S rRNA and COI genes, respectively. The PCR conditions were those described in Dorchin et al. (2019). The PCR products were purified using the ExoSAP-IT cleanup kit (Thermo Fisher Scientific), and sequencing was outsourced to FASMAC (Kanagawa, Japan). Electropherograms and multiple sequence alignments were assessed using MEGA v. 11 software (Tamura et al. 2021). Multiple sequence alignments were conducted using ClustalW, as implemented in MEGA, with default settings; obvious misalignments were corrected by visual inspection. A maximum-likelihood (ML) analysis of the concatenated 28S and COI dataset was performed using raxmlGUI 2.0 software (Edler et al. 2021).

The nucleotide substitution model that best fit each gene partition was selected under default settings, and the resulting TPM3uf+I+G4 and GTR+I+G4 models were used for the 28S and COI gene partitions, respectively. Branch support was evaluated in a bootstrap analysis with 1,000 replications. Newly obtained sequences were deposited in GenBank under accession numbers PV203684 and PV199165–PV199177 (see the Suppl. material 1 for the accession numbers of all sequences used in the ML analysis).

Results

Pollination mutualism

Heterosmilax japonica is a woody, dioecious climber growing along the edges of evergreen forests, with flowers on solitary umbels at the basal leaf axils of branches (Fig. 1A). The flowering season is from March to July, but in this study male flowers were observed only in March. On each umbel, 10–30 male and 8–20 female flowers are borne on long peduncles (Fig. 1B, C). Both male and female flowers are ellipsoid, with three fused perianths: male flowers (Fig. 1B) are ellipsoid and slenderer than the ovoid female flower (Fig. 1C). A male flower has three (rarely six) stamens, whose filaments are fused at the basal 1/4–1/2 portion (Fig. 1D). At flowering, the connate perianth dehisces only at the tip, and anthers are concealed in the connate perianths. A female flower has three stigmas, which protrude slightly from the connate perianths at flowering (Fig. 1F, G). Both male and female flowers are pendent and almost closed at flowering (Fig. 1B, C).

Our observation of insect visits to *Heterosmilax* flowers showed that both male and female flowers were seldom visited by any insects, except during the early morning. Just before sunrise, male flowers started dehiscing the tip of the perianth tube. Around the same time, minute gall midges started to swarm around male *Heterosmilax* flowers, visiting them successively (Fig. 1H). The midge belongs to the genus *Dasineura* (Cecidomyiidae) and is described as a new species in the following section. Male flowers were visited only by this species of gall midge (Cecidomyiidae, genus *Dasineura*), but the gregarious visits of the midges to the flowers ended within an hour. Midge visits to *Heterosmilax* flowers were observed from 6:12 to 6:52 on 15 April 2023 at Funaura, Iriomote Island, from 7:15 to 7:33 on 6 April 2024 at Komi, Iriomote Island, and from 7:34 to 8:25 on 5 March 2019 at Mt Kubura, Yonaguni Island. Each female midge visited a newly opened pendent male flower, walked to the opening of the perianth, extended its abdomen, and then inserted it into the perianth tube from the apical opening to lay eggs. The average time spent by a *Dasineura* midge on a male flower was 109 ± 46 s on 6 April 2024 at Iriomote Island and 97 ± 41 s on 5 March 2019 at Yonaguni Island.

All *Dasineura* midges that visited male *Heterosmilax* flowers were females, whose bodies, especially the abdomen, were dusted by plant pollen (Figs 1K, M, 2B–D). Dipteran eggs were found on the inner walls of the connate perianths of male flowers that had been visited by the *Dasineura* midge.

Almost all male flowers, together with their peduncles, fell the day after anthesis, i.e., the flowering period of a male flower is 24–36 h. Dissecting the fallen male flowers revealed that most contained one or two (rarely three) midge larvae (Fig. 2F, G), and rarely thrips (Fig. 1E). The midge larvae were initially

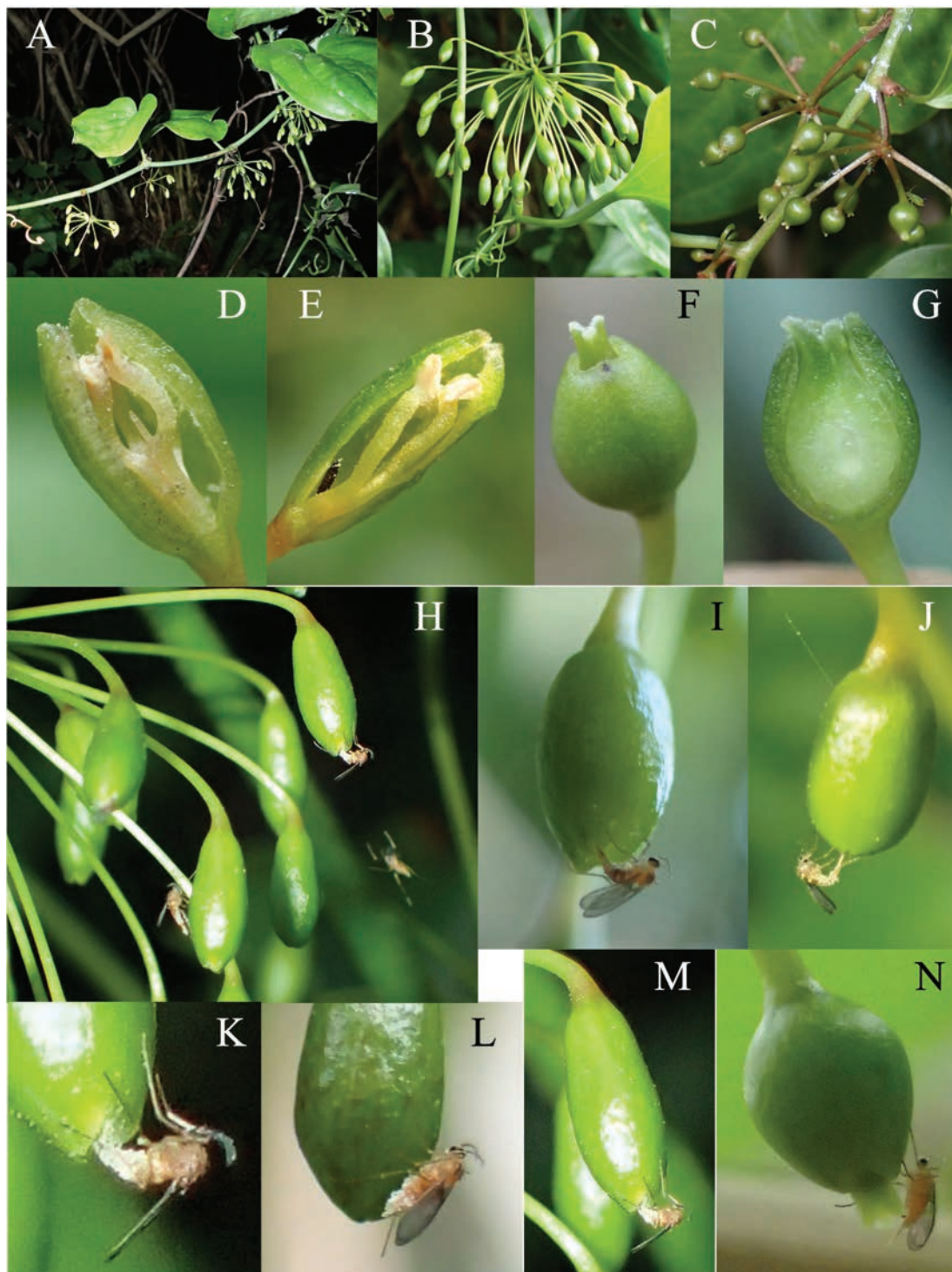


Figure 1. Male and female flowers of *Heterosmilax japonica* visited by a *Dasineura* midge **A** male plant with male inflorescences **B** male inflorescence **C** female inflorescence **D** cross section of a male flower **E** male flower visited by thrips **F** female flower **G** cross-section of a female flower **H–M** male flowers visited by *Dasineura* gall midges **N** female flower visited by a *Dasineura* midge. Observations were made on Amami-Ōshima Island (**A**, **C**, **L**, **N**), Iriomote Island (**D**, **F–K**), and Yonaguni Island (**B**, **E**, **M**).

found feeding on pollen and later infesting the perianth and filaments of the fallen flowers. Full-grown larvae were left the flowers and pupated in vermiculite in a plastic case. From the rearing case containing the flowers that bloomed on 5 March 2019, adults emerged on 29–31 March. Thus, the time spent for growth,

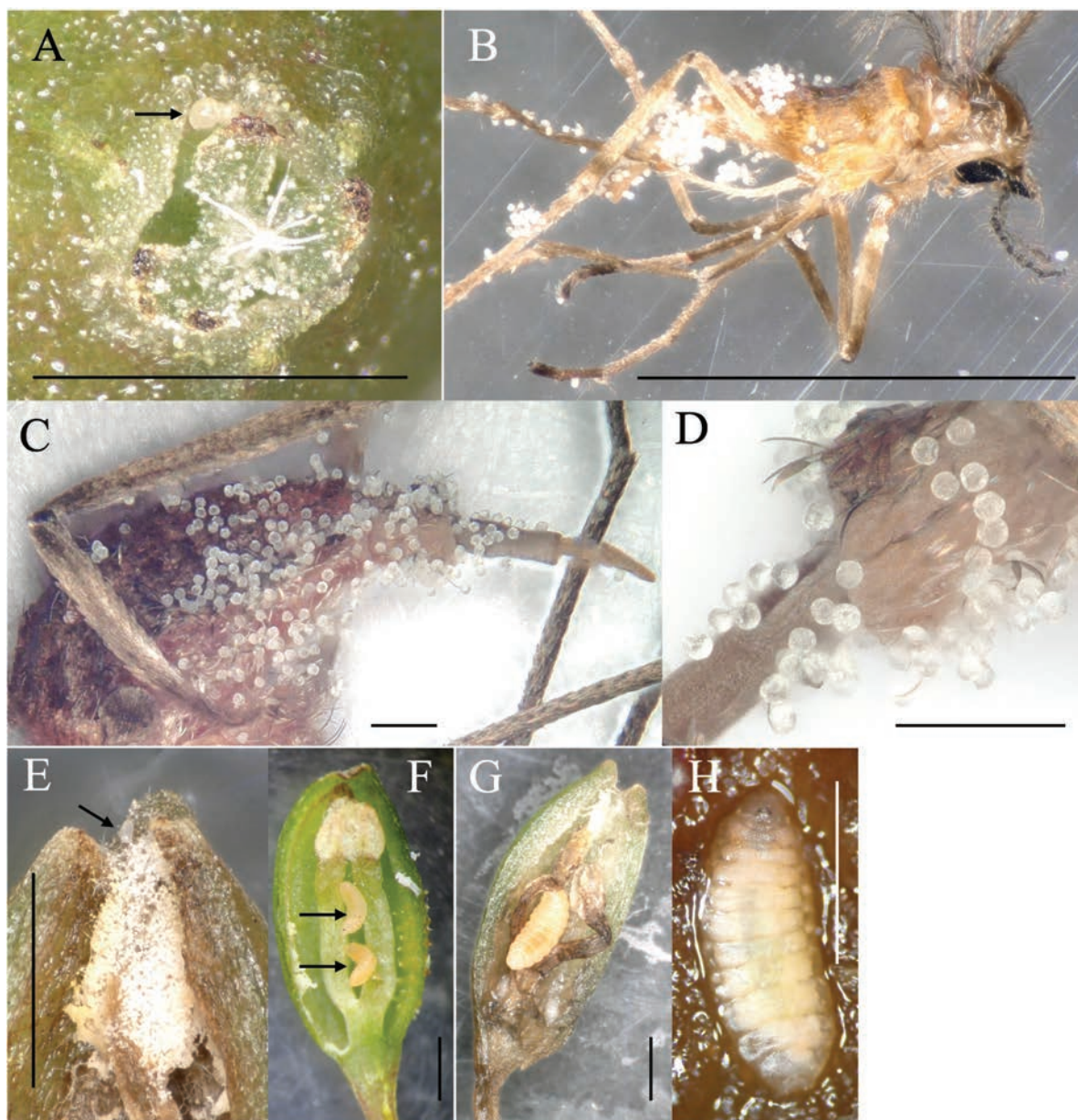


Figure 2. Attachment of *Heterosmilax japonica* pollen on the stigma and pollinator body, and larvae of the pollinator *Dasineura* midge breeding within male flowers **A** stigma of a female flower visited by the midge (arrow points to a deposited egg) **B–D** *Dasineura* gall midges that have visited female flowers (**B** body **C** abdomen **D** 7–8 segments of abdomen) **E** cross-section of a male flower visited by a *Dasineura* midge (arrow points to a deposited egg) **F** two larvae (arrows) feeding on pollen in a male flower **G** third instar larva having infested pollen and floral tissue **H** midge larva in dorsal view. Scale bars: 1 mm (**A, B, E–H**); 0.1 mm (**C, D**).

from egg deposition to adult emergence, was 24–26 days. The emerged midges were morphologically identical to those that had visited the flower, suggesting that the midge utilizes male *Heterosmilax* flowers as a brooding site.

Female flowers were visited by the *Dasineura* midge in the evening, but its visits were rarely observed. The female midge visited female flowers, extended its abdomen, touched stigma (Fig. 1N), and engaged in pollination (Fig. 2A). While oviposition was not confirmed, eggs resembling those deposited on male flowers were observed deposited on the inner wall of the perianth tube (Fig. 2A). The infestation of female flower tissue by midge larvae was not observed.

Taxonomy of the pollinator midge

Dasineura heterosmilacicola sp. nov.

<https://zoobank.org/A0D631C9-74F4-42EA-ABB3-83B4087DD40C>

Figs 3–7

Material examined. Holotype: JAPAN • 1 ♂, NSMT-I-Dip 36246, microscopic slide; Mt Kubura, Yonaguni Island, Yonaguni-chô, Yaeyama-gun, Okinawa Prefecture; 24.4572°N, 122.9586°E; altitude 90 m; 5-III-2019 (as larva in male flower of *Heterosmilax japonica*), emerged on 30-III-2019; M. Kato leg.

Paratypes: JAPAN • 2 ♂ 3 ♀, NSMT-I-Dip 36241–36245, freeze-dried specimens; NSMT-I-Dip 36247, microscopic slide; same data as holotype, emerged on 30–31-III-2019 M. Kato leg. • 2 ♂ 3 ♀, NSMT-I-Dip 36248–36250, freeze-dried specimens & NSMT-I-Dip 36251–36252, microscopic slides; Funaura, Iriomote Island, Taketomi-chô, Yaeyama-gun, Okinawa Prefecture; 16-IV-2023 (as larva in male flowers), emerged on 5–8-V-2023; M. Kato leg. • 1 ♂ 2 ♀, NSMT-I-Dip 36253–36255, freeze-dried specimens; Funaura, Iriomote Island, Taketomi-chô, Yaeyama-gun, Okinawa Prefecture; 5-VI-2018 (as larva in male flowers), emerged on 19–20-VI-2018; M. Kato leg.

Other material. JAPAN • 1 ♂ 3 ♀; same data as holotype, emerged on 30–31-III-2019 • 1 ♂ 3 ♀; Funaura, Iriomote Island, Taketomi-chô, Yaeyama-gun, Okinawa Prefecture; 5-VI-2018 (as larva on male flower), emerged on 19–22-VI-2018 • 1 ♂ 3 ♀; Funaura, Iriomote Island, Taketomi-chô, Yaeyama-gun, Okinawa Prefecture; 16-IV-2023 (as larva on male flower), emerged on 8-V-2023 • 1 ♂ 4 ♀; Higashinakama, Amami-Ôshima Island, Kagoshima Prefecture; 13-VI-2018 (as larva on male flower), emerged on 1-VII-2018; all these non-types M. Kato leg.

Diagnosis. A small species (wing length 1.2–1.5 mm); antenna with 12–13 flagellomeres in males, 11–12 in females. Eyes holoptic, with a distinct constriction at the middle. Tarsal claws bifid, each strongly curved downward beyond mid length. Male gonostylus basal 1/3 swollen, apically forming a dark brown sclerotized claw. Female abdomen with segments 7–8 protrusive; extended ovipositor 9–10× as long as 7th tergite; eighth tergite divided into two separate, narrow longitudinal sclerites, with a pair of anterior granular sensillae. Larva feeds on internal tissue of fallen male flower of *Heterosmilax japonica* (Smilacaceae).

Description. Adult male (Figs 3, 4):

Head (Fig. 3E, H, M): eyes holoptic, with a distinct constriction at the middle, along the frontal margin around antennae sockets. Eye facets circular; eye bridge 5–6 facets long. Antenna (Fig. 3C): scape and pedicel white and rounded; pedicel 2/3 as long as the scape (Fig. 3H); flagellomeres 12–13, brownish, with short, naked neck; neck length about 1/4 as long as node; circumfila composed of a continuous sub-basal band joined with a partial subapical band; 13–15 long subapical and 12–14 short sub-basal setae with enlarged alveoli (Fig. 3G, J–L). Palpus 4-segmented; segments 2–3 of similar length, 1.7 times as long as the 1st and 0.66 times as long as the 4th (Fig. 3I, M); each segment with several strong setae and covered by brownish scales (Fig. 3H).

Thorax: wing (Fig. 3B) length 1.3–1.4 mm; R1 joining C before mid-length of wing; R5 curving anteriorly and joining C before wing apex. M3+4 connected with Cu, forming a fork. Wing membrane with dense, dark microtrichia. Halter brownish. Scutum, scutellum, mediotergite, propleuron, anepisternum, katapisternum,

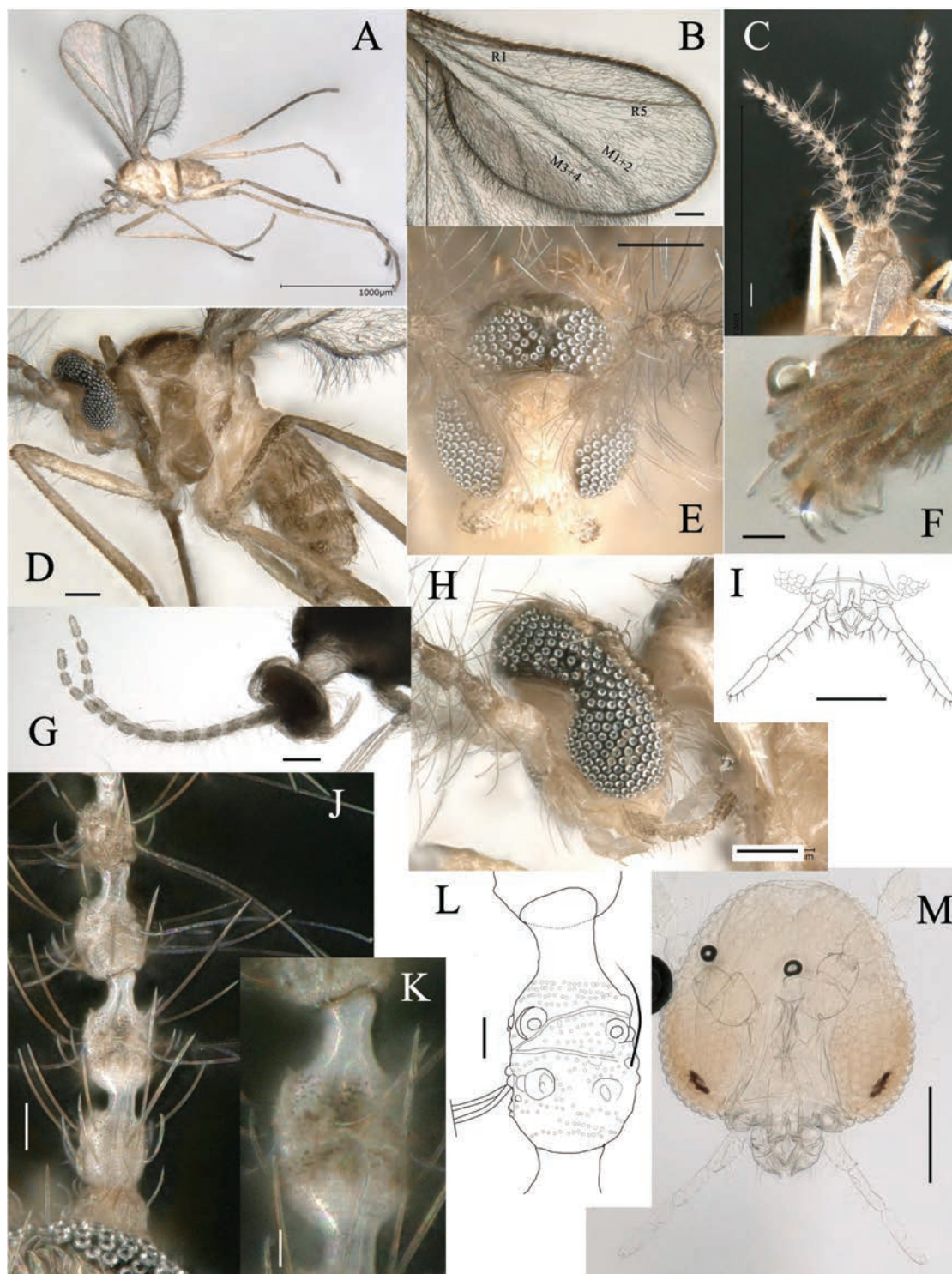


Figure 3. *Dasineura heterosmilacicola* sp. nov. male **A** habitus, lateral **B** wing **C** head and thorax, dorsal **D** body, lateral **E** head, frontal **F** tarsal claw of foreleg **G** antenna, lateral **H** head, lateral **I** mouthpart, frontal **J** segments 2–6 of an antenna, dorsal **K**, **L** 5th segment of an antenna, dorsal and lateral **M** head, frontal. Scale bars: 1 mm (**A**); 0.1 mm (**B–E**, **G–I**, **M**); 0.01 mm (**F**, **J–L**).

and katatergite brown; other parts whitish (Fig. 3D). Anepisternum with 5–6 setae on dorsal third; anepimeron with 7–8 setae; remaining pleura bare.

Legs slender and brown, but inner sides paler. Tarsal claws bifid on all legs; each claw strongly curved downward beyond mid-length; empodia as long as tarsal claws (Fig. 3F).

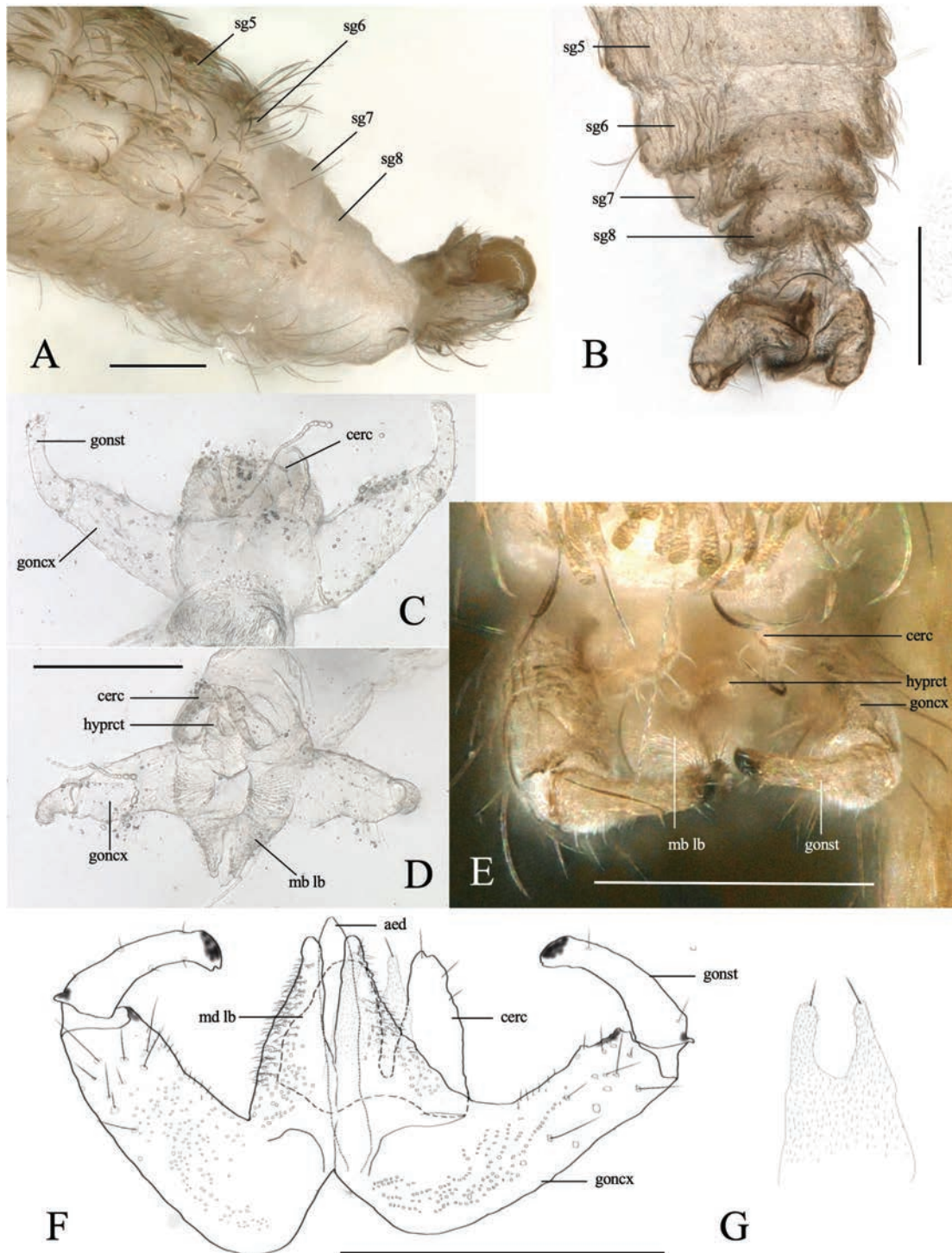


Figure 4. *Dasineura heterosmilacicola* sp. nov. male abdomen **A** abdomen, lateral **B** abdomen ventral **C–F** genitalia in dorsal (**C**, **E**), posterior (**D**) and ventral (**F**) views **G** hypoproct. Abbreviations: aed, aedeagus; cerc, cercus; goncx, gonocoxite; gonst, gonostylus; hyprect, hypoproct; mb lb, mediobasal lobe. Scale bars: 0.1 mm.

Abdomen: tergites 1–6 rectangular, each with a single row of setae along posterior margin and lateral setae, elsewhere mostly covered with brownish scales; 7th tergite unsclerotized, with a pair of medial setae (Figs 3D, 4A); 8th tergite unsclerotized. Sternites 1–7 rectangular, divided transversely, sclerotized as two pigmented transversal bands, each bearing a row of setae; 8th sternite smaller than others, emarginate posteromedially (Fig. 4A, B), setulose.

Terminalia (Fig. 4C–G): gonocoxite stout cylindrical, setulose, with setae on apical half and densely setose inward. Gonostylus tapering distally, weakly arched inward, sparsely setulose, apically forming dark-brown sclerotized claw. Mediobasal lobe subdivided, sheathing aedeagus, slightly shorter than aedeagus, densely covered with setulae directed backward. Hypoproct shorter than cerci, with narrow lobes, U-shaped incision about 1/3 length of hypoproct, uniformly covered with microtrichia and with one apical seta on each lobe (Fig. 4G). Cerci ovate, deeply separated, setose distally. Aedeagus with subtriangular apex.

Adult female (Figs 5, 6)

Head: similar to male except the antenna. Antenna (Fig. 5C); scape and pedicel pale and rounded, pedicel 2/3 as long as scape (Fig. 5D, G); 11–12 flagellomeres (Fig. 4C), brownish without neck; circumfila composed of a continuous sub-basal band and a partial subapical band joined by two connectives: dorsally with 6–7 basal setae with large alveoli; ventrally with 6–7 long subapical and 6–7 short sub-basal setae with enlarged alveoli (Fig. 5I, J).

Thorax: wing (Fig. 5E) length 1.2–1.5 mm. Wing venation similar to male. Notum pale brown with a pair of dark longitudinal stripes covered by long setae and brownish scales (Fig. 5C). Legs similar to male (Fig. 5K).

Abdomen: tergites 1–6 rectangular, 5th–6th each narrower than the previous one; all with single row of posterior setae, elsewhere mostly covered with scales (Fig. 5B, D); 7th tergite narrow, with many setae on posterior margin, covering only the anterior half of 7th segment; posterior half naked without scale; 8th tergite divided into two separate, narrow longitudinal sclerites; sclerites slightly divergent anteriorly and subparallel posteriorly, with a pair of anterior granular sensillae (Fig. 5B). Sternites 1–7 rectangular, divided transversely, sclerotized as two pigmented transversal bands, each bearing a row of setae (Fig. 6C). Long tubular ovipositor, usually housed in segments 6–8, but protruding and extended at oviposition (Fig. 6F, G); extended ovipositor (from base of 8th segment to cercus apex) 9–10× as long as 7th tergite. Cerci as long as 7th tergite, fused medially into a single terminal lamella, evenly microtrichose; hypoproct narrow, microtrichose, with a pair of distal setae (Fig. 6E).

Larva. full-grown larva (Figs 2H, 7): yellowish white, cylindrical, slightly flattened dorso-ventrally, pointed anteriorly, blunt posteriorly (Fig. 2H). Head capsule hemispherical, cephalic apodemes about as long as head capsule, antennae about twice as long as wide (Fig. 7A, B). Sternal spatula anteriorly bidentate with V-shaped emargination, slightly extended laterally just posterior to teeth; length/width ratio is 3–4 (Fig. 7C, D). Thoracic and abdominal segments dorsally with three inner and two outer lateral papillae on each side; each papilla with seta, except the central inner papilla (Fig. 7A, E). Terminal segment dorsally with eight terminal papillae, each with seta (Fig. 7E).

Etymology. The name *heterosmilacicola* denotes living on *Heterosmilax*.

Japanese name. Karasukibasankirai-hana-tamabae.

Host plant. Male flower of *Heterosmilax japonica* (Smilacaceae).

Biological notes. An adult female visits a male flower of the host plant species and lays an egg in the perianth tube. The larva grows by feeding on the pollen and the floral tissue of the fallen male flower. This species is the obligate pollinator of the host plant, breeding in fallen male flowers.

Distribution. Japan: Ryukyu Archipelago.

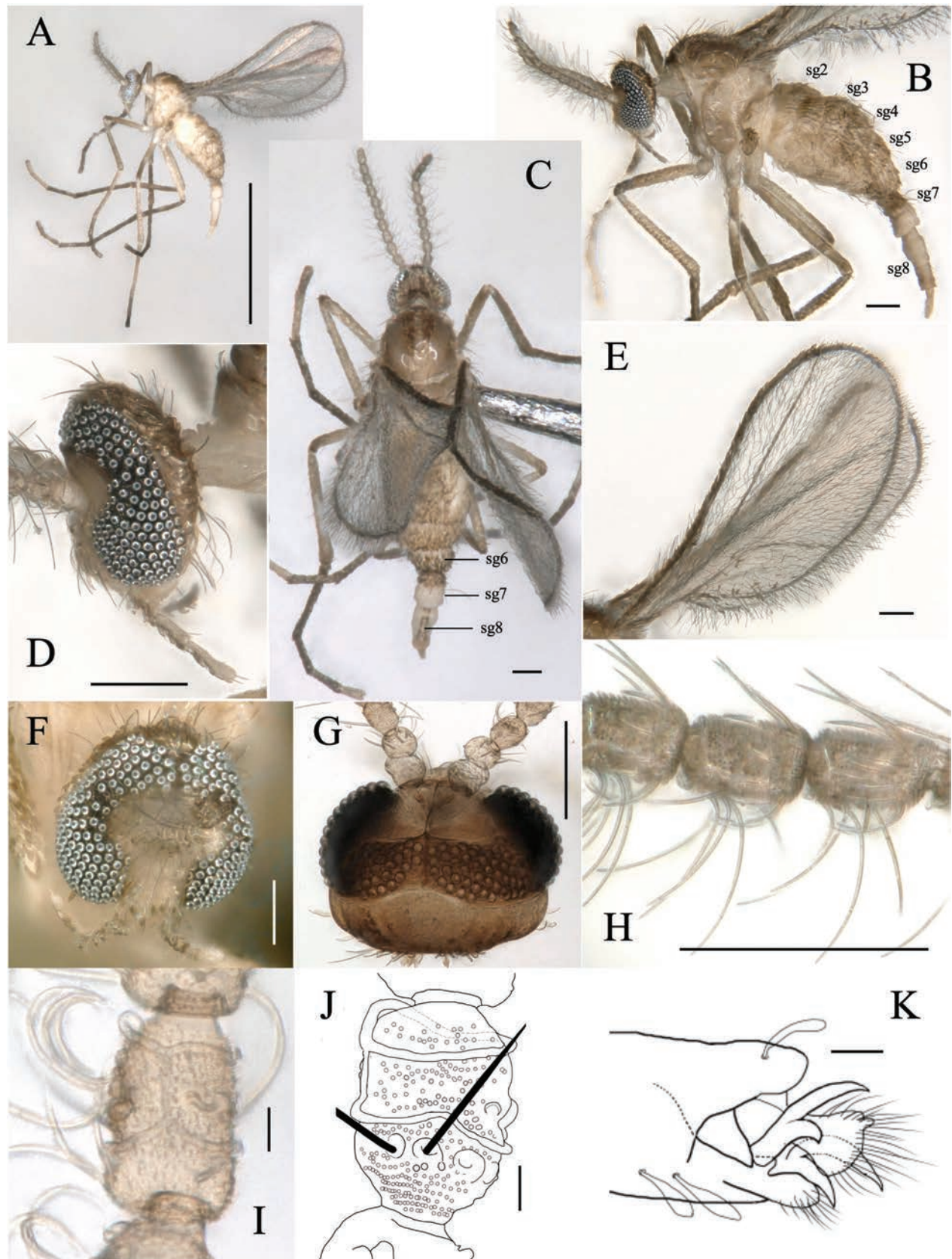


Figure 5. *Dasineura heterosmilacicola* sp. nov. female **A** habitus, lateral **B** body, lateral **C** habitus dorsal **D** head, lateral **E** wing **F** head, frontal **G** head, dorsal **H** segments 3–5 of an antenna, dorsal **I**, **J** 5th segment of an antenna, dorsal and ventral **K** tarsal claw of hindleg, lateral. Abbreviations: sg2–sg8, 2nd–8th segments. Scale bars: 1 mm (**A**); 0.1 mm (**B**–**H**); 0.01 mm (**I**–**K**).

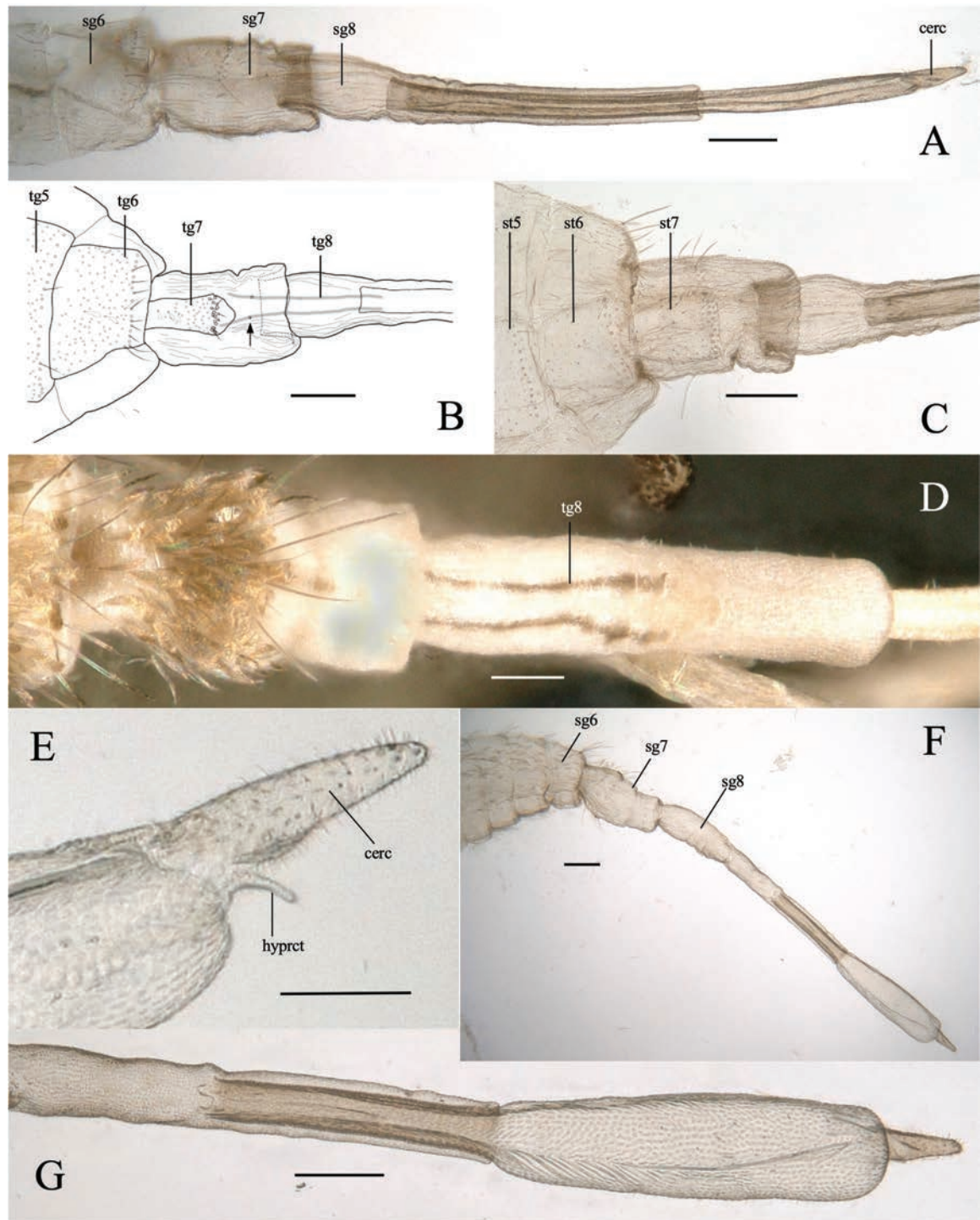


Figure 6. *Dasineura heterosmilacicola* sp. nov. female abdomen **A** segments 6–8, lateral **B**, **C** segments 5–8, dorsal and ventral **D** segments 7–8, dorsal **E** cercus, lateral **F** post-abdomen with fully protruded ovipositor, lateral **G** protruded ovipositor. Abbreviations: cerc, cercus; hypprct, hypoproct; sg6–sg8, 6–8th segments; st5–st7, 5–7th sternites; tg5–tg8, 5–8th tergites. The arrow indicates sensilla on the 8th tergite. Scale bars: 0.1 mm (**A–D**, **F**); 0.01 mm (**E**, **G**).

Remarks. So far, 10 *Dasineura* species are known from Japan (host plant: Pinaceae 3 spp., Fabaceae 3 spp., Symplocaceae, 1 sp., Rubiaceae 1 sp., Asteraceae 1 sp., Adoxaceae 1 sp.: Yukawa 1971; Elsayed et al. 2017). No species has been collected from monocots, and there are no described species closely related to this one. The species resembles *D. wisteriae*, which induces

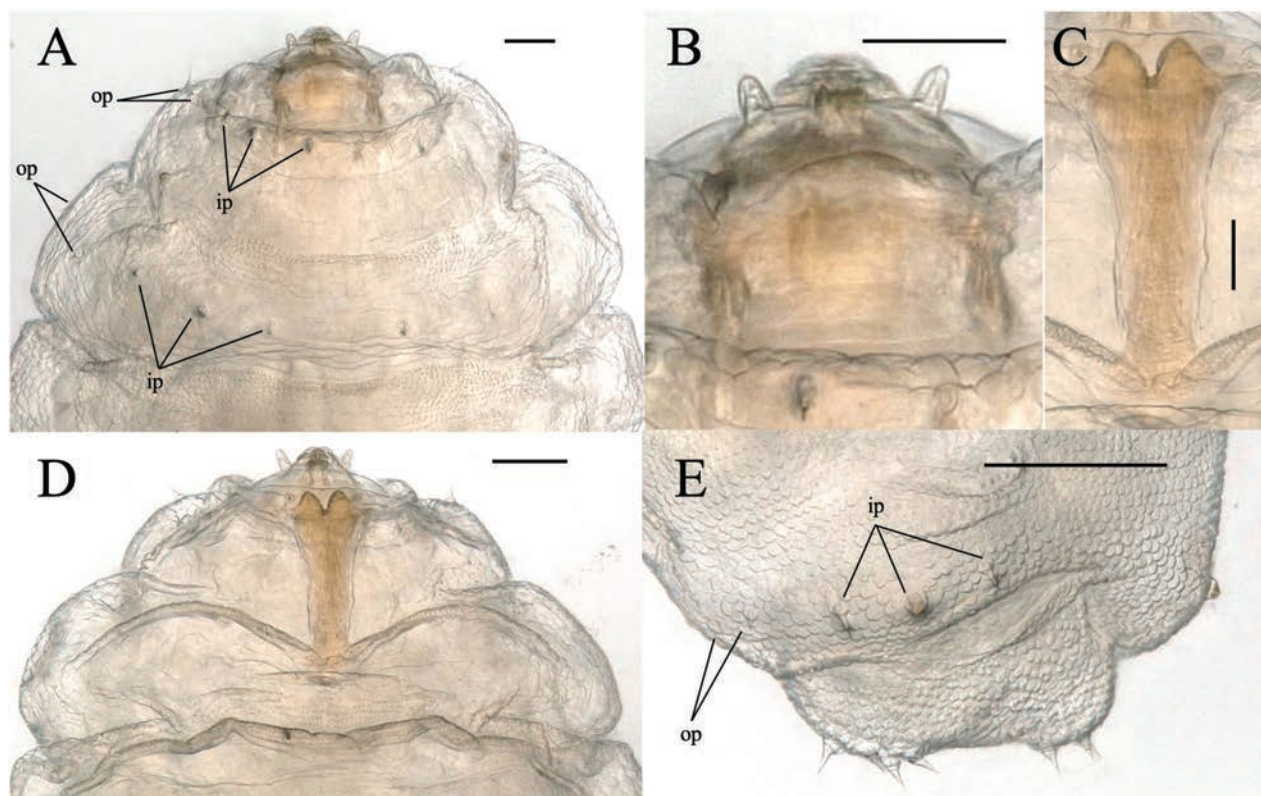


Figure 7. *Dasineura heterosmilacicola* sp. nov. full-grown larva **A** head and thorax, dorsal **B** head, dorsal **C** sternal spatula, ventral **D** head and thorax, ventral **E** 8th and terminal segments, left dorso-lateral. Abbreviations: ip, inner papilla; op, outer papilla. Scale bars: 0.1 mm.

gall formation on flower buds of *Wisteria* (Fabaceae) (Nakawatase and Yukawa 1984), but there are fewer flagellomeres than in the latter (male: 12–13 vs 14–15), and the life cycle is multivoltine (the latter univoltine). This species most closely resembles *D. camassiae*, whose larva grows in the flower bud galls of two monocot species of *Camassia* (Asparagaceae, Agavoideae), but is discriminated from the latter by the number of flagellomeres (male: 12–13 in this species, 13–15 in the latter; female: 11–12 in this species, 13–14 in the latter), the morphology of the male terminalia (cerci deeply incised in this species, but shallowly incised in the latter), the morphology of the female 7th tergite (subparallel in the former, but distinctly constricted at the middle in the latter), and the larval morphology (tergite dorsally in each side, with five papillae in the former and four in the latter; length/width ratio of sternal spatula is 3–4 in this species and 7–8 in the latter).

Phylogeny of the pollinator gall midge

Molecular phylogenetic analysis of the 28S rRNA and COI genes revealed that the pollinator midge is closely related to *Dasineura miki*, a flower parasite on Asteraceae (Fig. 8). The 615-bp COI sequences of the three adults and 10 larvae were all identical, except for one adult and one larval sequence that differed by a single base, confirming that all sampled adults and larvae belonged to a single species.

Discussion

Brood-site pollination mutualism

A mutualistic interaction between *Heterosmilax japonica* and a newly identified flower-parasitic gall midge, *Dasineura heterosmilacicola* sp. nov., which breeds in the male flowers, was observed on several islands of the Ryukyu Archipelago, Japan. This example of brood-site pollination mutualism associated with a gall midge is the second to be observed in monocots, and the first report of mutualism associated with the cecidomyiid supertribe Lasiapteridi (Table 1). Similar to other examples of gall-midge-associated brood-site pollination mutualism, *Heterosmilax* has unisexual flowers, and pollinator larvae breed only in fallen male flowers (Table 1).

In contrast to other descriptions of mutualism, the female pollinator gall midge identified in this study visited male flowers almost exclusively during the early morning, and male flowers fell the day after anthesis, whether or not they had been visited by gall midges. When the post-abdomen of a female midge is inserted into a male ellipsoid flower from the narrow flower entrance, it becomes dusted with pollen. The fallen male flower must therefore be the brood site for the pollinator gall midge larvae, with the larvae initially feeding on pollen and later on floral tissue. Thus, the sympetalous ellip-

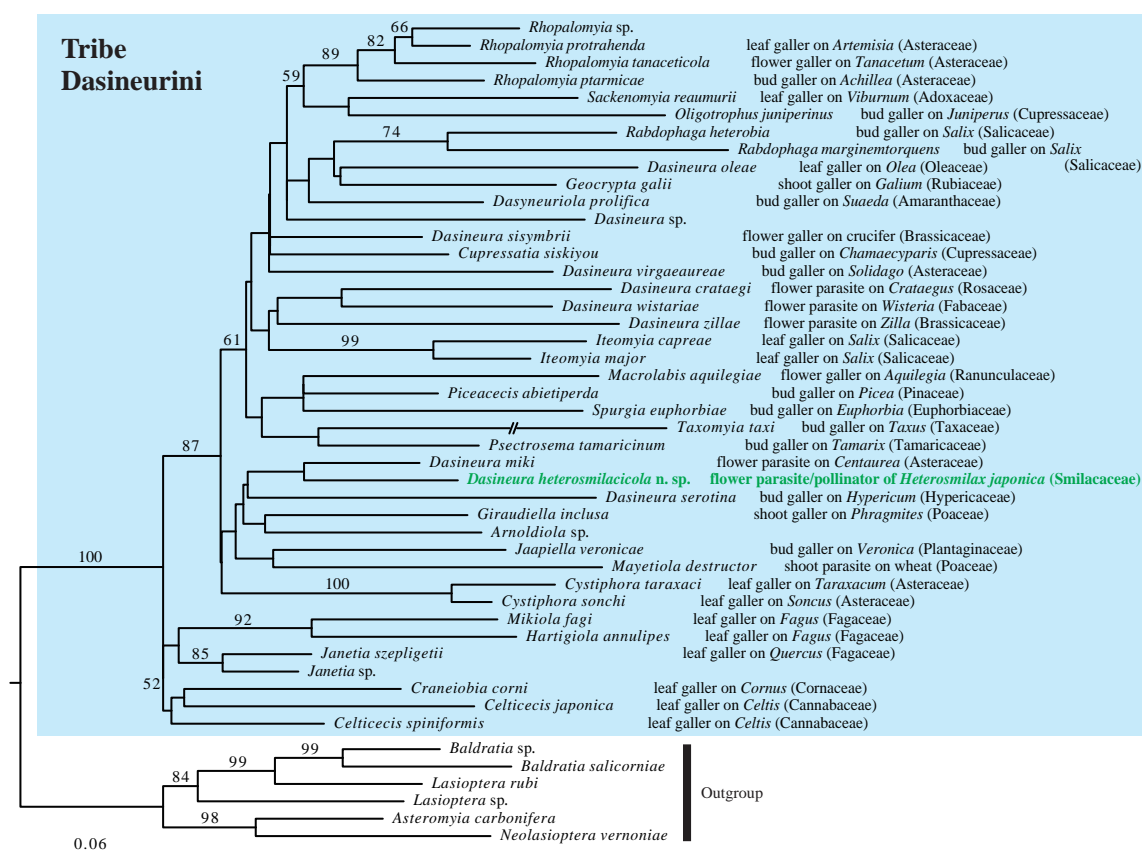


Figure 8. Maximum-likelihood tree of the gall midge tribe Dasineurini based on combined 28S rRNA and COI gene sequences, showing the phylogenetic position of the *Dasineura* gall midge that pollinates *Heterosmilax japonica*. Numbers above the branches are bootstrap values based on 1,000 replications. Sequence data are from Dorchin et al. (2019), except the newly obtained sequence for the pollinator of *Heterosmilax japonica*. The long terminal branch of *Taxomyia taxi* was trimmed.

soid flower seems to have adapted to allow pollen dusting on the elongated post-abdomen of the female gall midge while also protecting and incubating gall midge larvae. This example of brood-site pollination mutualism therefore differs from other mutualisms in the sexual expression of the flowers, the morphology and persistence of the male flowers, the brood site for pollinator larvae, and the food of those larvae.

As a female gall midge that has visited female flowers is dusted with pollen (Fig. 2B–D), it acts as a potential pollination agent if other such midges also visit female flowers. While visits to female flowers were rarely observed (Fig. 1N), the eggs that were presumably laid by the female gall midges were often deposited on pollinated flowers (Fig. 2A), suggesting that female flowers also attract female gall midges via floral odor by deceit. The absence of larvae on female flowers suggests that larvae are unable to grow in female flowers. Rather, female gall midges visit both male and female *Heterosmilax* flowers to oviposit, with the deposited eggs able to grow only on fallen male flowers. In addition, the observation that *Heterosmilax* flowers on all three islands (Yonaguni, Iriomote, and Amami-Ōshima) were visited exclusively by the same gall midge species suggests that the mutualism is highly specific and obligate.

Because male flowers contribute to the production of pollinator gall midges, pollination efficiency presumably depends on their abundance. The flowering season of *Heterosmilax* is long, lasting up to five months (from March to July), and only male flowers bloom during the early flowering season. This flowering pattern can be understood as reproductive strategy of male plants.

Heterosmilax is monophyletic (Qi et al. 2013) and comprises 11 species found in Southeast and East Asia (Koyama 1984). Further studies on other congeneric species will reveal whether sympetalous ellipsoid flowers have evolved to allow similar brood-site pollination mutualism, and whether parallel cospeciation has occurred in the plant and pollinator lineages.

Evolution of the pollinator gall midge

The pollinator gall midge is a newly discovered species within the diverse genus *Dasineura*; it is also the first pollinator species recognized within the tribe Dasineurini and the supertribe Lasiopteridi. All previously known pollinating gall midge species belong to the supertribe Cecidomyiidi (Table 1).

The phylogenetic tree (Fig. 8) suggests the evolution from flower-galler/parasite to mutualistic flower parasite on *Heterosmilax* flowers. For example, *D. camassiae* is a flower bud galler of *Camassia leichtlinii* (Asparagaceae, Agavoideae) that reduces the fitness of the host plant by feeding on the ovules of bisexual flowers (Gagné et al. 2014). A comparison of the two *Dasineura* species shows that tergites 6 and 7 are much wider in *D. heterosmilacicola* than in *D. camassiae*, such that the post-abdomen is covered by larger numbers of setae and scales, which may promote pollen attachment. *D. camassiae* females oviposit on the flower buds of the host plant, with the larvae that leave the bud galls entering hibernation until the next flower season, in spring, indicative of a univoltine life cycle. *Dasineura heterosmilacicola*, by contrast, is multivoltine, with several generations occurring during the long (up to 5 months) flowering season.

The timing of flower visitation would be expected to differ between parasitic and mutualistic gall midges. Many females of *D. heterosmilacicola* were seen to gregariously visit newly opened male flowers in the morning, while *D. camassiae* visits flower buds before anthesis. Further studies on the temporal changes in floral odor from flower bud formation to anthesis and the corresponding responses of gall midges are needed. Furthermore, assuming that the genus *Dasineura* is highly diverse, reflecting its associations with a diverse group of angiosperm flowers, comparisons based on phylogenetic relationships will provide insights into the transition from flower parasites to brood-site pollinators.

Acknowledgements

We thank N. Dorchin for invaluable and helpful advice on our manuscript, and L. Yamamori and T. Nishioka for help with fieldwork on Amami-Ōshima Island. We also thank H. Nagamasu and H. Motokawa of Kyoto University Museum for storing our herbarium/insect specimens and for helping in studies of the specimens.

Additional information

Conflict of interest

The authors have declared that no competing interests exist.

Ethical statement

No ethical statement was reported.

Funding

This work was supported by a Japan Ministry of Education, Culture, Science, Sports, and Technology Grant-in-Aid for Scientific Research (#15H02420, #20H03321 for MK; 24K02084 for AK).

Author contributions

Conceptualization: MK. Data curation: MK. Funding acquisition: MK, AK. Investigation: AK, MK. Writing - original draft: MK. Writing - review and editing: AK.

Author ORCIDs

Makoto Kato  <https://orcid.org/0000-0002-0602-7082>

Atsushi Kawakita  <https://orcid.org/0000-0002-4864-7423>

Data availability

All of the data that support the findings of this study are available in the main text or Supplementary Information.

References

- Armstrong JE, Irving HK (1990) Functions of staminodia in the beetle-pollinated flowers of *Eupomatia laurina*. *Biotropica* 22: 429–431. <https://doi.org/10.2307/2388563>
- Belshaw R, Lopez-Vaamonde C, Degerli N, Quicke, DJ (2001) Paraphyletic taxa and taxonomic chaining: evaluating the classification of braconine wasps

- (Hymenoptera: Braconidae) using 28S D2–3 rDNA sequences and morphological characters. *Biological Journal of the Linnean Society* 73: 411–424. <https://doi.org/10.1111/j.1095-8312.2001.tb01370.x>
- Carneiro MAA, Branco CS, Braga CE, Almada ED, Costa M, Maia VC, Fernandes, GW (2009) Are gall midge species (Diptera, Cecidomyiidae) host-plant specialists? *Revista Brasileira de Entomologia* 53: 365–378. <https://doi.org/10.1590/S0085-56262009000300010>
- Carson HL, Okada T (1980) Drosophilidae associated with flowers in Papua New Guinea. I. *Colocasia esculenta*. *Kontyû* 48: 15–29.
- Dorchin N, Harris KM, Stireman III JO (2019) Phylogeny of the gall midges (Diptera, Cecidomyiidae, Cecidomyiinae): systematics, evolution of feeding modes and diversification rates. *Molecular Phylogenetics and Evolution* 140: 106602. <https://doi.org/10.1016/j.ympev.2019.106602>
- Edler D, Antonelli AKJ, Silvestro D (2021) raxmlGUI 2.0: a graphical interface and toolkit for phylogenetic analyses using RAxML. *Methods in Ecology and Evolution* 12: 373–377. <https://doi.org/10.1111/2041-210X.13512>
- Elsayed AK, Kawakita A (2022) Two new species of mutualistic gall midges (Diptera: Cecidomyiidae) responsible for the pollination of *Phyllanthus flexuosus* (Phyllanthaceae) and using its male flower buds as brood-sites. *Proceedings of the Entomological Society of Washington* 124(3): 499–415. <https://doi.org/10.4289/0013-8797.124.3.499>
- Elsayed AK, Ogata K, Kaburagi K, Yukawa J, Tokuda M (2017) A new *Dasineura* species (Diptera: Cecidomyiidae) associated with *Symplocos cochinchinensis* (Loureiro) (Symplocaceae) in Japan. *Japanese Journal of Systematic Entomology* 23(1): 81–86.
- Essig FB (1973) Pollination in some New Guinea palms. *Principes* 17(3): 75–83.
- Etl F, Francke W, Schönenberger J, Dötterl S (2022) Chemical attraction of gall midge pollinators (Cecidomyiidae: Cecidomyiinae) to *Anthurium acutangulum* (Araceae). *Journal of Chemical Ecology* 48(3): 263–269. <https://doi.org/10.1007/s10886-022-01349-3>
- Fan JH, Thien LB, Luo YB (2011) Pollination systems, biogeography, and divergence times of three allopatric species of *Schisandra* in North America, China, and Japan. *Journal of Systematics and Evolution* 49(4): 330–338. <https://doi.org/10.1111/j.1759-6831.2011.00125.x>
- Feil JP (1992) Reproductive ecology of dioecious *Siparuna* (Monimiaceae) in Ecuador—a case of gall midge pollination. *Botanical Journal of the Linnean Society* 110(3): 171–203. <https://doi.org/10.1111/j.1095-8339.1992.tb00290.x>
- Folmer O, Black M, Hoeh W, Lutz R, Vrijenhoek R (1994) DNA primers for amplification of mitochondrial cytochrome c oxidase subunit I from diverse metazoan invertebrates. *Molecular Marine Biology and Biotechnology* 3: 294–297.
- Gagné RJ (1989) *The plant-feeding gall midges of North America*. Cornell University Press, Ithaca, 356 pp.
- Gagné RJ, Jaschhof M (2021) *A Catalog of the Cecidomyiidae (Diptera) of the World*. 5th Edn. Digital, 814 pp.
- Gagné RJ, Barosh T, Kephart S (2014) A new species of *Dasineura* Rondani (Diptera: Cecidomyiidae) in flower galls of *Camassia* (Asparagaceae: Agavoideae) in the Pacific Northwest, USA. *Zootaxa* 3900(2): 271–278. <https://doi.org/10.11646/zootaxa.3900.2.7>
- Gardner EM, Gagné RJ, Kendra PE, Montgomery W, Raguso RA, McNeil TT, Zerega NJ (2018) A flower in fruit's clothing: Pollination of jackfruit (*Artocarpus heterophyllus*, Moraceae) by a new species of gall midge, *Clinodiplosis ultracrepidata* sp. nov.

- (Diptera: Cecidomyiidae). International Journal of Plant Sciences 179(5): 350–367. <https://doi.org/10.1086/697115>
- Henderson A (1986) A review of pollination studies in the Palmae. The Botanical Review 52: 221–259. <https://doi.org/10.1007/BF02860996>
- Kato M, Kawakita A [Eds] (2017) Obligate pollination mutualism. Springer, Tokyo, 321 pp. <https://doi.org/10.1007/978-4-431-56532-1>
- Kawakita A, Elsayed AK, Mochizuki K, Vandrot H (2022) Pollination of *Phyllanthus* (Phyllanthaceae) by gall midges that use male flower buds as larval brood sites. Flora 293: 152115. <https://doi.org/10.1016/j.flora.2022.152115>
- Koyama T (1984) A taxonomic revision of the genus *Heterosmilax* (Smilacaceae). Brittonia 36: 184–205. <https://doi.org/10.2307/2806629>
- Luo YB, Li ZY (1999) Pollination ecology of *Chloranthus serratus* (Thunb.) Roem. et Schult. and *Ch. fortunei* (A.Gray) Solms-Laub. (Chloranthaceae). Annals of Botany 83: 489–499. <https://doi.org/10.1006/anbo.1998.0845>
- Luo SX, Chaw SM, Zhang D, Renner SS (2010) Flower heating following anthesis and the evolution of gall midge pollination in Schisandraceae. American Journal of Botany 97(7): 1220–1228. <https://doi.org/10.3732/ajb.1000077>
- Luo SX, Liu TT, Cui F, Yang ZY, Hu XY, Renner SS (2017) Coevolution with pollinating resin midges led to resin-filled nurseries in the androecia, gynoecia and tepals of *Kadsura* (Schisandraceae). Annals of Botany 120(5): 653–664. <https://doi.org/10.1093/aob/mcx024>
- Luo SX, Zhang LJ, Yuan S, Ma ZH, Zhang DX, Renner SS (2018) The largest early-diverging angiosperm family is mostly pollinated by ovipositing insects and so are most surviving lineages of early angiosperms. Proceedings of the Royal Society B: Biological Sciences 285(1870): 20172365. <https://doi.org/10.1098/rspb.2017.2365>
- McAlpine JF, Peterson BV, Shewell GE, Teskey HJ, Vockeroth JR, Wood M [Eds] (1981) Manual of Nearctic Diptera. Vol. 1. Research Branch, Agriculture Canada. Monograph No. 27. Agriculture Canada, Ottawa, 674 pp.
- Mochizuki K, Kawakita A (2018) Pollination by fungus gnats and associated floral characteristics in five families of the Japanese flora. Annals of Botany 121(4): 651–663. <https://doi.org/10.1093/aob/mcx196>
- Nakawatase A, Yukawa J (1984) Redescription of the wisteria flower bud midge, *Dasi-neura wisteriae* Mani (Diptera: Cecidomyiidae). Bulletin of the Kitakyushu Museum of Natural History 5: 85–90.
- Qi Z, Cameron KM, Li P, Zhao Y, Chen S, Chen G, Fu C (2013) Phylogenetics, character evolution, and distribution patterns of the greenbriers, Smilacaceae (Liliales), a near-cosmopolitan family of monocots. Botanical Journal of the Linnean Society 173(4): 535–548. <https://doi.org/10.1111/boj.12096>
- Riley CV (1892) The Yucca Moth and Yucca Pollination. Missouri Botanical Garden, St. Louis, 94 pp. <https://doi.org/10.2307/2992075>
- Sakai S (2002a) A review of brood-site pollination mutualism: plants providing breeding sites for their pollinators. Journal of Plant Research 115: 161–168. <https://doi.org/10.1007/s102650200021>
- Sakai S (2002b) *Aristolochia* spp. (Aristolochiaceae) pollinated by flies breeding on decomposing flowers in Panama. American Journal of Botany 89(3): 527–534. <https://doi.org/10.3732/ajb.89.3.527>
- Sakai S, Kato M, Nagamasu H (2000) *Artocarpus* (Moraceae)–gall midge pollination mutualism mediated by a male-flower parasitic fungus. American Journal of Botany 87(3): 440–445. <https://doi.org/10.2307/2656640>

- Sawyer NW, Anderson GJ (1998) Reproductive biology of the carrion-flower, *Smilax herbacea* (Smilacaceae). *Rhodora* 100: 1–24.
- Takano KT, Repin R, Mohamed MB, Toda MJ (2012) Pollination mutualism between *Alocasia macrorrhizos* (Araceae) and two taxonomically undescribed *Colocasiomyia* species (Diptera: Drosophilidae) in Sabah, Borneo. *Plant Biology* 14(4): 555–564. <https://doi.org/10.1111/j.1438-8677.2011.00541.x>
- Takenaka K, Yin JT, Wen SY, Toda MJ (2006) Pollination mutualism between a new species of the genus *Colocasiomyia* de Meijere (Diptera: Drosophilidae) and *Steudnera colocasiifolia* (Araceae) in Yunnan, China. *Entomological Science* 9(1): 79–91. <https://doi.org/10.1111/j.1479-8298.2006.00156.x>
- Tamura K, Stecher G, Kumar S (2021) MEGA11: Molecular Evolutionary Genetic Analysis version 11. *Molecular Biology and Evolution* 38: 3022–3027. <https://doi.org/10.1093/molbev/msab120>
- Tang W (1987) Insect pollination in the cycad *Zamia pumila* (Zamiaceae). *American Journal of Botany* 74: 90–99. <https://doi.org/10.1002/j.1537-2197.1987.tb08582.x>
- Thien LB, Sage TL, Jaffré T, Bernhardt P, Pontieri V, Weston PH, Malloch D, Azuma H, Graham SW, McPherson MA, Rai HS, Sage RF, Dupre JL (2003) The population structure and floral biology of *Amborella trichopoda* (Amborellaceae). *Annals of the Missouri Botanical Garden* 90: 466–490. <https://doi.org/10.2307/3298537>
- Vislobokov NA, Galinskaya TV, Degtjareva GV, Valiejo-Roman CM, Samigullin TH, Kuznetsov AN, Sokoloff DD (2014) Pollination of Vietnamese *Aspidistra xuansonsensis* (Asparagaceae) by female Cecidomyiidi flies: larvae of pollinator feed on fertile pollen in anthers of anthetic bisexual flowers. *American Journal of Botany* 101(9): 1519–1531. <https://doi.org/10.3732/ajb.1400359>
- Yuan LC, Luo YB, Thien LB, Fan JH, Xu H, Chen ZD (2007) Pollination of *Schisandra henryi* (Schisandraceae) by female, pollen-eating *Megommata* species (Cecidomyiidae, Diptera) in south-central China. *Annals of Botany* 99(3): 451–460. <https://doi.org/10.1093/aob/mcl287>
- Yuan LC, Luo YB, Thien LB, Fan JH, Xu HL, Yukawa J, Chen ZD (2008) Pollination of *Kadsura longipedunculata* (Schisandraceae), a monoecious basal angiosperm, by female, pollen-eating *Megommata* sp. (Cecidomyiidae: Diptera) in China. *Biological Journal of the Linnean Society* 93(3): 523–536. <https://doi.org/10.1111/j.1095-8312.2007.00897.x>
- Yukawa J (1971) A revision of the Japanese gall midges: Diptera: Cecidomyiidae. *Memoirs of the Faculty of Agriculture, Kagoshima University* 8(1): 1–203.

Supplementary material 1

Taxa used in the phylogenetic analysis, with GenBank accession numbers

Authors: Makoto Kato, Atsushi Kawakita

Data type: docx

Explanation note: Sequences of *Dasineura heterosmilacicola* sp. nov. (shown with asterisk) were newly obtained; other sequences are from Dorchin et al. (2019).

Copyright notice: This dataset is made available under the Open Database License (<http://opendatacommons.org/licenses/odbl/1.0/>). The Open Database License (ODbL) is a license agreement intended to allow users to freely share, modify, and use this Dataset while maintaining this same freedom for others, provided that the original source and author(s) are credited.

Link: <https://doi.org/10.3897/zookeys.1234.146453.suppl1>